frontiers | Research Topics

# Women in biogeochemical dynamics research 2022

**Edited by**
Claudia Cosio, Andrea G. Bravo and Marta Sebastian

**Published in**
Frontiers in Environmental Science
Frontiers in Marine Science

ISSN 1664-8714
ISBN 978-2-8325-4862-2
DOI 10.3389/978-2-8325-4862-2

## About Frontiers

Frontiers is more than just an open access publisher of scholarly articles: it is a pioneering approach to the world of academia, radically improving the way scholarly research is managed. The grand vision of Frontiers is a world where all people have an equal opportunity to seek, share and generate knowledge. Frontiers provides immediate and permanent online open access to all its publications, but this alone is not enough to realize our grand goals.

## Frontiers journal series

The Frontiers journal series is a multi-tier and interdisciplinary set of open-access, online journals, promising a paradigm shift from the current review, selection and dissemination processes in academic publishing. All Frontiers journals are driven by researchers for researchers; therefore, they constitute a service to the scholarly community. At the same time, the *Frontiers journal series* operates on a revolutionary invention, the tiered publishing system, initially addressing specific communities of scholars, and gradually climbing up to broader public understanding, thus serving the interests of the lay society, too.

## Dedication to quality

Each Frontiers article is a landmark of the highest quality, thanks to genuinely collaborative interactions between authors and review editors, who include some of the world's best academicians. Research must be certified by peers before entering a stream of knowledge that may eventually reach the public - and shape society; therefore, Frontiers only applies the most rigorous and unbiased reviews. Frontiers revolutionizes research publishing by freely delivering the most outstanding research, evaluated with no bias from both the academic and social point of view. By applying the most advanced information technologies, Frontiers is catapulting scholarly publishing into a new generation.

## What are Frontiers Research Topics?

Frontiers Research Topics are very popular trademarks of the *Frontiers journals series*: they are collections of at least ten articles, all centered on a particular subject. With their unique mix of varied contributions from Original Research to Review Articles, Frontiers Research Topics unify the most influential researchers, the latest key findings and historical advances in a hot research area.

Find out more on how to host your own Frontiers Research Topic or contribute to one as an author by contacting the Frontiers editorial office: frontiersin.org/about/contact

# Women in biogeochemical dynamics research: 2022

**Topic editors**

Claudia Cosio — Université de Reims Champagne-Ardenne, France

Andrea G. Bravo — Institute of Marine Sciences, Spanish National Research Council (CSIC), Spain

Marta Sebastian — Institut de Ciències del Mar, CSIC, Spain

**Citation**

Cosio, C., Bravo, A. G., Sebastian, M., eds. (2024). *Women in biogeochemical dynamics research: 2022*. Lausanne: Frontiers Media SA.

doi: 10.3389/978-2-8325-4862-2

# Table of contents

frontiers | Frontiers in Environmental Science

TYPE Editorial
PUBLISHED 24 April 2024
DOI 10.3389/fenvs.2024.1414689



OPEN ACCESS

EDITED AND REVIEWED BY
Vera I. Slaveykova,
University of Geneva, Switzerland

*CORRESPONDENCE
Claudia Cosio,
claudia.cosio@univ-reims.fr

RECEIVED 09 April 2024
ACCEPTED 11 April 2024
PUBLISHED 24 April 2024

CITATION
Cosio C, Bravo AG and Sebastian M (2024), Editorial: Women in biogeochemical dynamics research: 2022.
*Front. Environ. Sci.* 12:1414689.
doi: 10.3389/fenvs.2024.1414689



# Editorial: Women in biogeochemical dynamics research: 2022

Claudia Cosio[1]*, Andrea G. Bravo[2] and Marta Sebastian[2]

[1]Université de Reims Champagne-Ardenne, Reims, France, [2]Institute of Marine Sciences, Spanish National Research Council (CSIC), Barcelona, Spain

KEYWORDS

**women in STEM, environmental science, biogeochemical dynamics research, gender equality, diversity in science**

Editorial on the Research Topic
Women in biogeochemical dynamics research: 2022

At present, less than 30% of researchers worldwide are women. Long-standing biases and gender stereotypes are discouraging girls and women away from science-related fields, and STEM research in particular. Science and gender equality are, however, essential to ensure sustainable development as highlighted by UNESCO. In order to change traditional mindsets, gender equality must be promoted, stereotypes defeated, and girls and women should be encouraged to pursue STEM careers.

Therefore, we are proud to offer this platform in *Frontiers in Environmental Science* to promote the work of women scientists. To be considered for this Research Topic, the first, last, or corresponding author should be a researcher who identifies as a woman The papers presented here highlight the diversity of research performed across the entire breadth of Biogeochemical Dynamics research and the advances in theory, experiment, and methodology with applications to compelling problems. Contributions to this journal showcase the breadth and depth of investigations aimed at understanding and mitigating human impacts on our planet.

One significant study by Chua and Fulweiler highlights the importance of high-temporal-resolution gas concentration measurements in capturing the rapid response of sediments to low-oxygen conditions. This research sheds light on the dynamic nature of sedimentary processes and underscores the necessity of precise monitoring techniques in studying environmental phenomena.

In another investigation, Forsyth et al. delve into the bioconcentration and translocation of rare earth elements in plants from legacy mine sites in Portugal. Their findings not only contribute to our understanding of plant-metal interactions but also have implications for environmental management strategies in areas affected by mining activities.

Meanwhile, Ismail and Al-Shehhi offer a comprehensive review of biogeochemical models' applications in various marine environments. By synthesizing existing knowledge, the authors provide valuable insights into the role of these models in elucidating complex biogeochemical processes and guiding sustainable marine resource management practices.

Lavergne et al. draw attention to the importance of conserving microorganisms in terrestrial ecosystems, focusing on soil microbial diversity in Chile and the Antarctic Peninsula. Their work underscores the need for heightened awareness and proactive conservation efforts to safeguard these essential components of ecosystem functioning.

In a study with implications for land management practices, Rissanen et al. investigate the vegetation impacts on methane emissions from boreal forestry-drained peatlands. Their findings highlight the role of moss cover in modulating emissions and emphasize the importance of considering vegetation dynamics in peatland management strategies.

Addressing the pervasive Research Topic of plastic pollution in marine environments, Romera-Castillo et al. quantify the leaching of dissolved organic matter from aged plastic and its impact on microbial activity. This research underscores the urgent need to mitigate plastic pollution and its cascading effects on marine ecosystems.

Furthermore, Santos et al. employ leaf wax biomarkers to reconstruct environmental conditions in a high-mountain lake area in western Iberia. Their work illustrates the utility of biomarker analysis in paleoenvironmental reconstructions and contributes to our understanding of past environmental changes.

Sun et al. investigate the release of inorganic Mercury and subsequent methylmercury production in boreal peatlands due to ground warming. Their findings underscore the complex interactions between climate change and Mercury cycling in peatland ecosystems, highlighting the need for integrated approaches to mitigate Mercury pollution.

Lastly, Vila-Costa et al. data represent a significant step forward in unraveling the intricate interactions between pelagic marine bacteria and organic pollutants. By conducting comprehensive field studies in the tropical Pacific and subtropical Atlantic Oceans, the researchers provide invaluable insights into the responses of these bacteria to various pollutants.

Collectively, these studies exemplify the diverse and interdisciplinary nature of research featured by women in Environmental Science. By advancing our understanding of environmental processes and informing evidence-based management strategies, these contributions play a crucial role in addressing the myriad challenges facing our planet. As we navigate the complexities of the Anthropocene, women scientists are at the forefront of fostering dialogue and innovation to promote environmental sustainability and stewardship. In the realm of biogeochemical dynamics research, women scientists have long been making significant contributions, yet their achievements and perspectives are sometimes overlooked or underrepresented. As we strive for inclusivity and diversity in the scientific community, it's imperative to shine a spotlight on the invaluable work of women researchers in this field. It's essential to amplify their voices, recognize their contributions, and support their career advancement. By fostering an inclusive and supportive environment that values diversity, we can harness the full potential of women scientists and unlock new insights into the complex dynamics of our planet's biogeochemical cycles. In conclusion, women scientists are driving innovation, discovery, and progress in biogeochemical dynamics research. Their expertise, leadership, and dedication are indispensable assets in tackling the environmental challenges of the 21st century. Let us continue to celebrate and uplift the contributions of women in science, paving the way for a more equitable and sustainable future.

## Author contributions

CC: Writing–original draft, Writing–review and editing. AB: Writing–review and editing. MS: Writing–review and editing.

## Funding

The author(s) declare that no financial support was received for the research, authorship, and/or publication of this article.

## Conflict of interest

The authors declare that the research was conducted in the absence of any commercial or financial relationships that could be construed as a potential conflict of interest.

The author(s) declared that they were an editorial board member of Frontiers, at the time of submission. This had no impact on the peer review process and the final decision.

## Publisher's note

frontiers in Marine Science

ORIGINAL RESEARCH
published: 31 March 2022
doi: 10.3389/fmars.2022.861557

# Aged Plastic Leaching of Dissolved Organic Matter Is Two Orders of Magnitude Higher Than Virgin Plastic Leading to a Strong Uplift in Marine Microbial Activity

*Cristina Romera-Castillo[1]*, Stéphanie Birnstiel[1], Xosé Antón Álvarez-Salgado[2] and Marta Sebastián[1]*

[1] Instituto de Ciencias del Mar-CSIC, Barcelona, Spain, [2] Instituto de Investigaciones Marinas-CSIC, Vigo, Spain

Plastic debris reaching the ocean is exponentially increasing in parallel with plastic production. Once into seawater, plastic starts to leach organic compounds that are presumably additives and plastic oligomers, and that process is enhanced by solar radiation. From previous studies with virgin plastic, it has been estimated that up to 23,600 metric tons of dissolved organic carbon (DOC) can be released into seawater every year from all the plastic entering the ocean. However, most plastic found in the ocean has been aged through weathering and sunlight radiation, which could result in enhanced leaching. Despite this, dissolved organic matter (DOM) leaching from aged plastic and the effect on microbial communities and their activity has never been explored. Here we studied DOM leaching by aged plastic collected from a sand beach and how it compares with that from virgin plastic. After characterizing the DOM leached from plastic through fluorescence techniques, we also explored the bioavailability of the DOM leached and its fluorescent fraction through biodegradation experiments. Finally, we determined single cell activities of the prokaryotic community growing on the plastic leachates. We found that the release of DOC by aged plastic was two order of magnitude higher than that leached by virgin new plastic. Extrapolating that into the ocean and assuming that most of the plastic arriving there is not new, we estimated that up to 57,000 metric tons of DOC can be released by plastic debris every year. A fraction of the DOM released by plastic was fluorescent (FDOM), especially in the protein-like region, and bioavailable to microbial uptake, as it is also shown by the increase in the single cell activities of the bacteria growing on the leachates. Since most plastics in the ocean have been exposed to sunlight radiation provoking aging, our results unveil that the amount of carbon released by plastics is much higher than hitherto recognized, and thus will have a stronger impact in the oceanic carbon cycle and in marine ecosystems.

**Keywords: plastic leaching, FDOM, DOM, aged microplastics, BONCAT**

OPEN ACCESS

***Edited by:***
*Meilian Chen,*
*Guangdong Technion-Israel Institute of Technology, China*

***Reviewed by:***
*Jin Hur,*
*Sejong University, South Korea*
*Nagamitsu Maie,*
*Kitasato University, Japan*

****Correspondence:***
*Cristina Romera-Castillo*
*crisrc@icm.csic.es*

***Specialty section:***
*This article was submitted to Marine Biogeochemistry, a section of the journal Frontiers in Marine Science*

***Received:*** *24 January 2022*
***Accepted:*** *21 February 2022*
***Published:*** *31 March 2022*

***Citation:***
*Romera-Castillo C, Birnstiel S, Álvarez-Salgado XA and Sebastián M (2022) Aged Plastic Leaching of Dissolved Organic Matter Is Two Orders of Magnitude Higher Than Virgin Plastic Leading to a Strong Uplift in Marine Microbial Activity. Front. Mar. Sci. 9:861557. doi: 10.3389/fmars.2022.861557*

## INTRODUCTION

In 2020, 367 million metric tons of plastic were produced worldwide (Plastic Europe, 2021). From that, about 4% ended in the ocean and the predictions are that this amount will increase twice by 2025, in parallel with the increasing plastic production (Jambeck et al., 2015).

Marine plastic debris is known to negatively affect marine fauna through entangling and affecting their health after ingestion (Wesch et al., 2016). When plastics enter in contact with seawater where organic pollutants are present, they may adsorb and absorb these pollutants, which can be posteriorly released into the surrounding environment (Chen et al., 2018). Also, during plastic manufacture, different types of additives are added to the polymer to provide it with the properties required for its use, such as color, durability, and elasticity, among others. Up to 60% of plastic weight can be due to additives (Hermabessiere et al., 2017), which may be released into seawater (Suhrhoff and Scholz-Böttcher, 2016), but also inside the organisms once the plastic is ingested (Hermabessiere et al., 2017). The impact of these organic compounds in the carbon cycle has recently started to be studied. A previous work found that plastic entering the ocean can release up to 23,600 metric tons of dissolved organic carbon every year (Romera-Castillo et al., 2018), but this value was estimated using new commercial plastic. Plastic found in the ocean has been exposed to environmental factors such as UV radiation, oxidation, and erosion which contribute to its aging (Andrady, 2011). This causes degradation in form of scratches and fragmentation of the plastic into smaller pieces. Therefore, it is crucial to study aged plastic leaching into seawater and how it compares with new plastic. Only one work studied the leaching from aged plastic collected in the North Pacific but it did not determine the optical characterization of the leachates nor the biodegradation of the material released (Zhu et al., 2020). Fluorescence spectroscopy has been widely applied to the study of natural dissolved organic matter in aquatic systems (Stedmon and Nelson, 2015). Its application to the DOM leached from plastic gives information about the optical and chemical characteristics of the material released into seawater in a fast and non-expensive way. Also, this technique could show if the fluorescent signal associated to the DOM leached from plastic is distinguishable from that naturally occurring in aquatic systems.

Only a few studies have focused on the impact of plastic leaching on the microbial food web. For instance, dissolved organic compounds leached by plastic can enhance heterotrophic microbial growth (Romera-Castillo et al., 2018) but they have also been found to inhibit *Procchlorochoccus* photosynthesis and growth (Tetu et al., 2019). However, the effect of aged plastic leachates on marine prokaryotes is mostly unknown. Also, among the few works studying the microbial bioavailability of DOM leached from plastic (Romera-Castillo et al., 2018; Zhu et al., 2020), no one has studied the activity of prokaryotes growing in the leachates and how the leachates from aged plastic compare with new virgin plastic.

The aim of this work is to compare the amount of DOC and fluorescent characteristics of the DOM leached from a mix of naturally aged plastics with that from virgin low density polyethylene (LDPE) as well as other plastic types from the literature. It also investigates the response of a natural bacterial community to these different leachates. To this end, we measured the single-cell protein synthesis capacity of a natural bacterial community growing in plastic leachates applying Bioorthogonal non-canonical amino acid tagging (BONCAT, Dieterich et al., 2006; Hatzenpichler et al., 2014; Leizeaga et al., 2017). We hypothesize that aged plastics leach more DOC in contact with water due to the degradation of their surface and that their leachates will have a stronger impact on the marine bacterial communities than those from virgin commercial plastic.

# MATERIALS AND METHODS

## Plastic Leaching Photodegradation (Abiotic Production)

The plastic types used in this study were low density polyethylene (LDPE) film (0.5 mm thickness, Goodfellow), cut in 5 × 5 mm side squares, and a mix of aged plastics collected in Famara Beach, Lanzarote (Canary Islands, Spain). This beach is affected by predominant N-NE winds and swells which bring large amounts of plastic debris into its sand. This plastic is probably allochthonous, reaching Famara Beach with the Canary Current, which is fed by the Azores Current, coming from the western North Atlantic, and the Portugal Current, coming from the Iberian basin (Pérez-Hernández et al., 2013). The mix of aged plastics was composed by irregular flat pieces between 0.4 and 1 cm size. The total weight of plastic added to each flask was of 2.48 g for the new LDPE and ∼7.5 g for aged plastic. The amount of LDPE added was chosen following the methodology in Romera-Castillo et al. (2018), who determined the optimal plastic surface values, for a better comparison of the results. Adding the same surface of the aged plastic would have resulted in too few pieces with the risk of not having enough signal. Therefore, for aged plastic, we added ∼180 items $L^{-1}$ which is a concentration within the range commonly found in very polluted coastal areas such as Jade Bay in the Sourthern North Sea (64 items $L^{-1}$ on average, Dubaish and Liebezeit, 2013) or Mumbai coast (372 items $L^{-1}$ on average, Gurjar et al., 2022).

Aged plastic was characterized by FTIR using a Nicolet iS10 coupled with a ATR Smart iTR-Diamond. The mix was composed of 65% of polyethylene, 30% polypropylene, and 5% polyvinyl chloride. We decided to use new LDPE for comparison since polyethylene is the most abundant plastic found in the ocean (e.g., Cózar et al., 2014) and it represented 65% of the aged sample. A few plastic pieces were observed on the scanning electronic microscope (Hitachi S-3500N) and no bacteria or microorganisms were observed on their surface. The pictures also show that the plastic presented signs of aging with multiple fractures and scaly surface (**Supplementary Figure 1**). Before the experiment, the aged plastics were sonicated (Cole Parmer 8890, 42 KHz, 80 W) three times with MQ water for 10 min. Then, they were soaked in 1% oxygen peroxide for 1 h, to remove any organic debris and any potential bacterial contamination (e.g., Zhu et al., 2020). After that, the plastics were sonicated three times in MQ water for 5 min.

For the photodegradation experiment, plastic pieces were placed in 500 mL quartz tubes filled with 400 mL of 0.2 μm filtered and autoclaved aged seawater (AAS). This AAS had been collected at 2000 m depth in the NW Mediterranean Sea and aged in the dark for 2 years to ensure a low concentration of DOC (down to 52.0 μmol $L^{-1}$ at the beginning of our experiment). Non-irradiated treatments were placed in 500 mL borosilicate

bottles wrapped with aluminum foil. Controls of AAS without plastic were also incubated. All the treatments were performed in triplicates. The flasks were incubated for 6 days in a solar simulator placed in a flow-through water bath maintaining the temperature of the incubation at 28°C, similar to the water temperature in the tropics. The solar simulator provided artificial photosynthetic active radiation (PAR) by a HQI-T Powerstar lamp (250 W, Osram), UV-A radiation by 2 Philips TL100W/10 R fluorescent tubes and, and UV-B radiation by 2 UVA-340 fluorescent lamps (Q-Panel Company, United Kingdom). The radiation intensity for each wavelength or wavelength range was as follows: PAR (400–700 nm), 700 $\mu$mol $m^{-2}$ $s^{-1}$; 380 nm, 28.47 $\mu$W $cm^{-2}$ $nm^{-1}$; 340 nm, 16.31 $\mu$W $cm^{-2}$ $nm^{-1}$; 320 nm, 7.95 $\mu$W $cm^{-2}$ $nm^{-1}$; 305 nm, 1.09 $\mu$W $cm^{-2}$ $nm^{-1}$. The radiation dose rate represents the solar radiation in the subtropical North Atlantic Gyre measured at noon at 15 m depth. Artificial solar radiation was measured at 305, 320, 340, 380 nm, and PAR with a Biospherical PUV-510 radiometer. The light treatments received continuous artificial solar radiation.

Dissolved organic carbon and fluorescent dissolved organic matter (FDOM) were measured before and after the incubation period from the irradiated and non-irradiated treatments to estimate the DOM leaching from the plastic material and the effect of the radiation on it. The treatments with aged plastic were filtered through a pre-combusted (4 h, 450°C) Whatman GF/F filter at the end of the incubation since some plastic particles were observed in the water. In the controls of AAS without plastic, DOC variation during the leaching time was not significant ($p > 0.05$), being $1.16 \pm 0.86$ $\mu$mol $L^{-1}$ for irradiated and $1.57 \pm 1.09$ for non-irradiated treatments. DOC release was normalized to the surface area of the plastic used in every flask (8,000 $mm^2$ for LDPE and 15,000 $mm^2$ for aged plastic). The total surface area for each treatment was calculated from pictures using the software ImageJ. Bacterial abundance was measured at the end of the experiment to check that microbial growth did not take place during this photodegradation phase.

## Prokaryotic Degradation of Plastic Leachates

After exposure to irradiation, plastic pieces were removed and the leachates obtained in the photodegradation experiment were inoculated with fresh surface seawater from the Blanes Bay Microbial Observatory, in the coastal NW Mediterranean Sea (41°40′N, 2°48′E), at a ratio of 9:1 (leachate: inoculum). The inoculum was collected the same day of the experiment and was filtered by 0.8 $\mu$m to remove grazers and other eukaryotic cells, since they could mask the prokaryotic response to leachates. The water for the inoculum was collected on January 30, 2020. The treatments were amended with $NH_4Cl$ and $NaH_2PO_4$ to a final concentration of 10 and 2 $\mu$mol $mL^{-1}$, respectively, to avoid growth limitation by either nitrogen or phosphorus availability. The flasks were incubated in the dark at 23°C until the prokaryotic community reached the stationary phase. Samples for prokaryotic abundance were collected daily. DOC and FDOM samples were collected at the beginning of the incubation and at the end of the exponential growth phase. At the end of the experiment, samples for DOC and FDOM were filtered through pre-combusted Whatman GF/F filters to remove cells. Samples for BONCAT analyses were collected at 24 h and 96 h after the inoculation.

## Analyses

Dissolved organic carbon samples were collected in pre-combusted 20 mL glass vials, acidified with concentrated HCl to pH < 2 and stored at 4°C until analysis. DOC was measured on a Shimatzu TOC-V organic carbon analyzer (Álvarez-Salgado and Miller, 1998) after the removal of $CO_2$ by vigorous sparging with high purity $N_2$. Therefore, only the non-volatile fraction of DOC was measured. The accuracy was tested daily with the DOC reference materials provided by D.A. Hansell (University of Miami). We obtained average concentrations of $44.3 \pm 0.8$ $\mu$mol $L^{-1}$ for the deep ocean reference (Batch 18–Lot 08–18) minus blank reference materials. The nominal range of DOC values provided by the reference laboratory was 43.2–45.2 $\mu$mol $L^{-1}$.

Plastic carbon loss in the form of DOC was calculated as the mg of DOC leached per kg of plastic carbon (ppm). The carbon content for the plastics used in this work was determined on an Elemental Analyzer Perkin Elmer 2400. We obtained that carbon represented 85.3% for LDPE, and an average of 82.7% for aged beach plastic.

Excitation Emission matrices (EEMs) were performed with a LS 55 PerkinElmer Luminescence spectrometer, equipped with a xenon discharge lamp, equivalent to 20 kW for 8-ms duration. The detector was a red-sensitive R928 photomultiplier, and a photodiode worked as a reference detector. Measurements were performed at a constant room temperature of 20°C in a 1-cm quartz fluorescence cell. The excitation wavelength ranged from 240 to 440 nm at 10 nm steps increments and emissions wavelength from 300 to 560 nm at 0.5 nm increments, with a bandwidth of 5 nm, and the integration time was 0.1 s (scan speed was 250 nm min). Data was standardized and normalized to the Raman area. Raman area and its baseline correction was performed with the emission scan at 350 nm of the MQ blanks and the area was calculated based on measurements of Raman peak at 350 nm (Lawaetz and Stedmon, 2009). Samples were not diluted since the absorbance was always lower than 10 $m^{-1}$ both at 240 nm and 254 nm (Stedmon and Bro, 2008). Raman-normalized MQ blanks were subtracted to remove the Raman scattering signal (e.g., Stedmon et al., 2003). The drEEM 0.2.0 toolbox was used to standardize the EEMs (Murphy et al., 2013).

Integrated fluorescence was calculated as the sum of the fluorescence intensity values inside the range Ex: 300–400 and Em: 370–500, for the humic-like region, and Ex: 240–300 and Em: 300–370, for the protein-like region. Although the fluorescence observed due to the plastic leaching is not due to the humic- or protein-like substances present in natural DOM, we will keep the terms humic- and protein-like regions for an easier comparison with the Ex:Em regions where the natural dissolved organic matter fluoresces.

Bacterial abundances were determined daily by flow cytometry as described in Gasol and Del Giorgio (2000). Bacterial carbon

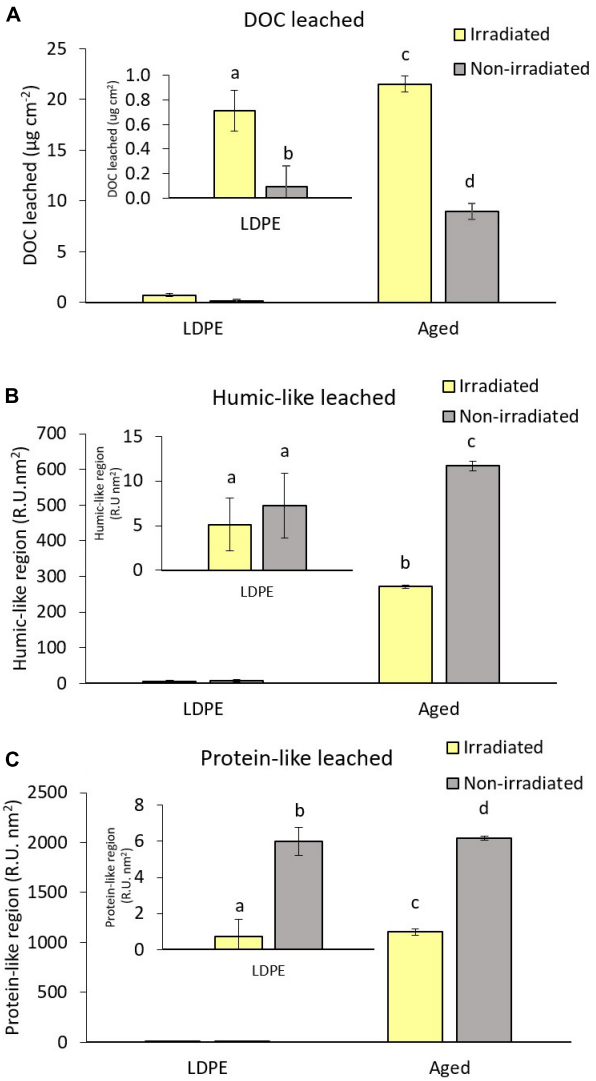


**FIGURE 1 |** Dissolved organic matter leached from LDPE and aged plastics in the irradiated and non-irradiated treatments during the photodegradation experiment **(A)** dissolved organic carbon; **(B)** fluorescent dissolved organic matter integrated in the humic-like region; **(C)** fluorescent dissolved organic matter integrated in the protein-like region. An enlargement of the LDPE values during the leaching incubation is included in all panels. The same letter over different bars indicate non-significant differences between them. Error bars represent the standard deviation of the mean of the triplicate cultures.

**TABLE 1 |** Total dissolved organic carbon ($\mu g \cdot cm^{-2}$) leached by different types of virgin plastic and aged plastics.

| Plastic type | Incubation time (d) | Treatment | Total DOC leached ($\mu g \cdot cm^{-2}$) | References |
|---|---|---|---|---|
| Virgin LDPE | 6 | Light | 5.80 ± 0.51 | Romera-Castillo et al., 2018 |
| | | Dark | 6.02 ± 1.75 | Romera-Castillo et al., 2018 |
| Virgin HDPE | 6 | Light | 2.41 ± 0.94 | Romera-Castillo et al., 2018 |
| | | Dark | 2.74 ± n.d. | Romera-Castillo et al., 2018 |
| Virgin LDPE | 33 | Light | 6.67 ± 0.90 | Romera-Castillo et al., 2018 |
| | | Dark | 8.92 ± 0.29 | Romera-Castillo et al., 2018 |
| Virgin HDPE | 33 | Light | 6.28 ± 0.96 | Romera-Castillo et al., 2018 |
| | | Dark | 2.79 ± 0.34 | Romera-Castillo et al., 2018 |
| Virgin PE packaging | 30 | Light | 0.31 ± 0.16 | Romera-Castillo et al., 2018 |
| | | Dark | 0.26 ± 0.20 | Romera-Castillo et al., 2018 |
| Virgin PP packaging | 30 | Light | 2.17 ± 0.13 | Romera-Castillo et al., 2018 |
| | | Dark | 1.61 ± 0.15 | Romera-Castillo et al., 2018 |
| Virgin LDPE | 6 | Light | 0.71 ± 0.17 | This work |
| | | Dark | 0.09 ± 0.09 | This work |
| Virgin EPS | 6 | Light | 0.72 ± 0.01 | Romera-Castillo et al., in press |
| | | Dark | 0.33 ± 0.05 | Romera-Castillo et al., in press |
| Virgin PS | 6 | Light | 0.46 ± 0.06 | Romera-Castillo et al., in press |
| | | Dark | −0.02 ± 0.12 | Romera-Castillo et al., in press |
| Aged LDPE | 6 | Light | 125.67 ± 20.66 | Romera-Castillo et al., in press |
| Aged mix | 6 | Light | 21.50 ± 0.78 | This work |
| | | Dark | 8.93 ± 0.09 | This work |

*LDPE, low density polystyrene; HDPE, high density polystyrene; PP, polypropylene; EPS, expanded polystyrene; PS, polystyrene; PLA, polylactic acid; Aged mix, aged plastic collected in a sand beach in Lanzarote.*

biomass was calculated from bacterial abundance using the conversion factor 20 fg C $cell^{-1}$ (Lee and Fuhrman, 1987). Bacterial growth efficiency (BGE, as%) was calculated as the increase in bacterial carbon biomass and the decrease in DOC during the incubation time.

Single-cell activity was estimated using BONCAT (Bioorthogonal non-canonical amino acid tagging, Dieterich et al., 2006) following the protocol detailed in Leizeaga et al. (2017). This protocol consists on the incubation of a natural sample with an artificial amino acid (*L*-homopropargylglycine, HPG) that is structurally analogue to L-methionine, which is incorporated into the newly synthesized proteins. The HPG-containing cells can get later fluorescently labeled *via* copper-catalyzed azide-alkyne click chemistry, and visualized and quantified with epifluorescence microscopy.

Samples for BONCAT were collected 24 h and 96 h after inoculation. Nine mL samples were incubated with L-homopropargylglycine (HPG) (1 µM final concentration) during 2 h. The incubation was stopped by fixing the samples with 0.2 µm-filtered formaldehyde (final concentration 4% [v/v]) overnight at 4°C. Samples were gently filtered through a 0.2 µm pore size polycarbonate filter placed on top of a 0.8 µm cellulose acetate membrane filter, washed three times with sterile milliQ

water, and kept frozen at −80°C until further processing. Samples were processed following Leizeaga et al. (2017) with small modifications (see **Supplementary Material** for details).

Images were acquired in black and white using an Axio Imager.Z2m epifluorescence microscope connected to a Zeiss camera (AxioCam MRm, Carl Zeiss MicroImaging, S.L., Barcelona, Spain) at 630 × magnification through the Axiovision software, and analyzed using ACMEtool. A Colibri LED light source was used (Carl Zeiss) with two light-emitting diodes (UV-emitting LED 365 for DAPI; red-emitting LED 590 for the tyramide Alexa Fluor 594), combined with the HE-62 multifilter module (Carl Zeiss). 100 ms exposure time was used for DAPI, and 120 ms for the BONCAT images. On average, 5,000 cells were counted per portion of filter. Image analyses were performed with ACMEtool over two black and white pictures of the same visual field: one for the DAPI stain and one for the BONCAT+ cells. The percentage of BONCAT+ cells was calculated in relation to the DAPI counts.

The intensity of the BONCAT+ cells was assessed using the mean gray value (MGV), which is the sum of the gray values of all the pixels in the cell divided by the number of pixels. Cells were categorized as displaying high, medium or low activity based on this signal intensity. To this end, all the BONCAT+ labeled cells were first rank-ordered by intensity. Then the maximum intensity and the minimum intensity were obtained. This intensity range (between the maximum and minimum intensity) was equally divided in three groups: high intensity (top third), medium intensity (middle third), and low intensity cells (bottom third). Finally, the percentage of each category within the BONCAT+ cells was calculated at each time point.

## Statistical Tests

We used ANOVA followed by Tukey's Honestly Significant Difference (HSD) test to explore differences in cell activity between the different treatments.

# RESULTS

## Photodegradation of Plastic Leachates (Abiotic Production)

All the plastic treatments showed leaching of DOC ranging from $0.09 \pm 0.09$ μg $cm^{-2}$ of plastic surface, for non-irradiated LDPE, to $21.50 \pm 0.78$ μg $cm^{-2}$ of plastic surface, for irradiated aged plastic (**Figure 1A** and **Table 1**). The aged plastic collected on the beach released between 30 and 94 times more DOC than the commercial LDPE for irradiated and non-irradiated treatments, respectively. Irradiation significantly enhanced the release of DOC in both plastic types, particularly in the LDPE that released 8 times more DOC after irradiation than its dark counterpart. After 6 days, all plastic types lost weight in form of DOC. The highest loss corresponded to the aged plastic with $542 \pm 20$ mg of DOC per kg of plastic carbon (ppm), for the irradiated, and $225 \pm 2$ ppm, for the dark treatments. After irradiation, LDPE lost only $29 \pm 7$ ppm while this plastic kept in the dark lost $3.9 \pm 4$ ppm.

Both new LDPE and aged plastics released fluorescent dissolved organic matter (FDOM) in the humic-like region (**Figure 1B**). The highest release was observed in the aged plastic treatments with $271.1 \pm 4.2$ R.U.· $nm^2$, for the irradiated treatments, and $609.8 \pm 13.4$ R.U. · $nm^2$, for the non-irradiated ones. The non-irradiated treatments presented higher FDOM in the humic-like region than irradiated ones, being not significant for LDPE but more than double in the aged plastic. Regarding FDOM in the protein-like region, only irradiated LDPE did not show a net release (**Figure 1C**). Aged plastic leached the highest amount being $1105.4 \pm 31.9$ R.U. · $nm^2$, for the irradiated treatments, and almost twice that amount ($2042.3 \pm 20.8$ R.U. · $nm^2$) for the non-irradiated ones.

The leached material of the aged plastic showed Excitation Emission Matrices (EEMs) characterized by two well-defined peaks: one in the protein-like region at Ex:Em around 268 nm:352 nm and a smaller one, around 3 times lower than the former, at Ex:Em around 312 nm:362 nm (**Figures 2A,B**). Both peaks were absent in the LDPE and control treatments. The intensity of these peaks was higher in the non-irradiated treatments (about 0.61 and 0.2 R.U., respectively) than in the irradiated ones (about 0.10 and 0.03 R.U., respectively) indicating that irradiation could have photodegraded both peaks. In the humic-like region it is also observable a fluorescent signal in the non-irradiated treatments that almost disappeared in the irradiated ones, showing that it was also photodegraded.

## Biodegradation of Plastic Leachates

All treatments showed an increase in the bacterial abundance that reached between $2.71 \times 10^6 \pm 2.32 \times 10^5$ cell $mL^{-1}$ in the non-irradiated control, and $1.34 \times 10^7 \pm 2.75 \times 10^6$ cell $mL^{-1}$ in the irradiated aged plastic leachates (**Figure 3**). The exponential phase started after 20 h of incubation. We stopped the incubations at day 4 when the communities reached the stationary phase. Bacterial growth on aged plastic leachates was one order of magnitude higher than in the control without plastic and in the LDPE leachates, for both, irradiated and non-irradiated treatments. The bacterial abundance reached in the LDPE leachates did not show a significant difference compared to the control without plastic for both irradiated (about $3.10 \times 10^6$ cell $mL^{-1}$) and non-irradiated treatments (about $2.75 \times 10^6$ cell $mL^{-1}$). At the end of the biodegradation experiment, all the previously irradiated treatments presented higher bacterial abundance compared to their non-irradiated counterparts, although the difference was not significant for the treatments with aged plastic leachates.

Dissolved organic carbon consumption during the biodegradation experiments ranged between $15.4 \pm 5.4$ μmol $L^{-1}$ in the non-irradiated control, and $194.9 \pm 12.8$ μmol $L^{-1}$ in the irradiated aged plastic leachates (**Figure 4A**). The consumption of DOC in the aged plastic leachates was significantly higher than in the LDPE and control, which showed similar values between them for both the irradiated and non-irradiated treatments. All the irradiated treatments presented a significantly ($p < 0.05$) higher DOC consumption than their non-irradiated counterparts. Since the DOC concentration at the beginning of the biodegradation experiment was different in each

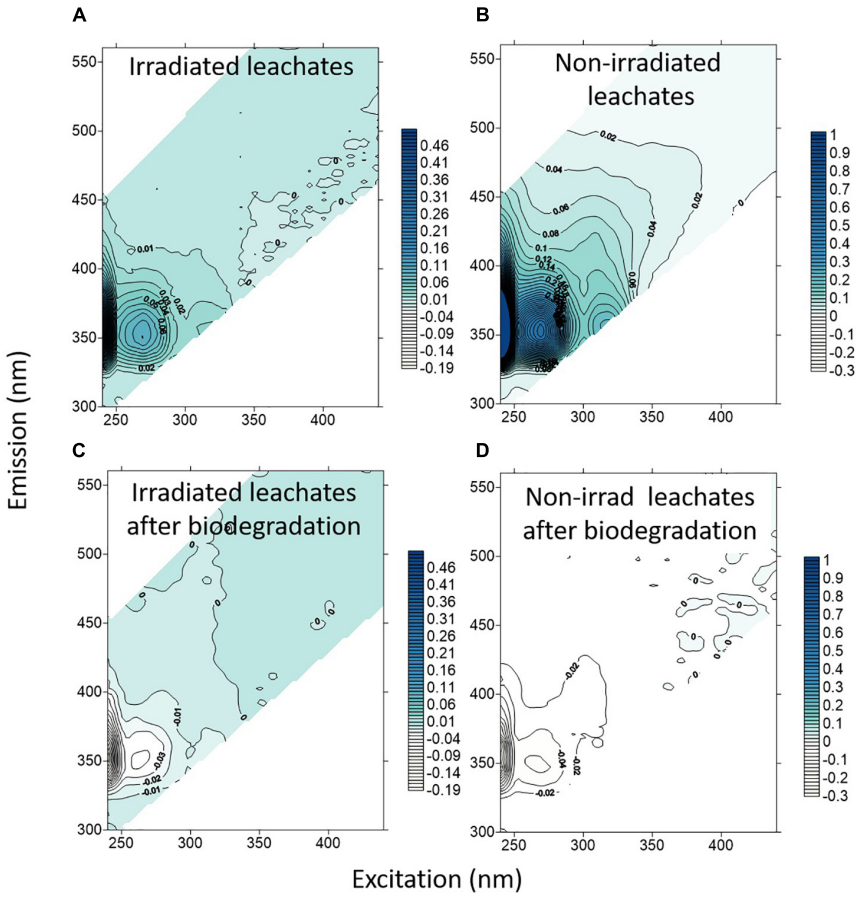


**FIGURE 2 |** Net Excitation Emission matrices (EEMs) variation in the leachates from aged plastic, as the difference between final and initial time points after **(A)** 6 days of abiotic irradiation; **(B)** 6 days of abiotic incubation with no irradiation; **(C)** 4 days of biodegradation by a marine natural community of the irradiated leachates; and **(D)** 4 days of biodegradation by a marine natural community of the non-irradiated leachates. Note the difference in the color scale for the irradiated and non-irradiated treatments.

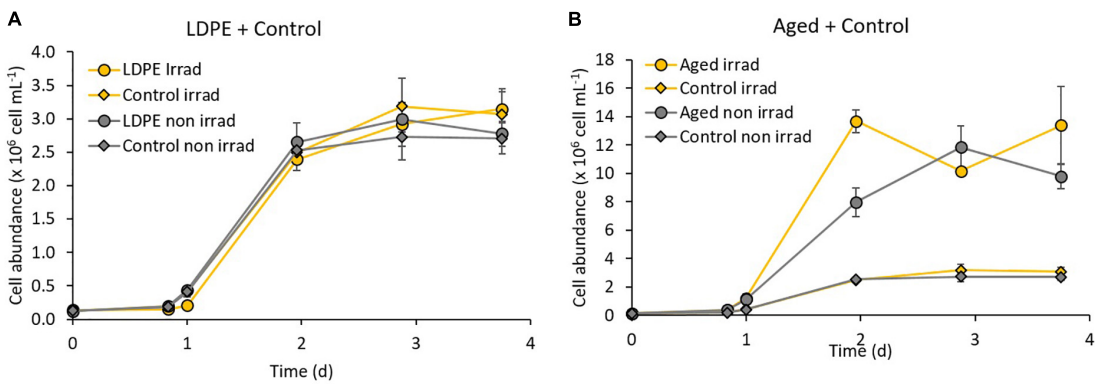


**FIGURE 3 |** Growth of natural bacterial communities on **(A)** LDPE leachates and **(B)** aged plastic leachates produced during the abiotic degradation experiment (irradiated and non-irradiated). The controls with no plastics are also shown. Error bars represent the standard deviation of the mean of the triplicate cultures. Note the different scales of cell abundance in panels **(A,B)**.

treatment, we also calculated the fraction of DOC consumed in relation to the initial concentration. In the irradiated treatments, between 35.7 and 30.0% of the available DOC was utilized with no significant differences between treatments. The fraction of DOC consumed in the non-irradiated treatments (between 25.7 and 20.7%) was significantly lower ($p < 0.05$) than in the

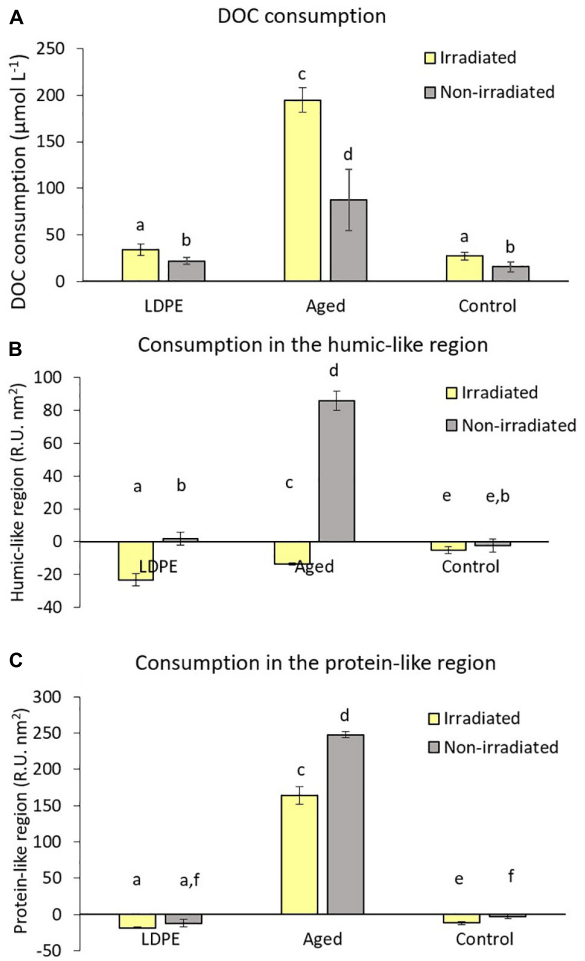


**FIGURE 4 |** Net variation of dissolved organic matter leached by LDPE and aged plastic after 4 days of bacterial biodegradation, calculated as the difference between the initial and final time points for **(A)** dissolved organic carbon consumption; Integrated fluorescence of dissolved organic matter in the **(B)** humic-like region and **(C)** protein-like region. Positive values indicate consumption while negatives indicate production. The same letter over different bars indicate non-significant differences between them. Error bars represent the standard deviation of the mean of the triplicate cultures.

irradiated ones but with no significant differences between plastic types or controls.

For the treatments with plastic, average bacterial growth efficiency (BGE) was 19 ± 10% while for the controls without plastic, it was 25 ± 8%. No significant differences were observed between both. Our BGE values are within the range of those found in coastal waters (Del Giorgio and Cole, 1998), but slightly higher than those found in similar experiments using a natural bacterial inoculum from the Adriatic Sea (Romera-Castillo et al., 2018). In the irradiated treatments, the average BGE was 15 ± 4%, not significantly different from the one observed in the non-irradiated treatments (27 ± 14%).

During the biodegradation phase, both irradiated plastic treatments showed a significantly ($p < 0.05$) higher production of FDOM in the humic-like region than the irradiated control without plastic with the highest value observed in the LDPE leachates (23.2 ± 3.7 R.U. · nm$^2$) followed by the aged plastic leachates (13.6 ± 0.6 R.U. · nm$^2$) (**Figure 4B**). The non-irradiated LDPE and control treatments did not show a significant change in the humic-like material over the biodegradation experiment. However, the non-irradiated aged plastic leachates experienced a notable decrease of 86.0 ± 5.8 R.U. · nm$^2$, showing the consumption of compounds fluorescing in the humic-like region by the marine prokaryote community. We also normalized the FDOM values to the DOC concentration at the beginning of the biodegradation experiment and the consumption/production trends were the same than those before the normalization.

A production of FDOM in the protein-like region was observed in all the treatments except in those with the aged plastic leachates, where consumption took place instead (**Figure 4C**). The production of these compounds in the irradiated LDPE treatments (18.5 ± 1.0 R.U. · nm$^2$) was significantly ($p < 0.05$) higher than in the irradiated control (11.5 ± 2.1 R.U. · nm$^2$). However, although the non-irradiated LDPE leachates showed higher production (12.2 ± 5.3 2.45 ± 0.10 R.U. · nm$^2$) than the non-irradiated control (2.7 ± 2.7 R.U. · nm$^2$), the differences between them were not significant. The production of protein-like material was similar in both irradiated and non-irradiated LDPE plastic leachates while in the control without plastic, the production was significantly higher in the irradiated than in its non-irradiated counterpart. In the aged plastic leachates, the consumption of protein-like FDOM was higher ($p < 0.05$) in the non-irradiated treatments (248.0 ± 4.4 R.U. · nm$^2$) than in the irradiated ones (164.0 ± 12.5 R.U. · nm$^2$).

During the biodegradation experiment, the peak observed in the protein-like region (Ex:Em around 268 nm:352 nm) of the aged plastic leachates decreased in intensity (**Figures 2C,D**) by 0.042 R.U. in the irradiated treatment and by 0.060 R.U. in the non-irradiated one. For the peak centered at Ex:Em around 312 nm:362 nm, the consumption was 0.012 R.U. in the irradiated and 0.020 R.U. in the non-irradiated treatments. Consumption at the boundary between the protein- and humic-like regions was also observed centered at 305nm:395 nm with higher variation in the dark.

To further investigate the response of the bacterial community to the plastic leachates we used Bioorthogonal non-canonical amino acid tagging (BONCAT, Dieterich et al., 2006; Hatzenpichler et al., 2014; Leizeaga et al., 2017), which achieves the fluorescent labeling of proteins that have been synthesized during the incubation with a methionine surrogate, allowing the quantification of translationally active cells. The aged plastic leachates resulted in a 4–5-fold-increase in the number of active cells compared to the LDPE leachates and the control treatment at the end of the experiment (**Figure 5A**). However, no significant differences were found in the number of active cells between the irradiated and the non-irradiated treatments in the control or any of the plastics leachates (ANOVA test, $p > 0.05$). The number of active cells in the LDPE leachates was not significantly different to that in the control treatment at any of the sampled time-points.

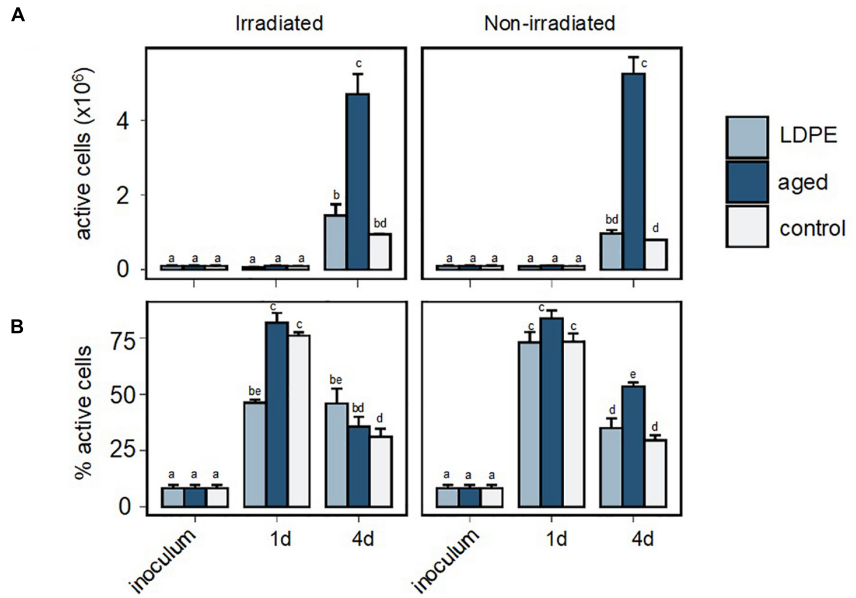


**FIGURE 5 |** Bacterial single-cell activity estimated with BONCAT in the inoculum and during the incubation with plastic leachates on day 1 and 4. **(A)** Number of active cells in the incubations. **(B)** Proportion of active cells. Different letters indicate significant differences among treatments. Error bars represent the standard deviation of the mean of the triplicate cultures.

Although the number of active cells was low one day after bacterial inoculation, the increase in the proportion of active cells observed from the inoculum to the control and plastic treatments (**Figure 5B**) indicated that the prokaryotic cells were rapidly stimulated by the 1:9 dilution. Nonetheless, this stimulation was significantly lower in the irradiated LDPE leachates, where 50% of the cells were active, than in the control and aged plastic leachates, where ∼75% of the cells were active (Tukey's *post hoc* test, $p < 0.001$). On day 4, the proportion of active cells significantly decreased in all treatments except in the irradiated LDPE leachates, where it barely changed. Furthermore, the proportion of active cells was lower in the irradiated aged plastic leachates than in the non-irradiated counterpart ($p = 0.00006$), whereas the opposite trend was observed with the LDPE leachates ($p = 0.04$).

Besides the decrease in the proportion of active cells, we also observed a drop in the single-cell translational activity of the individual cells in the aged plastic leachates on day 4, as evidenced by the fact that low activity cells accounted for most of the active pool of cells in both, irradiated and non-irradiated treatments (>75% of the cells, **Figure 6**). However, the proportion of low activity cells was significantly higher in the irradiated treatments than in the non-irradiated ones ($p = 0.01$). In contrast, medium and high activity cells represented roughly half of the active cells in the LDPE leachates and the control. These findings may indicate that in the aged-plastic leachates bacteria used all the biodegradable DOC faster, and the remaining DOC on day 4 (particularly in the irradiated treatment) was more resistant to utilization than the one in the LDPE leachates or the control treatment.

# DISCUSSION

## Plastic Leaching of Dissolved Organic Matter

The amounts of DOC leached from LDPE were within the low range of those previously reported for the same plastic type (Romera-Castillo et al., 2018; **Table 1**). Similar experiments were performed in our lab, as part of another work, with virgin expanded polystyrene (EPS), virgin polystyrene (PS), and artificially aged LDPE (exactly the same used as virgin in this experiment, **Table 1**). The aged plastic collected on the sand beach leached an amount of DOC up to two order of magnitude higher than those virgin plastic types, including PE and PP which made the 95% of the aged mix composition. Finally, the DOC leaching from the artificially aged LDPE was three order of magnitude higher than the virgin LDPE. This indicates that aged plastic releases much more DOM than virgin plastic.

In our study, between 3.9 and 542 ppm of carbon was lost from plastic in form of DOC after 6 days of abiotic incubation. The highest loss corresponded to the irradiated aged plastic. The amounts of plastic carbon lost in form of DOC (225–542 ppm) in the aged plastic treatments were one order of magnitude higher than the previously reported for new plastic after 6 days of irradiation which showed a loss of 86.7 ppm for expanded polystyrene and 28 ppm for LDPE (Romera-Castillo et al., in press). However, these values were lower than those reported by Zhu et al. (2020) of 4.8 g $kg^{-1}$ (ppt) for standard polyethylene

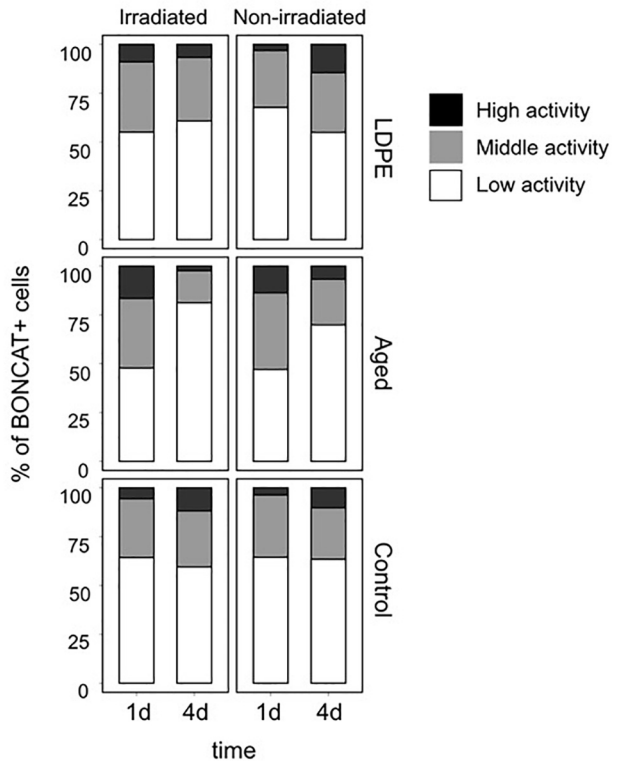


**FIGURE 6 |** Distribution of activity in the pool of active cells. Active cells were categorized as having low, medium, or high activity based on their BONCAT signal intensity, as in Sebastián et al. (2019) (see Section "Materials and Methods").

and 68 ppt for EPS after 54 days of irradiation. This could be because the amount of DOC leached from plastic was found to increase exponentially with incubation time (Zhu et al., 2020). New plastic has been shown to leach out the highest DOC amount right after the plastic get in touch with the water (Romera-Castillo et al., 2018). However, in longer incubation experiments using post-consumed plastic, the leaching increased exponentially at different rates depending on the plastic type, but accelerating after 54 days of light exposure (Zhu et al., 2020). The chemical composition of the commercial plastic includes antioxidants and other additives to prevent or retard degradation. Most of those additives are not chemically bound and can easily migrate to the fluid (Hermabessiere et al., 2017). Cracks and fragmentation make accessible light and oxygen to internal layers accelerating the aging process (Luo et al., 2020). Therefore, after a long time exposure to UV radiation, the additives can be lost making plastic even more vulnerable to degradation and leaching. After certain point, the plastic could be constantly leaking chemical compounds. This agrees with a previous experiment using a mix of plastic collected in the North Pacific Subtropical Gyre (NPSG), presumably old, which showed a lineal increase of DOC leached with time of exposure to irradiation (Zhu et al., 2020). All this explains why our new plastic released much less amount of DOC than the aged plastic which had been exposed to radiation for longer than 54 days. The previous estimate of 23,600 metric tons of DOC released by plastic in the ocean every year (Romera-Castillo et al., 2018) could be markedly underestimated, as it was derived from experiments with virgin plastic. Considering that aged plastic leached 21.50 $\mu g\ cm^{-2}$, which is 2.4 times the maximum leaching previously obtained with virgin plastics (Romera-Castillo et al., 2018), the amount of DOC released by plastic entering the ocean would increase up to 56,882 metric tons of DOC every year. The amount of plastic debris floating in the NPSG, one of the most polluted areas of the open ocean, is meant to be 96,400 metric tons (Eriksen et al., 2014). That plastic is known to be aged, since it takes about 1 year to arrive there from the closest coast (Lebreton et al., 2018) but they can be retained in the gyre for more than 3 years (Ebbesmeyer et al., 2007). Along that journey, it has been exposed to weathering factors such as sunlight radiation, oxidation and erosion. Therefore, the amount of DOC released per year from the plastic accumulated in that "garbage patch" is estimated to be, at least, 432 metric tons.

Here, the aged plastic collected on the beach released between 30 times more DOC, for irradiated, and 94 times more DOC, for non-irradiated treatments, than the commercial LDPE showing that sunlight radiation had more effect on the release of DOC from new than from aged plastic. The higher release of DOC after irradiation of plastic found here has been previously observed (Lee et al., 2020a). However, other studies reported contrasting results on plastic leaching (Suhrhoff and Scholz-Böttcher, 2016; Romera-Castillo et al., 2018). This difference could be due to the chemical composition of the material used, its degree of degradation and, maybe, the matrix where the plastic is releasing its compounds (fresh, brackish, or marine waters).

Possible compounds within plastic leachates could be the same oligomers from the polymer or additives (e.g., plasticizers or antioxidants). Some of these additives are known to present aromatic moieties that emit fluorescence, such as bisphenol A (BPA, Em/Em 220/309) and diethylhexyl phthalate (Em/Em 220/340, Lee et al., 2020b). Fluorescent additives would explain the FDOM observed in this work in both LDPE and aged plastics leachates, which was especially higher in the latter. Irradiated treatments showed lower values of leached FDOM than their non-irradiated counterparts both in the humic- and protein-like regions. This indicates that the FDOM leached from plastics was partially photodegraded during irradiation. The effect of irradiation on the FDOM was the opposite than on DOC which presented higher release in irradiated treatments. Therefore, DOM released by plastic under sunlight will have a higher proportion of less fluorescent material than that released in the dark. In the aged plastic leachates, the main fluorescing area was the protein-like region while in the humic-like region the intensity was lower. The ratio between the integrated fluorescence in the humic-like region of the irradiated aged plastic leachates vs. those from the non-irradiated aged plastic leachates was lower ($0.34 \pm 0.09$) than the same ratio for the protein-like region ($0.54 \pm 0.09$). This suggests that the compounds fluorescing in the humic-like region were more photo-labile than those in the protein-like area. This agrees with the fact that the UV radiation reaching the Earth surface starts at wavelengths $> 295$ nm. Since the protein-like fluorophores are usually excited bellow that

value, they do not undergo a direct photochemical decomposition and the effect of radiation on them is lower.

Aged plastic leachates EEMs showed two characteristic peaks that were not present in the LDPE leachates. Those peaks presented an intensity about six times higher in the non-irradiated than in the irradiated treatments, indicating, again, that irradiation photodegraded them. There are two typical protein-like peaks commonly found in natural organic matter: peak-B (Ex:Em 275 nm:310 nm) and peak-T (275 nm:340 nm, Coble, 1996). The highest peak observed in the aged plastic leachates (Ex:Em about 268 nm:352 nm) is close to the peak-T, but shifted to longer emission wavelengths. In a previous experiment with expanded polyestyrene (EPS) leachates, a predominant peak was also found in the protein-like region but shifted to shorter excitation and emission wavelengths (Ex:Em ∼250 nm:306 nm, Romera-Castillo et al., in press). This peak was attributed to polycyclic aromatic hydrocarbons (PAHs) from plastic impurities or additives, since those compounds fluoresce in that region (Ferretto et al., 2014). A recent study using new grinded virgin polyvinyl chloride (PVC) and polystyrene plastics, but in artificial freshwater, observed two peaks also in the protein-like region but their Ex:Em maxima did not coincide with ours (Lee et al., 2020b; Lee et al., 2021), being ours shifted to longer emission wavelengths. Agostino et al. (2021) found two peaks in the protein-like region coinciding with peak-T and peak-B in leachates from PP in MQ water. However, the peak found here at Ex:Em 312nm:362 nm seems to not coincide with any other peak previously found in natural organic matter nor in leachates from new plastic. This indicates that the mix of aged plastics, which is the most representative plastic debris found in the ocean (e.g., Cózar et al., 2014), releases much more FDOM than virgin plastic and presents a unique fluorescence fingerprint. However, more research needs to be done to see if that signal is observed with other plastic samples.

In any case, according to this work and to similar studies mentioned above, it seems that plastic releases FDOM with a characteristic signal in the protein-like region. So, special care should be taken when sampling for DOM, and particularly for FDOM, in very polluted areas such as some regions of the Mediterranean Sea or some very polluted coastal areas, since plastic signal could mask natural FDOM.

## Biodegradation of Plastic Leachates and Bacterial Activity

Bacterial abundance and single-cell activity in the LDPE treatments were similar to those in the control without plastic, with no significant differences among them. This contrasts with previous studies, which found a significantly higher bacterial abundance in LDPE treatments than in control without plastics (Romera-Castillo et al., 2018). On the other hand, DOC consumption was higher in those treatments where the plastic leaching was higher, which agrees with previous studies (Romera-Castillo et al., 2018), indicating that DOC leachates were labile to microbial uptake. This is supported by the observation of a significantly positive correlation between the bacterial abundance ($p < 0.05$; $R^2 = 0.97$) and single-cell activity ($p < 0.05$; $R^2 = 0.76$) at the end of the experiment with the amount of DOC leached, indicating that the prokaryotic response depended on the amount of DOC released. Since LDPE released a low amount of DOC in this experiment, it seems it was not high enough to provoke a big change in the bacterial abundance and single-cell activity regarding the control without plastic. The fluorescent fraction of the material leached by the aged plastic was also found to be bioavailable, as evidenced by a decrease of the DOM fluorescing in the protein-like region and in the humic-like region. This is also supported by the decrease of the two peaks observed in the EEMs of the aged plastic leachates, indicating a consumption during the bacterial incubation. All this shows that the fluorescent material released by aged plastic was labile to microbial uptake. The aged plastic was a mix of plastic types with a 65% of them being polyethylene, but remarkably, we did not observe those protein-like peaks in the LDPE treatment. Thus, probably, it was not the plastic type but the aging condition that made plastic release that labile fluorescent material.

Compounds fluorescing in the protein-like region were preferentially consumed by bacteria compared to those in the humic-like region. Coincidently, in natural DOM, protein-like compounds are also usually more labile than humic-like compounds (e.g., Lønborg et al., 2010; Cory and Kaplan, 2012). FDOM consumption was higher in the non-irradiated than in the irradiated treatments, but the opposite occurred for the DOC. This indicates that the DOM consumed by prokaryotes in the non-irradiated treatments was richer in fluorescent compounds than the DOM in the irradiated leachates. This could be due to the fact that fluorescent compounds were previously photodegraded in the irradiated treatments, so less amounts of FDOM were left there and prokaryotes used different compounds than in the treatments non-exposed to radiation. This shows that photodegradation makes the FDOM leached from aged plastic less labile to microbial uptake. For general DOC instead, photo-reactions could be rendering the non-fluorescent fraction of the DOM more labile to microbial uptake that would explain the higher consumption in the irradiated treatments. This agrees with the observation that sunlight can change the lability of natural DOM, turning the labile DOM into recalcitrant and making the recalcitrant DOM into labile (Obernosterer et al., 1999).

The presence of microplastics has been shown to stimulate marine microbial production of chromophoric DOM (CDOM) during a microcosm experiments containing microplastics and bacteria simultaneously (Galgani et al., 2018). In our study, in which marine bacteria were never in contact with plastic but only with the plastic leachates, we only observed a higher production of FDOM by bacteria, both in humic- and protein-like regions, in plastic leachates of the virgin LDPE treatments, especially in the irradiated samples. However, in the aged plastic leachates, only production of FDOM in the humic-like region of the irradiated treatments was observed. This could indicate that marine bacteria produce FDOM during the reworking of new virgin plastic leachates. It is likely that they also produce it during the biodegradation of the aged plastic leachates, but the consumption is probably masking the production.

Despite the amount of DOC released in the irradiated aged plastic was higher than in its non-irradiated counterpart, no

significant differences were found in the number of active cells between both treatments. Looking at the quality of DOM, the protein-like FDOM to DOC ratio was higher in the non-irradiated aged plastic treatment than in the irradiated one, both at the beginning and at the end of the biodegradation experiments. The lack of differences in the number of active cells between both treatments may indicate that the response of the bacterial community is driven by the interplay between both quantity and quality of DOM. The drop in the percentage of active cells and their corresponding single cell-activity observed in all treatments on day 4 of the experiment suggests that a large fraction of the DOM amenable to utilization had been consumed by then (**Figures 5B**, **6**) or, alternatively, that the bacterial community became limited by some micronutrient (i.e., vitamins or cofactors), as inorganic nutrients were added to prevent nutrient limitation. This drop in single-cell activity was more remarkable with the aged plastic leachates (and particularly in the irradiated treatment), where DOC consumption had been the highest compared to the other treatments. At the end of the biodegradation experiment, the remaining DOM in the irradiated aged plastic leachates presented a protein-like to DOC ratio significantly lower than the non-irradiated aged plastic leachates ($0.38 \pm 0.14$ vs. $0.99 \pm 0.13$, respectively). This suggests that the remaining DOM could have a higher quality in the non-irradiated aged plastic treatment than in the irradiated one, which explains why bacterial cells in the non-irradiated aged plastic treatment displayed comparatively higher per cell activity. In any case, bacterial cells were remarkably stimulated by the aged plastic leachates, with the number of active cells increasing 5-fold relative to the control (**Figure 5**). This stimulation is similar in magnitude to the one observed with a long-term carbon starved dark ocean prokaryotic community upon fresh organic carbon inputs (Sebastián et al., 2019). Thus, these findings suggest that leachates of ocean plastic debris may have a strong impact on microbial metabolism.

## CONCLUSION

Here we have seen that aged plastic releases much more DOC than virgin plastic into seawater. Such DOM presents a characteristic fluorescent signal in the protein-like region, which is photodegradable under the sunlight. The fluorescent material released by aged plastic was labile to microbial uptake, specially that fluorescing in the protein-like region. The aged plastic leachates showed a characteristic fluorescent signal at Ex:Em 312 nm:362 nm, which could potentially be used to track unseen plastic pollution in areas of the oceans that are heavily polluted. However, this signal could be masked by photodegradation and microbial processes. The single cell activity of marine bacteria was notably enhanced by the DOM released by aged plastic. Since plastic can last in the ocean for many years becoming old and smaller in size, most of the plastic that is found in the ocean is presumably aged and it is releasing more DOC into the ocean than previously thought, stimulating prokaryote activity. This means that DOM released by plastic has the capacity to alter the biogeochemistry of the carbon cycle in the ocean.

## DATA AVAILABILITY STATEMENT

The original contributions presented in the study are included in the article/**Supplementary Material**, further inquiries can be directed to the corresponding author.

## AUTHOR CONTRIBUTIONS

CR-C, MS, and XAÁ-S designed the research. CR-C and SB performed the experimental work. CR-C run the FDOM and bacterial abundance analyses and wrote the first draft of the manuscript. SB and MS performed the BONCAT analyses. XAÁ-S run the DOC samples. All authors made comments and amendments, and approved the final version.

## FUNDING

This work and CR-C involvement was supported by ComFuturo Program from Fundación General CSIC and a JIN-2019 project (PID2019-109889RJ-I00) from the Spanish Ministry of Science and Innovation and the Agencia Estatal de Investigación. CR-C also thanks the support by the Spanish Ministry of Science and the Agencia Estatal de Investigación through the Thematic Network of Micro- and Nanoplastics in the Environment (RED2018-102345-T, EnviroPlaNet) as well as the support provided by ISDIN. MS was supported by MIAU (RTI2018-101025-B-I00) from the Spanish Ministry of Science and Innovation. SB was funded by the Erasmus+ Program.

## ACKNOWLEDGMENTS

We acknowledges the "Severo Ochoa Centre of Excellence" accreditation (CEX2019-000928-S). We also thank Roberto Rosal García and Carlos Edo for the FTIR measurements of the sand beach plastic mix, Ariadna Martínez-Dios for provide the plastics from the sand beach in Lanzarote and Marola Lourdes Saá Yanez for lab assistance.

## SUPPLEMENTARY MATERIAL

The Supplementary Material for this article can be found online at: https://www.frontiersin.org/articles/10.3389/fmars.2022.861557/full#supplementary-material

## REFERENCES


Agostino, A., Rao, N. R. H., Paul, S., Zhang, Z., Leslie, G., Le-Clech, P., et al. (2021). Polymer leachates emulate naturally derived fluorescent dissolved organic matter: understanding and managing sample container interferences. *Water Res.* 204:117614. doi: 10.1016/j.watres.2021.117614

Álvarez-Salgado, X. A., and Miller, A. E. J. (1998). Simultaneous determination of dissolved organic carbon and total dissolved nitrogen in seawater by high temperature catalytic oxidation: conditions for precise shipboard measurements. *Mar. Chem.* 62, 325–333. doi: 10.1016/s0304-4203(98)00037-1

Andrady, A. L. (2011). Microplastics in the marine environment. *Mar. Pollut. Bull.* 62, 1596–1605.

Chen, Q., Reisser, J., Cunsolo, S., Kwadijk, C., Kotterman, M., Proietti, M., et al. (2018). Pollutants in plastics within the North Pacific subtropical gyre. *Environ. Sci. Technol.* 52, 446–456. doi: 10.1021/acs.est.7b04682

Coble, P. G. (1996). Characterization of marine and terrestrial DOM in seawater using excitation-emission matrix spectroscopy. *Mar. Chem.* 51, 325–346. doi: 10.1016/0304-4203(95)00062-3

Cory, R. M., and Kaplan, L. A. (2012). Biological lability of streamwater fluorescent dissolved organic matter. *Limnol. Oceanogr.* 57, 1347–1360. doi: 10.1038/nature08580

Cózar, A., Echevarría, F., González-Gordillo, J. I., Irigoien, X., Úbeda, B., Hernández-León, S., et al. (2014). Plastic debris in the open ocean. *Proc. Natl. Acad. Sci. U.S.A.* 111, 10239–10244. doi: 10.1073/pnas.1314705111

Del Giorgio, P. A., and Cole, J. J. (1998). Bacterial growth efficiency in natural aquatic systems. *Annu. Rev. Ecol. Syst.* 29, 503–541.

Dieterich, D. C., Link, A. J., Graumann, J., Tirrell, D. A., and Schuman, E. M. (2006). Selective identification of newly synthesized proteins in mammalian cells using bioorthogonal noncanonical amino acid tagging (BONCAT). *Proc. Natl. Acad. Sci. U.S.A.* 103, 9482–9487. doi: 10.1073/pnas.0601637103

Dubaish, F., and Liebezeit, G. (2013). Suspended microplastics and black carbon particles in the jade system, Southern North Sea. *Water Air Soil Pollut.* 224:1352.

Ebbesmeyer, C. C., Ingraham, W. J., Royer, T. C., and Grosch, C. E. (2007). Tub toys orbit the Pacific subarctic gyre. *EOS* 88, 1–4.

Eriksen, M., Lebreton, L. C. M., Carson, H. S., Thiel, M., Moore, C. J., Borerro, J. C., et al. (2014). Plastic pollution in the world's oceans: more than 5 trillion plastic pieces weighing over 250,000 tons Afloat at Sea. *PLoS One* 9:e111913. doi: 10.1371/journal.pone.0111913

Ferretto, N., Tedetti, M., Guigue, C., Mounier, S., Redon, R., and Goutx, M. (2014). Identification and quantification of known polycyclic aromatic hydrocarbons and pesticides in complex mixtures using fluorescence excitation–emission matrices and parallel factor analysis. *Chemosphere* 107, 344–353. doi: 10.1016/j.chemosphere.2013.12.087

Galgani, L., Engel, A., Rossi, C., Donati, A., and Loiselle, S. A. (2018). Polystyrene microplastics increase microbial release of marine chromophoric dissolved organic matter in microcosm experiments. *Sci. Rep.* 8:14635. doi: 10.1038/s41598-018-32805-4

Gasol, J. M., and Del Giorgio, P. A. (2000). Using flow cytometry for counting natural planktonic bacteria and understanding the structure of planktonic bacterial communities. *Sci. Mar.* 64, 197–224. doi: 10.3989/scimar.2000.64n2197

Gurjar, U. R., Xavier, K. A. M., Shukla, S. P., Jaiswar, A. K., Deshmukhe, G., and Nayak, B. B. (2022). Microplastic pollution in coastal ecosystem off Mumbai coast, India. *Chemosphere* 288:132484. doi: 10.1016/j.chemosphere.2021.132484

Hatzenpichler, R., Scheller, S., Tavormina, P. L., Babin, B. M., Tirrell, D. A., and Orphan, V. J. (2014). In situ visualization of newly synthesized proteins in environmental microbes using amino acid tagging and click chemistry. *Environ. Microbiol.* 16, 2568–2590. doi: 10.1111/1462-2920.12436

Hermabessiere, L., Dehaut, A., Paul-Pont, I., Lacroix, C., Jezequel, R., Soudant, P., et al. (2017). Occurrence and effects of plastic additives on marine environments and organisms: a review. *Chemosphere* 182, 781–793. doi: 10.1016/j.chemosphere.2017.05.096

Jambeck, J. R., Geyer, R., Wilcox, C., Siegler, T. R., Perryman, M., Andrady, A., et al. (2015). Plastic waste inputs from land into the ocean. *Science* 347, 768–771. doi: 10.1126/science.1260352

Lawaetz, A. J., and Stedmon, C. A. (2009). Fluorescence intensity calibration using the Raman scatter peak of water. *Appl. Spectrosc.* 63, 936–940. doi: 10.1366/000370209788964548

Lebreton, L., Slat, B., Ferrari, F., Sainte-Rose, B., Aitken, J., Marthouse, R., et al. (2018). Evidence that the Great Pacific Garbage Patch is rapidly accumulating plastic. Sci. Rep. 8:4666. doi: 10.1038/s41598-018-22939-w

Lee, S., and Fuhrman, J. A. (1987). Relationships between biovolume and biomass of naturally derived marine bacterioplankton. *Appl. Environ. Microbiol.* 53, 1298–1303. doi: 10.1128/aem.53.6.1298-1303.1987

Lee, Y. K., Hong, S., and Hur, J. (2021). A fluorescence indicator for source discrimination between microplastic-derived dissolved organic matter and aquatic natural organic matter. *Water Res.* 207:117833. doi: 10.1016/j.watres.2021.117833

Lee, Y. K., Romera-Castillo, C., Hong, S., and Hur, J. (2020a). Characteristics of microplastic polymer-derived dissolved organic matter and its potential as a disinfection byproduct precursor. *Water Res.* 175:115678. doi: 10.1016/j.watres.2020.115678

Lee, Y. K., Murphy, K. R., and Hur, J. (2020b). Fluorescence signatures of dissolved organic matter leached from microplastics: polymers and additives. *Environ. Sci. Technol.* 54, 11905–11914. doi: 10.1021/acs.est.0c00942

Leizeaga, A., Estrany, M., Forn, I., and Sebastián, M. (2017). Using click-chemistry for visualizing in situ changes of translational activity in planktonic marine bacteria. *Front. Microbiol.* 8:2360. doi: 10.3389/fmicb.2017.02360

Lønborg, C., Álvarez-Salgado, X. A., Davidson, K., Martínez-García, S., and Teira, E. (2010). Assessing the microbial bioavailability and degradation rate constants of dissolved organic matter by fluorescence spectroscopy in the coastal upwelling system of the Ría de Vigo. *Mar. Chem.* 119, 121–129.

Luo, H., Zhao, Y., Li, Y., Xiang, Y., He, D., and Pan, X. (2020). Aging of microplastics affects their surface properties, thermal decomposition, additives leaching and interactions in simulated fluids. *Sci. Total Environ.* 714:136862. doi: 10.1016/j.scitotenv.2020.136862

Murphy, K. R., Stedmon, C. A., Graeber, D., and Bro, R. (2013). Fluorescence spectroscopy and multi-way techniques. PARAFAC. *Anal. Methods* 5, 6557–6566.

Obernosterer, I., Reitner, B., and Herndl, G. J. (1999). Contrasting effects of solar radiation on dissolved organic matter and its bioavailability to marine bacterioplankton. *Limnol. Oceanogr.* 44, 1645–1654.

Pérez-Hernández, D. M., Hernández-Guerra, A., Fraile-Nuez, E., Comas-Rodríguez, I., Benítez-Barrios, V. M., Domínguez-Yanes, J. F., et al. (2013). The source of the canary current in fall 2009. *J. Geophys. Res. Oceans* 118, 2874–2891. doi: 10.1002/jgrc.20227

Plastic Europe (2021). *Plastic Europe*. Available Online at: https://plasticseurope.org/wp-content/uploads/2021/12/Plastics-the-Facts-2021-web-final.pdf

Romera-Castillo, C., Mallenco-Fornies, R., Saá-Yánez, M., and Alvarez-Salgado, X. A. (in press). Leaching and bioavailability of dissolved organic matter from petrol-based and biodegradable plastics. *Mar. Environ. Res.* doi: 10.1016/j.marenvres.2022.105607

Romera-Castillo, C., Pinto, M., Langer, T. M., Álvarez-Salgado, X. A., and Herndl, G. J. (2018). Dissolved organic carbon leaching from plastics stimulates microbial activity in the ocean. *Nat. Commun.* 9:1430. doi: 10.1038/s41467-018-03798-5

Sebastián, M., Estrany, M., Ruiz-González, C., Forn, I., Sala, M. M., Gasol, J. M., et al. (2019). High growth potential of long-term starved deep ocean opportunistic heterotrophic bacteria. *Front. Microbiol.* 10:760. doi: 10.3389/fmicb.2019.00760

Stedmon, C., and Nelson, N. B. (2015). "The optical properties of DOM in the ocean," in *Biogeochemistry of Marine Dissolved Organic Matter*, 2nd Edn, eds D. A. Hansell and C. A. Carlson (Amsterdam: Elsevier), 481–508. doi: 10.1016/b978-0-12-405940-5.00010-8

Stedmon, C. A., and Bro, R. (2008). Characterizing dissolved organic matter fluorescence with parallel factor analysis: a tutorial. *Limnol. Oceanogr. Methods* 6, 572–579. doi: 10.4319/lom.2008.6.572b

Stedmon, C. A., Markager, S., and Bro, R. (2003). Tracing dissolved organic matter in aquatic environments using a new approach to fluorescence spectroscopy. *Mar. Chem.* 82, 239–254. doi: 10.1021/acs.est.8b02648

Suhrhoff, T. J., and Scholz-Böttcher, B. M. (2016). Qualitative impact of salinity, UV radiation and turbulence on leaching of organic plastic additives from four common plastics — a lab experiment. *Mar. Pollut. Bull.* 102, 84–94. doi: 10.1016/j.marpolbul.2015.11.054

Tetu, S. G., Sarker, I., Schrameyer, V., Pickford, R., Elbourne, L. D. H., Moore, L. R., et al. (2019). Plastic leachates impair growth and oxygen production in *Prochlorococcus*, the ocean's most abundant photosynthetic bacteria. *Commun. Biol.* 2:184. doi: 10.1038/s42003-019-0410-x

Wesch, C., Bredimus, K., Paulus, M., and Klein, R. (2016). Towards the suitable monitoring of ingestion of microplastics by marine biota: a review. *Environ. Pollut.* 218, 1200–1208. doi: 10.1016/j.envpol.2016.08.076

Zhu, L., Zhao, S., Bittar, T. B., Stubbins, A., and Li, D. (2020). Photochemical dissolution of buoyant microplastics to dissolved organic carbon: rates and microbial impacts. *J. Hazard. Mater.* 383:121065. doi: 10.1016/j.jhazmat.2019.121065

**Conflict of Interest:** The authors declare that the research was conducted in the absence of any commercial or financial relationships that could be construed as a potential conflict of interest.

frontiers | Frontiers in Environmental Science

TYPE Original Research
PUBLISHED 29 November 2022
DOI 10.3389/fenvs.2022.994377



OPEN ACCESS

EDITED BY
Andrea G. Bravo,
Institute of Marine Sciences, Spanish National Research Council (CSIC), Spain

REVIEWED BY
Weiwei Sun,
Nanjing Institute of Geography and Limnology (CAS), China
Sandro Froehner,
Federal University of Paraná, Brazil
Mingda Wang,
Liaoning Normal University, China

*CORRESPONDENCE
Ricardo N. Santos,
ricardo.s.16@hotmail.com
Teresa Rodrigues,
teresa.rodrigues@ipma.pt

SPECIALTY SECTION
This article was submitted to Biogeochemical Dynamics, a section of the journal Frontiers in Environmental Science

RECEIVED 14 July 2022
ACCEPTED 03 November 2022
PUBLISHED 29 November 2022

CITATION
Santos RN, Schefuß E, Cordeiro LGMS, Oliveira D, Hernández A, Ramos AM and Rodrigues T (2022), Leaf wax biomarkers of a high-mountain lake area in western iberia—Implications for environmental reconstructions. *Front. Environ. Sci.* 10:994377. doi: 10.3389/fenvs.2022.994377



# Leaf wax biomarkers of a high-mountain lake area in western iberia—Implications for environmental reconstructions

Ricardo N. Santos[1,2,3]*, Enno Schefuß[4], Lívia Gebara M. S. Cordeiro[2,3], Dulce Oliveira[2,3], Armand Hernández[5], Alexandre M. Ramos[1,6] and Teresa Rodrigues[2,3]*

[1]IDL—Instituto Dom Luiz, Faculty of Sciences of the University of Lisbon, Lisbon, Portugal, [2]IPMA—Portuguese Institute for the Sea and Atmosphere, Lisbon, Portugal, [3]CCMAR—Algarve Centre of Marine Sciences, Algarve University, Faro, Portugal, [4]MARUM—Center for Marine Environmental Sciences, University of Bremen, Bremen, Germany, [5]CICA—Centre for Advanced Scientific Research, University of Coruña, GRICA Group, A Coruña, Spain, [6]Institute of Meteorology and Climate Research, Karlsruhe Institute of Technology, Karlsruhe, Germany

Leaf wax *n*-alkane biomarkers are widely used to infer past vegetation dynamics and hydroclimate changes. The use of these compounds strongly relies on the characterization of modern plants. However, few studies have explored leaf waxes of modern plants and their application to reconstructing climate and environmental changes in the Iberian Peninsula, a region known for its high vulnerability to climate change. In this study, we characterize the distributions and compound-specific isotopic compositions of the leaf waxes of dominant plants in the vegetation cover, soil, and surface sediment of the Lake Peixão area, a high-mountain glacial lake in Serra da Estrela (central Portugal). Our results show that the modern oro-Mediterranean (subalpine) vegetation of the study area is dominated by $C_3$ grasses/herbs and shrubs that preferentially produce long-chain leaf waxes ($\geq C_{27}$). The $C_{31}$ *n*-alkane display the overall highest concentration, produced by some grasses and shrubs, but especially *Erica* sp (heather), which is highlighted as a major source for the total *n*-alkane pool in the lake sediments. $C_{29}$ is the second-most abundant and the most equally produced *n*-alkane of the vegetation cover; $C_{25}$ and $C_{27}$ homologs are mainly associated with aquatic-related grasses/herbs, while $C_{33}$ and $C_{35}$ are particularly linked to cold-drought tolerant *Juniperus* sp. shrubs. Shrubs show higher but proportional values than grasses/herbs in the isotopic space, suggesting a directly proportional physiological adaptation of the two ecological forms to the prevailing climatic and environmental factors of the study area. $C_{29}$ is pointed as the most representative (or less plant-biased) leaf wax *n*-alkane in the lake sediments. Thus, δD of $C_{29}$ *n*-alkane is interpreted as a robust terrestrial hydrological indicator ($\delta D_{terr}$), which signal is believed to be strongly influenced by the mean air temperature and/or precipitation amount. Despite the sparse vegetation and small catchment area, the apparent hydrogen fractionation factor, determined from $\delta D_{terr}$ of the lake surface sediment, is in line with the modeled global mean values for the latitude of the study area. The different molecular and compound-specific signatures of the studied

oro-Mediterranean species have the potential to support future interpretations of leaf wax biomarkers in the Iberian Peninsula.

KEYWORDS

**leaf wax *n*-alkanes, terrestrial biomarkers, stable isotopes, western iberia, high-mountain lake**

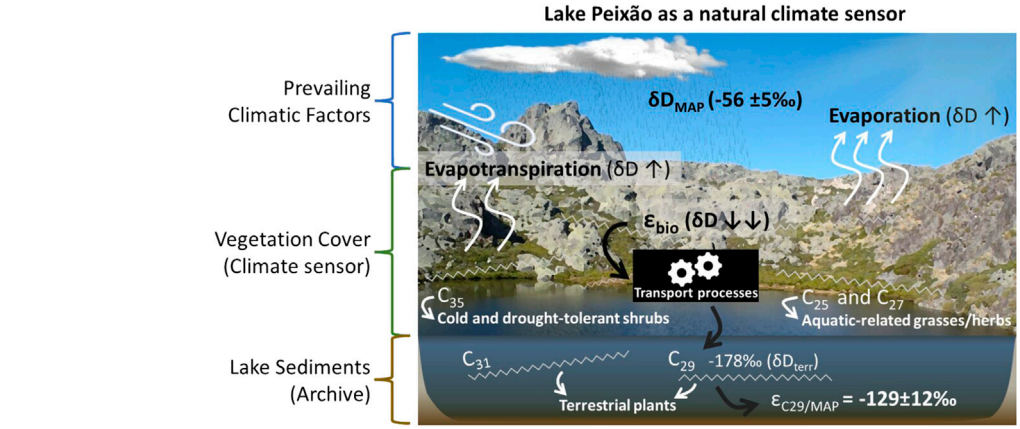


GRAPHICAL ABSTRACT

## 1 Introduction

Reconstruction of past climate and environmental conditions requires a thorough characterization and understanding of how modern ecosystems produce physical, chemical, or biological indicators, known as proxies, in response to specific climatic and environmental conditions. An ecosystem that promptly responds to climate change is often referred to as a "climatic sensor" (Evans et al., 2013). An excellent example of this type of sensor is the vegetation cover of the Iberian high mountains, known as sensitive ecosystems and natural laboratories (Toro et al., 2006). The lakes of these high mountains can act as sentinels of climate and environment changes and are capable of archiving evidence of the temporal evolution of the surrounding landscape in their sediments (Adrian et al., 2009). The Iberian Peninsula (IP) displays a wide range of climatic conditions due to its mid-latitude location, between the Eastern North Atlantic and the western Mediterranean regions, its complex orography, and the interplay between sub-tropical and sub-polar air masses. These features make IP bioclimatic diverse and particularly sensitive to climate changes and a recognized "hot spot" for the study of past climate, especially in quaternary studies (e.g., Sánchez-López et al., 2016; Abrantes et al., 2017; Baldini et al., 2019; Thatcher et al., 2020).

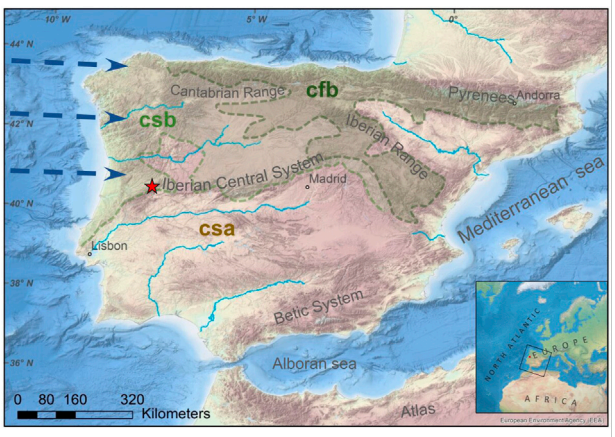


FIGURE 1
Morphological map of the Iberian Peninsula. The red star indicates the Lake Peixão location (Serra da Estrela, Portugal). Csa: Hot summer Mediterranean climate; Csb: Mild summer Mediterranean climate; Cfb: Oceanic. The dark blue arrows represent the moist rich prevailing westerlies from the Atlantic Ocean entering Iberia. Sources: European map from shadedrelief.com. River network from the European Environment Agency (EEA). Topography and bathymetry, sourced from portal.emodnet-bathymetry.eu, overlapped with the simplified Köppen-Geiger climate classification for the Iberian Peninsula (1971–2000) (adapted from the Iberian Climate Atlas, 2011).

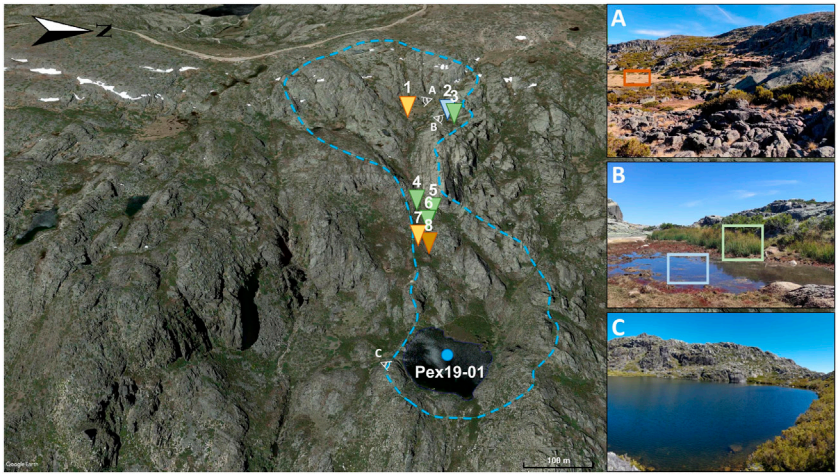


FIGURE 2
The Lake Peixão area. The light-blue dashed line represents the upslope watershed contour obtained from the elevation model of Google Earth Pro. The enumerated triangles represent sites of sample collection: 1—*Agrostis* sp.; 2—*Antinoria* sp.; 3—*Juncus* sp.; 4—*Cytisus* sp.; 5—*Juniperus* sp. and respective litter; 6—*Erica* sp. and respective litter; 7—*Nardus* sp. and respective litter; 8—Soil sample. Colors represent orange–grasses; light blue–aquatic grass; light green–soft rush; dark green–shrub; brown–soil. The eye-view symbol point to the view seen in the respective photos **(A,B)**, and **(C)**. Satellite imagery from Google Earth (date: 26 May 2019).

Plants produce a wide range of organic compounds, including leaf wax biomarkers, which are used as climate and environmental proxies (Peters et al., 2005; Castañeda and Schouten, 2011; Berke, 2018). However, the use of these compounds requires a comprehensive characterization of modern plants composition and understanding of their respond to the prevailing climate and environment factors (e.g., Bush and McInerney, 2013; Howard et al., 2018; Liu et al., 2018; Wang et al., 2018). The characterization of modern leaf wax compositions in the IP is still understudied (Ferreira et al., 2007; Ortiz et al., 2010, 2011, 2016; López-Días et al., 2013), despite the increasing number of past reconstructions using these compounds in both marine and lacustrine records (e.g., Jambrina-Enríquez et al., 2016; Taylor et al., 2018; Schirrmacher et al., 2020; Toney et al., 2020). Here, we focus on leaf wax *n*-alkanes, *n*-alkyl lipids with the general formula of $C_nH_{2n+2}$ (where *n* is the carbon number in the chemical chain), synthesized by plants to act as a protective barrier from the external environment and prevent water loss (Eglinton and Hamilton, 1967; Cranwell et al., 1987; Post-Beittenmiller, 1996; Shepherd and Griffiths, 2006). The high resistance to degradation and strong isotopic relationship of *n*-alkanes with vegetation type and water sources make compound-specific stable isotope analysis (CSIA) a valuable tool to infer past organic matter sources and hydrologic changes (e.g., Leider et al., 2013; Curtin et al., 2019; Hahn et al., 2021; Imfeld et al., 2022). Temporal variations in the stable carbon isotope ratio ($^{13}C/^{12}C$) of *n*-alkanes ($\delta^{13}C_{n\text{-alk}}$) in sedimentary records generally reflect changes in vegetation sources and water use efficiency of a catchment area (e.g., Freeman and Colarusso, 2001; Schefuß et al., 2003; Rommerskirchen et al., 2006; Diefendorf and Freimuth, 2017). The hydrogen isotopic ratios (D/H) of leaf wax *n*-alkanes ($\delta D_{n\text{-alk}}$) ultimately reflect the isotopic composition of precipitation. However, this signal results from a net fractionation process involving isotopic signatures of groundwater, lake water, soil, plant transpiration, and biosynthetic fractionation (see Sachse et al., 2012 for review).

In this work, we aim to fill the gap in studies of modern plants and their relationship as precursors of hydrocarbon biomarkers in IP. For that, we explored leaf wax *n*-alkanes of predominant species in the vegetation cover and surface sediment of Lake Peixão. This study area, located on top of the Serra da Estrela Mountain, lies between the Atlantic and Mediterranean bioclimatic zones, being considered a sensitive place to explore past hydrological changes and is in one of the most vulnerable regions to current climate changes (Allan et al., 2021). These results will add new insights about leaf wax biomarkers in IP and ultimately contribute to more reliable and robust interpretations of their sedimentary records in this key-region for reconstructing past climate and environmental changes.

# 2 Materials and methods

## 2.1 Study area

The study area is located in the Serra da Estrela Mountain, a NE–SW-directed intraplate mountain range in the westernmost sector of the Iberian Central System (Figure 1), central Portugal. This alpine range of the granitic basement (Ribeiro et al., 1990)

comprises the highest point (1,993 m above mean sea level, amsl) and the largest nature conservation area of continental Portugal. Here, a remarkable and unique set of glacial landforms and deposits (e.g., see Vieira, 2004, 2008) promoted the recognition of this region as a UNESCO Global Geopark. One of these glacial features is the study site, Lake Peixão (Figure 1) (40°20′35″N; 7°36′19″W), a relatively small (0.015 $km^2$) and subcircular lake (ca. 140 m diameter) at 1,677 m amsl. This alpine lake has a glacial origin, formed after the melting of the last icesheets ca. 14.7 ± 0.32 ka cal BP, which the small catchment area (ca. 0.30 $km^2$) is characterized by enclosed and steep granitic rocks (Figure 2) [Hernández et al., (2022) (in review)]. Few and small ephemeral streams flow into the lake, which has slightly acidic, oligotrophic, and monomitic waters (Boavida and Gliwicz, 1996). A spill point in the southern part can control the maximum lake level, draining into the Candeira valley (Figure 2). The landscape near the lake is characterized by sparse but well-constrained oro-Mediterranean vegetation patches dominated by shrubs such as *Erica* spp., *Juniperus communis*, *Genista* spp., *Cytisus* spp., and *Calluna vulgaris* (Connor et al., 2021), and grasslands mainly composed by *Agrostis delicatula* and *Nardus stricta*. Soils are rare and poorly developed; aquatic plants are sparse and mainly located near ponds and the lake, while trees are absent.

In general, Serra da Estrela region is characterized by a Mediterranean climate, with warm/dry summers and cold/wet winters, and is marked by strong vertical gradients in temperature and precipitation (Vieira et al., 2005; Mora, 2010). The ensemble historical climate of the region, from 1971 to 2000 [see http://portaldoclima.pt/en (Accessed 29 March 2022)], shows that the warmest and driest months are July and August, with mean values of approximately 20°C and 17 mm of rainfall. The coldest and wettest months are December and January, with a mean temperature of approximately 5°C and 150 mm precipitation, where precipitation often falls in the form of snow on the top of the mountain (Carreira et al., 2009, 2011).

The spatial variability of precipitation in this mountain range is highly controlled by altitude and slope orientation, with the basal areas receiving approximately half of the precipitation amount of the mountain summit, which can reach values of approximately 2,500 mm/year (Mora, 2010). The mountain range roughly defines a boundary between two Mediterranean climates (following the Köppen–Geiger climate classification system), one to the north characterized by mild summers (csb) and the other to the south characterized by hot and dry summers (csa) (Figure 1). The moisture-rich westerlies are predominant during winters and show a gradual D-depletion from the coast inland (Carreira et al., 2009). The atmospheric moisture sources of this part of the IP are almost exclusively derived from the prevailing westerly Atlantic air masses (Carreira et al., 2009; Cortesi et al., 2013; Thatcher et al., 2020), contrasting with other regions, such as the southeastern, which can also be significantly influenced by Mediterranean sources (Cortesi et al., 2013; Taylor et al., 2018; Schirrmacher et al., 2020; Toney et al., 2020). The high-altitude setting of Serra da Estrela results in temperature being an important driver of moisture condensation and the δD value of precipitation ($\delta D_{prc}$) (Carreira et al., 2009; Oliveira and Lima, 2010). This is reflected by a strong relationship between mean values of $\delta^{18}O$ and δD vs. temperature of monthly rainfall for Portugal's mainland (Carreira et al., 2009), which is also observed in other Iberian mountains (Giménez et al., 2021). The combination of the settings mentioned above and climatic and environmental factors makes Serra da Estrela one of the most biodiverse in Europe (Jansen, 2011) and a prime location to investigate the relationship between climate and ecology (Connor et al., 2021).

## 2.2 Material

A total of seven samples of dominant vegetation (four grass/herbs and three shrubs), three vegetation litters (one grass/herbs and two shrubs), a soil sample collected from the Lake Peixão catchment area (Figure 2), and a lake surface sediment. Modern plant samples were collected in September 2020; each plant sample was composed of several branches or leaves from different plants near the same collecting spot. These samples were wrapped in aluminum foil and sealed in an airtight bag. The vegetation litter samples were collected beneath the respective plant to ensure their source, and the soil sample comprises the top 2 cm of one of the few places in the lake's catchment where soils were available (Figure 2). Both litter and soil samples were collected directly with precombusted jar glasses. All samples were stored in a cool bag, directly transported to the Portuguese Institute of Sea and Atmosphere (IPMA, Portugal), and stored in a cool room (~5°C) until analysis. The lake surface sediment sample correspond to the 0 cm–1 cm depth of 8.63 m long core retrieved from the center of the Lake Peixão in June 2019 (PEX19-01) using a UWITEC® Piston Corer. Based on $^{210}Pb$ measurements, this surface sediment sample comprises 11 ± 4 years [Hernández et al. (2022) in review].

## 2.3 *n*-alkane analyses and characterization

All samples were freeze-dried, homogenized, and analyzed in the Biogeochemistry laboratory at IPMA. The vegetation samples were composed of leaves and stems from seven samples. Depending on the vegetation type, wood and stems were removed as much as possible. The samples were cut into small pieces with clean metal scissors. The three samples of the vegetation litter, the soil sample, and the lake surface sediment sample presented minimal clastic material (silt and clays), and no sieving was needed. Before extraction, 1,000 ng of an internal standard solution (hexatriacontane, tetracontane, and

nonadecanol-1-ol) was added to approximately 2.5 g of the sample. The lipid compounds were extracted three times using dichloromethane in an ultrasonic bath.

The total lipid extract (TLE) was hydrolyzed with potassium hydroxide in methanol (KOH/MeOH 6%, ~12 h, at room temperature). The neutral fraction containing *n*-alkanes was recovered with *n*-hexane by liquid–liquid extraction and cleaned with ultrapure water to remove traces of KOH. The *n*-alkanes were fractionated from the neutral extracts using 5 cm of deactivated silica gel (0.040 μm–0.063 μm mesh) and $AgNO_3$-silica gel Pasteur pipette columns with *n*-hexane as eluent. The *n*-alkane extracts were dried and diluted with toluene, and 1 μl was injected into a gas chromatography-flame ionization detector (GC-FID; Varian Model 3,800) equipped with a 1,079 programmable temperature vaporizing injector (PTV) for cold on-column with a CPSIL-5 CB column coated with 100% dimethylsiloxane capillary column (50 m × 0.32 mm × 0.12 μm film coating) connected to a fused silica precolumn (5 m × 0.25 mm × 0.25 μm). The oven temperature was programmed from 90° (holding time of 1 min) to 170°C at 20°C/min, then to 280°C at 6°C/min (holding time 25 min), and finally, to 315°C at 10°C/min (holding time of 12 min). The injector was programmed from 90°C (holding time of 0.5 min) to 310°C at 200°C/min. Samples were injected (1 μl) in split mode using $H_2$ as the carrier gas (~2.5 ml/min). The temperature of the detector was constant at 320°C with 35 ml/min of $H_2$ flow, 300 ml/min of airflow, and 30 ml/min of $N_2$ flow. The total run time for each sample was 63.83 min.

The *n*-alkanes were identified by comparing the retention times to an external standard mixture (*n*-alkanes ranging from $C_{17}$-$C_{36}$). The *n*-alkane concentrations (ng/g, dry weight sample) were determined based on the internal standard *n*-hexatriacontane ($C_{36}$).

Several indices have been developed to characterize the *n*-alkane distributions of samples (see Li et al., 2020). The most widely used are (a) the average chain length (ACL, Poynter, 1989); (b) the carbon preference index (CPI, Bray and Evans, 1961; Marzi et al., 1993), and (c) the proportion of aquatic plants ($P_{aq}$, Ficken et al., 2000).

(a) The ACL is used to identify the preferentially produced *n*-alkane length chains in a sample (Poynter, 1989) based on a weighted average of the *n*-alkane concentrations from $C_{27}$ to $C_{33}$, calculated as:

$$ACL_{27-33} = odd\sum_{n=27}^{33}(Cn \times n)\Big/\sum_{n=27}^{33}(Cn) \quad (1)$$

where $C_n$ is the concentration of a given *n*-alkane and *n is* the number of carbons in its chain.

(b) The CPI is the concentration weighted ratio of odd to even *n*-alkane chain lengths, which is normally used to examine the general source of sedimentary biomarkers and/or degradation processes. It can be calculated as follows:

$$CPI_{27-33} = 1\Big/2\left[odd\sum_{n=27}^{33}(Cn)\Big/even\sum_{n=26}^{32}(Cn) + \left(odd\sum_{n=27}^{33}(Cn)\Big/even\sum_{n=28}^{34}(Cn)\right)\right] \quad (2)$$

where $C_n$ is the concentration of a given *n*-alkane.

(c) The $P_{aq}$ commonly used to evaluate the relative contributions of *n*-alkanes from aquatic versus terrestrial plants in the lake sediments: $P_{aq}=(C_{23} + C_{25})/(C_{23} + C_{25} + C_{29} + C_{31})$, where $C_{23}$ and $C_{25}$ are considered from aquatic-related plant origins, whereas $C_{29}$ and $C_{31}$ are from terrestrial plants (Ficken et al., 2000).

CSIA was conducted on the *n*-alkanes when amounts were allowed by gas chromatography-isotope ratio mass spectrometry (GC-IRMS) at the MARUM Center for Marine Environmental Science, University of Bremen (Germany).

The $\delta^{13}C_{n\text{-alk}}$ values were measured with a Thermo Trace GC Ultra coupled to a Finnigan MAT 252 mass spectrometer. The *n*-alkane extracts were injected in splitless mode before being oxidized to $CO_2$ by a combustion reactor at 1,000°C. The instrument was equipped with an HP-5ms capillary column (30 m × 0.25 mm × 0.25 μm film coating); helium was the carrier gas (purity 99.999%) at a constant flow of 1.5 ml/min. The produced $CO_2$ was then injected into the mass spectrometer for analysis. The injector temperature was programmed to be constant at 250°C. The GC temperature was set from 120°C (hold time of 3 min) to 320°C at a heating rate of 5°C/min (hold time of 15 min). The $\delta^{13}C_{n\text{-alk}}$ values of the individual compounds were calibrated by injecting pulses of $CO_2$ from an external reference gas that was automatically introduced into IRMS at the beginning and end of each analysis. The $\delta^{13}C$ values are reported in ‰ relative to the Vienna Pee Dee Belemnite (VPDB) standard and represent an average of duplicates with a standard deviation less than 0.5‰ whenever *n*-alkane amounts allowed for multiple runs.

Standard $\delta D_{n\text{-alk}}$ was performed on a Thermo Trace GC equipped with an HP-5ms column (30 m × 0.25 mm × 0.10 μm film coating) coupled to a Thermo Fisher MAT 253 (IRMS) *via* a pyrolysis reactor (operated at 1,420°C). The GC oven program was similar to the conditions used to analyze the carbon isotopic composition. The injection of known isotopic composition standards after every six measurements and the daily determination of the $H^{3+}$ factor using $H_2$ reference gas were used to control measurement accuracy. The $\delta D_{n\text{-alk}}$ was calibrated against an external $H_2$ reference gas and reported

TABLE 1 – *n*-Alkane concentrations* and indices ($ACL_{27-33}$, $CPI_{27-33}$, $P_{aq}$) of plant leaves and stems and soil and surface sediment samples from the Lake Peixão (Serra da Estrela, Portugal).

| Sample | Ecological form | Environment | (*n*-alkanes ng/g) | | | | | | | | | | | | | | | | | | | (*n*-alkanes ng/g) | *n*-alkane indices | | |
|---|---|---|---|---|---|---|---|---|---|---|---|---|---|---|---|---|---|---|---|---|---|---|---|---|---|
| | | | Sample type** | $C_{17}$ | $C_{18}$ | $C_{19}$ | $C_{20}$ | $C_{21}$ | $C_{22}$ | $C_{23}$ | $C_{24}$ | $C_{25}$ | $C_{26}$ | $C_{27}$ | $C_{28}$ | $C_{29}$ | $C_{30}$ | $C_{31}$ | $C_{32}$ | $C_{33}$ | $C_{34}$ | $C_{35}$ | Total *n*-alk*** | $ACL_{27-33}$ | $CPI_{27-33}$ | $P_{aq}$ |
| *Agrostis* sp. | grass/herb | terrestrial | Veg | 11 | 326 | 65 | 193 | 354 | 145 | 2,857 | 1912 | 45,038 | 4,765 | 96,331 | 15,640 | **130,298** | 9,927 | 112,330 | 5,719 | 15,198 | 833 | 563 | $4.43 \times 10^5$ | 29.3 | 10.4 | 0.2 |
| *Nardus* sp. | grass/herb | terrestrial | Veg | 155 | 286 | 5 | 200 | 39 | 102 | 910 | 948 | 14,346 | 3,420 | 19,565 | 8,361 | 106,318 | 7,281 | **307,444** | 4,367 | 56,622 | 184 | 1,332 | $5.32 \times 10^5$ | 30.6 | 22.6 | 0.0 |
| *Antinoria* sp. | grass/herb | aquatic-related | Veg | 128 | 266 | 159 | 250 | 1,523 | 1,163 | 5,795 | 4,868 | **33,311** | 2,985 | 18,591 | 2074 | 16,629 | 1,349 | 25,081 | 1,054 | 22,256 | 186 | 1703 | $1.39 \times 10^5$ | 30.2 | 14.4 | 0.5 |
| *Juncus* sp. | grass/herb | aquatic-related | Veg | 28 | 218 | 263 | 89 | 830 | 690 | 3,685 | 1,222 | 2,905 | 1892 | **12,554** | 1,040 | 5,212 | 239 | 2,775 | 203 | 300 | 78 | 168 | $3.44 \times 10^4$ | 28.1 | 9.8 | 0.5 |
| *Erica* sp. | shrub | terrestrial | Veg | 45 | 204 | 188 | 201 | 4,360 | 1,018 | 6,152 | 1,411 | 12,809 | 3,831 | 84,604 | 13,728 | 311,759 | 42,497 | **659,377** | 41,027 | 178,062 | 2,669 | 845 | $1.36 \times 10^6$ | 30.5 | 12.3 | 0.0 |
| *Juniperus* sp. | shrub | terrestrial | Veg | 5 | 7 | 0 | 33 | 4 | 78 | 275 | 103 | 413 | 171 | 1,225 | 453 | 6,556 | 1,196 | 33,999 | 15,430 | **373,934** | 23,653 | 88,742 | $5.46 \times 10^5$ | 32.8 | 17.2 | 0.0 |
| *Cytisus* sp. | shrub | terrestrial | Veg | 4 | 322 | 32 | 206 | 255 | 681 | **39,449** | 3,532 | 24,616 | 757 | 6,830 | 756 | 13,283 | 1,447 | 18,675 | 369 | 538 | 55 | 80 | $1.12 \times 10^5$ | 29.7 | 13.4 | 0.7 |
| *Nardus* sp. (L.) | grass/herb | terrestrial | Veg. litter | 28 | 63 | 2 | 30 | 43 | 56 | 100 | 58 | 253 | 50 | 504 | 160 | 3,635 | 430 | **17,934** | 579 | 7,780 | 113 | 402 | $3.22 \times 10^4$ | 31.2 | 23.9 | 0.0 |
| *Erica* sp. (L.) | shrub | terrestrial | Veg. litter | 61 | 134 | 8 | 59 | 50 | 48 | 95 | 67 | 207 | 65 | 590 | 142 | 2,365 | 365 | **11,105** | 690 | 5,552 | 86 | 137 | $2.18 \times 10^4$ | 31.2 | 15.4 | 0.0 |
| *Juniperus* sp. (L.) | shrub | terrestrial | Veg. litter | 25 | 156 | 0 | 61 | 318 | 113 | 430 | 80 | 664 | 153 | 2,755 | 519 | 10,323 | 1870 | 37,055 | 6,652 | **118,922** | 3,845 | 15,050 | $1.99 \times 10^5$ | 32.2 | 15.8 | 0.0 |
| Soil sample | - | terrestrial | soil | 1 | 3 | 8 | 5 | 27 | 29 | 57 | 19 | 105 | 30 | 312 | 81 | 1,117 | 103 | **1,561** | 124 | 790 | 33 | 46 | $4.45 \times 10^3$ | 30.5 | 11.2 | 0.1 |
| Lake surface sediment | - | lake | sediment | 392 | 421 | 1,161 | 695 | 2,968 | 1,504 | 5,482 | 2,702 | 8,899 | 4,231 | 15,116 | 3,975 | 22,677 | 3,251 | **37,111** | 3,069 | 19,609 | 841 | 1921 | $1.36 \times 10^5$ | 30.3 | 7.5 | 0.2 |

*Highest concentrations values in bold; **Veg. meaning vegetation; ***sum of *n*-alkane concentrations from $C_{17}$ to $C_{35}$.





10.3389/fenvs.2022.994377

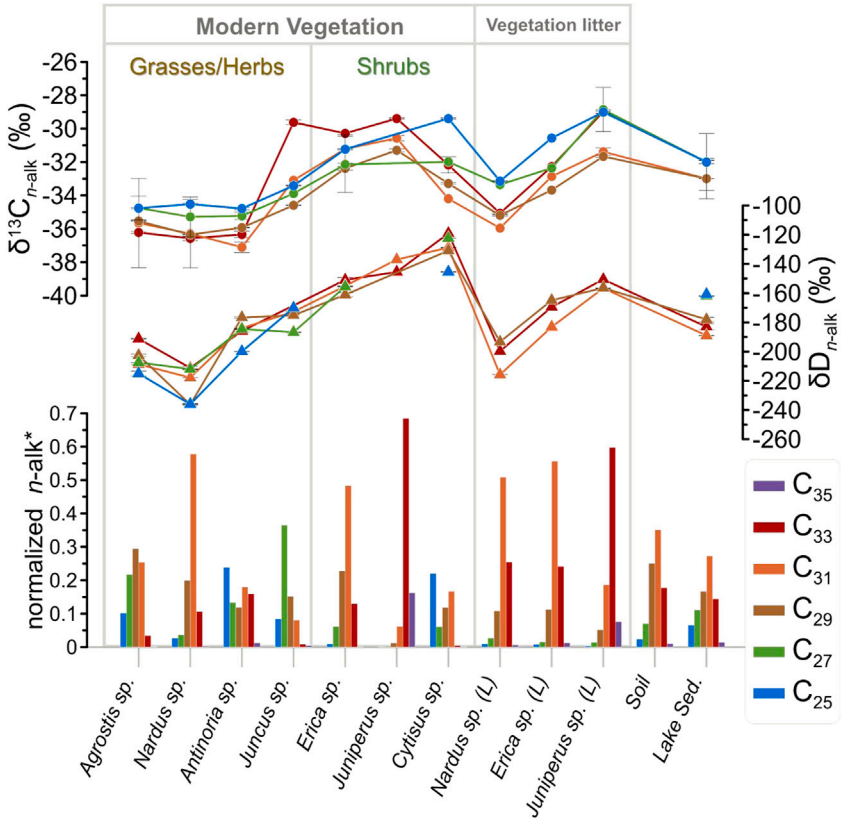


FIGURE 3
*n*-alkane distributions and compound-specific isotopic values ($C_{25}$—$C_{35}$) of the dominant plants, vegetation litter (L.), soil and surface sediment samples of the Lake Peixão area. The whiskers correspond to 1 SD, where multiple measurements on the respective compound were performed. *Normalization against the total *n*-alkane concentration of each sample.

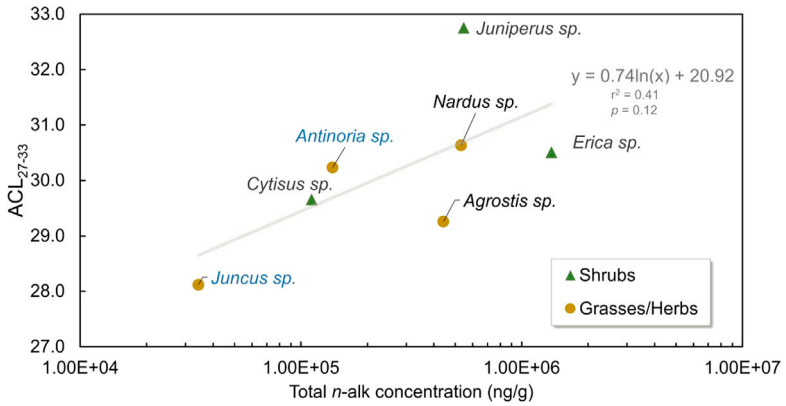


FIGURE 4
$ACL_{27\text{-}33}$ vs. total *n*-alkane concentrations (ng/g, in logarithmic scale) of the two dominant ecological forms of the Lake Peixão catchment. The overall trend is represented by a logarithm regression line in gray. Green triangles represent shrubs; colored circles represent grasses/herbs, aquatic-related plants in blue, and nonaquatic plants in yellowish.

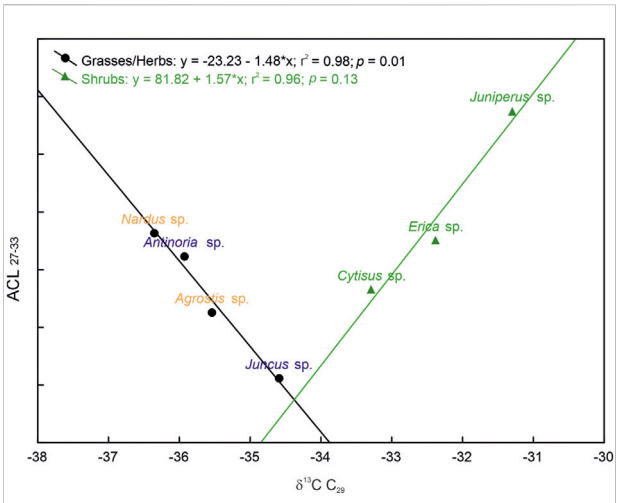


FIGURE 5
$ACL_{27-33}$ vs. $\delta^{13}C$ of $C_{29}$ *n*-alkane in modern plants of the Lake Peixão area. Blue names correspond to aquatic-related grasses, and yellowish names correspond to nonaquatic-related grasses/herbs plants.

in ‰ Vienna Standard Mean Ocean Water (VSMOW). When *n*-alkane amounts allowed multiple runs, the samples were run in duplicate, and the reported values represent the mean with a standard deviation less than 3‰.

The apparent fractionation ($\varepsilon_{app}$) between δD of leaf wax *n*-alkanes ($\delta D_{n\text{-alk}}$) and precipitation ($\delta D_{prc}$) was calculated using the equation described in Sessions et al. (1999): $\varepsilon_{n\text{-alk/water}} = 1{,}000\ [(\delta D_{n\text{-alk}}+1{,}000)/(\delta D_{prc}+1{,}000)] - 1$, in ‰. The $\delta D_{prc}$ used as a reference for the mean annual precipitation was estimated using the Online Isotopes in Precipitation Calculator (OIPC3.1; Bowen and Revenaugh, 2003) by constraining the central altitude, longitude, and elevation of the lake catchment area. This modeled $\delta D_{prc}$ value was then compared with the hydrogen isotopic value of nearby spring water.

# 3 Results

## 3.1 Distribution and concentration of *n*-alkanes

The modern vegetation samples exhibit the typical strong odd over even chain length predominance, with a wide range of total *n*-alkane concentration (sum of concentrations from $C_{17}$ to $C_{35}$ *n*-alkane), varying from $3.4 \times 10^4$ to $1.4 \times 10^6$ ng/g (dry weight) (Table 1). Most of the analyzed plants show a predominance of long-chain n-alkanes (≥$C_{27}$), particularly $C_{31}$ and $C_{29}$ homologs (Figure 3).

Principal component analysis (PCA) of the *n*-alkanes (concentration and isotopic compositions) performed in PAST4.07 free software (Hammer et al., 2001) (Supplementary Figure S1) suggests that samples can be grouped according to the ecological forms: grasses/herbs and shrubs (see Figure 3). On the other hand, for $ACL_{27-33}$ (U, $p = 0.12$) and $CPI_{27-33}$ (U, $p = 0.35$) the Mann-Whitney U tests, performed in STATISTICA 7.0, suggests no statistical difference in between the two forms (Supplementary Figure S2). In addition, grasses/herbs and shrubs appear to share a generally positive trend between $ACL_{27-33}$ and total *n*-alkane concentration, however under low statistical significance (Figure 4). *Nardus* sp. and *Agrostis* sp. presented the highest *n*-alkane concentrations in this ecological form, preferentially producing $C_{31}$ and $C_{29}$, respectively (Table 1). *Antinoria* sp (aquatic-related grass) exhibits proportional amounts of $C_{25}$, $C_{31}$, $C_{33}$, and $C_{27}$ homologs (decrescent in this order) (Figure 3). *Juncus* sp (herb) has the lowest total *n*-alkane concentration and a maximum at $C_{27}$. *Erica* sp. is highlighted as having the highest total *n*-alkane concentration of among all the studied plants (Table 1). These species preferentially produce $C_{31}$, twenty times more than the other investigated shrubs. On the other hand, *Cytisus* sp. is the shrub with the lowest total *n*-alkane concentration but produces considerably more mid-chains than the other shrubs, particularly the $C_{23}$ homolog (Figure 3; Table 1).

The decrease in *n*-alkane concentration from vegetation to the respective litter samples was significant, although the dominant homolog is preserved from its vegetation source (Table 1). For example, *Juniperus* sp. displays a decrease of 68% in the dominant homolog ($C_{33}$), *Nardus* sp. a decrease of 96% in $C_{31}$, while *Erica* sp. a decrease of 97% in $C_{31}$. The soil sample exhibits a strong odd over even chain length dominated by long-chain *n*-alkanes, resulting in $ACL_{27-33}$ and $CPI_{27-33}$ values of 30.5 and 11.2, respectively (Table 1). The total concentration of odd $C_{27}$—$C_{33}$ chains is $3.8 \times 10^3$ ng/g (dry weight) and accounts for ~85% of the total *n*-alkane concentration. The lake surface sediment and soil samples share the same dominance and long-chain *n*-alkane distribution (Table 1) ($C_{31} > C_{29} > C_{33} > C_{27} > C_{25} > C_{35}$) and similar $ACL_{27-33}$ (30.3). However, the lake sediments have a considerably larger concentration (thirty times more) of *n*-alkanes, lower $CPI_{27-33}$ (7.5), and higher $P_{aq}$ (0.19) than the soil sample (Table 1).

## 3.2 Compound-specific $\delta^{13}C_{n\text{-alk}}$ (odd $C_{25}$—$C_{33}$)

The $\delta^{13}C_{n\text{-alk}}$ values of the dominant plants of the Lake Peixão catchment area show an overall range of −37 to −29‰ (Supplementary Table S1), with minor differences between homologs but considerable interspecific variability (Figure 3). In general, longer carbon chains show the lowest $\delta^{13}C$ values, mainly $C_{29}$ and $C_{31}$ homologs (Figure 3). Grasses/herbs

display the most negative $\delta^{13}C$ values, ranging from −37 to −30‰. From those, *Juncus* sp. showed the highest values (−35 to −30‰) (Supplementary Table S1). The $\delta^{13}C_{n\text{-alk}}$ of shrubs varies from −34 to −29‰. *Juniperus* sp. and *Erica* sp. exhibit particularly narrow $\delta^{13}C$ ranges, the latter ranging from −32 to −30‰, whereas *Cytisus* sp. has a broader range (−34 to −29‰) (Supplementary Table S1). The $\delta^{13}C$ values of $C_{29}$ in the two dominant ecological forms in the study area showed clear and opposite linear relationships with $ACL_{27\text{-}33}$ (Figure 5) and CPI (Supplementary Figure S3). The $\delta^{13}C_{n\text{-alk}}$ values of vegetation litter vary from −35 to −30‰, generally displaying similar values to their respective vegetation sources (Supplementary Table S1). The lake surface sediment shows similar $\delta^{13}C_{n\text{-alk}}$ values among homologs (−33 to −32‰), with the lowest values of $C_{29}$ and $C_{31}$ (Figure 3).

## 3.3 Compound-specific $\delta D_{n\text{-alk}}$ (odd $C_{25}$—$C_{33}$)

The $\delta D_{n\text{-alk}}$ of the analyzed vegetation shows a wide range of values, from −236 to −119‰, with, grasses displaying lower $\delta D_{n\text{-alk}}$ values than shrubs (Supplementary Table S1). There is a remarkable difference between nonaquatic and aquatic-related grasses/herbs, with the latter showing higher $\delta D_{n\text{-alk}}$ values than their terrestrial counterparts. For example, for $C_{27}$, the terrestrial grasses *Agrostis* sp. and *Nardus* sp. display values of ca. −210‰, while *Antinoria* sp. and *Juncus* sp. show values of ca. -180‰ (Figure 3). In addition, *Cytisus* sp. showed higher and more variable values among homologs (−146 to −119‰) than plants such as *Erica* sp (−161 to −151‰) (Figure 3). Litter of Nardus sp. exhibits higher $\delta D_{n\text{-alk}}$ values than its source; in $C_{29}$, this relative increase corresponds to ca. 18%, from −236 to −193‰. This contrasts with shrub litter, which shows lower values than their sources (Figure 3). The δD values of $C_{31}$ in *Erica* sp. represent a decrease of 18%, from −155 to −183‰, and in *Juniperus* sp., a similar decrease from −137 to −157‰ (Figure 3; Supplementary Table S1). The $\delta D_{n\text{-alk}}$ from lake surface sediment displays values ranging from −189 to −161‰, with $C_{25}$ and $C_{27}$ homologs showing the highest (similar) values (Figure 3). In contrast, longer chains, particularly $C_{31}$, displayed the lowest values.

## 3.4 Apparent hydrogen isotope fractionation

The modern δD of the mean annual precipitation ($\delta D_{MAP}$) estimated using OIPC3.1 for the study area is −56 ± 5‰, a value similar to the −53‰ mean value for the wetter months during the main growing season (from March to May) and within the range of the near-annual mean value of −51 ± 2‰ from the Fonte dos Perús spring, which is ca. 1 km of the study area but in the opposite façade of the mountain (Carvalho, 2013).

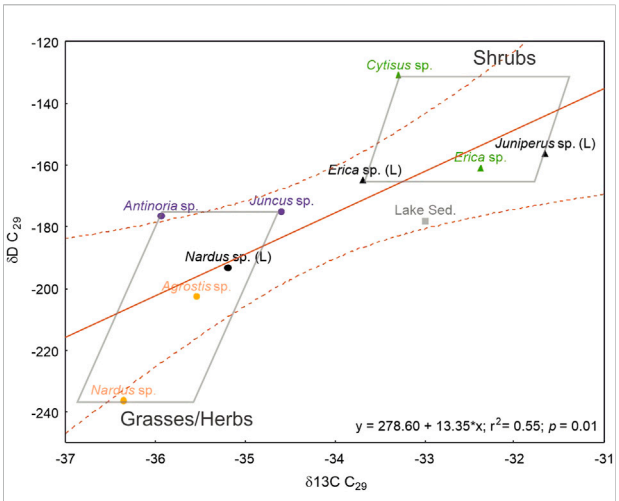


FIGURE 6
Isotopic space ($\delta^{13}C$ and δD values) of $C_{29}$ *n*-alkane in the analyzed samples from the Lake Peixão area. Circles correspond to samples form grass/herb ecological forms, where blue circles relate to aquatic-related plants and yellowish circles relate to nonaquatic-related plants; triangles correspond to samples from shrub ecological forms (L) indicating litter sample from the respective plant. Lake Sed. (black square) corresponds to the surface lake sediment sample.

The specific fractionation factors ($\varepsilon_{n\text{-alk/MAP}}$) determined for the modern vegetation range from −191 ± 17‰ to −67 ± 6‰ (Table 1) values constrained by a common $\delta D_{MAP}$ value of the study area; error is given by the standard deviation of measurements in *n*-alkanes and $\delta D_{MAP}$. Therefore, *Agrostis* sp. and *Nardus* sp. display mean $\varepsilon_{app}$ values (from $C_{25}$ to $C_{33}$) of −158 ± 32‰ and −177 ± 35‰, respectively, whereas the aquatic-related counterparts, *Antinoria* sp. and *Juncus* sp., show higher values of −138 ± 28‰ and −127 ± 23‰, respectively. $C_{31}$ was the only compound present in sufficient quantities in all three shrub species for reliable $\delta^{13}C/\delta D$ measurements; thus, using this component as a reference, *Erica* sp. shows the highest fractionation ($\varepsilon_{C31/MAP}$ = −105 ± 9‰), while *Cytisus* sp. the lowest ($\varepsilon_{C31/MAP}$ = −77 ± 7‰). The surface sediment of the lake also shows an increase in $\varepsilon_{n\text{-alk/MAP}}$ from $C_{29} > C_{33} > C_{31}$, ranging from −129 ± 12‰ to −141 ± 13‰, and $C_{25}$ and $C_{27}$ homologs display the lowest $\varepsilon_{n\text{-alk/MAP}}$, approximately −112 ± 10‰.

# 4 Discussion

## 4.1 Leaf wax *n*-alkane biomarkers of modern plants

The small and well-constrained catchment area of the Lake Peixão presents ideal characteristics for assessing the vegetation cover inputs into lake sediments. The $C_{31}$ and $C_{29}$ are the predominant *n*-alkanes of the modern plants in the vegetation

cover. Grasses/herbs and shrubs display similar $ACL_{27\text{-}33}$ and $CPI_{27\text{-}33}$ values (Supplementary Figure S2) that can suggest traits of a common physiological adaptation of this vegetation type, but also that the application of such indicators alone may be questionable to differentiate between the two terrestrial forms. This common physiological response may also be reflected in the suggested positive trend between $ACL_{27\text{-}33}$ and *n*-alkane concentration (Figure 4); however, the limited dataset appears to constraint the statistical significance of this hypothesis, which will be likely addressed in future studies.

The high amount of *n*-alkanes produced by *Erica* sp. suggests that these plants are significant sources of leaf waxes in the study area, particularly the $C_{31}$ *n*-alkane. These findings agree with other modern vegetation studies in the IP (Ferreira et al., 2007; Ortiz et al., 2016), where $C_{31}$ *n*-alkane is pointed out as a possible indicator of heather inputs (Loidi et al., 2007; Ortiz et al., 2016). Our results also suggest that *Juniperus* sp. is another important source of long-chain *n*-alkanes ($\geq C_{33}$), accounting almost exclusively for the production of $C_{35}$ in the vegetation cover (Figure 3; Table 1). These observations align with the results obtained for other species of *Juniperus* sp. in central Spain (Schäfer et al., 2016a), suggesting that these especially long-chains compounds can be used as an ecological proxy and indicators of arid and cold conditions (Thomas et al., 2007; Dasgupta et al., 2022). In Iberian heathlands, the relative increase in grasses/herbs over shrubs can reflect an increase in water availability, as they are often in contact with mires (Loidi et al., 2007). In the study area, the aquatic-related plants are restricted to the grass/herb ecological form, such as *Antinoria* sp. and *Juncus* sp., which are relatively abundant in small ponds and streams. The *n*-alkane analyses of these species suggest $C_{27}$ and $C_{25}$ as indicators of aquatic or aquatic-related plants matter and water availability in the lake Peixão ecosystem.

The relatively high contribution of mid-chain compounds of some shrubs, such as Cytisus sp., (Figure 3; Table 1), highlights that caution is needed when applying distributions *n*-alkane, such as $P_{aq}$, to infer past aquatic inputs or lake levels in downcore paleoreconstructions (Xie et al., 2020). However, the relative deviation in the n-alkane distribution of Cytisus sp. relative to other shrubs is not reflected in the isotopic space ($\delta^{13}C_{n\text{-alk}}$ and $\delta D_{n\text{-alk}}$) (Figures 3, 6), which encourages the application of CSIA to better assess vegetation sources in lake sediments. In fact, the two ecological forms are well-separated in the isotopic space (Figure 6), where the observed linear proportionality may result from the inferred common physiological response to the shared climatic and environmental conditions of the study area, i.e., precipitation, temperature, humidity, and water source. For example, the lower $\delta D_{n\text{-alk}}$ of grasses/herbs may imply lower transpiration rates and lower water loss than shrubs, but on the other hand, its lower $\delta^{13}C_{n\text{-alk}}$ values may also imply that grasses/herbs have less water use efficiency than shrubs (Hou et al., 2007; Gao et al., 2014). While the similar $ACL_{27\text{-}33}/CPI_{27\text{-}33}$, along with the proportionally distinct isotopic values, are inferred to be the reason for the opposite trends between the two ecological forms in ACL/CPI vs. $\delta^{13}Cn_{\text{-alk}}$ (e.g., Figure 5; Supplementary Figure S3).

## 4.2 The source of Lake Peixão *n*-alkanes and its implications for paleo-reconstructions

The strong predominance of odd-over-even carbon chain compounds, high $ACL_{27\text{-}33}$, and low $P_{aq}$ values (Table 1) in the surface sediment of Lake Peixão suggests that the *n*-alkanes were primarily derived from terrestrial plants from the catchment area. Additionally the high $CPI_{27\text{-}33}$ values (> 5) in the lake sediments suggest good preservation of the *n*-alkane content which gives confidence in the use of leaf waxes record in the lake sediments (Pancost and Boot, 2004).

Our results show that from plants to vegetation litter, and lake surface sediment the isotopic signal is well preserved despite important changes in *n*-alkane concentrations (Table 1). Moreover, the relative proportion of dominant chains (Figure 3) is also maintained The $ACL_{27\text{-}33}$ and *n*-alkane distribution of modern soil and the lake surface sediment remain identical even though the latter reflects higher contribution of aquatic or aquatic-related plants (Figure 3; Table 1). On the other hand, the $CPI_{27\text{-}33}$ offset between plants, vegetation litter, and the lake surface sediment reflects the complex plant-to-sediment transfer processes, which involve a series of admixtures of different plant inputs and biodegradation; for instance, by microbes (Zech et al., 2010; Schäfer et al., 2016b; Stout, 2020; Thomas et al., 2021).

The $\delta^{13}C_{n\text{-alk}}$ values (ca. −33‰) of lake surface sediment suggest a predominance of $C_3$ plants (Figure 3) and reinforce shrubs as a major source of waxes in the study area (Figure 3; Table 1). The two dominant ecological forms produce significant and relatively equivalent amounts of $C_{29}$, showing proportional values of carbon and hydrogen fractionation that may result from a consistent physiological response of plants to the same environment and climatic factors. Thus, we expect $C_{29}$ to provide a more holistic overview of the *n*-alkane composition of the terrestrial vegetation cover in the Lake Peixão sediments compared with other long-chain compounds, such as $C_{31}$, that appear to be particularly biased towards species like *Erica*. This hypothesis supports global compilations that report $C_{29}$ as a widely produced terrestrial *n*-alkane strongly and consistently associated with regional mean $\delta D_{prc}$ (Sachse et al., 2012; Liu and Liu, 2019; McFarlin et al., 2019). Moreover, the modern $\varepsilon C_{29}/_{MAP}$ value (−129 ± 12‰) of lake surface sediment is remarkably consistent with the global modeled values by Liu and An (2019) and McFarlin et al. (2019) for the latitude of the study area. Therefore, we suggest the δD of $C_{29}$ as a robust indicator of terrestrial hydrology, i.e., $\delta D_{terr}$, in paleostudies in both sediments of Lake Peixão and downstream areas.

The strong relationship between temperature and precipitation is an important paleo-hydrological factor in the study area since plants mostly synthesize their *n*-alkanes during early growing season or when water is available (Freimuth et al., 2017; Diefendorf et al., 2021), which in the IP occurs during spring-early summer and the during autumn-winter (Pérez Latorre and Cabezudo, 2002; García-Alix et al., 2021). Therefore, the downcore temporal variability in the values of $\delta D_{terr}$ in the Lake Peixão sediments is expected to mainly reflect bi-seasonal to annual changes in mean air temperature and/or precipitation amount. In the study site, lower temperatures often imply an increase in condensation, resulting in an inherent coupled effect of precipitation amount (amount effect) that may be imprinted in the $\delta D_{terr}$. Hence, low (high) $\delta D_{terr}$ values in downcore reconstructions are expected to reflect a decrease (increase) in temperatures and/or increase (decrease) in precipitation (snow or rainfall).

Moreover, based on the ecology of modern plants and the compositions of different *n*-alkanes analyzed, we expected the δD values of $C_{25}$ and $C_{27}$ in the lake sediments to better reflect changes in lake water sources. The scarcity of true aquatic plants in the study area makes it challenging to confirm this hypothesis. Aquatic plants typically show higher $\delta^{13}C_{n\text{-alk}}$ values than their terrestrial counterparts (e.g., Jiménez-Moreno et al., 2013; Hockun et al., 2016; Ortiz et al., 2021), which is not evident in the lake surface sediment nor in the analyzed plants, only *Juncus* sp. displaying relatively higher $\delta^{13}C_{n\text{-alk}}$ than their ecological counterparts (Figure 3; Table 1). The lack of evidence of less $\delta^{13}C$ depletion in mid-chains *n*-alkanes in the lake surface sediment supports terrestrial plant dominance over aquatic plant inputs in modern lake settings. This suggests that caution needs to be taken when using mid-chain *n*-alkanes without compound-specific $\delta^{13}C$ analyses in sedimentary archives to infer past changes in aquatic plant inputs and lake waters (Hockun et al., 2016; McFarlin et al., 2019). Moreover, it also highlights the importance of using $\delta^{13}C_{n\text{-alk}}$ over other indicators, such as $P_{aq}$, to better constrain aquatic inputs in the lake sediments. Beyond that, the distinct values of $\varepsilon_{app}$ between modern plants and lake surface sediment underline the importance of constraining the vegetation source when using specific fractionation factors in sediments (Yang et al., 2011).

## 5 Conclusion

Our results show that the oro-Mediterranean vegetation cover of the Lake Peixão area preferentially produces long-chain *n*-alkanes ($\geq C_{27}$) that control the *n*-alkane content in the lake. This vegetation is dominated by $C_3$ grasses/herbs and shrubs, two ecological forms that display similar $ACL_{27\text{-}33}$ and $CPI_{27\text{-}33}$ values but are clearly distinguished by their *n*-alkane isotopic signatures. Shrubs show proportionally higher $\delta^{13}C_{n\text{-alk}}$ and $\delta D_{n\text{-alk}}$ values than grasses/herbs, suggesting a congruent physiological response to the common climatic and environmental conditions. The *n*-alkane $C_{31}$ is the predominant leaf wax of the study area, produced by some grasses and shrubs, particularly by *Erica* sp. (heather), a shrub that is stands out as a major source for the total *n*-alkane pool. The $C_{29}$ is the second-most abundant and the more equally produced leaf *n*-alkane of the two dominant ecological forms. The *n*-alkanes $C_{33}$ and $C_{35}$, although less abundant than other long chains homologs, are also important in the study area since they are particularly associated with cold and drought-tolerant vegetation such as *Juniperus* sp. Finally, $C_{27}$ and $C_{25}$ *n*-alkanes are mainly linked to aquatic-related grasses/herbs and are inferred to better reflect changes in the water availability of the study area and the isotopic compositions of lake water. However, the aquatic origin of these homologs should be ensured in downcore reconstructions, for instance, performing compound-specific carbon isotopic analysis. The use δD of $C_{29}$ in the lake sediments ($\delta D_{terr}$) is interpreted as a robust terrestrial hydrology indicator. Despite the small number of plant species and different $\varepsilon_{app}$ among modern plants, the integrated $\varepsilon_{app}$ value of Lake Peixão's climatic sensor, determined from $\delta D_{terr}$ ($\varepsilon_{C29/MAP} = -129 \pm 12‰$), is in line with the projected values of global compilation studies. Overall, this dataset establishes a baseline for interpreting the leaf wax biomarkers in the region and Lake Peixão sediments, which is a valuable archive to reconstruct regional past hydroclimate changes in the region.

## Data availability statement

The original contributions presented in the study are included in the article/Supplementary Material, further inquiries can be directed to the corresponding authors.

## Author contributions

RS collected the data. RS, ES, LC, and TR produced the data. RS wrote the manuscript. DO, AH, and AR contributed to improving the manuscript. All authors contributed to the discussion and interpretation of the data and provided comments and suggestions to the manuscript.

## Funding

This work has been supported by the Portuguese Foundation for Science and Technology–FCT, through the HOLMODRIVE project (PTDC/CTA494 GEO/29029/2017).

The authors would like to express their gratitude for the data and contributions to the following projects/institutions: WarmWorld (PTDC/CTA-GEO/29897/2017), IF/01489/2015, EMSO-PT–INFRA/22157/2016, CCMAR UIDB/04326/2020, UIDP/04326/2020, LA/P/0101/2020, DO thanks to FCT through the contract CEECIND/02208/2017. AH thanks to the Spanish Ministry of Science and Innovation through the Ramón y Cajal Scheme (RYC2020–501 029253-I).

## Acknowledgments

RS and AR acknowledges the Portuguese Fundação para a Ciência e a Tecnologia (FCT) I.P./MCTES through national funds (PIDDAC) – UIDB/50019/2020- IDL. We are thankful to Mária Padilha for the help in n-alkane extraction at IPMA and Ralph Kreutz for the CSIA at MARUM. Marta Melissa Almeida for assisting during the vegetation collection campaign. Pedro Raposeiro, Pedro J. M. Costa, Ricardo M. Trigo, Alberto Sáez, Santiago Giralt, and personal of the Estrela UNESCO Global Geopark for the field work during the coring campaign.

## Conflict of interest

The authors declare that the research was conducted in the absence of any commercial or financial relationships that could be construed as a potential conflict of interest.

## Publisher's note



## Supplementary material

The Supplementary Material for this article can be found online at: https://www.frontiersin.org/articles/10.3389/fenvs.2022.994377/full#supplementary-material

## References

Abrantes, F., Rodrigues, T., Rufino, M., Salgueiro, E., Oliveira, D., Gomes, S., et al. (2017). The climate of the common era off the iberian Peninsula. *Clim. Past.* 13, 1901–1918. doi:10.5194/cp-13-1901-2017

Adrian, R., O'Reilly, C. M., Zagarese, H., Baines, S. B., Hessen, D. O., Keller, W., et al. (2009). Lakes as sentinels of climate change. *Limnol. Oceanogr.* 54, 2283–2297. doi:10.4319/lo.2009.54.6_part_2.2283

Allan, R. P., Hawkins, E., Bellouin, N., and Collins, B. (2021). "IPCC, 2021: Summary for policymakers," in *Climate change 2021: The physical science basis. Contribution of working group I to the sixth assessment report of the intergovernmental panel on climate change*. V. Masson-Delmotte, P. Zhai, A. Pirani, S. L. Connors, C. Péan, S. Berger, et al. (Cambridge University Press).

Baldini, L. M., Baldini, J. U. L., McDermott, F., Arias, P., Cueto, M., Fairchild, I. J., et al. (2019). North iberian temperature and rainfall seasonality over the younger dryas and holocene. *Quat. Sci. Rev.* 226, 105998. doi:10.1016/j.quascirev.2019.105998

Berke, M. A. (2018). "Reconstructing terrestrial paleoenvironments using sedimentary organic biomarkers BT - methods in paleoecology," in *Reconstructing cenozoic terrestrial environments and ecological communities*. Editors D. A. Croft, D. F. Su, and S. W. Simpson (Cham: Springer International Publishing), 121–149. doi:10.1007/978-3-319-94265-0_8

Boavida, M. J., and Gliwicz, Z. M. (1996). Limnological and biological characteristics of the alpine lakes of Portugal. *Limnetica* 12, 39–45. doi:10.23818/limn.12.11

Bowen, G. J., and Revenaugh, J. (2003). Interpolating the isotopic composition of modern meteoric precipitation. *Water Resour. Res.* 39, 1299. doi:10.1029/2003WR002086

Bray, E. E., and Evans, E. D. (1961). Distribution of n-paraffins as a clue to recognition of source beds. *Geochim. Cosmochim. Acta* 22, 2–15. doi:10.1016/0016-7037(61)90069-2

Bush, R. T., and McInerney, F. A. (2013). Leaf wax n-alkane distributions in and across modern plants: Implications for paleoecology and chemotaxonomy. *Geochim. Cosmochim. Acta* 117, 161–179. doi:10.1016/j.gca.2013.04.016

Carreira, P. M., Marques, J. M., Marques, J. E., Chaminé, H. I., Fonseca, P. E., Santos, F. M., et al. (2011). Defining the dynamics of groundwater in Serra da Estrela Mountain area, central Portugal: An isotopic and hydrogeochemical approach. *Hydrogeol. J.* 19, 117–131. doi:10.1007/s10040-010-0675-0

Carreira, P. M., Nunes, D., Valério, P., and Araújo, M. F. (2009). A 15-year record of seasonal variation in the isotopic composition of precipitation water over continental Portugal. *J. Radioanal. Nucl. Chem.* 281, 153–156. doi:10.1007/s10967-009-0064-0

Carvalho, A. M. M. (2013). *Hidrogeologia ambiental da região do Parque Natural da Serra da Estrela ( setor de Seia - Torre - Covilhã ): uma abordagem multidisciplinar*, 336.

Castañeda, I. S., and Schouten, S. (2011). A review of molecular organic proxies for examining modern and ancient lacustrine environments. *Quat. Sci. Rev.* 30, 2851–2891. doi:10.1016/j.quascirev.2011.07.009

Connor, S. E., van Leeuwen, J. F. N., van der Knaap, W. O., Pim)Akindola, R. B., Adeleye, M. A., et al. (2021). Pollen and plant diversity relationships in a Mediterranean montane area. *Veg. Hist. Archaeobot.* 30, 583–594. doi:10.1007/s00334-020-00811-0

Cortesi, N., Trigo, R. M., Gonzalez-Hidalgo, J. C., and Ramos, A. M. (2013). Modelling monthly precipitation with circulation weather types for a dense network of stations over Iberia. *Hydrol. Earth Syst. Sci.* 17, 665–678. doi:10.5194/hess-17-665-2013

Cranwell, P. A., Eglinton, G., and Robinson, N. (1987). Lipids of aquatic organisms as potential contributors to lacustrine sediments—II. *Org. Geochem.* 11, 513–527. doi:10.1016/0146-6380(87)90007-6

Curtin, L., Andrea, W. J. D., Balascio, N., Pugsley, G., Wet, G. De, and Bradley, R. (2019). Holocene and Last Interglacial climate of the Faroe Islands from sedimentary plant wax hydrogen and carbon isotopes. *Quat. Sci. Rev.* 223, 105930. doi:10.1016/j.quascirev.2019.105930

Dasgupta, B., Ajay, A., Prakash, P., and Sanyal, P. Understanding the disparity in n-alkane production among angiosperms and gymnosperms from the higher Himalayas: Inferences drawn from a Machine Learning approach. *Org. Geochem.* 171, 104463. doi:10.1016/J.ORGGEOCHEM.2022.104463

Diefendorf, A. F., Bickford, C. P., Schlanser, K. M., Freimuth, E. J., Hannon, J. S., Grossiord, C., et al. (2021). Plant wax and carbon isotope response to heat and drought in the conifer Juniperus monosperma. *Org. Geochem.* 153, 104197. doi:10.1016/j.orggeochem.2021.104197

Diefendorf, A., and Freimuth, E. (2017). Extracting the most from terrestrial plant-derived n-alkyl lipids and their carbon isotopes from the sedimentary record: A review. *Org. Geochem.* 103, 1–21. doi:10.1016/j.orggeochem.2016.10.016

Eglinton, G., and Hamilton, R. J. (1967). Leaf epicuticular waxes : The waxy outer surfaces of most plants display a wide diversity of fine structure and chemical constituents. *Sci. (80-. )* 156, 1322–1335. doi:10.1126/science.156.3780.1322

Evans, M. N., Tolwinski-Ward, S. E., Thompson, D. M., and Anchukaitis, K. J. (2013). Applications of proxy system modeling in high resolution paleoclimatology. *Quat. Sci. Rev.* 76, 16–28. doi:10.1016/j.quascirev.2013.05.024

Ferreira, L. M. M., Oliván, M., Celaya, R., Garcia, U., Rodrigues, M. A. M., and Osoro, K. (2007). The use of n-alkanes to estimate diet composition of ruminants grazing on species diverse plant communities - effect of feeding selectivity on diet composition estimates. *Livest. Sci.* 111, 114–123. doi:10.1016/j.livsci.2006.12.008

Ficken, K. J., Li, B., Swain, D. L., and Eglinton, G. (2000). An n-alkane proxy for the sedimentary input of submerged/floating freshwater aquatic macrophytes. *Org. Geochem.* 31, 745–749. doi:10.1016/S0146-6380(00)00081-4

Freeman, K. H., and Colarusso, L. A. (2001). Molecular and isotopic records of C4 grassland expansion in the late miocene. *Geochim. Cosmochim. Acta* 65, 1439–1454. doi:10.1016/S0016-7037(00)00573-1

Freimuth, E. J., Diefendorf, A. F., and Lowell, T. V. (2017). Hydrogen isotopes of n-alkanes and n-alkanoic acids as tracers of precipitation in a temperate forest and implications for paleorecords. *Geochim. Cosmochim. Acta* 206, 166–183. doi:10.1016/j.gca.2017.02.027

Gao, L., Edwards, E. J., Zeng, Y., and Huang, Y. (2014). Major evolutionary trends in hydrogen isotope fractionation of vascular plant leaf waxes. *PLoS One* 9, e112610. doi:10.1371/journal.pone.0112610

García-Alix, A., Camuera, J., Ramos-Román, M. J., Toney, J. L., Sachse, D., Schefuß, E., et al. (2021). Paleohydrological dynamics in the Western Mediterranean during the last glacial cycle. *Glob. Planet. Change* 202, 103527. doi:10.1016/j.gloplacha.2021.103527

Giménez, R., Bartolomé, M., Gázquez, F., Iglesias, M., and Moreno, A. (2021). Underlying climate controls in triple oxygen (16O, 17O, 18O) and hydrogen (1H, 2H) isotopes composition of rainfall (central pyrenees). *Front. Earth Sci.* 9, 1–16. doi:10.3389/feart.2021.633698

Hahn, A., Neumann, F. H., Miller, C., Finch, J., Frankland, T., Cawthra, H. C., et al. (2021). Mid-to late holocene climatic and anthropogenic influences in mpondoland, south Africa. *Quat. Sci. Rev.* 261, 106938. doi:10.1016/j.quascirev.2021.106938

Hammer, Ø., Harper, D., and Ryan, P. (2001). Past: Paleontological statistics software package for educaton and data anlysis. *Palaeontol. Electron.* 4, 1.

Hernández, A., Sáez, A., Santos, N. R., Rodrigues, T., Martin-Puertas, C., Gil-Romera, G., et al. (in review)). The timing of the deglaciation in the atlantic iberian mountains: Insights from the stratigraphic analysis on of a lake sediments sequence in Serra da Estrela (Portugal) (submitted). *Earth Surf. Process. Landforms*.

Hockun, K., Mollenhauer, G., Ling, S., Hefter, J., Ohlendorf, C., Zolitschka, B., et al. (2016). Using distributions and stable isotopes of n-alkanes to disentangle organic matter contributions to sediments of Laguna Potrok Aike, Argentina. *Org. Geochem.* 102, 110–119. doi:10.1016/j.orggeochem.2016.10.001

Hou, J., D'Andrea, W. J., MacDonald, D., and Huang, Y. (2007). Evidence for water use efficiency as an important factor in determining the δD values of tree leaf waxes. *Org. Geochem.* 38, 1251–1255. doi:10.1016/j.orggeochem.2007.03.011

Howard, S., McInerney, F. A., Caddy-Retalic, S., Hall, P. A., and Andrae, J. W. (2018). Modelling leaf wax n-alkane inputs to soils along a latitudinal transect across Australia. *Org. Geochem.* 121, 126–137. doi:10.1016/j.orggeochem.2018.03.013

Imfeld, A., Ouellet, A., Douglas, P. M. J., Kos, G., and Gélinas, Y. (2022). Molecular and stable isotope analysis (δ13C, δ2H) of sedimentary n-alkanes in the St. Lawrence Estuary and Gulf, Quebec, Canada: Importance of even numbered n-alkanes in coastal systems. *Org. Geochem.* 164, 104367. doi:10.1016/j.orggeochem.2022.104367

Jansen, J. (2011). *Managing Natura 2000 in a changing world the case of the Serra da Estrela*.

Jambrina-Enríquez, M., Sachse, D., and Valero-Garcés, B. L. (2016). A deglaciation and holocene biomarker-based reconstruction of climate and environmental variability in NW iberian Peninsula: The sanabria lake sequence. *J. Paleolimnol.* 56, 49–66. doi:10.1007/s10933-016-9890-6

Jiménez-moreno, G., García-alix, A., Hernández-corbalán, M. D., Anderson, R. S., and Delgado-huertas, A. (2013). Vegetation, fire, climate and human disturbance history in the southwestern Mediterranean area during the late Holocene. *Quat. Res.* 79, 110–122. doi:10.1016/j.yqres.2012.11.008

Leider, A., Hinrichs, K. U., Schefuß, E., and Versteegh, G. J. M. (2013). Distribution and stable isotopes of plant wax derived n-alkanes in lacustrine, fluvial and marine surface sediments along an Eastern Italian transect and their potential to reconstruct the hydrological cycle. *Geochim. Cosmochim. Acta* 117, 16–32. doi:10.1016/j.gca.2013.04.018

Li, Z., Sun, Y., and Nie, X. (2020). Biomarkers as a soil organic carbon tracer of sediment: Recent advances and challenges. *Earth. Sci. Rev.* 208, 103277. doi:10.1016/j.earscirev.2020.103277

Liu, H., and Liu, W. (2019). Hydrogen isotope fractionation variations of n-alkanes and fatty acids in algae and submerged plants from Tibetan Plateau lakes: Implications for palaeoclimatic reconstruction. *Sci. Total Environ.* 695, 133925. doi:10.1016/j.scitotenv.2019.133925

Liu, J., An, Z., and Liu, H. (2018). Leaf wax n-alkane distributions across plant types in the central Chinese Loess Plateau. *Org. Geochem.* 125, 260–269. doi:10.1016/j.orggeochem.2018.09.006

Liu, J., and An, Z. (2019). Variations in hydrogen isotopic fractionation in higher plants and sediments across different latitudes: Implications for paleohydrological reconstruction. *Sci. Total Environ.* 650, 470–478. doi:10.1016/j.scitotenv.2018.09.047

Loidi, J., Biurrun, I., Campos, J. A., García-Mijangos, I., and Herrera, M. (2007). A survey of heath vegetation of the iberian Peninsula and northern Morocco: A biogeographic and bioclimatic approach. *phyto.* 37, 341–370. doi:10.1127/0340-269X/2007/0037-0341

López-Días, V., Blanco, C. G., Bechtel, A., Püttmann, W., and Borrego, A. G. (2013). Different source of n-alkanes and n-alkan-2-ones in a 6000cal. yr BP Sphagnum-rich temperate peat bog (Roñanzas, N Spain). *Org. Geochem.* 57, 7–10. doi:10.1016/j.orggeochem.2013.01.006

Marzi, R., Torkelson, B. E., and Olson, R. K. (1993). A revised carbon preference index. *Org. Geochem.* 20, 1303–1306. doi:10.1016/0146-6380(93)90016-5

McFarlin, J. M., Axford, Y., Masterson, A. L., and Osburn, M. R. (2019). Calibration of modern sedimentary δ2H plant wax-water relationships in Greenland lakes. *Quat. Sci. Rev.* 225, 105978. doi:10.1016/j.quascirev.2019.105978

Mora, C. (2010). A synthetic map of the climatopes of the Serra da Estrela (Portugal). *J. Maps* 6, 591–608. doi:10.4113/jom.2010.1112

Oliveira, A., and Lima, A. (2010). Spatial variability in the stable isotopes of modern precipitation in the northwest of Iberia. *Isot. Environ. Health Stud.* 46, 13–26. doi:10.1080/10256010903388154

Ortiz, J. E., Borrego, Á. G., Gallego, J. L. R., Sánchez-Palencia, Y., Urbanczyk, J., Torres, T., et al. (2016). Biomarkers and inorganic proxies in the paleoenvironmental reconstruction of mires: The importance of landscape in Las Conchas (Asturias, Northern Spain). *Org. Geochem.* 95, 41–54. doi:10.1016/j.orggeochem.2016.02.009

Ortiz, J. E., Díaz-Bautista, A., Aldasoro, J. J., Torres, T., Gallego, J. L. R., Moreno, L., et al. (2011). N-Alkan-2-ones in peat-forming plants from the Roñanzas ombrotrophic bog (Asturias, northern Spain). *Org. Geochem.* 42, 586–592. doi:10.1016/j.orggeochem.2011.04.009

Ortiz, J. E., Torres, T., Delgado, A., Llamas, J. F., Soler, V., Valle, M., et al. (2010). Palaeoenvironmental changes in the Padul Basin (Granada, Spain) over the last 1Ma based on the biomarker content. *Palaeogeogr. Palaeoclimatol. Palaeoecol.* 298, 286–299. doi:10.1016/j.palaeo.2010.10.003

Ortiz, J. E., Torres, T., Delgado, A., Valle, M., Soler, V., Araujo, R., et al. (2021). Bulk and compound-specific δ13C and n-alkane indices in a palustrine intermontane record for assessing environmental changes over the past 320 ka: The padul basin (southwestern mediterranean realm). *J. Iber. Geol.* 47, 625–639. doi:10.1007/s41513-021-00175-y

Pancost, R. D., and Boot, C. S. (2004). The palaeoclimatic utility of terrestrial biomarkers in marine sediments. *Mar. Chem.* 92, 239–261. doi:10.1016/j.marchem.2004.06.029

Pérez Latorre, A. V., and Cabezudo, B. (2002). Use of monocharacteristic growth forms and phenological phases to describe and differentiate plant communities in Mediterranean-type ecosystems. *Plant Ecol.* 161, 231–249. doi:10.1023/A:1020327522487

Peters, K. E., Peters, K. E., Walters, C. C., and Moldowan, J. M. (2005). *The biomarker guide*. Cambridge University Press.

Post-Beittenmiller, D. (1996). Biochemistry and molecular biology of wax production in plants. *Annu. Rev. Plant Physiol. Plant Mol. Biol.* 47, 405–430. doi:10.1146/annurev.arplant.47.1.405

Poynter, J. G. (1989). *Molecular stratigraphy: The recognition of palaeoclimatic signals in organic geochemical data*. Bristol: School of Chemistry, University of Bristol. PhD Thesis.

Ribeiro, A., Kullberg, M. C., Kullberg, J. C., Manuppella, G., and Phipps, S. (1990). A review of Alpine tectonics in Portugal: Foreland detachment in basement and cover rocks. *Tectonophysics* 184, 357–366. doi:10.1016/0040-1951(90)90448-H

Rommerskirchen, F., Eglinton, G., Dupont, L., and Rullkötter, J. (2006). Glacial/interglacial changes in southern Africa: Compoundspecific δ13C land plant biomarker and pollen records from southeast Atlantic continental margin sediments. *Geochem. Geophys. Geosyst.* 7. doi:10.1029/2005GC001223

Sachse, D., Billault, I., Bowen, G. J., Chikaraishi, Y., Dawson, T. E., Feakins, S. J., et al. (2012). Molecular paleohydrology: Interpreting the hydrogen-isotopic composition of lipid biomarkers from photosynthesizing organisms. *Annu. Rev. Earth Planet. Sci.* 40, 221–249. doi:10.1146/annurev-earth-042711-105535

Sánchez-López, G., Hernández, A., Pla-Rabes, S., Trigo, R. M., Toro, M., Granados, I., et al. (2016). Climate reconstruction for the last two millennia in central Iberia: The role of east atlantic (EA), North Atlantic oscillation (NAO) and their interplay over the iberian Peninsula. *Quat. Sci. Rev.* 149, 135–150. doi:10.1016/j.quascirev.2016.07.021

Schäfer, I. K., Bliedtner, M., Wolf, D., Faust, D., and Zech, R. (2016a). Evidence for humid conditions during the last glacial from leaf wax patterns in the loess-paleosol sequence El Paraíso, Central Spain. *Quat. Int.* 407, 64–73. doi:10.1016/j.quaint.2016.01.061

Schäfer, I. K., Lanny, V., Franke, J., Eglinton, T. I., Zech, M., Vysloužilová, B., et al. (2016b). Leaf waxes in litter and topsoils along a European transect. *Soil* 2, 551–564. doi:10.5194/soil-2-551-2016

Schefuß, E., Ratmeyer, V., Stuut, J. B. W., Jansen, J. H. F., and Sinninghe Damsté, J. S. (2003). Carbon isotope analyses of n-alkanes in dust from the lower atmosphere over the central eastern Atlantic. *Geochim. Cosmochim. Acta* 67, 1757–1767. doi:10.1016/S0016-7037(02)01414-X

Schirrmacher, J., Andersen, N., Schneider, R. R., and Weinelt, M. (2020). Fossil leaf wax hydrogen isotopes reveal variability of Atlantic and Mediterranean climate forcing on the southeast Iberian Peninsula between 6000 to 3000 cal. BP. *PLoS One* 15, 1–19. doi:10.1371/journal.pone.0243662

Shepherd, T., and Griffiths, D. W. (2006). The effects of stress on plant cuticular waxes. *New Phytol.* 171, 469–499. doi:10.1111/j.1469-8137.2006.01826.x

Stout, S. A. (2020). Leaf wax n-alkanes in leaves, litter, and surface soil in a low diversity, temperate deciduous angiosperm forest, Central Missouri, USA. *Chem. Ecol.* 0, 810–826. doi:10.1080/02757540.2020.1789118

Taylor, A. K., Benedetti, M. M., Haws, J. A., and Lane, C. S. (2018). Mid-holocene iberian hydroclimate variability and paleoenvironmental change: Molecular and isotopic insights from praia rei cortiço, Portugal. *J. Quat. Sci.* 33, 79–92. doi:10.1002/jqs.3000

Thatcher, D. L., Wanamaker, A. D., Denniston, R. F., Asmerom, Y., Polyak, V. J., Fullick, D., et al. (2020). Hydroclimate variability from Western Iberia (Portugal) during the Holocene: Insights from a composite stalagmite isotope record. *Holocene* 30, 966–981. doi:10.1177/0959683620908648

Thomas, C. L., Jansen, B., Van Loon, E. E., and Wiesenberg, G. L. B. (2021). Transformation of <i>n</i>-alkanes from plant to soil: A review. *SOIL* 7, 785–809. doi:10.5194/soil-7-785-2021

Thomas, P. A., El-Barghathi, M., and Polwart, A. (2007). Biological flora of the British isles: Juniperus communis L. *J. Ecol.* 95, 1404–1440. doi:10.1111/j.1365-2745.2007.01308.x

Toney, J. L., García-Alix, A., Jiménez-Moreno, G., Anderson, R. S., Moossen, H., and Seki, O. (2020). New insights into Holocene hydrology and temperature from lipid biomarkers in Western Mediterranean alpine wetlands. *Quat. Sci. Rev.* 240, 106395. doi:10.1016/j.quascirev.2020.106395

Toro, M., Granados, I., Robles, S., and Montes, C. (2006). High mountain lakes of the central range (iberian Peninsula): Regional limnology & environmental changes. *Limnetica* 25, 217–252. doi:10.23818/limn.25.17

Vieira, G. (2008). Combined numerical and geomorphological reconstruction of the Serra da Estrela plateau icefield, Portugal. *Geomorphology* 97, 190–207. doi:10.1016/j.geomorph.2007.02.042

Vieira, G. (2004). *Geomorfologia dos planaltos E altos vales da Serra da Estrela ambientes frios do plistocénico superior E dinâmica actual*. Lisbon: University of Lisbon. PhD Thesis.

Vieira, G., Jansen, J., and Ferreira, N. (2005). *Environmental setting of the Serra da Estrela, Portugal a short-note*. IALE UK: Landsc. Ecol. Ser.

Wang, J., Axia, E., Xu, Y., Wang, G., Zhou, L., Jia, Y., et al. (2018). Temperature effect on abundance and distribution of leaf wax n-alkanes across a temperature gradient along the 400 mm isohyet in China. *Org. Geochem.* 120, 31–41. doi:10.1016/j.orggeochem.2018.03.009

Xie, M., Sun, Q., Dong, H., Liu, S., Shang, W., Ling, Y., et al. (2020). n-Alkanes and compound carbon isotope records from Lake Yihesharwusu in the Hulun Buir sandy land, northeastern China. *Holocene* 30, 1451–1461. doi:10.1177/0959683620932968

Yang, H., Liu, W., Leng, Q., Hren, M. T., and Pagani, M. (2011). Variation in n-alkane δD values from terrestrial plants at high latitude: Implications for paleoclimate reconstruction. *Org. Geochem.* 42, 283–288. doi:10.1016/j.orggeochem.2011.01.006

Zech, M., Buggle, B., Leiber, K., Marković, S., Glaser, B., Hambach, U., et al. (2010). Reconstructing Quaternary vegetation history in the Carpathian Basin, SE-Europe, using n-alkane biomarkers as molecular fossils: Problems and possible solutions, potential and limitations. *E&G Quat. Sci. J.* 58, 148–155. doi:10.3285/eg.58.2.03

frontiers | Frontiers in Environmental Science

TYPE Original Research
PUBLISHED 04 January 2023
DOI 10.3389/fenvs.2022.1028405



OPEN ACCESS

EDITED BY
Marta Sebastian,
Institut de Ciències del Mar, CSIC, Spain

REVIEWED BY
Moritz Felix Lehmann,
University of Basel, Switzerland
Haryun Kim,
Korea Institute of Ocean Science and Technology (KIOST), South Korea

*CORRESPONDENCE
Emily J. Chua,
ejchua@bu.edu
Robinson W. Fulweiler,
rwf@bu.edu

SPECIALTY SECTION
This article was submitted to Biogeochemical Dynamics, a section of the journal Frontiers in Environmental Science

RECEIVED 26 August 2022
ACCEPTED 12 December 2022
PUBLISHED 04 January 2023

CITATION
Chua EJ and Fulweiler RW (2023), Capturing the rapid response of sediments to low-oxygen conditions with high temporal resolution gas concentration measurements. *Front. Environ. Sci.* 10:1028405. doi: 10.3389/fenvs.2022.1028405



# Capturing the rapid response of sediments to low-oxygen conditions with high temporal resolution gas concentration measurements

Emily J. Chua[1]* and Robinson W. Fulweiler[1,2]*

[1]Department of Earth and Environment, Boston University, Boston, MA, United States, [2]Department of Biology, Boston University, Boston, MA, United States

Low-oxygen conditions plague coastlines worldwide. At present, little is known about how the transition from normoxic to low or even no oxygen conditions alters sediment biogeochemical cycling and ultimately ecosystem functioning. Conventional sediment core incubations cannot capture rapid (<hourly) changes in biogenic gas fluxes that may occur due to oxygen depletion. To better constrain the response of sediments to hypoxia, we employed a novel flow-injection system coupled to a membrane inlet mass spectrometer to quantify fluxes oxygen, dinitrogen, and methane across the sediment-water interface from a temperate estuary (Narragansett Bay, Rhode Island, United States). We evaluated how sediments from a site more impacted by nitrogen pollution compare to one less impacted by nitrogen in response to organic matter addition. Our system is able to sample every 10 minutes, allowing us to cycle through triplicate core measurements roughly every 30 minutes to track the response of sediments to increasing hypoxic severity. The high temporal-resolution data revealed dynamic changes in sediment-water gas fluxes, suggesting that reactive nitrogen removal is enhanced under mild hypoxia but dampened under prolonged hypoxia to anoxia. Further we found that organic matter loading enhances both net denitrification and methane emissions. Ultimately, our approach represents a powerful new tool for advancing our knowledge of short-term temporal dynamics in benthic biogeochemical cycling.

KEYWORDS

**estuary, hypoxia, nitrogen, methane, greenhouse gas, mass spectrometry**

## 1 Introduction

In coastal waters worldwide, oxygen levels are declining. Zones of low oxygen overwhelmingly occur near human population centers and developed watersheds that discharge nutrient-laden water into the ocean. These low oxygen conditions are primarily driven by excess nutrient loading and rising temperatures (Breitburg et al., 2018). In

particular, elevated nutrient concentrations in coastal waters stimulate the growth of phytoplankton and macroalgae, which in turn promotes microbial respiration and the drawdown of water column oxygen. This enhanced respiration is exacerbated by warming water temperature, which stratifies the water column, decreasing oxygen replenishment from mixing. Rising water temperatures also decreases the solubility of oxygen, lowering water column oxygen concentrations while simulatenously increasing metabolic oxygen demands (Breitburg et al., 2018).

Oxygen availability dictates the survival of marine life and exerts a strong influence on the cycling of nutrients and gases important for both local ecosystem function and global climate. As such, waters that are hypoxic (low in oxygen, Vaquer-Sunyer and Duarte, 2008) or anoxic (devoid of oxygen) can lead to the loss of biomass, biodiversity, and habitat, as well as alter energy and biogeochemical cycling in coastal systems (Diaz et al., 2019). While overlooked in global ocean nutrient budgets (Chua et al., 2022), coastal and continental shelf sediments are key sites of nitrogen and carbon cycling. Low dissolved oxygen in bottom waters can interfere with the ability of sediments to provide key ecosystem services such as reactive nitrogen removal and greenhouse gas regulation.

In general, the magnitudes and mechanisms behind marine sediment nitrogen and carbon cycling are not well constrained (e.g., Rosentreter et al., 2021; Chua et al., 2022), and even less is known about how coastal hypoxia impacts sediment biogeochemical processes. The available work suggests that biogeochemical responses vary widely and depend on the severity and duration of oxygen depletion. For example, previous studies have found that sediment nitrogen removal through denitrification can be enhanced (e.g., Gardner and McCarthy, 2009), diminished (e.g., McCarthy et al., 2015), or remain unchanged (e.g., Foster and Fulweiler, 2019) by hypoxic conditions. Similarly, sediment methane emissions exhibit variable responses to low oxygen (e.g., Damgaard, Revsbech and Reichardt, 1998; Foster and Fulweiler, 2019). Moreover, a recent metaanalysis found that methane emissions from estuaries, mangroves, and salt marshes increase with eutrophication (Rosentreter et al., 2021). It is likely that sediment denitrification and methane production respond dynamically and non-linearly to increasing oxygen depletion, and that factors such as the environmental legacy of the sediment (i.e., whether it is accustomed to received high organic matter loads or not) can influence this response.

Measuring sediment fluxes is challenging for a host of reasons, one of which is that current methods do not allow us to examine fluxes of multiple biogeochemically important gases over time as conditions change. In fact, we often assume and/or wait for steady state conditions. Thus, when we try to determine how sediments respond to low oxygen (or any perturbation) we often treat it as a binary—normal condition *versus* impacted condition. While useful, this misses critical transition periods and leaves us with an incomplete picture of how sediments respond to the dynamic conditions they experience. Here we had an opportunity to apply a previously described, novel mass spectrometer-based system (Chua et al., 2021) that analyzes dissolved gas content in near real time, enabling us to obtain measurements at a much higher temporal resolution than possible in conventional laboratory incubations. We used this system to assess the influence of oxygen depletion on reactive nitrogen removal and methane emission in coastal sediments by quantifying sediment fluxes of dissolved oxygen ($O_2$), dinitrogen ($N_2$), and methane ($CH_4$) continuously over 24 h in a series of laboratory experiments. We compared differences in emissions of these gas fluxes over time from sediments collected from a more nutrient-enriched and productive site to a less nutrient-impacted site. Additionally, we investigated how sediment fluxes from each site would respond to a pulse of labile organic matter. Using these high-resolution gas concentration data we modeled gas fluxes over time, capturing the response of sediments as they crossed hypoxic and anoxic thresholds. Based on these results and the current literature we then discuss possible explanations for what we observed to stimulate future research.

# 2 Materials and methods

## 2.1 Field site description

For these experiments we used sediments from Narragansett Bay, Rhode Island, United States. Narragansett Bay is a small (328 $km^2$), well-mixed, phytoplankton-dominated temperate estuary (Nixon et al., 2008). Narragansett Bay is characterized by a strong north-to-south gradient in anthropogenic pollutants as most of the wastewater and land drainage enters at the head of the bay. Low-oxygen conditions occur intermittently in upper Narragansett Bay, especially in Providence River Estuary bottom waters (Bergondo et al., 2005; Codiga et al., 2009). The bay has a mean low water depth of 8.6 m and a mean residence time of 26 days (Pilson, 1985; Nixon et al., 1995). The majority of the sediments are clayey silt and sand-silt-clay (McMaster, 1960).

We collected intact, subtidal sediment cores from Narragansett Bay for laboratory measurements from two sites: one in the Providence River Estuary (PRE) and one in mid-Narragansett Bay (MNB). PRE is an urban estuary where 60%–70% of the total sewage load that enters Narragansett Bay was directly discharged to this estuary. Because of this major anthropogenic perturbation, a variety of environmental factors such as chlorophyll and nutrient concentrations (Oviatt et al., 2002) are highest here and decrease down the bay. Additionally low oxygen conditions are more frequent in PRE compared to MNB (Codiga et al., 2009). PRE and MNB have similar sediment characteristics (~75% silt/coarse silt) but C:N is more variable (Fulweiler and Nixon 2012). Six intact cores were collected by divers from MNB on 9 November 2021, and another six cores

were collected using a pull corer off the side of a boat from PRE on 19 November 2021. The cores were collected in clear PVC tubes measuring 10 cm (inner diameter) and 30 cm (height). Following collection, cores were loosely capped and placed upright in a cooler. Bottom water was also collected from each site and immediately filtered (0.2 micron) to remove water column biota, as our subsequent measurements were focused on processes occurring at the sediment-water interface. On both dates, the cores and filtered site water were immediately transported from the field to the laboratory (within 6 h), where they were kept in the dark at room temperature (~20°C).

## 2.2 Benthic flux incubations

Following both field sampling events, we conducted 24-h incubations on the collected cores in the laboratory to measure fluxes of dissolved gases across the sediment-water interface. For each site, we conducted an "amended" incubation, in which labile organic matter was added to the cores ($n$ = 3), and a "control" incubation, in which the cores ($n$ = 3) were left unamended. Cores were stored uncapped in a cooler with the overlying water gently bubbled with air at least overnight to equilibrate to laboratory conditions (e.g., Hopkinson, Giblin and Tucker, 2001; Fulweiler et al., 2007). The carboy of site water was also gently bubbled with air.

During the incubations, we employed a newly developed flow-injection mass spectrometer system (Chua et al., 2021) to make measurements of dissolved gases directly in the overlying water of the cores in near-real time and at high temporal resolution. While we originally developed this instrument to measure porewater dissolved gases in highly permeable sandy sediments, it can also be used to make measurements in the overlying water of sediment with no modification. The instrument has been described elsewhere in detail (Chua et al., 2021). In brief, it comprises a flow-injection system that collects water samples, and a commercially available mass spectrometer (Transpector MPH, Inficon) that analyzes the dissolved gas content of the collected samples in real-time. The instrument measures sample dissolved gas concentrations relative to some known reference, e.g., air-equilibrated deionized water. While it can measure a suite of dissolved gases simultaneously, here we were interested in capturing net changes in dissolved oxygen ($O_2$), methane ($CH_4$), and dinitrogen gas ($N_2$). Quantifying net fluxes of these gases across the sediment-water interface provides insights into key benthic biogeochemical processes: $O_2$ provides a measure of photosynthesis and respiration, net $N_2$ production indicates denitrification (i.e., the $N_2$/Ar technique gives a net measurement of denitrification minus nitrogen fixation), and $CH_4$ production suggests methanogenesis.

At the start of an incubation, the overlying water of each core was carefully siphoned off, leaving the surface sediment undisturbed (Fulweiler et al., 2007). For the amended incubations, 1 g of commercial spray-dried marine phytoplankton with a C:N ratio of 8.0 (PhytoPlan, Two Little Fishies, Inc.) was added to each core (Fulweiler et al., 2007). The cores were then slowly refilled with water from the carboy of site water to ensure the same initial conditions for the overlying water. The cores were sealed with air-tight caps, taking care to avoid introducing bubbles. The caps had an outlet port with tubing leading to the automated flow-injection sampling system, and an inlet port connected to an elevated reservoir of site water open to air. As the flow-injection system extracted discrete samples of overlying water (~1.5 ml volume), the water was replenished by the gravity feed. The overlying water was gently mixed (~45 rpm) with magnetic stirrer bars to prevent concentration gradients from forming (Foster and Fulweiler, 2019). Air-equilibrated deionized water, contained in the same cooler as the cores, was used as the reference. Reference water temperature was monitored continuously (1 s resolution) with a FireSting probe (Ohio Lumex). Flow-injection measurements were automated with a custom MATLAB routine (Chua et al., 2021) that produced a time-stamped sampling log upon termination. Each of the three replicate cores was sampled every 10 min, resulting in timeseries data for each core at half-hour resolution. Incubations were left to run for 24 h in the dark and monitored intermittently (e.g., to measure flow rate to the mass spectrometer).

Following the control and amended incubations for each site, calibrations for $O_2$ and $CH_4$ were conducted using the water collected from that site. Calibration conditions were kept as similar as possible to incubation conditions—i.e., the calibrations were conducted at room temperature and using the same flow-injection timing and mass spectrometer parameters as during the incubations. Calibration standards were created by bubbling site water with dry gas mixtures containing known mole fractions of $O_2$ and $CH_4$. For each gas, five calibration standards spanning the expected concentration range for that gas were created. The corresponding dissolved gas concentrations for each calibration standard were calculated using solubility equations for $O_2$ (Garcia and Gordon, 1992) and $CH_4$ (Wiesenburg and Guinasso, 1979). Each calibration standard was sampled by flow injection (three replicate measurements per standard), and the impulse inputs were integrated to relate peak areas to concentration differentials. Linear regressions fit to the calibration data were used to relate flow-injection mass spectrometer measurements to gas concentrations in the subsequent data analysis. For $N_2$, we used a modified $N_2$/Ar method that did not require calibration (see below).

## 2.3 Flow injection-mass spectrometer data analysis

The data from the flow-injection mass spectrometer system were processed using custom scripts written in MATLAB. We used the peak area (as opposed to peak height) to characterize peak size, as this metric is less sensitive to factors such as sample dispersion (O'Haver, 2020).

The data processing for $O_2$ and $CH_4$ proceeded as follows. First, the log from the automated MATLAB sampling routine was used to locate the start and stop indices and baseline signals for each peak in the mass spectrometer data. Next, the peaks were baseline-corrected and integrated to obtain peak areas (units: Coulombs). Then, the flow-injection calibration curves were applied to the raw peak area data to obtain gas concentration differentials from the reference water (units: μmol $L^{-1}$). Reference water gas concentrations as a function of time were calculated with gas-specific solubility equations ($O_2$: Garcia and Gordon, 1992; $CH_4$: Wiesenburg and Guinasso, 1979), using the measured salinity and the FireSting temperature timeseries data. Absolute gas concentrations ($C$) were then computed by adding the concentration differential ($\Delta C$) to the reference water concentration ($C_{Ref}$):

$$C = C_{Ref} + \Delta C \quad (1)$$

For $N_2$, we modified the $N_2$/Ar technique for conventional membrane inlet mass spectrometry data (Kana et al., 1994) for our flow-injection data. Argon is an inert gas that is not influenced by biological processes; changes in its concentration are therefore diagnostic of changing physical conditions. Because $N_2$ typically has a low flux compared to its background concentration, normalizing the $N_2$ signal to the Ar signal permits measurements with higher precision. Analysis of the $N_2$/Ar ratio data is similar as for the other gases, except that after integrating the peaks (units: seconds), the peak areas are divided by the integration time period. This quantity is then multiplied by the Ar concentration, which is assumed to be at equilibrium at the measured temperature and salinity of the sample water, to obtain $\Delta N_2$ (μmol $L^{-1}$).

## 2.4 Flux modeling

We used the concentration timeseries data to estimate continuous fluxes of the gases over the 24-h incubation period. This flux modelling was conducted in MATLAB. To better reveal overall trends in the timeseries, we first smoothed the raw concentration data using the *smoothn* function (Garcia, 2010, 2011) which automatically determines the smoothing parameter by minimizing the generalized cross-validation score, with the "robust" option specified. Next, we fit curves to the smoothed concentration data using the built-in *fit* function, with smoothing splines as the model type. We selected a smoothing parameter of one so that the curves fit through all of the smoothed data. The fitted curves were then differentiated at 0.01 h intervals to estimate rates of change as a function of time [$C'(t)$; μmol $L^{-1}$ $h^{-1}$] over the 24-h incubation period, starting at hour two. To convert to fluxes ($J(t)$; μmol $m^{-2}$ $h^{-1}$), the first derivatives were multiplied by the height of the overlying water ($h_{OLW}$; m) for the respective core and a volume conversion factor of $10^3$ (from L to $m^3$):

$$J(t)\left(\frac{\mu mol}{m^2 \cdot h}\right) = C'(t)\left(\frac{\mu mol}{L \cdot h}\right) \times h_{OLW}\,(m) \times 10^3\left(\frac{L}{m^3}\right) \quad (2)$$

Positive fluxes indicate net production of the gas by the sediment (i.e., an efflux from the sediment into the water column), while negative fluxes indicate net sediment consumption (i.e., an influx into the sediment).

In order to put our results into context with the literature, we took our fitted concentration curves and calculated average fluxes for three oxygen "regimes". We defined the "normoxic" regime as measurements made above the hypoxic threshold ($O_2$ > 94 μM; Vaquer-Sunyer and Duarte, 2008), the "hypoxic" regime between the hypoxic and anoxic thresholds (0 < $O_2$ < 94 μM), and the "anoxic" regime below the anoxic threshold ($O_2$ = 0 μM). Hypoxia is often operationally defined as water with an oxygen concentration at or below 63 μM, based on when fisheries collapse (Renaud et al., 1986). We chose a marginally higher oxygen concentration because other studies demonstrate that a variety of organisms experience hypoxia at higher oxygen levels (Vaquer-Sunyer and Duarte, 2008). The averaged fluxes for each gas were estimated from the difference in fitted concentrations between the beginning and end of each oxygen regime.

# 3 Results and discussion

## 3.1 Concentration and flux timeseries

The high-resolution gas concentration measurements (Figures 1, 2) enabled calculation of continuous fluxes of $O_2$, $N_2$, and $CH_4$ over the 24-h experiments, which in turn revealed complex, dynamic changes (Figure 2; Tables 1, 2).

While aerobic respiration led to declines in $O_2$ in all cores, there were large variations in whether and when a core reached hypoxia or anoxia, even within a given site and treatment (Figures 1, 2; Table 2). All three control cores from MNB reached hypoxia, after 15.6 ± 1.2 h, while only one PRE control core went hypoxic, after 19.3 h. As expected, our addition of organic matter to cores in the amended treatment intensified aerobic respiration, resulting in a rapid $O_2$ depletion to anoxia in sediments from both sites (2Figures 1B, D and Figures 2B, D). Amended cores from the less impacted site

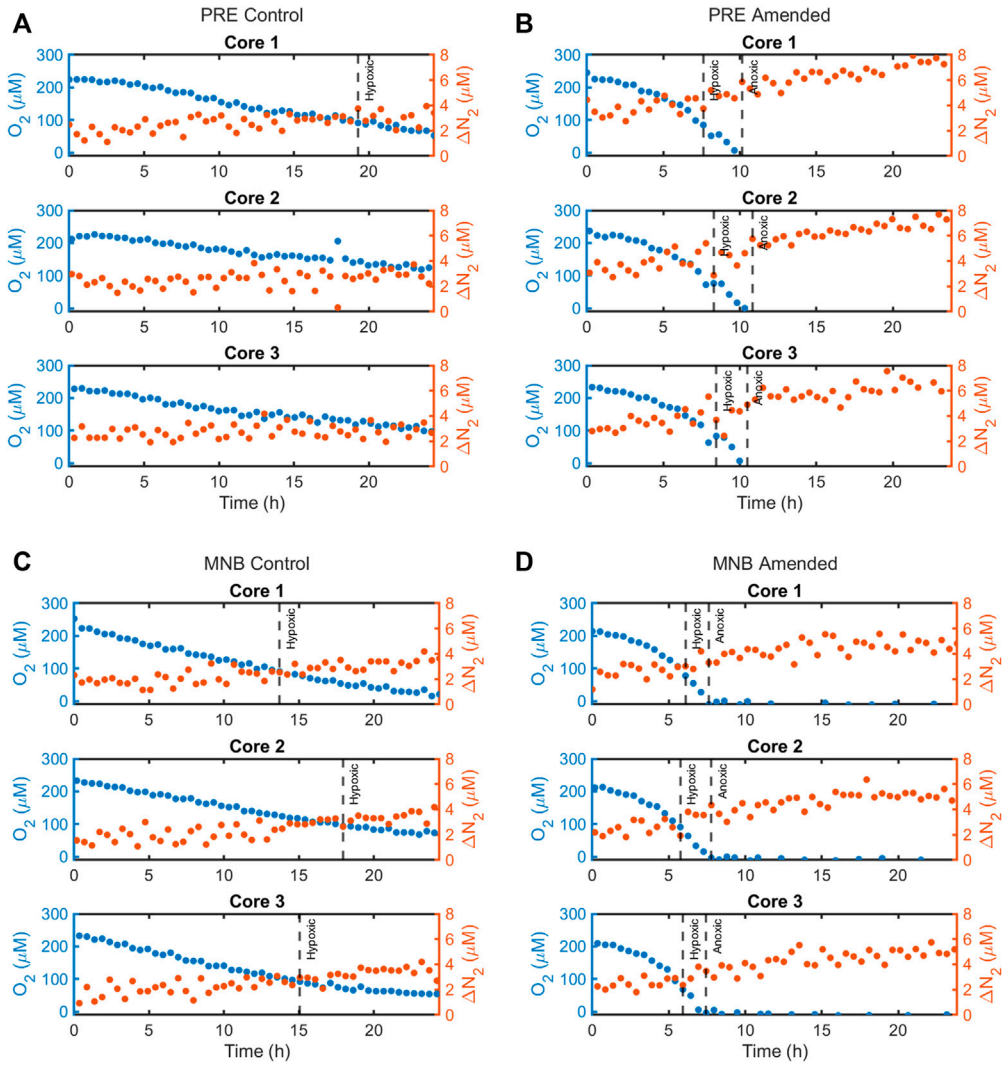


FIGURE 1
Calibrated concentration timeseries data for $\Delta N_2$ (in red) compared to $O_2$ (blue), as measured by the flow-injection mass spectrometer system during the 24-h incubations for the four site and treatment combinations: **(A)** Providence River Estuary—Control treatment, **(B)** Providence River Estuary—Amended treatment, **(C)** Mid-Narragansett Bay—Control treatment, and **(D)** Mid-Narragansett Bay—Amended treatment. $\Delta N_2$ represents the difference in concentration from the reference and was calculated from the modified $N_2$/Ar technique (described in the main text).

(MNB) reached the hypoxic and anoxic timepoints on average 1.7 and 2.4 h faster respectively than those from the more impacted site (PRE). For the control cores, the $O_2$ consumption rate reached maximal values of −1,541 ± 133 μmol $m^{-2}$ $h^{-1}$ (MNB) and −1,733 ± 228 μmol $m^{-2}$ $h^{-1}$ (PRE). For the amended cores, the $O_2$ consumption rate peaked at −6,653 ± 74 μmol $m^{-2}$ $h^{-1}$ at 5.9 ± 0.2 h into the incubation for MNB, and −8,689 ± 694 μmol $m^{-2}$ $h^{-1}$ at 9.5 ± 0.2 h for PRE (Figure 3).

$N_2$ production was measured in all sites and treatments, indicating that net denitrification occurred throughout the incubation period (Figure 3B). The general trend of the $N_2$ fluxes for MNB control and both amended treatments was similar: all initially showed an increase in $N_2$ flux, which continued until the onset of hypoxia (for MNB control) or anoxia (for the amended treatments), at which point the $N_2$ efflux started to decline. However, between both sites and treatments, there were differences in the magnitudes of $N_2$ fluxes and the timing of maximum efflux. The MNB control cores had low initial $N_2$ flux of 1.7 ± 0.2 μmol $m^{-2}$ $h^{-1}$ which increased to a maximum of 16.0 ± 1.1 μmol $m^{-2}$ $h^{-1}$, then declined again to 1.0 ± 0.1 μmol $m^{-2}$ $h^{-1}$. These rates are on par with those measured previously at this site (Fulweiler and Heiss 2014). The PRE control core $N_2$ efflux started at 1.9 ± 1.3 μmol $m^{-2}$ $h^{-1}$, increased to 8.7 ± 3.6 μmol $m^{-2}$ $h^{-1}$, then returned to 0.4 ±

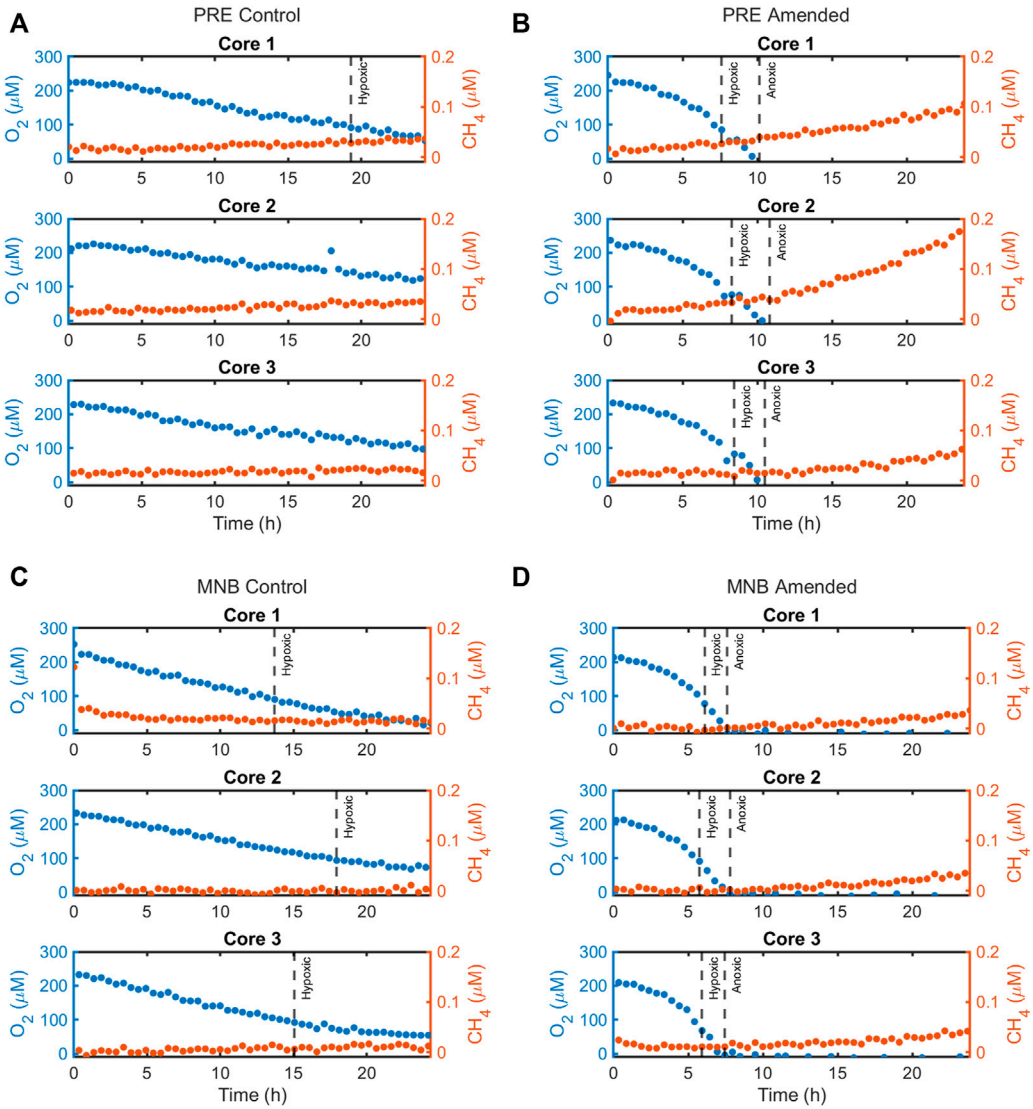


FIGURE 2
Calibrated concentration timeseries data for $CH_4$ (in red) compared to $O_2$ (blue), as measured by the flow-injection mass spectrometer system during the 24-h incubations for the four site and treatment combinations: **(A)** Providence River Estuary—Control treatment, **(B)** Providence River Estuary—Amended treatment, **(C)** Mid-Narragansett Bay—Control treatment, and **(D)** Mid-Narragansett Bay—Amended treatment.

0.2 μmol $m^{-2}$ $h^{-1}$. Overall, the control cores from MNB displayed elevated $N_2$ fluxes compared to those from PRE. In contrast, the amended cores from PRE showed more rapid and higher $N_2$ production than those from MNB. For MNB amended, $N_2$ fluxes reached 28.8 ± 0.6 μmol $m^{-2}$ $h^{-1}$ after 7.7 ± 0.6 h, and the PRE amended cores attained an even higher level of 45.5 ± 0.8 μmol $m^{-2}$ $h^{-1}$ after 10.5 ± 0.5 h. These amended rates represent a 180% and 523% increase over the maximum $N_2$ fluxes in the control treatment for MNB and PRE, respectively.

$CH_4$ fluxes exhibited dramatic responses to organic matter loading (Figure 3C). Under the initially oxic conditions, the MNB cores in both treatments had negative fluxes (at hour one: 0.112 ± 0.119 μmol $m^{-2}$ $h^{-1}$ (control) and −0.105 ± 0.054 μmol $m^{-2}$ $h^{-1}$ (amended)), indicating methane consumption within the core. After the onset of hypoxia approximately 6 hours into the incubation, the amended cores switched to a net $CH_4$ efflux. At around the same time for the control cores, the $CH_4$ consumption ceased and the $CH_4$ flux remained near zero for the duration of the incubation. In contrast, the PRE control cores started out with zero $CH_4$ fluxes, then increased to a fairly constant level (maximum flux: 0.209 ± 0.062 μmol $m^{-2}$ $h^{-1}$). PRE amended cores emitted $CH_4$ even under oxic conditions, and $CH_4$ production ramped up around the time at which the anoxic threshold was crossed (10.5 ± 0.5 h), reaching a maximum

**TABLE 1 Comparison of benthic gas fluxes for each site and treatment during normoxic, hypoxic (≤94 μM), and anoxic conditions. Values represent the mean ± standard error of the fluxes measured for the up to three replicate cores in each incubation. For the timeseries fluxes, the initial flux is that measured 1 h into the incubation, the final flux is that measured at the end of the incubation, and the maximum flux is the maximum influx ($O_2$) or efflux ($N_2$ and $CH_4$) attained during the incubation. The regime-averaged fluxes were calculated from the difference in fitted concentrations between the beginning and end of each oxygen regime. If no standard error is reported then only one core reached hypoxia. If no value is reported then none of the cores reached anoxia.**

| | Timeseries fluxes (μmol $m^{-2}$ $h^{-1}$) | | | | Regime-averaged fluxes (μmol $m^{-2}$ $h^{-1}$) | | |
|---|---|---|---|---|---|---|---|
| Gas | Description | Initial | Final | Maximum | Normoxic | Hypoxic | Anoxic |
| $O_2$ | PRE Control | −350 ± 117 | −200 ± 14 | −1733 ± 228 | −1,177 ± 154 | −1,025 | — |
| | PRE Amended | −1,239 ± 173 | −7,490 ± 781 | −8,689 ± 694 | −3,949 ± 73 | −8,228 ± 531 | — |
| | MNB Control | −743 ± 94 | −112 ± 21 | −1,541 ± 133 | −1,325 ± 94 | −706 ± 120 | — |
| | MNB Amended | −1,220 ± 99 | −3,728 ± 439 | −6,653 ± 74 | −3,688 ± 181 | −5,576 ± 125 | — |
| $N_2$ | PRE Control | 1.9 ± 1.3 | 0.4 ± 0.2 | 8.7 ± 3.6 | 6.1 ± 2.7 | 3.4 | — |
| | PRE Amended | 8.4 ± 0.3 | 3.0 ± 0.3 | 45.5 ± 0.8 | 29.3 ± 1.9 | 44.2 ± 1.2 | 29.7 ± 1.2 |
| | MNB Control | 1.7 ± 0.2 | 1.0 ± 0.1 | 16.0 ± 1.1 | 10.8 ± 1.0 | 9.6 ± 0.4 | — |
| | MNB Amended | 6.6 ± 0.8 | 0.2 ± 0.2 | 28.8 ± 0.6 | 18.0 ± 0.8 | 28.0 ± 0.6 | 13.7 ± 0.8 |
| $CH_4$ | PRE Control | −0.009 ± 0.029 | 0.021 ± 0.014 | 0.209 ± 0.062 | 0.116 ± 0.028 | 0.194 | — |
| | PRE Amended | 0.155 ± 0.068 | 0.312 ± 0.183 | 1.525 ± 0.626 | 0.307 ± 0.149 | 0.447 ± 0.194 | 1.040 ± 0.416 |
| | MNB Control | −0.112 ± 0.119 | −0.002 ± 0.005 | 0.045 ± 0.027 | −0.047 ± 0.085 | 0.008 ± 0.021 | — |
| | MNB Amended | −0.105 ± 0.054 | 0.080 ± 0.007 | 0.420 ± 0.029 | −0.103 ± 0.026 | 0.073 ± 0.020 | 0.244 ± 0.002 |

**TABLE 2 Times at which each incubation reached the hypoxic (≤94 μM) and anoxic thresholds. Values represent the mean ± standard error of up to three replicate cores.**

| Description | Hypoxic (h) | Anoxic (h) |
|---|---|---|
| MNB Control | 15.6 ± 1.2 ($n$ = 3) | — |
| MNB Amended | 5.9 ± 0.1 ($n$ = 3) | 7.6 ± 0.1 ($n$ = 3) |
| PRE Control | 19.3 ($n$ = 1) | — |
| PRE Amended | 8.1 ± 0.3 ($n$ = 3) | 10.5 ± 0.2 ($n$ = 3) |

of 1.525 ± 0.626 μmol $m^{-2}$ $h^{-1}$ before rapidly decreasing in magnitude to 0.312 ± 0.183 μmol $m^{-2}$ $h^{-1}$ at the end of the incubation.

Our observation of faster $O_2$ depletion in MNB sediments compared to PRE is perhaps surprising. One possible explanation could be due to legacy effects from varying organic matter loads. Since the 1800s, PRE has been intensively fertilized with nitrogen from anthropogenic sources, primarily wastewater (Nixon et al., 2008). Management efforts to reduce nitrogen inputs only began in 2006, and while N loads have since decreased to the lowest ever measured in Narragansett Bay, the system is still contending with a long history of human impacts (Oczkowski et al., 2018). We hypothesize that the sediment microbial community in PRE has adapted to process high loads of organic matter more efficiently than in MNB. Traditionally, the assumption has been that dissolved $O_2$ must be depleted before facultative anaerobes (organisms that can switch between aerobic and anaerobic respiration) will begin to use alternative electron acceptors such as nitrate ($NO_3^-$). However, recent work in permeable sediments, which are supplied with organic- and oxygen-rich overlying water *via* advective flows, has found that denitrification can occur under oxic conditions (Rao et al., 2008; Marchant et al., 2017)—in other words, denitrifiers can co-respire $O_2$ and $NO_3^-$ in order to capitalize on changing supplies of electron acceptors. By extension we propose that at PRE, denitrifiers may have adapted by adjusting their respiratory strategies and using $O_2$ and $NO_3^-$ concurrently to process high loads of organic matter. This may explain the slower $O_2$ depletion and faster $N_2$ production that we observed in PRE sediments. Because MNB is located farther down bay, it receives less of the brunt of nutrients; moreover, organic matter must sink through a deeper water column before reaching the sediments (Fulweiler and Nixon, 2012). Since MNB sediments are typically more starved in organic carbon and nitrogen, a sudden pulse of labile organic matter may fuel high rates of aerobic respiration, inducing the observed faster oxygen depletion.

We hypothesize that the variations in $N_2$ effluxes over time can be explained by a competition between aerobic and anaerobic processes whose predominance is influenced by dissolved oxygen levels. Under normoxic and even hypoxic conditions, nitrification can occur, supplying the nitrate required for dentrification. We propose that in the amended treatments,

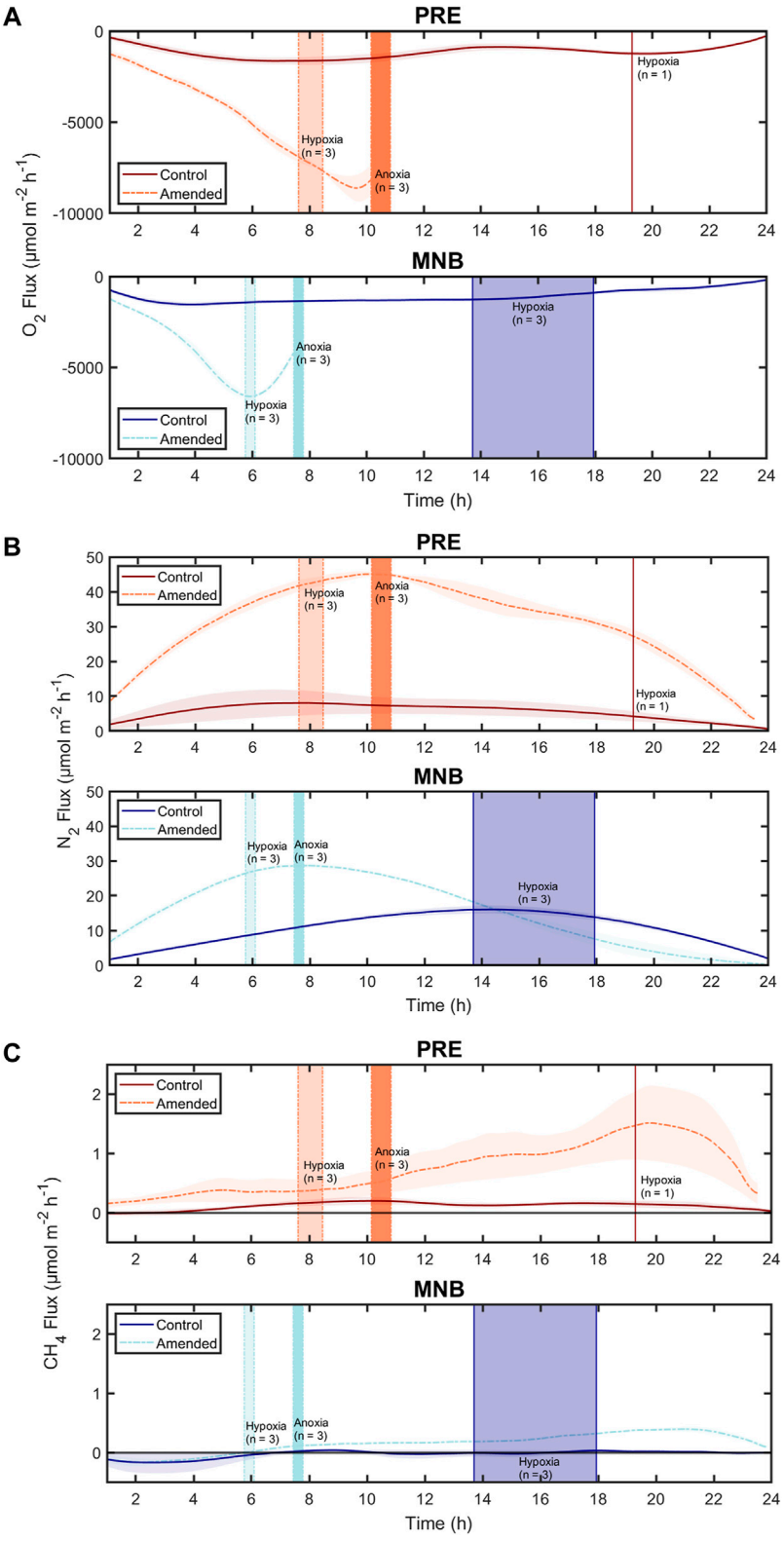


FIGURE 3
Variation of fluxes of **(A)** oxygen ($O_2$), **(B)** dinitrogen ($N_2$), and **(C)** methane ($CH_4$) from sediments incubated over 24 h. Sediments were collected either from a more nutrient-enriched and productive site (Providence River Estuary, PRE) or a less productive site (Mid-Narragansett Bay, MNB) and incubated under ambient conditions (control) or treated with an initial pulse of organic matter (amended). Curve shading around the continuous

(*Continued*)

FIGURE 3 (Continued)
fluxes represents the standard error (for up to three cores). The vertical bars highlight the times at which hypoxia or anoxia was reached for the cores in each treatment. While each treatment included three cores, not all cores in each treatment reached hypoxia or anoxia so we include the number of cores (n) represented by each vertical line. The thickness of the vertical bars corresponds to the range in time for when the cores reached hypoxia or anoxia. Here we define hypoxia as water column dissolved oxygen of ≤94 μM and anoxia as 0 μM.

the pulse of labile organic matter was degraded by aerobic bacterial respiration, providing another source of reactive nitrogen to fuel high rates of coupled nitrification-denitrification. As oxygen depletion increased in severity, however, nitrification would have ceased, any remaining nitrate would have be consumed and thus denitrification would decline. It is also important to remember that here we measured a net flux of $N_2$ across the sediment-water interface. Thus it is possible that sediment nitrogen fixation could have increased, which would show up first as a decline in $N_2$ production. Sediment nitrogen fixation has been measured at both sites previously (Fulweiler and Heiss 2014). Additionally, the pulse of organic matter could have stimulated dissimilatory nitrate reduction to ammonium (DNRA), which may begin to outcompete denitrification for the remaining nitrate (An et al., 2001; Gardner and McCarthy, 2009). Of course, none of these is mutually exclusive and thus it is possible that any or a combination of these processes were occurring. Future work capturing the microbial composition and activity or using isotopic labels would help untangle these processes.

At PRE, both the control and amended cores exhibit $CH_4$ efflux, while at MNB we observed a small uptake of $CH_4$ in the control core at the beginning of the incubation, and small effluxes in the amended cores (similar to the efflux in the PRE control cores). Because we measured a net flux of $CH_4$ across the sediment water interface, we cannot know what mechanism are driving these results. $CH_4$ fluxes are ultimately controlled by methane-producing processes (i.e., methanogenesis) and methane-consuming processes (i.e., methanotrophy). While it has traditionally been assumed that coastal sediments will not produce $CH_4$ because sulfate is abundant and sulfate reducers will outcompete methanogens for organic matter, a variety of newer studies have highlighted that this might not be the case. For example, methylotrophic methanogenesis can readily occur, especially in organic-rich muddy sediments (Schorn et al., 2022). When oxygen is present either at the sediment-water interface or within the overlying water then it is likely that aerobic methane oxidation is occurring (Fenchel et al., 1995). However, when the overlying water becomes anoxic then other methane consuming processes are likely dominating such anaerobic oxidation of methane (AOM). AOM can occur *via* different electron acceptors, such as nitrate and nitrite (AOM coupled to $NO_x^-$ reduction), sulfate (AOM coupled to sulfate reduction), and metals.

There is an unusual pattern in $CH_4$ efflux in the PRE cores and the MNB amended core—methane appears to decrease towards the end of the 24-h incubation. This is unexpected because we would assume that the low to no oxygen conditions in the cores would stimulate $CH_4$ production. We do not know why this decrease occurred. But we note that we see a similar decline in $N_2$ production and in sediment oxygen uptake. We propose that this decline could indicate the labile organic matter was rapidly consumed leaving more recalcitrant material behind, thus slowing the overall pace of benthic metabolism (Henrichs and Reeburgh, 1987).

## 3.2 Influence of oxygen on gas fluxes

Because $O_2$ concentration is easier to measure than $N_2$ or $CH_4$ concentrations, and $O_2$ data is more prevalent We examined the ability of $O_2$ concentrations as a function of $N_2$ and $CH_4$ fluxes. This is helpful to show any relationships between $O_2$ and other gas fluxes as. If strong relationships existed, they could help inform benthic models. Accordingly, we plotted the flux data pooled for the cores in each site and treatment combination against the respective oxygen concentrations until the onset of anoxia (Figure 4). This analysis revealed that changing $O_2$ conditions induce different behaviors for the control vs. amended cores. In the control treatment, $N_2$ effluxes were low to zero at normoxic and anoxic conditions, and attained maxima at an $O_2$ concentration of ~200 μM for PRE (Figure 4A) and ~120 μM for MNB (Figure 4C). For the amended treatment, the $N_2$ effluxes were low under oxic conditions, then displayed an increase to a high, constant level upon crossing the hypoxic threshold for both sites Figures 4B, D). These data suggest that organic matter and or nitrate may be limiting denitrification at these sites and may hint at the reason why studies on the impact of low oxygen events on sediment denitrification report such variable results. For example, some studies report an increase in denitrification under hypoxia (Neubacher et al., 2011; Caffrey et al., 2019; Huang and An, 2022) while others found a decrease in denitrification (Song et al., 2021), and others no change at all (Foster and Fulweiler 2019). One potential reason for this variation could be the availability of organic matter during the hypoxic episodes. For example, in the unamended sediment cores here we see low rates of dentification that rapidly decline under hypoxia (Figures 3A, C). Conversely, when fresh, labile organic matter was present denitrification increases as oxygen levels

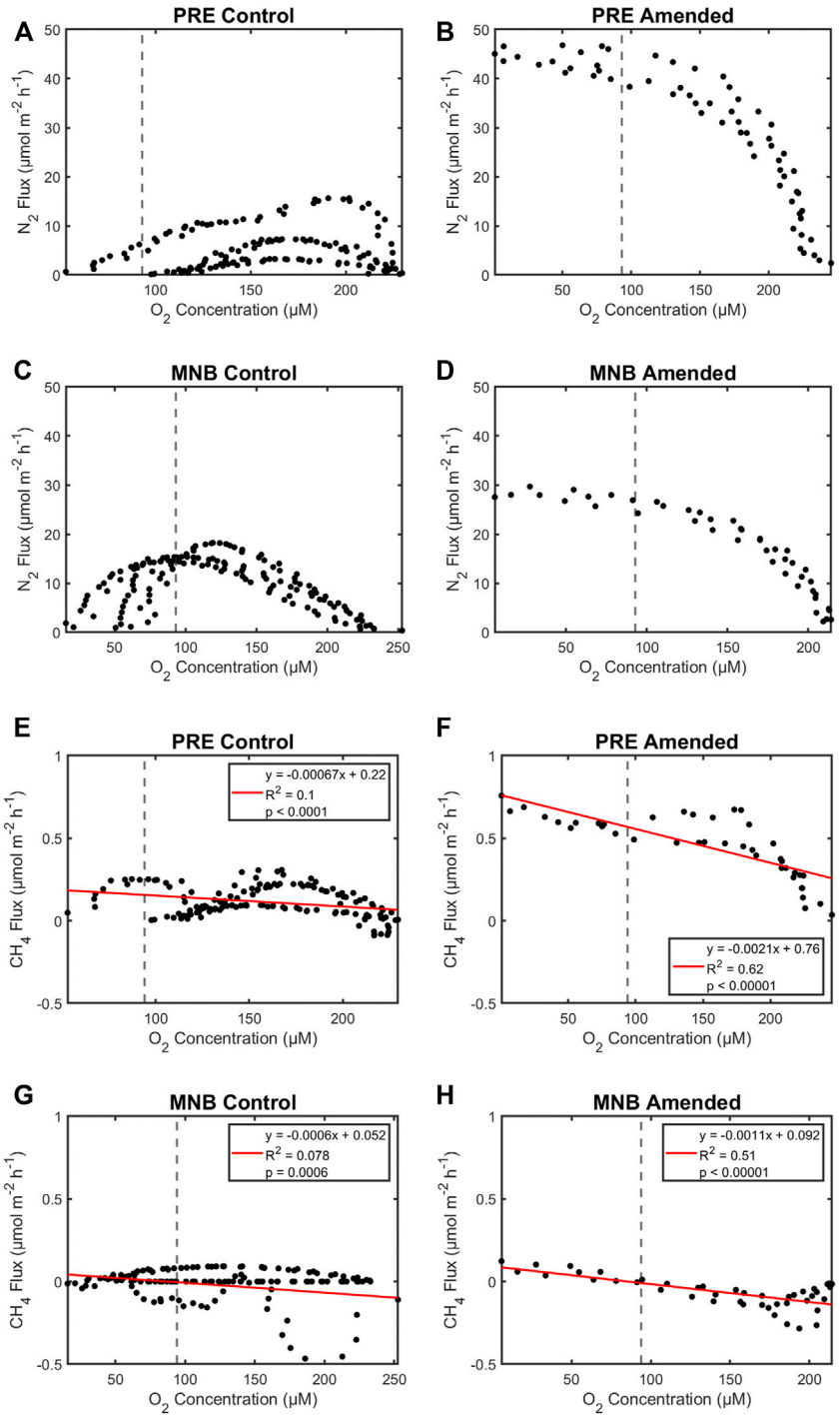


FIGURE 4
Dinitrogen ($N_2$; **A–D**) and methane ($CH_4$; **E–H**) fluxes as a function of oxygen concentration. Data from triplicate cores in each site and organic matter treatment are pooled. Vertical dashed lines denote the defined hypoxic threshold used in this study (≤94 μM). Here we do not show any fluxes that occurred once the cores went anoxic (Supplementary Figure S1 has all the fluxes).

decline (Figures 3B, D). This organic matter could fuel the heterotrophic process of denitrification directly. Additionally, aerobic organic matter decomposition could release ammonium that is subsequently nitrified thus stimulating coupled nitrification-denitrification. A recent paper found that their observed increase in sediment denitrification under hypoxia

was driven by enhanced nitrification that was not inhibited by weak hypoxia (Huang and An 2022).

We observed a similar pattern for $CH_4$, where methane fluxes were low regardless of oxygen concentrations in the control cores (Figures 4E, G). Yet in the amended cores methane flux significantly increased at low oxygen conditions (Figures 4F, H). In fact, water column oxygen concentration was able to predict more than 50%–60% of the variability in $CH_4$ fluxes in the amended cores. The increase in organic matter appears to be a mechanism for decreasing the filters (i.e., aerobic and anerobic oxidation of methane) that usually keep methane fluxes low in estuaries (Myllykangas et al., 2020).

Together these data have important implications for how we understand how hypoxia and anoxia will alter nitrogen removal and greenhouse gas emissions. For example, if the low oxygen event is driven by phytoplankton bloom senescence, then that pulse of organic matter might stimulate denitrification and methane emissions. In contrast, if the low oxygen event is the product of warming induced water column stratification, then we might expect a decrease in dentification and methane emissions. Unfortunately, in this study we do not have additional data (e.g., nutrient fluxes, microbial community activity) that can help us elucidate these mechanisms—But the patterns are interesting and provide strong motivation for future research.

## 4 Conclusion

As coastal hypoxia increases in intensity and duration globally, there will be profound impacts on benthic biogeochemical cycling. These may include changes to microbial processes occurring in the sediment, and in the magnitude and direction of sediment-water nutrient fluxes (e.g., Jilbert et al., 2011; Pratihary et al., 2014; Foster and Fulweiler, 2019). At present, there is insufficient evidence to conclude whether hypoxia hinders the ability of sediments to provide important ecosystem services, such as nutrient recycling, carbon sequestration, and greenhouse gas emission regulation (Middelburg and Levin, 2009). Here, we have demonstrated that benthic fluxes of $N_2$ and $CH_4$ respond rapidly and in complex ways to oxygen depletion. These responses vary depending on the organic matter availability (i.e., whether the sediments are provided with a source of labile organic matter or not) and legacy (i.e., whether the sediments were collected from a more or less productive site). Our results suggest that reactive nitrogen removal may initially be enhanced under short-term hypoxia but that this effect is temporary and diminishes under prolonged hypoxia to anoxia, and that organic matter loading enhances methane effluxes from sediments, especially as oxygen depletion increases in severity.

Our use of a novel flow-injection mass spectrometer system for gas concentration measurements during the laboratory incubations enabled us to capture transient changes as the sediments crossed various oxygen thresholds. While we cannot quantify the individual processes responsible for the observed biogeochemical responses from net gas flux measurements alone, our data do reflect the changing overall balance in the competition between aerobic and anaerobic processes across a spectrum of dissolved oxygen levels. Given our findings that gas fluxes can change depending on whether the sediment is experiencing normoxic, hypoxic, or anoxic conditions, our results highlight the nuances not represented by one flux number across oxygen regimes, as typically reported. Application of our method in future benthic flux incubation studies has considerable potential to improve our understanding of how key sediment biogeochemical processes respond to oxygen depletion.

## Data availability statement

The raw data supporting the conclusions of this article will be made available by the authors, without undue reservation.

## Author contributions

RF conceived of this study. EC and RF modified the study. EC carried out the experiment and performed the data analysis. EC wrote the initial draft of the manuscript with contributions from RF. RF and EC edited the manuscript. All authors contributed to the critical review of this manuscript.

## Funding

This work was funded by the National Science Foundation through a grant (OCE-1435690) to RF in Ocean Technology and Interdisciplinary Coordination. EC was supported in part by a Graduate Writing Fellowship from Boston University. EC and RF were supported by NOAA ECOHAB grant. RF was supported by a grant from RI Sea Grant.

## Acknowledgments

The authors thank Amanda Vieillard, Cat Mahoney, and Melissa Hagy for assistance in the field, Joel Sparks for technical support, Tim Short for helpful discussions about the mass spectrometer data analysis, and Russell Goebel for invaluable guidance on the statistical analysis.

## Conflict of interest

The authors declare that the research was conducted in the absence of any commercial or financial relationships that could be construed as a potential conflict of interest.

## Publisher's note

All claims expressed in this article are solely those of the authors and do not necessarily represent those of their affiliated organizations, or those of the publisher, the editors and the reviewers. Any product that may be evaluated in this article, or claim that may be made by its manufacturer, is not guaranteed or endorsed by the publisher.

## Supplementary material

The Supplementary Material for this article can be found online at: https://www.frontiersin.org/articles/10.3389/fenvs.2022.1028405/full#supplementary-material

## References


An, S., Gardner, W. S., and Kana, T. (2001). Simultaneous measurement of denitrification and nitrogen fixation using isotope pairing with membrane inlet mass spectrometry analysis. *Appl. Environ. Microbiol.* 67, 1171–1178. doi:10.1128/aem.67.3.1171-1178.2001

Bergondo, D. L., Kester, D. R., Stoffel, H. E., and Woods, W. L. (2005). Time-series observations during the low sub-surface oxygen events in Narragansett Bay during summer 2001. *Marine Chemistry*. 97. doi:10.1016/j.marchem.2005.01.006

Breitburg, D., Levin, L. A., Oschlies, A., Grégoire, M., Chavez, F. P., Conley, D. J., et al. (2018). Declining oxygen in the global ocean and coastal waters. *Science* 80, eaam7240. doi:10.1126/science.aam7240

Caffrey, J. M., Bonaglia, S., and Conley, D. J. (2019). Short exposure to oxygen and sulfide alter nitrification, denitrification, and DNRA activity in seasonally hypoxic estuarine sediments. *FEMS Microbiol. Lett.* 366, fny288. doi:10.1093/femsle/fny288

Hopkinson, C., Giblin, A. E., and Tucker, J. (2001). Benthic metabolism and nutrient regeneration on the continental shelf of Eastern Massachusetts. *USA* 224, 1–19.

Chua, E. J., Huettel, M., Fennel, K., and Fulweiler, R. W. (2022). A case for addressing the unresolved role of permeable shelf sediments in ocean denitrification. *Limnol. Oceanogr. Lett.* 7, 11–25. doi:10.1002/lol2.10218

Chua, E. J., Short, R. T., Cardenas Valencia, A. M., Savidge, W., and Fulweiler, R. W. (2021). A mass spectrometer based pore water sampling system for sandy sediments. *Limnol. Oceanogr. Methods.* 19, 769–784. doi:10.1002/lom3.10460

Codiga, D. L., Stoffel, H. E., Deacutis, C. F., Kiernan, S., and Oviatt, C. A. (2009). Narragansett Bay hypoxic event characteristics based on fixed-site monitoring network time series: Intermittency, geographic distribution, spatial synchronicity, and interannual variability. *Estuaries Coasts* 32, 621–641. doi:10.1007/S12237-009-9165-9

Damgaard, L. R., Revsbech, N. P., and Reichardt, W. (1998). Use of an oxygen-insensitive microscale biosensor for methane to measure methane concentration profiles in a rice paddy. *Appl. Environ. Microbiol.* 64, 864–870. doi:10.1128/AEM.64.3.864-870.1998

Diaz, R. J., Rosenberg, R., and Sturdivant, K. (2019). Ocean deoxygenation everyone's probl, 20. Available at: https://portals.iucn.org/library/node/48892.

Fenchel, T., Bernard, C., Esteban, G., Finlay, B. J., Hansen, P. J., and Iversen, N. (1995). Microbial diversity and activity in a Danish fjord with anoxic deep water. *Ophelia* 43, 45–100. doi:10.1080/00785326.1995.10430576

Foster, S. Q., and Fulweiler, R. W. (2019). Estuarine sediments exhibit dynamic and variable biogeochemical responses to hypoxia. *J. Geophys. Res. Biogeosciences* 124, 737–758. doi:10.1029/2018JG004663

Fulweiler, R. W., Nixon, S. W., Buckley, B. A., and Granger, S. L. (2007). Reversal of the net dinitrogen gas flux in coastal marine sediments. *Nature* 448, 180–182. doi:10.1038/nature05963

Fulweiler, R. W., and Nixon, S. W. (2012). Net sediment N2 fluxes in a southern New England estuary: Variations in space and time. *Biogeochemistry* 111, 111–124. doi:10.1007/s10533-011-9660-5

Fulweiler, R. W., and Heiss, E. M. (2014). (Nearly) a decade of directly measured sediment N2 fluxes: What can Narragansett Bay tell us about the global ocean nitrogen budget? *Oceanography* 27 (1), 184–195. doi:10.5670/oceanog.2014.22

Garcia, D. (2011). A fast all-in-one method for automated post-processing of PIV data. *Exp. Fluids* 50, 1247–1259. doi:10.1007/s00348-010-0985-y

Garcia, D. (2010). Robust smoothing of gridded data in one and higher dimensions with missing values. *Comput. Stat. Data Anal.* 54, 1167–1178. doi:10.1016/j.csda.2009.09.020

Garcia, H. E., and Gordon, L. I. (1992). Oxygen solubility in seawater: Better fitting equations. *Limnol. Oceanogr.* 37, 1307–1312. doi:10.4319/lo.1992.37.6.1307

Gardner, W. S., and McCarthy, M. J. (2009). Nitrogen dynamics at the sediment-water interface in shallow, sub-tropical Florida Bay: Why denitrification efficiency may decrease with increased eutrophication. *Biogeochemistry* 95, 185–198. doi:10.1007/s10533-009-9329-5

Henrichs, S. M., and Reeburgh, W. S. (1987). Anaerobic mineralization of marine sediment organic matter: Rates and the role of anaerobic processes in the oceanic carbon economy. *Geomicrobiol. J.* 5, 191–237. doi:10.1080/01490458709385971

Huang, Y., and An, S. (2022). Weak hypoxia enhanced denitrification in a dissimilatory nitrate reduction to ammonium (DNRA)-Dominated shallow and eutrophic coastal waterbody, jinhae bay, South Korea. *Mar. Sci.* 9, 897474doi:10.3389/fmars.2022.897474

Jilbert, T., Slomp, C. P., Gustafsson, B. G., and Boer, W. (2011). Beyond the Fe-P-redox connection: Preferential regeneration of phosphorus from organic matter as a key control on Baltic Sea nutrient cycles. *Biogeosciences* 8, 1699–1720. doi:10.5194/BG-8-1699-2011

Kana, T. M., Darkangelo, C., Hunt, M. D., Oldham, J. B., Bennett, G. E., and Cornwell, J. C. (1994). Membrane inlet mass spectrometer for rapid high-precision determination of N2, O2, and Ar in environmental water samples. *Anal. Chem.* 66, 4166–4170. doi:10.1021/ac00095a009

Marchant, H. K., Ahmerkamp, S., Lavik, G., Tegetmeyer, H. E., Graf, J., Klatt, J. M., et al. (2017). Denitrifying community in coastal sediments performs aerobic and anaerobic respiration simultaneously. *ISME J.* 11, 1799–1812. doi:10.1038/ismej.2017.51

McCarthy, M. J., Newell, S. E., Carini, S. A., and Gardner, W. S. (2015). Denitrification dominates sediment nitrogen removal and is enhanced by bottom-water hypoxia in the northern gulf of Mexico. *Estuaries Coasts* 38, 2279–2294. doi:10.1007/s12237-015-9964-0

McMaster, R. (1960). Sediments of Narragansett bay system and Rhode Island sound, Rhode Island. *SEPM J. Sediment. Res.* 30, 249–274. doi:10.1306/74d70a15-2b21-11d7-8648000102c1865d

Middelburg, J. J., and Levin, L. A. (2009). Coastal hypoxia and sediment biogeochemistry. *Biogeosciences* 6, 1273–1293. doi:10.5194/bg-6-1273-2009

Myllykangas, J.-P., Hietanen, S., and Jilbert, T. (2020). Legacy effects of eutrophication on modern methane dynamics in a boreal estuary. *Estuaries Coasts* 43, 189–206. doi:10.1007/s12237-019-00677-0

Neubacher, E. C., Parker, R. E., and Trimmer, M. (2011). Short term hypoxia alters the balance of the nitrogen cycle in coastal sediments. *Limnol. Oceanogr.* 56, 651–665. doi:10.4319/lo.2011.56.2.0651

Nixon, S. W., Buckley, B. A., Granger, S. L., Harris, L. A., Oczkowski, A. J., Fulweiler, R. W., et al. (2008). "Nitrogen and phosphorus inputs to Narragansett bay: Past, present, and future," in *Science for ecosystem-based management* (New York, NY: Springer), 101–175. doi:10.1007/978-0-387-35299-2_5

Nixon, S. W., Granger, S. L., and Nowicki, B. L. (1995). An assessment of the annual mass balance of carbon, nitrogen, and phosphorus in Narragansett Bay. *Biogeochemistry* 33, 217. doi:10.1007/bf00000805

Oczkowski, A., Schmidt, C., Santos, E., Miller, K., Hanson, A., Cobb, D., et al. (2018). How the distribution of anthropogenic nitrogen has changed in Narragansett Bay (RI, USA) following major reductions in nutrient loads. *Estuaries Coasts* 41, 2260–2276. doi:10.1007/s12237-018-0435-2

O'Haver, T. (2020). Pragmatic introduction to signal processing A retirement project by. Available at: http://bit.ly/1TucWLfWebaddresshttp://bit.ly/

1NLOlLRInteractiveMatlabTools:http://bit.ly/1r7oN7bSoftwaredownloadlinkshttp://tinyurl.com/cey8rwhAnimatedexampleshttps://terpconnect.umd.edu/%7B~%7Dtoh/spectrum/ToolsZoo.html.

Oviatt, C. A., Keller, A., and Reed, L. (2002). Annual primary production in Narragansett Bay with no bay-wide winter–spring phytoplankton bloom Estuar. *Coast Shelf Sci* 54 (6), 1013–1026. doi:10.1006/ecss.2001.0872

Pilson, M. E. Q. (1985). On the residence time of water in Narragansett Bay. *Estuaries* 8, 2–14. doi:10.2307/1352116

Pratihary, A. K., Naqvi, S. W. A., Narvenkar, G., Kurian, S., Naik, H., Naik, R., et al. (2014). Benthic mineralization and nutrient exchange over the inner continental shelf of Western India. *Biogeosciences* 11, 2771–2791. doi:10.5194/BG-11-2771-2014

Rao, A. M. F., McCarthy, M. J., Gardner, W. S., and Jahnke, R. A. (2008). Respiration and denitrification in permeable continental shelf deposits on the south atlantic bight: N2:Ar and isotope pairing measurements in sediment column experiments. *Cont. Shelf Res.* 28, 602–613. doi:10.1016/j.csr.2007.11.007

Rosentreter, J. A., Borges, A. V., Deemer, B. R., Holgerson, M. A., Liu, S., Song, C., et al. (2021). Half of global methane emissions come from highly variable aquatic ecosystem sources. *Nat. Geosci.* 14, 225–230. doi:10.1038/s41561-021-00715-2

Schorn, S., Ahmerkamp, S., Bullock, E., Weber, M., Lott, C., Liebeke, M., et al. (2022). Diverse methylotrophic methanogenic archaea cause high methane emissions from seagrass meadows. *Proc. Natl. Acad. Sci. U. S. A.* 119, 21066281199–e2106628212. doi:10.1073/pnas.2106628119

Song, G., Liu, S., Zhang, J., Zhu, Z., Zhang, G., Marchant, H. K., et al. (2021). Response of benthic nitrogen cycling to estuarine hypoxia. *Limnol. Oceanogr.* 66, 652–666. doi:10.1002/lno.11630

Vaquer-Sunyer, R., and Duarte, C. M. (2008). Thresholds of hypoxia for marine biodiversity. *Proc. Natl. Acad. Sci. U. S. A.* 105, 15452–15457. doi:10.1073/pnas.0803833105

Wiesenburg, D. A., and Guinasso, N. L. (1979). Equilibrium solubilities of methane, carbon monoxide, and hydrogen in water and Sea water. *J. Chem. Eng. Data* 24, 356–360. doi:10.1021/je60083a006

frontiers | Frontiers in Environmental Science

TYPE Original Research
PUBLISHED 30 March 2023
DOI 10.3389/fenvs.2023.1110169



OPEN ACCESS

EDITED BY
Claudia Cosio,
Université de Reims Champagne-Ardenne, France

REVIEWED BY
Eleanor Arrington,
University of California, Santa Barbara, United States
Michael Hügler,
Technologiezentrum Wasser, Germany

*CORRESPONDENCE
Maria Vila-Costa,
maria.vila@idaea.csic.es

†PRESENT ADDRESS
Maria-Carmen Fernández-Pinos,
Ministry for the Ecological Transition and the Demographic challenge of Spain, Madrid, Spain

SPECIALTY SECTION
This article was submitted to Biogeochemical Dynamics, a section of the journal Frontiers in Environmental Science

RECEIVED 28 November 2022
ACCEPTED 14 March 2023
PUBLISHED 30 March 2023

CITATION
Vila-Costa M, Lundin D, Fernández-Pinos M-C, Iriarte J, Irigoien X, Piña B and Dachs J (2023), Responses to organic pollutants in the tropical Pacific and subtropical Atlantic Oceans by pelagic marine bacteria. *Front. Environ. Sci.* 11:1110169. doi: 10.3389/fenvs.2023.1110169



# Responses to organic pollutants in the tropical Pacific and subtropical Atlantic Oceans by pelagic marine bacteria

Maria Vila-Costa[1]*, Daniel Lundin[2], Maria-Carmen Fernández-Pinos[1†], Jon Iriarte[1], Xavier Irigoien[3,4], Benjamin Piña[1] and Jordi Dachs[1]

[1]Department of Environmental Chemistry, IDAEA-CSIC, Barcelona, Catalonia, Spain, [2]Centre for Ecology and Evolution in Microbial Model Systems—EEMiS, Linnaeus University, Kalmar, Sweden, [3]IKERBASQUE, Basque Foundation for Science, Bilbao, Spain, [4]AZTI Marine Research, Basque Research and Technology Alliance (BRTA), Herrera Kaia, Bilbao, Spain

Background and chronic pollution by organic pollutants (OPs) is a widespread threat in the oceans with still uncharacterized effects on marine ecosystems and the modulation of major biogeochemical cycles. The ecological impact and toxicity of this anthropogenic dissolved organic carbon (ADOC) is not related to the presence of a single compound but to the co-occurrence of a myriad of synthetic chemicals with largely unknown effects on heterotrophic microbial communities. We have analyzed the metabolic capacity of metagenome-assembled genomes (MAGs) of natural oceanic communities from the north Pacific (Costa Rica dome) and Atlantic oceans challenged with environmentally relevant levels of ADOC. In the Atlantic, ADOC-exposed MAGs responded transcriptionally more strongly compared to controls than in the Pacific, possibly mirroring the higher relevance of ADOC compounds as carbon source in oligotrophic environments. The largest proportions of transcripts originated from MAGs belonging in the families *Rhodobacteraceae* and *Flavobacteriaceae*, known to play a role on consumption of several OPs. In the Atlantic, archaeal *Poseidoniales* showed the highest transcription levels after 2 h of ADOC exposure, although no increase of relative abundances in the DNA pool was recorded after 24 h, whereas *Methylophaga* showed the opposite pattern. Both taxa are suggested to be actively involved in the consumption of biogenic alkanes produced by cyanobacteria. We observed similar gene expression profiles of alkane degradation and methylotrophy signature genes. These findings, plus the chemical degradation of alkanes measured in the experiments, provides experimental evidence of the consumption of anthropogenic hydrocarbons and synthetic chemicals at the low concentrations found in the ocean, and modulation of microbiomes by ADOC.

KEYWORDS

**organic pollutants, surface seawater, anthropogenic organic matter, alkane biodegradation, polycyclic aromatic hydrocarbon degradation, Poseidonales, Methylophaga**

# 1 Introduction

Anthropogenic dissolved organic carbon (ADOC) is among the most under-studied anthropogenic perturbation in the environment under the current scenario of global change (Vila-Costa et al., 2020), specifically in terms of its influence on the major biogeochemical cycles, and thus the functioning of the Earth system. ADOC is composed by the mixture of the thousands of synthetic organic compounds used by humans, as well as hydrocarbons from incomplete combustion of fossil fuels, released to the environment. This pool of organic carbon includes flame retardants, pesticides and herbicides, plasticizers and other leachates from plastics, hydrocarbons, surface active substances, among other chemicals used in a myriad of industrial, agricultural and domestic applications. Currently, there are 300,000 synthetic chemicals in use (Wang et al., 2020) with an unquantified release to the marine environment. Even though the absolute concentrations of ADOC may account for a small percentage of the overall dissolved organic carbon (DOC), this pool is important due to their persistence, which allow them to distribute in the global oceans, and eventually inducing an effect on cells due to their accumulation in lipids at concentrations many orders of magnitude above the seawater levels (Lohmann et al., 2007; Vila-Costa et al., 2020). Nevertheless, some components of ADOC, such as hydrocarbons or organophosphate esters are degraded in the environment, and thus used as a source of C and P (González-Gaya et al., 2019; Vila-Costa et al., 2019). The subtle influence of ADOC modulating the major biogeochemical cycles remains uncharacterized, even though it is presumably increasing in pace with social and economic development, as more and more synthetic chemicals are used by the contemporary society.

Organic pollutants contributing to ADOC are ubiquitous in the ocean, including the remote regions of the Pacific, Indian, Southern and Atlantic oceans (Galbán-malagón, 2012; González-Gaya et al., 2014; González-Gaya et al., 2016; Casal et al., 2019; Muir and Miaz 2021). Many of the organic pollutants reaching the ocean are semivolatile, such as polycyclic aromatic hydrocarbons (PAHs), alkanes, organophosphate esters, organochlorine compounds, etc. These chemicals reach the ocean through atmospheric transport and subsequent deposition. However, some chemicals such as perfluoroalkyl substances are prone to oceanic transport due to their low volatility and high solubility in water (Muir and Miaz 2021). The transport mechanism, as well the biogeochemistry of the pollutant once in the water column, determines their spatial and vertical distribution. The oceanic sinks of ADOC are accounted mainly by the biological pump and degradation (Galbán-malagón, 2012; González-Gaya et al., 2019). In coastal waters, strong gradients and high concentrations of pollutants can be found locally. On the contrary, low variability of pollutant levels is found in the large open oceanic regions as atmospheric transport can re-distribute pollutants over large regions and to the low lability of these chemicals. Indeed, highly labile pollutants do not reach open sea waters as they are degraded during their transport from land. Nevertheless, there are some global trends, such as generally lower concentrations in the open Pacific than the Atlantic, or higher concentrations in the northern hemisphere than the southern hemisphere (González-Gaya et al., 2016; Muir and Miaz 2021; Xie et al., 2022). Importantly, some alkanes with lower carbon number can have biogenic sources, especially from cyanobacteria (Dachs et al., 1998; Love et al., 2021). A cryptic but ubiquitous and fast consumption cycle for these biogenic alkanes has been suggested (Love et al., 2021). Whether or not the same genetic machinery is used for the degradation of both biogenic and anthropogenic alkanes, remains unknown.

Even though there are several previous studies assessing the influence of given individual or families of organic pollutants on phytoplankton and bacteria (Echeveste et al., 2016; Cerro-Galvez et al., 2019; Martinez-Varela et al., 2021), very few of these works have addressed the influence of the overall ADOC on microbiomes. For phytoplankton, it has been shown that ADOC concentrations slightly above the background oceanic levels induce a decrease of the abundance of *Prochlorococcus* and *Synechococcus*, their viability, as well as that the expression of genes related to carbon fixation, such as Rubisco (Echeveste et al., 2016; Fernández Pinos et al., 2017). In these works, in order to simulate the influence of ADOC, microbial communities were exposed to extracts of seawater, following the standard procedures usually used for the analysis of a wide range of organic pollutants, which concentrates the hydrophobic and non-ionic fraction of DOC. Similar effects of mixtures of organic pollutants on cyanobacteria have been described for leachates from microplastics (Tetu et al., 2020). The influence of ADOC on heterotrophic prokaryotes (Bacteria and Archaea) have received much less attention. Recent works suggested a range of subtle effects of low concentrations of ADOC on Arctic, Antarctic and Mediterranean Bacteria (Cerro-Gálvez et al., 2019, 2020). In these works, metagenomic and metatranscriptomic approaches allowed to identify cellular to small variations in exposure ADOC concentrations. High-throughput sequencing is a useful tool to access the genomic repository of the uncultured Bacteria and Archaea that account for most species in the oceans, and how it respond to environmental stressors. The current exponential number of works reconstructing high-quality metagenome-assembled genomes (MAGs) from oceanic microbiomes is expanding the knowledge on microbial metabolisms, enzymatic capabilities and habitat distributions (e.g., Tully et al., 2018), including MAGs retrieved from sites influenced by oil spilled accidents (Karthikeyan et al., 2021). However, no attempts have been made to reconstruct MAGs in manipulated experiments to analyze responses to specific conditions, for instance, to exposure of background concentrations of pollutants.

The objectives of this work were 1) to explore the subtle effects of small variations in concentrations of ADOC (less than a factor of 2) by exposing microbial communities to extracts of hydrophobic compounds in seawater 2) prove the utility of assessing metagenome assembled genomes (MAGs) resolved from exposure experiments as indicators of subtle effects of ADOC on microbiomes, 3) to provide evidences on the interactions between ADOC, trophic status and microbiomes for some sectors of the North Pacific and Atlantic oceans.

# 2 Materials and methods

## 2.1 Exposure experiments

The experiments were done during the Malaspina circumnavigation cruise in 2011. Four experiments were performed, two in the North Pacific, on the Costa Rica dome off-

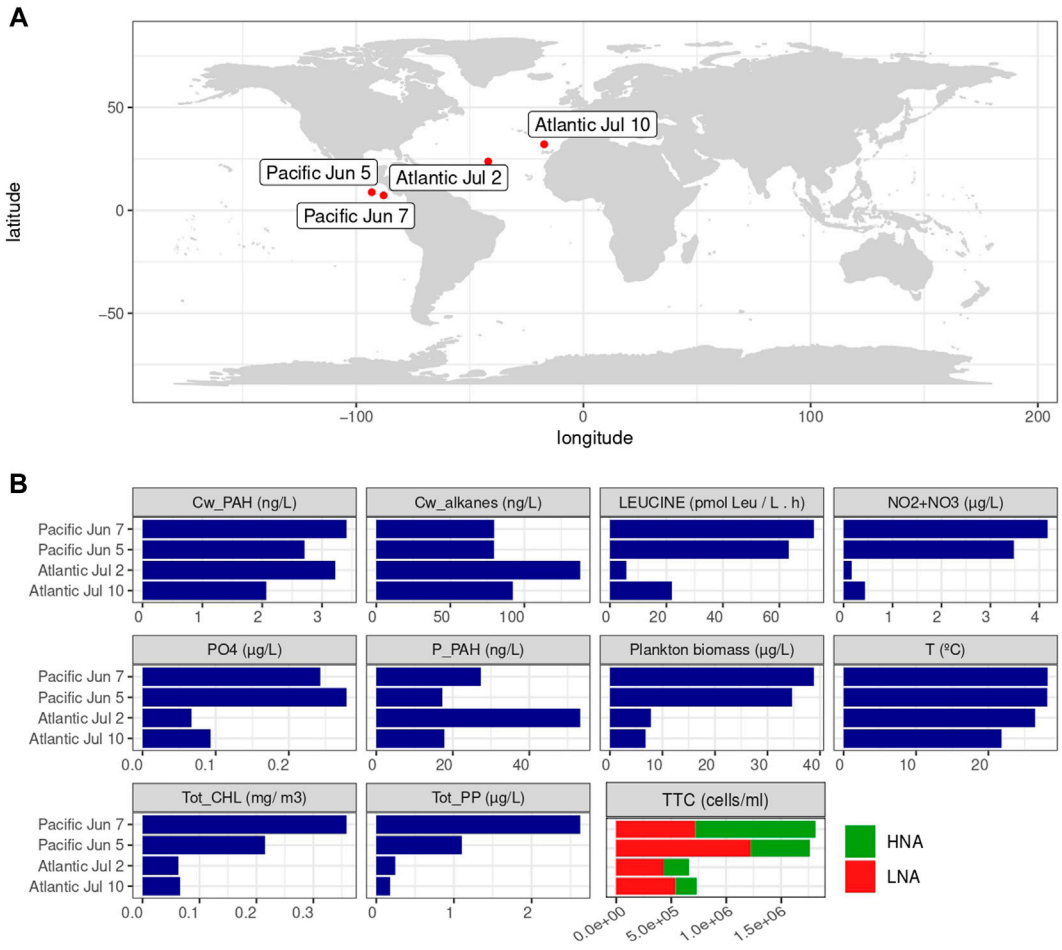


FIGURE 1
Water sampling stations and *in situ* measurements. **(A)** Stations where samples were taken for the experiments. **(B)** Measurements of nutrients, chlorophyll, cell abundances and pollutants. "Cw_PAH", "*p*_PAH": PAH concentrations in the dissolved phase (ng/L) and plankton (ng/g) respectively, "Cw_alkanes": alkane concentrations in the dissolved phase (ng/L), "LEUCINE": leucine incorporation rates (pmol Leu/L h), "NO2+NO3" and "PO4": concentrations of $NO_2^-$ + $NO_3^-$ and $PO_4$ respectively (µg/L), "Plankton biomass" (µg/L), "Tot_CHL": total chlorophyll A (mg/m$^3$) and "Tot_PP": total primary production (mg C/m$^3$ h), "TCC": total cell counts, that include "HNA" and "LNA": high and low nucleic acid content bacteria (cells/ml).

shore central America. The other two experiments were performed in the North Atlantic (Figure 1, Supplementary Table S1). Experiments consisted in spiking 1 L of seawater from the deep chlorophyll maximum (DCM) with a mixture of hydrophobic organic pollutants obtained by concentrating the hydrophobic DOC on a XAD-2 column. Control experiments using the same seawater, but with no addition of organic pollutants, were carried out in parallel to the treatments. Details of the preparation of these complex mixtures are given elsewhere (Fernández-Pinos et al., 2017). This mixture contained 50.9 ng/L of PAHs, 137 pg/L of polychlorinated biphenyls (PCBs), 8 pg/L of hexachlorobenzene, and 3.2 pg/L of hexachlorocyclohexanes. In addition to these chemicals, the mixture also contained other pollutants such as n-alkanes and chlorinated-alkanes, that were at tens of ng/L, and polybrominated diphenyl ethers (PBDEs), polychlorinated dibenzo-p-dioxins and dibenzofurans, dechlorane plus, chlorinated naphthalene at concentrations between 1 and 50 pg/L, as well the unresolved complex mixture of aliphatic and aromatic hydrocarbons at concentrations of few ug/L These chemical mixtures also contain unknown POPs which have not been described yet in the literature due to lack of appropriate analytical methods (Muir and Howard, 2006), and which can contribute significantly to the overall mixture toxicity as found in other studies (Tang et al., 2013). PAHs and n-alkanes were analyzed in the treatments and controls for the initial and final time (24 h, Figure 1, Supplementary Figure S1). The addition of this mixture of pollutants to seawater, resulted in a final concentration less than 2-fold increase with respect to the *in-situ* concentrations (comparison of concentration in treatments *versus* controls). During the course of experiments, there was no apparent degradation of PAHs, but a reduction of n-alkane concentrations to half of the initial values (Figure 1, Supplementary Figure S1 and details in Supplementary Table S3 in Fernández-Pinos et al., 2017). The incubations were performed in baked 1-L glass bottles. The pollutant mixtures were added to the treatment bottles and the solvent (acetone) to the control bottles 1 h before adding the seawater to allow for

**TABLE 1 Profiles used to identify signature genes. Gen *alkB* (alkane-1-monooxygenase) was selected as surrogates of genes associated with the degradation of mid-chain alkanes. File of alkB profile can found in Supplemental Material.**

| Profile accession/gene name | Pathway | Gene product |
|---|---|---|
| *alkB*[a] | Alkane degradation | alkane-1-monooxygenase |
| PF00141 | Oxidative stress | Peroxidase |
| PF00464 | Methylotrophy | Serine hydroxymethyltransferase |

[a]inhouse profile.

evaporation and avoid potential toxic effects of the solvents used to prepare the POPs mixtures. After addition of seawater from the DCM, the bottles were manually stirred and immediately placed in an incubator located on the deck of the vessel that maintained the surface temperature (Supplementary Table S1). No further stirring was performed. The light radiation at the sampled depth was simulated using a net covering the bottles. All experiments started between 10 and 12:30 h local time and we used one pair of treatment and control for each time point. After 30 min, 2 h and 24 h, we collected samples for DNA and mRNA.

## 2.2 Nucleic acids extraction and sequencing

After 0.5, 2 h and 24 h incubations, seawater from experimental bottles was pre-filtered through a 3 µm pore-size 47 mm diameter polytetrafluoroethylene filter and bacterial cells were collected onto a 0.2 µm pore-size 47 mm polytetrafluoroethylene filter under low vacuum pressure. The duration of the filtration step was no longer than 15 min to minimize RNA degradation. Each filter was cut in two-halves, one was placed in 1 ml RNAlater (Sigma-Aldrich, Saint Louis, MO) and the other one into 1 ml lysis buffer (50 mM Tris HCl, 40 mM EDTA, 0.75 M Sucrose) and stored at -80°C to preserve RNA and DNA respectively. DNA extraction was performed following the protocol described in Cerro-Gálvez et al. (2019). mRNA was extracted and amplified as described in Poretsky et al. (2010) with the modification of the use of mirVana isolation kit (Ambion) to extract the total RNA. Resulting DNA and amplified RNA were sequenced at the National Center for Genomic Analysis (CNAG, Barcelona, Spain) using Illumina high output mode HS200 2 × 100 bp v4.

## 2.3 Bioinformatics

DNA and cDNA sequences were quality trimmed and internal standard sequences removed using the ERNE mapping program (v. 2.1.1, Del Fabbro et al., 2013) using default parameters (--fast mode, --min-size 25, --min-mean-phred-quality 20, --errors-rate 15, --indels-max). For cDNA sequences, ERNE was run twice, to also remove stable RNA sequences using an in-house database. After quality trimming and removal of sequences, an average of 4.00 e + 07 reads remained per sample (Supplementary Table S2).

Genomes were constructed from DNA reads to create metagenome assembled genomes (MAGs) using the MetaWrap tool (v. 1.0, Uritskiy et al., 2018)), with MEGAHIT (v. 1.1.2, default settings, i.e. 21, 29, 39, 59, 79, 99, 119 and 141 kmer sizes, Li et al., 2015) for assembly and Metabat2 (v. 2.12.1, Kang et al., 2019) as the binning tool. MAGs were quality checked with CheckM (v. 1.0.12, Parks et al., 2015) (Supplementary Table S3), taxonomy determined with GTDB-Tk (v. 1.5.1, Chaumeil et al., 2020) using release r06-rs202 of the GTDB database (Parks et al., 2018) and functionally annotated with Prokka (v. 1.12, Seemann 2014), all using default settings. MAG abundances in the samples were calculated by mapping DNA reads back to the MAGs using Bowtie 2 (v. 2.3.4.1, Langmead and Salzberg 2012) and Samtools to create idxstats files (v. 1.7, Li et al., 2009). Bowtie 2 was run with default settings, i.e., in paired end "end-to-end" mode to map the full length of reads to contigs. Genes were quantified using the Bowtie 2 mapping results and feature Count from the Subread package (v. 2.0.1, Liao et al., 2014) with gff files from the Prokka annotation. An average of 52% of reads mapped to contigs, and 22% of reads mapped to MAGs. Transcripts per million (tpm) was used as the unit of abundance of genes and MAGs. This was calculated by taking the ratio of counts per gene/genome to the length of the gene/genome and dividing that by the sum of the ratio over the sample. Finally, the number was multiplied by a million. The proportion of reads mapping to MAGs made up on average 42% of reads mapping to contigs (SupplementaryTable S1). Selected specific signature genes coding for enzymes involved in the interaction between ADOC and microorganisms were searched for against genes in the MAGs using HMMER (v. 3.1. b. 2, Eddy, 2011) with a set of inhouse and Pfam (Finn et al., 2016; Table 1) profiles. In-house alkB profile can be found in Supplemental Material. R (v. 4.1.2, R Core Team. 2021), RStudio (v. 2022.7.2.576, RStudio Team 2022) and the Tidyverse (v. 1.3.0, Wickham et al., 2019) were used to create all figures, except for the Anvi'o (v. 7.1, Eren et al., 2021) figures.

To analyze the effects of treatments (controls vs. ADOC addition), experiments and ocean basin on both community structure (DNA relative abundances) and community transcriptional activities (RNA relative abundances), a Permanova using a Bray–Curtis distance matrix (Anderson, 2001) was performed. Variance in community structure and transcription described by Bray–Curtis dissimilarities was visualized using principal component analysis in R.

# 3 Results and discussion

## 3.1 Characterization of sampling sites

Several families of organic compounds were analyzed in seawater and plankton at the sites and in the regions, where experiments were carried out, as reported previously (González-

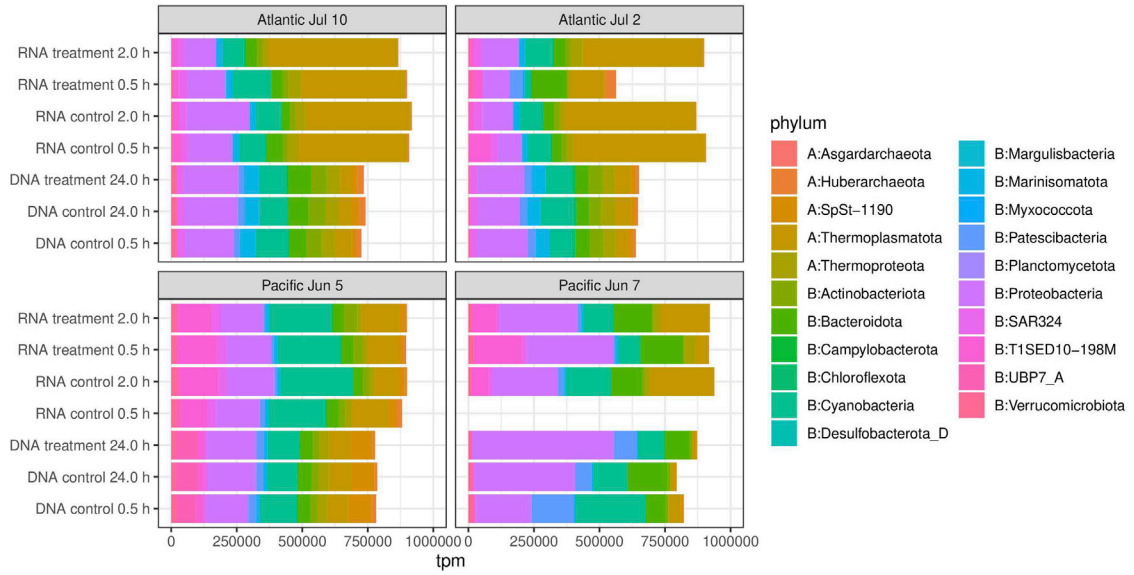


FIGURE 2
Overall taxonomic composition of microbial communities. Transcripts per million (tpm) were used as the unit of abundance. See materials and methods for details on tpm calculation.

Gaya et al., 2014; Morales et al., 2015; Casal et al., 2017; González-Gaya et al., 2019), which include PAHs, PCBs, dioxins, and perfluoroalkyl substances. Here we use 64 PAHs (González-Gaya et al., 2019) and alkanes ranging from 21 to 35 carbon chains (previously unpublished, see Materials and Methods) as surrogates or chemical indicators of hydrophobic ADOC to characterize the level of pollution at each sampling site. Concentrations of PAH and alkanes in the dissolved and plankton phase (Figure 1, Supplementary Figure S1) were similar at the four experiment sites. Even though the North Pacific Ocean is generally less polluted than the North Atlantic for a wide range of pollutants (González-Gaya et al., 2014, 2019; Muir and Miaz, 2021; Xie et al., 2022), the similarity in concentrations is consistent with the fact that experiments in the Pacific Ocean were performed on the Coastal Rica Dome, which is influenced by a regional upwelling, while the experiments in the Atlantic were performed in oligotrophic regions remote from primary sources. Concentrations of pollutants in surface seawater in the Costa Rica dome are comparable to those reported for the North Atlantic, probably due to the influence of proximate continental sources and the regional upwelling re-mobilizing previously deposited chemicals in deep waters (Casal et al., 2017; González-Gaya et al., 2019). The more eutrophic conditions of this upwelling region were mirrored by the higher nutrient concentrations at Pacific sites compared to North Atlantic sites (Figure 1). In consequence, this location harbors dynamic biological communities. Consistently, total Chl *a* concentration, primary production, bacterial production and concentration of heterotrophic cells were significantly higher in the Pacific than in the Atlantic sites. The two experiments in the Pacific ocean were carried out under identical surface seawater temperatures (28°C) which were above those in the subtropical Atlantic Ocean experiments (26°C and 22°C respectively).

## 3.2 MAGs recovered from experiments

From the DNA samples, we constructed 976 metagenome assembled genomes (MAGs) representing both Archaea and Bacteria (Supplementary Table S2). The majority were of low quality, following Bowers et al. classification (Bowers et al., 2017), and nearly half of them lacked sufficient markers for taxonomy classification. MAGs were quite fragmented (Supplementary Table S3) with a median number of contigs of 159, 331 and 355 for high, medium and low quality respectively (excluding MAGs without taxonomy). The corresponding median N50 values were 27,831, 8,161 and 9,678. Nevertheless, we found 24 archaeal and 208 bacterial MAGs of medium or high quality, i.e. with an estimated degree of contamination less than 10%. In addition, we used 25 archaeal and 209 bacterial low-quality MAGs that were less than 10% contaminated and were possible to assign taxonomically. While incomplete and not suitable for analysis of their full genetic potential, these low-quality MAGs could still provide taxonomic information about key functional responses in our experiments.

We recovered several species known to be important in marine surface waters, such as the unicellular *Cyanobacteria Synechococcus* spp. and *Prochlorococcus* spp, as well as the alphaproteobacterial Pelagibacteraceae spp. ("SAR11"; all unfortunately of low quality) and Rhodobacteraceae spp, the gammaproteobacterial SAR86 order, Alteromonadaceae spp. and *Pseudomonadales* spp, as well as several *Flavobacteriales* (Sunagawa et al., 2015). The recently named *Poseidonales* order of Archaea, formerly known as "Marine Group II Archaea" (Rinke et al., 2019), was also well represented by MAGs.

In terms of relative abundances of MAGs, both from DNA and RNA samples, communities were dominated by a few phyla: the archaeal *Thermoplasmatota*, and the bacterial *Bacteriodota*, *Cyanobacteria*, *Patescibacteria*, *Proteobacteria* and the automatically named phylum *T1SED10-198M*, recently named as

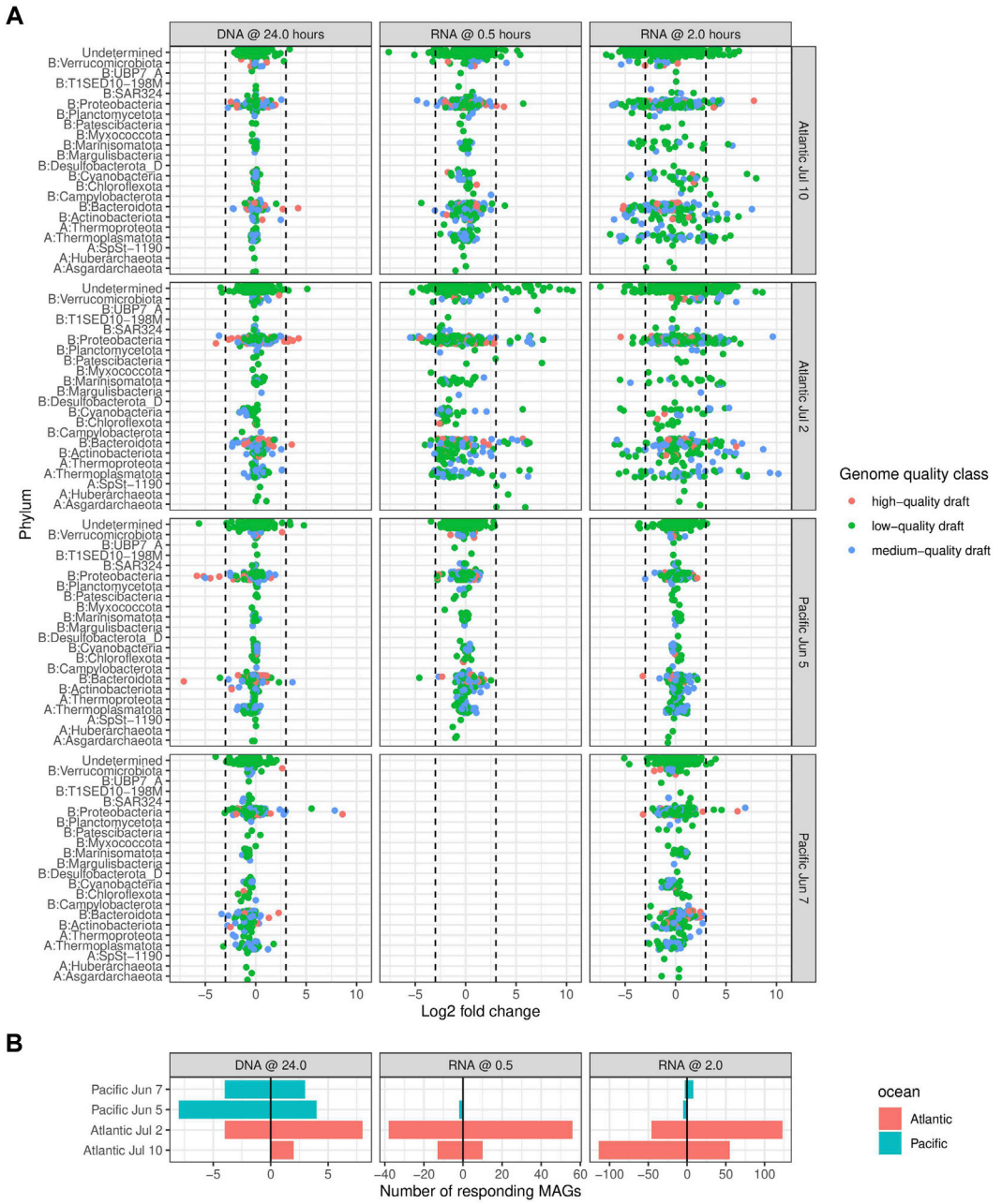


FIGURE 3
Log 2 fold changes of relative abundances of MAGs between treatments and controls in the DNA pool (indicating enrichment) and in the RNA pool (indicating transcriptional activity) in each experiment. To be included, a MAG needed to be present both in the treatment and control samples. Phyla are prepended with an **(A, B)** to denote Bacteria and Archaea respectively. Dashed lines at log 2 fold changes of -3 and 3, corresponding to eight-fold decrease and increase respectively, indicate limits for inclusion in further analyses below. MAGs appearing to the left of the leftmost or right of the rightmost line were considered as "responders" to treatment.

*Candidatus* Gulusiota (Pallen et al., 2022) (Figure 2 and Supplementary Table S4). A few MAGs from *Thermoplasmatota*, particularly from the order *Poseidoniales*, dominated gene expression in the two experiments performed in the Atlantic, but not for the Pacific sites. The proportion of reads mapping to contigs from taxonomy-assigned MAGs, was considerably smaller in the RNA than in the DNA samples, suggesting that our MAGs were representative of the active part of the community.

## 3.3 Responses of MAGs in ADOC exposed communities

To analyze populations that were transcriptionally responding to exposure to ADOC, we identified 331 MAGs that contributed at least eight-fold more, or less, to the total RNA in the treatment than in the control sample for at least one experiment and sampling time (Figure 3; Table 2, Supplementary Table S4). In general, we detected

**TABLE 2** Number of transcriptionally responding MAGs per experiment and time point. Transcriptionally responding was defined as MAGs being at least eight-fold more or less abundant in the treatment than in the control. Only low-quality draft genomes with at most 10% contamination and determined taxonomy included.

| | High-quality draft | | Medium-quality draft | | Low-quality draft | |
|---|---|---|---|---|---|---|
| Experiment/time | Down | Up | Down | Up | Down | Up |
| Atlantic July 10 RNA 0.5 | 2 | 0 | 4 | 1 | 0 | 1 |
| Atlantic July 10 RNA 2.0 | 13 | 6 | 29 | 24 | 2 | 2 |
| Atlantic July 2 RNA 0.5 | 17 | 6 | 62 | 11 | 10 | 1 |
| Atlantic July 2 RNA 2.0 | 2 | 16 | 19 | 39 | 1 | 3 |
| Pacific June 5 RNA 0.5 | 0 | 0 | 1 | 0 | 0 | 0 |
| Pacific June 7 RNA 2.0 | 0 | 0 | 0 | 3 | 1 | 1 |

a higher number of responding MAGs in the Atlantic than in the Pacific, although the number varied considerably between experiments and time points, from 0 to 5 Pacific June 5 experiments, to 107 after half an hour at the Atlantic July 2 experiment and around 80 after 2 h of exposure in both of the Atlantic experiments. The balance between increasing and decreasing MAGs also varied considerably between experiments and time points. In the Atlantic experiments, most of the transcriptionally responding MAGs belonged to *Proteobacteria, Thermoplasmatota, Actinobacteriota* and *Bacteroidota* (Supplementary Table S5). In the Pacific experiments, transcriptionally responding MAGs were from the Bacteroidota and the Proteobacteria. The higher number of transcriptionally responding MAGs in the Atlantic than in the Pacific experiments can be related to the more oligotrophic status of Atlantic waters, where ADOC addition represented a more relevant pulse of carbon than in the Pacific. This is consistent with the higher sensitivity of oligotrophic systems to external anthropogenic inputs (Shai et al., 2021). Our results indicate that this is also true at ADOC concentrations relevant for the open ocean, as previously reported for coastal Mediterranean waters (Cerro-Gálvez et al., 2021). The changes in community structure using DNA relative abundances of all MAGs assessed using a Permanova test significantly differed between experiments ($p < 0.01$) and oceans ($p < 0.01$). The same pattern was observed for transcriptional activities (Supplementary Table S6). The microbial responses in Atlantic experiments were more similar to each other than to either of the Pacific experiments consistent with a minor effect of temperature on the microbial responses to ADOC additions (Supplementary Figure S2).

## 3.4 Patterns of gene expression and enrichments in ADOC exposed communities of responding MAGs

Among all the transcriptionally more active MAGs, up to 86 had not only a fold-change in gene expression higher than eight between treatments and controls, but also a quality classification of at least "medium-quality draft". These included 77 Bacteria (9 *Actinobacteriota*, 18 *Bacteroidota*, four *Synechococcus*, 2 *Marinisomatota*, 22 *Alphaproteobacteria*, 17 *Gammaproteobacteria* and five *Verrucomicrobiota*) and nine Archaea (8 *Thermoplasmatota* and one *Thermoproteota*) (Supplementary Table S5). We labeled them as "responding MAGs" and selected them for deeper gene content and transcriptional analyses in ADOC exposed communities. In the Pacific experiments, we observed some high contributions of specific taxa to the DNA and RNA pool. These were, for instance, MAGs from *Cyanobacteria* and some from *Flavobacteriales* and *Rhodobacterales*. The Atlantic experiments had a more equal distribution of contributions from several bacterial groups. Three archaeal MAGs belonging to *Thalassarchaeaceae* within the *Thermoplasmatota* phylum contributed considerably to the DNA and RNA pools. (Figure 4).

Contrasting how individual MAGs responded to ADOC addition in terms of transcriptional activity and increase of contribution to the DNA pool (called enrichment hereafter) respectively, we detected different patterns: 1) increased transcription in treatments compared to controls during the first 2 h of exposure but not a concurrent growth after 24 h, 2) stable or increased transcription with growth after 24 h, 3) stable transcription and no enrichment, 4) decreases in community size, i.e., DNA contribution, after 24 h, and v) no clear responses neither in transcription nor enrichment. In the Atlantic Ocean, the highest number of MAGs fell into the "transcription increase, no enrichment" and "no clear response" categories, whereas in the Pacific most MAGs were in the "stable in both" category and, a lower number, in "decreases in community size". The top responding MAGs within all categories belonged to the families Rhodobacteraceae and Flavobacteriaceae but with an ocean dependent pattern, as these contributed the most to the active transcription categories (with and without growth) in Atlantic experiments, whereas they were stable in the Pacific experiments (Figure 5, Supplementary Figure S7). These two families of bacteria are generalists, known for their copiotrophic lifestyle and opportunistic activation of transcription after inputs of organic matter, including ADOC compounds, and thus capable of rapid growth in carbon-rich environments (Yooseph et al., 2010; Cerro-Gálvez et al., 2021). The different responses in contributions to the DNA pool in each ocean might be related to the importance of ADOC respect to the total pool of DOC, that was probably less labile and more limited in the oligotrophic Atlantic than in the Costa Rica Dome in the Pacific.

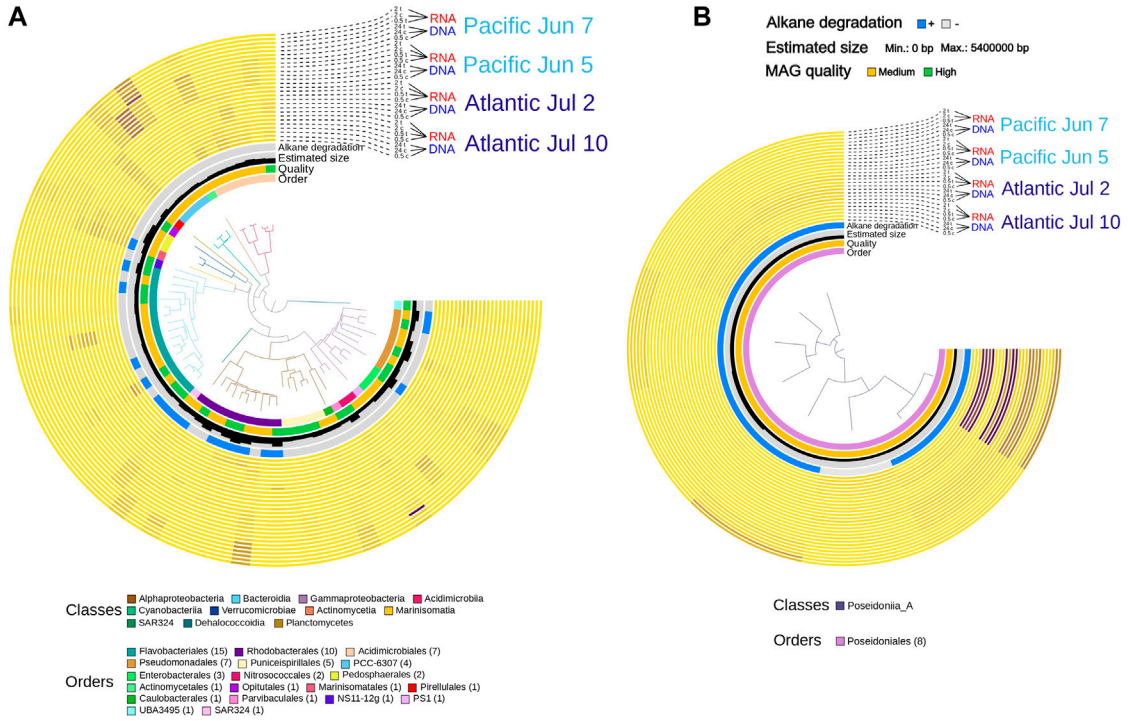


FIGURE 4
Phylogeny and abundance of strongly responding MAGs per sample together with genome statistics as well as presence and expression of signature genes for alkane oxidation. **(A)** bacteria, **(B)** archaea. Branches are colored according to taxonomic Classes. Abundances were normalized by calculating square root of tpm values. The color scale was set from 0 (min) to 290 (max).

Several MAGs belonging to the archaeal *Poseidoniales* order were found to have increasing transcriptional activity after 2 h of exposure to ADOC, although they did not get significantly enriched. This is a pattern already observed in *Alteromonadales* in coastal Mediterranean waters after exposures to low levels of ADOC concentrations (Cerro-Gálvez et al., 2021). *Poseidoniales* is the most abundant archaeal group in surface seawaters, with different genera present in both oligotrophic and eutrophic waters (Rinke et al., 2019). We observed similar behavior of two families, Poseidoniaceae and Thalassarchaeaceae, with a higher activity in the Atlantic experiments than in the Pacific. Importantly, this group has been found to commonly harbor *alkB*-like monooxygenase genes in the North Atlantic, and a role in degradation of biogenic medium chain alkanes has been suggested (Love et al., 2021). The activation of gene expression but lack of significant enrichment, however, suggests that *Poseidoniales* are able to quickly respond to ADOC presence, but that this capacity, at least in oligotrophic waters, does not always result in population growth likely due to nutrient limitation. This is consistent with an oligotrophic lifestyle, among other things characterized by expression of high-affinity transporters effective at low substrate concentrations (Lauro et al., 2009).

Interestingly, the responding MAGs that showed the highest increase in relative contributions to the DNA pool after 24 h (independent of the transcription patterns) in Atlantic July 2 and Pacific June 7 experiments belonged to Methylophagaceae (order *Nitrosococcales*). The capacity of species in the Methylophagaceae to degrade aliphatic hydrocarbons has been shown under oil spill scenarios (Mishamandani et al., 2014; 2016; Gutierrez and Aitken 2014; Kleindienst et al., 2016), as well for consumption of biogenic alkanes, such as those from cyanobacteria (Love et al., 2021). Although Methylophagaceae in most marine environments belong in the "rare biosphere", i.e., present, but at low abundances, this group was observed to bloom in polluted coastal Mediterranean waters after a pulse of ADOC at background concentrations (Cerro-Gálvez et al., 2021). A similar result was found in both the Pacific and the Atlantic experiments, providing field evidence on the high adaptation of Methylophagaceae to growth on ADOC chemicals at the low concentrations found in the global oceans.

On average, between 2 and 26 genes from each MAG from the four most characteristic orders of strongly responding MAGs—*Poseidonales*, *Flavobacteriales*, *Nitrosococcales* and *Rhodobacterales*—contributed at least two-fold more to the total RNA pool in treatments than in controls (Figure 6). Except for in *Rhodobacterales*, the number of responding genes varied considerably between experiments and for different time points. In order to assess the nature of the responses, these individual genes were classified into nine relevant classes—ATP synthase (energy conversion), DNA polymerase (replication), RNA polymerase (transcriptional activity), enzymes (overall metabolism; genes not included in more specific classes but having an EC number), stress, translation, transporters, hypothetical proteins and others. We observed a low

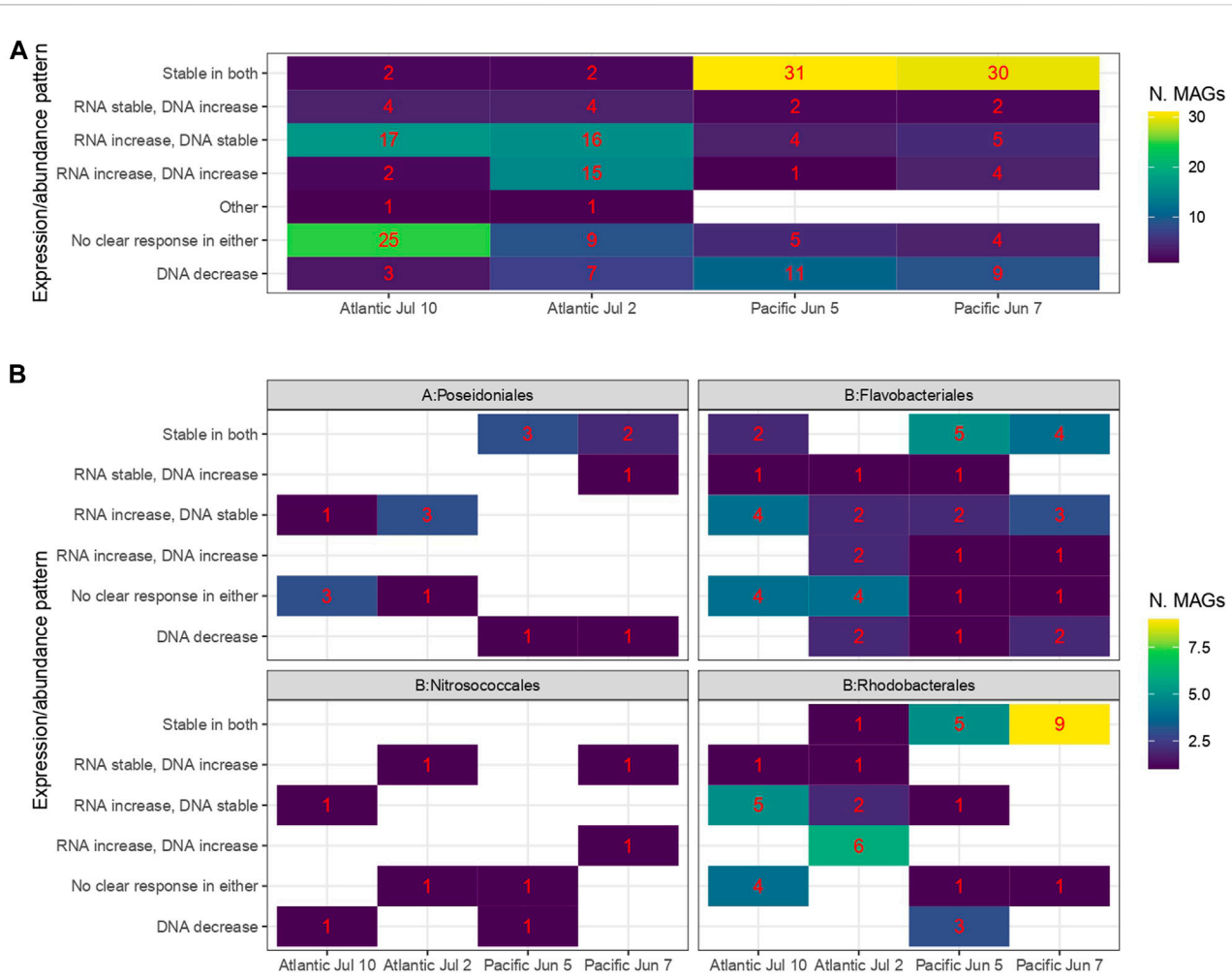


FIGURE 5
Overall patterns in RNA expression and DNA abundance in MAGs increasing at least eight-fold in at least one sample pair. The RNA 0.5, RNA 2.0 and DNA 24 h sample pairs were classified as increasing in the treatment if the treatment was at least two-fold higher than the control. Individual patterns were then classified in classes. **(A)** Overall, **(B)** Selected orders.

contribution of transporters, quite a small but consistently present contribution of genes involved in transcription and translation and conspicuously low numbers of genes involved in replication (Figure 6). We found a consistently high number of hypothetical genes in the *Poseidonales consistent with* the relatively recent discovery of the group and lack of cultures for phenotypic characterization of the group (Rinke et al., 2022).

To look for patterns of consistent gene expression between different populations of the same phylum, we searched for genes increasing at least two-fold in any of the experiments and counted the number of different MAGs that expressed genes with the same product name. Any genes occurring in the list at least twice were considered (Supplementary Table S8). Furthermore, we weighted the gene list by the product of each product's highest relative abundance and its highest fold-change. At the top of this list, appearing in five different MAGs at relative abundances between 0.2 and 230, and log 2 fold-changes between 1.0 and 3.7, we found "Serine hydroxymethyltransferase", an important enzyme in one-carbon metabolism or methylotrophy (Supplementary Table S8) (Rao et al., 2003). The species were representatives of the Alteromonadaceae, Rhodobacteraceae and SAR86 families. In the actinobacterial families *MedAcidi-G1, TK06* we found "Putative formate dehydrogenase", also involved in one-carbon metabolism (Ferry 1990), represented in two genomes. In alkane metabolism, "Alkane 1-monooxygenase" (3 species from Flavobacteriaceae, Schleiferiaceae and UBA10066 families of *Bacteroidota*), "Alkanesulfonate monooxygenase" (3 species from the actinobacterial families MedAcidi-G1, MedAcidi-G1 and TK06) and "Haloalkane dehalogenase" (3 species from the proteobacterial families Pseudohongiellaceae, Rhodobacteraceae and SAR86), were discovered. Other enzymes expressed in more than one species, and with a potential physiological role after addition of ADOC included the oxidative stress-related "Superoxide dismutase" (five species from Alteromonadaceae, Rhodobacteraceae and Methylophagaceae), "Catalase-peroxidase" (nine species from Flavobacteriaceae, Schleiferiaceae, Alteromonadaceae, Pseudohongiellaceae, Puniceispirillaceae and Rhodobacteraceae), "putative

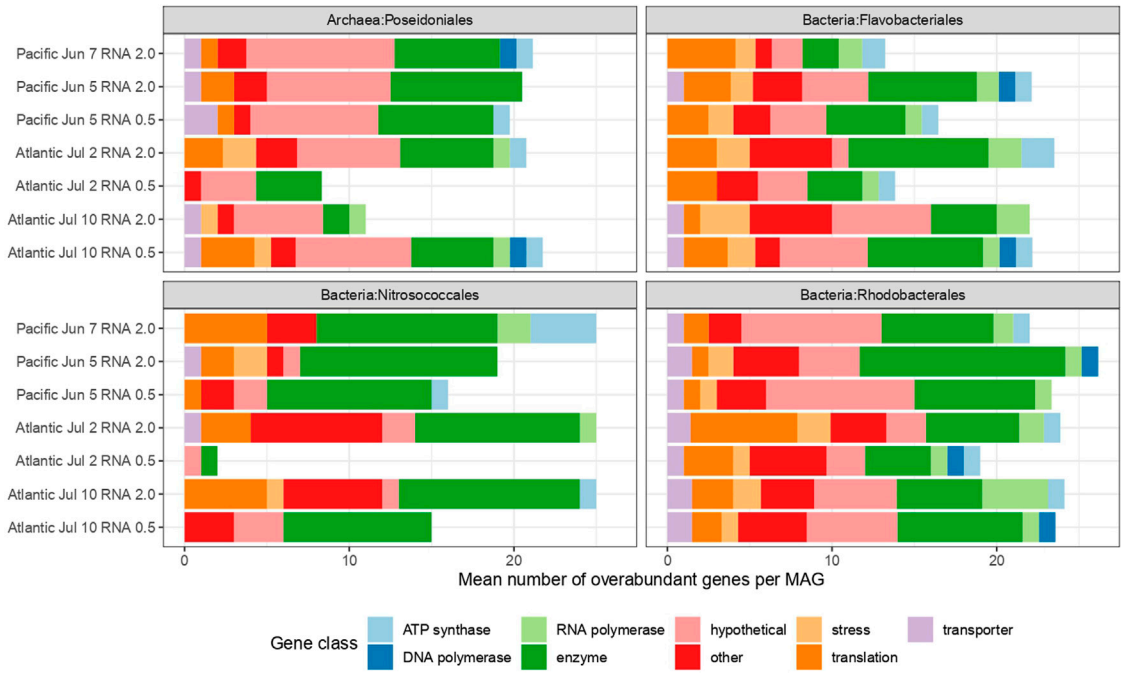


FIGURE 6
Mean number of overabundant genes in treatments compared with controls for selected orders. Genes reaching abundances in treatments at least two-fold higher than in controls. Genes were classified based on product names in the Prokka annotation.

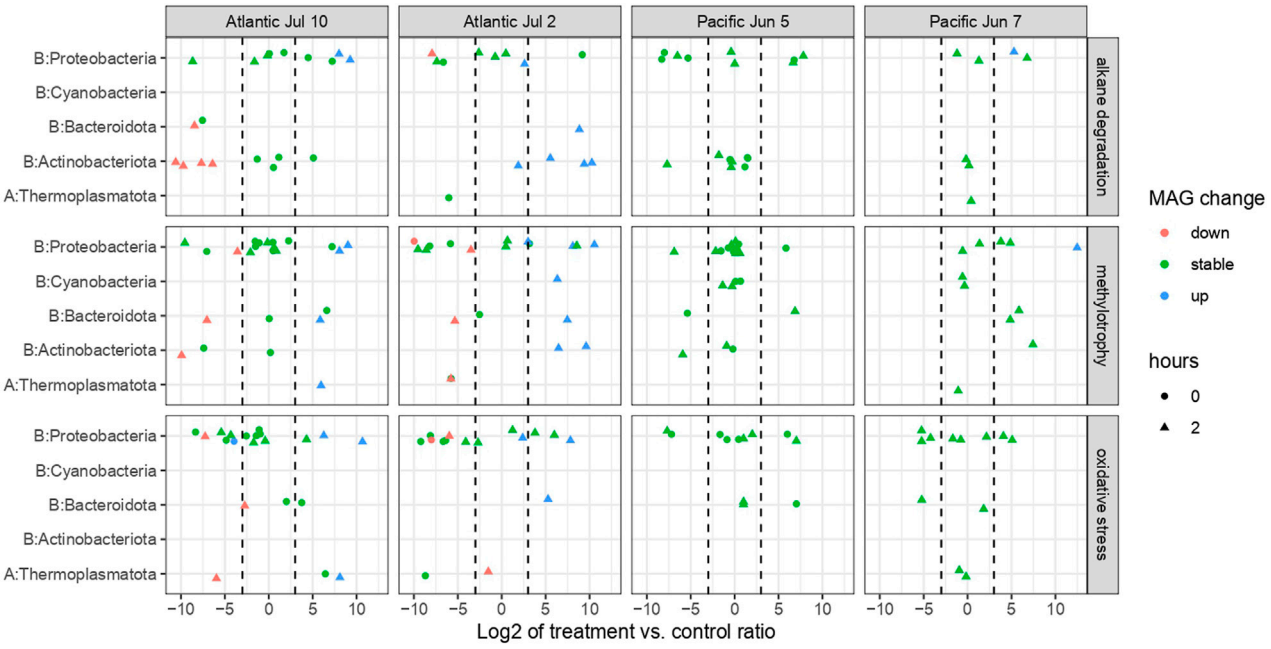


FIGURE 7
Expression of signature genes for alkane degradation, methylotrophy and oxidative stress in MAGs responding with growth or decrease in at least one experiment (panel **(A)**) and averaged changes in relative concentrations (treatment/controls) of PAHs and alkanes in the experiments after 0.5 and 24 h of incubation (panel **(B)**). On the top panel, the *x*-axis values show *gene* log 2 fold-changes, while the MAGs's response is encoded with color. When calculating ratios, a zero in either the treatment or control was replaced with 0.001. Specific changes in relative concentration ratios of each chemical within PAH and alkanes families is described in Supplementary Figure S1.

**TABLE 3 Number of genes increasing or decreasing in responding MAGs more than eight-fold between treatment and control. Responding MAGs were defined as those being at least eight-fold more abundant in treatments than in controls. Similarly, genes were defined as up or down if they were eight-fold more or less respectively abundant in treatments than in controls.**

| | Alkane degradation | | Methylotrophy | | Oxidative stress | |
|---|---|---|---|---|---|---|
| Experiment | Down | Up | Down | Up | Down | Up |
| Atlantic July 10 | 0 | 2 | 0 | 4 | 0 | 3 |
| Atlantic Jul 2 | 0 | 4 | 0 | 7 | 0 | 2 |
| Pacific Jun 7 | 0 | 1 | 0 | 1 | 0 | 0 |

peroxiredoxin" (24 species from *Actinobacteriota*, *Bacteroidota*, *Cyanobacteria* and *Proteobacteria*) and, in electron transport, a number of cytochrome c components (45 species from the phyla *Actinobacteriota*, *Bacteroidota*, *Marinisomatota* and *Proteobacteria*). Lastly, different components of ribonucleotide reductase, the enzyme catalyzing the only known *de novo* pathway for production of deoxyribonucleotides, building blocks of DNA (Torrents et al., 2008), was found to be highly expressed by 17 MAGs from the archaeal *Thermoplasmatota* phylum and the bacterial *Bacteroidota* and *Proteobacteria* phyla.

## 3.5 Signature gene responses in ADOC exposed communities

Whereas generic functional annotation of genomes is helpful for the identification of patterns without strong presumptions about which pathways are potentially affected by ADOC addition, the fact that alkane families are important components of hydrophobic ADOC suggests a more targeted approach. We screened the MAGs for the potential degradation of alkanes with sequence searches using profiles for the gene coding for the enzyme that catalyzes the committed step in degradation "alkane-1-monooxygenase" (*alkB*). Since PAH concentrations did not change significantly during our experiments and because it has been shown difficult to exactly identify the key enzyme involved in PAH degradation (CITE)—Aromatic ring-hydroxylating dioxygenase—we did not analyze our MAGs for the presence or expression of this gene. The highest number of presence of alkane degrading genes in Bacteria were found in *Alphaproteobacteria* (encoding genes for both pathways, four only for alkanes) and *Gammaproteobacteria* (with both pathways, six only alkanes) (Figure 4). These results are consistent with the reported geographical ubiquity of n-alkane degradation genes in the open ocean (Love et al., 2021).

For the study of differentially expressed genes in key metabolisms, we included specific markers for oxidative stress ("peroxidase") and methylotrophy ("Serine hydroxymethyltransferase"). The former because of the toxicity of these compounds on cells (Cerro-Gálvez et al., 2019), and the latter because methylotrophy has been implicated in ADOC degradation, probably alkyl PAHs and alkanes (Gutierrez and Aitken 2014; Cerro-Gálvez et al., 2019). We detected many responding signature genes for the four pathways with at least an eight-fold higher abundance in treatments than in controls, primarily from the experiments in the Atlantic and mostly in samples taken after 2 h incubation (Figure 7, Supplementary Table S9). Among MAGs that decreased or had a stable contribution to the RNA pool, we detected roughly equal numbers of signature genes going up as going down (Figure 7), whereas in MAGs that increased their contribution only increases, baring one exception, were observed (Figure 7; Table 3). In particular, several MAGs expressed genes for alkane degradation and methylotrophy more abundantly in treatments than in control, but only in the Atlantic experiments. This supports previous findings of the higher lability of alkanes within the ADOC pool, thanks to its simpler chemical structure, higher transcription of *alkB* genes in oil spills and widespread occurrence and divergence of *alkB*-harboring bacteria in marine microbiomes (Mason et al., 2012; Rivers et al., 2013; Karthikeyan et al., 2021; Love et al., 2021). The increasing alkane degradation signature genes in increasing MAGs were expressed by species from the archaeal *Poseidoniales* order, the actinobacterial *Acidimicrobiales* order, the *Bacteroidia* order *Flavobacteriales* and the proteobacterial Rhodobacteraceae, Saccharospirillaceae and Methylophagaceae families. Methylotrophy was expressed by the same groups plus the archaeal Nitrosopumilaceae family, the cyanobacterial Cyanobiaceae family, the *Marinisomatota* phylum and the gammaproteobacterial *Puniceispirillales* order (Figure 7 and Supplementary Table S9). The taxonomical connection between alkane oxidation on the one hand, and methylotrophy on the other hand, reflects the proposed role of methylotrophy in degradation of hydrocarbons in the ocean that has been analyzed under oil spill scenarios, but it is here evidenced at low oceanic concentrations. For instance, methylotrophs were enriched in the oil plume in late stages of the Deepwater Horizon oil spill (Gulf of Mexico) after the initial bloom of opportunistic hydrocarbonoclastic bacteria (Kessler. et al., 2011). Direct evidence of *Methylophaga* in consumption of hexadecane was obtained in experiments using stable isotope probing (Mishamandani et al., 2014). Further, *Methylophaga* have the capacity to remove methyl-groups from alkylated hydrocarbons, for example methyl phenanthrenes, that are generally abundant in the ADOC pool (Gutierrez and Aitken 2014; Cerro-Gálvez et al., 2019). Overall, our gene expression profiles support a fast consumption of alkanes, along with an activation of methylotrophy, at the low concentrations of ADOC ubiquitous in oceanic waters.

The signature gene for oxidative stress was enriched in a subset of the taxa that also expressed signature genes for the other three processes: *Poseidoniales, Acidimicrobiales, Flavobacteriales,*

*Puniceispirillales, Rhodobacterales* and *Pseudomonadales*. Similar correlations between metabolic responses at gene level to ADOC addition has been reported previously (Cerro-Gálvez et al., 2019, 2021). The higher metabolic rate that might be a consequence of oxidative metabolism of ADOC, either as a carbon source or as a defense mechanism against toxicity, can be expected to result in higher concentrations of reactive oxygen species, and hence trigger transcription of defense systems.

## 4 Conclusion

We performed different ADOC exposure experiments at background concentrations in the mesotrophic tropical Pacific (Costa Rica Dome) and the oligotrophic subtropical North Atlantic. During these experiments, there was degradation of n-alkanes with 21–35 carbons that are thought to be from fossil fuels (petroleum, coal), and thus have anthropogenic origin (Fernández-pinos et al., 2017). The most active MAGs responding to ADOC belonged to the families Rhodobacteraceae and Flavobacteriaceae. Recently, it has been suggested a fast cryptic cycle of C15 and C17 alkanes produced by cyanobacteria and consumed by some heterotrophic bacteria (including specialist hydrocarbonoclastic bacteria such as *Alcanivorax* and methylotrophs such as *Methylophaga* spp.) and archaeal *Poseidoniales*. Whether or not the recycling of anthropogenic and other biogenic n-alkanes is similar to that of the cryptic cycle remains unknown. In this study, besides high activities of MAGs from families Rhodobacteraceae and Flavobacteriaceae responding to ADOC after short-term exposures, we observed a high transcription activity of Poseidonales and growth of Methylophaga, and similar patterns of methylotrophy and alkane degradation gene expression. These observations, along with the efficient degradation of C21-C35 alkanes (Fernández-pinos et al., 2017) support the high lability of alkanes within the ADOC pool and the suggested role of several taxa consuming medium high chain alkanes. This can possibly be related to their capacity to outcompete other opportunistic bacteria at low alkane concentrations (and fail at high concentrations such as in initial stages of oil spill accidents), similar to the concentrations of alkanes produced by cyanobacteria. As the experiments were performed exposing the microbial communities to changes in ADOC concentrations by a factor of two, the results suggest that anthropogenic carbon introduction in the ocean could play a role modulating microbiomes, which will require extensive research efforts in the coming years.

## Data availability statement

All sequence data presented here can be downloaded from the European Nucleotide Archive (ENA) under the project accession PRJEB60184. Metagenome samples have accessions ERS14678684-ERS14678695 and metatranscriptome samples have ERS14678669-ERS14678683. Accessions for metagenome bins and MAGs (better quality bins) that were possible to annotate taxonomically and were less than 10% contaminated can be found in Supplementary Table S11.

## Author contributions

MV-C, DL, and JD wrote sections of the manuscript. M-CF-P, JD, and BP did the conceptualization of the experiments. M-CF-P performed the experiments. M-CF-P and MV-C processed DNA and RNA samples. DL and MV-C did the computational and bioinformatic analyses. JI did anvio analyses. All the authors contributed to provide feedback to the manuscript and approved the submitted version.

## Funding

This work was supported by the Spanish Ministry of Science and Innovation through projects MIQAS (PID2021-128084OB-I00) and PANTOC (PID2021-127769NB-I00). The research group of Global Change and Genomic Biogeochemistry receives support from the Catalan Government (2017SGR800). IDAEA-CSIC is a Centre of Excellence Severo Ochoa (Spanish Ministry of Science and Innovation, Project CEX2018-000794-S). DL was supported by the Faculty of Health and Life Sciences at Linnaeus University and the Swedish Research Council FORMAS Strong Research environment Eco Change.

## Acknowledgments

We thank the staff of the Marine Technology Unit (UTM-CSIC) for their logistical support during the sampling Malaspina campaign.

## Conflict of interest

The authors declare that the research was conducted in the absence of any commercial or financial relationships that could be construed as a potential conflict of interest.

## Publisher's note



## Supplementary material

The Supplementary Material for this article can be found online at: https://www.frontiersin.org/articles/10.3389/fenvs.2023.1110169/full#supplementary-material

# References


Anderson, M. J. (2001). A new method for non-parametric multivariate analysis of variance. *Austral Ecol.* 26, 32–46. doi:10.1111/j.1442-9993.2001.01070.pp.x

Bowers, R. M., Kyrpides, N. C., Stepanauskas, R., Harmon-Smith, M., Doud, D., Reddy, T. B. K., et al. (2017). Minimum information about a single amplified genome (MISAG) and a metagenome-assembled genome (MIMAG) of bacteria and archaea. *Nat. Biotechnol.* 35, 725–731. doi:10.1038/nbt.3893

Casal, P., Casas, G., Vila-Costa, M., Cabrerizo, A., Pizarro, M., Jiménez, B., et al. (2019). Snow amplification of persistent organic pollutants at coastal Antarctica. *Environ. Sci. Technol.* 53, 8872–8882. doi:10.1021/acs.est.9b03006

Casal, P., Zhang, Y., Reardon, F., Martin, J. W., and Dachs, J. (2017). Accumulation of perfluoroalkylated substances in oceanic plankton. *Environ. Sci. Technol.* 51, 2766–2775. doi:10.1021/acs.est.6b05821

Cerro-Gálvez, E., Dachs, J., Lundin, D., Fernández-Pinos, M. C., Sebastián, M., and Vila-Costa, M. (2021). Responses of coastal marine microbiomes exposed to anthropogenic dissolved organic carbon. *Environ. Sci. Technol.* 55, 9609–9621. doi:10.1021/acs.est.0c07262

Cerro-Gálvez, E., Sala, M. M., Marrasé, C., Gasol, J. M., Dachs, J., and Vila-Costa, M. (2019). Modulation of microbial growth and enzymatic activities in the marine environment due to exposure to organic contaminants of emerging concern and hydrocarbons. *Sci. Total Environ.* 678, 486–498. doi:10.1016/j.scitotenv.2019.04.361

Chaumeil, P. A., Mussig, A. J., Hugenholtz, P., and Parks, D. H. (2020). GTDB-tk: A toolkit to classify genomes with the genome taxonomy database. *Bioinformatics* 36, 1925–1927. doi:10.1093/bioinformatics/btz848

Dachs, J., Bayona, J. M., Fowler, S. W., Miquel, J. C., and Albaigés, J. (1998). Evidence for cyanobacterial inputs and heterotrophic alteration of lipids in sinking particles in the Alboran Sea (SW Mediterranean). *Mar. Chem.* 60, 189–201. doi:10.1016/s0304-4203(97)00105-9

Del Fabbro, D., Giorgi, F. M., Scalabrin, C., Morgante, S., and Giorgi, M. M. (2013). An extensive evaluation of read trimming effects on Illumina NGS data analysis. *PLoS One* 8, 85024. doi:10.1371/journal.pone.0085024

Echeveste, P., Galbán-Malagón, C., Dachs, J., Berrojalbiz, N., and Agustí, S. (2016). Toxicity of natural mixtures of organic pollutants in temperate and polar marine phytoplankton. *Sci. Total Environ.* 571, 34–41. doi:10.1016/j.scitotenv.2016.07.111

Eddy, S. R. (2011). Accelerated profile HMM searches. *PLoS Comput. Biol. 7* 7, e1002195. doi:10.1371/journal.pcbi.1002195

Eren, A. M., Kiefl, E., Shaiber, A., Veseli, I., Miller, S. E., Schechter, M. S., et al. (2021). Community-led, integrated, reproducible multi-omics with anvi'o. *Nat. Microbiol.* 6, 3–6. doi:10.1038/s41564-020-00834-3

Fernández-Pinos, M. C., Vila-Costa, M., Arrieta, J. M., Morales, L., González-Gaya, B., Piña, B., et al. (2017). Dysregulation of photosynthetic genes in oceanic Prochlorococcus populations exposed to organic pollutants. *Sci. Rep.* 7, 8029. doi:10.1038/s41598-017-08425-9

Ferry, J. G. (1990). Formate dehydrogenase. *FEMS Microbiol. Rev.* 87, 377–382. doi:10.1111/j.1574-6968.1990.tb04940.x

Finn, R. D., Coggill, P., Eberhardt, R. Y., Eddy, S. R., Mistry, J., Mitchell, A. L., et al. (2016). The Pfam protein families database: Towards a more sustainable future. *Nucleic Acids Res.* 44, D279–D285. doi:10.1093/nar/gkv1344

Galbán-malagón, C., Berrojalbiz, N., Ojeda, M-J., and Dachs, J. (2012). The oceanic biological pump modulates the atmospheric transport of persistent organic pollutants to the Arctic. Nature Communications 3, doi:10.1038/ncomms1858

González-Gaya, B., Dachs, J., Roscales, J. L., Caballero, G., and Jiménez, B. (2014). Perfluoroalkylated substances in the global tropical and subtropical surface oceans. *Environ. Sci. Technol.* 48, 13076–13084. doi:10.1021/es503490z

González-Gaya, B., Fernández-Pinos, M. C., Morales, L., Méjanelle, L., Abad, E., Piña, B., et al. (2016). High atmosphere-ocean exchange of semivolatile aromatic hydrocarbons. *Nat. Geosci.* 9, 438–442. doi:10.1038/ngeo2714

González-Gaya, B., Martínez-Varela, A., Vila-Costa, M., Casal, P., Cerro-Gálvez, E., Berrojalbiz, N., et al. (2019). Biodegradation as an important sink of aromatic hydrocarbons in the oceans. *Nat. Geosci.* 12, 119–125. doi:10.1038/s41561-018-0285-3

Gutierrez, T., and Aitken, M. D. (2014). Role of methylotrophs in the degradation of hydrocarbons during the Deepwater Horizon oil spill. *ISME J.* 8, 2543–2545. doi:10.1038/ismej.2014.88

Kang, D. D., Li, F., Kirton, E., Thomas, A., Egan, R., An, H., et al. (2019). MetaBAT 2: An adaptive binning algorithm for robust and efficient genome reconstruction from metagenome assemblies. *PeerJ* 7, e7359. doi:10.7717/peerj.7359

Karthikeyan, S., Hatt, J. K., Kim, M., Spain, J. C., Huettel, M., Kostka, J. E., et al. (2021). A novel, divergent alkane monooxygenase (*alkB*) clade involved in crude oil biodegradation. *Environ. Microbiol. Rep.* 13, 830–840. doi:10.1111/1758-2229.13018

Langmead, B., and Salzberg, S. L. (2012). Fast gapped-read alignment with Bowtie 2. *Nat. Methods* 9, 357–359. doi:10.1038/nmeth.1923

Lauro, F. M., McDougald, D., Thomas, T., Williams, T. J., Egan, S., Rice, S., et al. (2009). The genomic basis of trophic strategy in marine bacteria. *Proc. Natl. Acad. Sci. U. S. A.* 106, 15527–15533. doi:10.1073/pnas.0903507106

Li, H., Handsaker, B., Wysoker, A., Fennell, T., Ruan, J., Homer, N., et al. (2009). The sequence alignment/map format and SAMtools. *Bioinforma. Appl. NOTE* 25, 2078–2079. doi:10.1093/bioinformatics/btp352

Liao, Y., Smyth, G. K., and Shi, W. (2014). featureCounts: an efficient general purpose program for assigning sequence reads to genomic features. *Bioinformatics* 30, 923–930. doi:10.1093/bioinformatics/btt656

Lohmann, R., Breivik, K., Dachs, J., and Muir, D. (2007). Global fate of POPs: Current and future research directions. *Environ. Pollut.* 150, 150–165. doi:10.1016/j.envpol.2007.06.051

Love, C. R., Arrington, E. C., Gosselin, K. M., Reddy, C. M., Van Mooy, B. A. S., Nelson, R. K., et al. (2021). Microbial production and consumption of hydrocarbons in the global ocean. *Nat. Microbiol.* 6, 489–498. doi:10.1038/s41564-020-00859-8

Martinez-Varela, A., Cerro-Gálvez, E., Auladell, A., Sharma, S., Moran, M. A., Kiene, R. P., et al. (2021). Bacterial responses to background organic pollutants in the northeast subarctic Pacific Ocean. *Environ. Microbiol.* 23, 4532–4546. doi:10.1111/1462-2920.15646

Mason, O. U., Hazen, T. C., Borglin, S., Chain, P. S. G., Dubinsky, E. A., Fortney, J. L., et al. (2012). Metagenome, metatranscriptome and single-cell sequencing reveal microbial response to Deepwater Horizon oil spill. *ISME J.* 6, 1715–1727. doi:10.1038/ismej.2012.59

Mishamandani, S., Gutierrez, T., and Aitken, M. D. (2014). DNA-based stable isotope probing coupled with cultivation methods implicates Methylophaga in hydrocarbon degradation. *Front. Microbiol.* 5, 76–79. doi:10.3389/fmicb.2014.00076

Mishamandani, S., Gutierrez, T., Berry, D., and Aitken, M. D. (2016). Response of the bacterial community associated with a cosmopolitan marine diatom to crude oil shows a preference for the biodegradation of aromatic hydrocarbons. *Environ. Microbiol.* 18, 1817–1833. doi:10.1111/1462-2920.12988

Morales, L., Dachs, J., Fernándezfernández-Pinos, M.-C., Berrojalbiz, N., Mompean, C., Belén Gonzaíez-Gaya, B., et al. (2015). Oceanic sink and biogeochemical controls on the accumulation of polychlorinated dibenzo-p-dioxins, dibenzofurans, and biphenyls in plankton. *Environ. Sci. Technol.* 49, 13853–13861. doi:10.1021/acs.est.5b01360

Muir, D. C. G., and Howard, P. H. (2006). Are there other persistent organic pollutants? A challenge for environmental chemists. *Environ. Sci. Technol.* 40, 7157–7166. doi:10.1021/es061677a

Muir, D., and Miaz, L. T. (2021). Spatial and temporal trends of perfluoroalkyl substances in global ocean and coastal waters. *Cite This Environ. Sci. Technol.* 55, 9527–9537. doi:10.1021/acs.est.0c08035

Pallen, M. J., Rodriguez-R, L. M., and Alikhan, N.-F. (2022). Naming the unnamed: Over 65,000 Candidatus names for unnamed archaea and bacteria in the genome taxonomy database. *Int. J. Syst. Evol. Microbiol.* 72, 5482. doi:10.1099/ijsem.0.005482

Parks, D. H., Chuvochina, M., Waite, D. W., Rinke, C., Skarshewski, A., Chaumeil, P.-A., et al. (2018). A standardized bacterial taxonomy based on genome phylogeny substantially revises the tree of life. *Nat. Biotechnol.* 36, 996–1004. doi:10.1038/nbt.4229

Parks, D. H., Imelfort, M., Skennerton, C. T., Hugenholtz, P., and Tyson, G. W. (2015). CheckM: Assessing the quality of microbial genomes recovered from isolates, single cells, and metagenomes. *Genome Res.* 25, 1043–1055. doi:10.1101/gr.186072.114

Poretsky, R. S., Sun, S., Mou, X., and Moran, M. A. (2010). Transporter genes expressed by coastal bacterioplankton in response to dissolved organic carbon. *Environ. Microbiol.* 12, 616–627. doi:10.1111/j.1462-2920.2009.02102.x

Rao, N. A., Ambili, M., Jala, V. R., Subramanya, H. S., and Savithri, H. S. (2003). Structure-function relationship in serine hydroxymethyltransferase. *Biochim. Biophys. Acta - Proteins Proteomics* 1647, 24–29. doi:10.1016/s1570-9639(03)00043-8

Rinke, C., Rubino, F., Messer, L. F., Youssef, N., Parks, D. H., Chuvochina, M., et al. (2019). A phylogenomic and ecological analysis of the globally abundant Marine Group II archaea (Ca. Poseidoniales ord. nov.). *ISME J.* 13, 663–675. doi:10.1038/s41396-018-0282-y

Rivers, A. R., Sharma, S., Tringe, S. G., Martin, J., Joye, S. B., and Moran, M. A. (2013). Transcriptional response of bathypelagic marine bacterioplankton to the Deepwater Horizon oil spill. *ISME J.* 7, 2315–2329. doi:10.1038/ismej.2013.129

RStudio Team (2022). RStudio: Integrated development environment for R. *RStudio, PBC, Boston, MA URL*.

Seemann, T. (2014). Prokka: Rapid prokaryotic genome annotation. *Bioinformatics* 30, 2068–2069. doi:10.1093/bioinformatics/btu153

Shai, Y., Rubin-Blum, M., Angel, D. L., Sisma-Ventura, G., Zurel, D., Astrahan, P., et al. (2021). Response of oligotrophic coastal microbial populations in the SE Mediterranean Sea to crude oil pollution; lessons from mesocosm studies. *Estuar. Coast. Shelf Sci.* 249, 107102. doi:10.1016/j.ecss.2020.107102

Sunagawa, S., Coelho, L. P., Chaffron, S., Kultima, J. R., Labadie, K., Salazar, G., et al. (2015). Ocean plankton. Structure and function of the global ocean microbiome. *Sci. (80-. ).* 348, 1261359. doi:10.1126/science.1261359

Tang, J. Y. M., McCarty, S., Glenn, E., Neale, P. A., Warne, M. S. J., and Escher, B. I. (2013). Mixture effects of organic micropollutants present in water: Towards the

development of effect-based water quality trigger values for baseline toxicity. *Water Res.* 47, 3300–3314. doi:10.1016/j.watres.2013.03.011

Tetu, S. G., Sarker, I., Schrameyer, V., Pickford, R., Elbourne, L. D. H., Moore, L. R., et al. (2020). Plastic leachates impair growth and oxygen production in Prochlorococcus, the ocean's most abundant photosynthetic bacteria. Commun. Biol. 184. doi:10.1038/s42003-019-0410-x

Torrents, E., Sahlin, M., and Sjöberg, B. (2008). The ribonucleotide reductase family: Genetics and genomics. *Undefined*.

Uritskiy, G. V., Diruggiero, J., and Taylor, J. (2018). MetaWRAP-a flexible pipeline for genome-resolved metagenomic data analysis. Microbiome. 158. doi:10.1186/s40168-018-0541-1

Vila-Costa, M., Cerro-Gálvez, E., Martínez-Varela, A., Casas, G., and Dachs, J. (2020). Anthropogenic dissolved organic carbon and marine microbiomes. *ISME J.* 14, 2646–2648. doi:10.1038/s41396-020-0712-5

Vila-Costa, M., Sebastián, M., Pizarro, M., Cerro-Gálvez, E., Lundin, D., Gasol, J. M., et al. (2019). Microbial consumption of organophosphate esters in seawater under phosphorus limited conditions. *Sci. Rep.* 9, 233–311. doi:10.1038/s41598-018-36635-2

Wang, Z., Walker, G. W., Muir, D. C. G., and Nagatani-Yoshida, K. (2020). Toward a global understanding of chemical pollution: A first comprehensive analysis of national and regional chemical inventories. *Environ. Sci. Technol.* 54, 2575–2584. doi:10.1021/acs.est.9b06379

Wickham, H., Averick, M., Bryan, J., Chang, W., McGowan, L., François, R., et al. (2019). Welcome to the Tidyverse. *J. Open Source Softw.* 4, 1686. doi:10.21105/joss.01686

Xie, Z., Wang, P., Wang, X., Castro-Jiménez, J., Kallenborn, R., Liao, C., et al. (2022). Organophosphate ester pollution in the oceans. *Nat. Rev. Earth Environ.* 3, 309–322. doi:10.1038/s43017-022-00277-w

Yooseph, S., Nealson, K. H., Rusch, D. B., McCrow, J. P., Dupont, C. L., Kim, M., et al. (2010). Genomic and functional adaptation in surface ocean planktonic prokaryotes. *Nature* 468, 60–66. doi:10.1038/nature09530

frontiers | Frontiers in Environmental Science

TYPE Original Research
PUBLISHED 05 April 2023
DOI 10.3389/fenvs.2023.1121969



OPEN ACCESS

EDITED BY
David Widory,
Université du Québec à Montréal, Canada

REVIEWED BY
Gerald Jurasinski,
University of Rostock, Germany
Michelle Garneau,
Université du Québec à Montréal, Canada

*CORRESPONDENCE
Antti J. Rissanen,
antti.rissanen@tuni.fi

SPECIALTY SECTION
This article was submitted to Biogeochemical Dynamics, a section of the journal Frontiers in Environmental Science

RECEIVED 12 December 2022
ACCEPTED 24 March 2023
PUBLISHED 05 April 2023

CITATION
Rissanen AJ, Ojanen P, Stenberg L, Larmola T, Anttila J, Tuominen S, Minkkinen K, Koskinen M and Mäkipää R (2023), Vegetation impacts ditch methane emissions from boreal forestry-drained peatlands—Moss-free ditches have an order-of-magnitude higher emissions than moss-covered ditches. *Front. Environ. Sci.* 11:1121969. doi: 10.3389/fenvs.2023.1121969



# Vegetation impacts ditch methane emissions from boreal forestry-drained peatlands—Moss-free ditches have an order-of-magnitude higher emissions than moss-covered ditches

Antti J. Rissanen[1,2]*, Paavo Ojanen[1,3], Leena Stenberg[1], Tuula Larmola[1], Jani Anttila[1], Sakari Tuominen[1], Kari Minkkinen[3], Markku Koskinen[4,5] and Raisa Mäkipää[1]

[1]Natural Resources Institute Finland (Luke), Helsinki, Finland, [2]Faculty of Engineering and Natural Sciences, Tampere University, Tampere, Finland, [3]Department of Forest Sciences, University of Helsinki, Helsinki, Finland, [4]Environmental Soil Science, Department of Agricultural Sciences, University of Helsinki, Helsinki, Finland, [5]Institute of Atmospheric and Earth System Research (INAR)/Forest Sciences, University of Helsinki, Helsinki, Finland

Ditches of forestry-drained peatlands are an important source of methane ($CH_4$) to the atmosphere. These $CH_4$ emissions are currently estimated using the IPCC Tier 1 emission factor (21.7 g $CH_4$ $m^{-2}$ $y^{-1}$), which is based on a limited number of observations (11 study sites) and does not take into account that the emissions are affected by the condition and age of the ditches. Furthermore, the total area of different kinds of ditches remains insufficiently estimated. To construct more advanced ditch $CH_4$ emission factors for Finland, we measured $CH_4$ emissions in ditches of 3 forestry-drained peatland areas (manual chamber technique) and amended this dataset with previously measured unpublished and published data from 18 study areas. In a predetermined 2-type ditch classification scheme, the mean $CH_4$ emissions (±standard error) were 2.6 ± 0.8 g $CH_4$ $m^{-2}$ $y^{-1}$ and 20.6 ± 7.0 g $CH_4$ $m^{-2}$ $y^{-1}$ in moss-covered and moss-free ditches, respectively. In a more detailed 4-type classification scheme, the yearly emissions were 0.6 ± 0.3, 3.8 ± 1.1, 8.8 ± 3.2, and 25.1 ± 9.7 g $CH_4$ $m^{-2}$ $y^{-1}$ in *Sphagnum*-covered, *Sphagnum*- and vascular plant—covered, moss-free and vascular plant-covered, and plant - free ditches, respectively. Hence, we found that Tier 1 emission factor may overestimate ditch $CH_4$ emissions through overestimation of the emissions of moss-covered ditches, irrespective of whether they harbor potentially $CH_4$ conducing vascular plants. Based on the areal estimates and the $CH_4$ emission factors for moss-covered and moss-free ditches, $CH_4$ emissions of ditches of forestry-drained peatlands in Finland were 8,600 t $a^{-1}$, which is 63% lower than the current greenhouse gas inventory estimates for ditch $CH_4$ emissions (23,200 t $a^{-1}$). We suggest that the Tier 1 emission factor should be replaced with more advanced emission factors in the estimation of ditch $CH_4$ emissions of boreal forestry-drained peatlands also in other countries than in Finland. Furthermore, our results suggest that the current practice in Finland to

minimize ditch-network maintenance by ditch cleaning will likely decrease $CH_4$ emissions from ditches, since old moss-covered ditches have very low emissions.

KEYWORDS

methane, IPCC emission factor, greenhouse gas (GHG), peatland, ditch, drainage, forestry, moss

## 1 Introduction

The concentration of the greenhouse gas (GHG) methane ($CH_4$) has increased substantially since industrialization, with the current global yearly emissions averaging 576 Tg (550–594 Tg) based on top-down estimation (Saunois et al., 2020). Of these global emissions, approximately 60% stem from anthropogenic sources, mostly agriculture, waste treatment, biomass burning and fossil fuel industry (Saunois et al., 2020). In addition, drainage ditches and canals were recently estimated to contribute on average 1% to the global anthropogenic $CH_4$ emissions, yet, their contribution to anthropogenic $CH_4$ emissions can be much higher in densely drained areas (Peacock et al., 2021). Hence, inclusion of ditch and canal emissions into local and national GHG inventories will be crucial in assessing the impact of drained land on $CH_4$ budgets, especially in densely drained countries (Peacock et al., 2021), like in Finland, where approximately 5.9 million ha of peatlands (ca. 17% of total land area of Finland) have been drained for forestry since the 1920s, an area equal to as much as 40% of the global estimate of 15 million ha of forestry-drained peatlands (Paavilainen and Päivänen, 1995).

Drainage of peatlands typically decreases $CH_4$ emissions from soil and ground vegetation, but also creates ditches that have significant $CH_4$ emissions (Martikainen et al., 1995; Roulet and Moore, 1995; von Arnold et al., 2005; Koskinen et al., 2016; Minkkinen et al., 1997; Minkkinen and Laine, 2006). The methane emissions from drainage ditches in Finland are currently estimated using the Tier 1 emission factor of the Intergovernmental Panel on Climate Change (IPCC) for ditches of temperate and boreal drained forest land and drained wetland (Supplementary Table S1; IPCC, 2014). This emission factor, however, is based on a limited number of studies, covering only 11 study sites (Supplementary Table S1; Roulet and Moore, 1995; Minkkinen and Laine, 2006; Sirin et al., 2012; Glagolev et al., 2008; von Arnold et al., 2005; Cooper and Evans, 2013; Cooper et al., 2014) of which only one study is from Finland, covering drained fen and bog sites of one peatland complex (Minkkinen and Laine, 2006). Furthermore, the Tier 1 emission factor does not take into account that different types of ditches (e.g., vegetated vs. non-vegetated) could vary in their $CH_4$ emissions, and the information on the ditch types is impossible to extract for many of the study sites used in the calculations (Supplementary Table S1).

The currently published results of ditch $CH_4$ emission from Finnish forestry-drained peatlands are still scarce, but they already show that the emissions have considerable variation, explained by the hydrology and the type of vegetation cover. The emissions are larger from ditches with moving water than with standing water, which is probably explained by higher input of dissolved methane from surrounding soils *via* drainage and ground water flow into ditches with moving water (Minkkinen and Laine, 2006). In addition, ditches with aerenchymous plants may have higher $CH_4$ emissions than ditches with *Sphagnum* moss, as $CH_4$ conducted through the aerenchyma can bypass the methanotrophic filter in oxic surface water, moss, sediment and peat layers, and plant root exudates can also increase methane emissions through several mechanisms (e.g., increasing microbial metabolism) (Schimel, 1995; Frenzel and Karofeld, 2000; Minkkinen and Laine, 2006; Waldo et al., 2019). The scarce published results also hint towards lower $CH_4$ fluxes from moss-covered than moss-free ditches, but the effect of moss-cover remains to be confirmed as the sites of the previously studied moss-free and moss-covered ditches also differed in their nutrient status and forest harvesting treatment, both potentially affecting $CH_4$ production within ditches and strips as well as $CH_4$ transfer from strips to ditches (Minkkinen and Laine, 2006; Korkiakoski et al., 2020). In any case, moss-covered ditches have also shown to turn into occasional $CH_4$ sinks, probably due to activity of methanotrophs within *Sphagnum* layer or in the sediment and peat below the *Sphagnum* layer (Raghoebarsing et al., 2005; Larmola et al., 2010; Korkiakoski et al., 2020). As it takes time before ditches are covered by mosses after ditch digging or cleaning, it can be also suggested that ditch age affects $CH_4$ emissions.

As the forest floor of the forestry-drained peatlands is usually a small $CH_4$ sink (Roulet and Moore, 1995; Ojanen et al., 2010; Korkiakoski et al., 2020), the emissions from the ditches determine whether these lands are net sources or sinks of $CH_4$. Accurate methane budget calculations for forestry-drained peatlands followed by national greenhouse gas (GHG) inventories would greatly benefit from development of emission factors, which account the differences in $CH_4$ emissions between ditches of varied age and vegetation cover. Furthermore, a more accurate estimate of the total area of different types of ditches is needed for more accurate calculations of the national GHG inventory. In southern Finland, 35%–43% moss-coverage has been estimated for 5–10-year-old ditches (Silver and Joensuu, 2005), but otherwise publications on ditch vegetation distribution are lacking.

The current $CH_4$ emission data from ditches of forestry-drained boreal peatlands are still scarce and the accuracy of the peatland $CH_4$ emission estimates cannot be improved without further measurements. Using data from 21 study areas covering different ditch vegetation cover and site nutrient status and spanning from southern Finland to southern Lapland, we aimed at developing $CH_4$ emission factors that account for different types of ditches (in terms of vegetation cover), and thus should improve the accuracy of the $CH_4$ emission estimation of forestry-drained peatlands. To further improve the accuracy of the $CH_4$ emission estimation in the national GHG inventory, we also made an improved estimation of the total area of ditches and proportion of the different types of ditches in Finland.

**TABLE 1 Study areas (their location and nutrient status), year of $CH_4$ flux measurements, number of measurement timepoints during snow-free season (T.P.), the types of ditches, number of measurement points belonging to the particular type of ditch (N), and reference for the description of the study area. Site types from the nutrient richest to the nutrient poorest type with their abbreviations (Laine et al., 2012): Herb-rich (Rhtkg), *Vaccinium myrtillus* (Mtkg), *Vaccinium vitis-idaea* (Ptkg), Dwarf-shrub (Vatkg), Lichen (Jätkg). I and II describe the status of the tree stand prior drainage, if known: treed (I), sparsely treed or treeless (II). $CH_4$ flux data from four (i.e., Lakkasuo, Kalevansuo, Konilampi and Vesijako) out of the total of 21 study areas was previously published (see references in footnotes).**

| Study area | Latitude | Longitude | Site type | Year | T.P. | Type of ditch | N | Description of the study area |
|---|---|---|---|---|---|---|---|---|
| Lakkasuo[a] | 61°47′ | 24°18′ | Mtkg | 1996–97 | 19[b] | plant-free | 3 | Minkkinen and Laine. (2006) |
| | | | Ptkg | 1996–97 | 19[b] | plant-free | 6 | ” |
| | | | Vatkg | 1996–97 | 19[b] | *Sphagnum* + vascular | 2 | ” |
| | | | Vatkg | 1996–97 | 19[b] | *Sphagnum* | 1 | ” |
| Kalevansuo[c] | 60°38.82′ | 24°21.38′ | Vatkg | 2011 | 6 | *Sphagnum* + vascular | 3 | Minkkinen et al. (2018) |
| | | | Vatkg | 2011 | 6 | *Sphagnum* | 1 | ” |
| Konilampi[d] | 61°47.728′ | 24°17.713′ | Mtkg I | 2012 | 5 | *Calliergon*, *Polytrichum*, *Sphagnum* + vascular | 1 | Koskinen et al. (2016) |
| Vesijako[d] | 61°22.712′ | 25°06.615′ | Mtkg I | 2012 | 3 | plant-free | 1 | ” |
| Alkkianneva | 62° 9.50′ | 22° 46.24′ | Jätkg | 2014–15 | 11[b] | *Sphagnum* | 2 | Heikkinen (2016) |
| Huhdanneva | 62° 10.13′ | 22° 52.75′ | Jätkg | 2014–15 | 10[b] | *Sphagnum* + vascular | 2 | ” |
| Jylkky | 64°52.97′ | 26°06.07′ | Vatkg | 2014–15 | 10[b] | *Sphagnum* | 2 | Ojanen et al. (2019) |
| | | | Ptkg | 2014–15 | 10[b] | *Sphagnum* + vascular | 2 | ” |
| Koirasuo | 66° 26.54′ | 26° 44.96′ | Vatkg | 2014–15 | 11[b] | *Sphagnum* | 2 | Tolvanen et al. (2018)[e] |
| | 66° 26.62′ | 26° 44.42′ | Vatkg | 2014–15 | 12[b] | *Sphagnum* | 2 | ” |
| Könölä | 65° 57.77′ | 24°29.6′ | Rhtkg | 2014–15 | 13[b] | plant-free | 2 | Ojanen et al. (2019) |
| | | | Rhtkg | 2014–15 | 12[b] | plant-free | 2 | ” |
| Lahnalamminsuo | 60°40.69′ | 23°48.36′ | Jätkg | 2014–15 | 14[b] | *Sphagnum* + vascular | 2 | Heikkinen (2016) |
| Laitasuo | 64°36.65′ | 26°54.00′ | Vatkg | 2014–15 | 10[b] | *Sphagnum* + vascular | 2 | ” |
| Leppiniemi | 64°50.90′ | 26°03.51′ | Vatkg | 2014–15 | 10[b] | plant-free | 2 | Ojanen et al. (2019) |
| | | | Rhtkg | 2014–15 | 10[b] | plant-free | 2 | ” |
| Lylynneva | 62° 10.40′ | 22° 48.63′ | Jätkg | 2014–15 | 11[b] | *Sphagnum* + vascular | 2 | ” |
| | | | Vatkg | 2014–15 | 10[b] | *Sphagnum* + vascular | 2 | ” |
| Pelso | 64°29.58′ | 26°18.36′ | Vatkg | 2014–15 | 10[b] | vascular | 2 | ” |
| | | | Ptkg | 2014–15 | 10[b] | *Sphagnum* | 2 | ” |
| Rantasuo | 64°47.33′ | 26°29.95′ | Jätkg | 2014–15 | 9[b] | vascular | 2 | ” |
| | | | Vatkg | 2014–15 | 9[b] | vascular | 2 | ” |
| Stormossen | 60°17.76′ | 25°26.75′ | Vatkg | 2014–15 | 14[b] | *Sphagnum* + vascular | 2 | Tolvanen et al. (2018)[e] |
| Tolkansuo | 64°38.08′ | 26°49.55′ | Vatkg | 2014–15 | 10[b] | *Sphagnum* + vascular | 2 | ” |
| Ylimysneva | 62° 8.93′ | 22° 52.09′ | Jätkg | 2014–15 | 10[b] | *Sphagnum* + vascular | 2 | Heikkinen (2016) |
| Ränskälänkorpi | 61°10.966′ | 25°15.985′ | Rhtkg II and Mtkg II | 2021 | 8 | plant-free | 10 | Laurila et al. (2021) |
| | | | Rhtkg II and Mtkg II | 2021 | 8 | vascular | 2 | ” |
| | | | Rhtkg II and Mtkg II | 2021 | 8 | *Sphagnum* | 11 | ” |
| | | | Rhtkg II and Mtkg II | 2021 | 8 | *Sphagnum* + vascular | 1 | ” |

(Continued on following page)

**TABLE 1 (*Continued*) Study areas (their location and nutrient status), year of $CH_4$ flux measurements, number of measurement timepoints during snow-free season (T.P.), the types of ditches, number of measurement points belonging to the particular type of ditch (N), and reference for the description of the study area. Site types from the nutrient richest to the nutrient poorest type with their abbreviations (Laine et al., 2012): Herb-rich (Rhtkg), *Vaccinium myrtillus* (Mtkg), *Vaccinium vitis-idaea* (Ptkg), Dwarf-shrub (Vatkg), Lichen (Jätkg). I and II describe the status of the tree stand prior drainage, if known: treed (I), sparsely treed or treeless (II). $CH_4$ flux data from four (i.e., Lakkasuo, Kalevansuo, Konilampi and Vesijako) out of the total of 21 study areas was previously published (see references in footnotes).**

| Study area | Latitude | Longitude | Site type | Year | T.P. | Type of ditch | N | Description of the study area |
|---|---|---|---|---|---|---|---|---|
| Lettosuo | 60°38′ | 23°57′ | Mtkg II | 2021 | 7 | vascular | 6 | Korkiakoski et al. (2020) |
| | | | Mtkg II | 2021 | 7 | *Sphagnum* | 3 | ” |
| | | | Mtkg II | 2021 | 7 | *Sphagnum* + vascular | 1 | ” |
| | | | Mtkg II | 2021 | 7 | *Polytrichum*, *Sphagnum* | 2 | ” |
| | | | Mtkg II | 2021 | 7 | *Polytrichum* | 6 | ” |
| Paroninkorpi | 61° 0′ | 24° 45′ | Rhtkg II | 2021 | 7 | plant-free | 8 | Palviainen et al. (2022) |
| | | | Rhtkg II | 2021 | 7 | *Sphagnum* | 10 | ” |
| | | | Rhtkg II | 2021 | 7 | *Sphagnum* + vascular | 5 | ” |
| | | | Rhtkg II | 2021 | 7 | *Polytrichum*, *Sphagnum* | 1 | ” |

[a]$CH_4$ flux data is from Minkkinen and Laine, (2006).
[b]Total number of measurement timepoints for snow-free season during both study years, i.e., there were 9–10 timepoints per study year (1996 and 1997) in Lakkasuo and 3-8 timepoints per study year (2014 and 2015) in other denoted areas.
[c]$CH_4$ flux data is from Minkkinen et al. (2018).
[d]$CH_4$ flux data is from Koskinen et al. (2016).
[e]The reference report results on GHG measurements from the study areas but not description of the study areas.

# 2 Materials and methods

## 2.1 Study areas

Altogether, we used data from 21 forestry-drained peatland study areas representing different site types (nutrient status) and covering Finland from south to north (Table 1). The measurements were done within 25 years spanning 1996–2021 (Table 1). For four areas (Lakkasuo, Konilampi, Vesijako and Kalevansuo), data were obtained from previously published studies (Minkkinen and Laine, 2006; Koskinen et al., 2016; Minkkinen et al., 2018). For 14 areas, unpublished data measured in 2014–2015 were utilized (Table 1). Furthermore, for this study, we conducted $CH_4$ flux measurements at three study areas (Table 1: Ränskälänkorpi, Lettosuo, Paroninkorpi) in 2021. These areas were selected, because they represent nutrient-rich drained peatland forests [Herb-rich (Rhtkg) and *Vaccinium myrtillus* type (Mtkg)] that are scarce in the previously measured datasets (Table 1), even though they comprise almost 40% of the current forestry-drained peatland area in Finland (Korhonen et al., 2021).

## 2.2 $CH_4$ flux measurements

Depending on the study area, there were 1–24 measurement points from which the $CH_4$ emissions were measured 3–19 times during 1–2 snow-free seasons, mostly between May–October (Table 1). The $CH_4$ fluxes were measured using the manual closed chamber method at each study area. For Lakkasuo, Konilampi, Vesijako and Kalevansuo, the measurements, gas analyses [gas chromatograph (GC)] and flux calculation were reported previously (Minkkinen and Laine, 2006; Koskinen et al., 2016; Minkkinen et al., 2018). Measurements (using an opaque round closed floating chamber) and GC analyses for the dataset from 2014 to 15 (Table 1) were conducted as previously described (Ojanen et al., 2019). Furthermore, concentration-time graphs of the 2014–15 data were visually inspected for patterns indicating $CH_4$ ebullition events (i.e., release of $CH_4$ bubbles) or analyzer malfunction. Such flux estimates were excluded from the dataset. Altogether, on average 13.1% of the flux estimates, varying from 0% to 40.9% for single study areas, of the 2014–2015 dataset were excluded.

For the dataset measured in 2021 (Ränskälänkorpi, Lettosuo and Paroninkorpi), the gas analyses were made using a portable gas analyser (LI-COR LI-7810, 1 measurement per second) from the headspace of an opaque closed floating chamber (d 31.5 cm, h 31 cm, equipped with a fan) for a time period of 3 min after placing the chamber at the measurement point. After manual trimming of anomalies in the gas concentration data caused by placement and removal of the chamber in the beginning and at the end of the measurement period, respectively, fluxes were calculated based on linear fit between gas concentration and time [linregress routine of SciPy (v. 1.7.0); Virtanen et al., 2020], accounting for chamber temperature, volume and area, using an in-house script (available from https://github.com/janivaltteri/manual-chamber-data-server/blob/main/dataserver/application/fluxcalc.py).

We acknowledge that $CH_4$ measurements from wet surfaces are very sensitive to interferences. It is difficult to place the chamber firmly into the open water or plant-covered ditch surface in a gas-tight manner. Furthermore, pressing the chamber too hard on the measurement surface can disturb the water column and/or sediment surface and lead to inadvertently enhanced gas transfer or even

inadvertent $CH_4$ ebullition causing overestimation of the $CH_4$ fluxes (Matthews et al., 2003). This makes it impossible to determine whether disturbances detected in concentration-time data are due to natural $CH_4$ ebullition or the disturbances caused by the measurement procedure. Hence, the $CH_4$ concentration-time graphs of the portable analyser measurements were manually screened for patterns indicating interference of measurements, gas leaks, $CH_4$ ebullition events or analyser malfunctioning resulting in exclusion of such data (see examples in the Supplementary Material; Supplementary Figure S1). The possible anomalies in the concurrently measured $CO_2$ (data not shown) were used as to help in detecting the possible gas leaks, chamber interference and analyzer malfunctioning. We monitored $CH_4$ ebullition specifically using a bubble collector (Huttunen et al., 2001) in an open water (moss-free) ditch in one of the study areas, Ränskälänkorpi during June-October 2021, and found that ebullition was infrequent, occurring only in two occasions: mid July and early August.

In the plant-free, open water ditches, we also noticed that when a downstream measurement point was measured soon (within few minutes) after measurement of a nearby (only 1–2 m apart) upstream measurement point, the disturbance and mixing of the water upstream could lead to biased, comparatively high $CH_4$ flux estimates at the downstream point, which can be due to inadvertently enhanced gas transfer or even inadvertent $CH_4$ ebullition, as explained above (Matthews et al., 2003). There were one such occasion in Ränskälänkorpi (points 321/322 at 5 August 2021), one occasion in Lettosuo (points 121/122 at 21 July 2021) and four occasions in Paroninkorpi (points 421/422 at 24 August 2021 and 18 October 2021; points 431/432 at 28 July 2021 and 7 September 2021), where downstream point had 3.4, 2.9, and 2.0–28.4 times as high $CH_4$ flux as the upstream point, respectively. Hence, such data were also discarded from further analyses.

Altogether, the manual screening procedure removed 26 (13.7%), 43 (35.2%), and 37 (25.5%) flux estimates resulting in 164, 79, and 108 accepted flux estimates for Ränskälänkorpi, Lettosuo and Paroninkorpi, respectively. The accepted $CH_4$ fluxes used in this study are available in the Dataset 1 [All datasets (i.e., Datasets 1–6) are freely available from https://doi.org/10.5281/zenodo.7341325].

## 2.3 Water level, temperature and precipitation

Temperature in the ditches of Ränskälänkorpi, Lettosuo and Paroninkorpi in 2021 were measured using iButton loggers (Maxim Integrated, USA) (see Dataset 2). Furthermore, water table level (WT) of the measurement points was recorded during gas flux measurements using a measurement stick permanently attached to ditch bottom (with a measurement scale). WT was recorded as relative to the WT level in the beginning of June 2021 (see Dataset 3).

For all the datasets, the data on air temperature and precipitation for the study years and 30-year comparison period (1 January 1991–31 December 2020) were gathered from the nearest grid point in the 10 km × 10 km grid dataset of Finnish Meteorological Institute (Venäläinen et al., 2005) (see the Supplementary Material, Supplementary Figures S2–S22). In the Lakkasuo dataset in 1996–1997 (Supplementary Figure S2), the year 1997 was warmer and drier than 1996. The summer temperatures were higher than the 30-year average in 1997, while temperature did not differ from the 30-year average in 1996. Precipitation was similar with the 30-year average in 1997 but higher than that in July and November and lower than that in August and September in 1996. In the Kalevansuo dataset in 2011 (Supplementary Figure S3), the summer was warmer, and July, September and December had higher precipitation than the 30-year average. In the Konilampi and Vesijako dataset in 2012 (Supplementary Figures S4, S5), temperature was comparable to while precipitation was generally higher than the 30-year average. In the dataset of several study areas in 2014–2015 (Supplementary Figure S6–19), the year 2014 was generally warmer and drier than the year 2015. Compared to the 30-year average, the temperatures were slightly higher in summer 2014 but not in 2015. Precipitation was also generally higher than the 30-year average in 2015 whereas it was comparable to the 30-year average in 2014, except for some single rainy months, for example, August 2014 in Könölä, when precipitation was higher than the 30-year average (Supplementary Figure S10). In the Ränskälänkorpi, Lettosuo and Paroninkorpi datasets in 2021 (Supplementary Figures S20–22), the summer was warmer, and May and August had higher and July lower precipitation than the 30-year average.

## 2.4 Development of $CH_4$ emission factors

The measurement points in the study areas were classified into different ditch types utilizing field observations and photographs. The classification was based on the presence/absence of moss cover and vascular plants (Table 1). Finally, in the development of the $CH_4$ emission factors, 2-type and 4-type classification schemes were used. The 2-type scheme classified measurement points into 1. moss-covered and 2. moss-free, because presence or absence of moss-cover was the most conspicuous factor differing between the study ditches (Table 1). This classification scheme also best supported the estimation of the area of different types of ditches and total ditch $CH_4$ emissions of Finland (see below). The majority of the moss-covered measurement points were covered by *Sphagnum* mosses, yet some were covered also by other mosses (Table 1, Dataset 1). The ditch types in the 4-type classification scheme were: 1. *Sphagnum*-covered, vascular plant-free ditches (in short: *Sphagnum*), 2. *Sphagnum*- and vascular plant - covered ditches (*Sphagnum* + vascular), 3. moss-free, vascular plant—covered ditches (vascular), and 4) moss- and vascular plant-free ditches (plant-free). The purpose of the 4-type classification scheme was to develop the most detailed classification possible, considering also the effect of vascular plants in increasing ditch $CH_4$ emissions (e.g., Minkkinen and Laine, 2006), yet each ditch type still containing adequate number of replicates for statistical testing of differences in the $CH_4$ emissions between ditch types (Table 1, Dataset 1). Additionally, there were 10 measurement points, representing rare ditch types in the dataset, which were included in the 2-type classification scheme in the class of moss-covered ditches (Table 1, Dataset 1). These remained outside of the 4-type classification scheme, including ditches covered with *Polytrichum commune*

(common hair moss), co-covered with *P. commune* and *Sphagnum* mosses, and co-covered with *Calliergon stramineum* (calliergon moss), *P. commune*, *Sphagnum* mosses and vascular plants, due to too low number of replicates.

Annual $CH_4$ emissions were calculated separately for each measurement point. Emissions were calculated first for the snow-free season simply based on the mean of the measured fluxes during May–October. The only exception was Ränskälänkorpi where the autumn's last timepoint was at 19 November 2021, which, according to the weather data and field observation still represented snow-free season. For the datasets with two study years (1996–97 and 2014–15, see Table 1), the snow-free season emission was first calculated separately for each study year, after which the mean of the two snow-free seasons was considered as the snow-free season emission for the measurement point. Snowy season (November–April) daily emissions were calculated based on the published relationship between mean daily snow-free season and mean daily snowy season emissions/sinks estimated from data of forestry-drained and undrained peatland soils, which were measured throughout the year (Ojanen et al., 2019), as follows:

$$y = 0.29x \text{ (for } CH_4 \text{ sinks)} \quad (1)$$

$$y = -0.00015x^2 + 0.15853x \text{ (for } CH_4 \text{ emissions)} \quad (2)$$

where y is the snowy season daily emission/sink and x is the snow-free season daily emission/sink (Ojanen et al., 2019). Only the increasing part of the parabola resulting from equation 2 was considered. Snowy season $CH_4$ emission reached its maximum value, 41.89 mg $CH_4$ $m^{-2}$ $d^{-1}$, at snow-free season emission of 528.43 mg $CH_4$ $m^{-2}$ $d^{-1}$. Therefore, for snow-free season emissions >528.43 mg $CH_4$ $m^{-2}$ $d^{-1}$, the snowy season emission was set at 41.89 mg $CH_4$ $m^{-2}$ $d^{-1}$, which happened at only three plant-free measurement points in the Lakkasuo study area (with snow-free season emissions of 536.40, 631.69, and 677.60 mg $CH_4$ $m^{-2}$ $d^{-1}$). We acknowledge that the equations used to estimate the winter fluxes are based on data which are not from ditches but from soils of forestry-drained and undrained peatlands (Ojanen et al., 2019). This is because winter ditch measurements have been conducted only in Lakkasuo and Lettosuo (Minkkinen and Laine, 2006; Korkiakoski et al., 2020). However, according to Eq. 2, the snowy season emission is comparatively low, only approximately 8%–16% of the snow-free season emission. This agrees well with the previous ditch data from Lakkasuo, where mean emissions in February were on average 16% of the mean snow-free season emissions (Minkkinen and Laine, 2006), and from Lettosuo, where winter emissions were negligible (i.e., ~0% of the snow-free season emissions) (Korkiakoski et al., 2020).

The daily snow-free and snowy season emissions were converted into seasonal emissions [i.e., for snow-free (May-October, 184 days) and snowy season emission (Nov-April, 181 days)]. The yearly $CH_4$ emission factor was then calculated as a sum of snow-free and snowy-season emissions for each measurement point. Thereafter, a study area specific emission factor was calculated for each ditch type as mean of all the ditch-type specific measurement points of the particular study area (Table 1). For some study areas, several emission factors were calculated for the same ditch type, if the measurement points represented several site types (Lakkasuo, Leppiniemi, Lylynneva, and Rantasuo), or the area consisted of two separate study sites (Koirasuo, Könölä) (Table 1). The calculated yearly emission factors are available in Dataset 4.

We tested first if site type or dataset type affected the analysis of the differences in yearly $CH_4$ emission factors between different types of ditches. For that, we employed two-way analysis of variance (2-ANOVA). Two models were built, one with 2-type classification (i.e., between moss-covered and moss-free) and site type as factors, and another with 2-type classification and dataset type as factors. For the site type—factor, the study areas were grouped into two groups, 1. Nutrient-rich, including Herb-rich (Rhtkg I and Rhtkg II) and *V. myrtillus* type (Mtkg I and Mtkg II), and, 2. Nutrient-poor, including *Vaccinium vitis-idaea* (Ptkg), Dwarf-shrub (Vatkg), and Lichen type (Jätkg) (Table 1). For the dataset type—factor, there were also two groups, 1. Old data, measured during multiple years between 1996 and 2015, with long chamber closure time (20–35 min) and analyzed with GC, and, 2. New data, measured in 2021, with short chamber closure time (3 min) and analyzed with portable gas analyzer (See Table 1 and above for the description of the $CH_4$ flux measurements).

After the preliminary 2-ANOVA analyses showing non-significant effect of site type and dataset type on $CH_4$ emission factors (reported below in Results), the final tests on the differences in yearly $CH_4$ emission factors between different types of ditches were done using *t*-test and one way analysis of variance (1-ANOVA) for the 2-type and 4-type classification schemes, respectively. Pairwise analyses following 1-ANOVA were conducted *via t*-test with Holm-Bonferroni adjustment of the *p*-value. Before t-tests and ANOVA analyses (1-ANOVA and afore-mentioned 2-ANOVA), the data were boxcox-transformed to improve the normality and variance homoscedasticity, which were tested using Shapiro-Wilk and Levene tests, respectively, and also inspected visually from residuals. Before boxcox-transformation, a constant (2 $g/m^2/y$) was added to each value, to make all the values positive. In addition to *t*-test and 1-ANOVA, the differences in $CH_4$ emission factors between ditch types were assessed *via* comparison of 95% confidence intervals, which were computed using a non-parametric bootstrap method due to non-normal distribution of the data. All the analyses were conducted in R (v. 4.1.1) (R Core Team, 2021) *via* R studio (v. 1.4.1106) (RStudio Team, 2020) using the packages MASS (v. 7.3.54) (Venables and Ripley, 2002), stats (v. 4.1.1) (R Core Team, 2021), car (v. 3.1.0) (Fox and Weisberg, 2019) and Hmisc (v. 4.7.0) (Harrell, 2022), and results visualized using the package ggplot2 (v. 3.3.6) (Wickham, 2016).

## 2.5 Estimation of the areal extent of different types of ditches in Finland

We estimated the areal extent of different types of ditches by 1) building a model to classify ditches into moss-covered and moss-free ditches, and 2) applying the classification model across Finland. We used SINKA database (Penttilä and Honkanen, 1986) to build the classification model. The SINKA database consists of a systematic subsample of the 7th National Forest Inventory field plots on drained peatlands. The field measurements were carried out in 1984–2013 in Southern Finland and in 2001–2013 in Northern Finland. Detailed descriptions of the SINKA data can be found in

Penttilä and Honkanen (1986) and previous studies utilizing the data (Repola et al., 2018; Hökkä et al., 2020). In addition to tree stand properties, the field observations included various ditch properties such as depth, age, width, slope, ditch condition, and primary and secondary factors that diminish ditch condition (FDC). In this study, the FDCs were categorized into two classes: 1) *Sphagnum* mosses and 2) other reasons (such as grasses and weeds, erosion, siltation, logging residues, etc.). *Sphagnum* mosses were assumed to represent mosses in general as other moss species were not stated in the list of FDCs.

Before utilizing the SINKA data for model building, we checked the data to remove observations unsuitable for this study. In addition to the observations that were found suspicious by Hökkä et al. (2020), the following conditions were used in outlining the data. If ditch condition was marked as "good" or "almost good", the FDC was allowed to be empty, but otherwise empty FDC observations were removed from the data. Only the ditches made by excavator and ditches classified as drainage ditches (lateral ditches) were included in the model building. Older digging methods were excluded to keep the data consistent with the currently existing forest ditches. FDC was included in the list of observations in the SINKA data only after 1990, which also limits the amount of data.

For model building, the ditches were classified as moss-covered if either primary or secondary FDC was *Sphagnum*. The accepted data consisted of 2,922 observations of which 1,358 (46%) were moss-covered ditches. The data were shuffled, and similar amount of moss-covered and moss-free observations were picked for model building. The data were divided into training (70%) and validation (30%) data sets to build a random forest (RF) classification model. The model was built using the randomForest package (v. 4.7–1.1) (Liaw and Wiener, 2002) in R. We tested multiple variable combinations and calculated classification error for moss-covered and moss-free ditches using the validation data set (Dataset 5; Dataset 6). In addition, we calculated errors for Southern Finland (north coordinate <7,200 000 in EPSG:2,393 projection) and Northern Finland to make sure the model would not produce geographically biased results. As the tested models tended to overestimate moss-covered ditches in the south and underestimate them in north, we also calculated over/underestimation percentage for both areas. The model for classifying the ditches was chosen based on 1) the availability of data to apply the model across Finland, and 2) the ability of the model to produce accurate and unbiased results for both ditch types and in the south and the north.

To apply the classification model across Finland, we constructed a spatial dataset where forestry-drained peatlands were segmented and assigned with various properties, similar to that described by Haakana et al. (2022). The segmented dataset covered whole Finland. The properties of each segment included segment area, length of ditches, stand volume separately for tree species, site fertility class, elevation, and temperature sums. Stand data were obtained from multisource national forest inventory data. Ditch lengths were calculated as a sum of ditch lines overlapping each segment. Ditch lines and elevation were available as open data from the National Land Survey of Finland. Temperature sums (above 5°C) were obtained from Finnish Meteorological Institute open data and presented as mean values from years 1980–2010. Ditch ages (latest ditching years) were obtained from the Finnish Forest Centre open data. Ditch age was available for 47% of the total ditch area. The classification model was then applied for the segmented data, and as a result the shares of moss-covered and moss-free ditches within Finland were obtained. The areas of both ditch types were calculated assuming 1 m ditch width similarly to the procedure in national GHG inventory (NIR Finland, 2022).

# 3 Results

## 3.1 Measured $CH_4$ fluxes in 2021

In this study, we report the temporal variation of ditch $CH_4$ emissions in different types of ditches in detail for the dataset gathered in 2021. The other datasets (from 1996 to 97, 2011, 2012 and 2014–15, see Table 1) were only used in calculations of the $CH_4$ emissions factors (see further). To observe the temporal variation in different types of ditches of the other datasets, we encourage the reader to utilize the $CH_4$ flux data published in Dataset 1.

Overall variation in ditch $CH_4$ fluxes was high, ranging from −412–4,012 μg $CH_4$ $m^{-2}$ $h^{-1}$ across the whole dataset, and from −412–3,666 μg $CH_4$ $m^{-2}$ $h^{-1}$, from −287–3,816 μg $CH_4$ $m^{-2}$ $h^{-1}$ and from −165–4,012 μg $CH_4$ $m^{-2}$ $h^{-1}$ for the nutrient-rich peatland forests Ränskälänkorpi, Lettosuo and Paroninkorpi, respectively (Table 2). In addition to the considerable temporal dynamics, which was especially apparent in moss-free ditches, this variation was caused by differences in the vegetation community between the measurement points (Figure 1). The $CH_4$ fluxes were generally higher at moss-free (i.e., open water) measurement points than at moss-covered points (Figure 1). The latter ones could even turn into $CH_4$ sinks occasionally during July-August in Ränskälänkorpi and Lettosuo (Figures 1A, B), which was associated with dry conditions, i.e., high air and ditch temperature (Supplementary Figures S20–23) and lowered WT (Supplementary Figure S24). Furthermore, moss-covered points with vascular plants had occasionally higher $CH_4$ fluxes than moss-covered points which were vascular plant - free (Figure 1). The $CH_4$ fluxes at moss- and vascular plant - covered measurement points were even higher than at plant-free (i.e., moss- and vascular plant—free) points in Ränskälänkorpi in June and July and in Paroninkorpi in July (Figures 1A, C). In the Lettosuo study area, it was also possible to compare $CH_4$ flux between measurement points covered by two different moss genera (Figure 1B). The magnitude and temporal variation in $CH_4$ flux profiles were quite similar between points covered by *Polytrichum* and *Sphagnum* mosses (Figure 1B). Yet, $CH_4$ sink was slightly more efficient in *Polytrichum*- than in *Sphagnum*-covered measurement points during July, and *Polytrichum* - covered points had higher $CH_4$ emissions in late September (Figure 1B).

## 3.2 $CH_4$ emission factors

The ditches in the whole dataset consisting of 21 study areas were classified using 2-type and 4-type classification schemes (Table 1, Dataset 1). According to the preliminary 2-ANOVA analyses, ditch type (i.e., moss-free and moss-covered) had an

**TABLE 2 Average, median and range of $CH_4$ emission/sink measurements from ditches of boreal forestry-drained peatlands in Finland and in other countries.**

| Study area (country) | Year | $CH_4$ (μg $m^{-2}$ $h^{-1}$) | | | | References |
|---|---|---|---|---|---|---|
| | | Average | Median | min | Max | |
| Data used for $CH_4$ emission factor | | | | | | |
| Ränskälänkorpi (Finland) | 2021 | 179 | 36 | −412 | 3,666 | This study |
| Lettosuo (Finland) | 2021 | 502 | 120 | −287 | 3,816 | This study |
| Paroninkorpi (Finland) | 2021 | 324 | 68 | −165 | 4,012 | This study |
| 14 study areas (Finland)[a] | 2014–2015 | 1,302 | 217 | −2,283 | 30,739 | This study |
| Konilampi and Vesijako (Finland) | 2012 | 1,922 | 3 | −34 | 7,908 | Koskinen et al. (2016) |
| Kalevansuo (Finland) | 2011 | 234 | 34 | −98 | 1,757 | Minkkinen et al. (2018) |
| Lakkasuo (Finland) | 1996–1997 | 12,375 | 6,371 | −47 | 146,341 | Minkkinen and Laine. (2006) |
| Other data from Finland | | | | | | |
| Lettosuo (Finland) | 2015–2017 | 127/2,754[b] | n.d. | −238 | 10,894 | Korkiakoski et al. (2020) |
| Lakkasuo (Finland) | 1995 | 5,065 | 3,210 | 0 | 24,807 | Minkkinen et al. (1997) |
| Data from foreign study areas | | | | | | |
| Asa Experimental Forest (Sweden) | 1999–2002[c] | 300–520[d] | n.d. | n.d. | n.d. | von Arnold et al. (2005) |
| Tobo (Sweden) | 2018–2019 | 3–224[e] | 0–5[e] | −31 | 5,695 | Tong et al. (2022) |
| Wally Creek (Canada) | 1991 | 838–5,825[f] | n.d. | ~0 | 39,583 | Roulet and Moore (1995) |

[a]See Table 1 for the names of the 14 study areas in dataset from 2014 to 2015.
[b]Two average values reported: 1. moss-filled ditch, and 2. Water-filled ditch.
[c]The exact year of ditch measurements is not reported.
[d]Min – max of four reported average values from 1. Site with young trees 13th June, 2. Site with young trees 27th June, 3. Site with old trees 13th June, and 4. Site with old trees 27th June.
[e]Min – max of four reported average and median values from 1. Uncleaned ditch in 2018, 2. Uncleaned ditch in 2019, 3. Cleaned ditch in 2018, and 4. Cleaned ditch in 2019.
[f]Min – max of three reported average values from 1. Treed bog, 2. Forested bog, and 3. Treed fen.

effect ($p < 0.05$), while either the site type (nutrient-rich vs. nutrient-poor) or the dataset type (old data 1996–2015 vs. new data 2021) did not affect the $CH_4$ emission factor ($p > 0.05$, Supplementary Figures S25, S26). However, there was a tendency, albeit only marginally significant ($0.05 < p < 0.10$), for the $CH_4$ emission to be lower in nutrient-rich than in nutrient-poor sites (Supplementary Figure S25). In addition, based on visual observation of the Supplementary Figure S26, the $CH_4$ emission factor tended to be lower, albeit not statistically significantly, in the new than in the old dataset. As the new dataset consisted only of nutrient-rich sites (i.e., Rhtkg or Mtkg, Table 1), we cannot conclude to what extent the marginally significant differences in $CH_4$ emission factor between the nutrient-rich and the nutrient-poor sites stem from differences in fertility and to what extent from differences in methods between the old and the new datasets (see Materials and Methods). Therefore, and given the non-significant effects of site and dataset type on $CH_4$ emission factor, we decided to calculate the final $CH_4$ emission factors only for different ditch types irrespective of the site type (Table 3).

In the 2-type classification scheme, the $CH_4$ emission factor for moss-covered ditches was approximately 1/8 of that for moss-free ditches (Table 3; Figure 2). In the 4-type classification scheme, the $CH_4$ emission factor was lowest for *Sphagnum*-covered, vascular plant-free ditches, being approximately 1/6 of that for *Sphagnum*- and vascular plant-covered ditches. The highest emission factors were estimated for plant-free ditches (Table 3; Figure 3). They were approximately 41 and 7 times as high as for the *Sphagnum*-covered, vascular plant-free and *Sphagnum*- and vascular plant—covered ditches, respectively (Table 3; Figure 3). The second highest emission factor was observed for moss-free, vascular plant-covered ditches, which differed statistically significantly only from *Sphagnum*-covered, vascular plant-free ditches (Table 3; Figure 3). Emission factors were also calculated for rare ditch types (those represented by ≤ 2 replicate estimates) including ditches covered with *Polytrichum* (moss), co-covered with *Polytrichum* and *Sphagnum*, and co-covered with *Calliergon* (moss), *Polytrichum*, *Sphagnum* and vascular plants, with the values of same magnitude as *Sphagnum*-covered, vascular plant-free ditches in the 4-type classification scheme (Table 3). These data were included in analyses based on the 2-type classification (in the type of moss-covered ditches) but was left out from the analyses based on the 4-type classification.

The mean and 95% confidence interval of the default Tier 1 emission factor for $CH_4$ emissions of ditches of drained forest land and drained wetland of temperate and boreal area (IPCC, 2014) was compared with those developed in this study for different types of ditches of forestry-drained boreal peatlands of Finland (Table 3). Based on the comparison of means and overlapping 95% confidence intervals, the Tier 1 emission factor is similar to our estimates of average $CH_4$ emission factors for moss-free ditches in the 2-type classification scheme and *Sphagnum*-free vascular plant-covered and plant-free ditches in the 4-type classification schemes

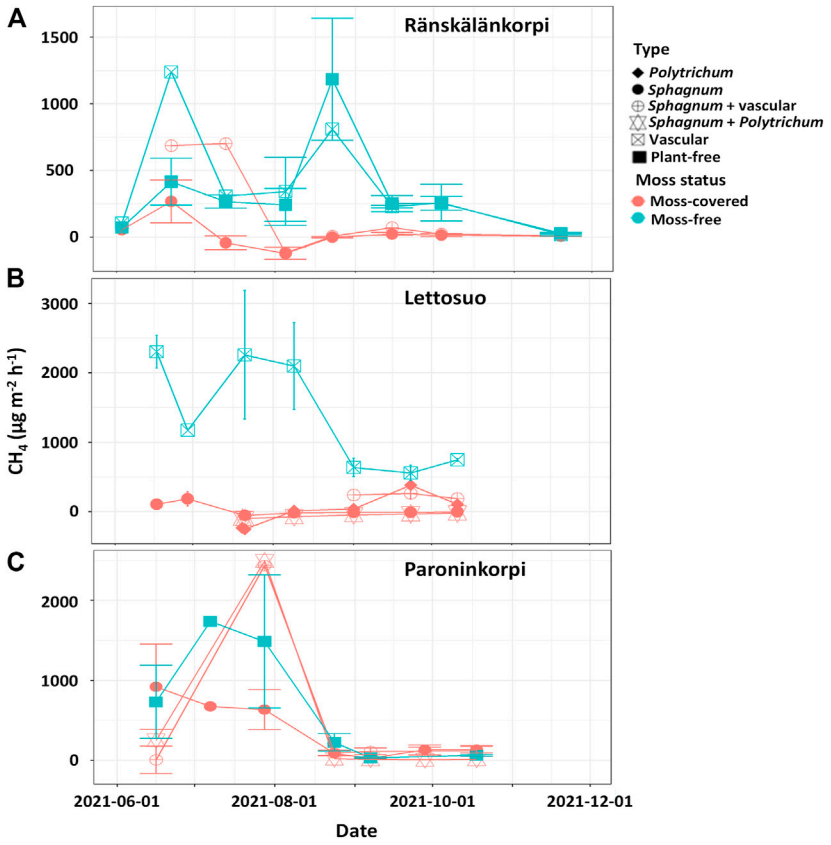


FIGURE 1
Temporal variation of measured $CH_4$ flux in different types of measurement points of ditches (average +/- SE) at **(A)** Ränskälänkorpi, **(B)** Lettosuo, and **(C)** Paroninkorpi forestry-drained peatland area in 2021.

(Table 3). In contrast, it is 8 times as high as our estimates for moss-covered ditches in the 2-type classification scheme, and 36 times as high as our estimates for *Sphagnum*-covered vascular plant-free ditches in the 4-type classification scheme (Table 3). It is also 6 times as high as our estimates for *Sphagnum*-and vascular plant - covered ditches in the 4-type classification scheme, yet there is slight overlap in the 95% confidence intervals (Table 3). The Tier 1 emission factor is also higher than those estimated for the rare ditch types, i.e., those including also other moss taxa than *Sphagnum* (Table 3).

## 3.3 Estimation of the areas of various ditch types

We estimated the area of moss-covered and moss-free ditches of forestry-drained peatlands of Finland. The tested RF classification models produced overall errors with validation data varying from 11% to 19%. Based on mean decrease in accuracy, the most important variables included ditch properties (age, depth, and width) and those related to climatic conditions (north coordinate, temperature sum, and elevation), and peat layer thickness (Dataset 5). In addition, including site fertility, tree species type (coniferous/deciduous), or ditch spacing among the variables improved model performance in many cases. Models RF1, RF3, RF5, and RF25 provided the lowest average of different error types (<12%). Most of the tested models had a tendency to underestimate the area of moss-covered ditches in the north. The model selected for application over Finland (RF25) was able to produce relatively unbiased results with low errors (11%–13%).

The selected model (RF25) included ditch age, north coordinate, elevation, and temperature sum as continuous variables and site fertility as a class variable (Figure 4, Supplementary Figure S27). In nutrient poor sites (*V. vitis-idaea* type (Ptkg), Dwarf-shrub type (Vatkg)), older age increased the probability of moss-coverage in a ditch until the ditch was 40 years old (Figure 4E). In more fertile sites (Herb-rich type (Rhtkg), *V. myrtillus* type (Mtkg)), moss-coverage increased until ditch was 30 years old (Figure 4F). North coordinate, elevation, and temperature sum together represent climate conditions in the classification model. The probability of moss coverage increased towards warmer conditions in all ditches (Figures 4A–D). However, the effect was more substantial in less fertile sites.

Ditch age was available for 47% of the total ditch area. Ditch age varied from 1 to 115 years with mean age being 37 years. The model RF25 was applied over these ditches, and model RF42 was applied to ditches with missing ditch age data. With an overall error of 19%, the model RF42 did not perform as well as models with ditch age as a variable (Dataset 5). A small percentage of ditches did not have all the required variables available for the selected models, and it was assumed that the proportions of moss-covered and moss-free

**TABLE 3** $CH_4$ emission factors [mean, standard error (SE), 95% confidence interval (CI), range and number of replicates (N)] for different types of ditches of boreal forestry-drained peatlands in Finland. Different letters in D column show statistical differences between ditch types in the 2-type (*t*-test, t (31) = −4.0336, $p < 0.001$) and 4-type classification schemes (1-ANOVA, F (3, 33) = 10.53, $p < 0.001$; Pairwise *t*-test with Holm-Bonferroni adjustment of the *p*-value, $p < 0.05$), which were also further confirmed by comparison of 95% CIs (i.e., non-overlapping 95% CIs indicate significant difference). The Tier 1 $CH_4$ emission factor (mean, 95% CI and N) for ditches of drained forest land and drained wetland of temperate and boreal area is shown for comparison.

| Classification scheme | Mean | SE | 95% CI[a] | | Range | | N | D |
|---|---|---|---|---|---|---|---|---|
| | (g $CH_4$ $m^{-2}$ $y^{-1}$) | | min | max | min | max | | |
| 2 types of ditches | | | | | | | | |
| moss-covered | 2.6 | 0.8 | 1.3 | 4.0 | −0.3 | 13.0 | 20 | a |
| moss-free | 20.6 | 7.0 | 9.3 | 34.0 | 0.9 | 77.8 | 13 | b |
| 4 types of ditches | | | | | | | | |
| *Sphagnum* | 0.6 | 0.3 | 0.1 | 1.1 | −0.3 | 2.4 | 10 | a |
| *Sphagnum* + vascular | 3.8 | 1.1 | 1.8 | 6.2 | 0.8 | 13.0 | 14 | b |
| vascular | 8.8 | 3.2 | 3.0 | 14.5 | 1.7 | 16.6 | 5 | bc |
| plant-free | 25.1 | 9.7 | 8.3 | 44.2 | 0.9 | 77.8 | 9 | c |
| Outside of 4-type classification[b] | 0.7 | 0.6 | n/d | n/d | −0.3 | 2.4 | 4 | |
| IPCC Tier 1 default[c] | 21.7 | n/d | 4.1 | 39.3 | n/d | n/d | 11[d] | |

[a]95% confidence interval was calculated using bootstrapping for ditches in the 2-type and 4-type classification schemes.
[b]Ditch types included in the 2-type (in moss-covered class) but not in the 4-type classification, including *Polytrichum*-covered (1), *Polytrichum* and *Sphagnum*-covered (2), and *Calliergon*, *Polytrichum*, *Sphagnum* and vascular plant—covered (1).
[c]IPCC, 2014.
[d]Number of study sites (IPCC, 2014).

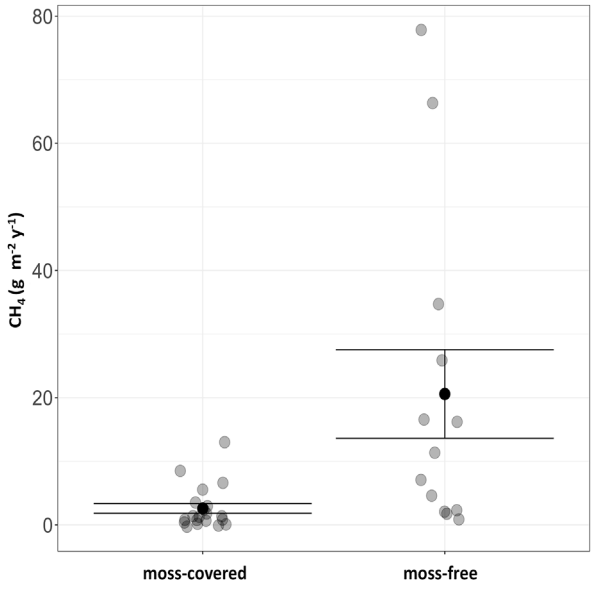


FIGURE 2
$CH_4$ emission factors in the 2-type classification scheme of ditches of boreal forestry-drained peatlands. Shown are average ± SE (in black) calculated from the replicate observations (in grey). The difference between the groups is statistically significant (*t*-test; t (31) = −4.0336, $p < 0.001$).

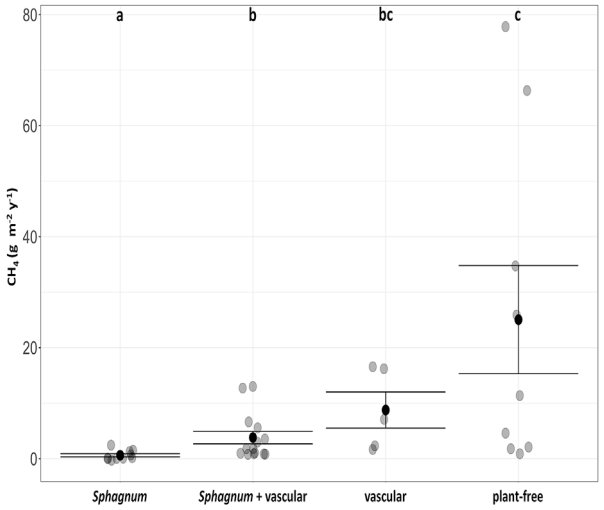


FIGURE 3
$CH_4$ emission factors in the 4-type classification scheme of ditches of boreal forestry-drained peatlands. Shown are average ± SE (in black) calculated from the replicate observations (in grey). Different letter (top-part of the figure) denote significant pairwise differences between groups (1-ANOVA, F (3, 33) = 10.53, $p < 0.001$; Pairwise *t*-test with Holm-Bonferroni adjustment of the *p*-value, $p < 0.05$).

ditches in the results also represent those ditches (Table 4). Applying the models for the segmented data over Finland resulted in 68,359 ha (67%) of moss-covered ditches and 33,349 ha (33%) of moss-free ditches. In southern Finland, 79% of the ditches were classified moss-covered, while in northern Finland 41% were moss-covered. 69% of the ditches were located in southern Finland (70,322 ha).

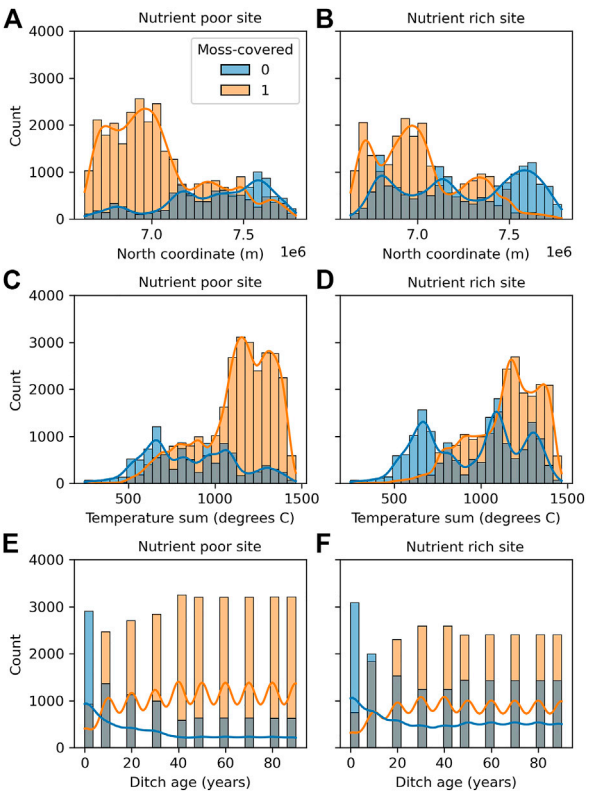


FIGURE 4
Demonstration of classification model RF25 results using regular point grid (10 km spacing within whole Finland, resulting in 3,829 grid points) and varying ditch age (0, 10, ..., 90 years) separately for nutrient poor **(A,C,E)** and nutrient rich sites **(B,D,F)**. In total, there were 76,580 points to classify. Note that the distributions demonstrate model performance within the 76,580 points, and thus the figures do not represent the real distributions of moss-coverage in Finland since the geographical distribution of ditches and their parameters are different in reality. Note also that the grey bars in the figure represent the areas where the orange and blue bars for moss-covered and moss-free ditches overlap.

**TABLE 4** Drained peatland areas and ditch areas in all segmented data and within the data where parameters were available for application for the random forest classifiers RF25 (segments with ditch age available) and RF42 (segments without ditch age available) (see Datasets 5 and 6).

| | | North[a] | South[b] | All |
|---|---|---|---|---|
| Drained peatland area | All data ($10^6$ ha) | 1.709 | 2.859 | 4.568 |
| | Available data ($10^6$ ha) | 1.638 | 2.777 | 4.415 |
| | All data (%) | 37% | 63% | 100% |
| | Available data (%) | 37% | 63% | 100% |
| Ditches, all types | All data (ha) | 31,387 | 70,322 | 101,709 |
| | Available data (ha) | 30,509 | 69,607 | 100,116 |
| | All data (%) | 31% | 69% | 100% |
| | Available data (%) | 30% | 70% | 100% |
| Ditches, moss-covered | All data (ha) | 12,910 | 55,449 | 68,359 |
| | Available data (ha) | 12,549 | 54,885 | 67,435 |
| | All data (%) | 41% | 79% | 67% |
| | Available data (%) | 41% | 79% | 67% |
| Ditches, moss-free | All data (ha) | 18,476 | 14,873 | 33,349 |
| | Available data (ha) | 17,960 | 14,722 | 32,681 |
| | All data (%) | 59% | 21% | 33% |
| | Available data (%) | 59% | 21% | 33% |

[a]North refers to North coordinate ≥7,200 000 in EPSG 2393 projection.
[b]South refers to North coordinate <7,200 000 in EPSG 2393 projection.

## 3.4 Ditch $CH_4$ emissions of forestry-drained boreal peatlands in Finland

With the mean emission factors (Table 3) and estimated ditch areas for moss-covered and moss-free ditches (Table 4), the total ditch $CH_4$ emissions for Finland were 8,600 t $a^{-1}$ (Table 5). Overall variation in $CH_4$ emissions caused by the 95% confidence level of the emission factor was from 4,000 t $a^{-1}$ (−54%) to 14,100 t $a^{-1}$ (+63%).

# 4 Discussion

Our results show that the currently used IPCC Tier 1 emission factor likely overestimates $CH_4$ emissions of ditches of boreal, forestry-drained peatlands in Finland through large overestimation of the emissions of moss-covered ditches, irrespective of whether they harbor potentially $CH_4$ conducing vascular plants (Table 3; Figures 2, 3). Consequently, the usage of the here-developed emission factors and the ditch-type specific areal estimates would lead to a 63% lower estimate of ditch $CH_4$ emissions than previously estimated for the greenhouse gas reporting in Finland (Table 5). Based on the comparison of hourly $CH_4$ fluxes between foreign datasets and the compiled Finnish dataset used for calculation of the $CH_4$ emission factors in this study, the magnitude of $CH_4$ fluxes from ditches of forestry-drained peatlands is not generally different between Finland and other countries (Table 2). This suggests that the Tier 1 emission factor overestimates $CH_4$ emissions of ditches of forestry-drained boreal peatlands also in other countries than in Finland.

## 4.1 $CH_4$ fluxes of ditches of Ränskälänkorpi, Lettosuo and Paroninkorpi

Overall, the $CH_4$ fluxes measured from the ditches of the three relatively nutrient-rich peatland forests in southern Finland (study sites in Ränskälänkorpi, Lettosuo and Paroninkorpi) in 2021 were of similar magnitude as measured previously for the Finnish site Kalevansuo and study areas in Sweden (Table 2). However, the fluxes were generally lower than measured previously for other Finnish sites as well as for study areas in Canada (Table 2). It is not in

**TABLE 5** Ditch areas and $CH_4$ emissions for moss-covered and moss-free ditches in Finland. The shares of moss-covered and moss-free ditch areas (Table 4) are based on the results from models RF25 and RF42 (see Datasets 5 and 6). For emission factors (mean and 95% confidence interval (CI)), see Table 3.

| Ditch area data source | Ditch type | Ditch area (ha) | $CH_4$ emissions (t $a^{-1}$) with different emission factors | | | | | |
|---|---|---|---|---|---|---|---|---|
| | | | Mean | 95% CI, min | 95% CI, max | IPCC Tier 1, mean | IPCC Tier 1, 95% CI, min | IPCC Tier 1, 95% CI, max |
| Segmented data | moss-covered | 68,359 | 1,771 | 882 | 2,748 | | | |
| | moss-free | 33,349 | 6,867 | 3,095 | 11,349 | | | |
| | all | 101,709 | 8,637 | 3,977 | 14,097 | 22,071 | 4,170 | 39,972 |
| Current $CH_4$ inventory | moss-covered[a] | 71,865 | 1,861 | 927 | 2,889 | | | |
| | moss-free[a] | 35,060 | 7,219 | 3,254 | 11,931 | | | |
| | all | 106 925[b] | 9,080 | 4,181 | 14,820 | 23,203 | 4,384 | 42,022 |

[a]Assuming a similar percentage of moss-covered (67%) and moss-free (33%) ditches as calculated in Table 4.
[b]From NIR finland, 2022.

the scope of this study to assess the factors affecting differences in $CH_4$ emissions between study areas. However, it can be speculated that the differences between our study and the study from Canada can be due to much younger ditches (ditches dug 7 years before sampling) in the Canadian study area (Roulet and Moore, 1995) than in Ränskälänsuo, Lettosuo and Paroninkorpi (>50 years) (Laurila et al., 2021; Palviainen et al., 2022) during the time of measurements. For Lettosuo, the fluxes measured in this study in 2021 were at the lower end of range measured previously in 2015–2017 (Table 2). This can be due to higher summer temperatures (higher than the 30-year average, Supplementary Figure S21) in 2021 than in 2015–2017 (generally lower than the 30-year average) (Korkiakoski et al., 2020).

The higher fluxes in moss-free than in moss-covered measurement points, and the occurrence of occasional $CH_4$ sinks in moss-covered points (Figure 1), agree with results from previous studies (Minkkinen and Laine, 2006; Korkiakoski et al., 2020). This may be explained by active $CH_4$ - consuming bacteria (methanotrophs) living in and on mosses, especially in and on *Sphagnum* mosses (Raghoebarsing et al., 2005; Kolton et al., 2022), and in water and sediments below the mosses. In fact, the moss-covered measurement points of two study areas, Ränskälänkorpi and Lettosuo, turned into net $CH_4$ sinks in mid-summer when the WT was at relatively low level (Figures 1A, B; Supplementary Figure S24). This was probably due to decreased WT inducing aerobic conditions and consequently increasing aerobic $CH_4$ oxidation and decreasing *in situ* methanogenesis. This condition agrees with that in the strips of forestry-drained peatlands which are usually net $CH_4$ sinks (e.g., Huttunen et al., 2003; Korkiakoski et al., 2020). Input of dissolved $CH_4$ from surrounding peat strips *via* drainage and ground water can be also expected to be lower during periods of low WT, which further decreases emissions from ditches. In addition, it has been shown that *Sphagnum* leachates potentially inhibit methanogenesis further decreasing methane emissions from moss-covered ditches (Medvedeff et al., 2015).

A slightly stronger occasional $CH_4$ sink was noticed in *Polytrichum*-covered than in *Sphagnum*-covered measurement points, and there was also general similarity in the extent and temporal variation in net $CH_4$ fluxes and sinks between *Polytrichum* and *Sphagnum*—covered points in Lettosuo (Figure 1B). This suggests that besides *Sphagnum*, methane oxidation may be associated also with *Polytrichum* mosses, but further studies are needed to confirm whether *Polytrichum* mosses harbor active methanotrophs in or on their cells, or whether methanotrophs inhabit the surface sediment or peat below the moss. The occasional high fluxes from moss-covered measurement points having vascular plants also agree with previous studies and is likely due to $CH_4$ being conducted through the aerenchyma of the plants into atmosphere, bypassing the sediment, peat, water and moss-associated methanotrophs (Figure 1) (Schimel, 1995; Frenzel and Karofeld, 2000; Minkkinen and Laine, 2006). Furthermore, plant root exudates can also increase methane production (Waldo et al., 2019).

In addition to the absence of moss-associated methanotrophs, the high $CH_4$ emissions from moss-free open water ditches can be also partially due to higher input of dissolved $CH_4$ from surrounding peat strips *via* drainage and ground water. Contribution of strip $CH_4$ in ditch emissions has been considered to be especially important in moss-free ditches with moving water, which have much higher $CH_4$ emissions than those with stagnant water (Minkkinen and Laine, 2006; Sirin et al., 2012).

## 4.2 $CH_4$ emission factors

$CH_4$ emissions from moss-free ditches were much higher than those from moss-covered ditches and the presence of vascular plants increased $CH_4$ emissions from moss-covered ditches (Table 3; Figure 2; Figure 3). These results are consistent with earlier studies (Minkkinen and Laine, 2006; Korkiakoski et al., 2020). Interestingly, there was also a tendency, albeit not statistically significant, for the presence of vascular plants decreasing $CH_4$ emissions from moss-free ditches compared to those without vascular plants (Table 3; Figure 3). As vascular plants can be speculated more likely to take root in stagnant than in flowing water, we assume that the presence and absence of vascular plants in

moss-free ditches can reflect water flow dynamics in ditches. Hence, the moss-free ditches with vascular plants more likely include ditches with stagnant water than those without vascular plants. As discussed above, the $CH_4$ emissions are lower from ditches with stagnant than with flowing water (Minkkinen and Laine, 2006; Sirin et al., 2012).

It should be noted here that our estimates on the $CH_4$ emission factors are based on diffusive fluxes, hence, excluding possible ebullition (see Material and Methods). The only existing studies on $CH_4$ ebullition of ditches of boreal forestry-drained peatlands were done in one of our study sites, Lakkasuo, and showed no ebullition in vegetated ditches (*Sphagnum* and vascular plants) but only in non-vegetated, open water ditches, yet contributing there only 0.2%–22% of the diffusive flux (Minkkinen et al., 1997; Minkkinen and Laine, 2006). Furthermore, our non-quantitative measurements in a non-vegetated, open water ditch in Ränskälänkorpi also suggest that ebullition occurs only infrequently (see Materials and Methods). Hence, our estimates on ditch $CH_4$ emissions can be underestimated, but we do not consider this to affect the major patterns detected in this study. However, due to the rarity of the ebullition data, we think that there is a need for further studies on the quantitative importance of ebullitive $CH_4$ fluxes of different types of ditches of boreal forestry-drained peatlands.

We also acknowledge that there are subjective factors causing uncertainty in the $CH_4$ emission results. As the $CH_4$ measurements from wet surfaces are prone to interferences (gas leaks, unwanted chamber movement, measurement-induced ebullition, and analyzer malfunction), the measurement quality can differ between different persons conducting the measurements. In addition, the post-measurement manual screening of the concentration-time graphs to detect and discard the interfered flux data is partially a subjective process. The visual but not statistically significant difference in $CH_4$ emissions between old data (1996–2015) and new data (2021) (Supplementary Figure S26) also hints towards the possibility that the new measurement method (i.e., short chamber closure time; portable gas analyzer) would lead to lower estimates of $CH_4$ emissions than the old method (long chamber closure time; GC) used in majority of the previous studies (Supplementary Table S1). This could be tested in future studies, because the new method is being increasingly used. We also acknowledge that the calculation of the $CH_4$ emission factors was based on a simplified approach, i.e., calculation of mean snow-free season $CH_4$ emission and estimation of the snowy season emission from the snow-free season emission using published equations (see Materials and Methods). Future studies could also measure snowy season emissions, despite they should not much affect the yearly $CH_4$ emission estimate (i.e., are only on average 0%–16% of snow-free season emissions) of ditches of boreal, forestry-drained peatlands (Minkkinen and Laine, 2006; Korkiakoski et al., 2020). In future, process-based modelling, taking into account factors known to affect microbial processes and ditch $CH_4$ emissions, e.g., temperature, hydrological conditions, water movement, water quality, vascular plant and moss community, and moss-associated methanotrophy, could be useful in even more accurate estimations of ditch $CH_4$ emissions and in predicting their changes under changing climate and forestry and land-use practices.

Within time, the majority of ditches of forestry-drained peatlands can be expected to be covered by mosses. For instance, in southwestern Finland mosses typically cover 35% and 43% of the ditches already 5 or 10 years after ditch cleaning, respectively (Silver and Joensuu, 2005). Also, in our model (RF25), age increased the probability of moss-coverage in a ditch until the ditch was 30–40 years old (Figures 4E, F; Supplementary Figure S27). Based on our results on the much lower $CH_4$ emissions estimated for moss-covered than for moss-free ditches, ditch age leads to decreased $CH_4$ emissions. Active ditch network maintenance *via* ditch cleaning, i.e., removal of soil, moss and other plants from ditches, is a typical forestry practice to sustain and improve the drainage conditions of forest soils (Nieminen et al., 2018). In rotation forestry, which is the most common forest management method in Finland and the other Nordic countries, ditch cleaning is applied to lower the increased water table level, caused by decreased evapotranspiration after clearcutting, to enhance growth of new tree seedlings. Based on our results, removing moss-cover of the ditches is expected to increase their $CH_4$ emissions. Hence, this suggests that the current practice in Finland, towards minimizing ditch network maintenance (i.e., ditch cleaning) to decrease the discharge of suspended solids, would also decrease the ditch $CH_4$ emissions.

However, according to the only existing study, a case study from Sweden, on the effects of post-harvest ditch cleaning on ditch $CH_4$ emissions in forestry-drained peatlands, cleaned ditches have lower $CH_4$ emissions than uncleaned ditches during the first 2 years after ditch cleaning (Tong et al., 2022). This can be due to higher occurrence of water-logged conditions in uncleaned than in cleaned ditches (Tong et al., 2022). Waterlogged conditions likely enhance methanogenesis *via* anaerobiosis. Furthermore, in uncleaned ditches, vascular plants likely conduct $CH_4$ to the atmosphere and generate labile methanogenic compounds. However, the ditches studied by Tong et al. (2022) were relatively dry, which may have had increased soil aeration leading to decreased $CH_4$ emissions *via* increased and decreased within-ditch $CH_4$ oxidation and methanogenesis, respectively. Dry conditions (low WT) can be also expected to have decreased ditch $CH_4$ emissions *via* decreasing $CH_4$ transport from strips to ditches. The contrary outcomes by our study and Tong et al. (2022) suggests that the effects of ditch cleaning on ditch $CH_4$ emissions depend on the hydrological conditions and the prior extent and quality of plant and moss coverage, and, thus, require further studies. However, it must be noted that while Tong et al. (2022) compared the $CH_4$ emissions of newly cleaned ditches to those of old ditches, the ditches in our dataset had not been cleaned lately making it difficult to directly compare the studies. Furthermore, in contrast to Tong et al. (2022) including only one study area, our dataset of 21 study areas covered ditches of varying hydrological conditions (from dry to wet) and study years with varying temperature and precipitation compared to the 30-year average (Supplementary Figures S2–S22). Hence, combining data from these 21 study areas, we can generalize to ditches of boreal forestry-drained peatlands to conclude that removal of moss-cover *via* ditch cleaning likely increases $CH_4$ emissions from ditches.

It should be, however, noted, that without ditch cleaning after clearcutting, the increase in the water table level can cause the $CH_4$

sink of forest floor to decrease and can even turn the forest floor to a $CH_4$ source (Korkiakoski et al., 2019). In contrast, in continuous cover forestry, where only part of the tree stand is removed in cuttings, ditch cleaning is not necessary, since the water level is kept at a sufficiently low level by sustained evapotranspiration (Leppä et al., 2020a; Leppä et al., 2020b). Consequently, as suggested by results of Korkiakoski et al. (2020), the forest floor $CH_4$ emissions do not increase after partial harvesting. Recent modelling results also suggest that financially profitable continuous cover forestry may be sustained without ditch network maintenance when the post-harvest basal area is higher than 10 $m^2$ $ha^{-1}$ (Juutinen et al., 2021).

Soil preparation after clearcuttings, *via* mounding and scalping, can also affect the forest floor $CH_4$ emissions (Pearson et al., 2012). In addition to mounding, ditch-mounding is an often-applied method to create mounds for tree seedlings to enhance their growth. Digging of the mound material results in shallow ditches, which can affect water flow directions but do not belong to the main ditch networks and hence have only marginal effects on the drying process of forestry-drained peatlands. The surface area of ditches resulting from ditch-mounding is currently not known but can be reasonably large. Their $CH_4$ emissions are also not taken into account in the national GHG inventory (NIR Finland, 2022). Given the high $CH_4$ emissions detected in this study for plant-free ditches, we suggest that the $CH_4$ emissions of the ditches resulting from ditch-mounding should be taken into account in future GHG inventories.

### 4.3 $CH_4$ emissions from ditches of forestry-drained peatlands in Finland

Our results suggest that ditch $CH_4$ emission estimate for Finland (Table 5) may be clearly smaller (8,637 t $a^{-1}$) than previously estimated for the greenhouse gas reporting (23,203 t $a^{-1}$) (NIR Finland, 2022). This is a result of the lower emission factors for moss-covered ditches that were discussed above, and the proportions of ditch area estimates for ditch types. We estimated that 67% of the ditches were moss-covered. Silver and Joensuu. (2005) found that in southwestern Finland mosses typically cover 35% and 43% of the ditches already 5 or 10 years after ditch cleaning, respectively. The average ditch in Finland is most likely older because ditch cleaning is recommended at 20–40-year intervals (Vanhatalo et al., 2019). Thus, it can be assumed that in southern Finland the moss-coverage would be clearly over 43%. Based on the restricted SINKA data, which covered wider geographic area, average ditch age was 18 and 19 years, and the share of moss-covered ditches was 53% and 38% in southern and northern Finland, respectively. The higher proportion of moss-covered ditches can be at least partly explained by the older ditches in the data used in this study. The occurrence of ditch cleaning has been strongly decreasing in Finland in the last 20 years (Natural Resources Institute Finland, 2022), which could explain the high mean age of ditches.

The random forest model was based on drainage ditches which leads to uncertainties in estimating other ditch types. Collector ditches and main ditches are typically deeper and carry more water which increases the possibility for erosion. Applying our classification model to such ditches could overestimate the moss-coverage because ditch depth data was not available. However, drainage ditches are the most typical ditch type in forestry drainage and thus the overall overestimation should not be large.

In the selected classification model (RF25), the probability for moss-covered ditches increased with ditch age until ditches were 30–40 years old (Figures 4E, F; Supplementary Figure S27). After that the situation was quite stable. This could indicate that moss-coverage is established within 40 years if it is established at all. In fertile sites, moss coverage was established sooner than in less fertile sites. However, it should also be noted that most of the ditches in the training data were less than 40 years old which could lead to stable classification results in older ditches. In the model results, the probability for moss-coverage was higher in less fertile sites (Figure 4). Such a trend can also be seen in the sites listed in Table 1. Silver and Joensuu. (2005) also found out that *Sphagnum* moss coverage in peatland ditches was higher in less fertile sites. Possible reasons could include that *Sphagnum* mosses typically grow in nutrient poor sites and light conditions in ditches are more favorable in less fertile sites with sparser tree stands. Sparser tree stand can also help in keeping water table level from falling below ditch bottom level during dry periods which can be beneficial for mosses. However, the specific mechanisms behind the differences caused by site fertility remain unclear and require further studies.

## 5 Conclusion

Moss-free ditches may have several times higher methane emissions than moss-covered ditches in forestry-drained boreal peatlands. The IPCC default Tier 1 emission factor significantly overestimates $CH_4$ emissions of moss-covered ditches of forestry-drained boreal peatlands in Finland and the use of ditch type-specific emission factors can improve substantially the accuracy of ditch emissions estimates. The majority of the ditches (67%) were classified as moss-covered ditches, which together with the new emission factors resulted in 63% lower $CH_4$ emission estimate for ditches of peatland forests in Finland than in the current GHG inventory. Furthermore, our results indicate that the current practice in Finland to minimize ditch-network maintenance by ditch cleaning will likely decrease $CH_4$ emissions from ditches, since old moss-covered ditches have very low $CH_4$ emissions.

## Data availability statement

The datasets presented in this study can be found online in Zenodo repository: https://doi.org/10.5281/zenodo.7341325.

## Author contributions

AR, Formal analysis, Investigation, Writing-Original Draft, Writing-Review and Editing, Visualization. PO, Conceptualization, Formal analysis, Investigation, Writing-Review and Editing, Project Administration, Funding acquisition. LS, Formal analysis, Investigation, Writing-Review and Editing, Visualization. TL, Conceptualization, Investigation, Writing-Review and Editing, Project Administration, Funding acquisition. JA, Software, Formal analysis, Resources, Data

curation, Writing-Review and Editing. ST, Methodology, Formal analysis, Investigation, Writing-Review and Editing. KM, Investigation, Writing-Review and Editing, Funding acquisition. MK, Investigation, Writing-Review and Editing. RM, Conceptualization, Writing-Review and Editing, Project Administration, Funding acquisition, Resources. All authors have read and agreed to the published version of the manuscript.

## Funding

This study was part of Maaperätiedon kehittäminen (MaaTi) project funded by Ministry of Agriculture and Forestry of Finland. The measurements of the 2014–2015 data were funded by LIFE+ (LIFEPeatLandUse, LIFE12ENV/FI/150). Open access funding was provided by Tampere University.

## Acknowledgments

We thank Timo Penttilä for providing us with data, Hannu Hökkä for supporting the processing of SINKA data and random forest model building, Petri Salovaara for coordinating the field measurements. We also want to thank Kyle Eyvindson, Aura Salmivaara, Andras Balazs, and Markus Haakana for providing and helping with the drained peatland segmented data. In addition, the following persons are acknowledged for their contribution in flux measurements in the field: Ilona Kerovuori, Juulia Suikula, Oona Keskisaari, Tiia Määttä, Tiina Heikkinen, Angela Lafuente, Kaisa Silvan, Mari Parkkari and Raimo Pikkupeura. The authors also wish to acknowledge CSC—IT Center for Science, Finland, for computational resources. Reviewers are acknowledged for their valuable comments and suggestions that improved the paper.

## Conflict of interest

The authors declare that the research was conducted in the absence of any commercial or financial relationships that could be construed as a potential conflict of interest.

## Publisher's note

All claims expressed in this article are solely those of the authors and do not necessarily represent those of their affiliated organizations, or those of the publisher, the editors and the reviewers. Any product that may be evaluated in this article, or claim that may be made by its manufacturer, is not guaranteed or endorsed by the publisher.

## Supplementary material

The Supplementary Material for this article can be found online at: https://www.frontiersin.org/articles/10.3389/fenvs.2023.1121969/full#supplementary-material

## References

Cooper, M. D. A., Evans, C. D., Zielinski, P., Levy, P. E., Gray, A., Peacock, M., et al. (2014). Infilled ditches are hotspots of landscape methane flux following peatland re-wetting. *Ecosystems* 17, 1227–1241. doi:10.1007/s10021-014-9791-3

Cooper, M., and Evans, C. (2013). "$CH_4$ emissions from ditches in a drained upland blanket bog, North Wales, UK," in *Emissions of greenhouse gases associated with peatland drainage waters. Report to Defra under project SP1205: Greenhouse gas emissions associated with non-gaseous losses of carbon from peatlands – fate of particulate and dissolved carbon* (Food and Rural Affairs, UK: Report to the Department of Environment).

Fox, J., and Weisberg, S. (2019). *An R companion to applied regression*. Third Edition. Thousand Oaks, California (USA): Sage. Avaliable At: https://socialsciences.mcmaster.ca/jfox/Books/Companion/.

Frenzel, P., and Karofeld, E. (2000). $CH_4$ emission from a hollow-ridge complex in a raised bog: The role of $CH_4$ production and oxidation. *Biogeochemistry* 51, 91–112. doi:10.1023/A:1006351118347

Glagolev, M. V., Chistotin, M. V., Shnyrev, N. A., and Sirin, A. A. (2008). The emission of carbon dioxide and methane from drained peatlands changed by economic use and from natural mires during the summer-fall period (on example of a region of Tomsk oblast). *Agrokhimija* 5, 46–58.

Haakana, M., Tuominen, S., Heikkinen, J., Peltoniemi, M., and Lehtonen, A. (2022). Spatial patterns of biomass change across Finland in 2009–2015. bioRxiv. doi:10.1101/2022.02.15.480479

Harrell, F. E. (2022). Hmisc: Harrell miscellaneous. R package version 4.7-0. Avaliable At: https://CRAN.R-project.org/package=Hmisc.

Heikkinen, T. K. (2016). Ennallistamisen vaikutus metsänkasvatuskelvottomien karujen keidassoiden metaanivirtoihin. Master thesis. Helsinki, Finland: University of Helsinki. Avaliable At: http://urn.fi/URN:NBN:fi:hulib-201606092345.

Hökkä, H., Stenberg, L., and Laurén, A. (2020). Modeling depth of drainage ditches in forested peatlands in Finland. *Balt. For.* 26, 453. doi:10.46490/BF453

Huttunen, J. T., Lappalainen, K. M., Saarijärvi, E., Väisänen, T., and Martikainen, P. J. (2001). A novel sediment gas sampler and a subsurface gas collector used for measurement of the ebullition of methane and carbon dioxide from a eutrophied lake. *Sci. Total Environ.* 266, 153–158. doi:10.1016/s0048-9697(00)00749-x

Huttunen, J. T., Nykänen, H., Martikainen, P. J., and Nieminen, M. (2003). Fluxes of nitrous oxide and methane from drained peatlands following forest clear-felling in southern Finland. *Plant Soil* 255, 457–462. doi:10.1023/A:1026035427891

IPCC (2014). *2013 supplement to the 2006 IPCC guidelines for national greenhouse gas inventories: Wetlands*. Switzerland: IPCC.

Juutinen, A., Shanin, V., Ahtikoski, A., Rämö, J., Mäkipää, R., Laiho, R., et al. (2021). Profitability of continuous-cover forestry in Norway spruce dominated peatland forest and the role of water table. *Can. J. For. Res.* 51, 859–870. doi:10.1139/cjfr-2020-0305

Kolton, M., Weston, D. J., Mayali, X., Weber, P. K., McFarlane, K. J., Pett-Ridge, J., et al. (2022). Defining the *Sphagnum* core microbiome across the North American continent reveals a central role for diazotrophic methanotrophs in the nitrogen and carbon cycles of boreal peatland ecosystems. *mBio* 13, e03714–e03721. doi:10.1128/mbio.03714-21

Korhonen, K., Ahola, A., Heikkinen, J., Henttonen, H., Hotanen, J., Ihalainen, A., et al. (2021). Forests of Finland 2014–2018 and their development 1921–2018. *Silva Fenn.* 55, 10662. doi:10.14214/sf.10662

Korkiakoski, M., Ojanen, P., Penttilä, T., Minkkinen, K., Sarkkola, S., Rainne, J., et al. (2020). Impact of partial harvest on $CH_4$ and $N_2O$ balances of a drained boreal peatland forest. *Agric. For. Meteorol.* 295, 108168. doi:10.1016/j.agrformet.2020.108168

Korkiakoski, M., Tuovinen, J., Penttilä, T., Sarkkola, S., Ojanen, P., Minkkinen, K., et al. (2019). Greenhouse gas and energy fluxes in a boreal peatland forest after clear-cutting. *Biogeosciences* 16, 3703–3723. doi:10.5194/bg-16-3703-2019

Koskinen, M., Maanavilja, L., Nieminen, M., Minkkinen, K., and Tuittila, E-S. (2016). High methane emissions from restored Norway spruce swamps in southern Finland over one growing season. *Mires Peat* 17, 1–13. doi:10.19189/MaP.2015.OMB.202

Laine, J., Vasander, H., Hotanen, J. P., Nousiainen, H., Saarinen, M., and Penttila, T. (2012). *Suotyypit ja turvekankaat – opas kasvupaikkojen tunnistamiseen*. Helsinki: Metsäkustannus Oy, 160.

Larmola, T., Tuittila, E., Tiirola, M., Nykänen, H., Martikainen, P. J., Yrjälä, K., et al. (2010). The role of *Sphagnum* mosses in the methane cycling of a boreal mire. *Ecology* 91, 2356–2365. doi:10.1890/09-1343.1

Laurila, T., Aurela, M., Hatakka, J., Hotanen, J., Jauhiainen, J., Korkiakoski, M., et al. (2021). Set-up and instrumentation of the greenhouse gas (GHG) measurements on experimental sites of continuous cover forestry. *Natural resources and bioeconomy studies 26*. Helsinki, Finland: Natural Resources Institute Finland.

Leppä, K., Hökkä, H., Laiho, R., Launiainen, S., Lehtonen, A., Mäkipää, R., et al. (2020b). Selection cuttings as a tool to control water table level in boreal drained peatland forests. *Front. Earth Sci.* 8, 576510. doi:10.3389/feart.2020.576510

Leppä, K., Korkiakoski, M., Nieminen, M., Laiho, R., Hotanen, J. P., Kieloaho, A. J., et al. (2020a). Vegetation controls of water and energy balance of a drained peatland forest: Responses to alternative harvesting practices. *Agric. For. Meteorol.* 295, 108198. doi:10.1016/j.agrformet.2020.108198

Liaw, A., and Wiener, M. (2002). Classification and regression by randomForest. *R. News* 2, 18–22. Avaliable At: https://CRAN.R-project.org/doc/Rnews/.

Martikainen, P. J., Nykänen, H., Alm, J., and Silvola, J. (1995). Change in fluxes of carbon dioxide, methane and nitrous oxide due to forest drainage of mire sites of different trophy. *Plant Soil* 168/169, 571–577. doi:10.1007/BF00029370

Matthews, C. J. D., Louis, St.V. L., and Hesslein, R. H. (2003). Comparison of three techniques used to measure diffusive gas exchange from sheltered aquatic surfaces. *Environ. Sci. Technol.* 37, 772–780. doi:10.1021/es0205838

Medvedeff, C. A., Bridgham, S. D., Pfeifer-Meister, L., and Keller, J. K. (2015). *Soil Biol. biochem.* 86, 34–41. doi:10.1016/j.soilbio.2015.03.016

Minkkinen, K., Laine, J., Nykänen, H., and Martikainen, P. J. (1997). Importance of drainage ditches in emissions of methane from mires drained for forestry. *Can. J. For. Res.* 27, 949–952. doi:10.1139/x97-016

Minkkinen, K., and Laine, J. (2006). Vegetation heterogeneity and ditches create spatial variability in methane fluxes from peatlands drained for forestry. *Plant Soil* 285, 289–304. doi:10.1007/s11104-006-9016-4

Minkkinen, K., Ojanen, P., Penttilä, T., Aurela, M., Laurila, T., Tuovinen, J., et al. (2018). Persistent carbon sink at a boreal drained bog forest. *Biogeosciences* 15, 3603–3624. doi:10.5194/bg-15-3603-2018

Natural Resources Institute Finland (2022). *Statistics database*. Finland: Natural Resources Institute Finland. Avaliable At: https://statdb.luke.fi/PXWeb/pxweb/en/LUKE/.

Nieminen, M., Piirainen, S., Sikström, U., Löfgren, S., Marttila, H., Sarkkola, S., et al. (2018). Ditch network maintenance in peat-dominated boreal forests: Review and analysis of water quality management options. *Ambio* 47, 535–545. doi:10.1007/s13280-018-1047-6

NIR Finland (2022). *Greenhouse gas emissions in Finland 1990 to 2021. National inventory report under the UNFCC and the kyoto protocol*. Finland: Statistics Finland. Avaliable At: https://unfccc.int/documents/461893.

Ojanen, P., Minkkinen, K., Alm, J., and Penttilä, T. (2010). Soil–atmosphere $CO_2$, $CH_4$ and $N_2O$ fluxes in boreal forestry-drained peatlands. *For. Ecol. Manag.* 260, 411–421. doi:10.1016/j.foreco.2010.04.036

Ojanen, P., Penttilä, T., Tolvanen, A., Hotanen, J., Saarimaa, M., Nousiainen, H., et al. (2019). Long-term effect of fertilization on the greenhouse gas exchange of low-productive peatland forests. *For. Ecol. Manag.* 432, 786–798. doi:10.1016/j.foreco.2018.10.015

Paavilainen, E., and Päivänen, J. (1995). *Peatland forestry*. Heidelberg: Springer Berlin. doi:10.1007/978-3-662-03125-4

Palviainen, M., Peltomaa, E., Laurén, A., Kinnunen, N., Ojala, A., Berninger, F., et al. (2022). Water quality and the biodegradability of dissolved organic carbon in drained boreal peatland under different forest harvesting intensities. *Sci. Total Environ.* 806, 150919. doi:10.1016/j.scitotenv.2021.150919

Peacock, M., Audet, J., Bastviken, D., Futter, M. N., Gauci, V., Grinham, A., et al. (2021). Global importance of methane emissions from drainage ditches and canals. *Environ. Res. Lett.* 16, 044010. doi:10.1088/1748-9326/abeb36

Pearson, M., Saarinen, M., Minkkinen, K., Silvan, N., and Laine, J. (2012). Short-term impacts of soil preparation on greenhouse gas fluxes: A case study in nutrient-poor, clearcut peatland forest. *For. Ecol. Manag.* 283, 10–26. doi:10.1016/j.foreco.2012.07.011

Penttilä, T., and Honkanen, M. (1986). *Suometsien pysyvien kasvukoealojen (SINKA) maastotyöohjeet* [Field work guide for measuring permanent peatland sample plots]. *Metsäntutkimuslaitoksen Tied.* 226, 98.

R Core Team (2021). *R: A language and environment for statistical computing*. Vienna, Austria: R Foundation for Statistical Computing. Avaliable At: https://www.R-project.org/.

Raghoebarsing, A. A., Smolders, A. J., Schmid, M. C., Rijpstra, W. I., Wolters-Arts, M., Derksen, J., et al. (2005). Methanotrophic symbionts provide carbon for photosynthesis in peat bogs. *Nature* 436, 1153–1156. doi:10.1038/nature03802

Repola, J., Hökkä, H., and Salminen, H. (2018). Models for diameter and height growth of Scots pine, Norway spruce and pubescent birch in drained peatland sites in Finland. *Silva Fenn.* 52, 10055. doi:10.14214/sf.10055

Roulet, N. T., and Moore, T. R. (1995). The effect of forestry drainage practices on the emission of methane from northern peatlands. *Can. J. For. Res.* 25, 491–499. doi:10.1139/x95-055

RStudio Team (2020). *RStudio*. Boston, Massachusetts (USA): Integrated Development for R. RStudio, PBC. Avaliable At: http://www.rstudio.com/.

Saunois, M., Stavert, A. R., Poulter, B., Bousquet, P., Canadell, J. G., Jackson, R. B., et al. (2020). The global methane budget 2000–2017. *Earth Syst. Sci. Data* 12, 1561–1623. doi:10.5194/essd-12-1561-2020

Schimel, J. P. (1995). Plant transport and methane production as controls on methane flux from arctic wet meadow tundra. *Biogeochemistry* 28, 183–200. doi:10.1007/BF02186458

Silver, T., and Joensuu, S. (2005). Ojien kunnon säilymiseen vaikuttavat tekijät kunnostusojituksen jälkeen [The condition and deterioration of forest ditches after ditch network maintenance]. *Suo* 56, 69–81. Avaliable At: http://www.suo.fi/article/9839.

Sirin, A. A., Suvorov, G. G., Chistotin, M. V., and Glagolev, M. V. (2012). Values of methane emission from drainage ditches. *Environ. Dyn. Glob. Clim. Change* 3, 1–10. doi:10.17816/edgcc321-10

Tolvanen, A., Saarimaa, M., Ahtikoski, A., Haara, A., Hotanen, J., Juutinen, A., et al. (2018). "Quantification and valuation of ecosystem services to optimize sustainable re-use for low-productive drained peatlands," in *LIFEPeatLandUse (LIFE12 ENV/FI/000150) 2013 – 2018, LAYMAN'S report* (Helsinki, Finland: ENVFI).

Tong, C. H. M., Nilsson, M. B., Sikström, U., Ring, E., Drott, A., Eklöf, K., et al. (2022). Initial effects of post-harvest ditch cleaning on greenhouse gas fluxes in a hemiboreal peatland forest. *Geoderma* 426, 116055. doi:10.1016/j.geoderma.2022.116055

Vanhatalo, K., Väisänen, P., Joensuu, S., Sved, J., Koistinen, A., and Äijälä, O. (2019). *Metsänhoidon suositukset suometsien hoitoon, työopas*. Tapion julkaisuja: Tapio. Avaliable At: https://tapio.fi/wp-content/uploads/2020/09/Metsanhoidon_suositukset_suometsien-hoitoon_TAPIO_2019.pdf.

Venables, W. N., and Ripley, B. D. (2002). *Modern applied statistics with S*. Fourth edition. New York: Springer.

Venäläinen, A., Tuomenvirta, H., Pirinen, P., and Drebs, A. (2005). *A Basic Finnish climate data set 1961–2000—description and illustrations*. Helsinki, Finland: Finnish Meteorological Institute. doi:10.13140/RG.2.2.24473.62567

Virtanen, P., Gommers, R., Oliphant, T. E., Haberland, M., Reddy, T., Cournapeau, D., et al. (2020). SciPy 1.0: Fundamental algorithms for scientific computing in Python. *Nat. Methods* 17, 261–272. doi:10.1038/s41592-019-0686-2

von Arnold, K., Weslien, P., Nilsson, M., Svensson, B. H., and Klemedtsson, L. (2005). Fluxes of $CO_2$, $CH_4$ and $N_2O$ from drained coniferous forests on organic soils. *For. Ecol. Manag.* 210, 239–254. doi:10.1016/j.foreco.2005.02.031

Waldo, N. B., Hunt, B. K., Fadely, E. C., Moran, J. J., and Neumann, R. B. (2019). Plant root exudates increase methane emissions through direct and indirect pathways. *Biogeochemistry* 145, 213–234. doi:10.1007/s10533-019-00600-6

Wickham, H. (2016). *ggplot2: Elegant graphics for data analysis*. New York: Springer-Verlag.

frontiers | Frontiers in Environmental Science

TYPE Original Research
PUBLISHED 14 April 2023
DOI 10.3389/fenvs.2023.1100443



OPEN ACCESS

EDITED BY
Andrea G. Bravo,
Institute of Marine Sciences (CSIC), Spain

REVIEWED BY
Bo Meng,
Institute of Geochemistry (CAS), China
Amanda J. Barker,
Cold Regions Research and Engineering Laboratory, United States
Douglas Burns,
United States Geological Survey (USGS), United States

*CORRESPONDENCE
Brian A. Branfireun,
bbranfir@uwo.ca

SPECIALTY SECTION
This article was submitted to Biogeochemical Dynamics, a section of the journal Frontiers in Environmental Science

RECEIVED 16 November 2022
ACCEPTED 06 March 2023
PUBLISHED 14 April 2023

CITATION
Sun T, Lindo Z and Branfireun BA (2023), Ground warming releases inorganic mercury and increases net methylmercury production in two boreal peatland types.
*Front. Environ. Sci.* 11:1100443.
doi: 10.3389/fenvs.2023.1100443



# Ground warming releases inorganic mercury and increases net methylmercury production in two boreal peatland types

Ting Sun[1,2,3], Zoë Lindo[4] and Brian A. Branfireun[4]*

[1]School of Environmental Science and Engineering, Shandong University, Qingdao, China, [2]Institute of Eco-Environmental Forensics, Shandong University, Qingdao, China, [3]Formerly at Department of Earth Sciences, University of Western Ontario, London, ON, Canada, [4]Department of Biology, University of Western Ontario, London, ON, Canada

Boreal peatlands are considered sinks for atmospheric mercury (Hg) and are important sources of methylmercury (MeHg) to downstream ecosystems. Climate change-driven increases in average annual temperature in coming decades will be amplified at higher latitudes and will modify many biogeochemical processes in high boreal and subarctic peatlands that are important landscape features in these regions. Changes in water quality are an important issue for Northern ecosystems and fish consumers, and the directionality of changes in mercury levels due to climate warming presents considerable uncertainty. Peatlands are key landscape hotspots for MeHg production, however, the impact of climate warming on Hg cycling in boreal peatlands is not well studied. We use a multi-year field-based warming experiment (2 years passive, 1 year active ground warming) across two boreal peatland types (moss and sedge dominated) to explore the effects of ground warming on inorganic Hg (IHg) release, net MeHg production, and biogeochemical controls on both of these processes including the availability of sulfate ($SO_4^{2-}$) and dissolved organic matter (DOM) quality and concentration. There were higher porewater IHg and MeHg concentrations under active ground warming conditions in both peatlands, likely related to both increased microbial metabolism, and changes in biogeochemical conditions that favor Hg methylation. Both $SO_4^{2-}$ (electron acceptor) and bioaccessible DOM (electron donor) are nutrients for sulfate-reducing bacteria which are dominant Hg methylators in freshwater environments, and increases in $SO_4^{2-}$ and/or bioaccessible DOM concentrations under warming played an important role in the observed changes in net MeHg production. Warming increased $SO_4^{2-}$ concentrations in the sedge-dominated but not in the moss-dominated fen likely because of a larger pool of groundwater derived $SO_4^{2-}$ in the sedge-dominated site. Warming increased DOM concentration in both peatland sites through enhanced decomposition of peat and increased release of root exudates from vascular plants, and the balance of these processes varied by peatland type and degree of warming. Experimentally increased ground temperatures increased microbial metabolism, organic matter turnover, and the availability of IHg all of which resulted in increases in porewater MeHg, indicating that climate-driven ground warming will increase MeHg production in northern peatlands in the future.

KEYWORDS

**mercury, methylmercury, climate change, wetland, sulfate, dissolved organic matter**

# 1 Introduction

The Earth's climate is warming due to the increase in atmospheric greenhouse gasses driven mainly by anthropogenic fossil fuel combustion (IPCC, 2018). The IPCC (2018) special report states that the mean global temperature will reach at least 1.5°C above pre-industrial levels between 2030 and 2052 and higher latitudes of the northern hemisphere are experiencing greater rates of change in air temperature with increases of 6°C or greater (Brigham et al., 2009). Northern peatlands are particularly vulnerable to warming due to changes in hydrology (Tarnocai, 2009), primary productivity (McPartland et al., 2020) and community composition (Dieleman et al., 2015; Kolari et al., 2021), and biogeochemical cycles, particularly carbon (Dieleman et al., 2016; Zhang et al., 2020). Much of this is through warming-induced drying of peatlands by increasing evapotranspiration (Tarnocai, 2009; Helbig et al., 2020) which can decrease carbon accumulation (Zhang et al., 2020). Warming is also shown to increase vascular plant abundance and biomass and decrease *Sphagnum* spp. cover (Buttler et al., 2015; Dieleman et al., 2015), modifying organic matter cycling and carbon storage potential.

Mercury (Hg) is a global pollutant due to its ubiquitous distribution and anthropogenic enrichment (Driscoll et al., 2013). Mining, coal combustion, and cement manufacturing are the largest sources of global Hg emissions and largely responsible for increasing Hg concentrations in the atmosphere many-fold above pre-industrial levels (Streets et al., 2019). Inorganic Hg (IHg) can be converted into the toxic and bioaccumulating form methylmercury (MeHg) in anaerobic environments (e.g., lake sediments and peatlands) by sulfate-reducing bacteria (SRB) (Gilmour et al., 1992), iron-reducing bacteria (FeRB) (Fleming et al., 2006; Kerin et al., 2006), methanogenic archaea (Hamelin et al., 2011), and other syntrophic and acetogenic bacteria (Gilmour et al., 2013) although SRB are primary methylators in most freshwater environments. MeHg is a potent neurotoxin that can affect the nervous, immune, and reproductive systems of vertebrates (see review by Clarkson and Magos, 2006). Owing to its lipophilic and protein-binding properties, MeHg bioaccumulates and biomagnifies in food webs, posing a threat to upper trophic level wildlife and humans (Mergler et al., 2007).

Climate change is expected to substantially change the cycling of Hg, with local to regional scale implications (Driscoll et al., 2013; Krabbenhoft and Sunderland, 2013). These impacts may be direct such as increasing the amount of IHg available for methylation, as well as amplifying the methylation process itself. A warming environment has been directly linked to the release of IHg from degrading permafrost to nearby aquatic ecosystems (Ci et al., 2020; Mu et al., 2020; Schaefer et al., 2020). As a microbial process, it is not surprising that both laboratory (King et al., 1999; St Pierre et al., 2014; Yang et al., 2016) and field studies (Hurley et al., 1998; Hudelson et al., 2020) have found that higher temperatures favor net MeHg production (Canario et al., 2007). Several studies have attributed increased water MeHg concentrations to global warming (MacMillan et al., 2015; Yang et al., 2016).

Boreal peatlands are important "hotspots" of net MeHg production (Branfireun et al., 1999; Mitchell et al., 2008a), and temperature-mediated changes in the metabolism of Hg methylators and Hg availability would be expected in these ecosystems as well.

In addition to these direct effects, climate warming can also indirectly affect Hg methylation through hydrologic fluctuation (Coleman-Wasik et al., 2015), drought-induced wetting and drying cycles can lead to cycling in redox conditions (Helbig et al., 2020), an important factor for net MeHg production (Ullrich et al., 2001). Furthermore, a receding water table driven by climate warming increases the oxidative release of Hg and Hg methylator nutrients, such as sulfate ($SO_4^{2-}$) and dissolved organic matter (DOM) (Haitzer et al., 2003). It has also been shown that higher temperatures may also increase the gaseous evasion of S compounds (e.g., hydrogen sulfide and carbonyl sulfides) from boreal peatlands and consequently decrease net MeHg production over time. Predicted changes in peatland plant biomass and community composition under climate warming (Dieleman et al., 2015; Mäkiranta et al., 2018) may also affect Hg methylation, given that plant biomass and community composition controls litter and root characteristics, which influence soil and pore water DOM quantity and bioaccessibility (Mastný et al., 2018).

Peatlands of the circum-boreal region of the northern hemisphere represent a relatively small but important land cover class with respect to carbon storage and the regulation of water quality. Moss-dominated (i.e., *Sphagnum*) and sedge-dominated (e.g., *Carex*) fen peatlands are both equally important types of boreal peatlands in Canada, however sedge-dominated more nutrient rich peat-accumulating wetlands are under-represented in the scientific literature relative to moss-dominated systems despite their nearly equal proportion by area in Canada (Wu and Roulet, 2014). Importantly, the potential shift of moss-dominated fens toward a much higher proportion of vascular plant (graminoid) cover due to warmer temperatures and elevated atmospheric $CO_2$ (Dieleman et al., 2015) has significant implications for not only carbon cycling, but other biogeochemical processes that are linked to microbial metabolic processes, such as Hg methylation.

Given the wide ranging implications of future warming on northern peatland biogeochemistry, this study was conducted to assess the impact of experimental ground warming on the net MeHg production in two boreal peatlands: a *Sphagnum* moss-dominated fen and a *Carex* sedge-dominated fen peatland. Specifically, this study sought to (1) determine the effect of ground warming on IHg and MeHg concentrations in pore waters, and the net MeHg production potentials of the two fens, (2) characterize the importance of pore water chemistry including $SO_4^{2-}$ concentrations and DOM concentrations on IHg and MeHg concentrations, and the characteristics that explain among-temperatures differences in pore water IHg and MeHg concentrations, and (3) compare the among-fens differences in concentrations of IHg, MeHg and $SO_4^{2-}$ and concentrations and characteristics of DOM.

# 2 Methods

## 2.1 Study sites

The Biological Response to A Changing Environment (BRACE) experiment was established in 2012 associated with two adjacent peatlands that differ in vegetation composition (moss vs. sedge-dominated), hydrology, and nutrient status (low vs. intermediate) maintained as long-term monitoring sites by the Ontario Ministry of

Natural Resources and Forestry–Ontario Forest Research Institute (OMNRF-OFRI). The peatlands are located ~2 km apart in an 817 ha sub-watershed of the Lake Superior basin near White River, Ontario, Canada (48°21' N, 84°20' W). Both peatlands are fen peatlands and share a surrounding catchment of mixed-wood coniferous and deciduous forests. The sedge-dominated fen has lower plant species richness with a high abundance of *Carex* spp. sedges and a low shrub overstory mainly of sweet gale [*Myrica gale* L.] with some leatherleaf [*Chamaedaphne calyculata* L. Moench]. The moss-dominated fen has a near-continuous groundcover of *Sphagnum* spp. mosses, with a low shrub cover of leatherleaf, Labrador tea [*Rhododendron groenlandicum* (Oeder) Kron & Judd] and lowbush blueberry [*Vaccinium angustifolium* Aiton], and a more species rich array of herbs (e.g., *Maianthemum trifolium* (L.) Sloboda) with a sparse overstory of coniferous trees including tamarack [*Larix laricina* (Du Roi) K. Koch] and black spruce [*Picea mariana* (Mill.) Britton, Sterns & Poggenburg]. A full description of the vegetation community can be found in Lyons and Lindo (2020). The sedge-dominated fen is relatively more nutrient-rich with a higher pH (~5.2) due to groundwater and surface water connections and has a generally higher water table (near soil surface) compared to the moss-dominated fen that has pH ~4.2 and water table approx. ~20 cm below the soil surface.

The sedge-dominated fen is 10.2 ha, while the moss-dominated fen is 4.5 ha; weather station data, including air temperature and precipitation, and water table depth is monitored continuously through the OMNRF-OFRI at both sites. Data collected from June to October in 2017, 2018, and 2019 report a mean air temperature of each year was 12.3°C, 8.7°C, and 12.9°C, respectively. The mean precipitation from June to October of each year was 299.05 mm, 277.15 mm, and 219.40 mm for 2017, 2018, and 2019, respectively.

## 2.2 Field experimental design

Sixteen experimental plots were established at each of the two peatland sites in 2015. At each site plots were established using cylindrical PVC collars (1 m diameter; 40 cm deep) inserted into the peat ~30 cm. Half the plots were designated as warmed and equipped with six vertical immersion heaters (60 W Watlow FireRod®) installed to a depth of 50 cm at the time of plot establishment while the other half were designated as control plots (ambient temperatures). Plots were arranged in a block design (four plots per block) at each site to account for any small-scale spatial factors (e.g., microtopography, vegetation biomass and composition, moisture variability). Additionally, two reference plots (without PVC collars) were established at each of the two sites for a total of 36 experimental plots (2 sites × 2 treatments (control, warming) × 8 replicates plus 2 reference plots per site = 36 plots); reference plots were located ~50 m away from the experimental plots in the sedge-dominated fen and ~25 m away from experimental plots in the moss-dominated fen to ensure minimal disturbance.

In 2016, an integrated groundwater sampling well was permanently installed in each experimental (control and warmed) and reference plots. Sampling wells were custom fabricated from Teflon® (5 cm O.D. 4 cm I.D. 50 cm long; slotted along the entire length), and capped at both ends to prevent contamination. An acid-washed (10% v/v) 6.35 mm (0.25 cm O.D.) Teflon sampling line was installed in each well secured with a Teflon compression fitting in the vented top cap for sampling pore water.

### 2.2.1 Experimental warming

Experimental ground warming was implemented in stages beginning with passive warming in 2017. Passive warming was accomplished using clear, 1.2 m tall, open-topped chambers (OTCs) that were fitted onto the PVC collars at each of the warmed plots. Teflon sampling lines from central wells passed through the sidewall of the plot collar to allow for water sampling without having to remove the OTCs or otherwise disturb the plot. Passive warming was implemented from June to October in 2017, 2018 and 2019. Passive warming increased the mean surface peat (5 cm) temperatures by 0.38°C and 0.27°C for the moss-dominated fen and sedge-dominated fen, respectively (Lyons et al., 2020).

In June 2019, active ground warming was enabled in addition to passive warming with a target temperature of + 4°C above ambient peat temperatures in the deeper peat (30 cm). Active heating of the peat profile *via* the immersion heaters was controlled by a custom system designed by Zesta Engineering (Mississauga, ON) using paired thermocouples installed inside and outside of each warming plot. Manual temperature measurements at 25 cm depth were used to validate the + 4°C warming temperature. Active warming was established in June through late September in 2019 at both sites. Active warming increased the soil temperature (25 cm) of warmed plots by + 4.5 (SD ± 0.9)°C and + 3.8 (SD ± 0.8)°C in the moss-dominated fen and sedge-dominated fen, respectively. Two plots at each site had active warming malfunctions during the 2019 experimental season, and data from these warmed plots are not included in the 2019 data analysis of active warming. These plots continued to receive passive warming under the OTCs consistent with previous years.

Manual measurements of soil temperature at 5, 10 and 25 cm soil depth were performed weekly at three random locations in each plot. Surface soil moisture (top 10 cm) was also measured weekly at three different locations for each plot using an HH2 Moisture Meter (Delta-T Devices, Burwell, Cambridge, United Kingdom). We also monitored site-level water table elevation (below peat surface, cm) based on OMNRF-OFRI weather stations established at each site and TD-Diver™ and Baro-Diver® data loggers deployed in four locations across each site that measured water table levels (cm, below peat soil surface) every 15 min.

## 2.3 Sampling and analysis

Sampling wells were pre-purged using a Geotech® GeoPump (Geotech Ltd. North Aurora, ON, Canada) and acid-washed Masterflex® C-FlexUltra tubing (Cole-Palmer Instrument Co.). Pore waters were collected weekly (2017 and 2019) or bi-weekly (2018) into a pre-acid washed 500 mL PETG (polyethylene terephthalate glycol-modified) bottle (Thermo Scientific™ Nalgene™). A second smaller volume was used for pH measurements (Mettler Toledo Seven2GO™Pro) in the field at the time of water sampling. All pore water samples were kept in a

clean cooler and transported each day to a local field laboratory for filtering and preservation. Sample lines were kept capped and clean between sampling times.

Standard ultraclean sampling protocols were used throughout sample collection (US EPA, 1996). Before sample collection, all sampling equipment and sample containers for Hg and DOM analysis were cleaned using Citranox® followed by a MilliQ water rinse and soaked in 10% (v:v) HCl overnight followed by a MilliQ water rinse in the university laboratory. Sample containers for ions analysis were cleaned using Citranox® followed by a MilliQ water rinse. After cleaning, sampling equipment and sample containers for Hg and MeHg sampling were individually double-bagged and shipped to the sampling site. Sample collection was compliant with EPA Method 1669, and is colloquially referred to as the "clean hands–dirty hands technique". There were two people in a sampling team with one person as "dirty hands" and another as "clean hands". All operations including preparation of sampling, operation of any machinery, and all other activities that do not directly contact with samples and the inner sample bottles were handled by "dirty hands". "Clean hands" was responsible for all operations involving contact with sample bottles and the transfer of samples from the sampling equipment to the sample bottles. Clean disposable nitrile gloves were worn all the time to avoid contamination.

All samples were filtered within 6 h with 0.5 μm glass-fiber filters in an enclosed vacuum filter apparatus with Teflon wetted surfaces and transferred to acid-cleaned 250 mL PETG bottles for total Hg (THg) and MeHg analysis, 60 mL HDPE (high-density polyethylene) bottles for ion analysis, and 60 mL amber glass bottles for total DOC and optical characterization analysis. Filtered pore waters for Hg analysis were preserved by acidifying to 0.5% (vol/vol) with OmniTrace® hydrochloric acid. All filtered samples were stored at 4°C in the dark until they were returned to the university analytical lab for analysis.

Blanks of field, equipment and filters, and duplicates of samples were collected on each sampling date. Sample duplicates were performed by randomly choosing one plot and then simultaneously collecting two-pore water samples. Field blanks were performed by directly pouring the deionized water (18.2 MΩ cm) into the 250 mL PETG bottles. Equipment blanks were performed by directly pumping deionized water (18.2 MΩ cm) into the 500 mL PETG bottles using the acid-cleaned Masterflex C-FlexUltra tube. Filter blanks were performed by filtering the deionized water (18.2 MΩ cm) into 250 mL PETG bottles, 60 mL HDPE bottles, and 60 mL amber glass bottles. All field blanks, filter blanks, equipment blanks, and sample duplicates were stored and handled in the same way as field samples. All sampling equipment and sample containers were cleaned carefully before each sampling event, and standard ultraclean sampling protocols were used throughout sample collection (US EPA, 1996).

Pore water samples were analyzed for THg, MeHg, $SO_4^{2-}$, and DOM concentrations and several DOM indices. Pore water THg concentrations were analyzed by cold vapor atomic fluorescence spectroscopy (CVAFS, Tekran 2600, Tekran Inc. Canada) using the Environmental Protection Agency (EPA) method 1631 (US EPA 2002). The pore water MeHg concentrations were determined by CVAFS (Tekran 2700, Tekran Inc. Canada) using the methods introduced by Bloom (1989) and Liang et al. (1994). The IHg concentration was calculated as the difference between THg and MeHg concentrations. Pore water $SO_4^{2-}$ concentrations were analyzed using ion chromatography on a Dionex ICS-1600 (Thermo Scientific™ Dionex™, Canada). Dissolved organic matter was quantified analytically as dissolved organic carbon (DOC); DOC concentrations in pore waters were determined by the persulfate wet oxidation method using the iTOC Aurora 1030 (OI Analytical, College Station, TX, United States).

The DOM in pore waters was characterized using several indices that are indicators of its molecular character and may be used to infer such things as its origin (e.g., microbial vs. detrital). These indices included the specific UV absorbance at 254 nm ($SUVA_{254}$) and three optical fluorescence excitation-emission matrices (EEMs) indices: the fluorescence index (FI), humification index ($HIX_{EM}$), and biological index or freshness index (BIX). The $SUVA_{254}$ is an indicator of DOM aromaticity (aromatic molecules content) (Weishaar et al., 2003); higher $SUVA_{254}$ values indicate higher DOM aromaticity. The values of $SUVA_{254}$ were measured and calculated using EPA methods (415.3). The FI also reflects aromaticity and indicates DOM origin source with higher FI values (>1.8) being suggestive of microbially-derived DOM that has lower aromaticity (i.e., originating from processes such as extracellular release and leachate of algae and bacteria), while lower FI values (<1.2) indicate DOM is terrestrially derived (originating from decomposition and leaching of plant and soil organic matter) and has higher aromaticity (Fellman et al., 2010). The $HIX_{EM}$ indicates the humic substance content or the extent of humification that converts simple organic matter derived from plants and animals to more condensed and higher molecular weights organic matter by microbes (Fellman et al., 2010). High $HIX_{EM}$ values (>1.0) indicate high humification of DOM that contains more highly condensed and complex molecules. The BIX denotes the freshness of DOM that is generally produced by microorganisms (Fellman et al., 2010); higher BIX values (>1.0) indicate that DOM is predominantly produced by microbes and is more bioaccessible. Fluorescence and absorbance measurements were made using a Horiba Aqualog® fluorescence spectrofluorometer with a xenon lamp.

## 2.4 Statistical analysis

All statistical analyses were performed using SPSS statistics software (IBM SPSS Inc. 24.0). The effects of ground warming on surface soil moisture content and concentrations of total (THg), inorganic (IHg), and methyl-mercury (MeHg), and $SO_4^{2-}$ in porewater alongside percent MeHg, and DOM characteristics (DOC, $SUVA_{254}$, FI, $HIX_{EM}$, and BIX) in pore water were analyzed using repeated measures analysis of variance (ANOVA) following examination of the data for parametric test assumptions using Levene's test and Q-Q plots; block effects were retained in the model only when significant. Separate statistical tests were used for each site as differences in pore water chemistry. Origin 9.3 (Microcal Software Inc. MA) software was used to visualize data. Data are shown as the mean ± standard deviation (SD).

Linear regression or non-parametric regression was used to test the relationships between the concentrations of THg, IHg and DOC.

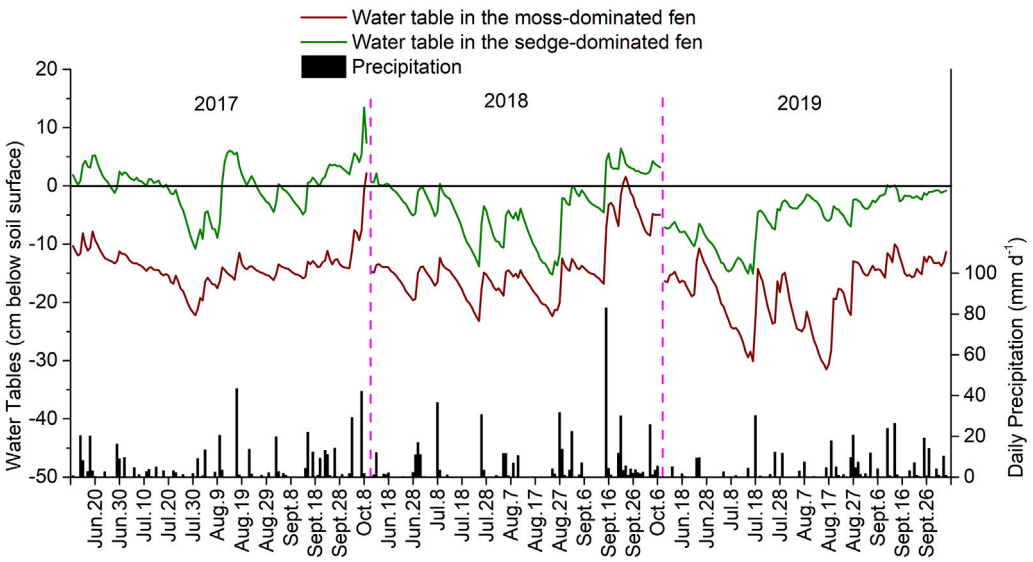


FIGURE 1
Water table levels and daily precipitation in the moss-dominated fen and the sedge-dominated fen over the experiment (2017–2019).

Coefficient of determination ($R^2$) and significance probabilities ($p$) are presented for linear regression fits, with a level of significance set at $p < 0.05$.

# 3 Results

## 3.1 Effects of ground warming on physical environmental conditions

Water table levels (cm, below peat soil surface) were approximately 10 cm lower in the moss-dominated fen than in the sedge-dominated fen (Figure 1). Mean water table level was generally lowest in July and August of the experimental years, while the relatively high water table levels in June are attributed to snow melt. The higher water table levels in September and October are attributed to late season precipitation events. The mean water table levels during the growing season from June to August in both fens were generally lower in 2019 than in 2017 and 2018 (the moss-dominated fen: −14.1 ± 2.1 cm (2017), −16.5 ± 2.6 cm (2018), and −19.7 ± 4.3 cm (2019); the sedge-dominated fen: −0.2 ± 3.5 cm (2017), −6.3 ± 1.0 cm (2018), and −7.5 ± 3.9 cm (2019)); this coincides with the total annual precipitation across those years which was approximately 598 mm, 554 mm, and 439 mm in 2017, 2018, and 2019, respectively.

Warming (passive or active) had no significant effect on soil moisture in the top 10 cm of the peat at the moss-dominated fen ($F_{1,6} = 0.133$, $p = 0.728$), however, active warming significantly decreased soil moisture at the sedge-dominated fen ($F_{1,12} = 5.52$, $p = 0.037$), which was driven by a 21% reduction in soil moisture during active warming (Table 1). Active warming also induced periods of drier conditions in the surface peat at the moss-dominated fen (reductions on average 13%), particularly as the season progressed (Table 1). This pattern of later season reductions in soil moisture was also observed in 2017 and 2018 at both sites under passive warming, albeit to a lesser extent.

## 3.2 Pore water mercury, methylmercury and sulfate concentrations

Total Hg concentrations were non-significantly higher in the warmed plots at both the moss-dominated site ($F_{1,11} = 3.41$, $p = 0.092$) and the sedge-dominated site ($F_{1,12} = 0.049$, $p = 0.828$) when all time points were considered together (Figure 2). In the moss-dominated site, passive warming had no significant effects on THg concentrations ($F_{1,14} = 2.66$, $p = 0.125$), while active warming significantly increased the concentrations of THg concentrations ($F_{1,11} = 5.21$, $p = 0.043$). Total Hg values were ~50% greater under active warming in 2019 compared to ~30% and ~20% greater under passive warming in 2018 and 2017, respectively. There was no effect of passive ($F_{1,14} = 0.36$, $p = 0.557$) or active ($F_{1,12} = 0.33$, $p = 0.578$) warming on THg concentrations in pore waters collected from the sedge-dominated site.

Inorganic Hg (IHg) largely drove the patterns observed for THg at the moss-dominated site across all years with a trend not statistically different between treatments ($F_{1,11} = 2.59$, $p = 0.136$) (Figure 3A). There were also no significant effects of both passive ($F_{1,14} = 2.44$, $p = 0.140$) and active ($F_{1,11} = 3.18$, $p = 0.102$) warming on IHg concentrations in pore water. In the sedge-dominated site, while there were peaks in IHg that were greater under warming, pore water IHg concentrations in control plots were not significantly different than those in warmed plots overall ($F_{1,12} = 0.10$, $p = 0.756$) (Figure 3B). Both passive warming ($F_{1,14} = 0.44$, $p = 0.517$) and active warming ($F_{1,12} = 0.64$, $p = 0.440$) had no significant effects on IHg concentrations. Indeed under active warming in July and August, pore water IHg concentrations were slightly lower in the actively warmed plots than in the control plots. Although the pattern

**TABLE 1 Average monthly soil moisture (± standard deviation; % v/v) in the control and warmed plots in the moss-dominated fen and the sedge-dominated fen over the experiment.**

| Year | Month | Moss-dominated fen | | Sedge-dominated fen | |
|---|---|---|---|---|---|
| | | Control plots | Warmed plots | Control plots | Warmed plots |
| 2017 | June | 41.9 ± 7.5 | 41.0 ± 10.5 | 68.1 ± 1.6 | 67.8 ± 2.0 |
| | July | 25.5 ± 9.3 | 23.7 ± 8.2 | 51.3 ± 12.7 | 46.4 ± 13.3 |
| | August | 34.4 ± 9.3 | 32.5 ± 10.4 | 56.1 ± 18.6 | 52.3 ± 16.6 |
| 2018 | June | 21.6 ± 8.4 | 21.0 ± 8.6 | 53.8 ± 7.9 | 48.9 ± 10.5 |
| | July | 20.2 ± 7.3 | 19.2 ± 5.5 | 42.1 ± 11.1 | 41.6 ± 12.1 |
| | August | 20.8 ± 6.5 | 19.8 ± 5.1 | 32.3 ± 10.0 | 28.9 ± 5.3 |
| 2019 | June | 16.2 ± 9.5 | 16.4 ± 1.6 | 32.1 ± 8.4 | 34.8 ± 8.7 |
| | July | 17.5 ± 4.2 | 15.2 ± 5.5 | 33.7 ± 11.1 | 26.2 ± 8.7 |
| | August | 16.9 ± 4.3 | 14.9 ± 4.0 | 41.9 ± 10.9 | 29.1 ± 10.7 |
| | September | 15.5 ± 5.4 | 12.3 ± 5.1 | 61.4 ± 6.6 | 61.8 ± 5.3 |
| | October | 18.2 ± 4.0 | 13.3 ± 5.8 | 65.5 ± 4.6 | 64.7 ± 3.4 |

of IHg was relatively consistent over time between years, an anomalous peak in mid-July 2018 in IHg in both control and passively warmed plots was notable, and inconsistent with the period prior and post measurement.

There were no statistical difference in MeHg concentrations between treatments at the moss-dominated site ($F_{1,11}$ = 2.51, $p$ = 0.141) (Figure 3C). Passive warming had no significant effects on MeHg concentrations ($F_{1,14}$ = 0.28, $p$ = 0.603) but active warming-induced increases in MeHg were evident ($F_{1,11}$ = 6.09, $p$ = 0.031) where concentrations were on average more than 2× greater than the control plots. In the sedge-dominated site, only active (not passive: $F_{1,13}$ = 1.63, $p$ = 0.224) warming in 2019 ($F_{1,11}$ = 9.94, $p$ = 0.009) significantly increased MeHg concentrations, such that the overall effect of warming across all years was statistically non-significant ($F_{1,10}$ = 3.63, $p$ = 0.086). Increases in MeHg concentrations under active warming were 2–2.5× greater than the control plots in 2019 (Figure 3D). Both the moss-dominated and the sedge-dominated sites showed significant time × warming treatment interactions (moss-dominated: $F_{29,319}$ = 3.52, $p$ < 0.001; sedge-dominated: $F_{29,290}$ = 8.69, $p$ < 0.001). The %MeHg showed similar trends as MeHg concentrations with significant time × warming treatment interactions at both sites as % MeHg was lower under the passive warming plots at both sites, but higher under active warming plots compared to control plots (moss-dominated: $F_{29,319}$ = 1.96, $p$ = 0.003; sedge-dominated: $F_{29,290}$ = 3.39, $p$ < 0.001) (Figures 3E, F).

Sulfate concentrations were generally low (<0.5 mg/L) but showed strong summer seasonal peaks in concentration in both control and warmed plots (Figure 4). This trend was more pronounced at the sedge-dominated site (Figure 4B) and in 2019 at both sites. During 2017 and 2018 under passive warming and in 2019 under active ground warming, these peaks in pore water $SO_4^{2-}$ concentrations were greater in the experimentally warmed plots, although peaks were observed at the same sampling periods in the control plots. Ultimately while warming-induced increases in $SO_4^{2-}$ concentrations at the moss-dominated site were not significant overall ($F_{1,10}$ = 0.10, $p$ = 0.761), the site showed a significant time × warming treatment interaction ($F_{25,175}$ = 2.42, $p$ = 0.015). While the sedge-dominated also showed a significant time × warming treatment interaction ($F_{25,175}$ = 4.83, $p$ < 0.001), there was also an overall effect of warming on $SO_4^{2-}$ concentrations ($F_{1,7}$ = 8.78, $p$ = 0.021).

## 3.3 Response of dissolved organic matter concentrations and characteristics to ground warming

Superimposed on annual cycles of higher concentrations during the summer months, increase in DOC under warming was small and the overall result was not statistically significant at either site (moss-dominated: $F_{1,10}$ = 1.59, $p$ = 0.235; sedge-dominated: $F_{1,11}$ = 1.76, $p$ = 0.211) (Figures 5A, B). Additionally, both passive warming (moss-dominated: $F_{1,13}$ = 1.14, $p$ = 0.306; sedge-dominated: $F_{1,13}$ = 0.73, $p$ = 0.408) and active warming (moss-dominated: $F_{1,11}$ = 3.40, $p$ = 0.092; sedge-dominated: $F_{1,12}$ = 3.21, $p$ = 0.099) had no significant effects on DOC concentrations at either site. There was a significant time × warming treatment interaction at the sedge-dominated site ($F_{29,319}$ = 1.69, $p$ < 0.05) but not at the moss-dominated site ($F_{29,290}$ = 1.21, $p$ = 0.212).

Both passive warming ($F_{1,12}$ = 3.44, $p$ = 0.088) and active warming ($F_{1,11}$ = 1.48, $p$ = 0.249) had no significant influences on $SUVA_{254}$ at the moss-dominated site leading to an overall non-significant effect of warming on $SUVA_{254}$ ($F_{1,9}$ = 0.14, $p$ = 0.716) (Table 2). $SUVA_{254}$ was consistently lower under warming at the sedge-dominated site ($F_{1,8}$ = 3.42, $p$ = 0.102), but only statistically significantly lower under active warming (passive: $F_{1,11}$ = 0.02, $p$ = 0.901; active: $F_{1,11}$ = 8.50, $p$ = 0.014). The fluorescence indices FI, $HIX_{EM}$, and BIX showed no significant difference between warming and control plots at the moss-dominated site. At the sedge-dominated site, FI was higher under warmed conditions (not significant: $F_{1,10}$ = 3.90, $p$ = 0.076) with the trend largely driven by increases under active warming in 2019

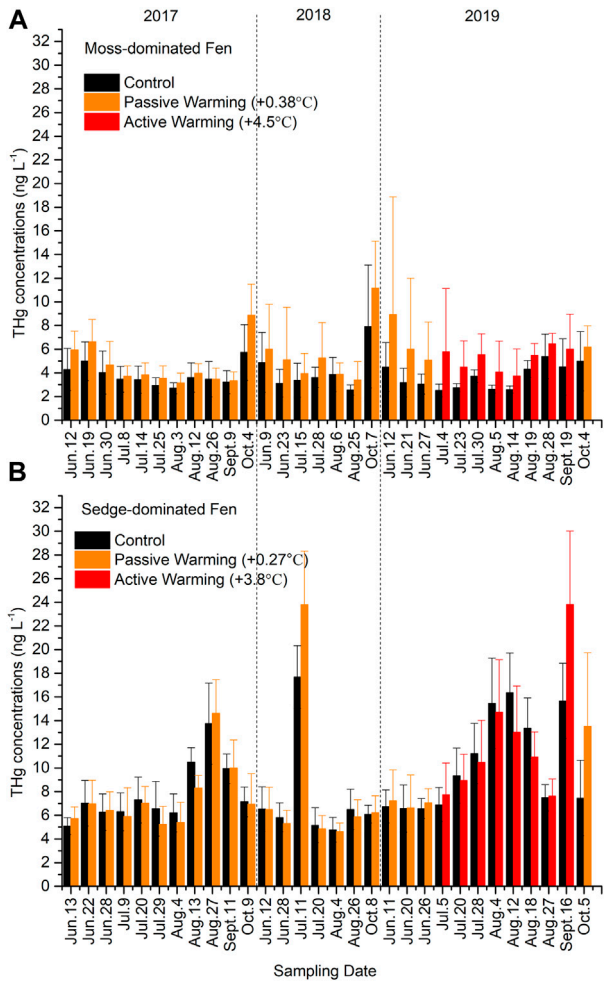


FIGURE 2
Total mercury (THg) concentrations in **(A)** the moss-dominated fen and **(B)** the sedge-dominated fen. Colors are different plot treatments: black for the control plots; orange for the passively warmed plots; red for the actively warmed plots. Bars are mean values and whiskers are ± ones tandard deviation. Note differences in *y*-axis scales.

(time × warming treatment interaction: $F_{29,290}$ = 2.0, $p$ = 0.003). The $HIX_{EM}$ index was not significantly different between warmed and control treatment plots ($F_{1,10}$ = 1.30, $p$ = 0.276) but was marginally lower during the period of active warming in 2019. The BIX index was significantly higher in the warming treatment plots ($F_{1,10}$ = 8.04, $p$ = 0.018), which was largely driven by increases during the 2019 active warming (time × warming treatment interaction: $F_{29,290}$ = 3.60, $p$ < 0.001) (Table 2 presents the summary data for DOM quality measures).

## 4 Discussion

Given the well-established geochemical and biological controls on Hg cycling and methylation in particular, it is perhaps not surprising that overall, ground warming resulted in increased concentrations of THg and MeHg through decomposition-mediated release from peats into pore waters, and through enhanced net Hg methylation. Higher temperatures increase microbial metabolism (Comeau, 2008), leading in this case to a subsequent increase in decomposition and net Hg methylation. The increased decomposition of soil organic matter (SOM) not only releases more DOM but also releases more Hg, given the strong binding between Hg and the reduced sulfur groups in DOM (Xia et al., 1999). Some of the increases in MeHg concentrations observed indeed may be because MeHg is more readily desorbed from soils than IHg, given that IHg is chemically bound more strongly to the reduced sulfur groups in SOM than MeHg (Skyllberg, 2008; Liem-Nguyen et al., 2017). This study could not differentiate between MeHg in porewaters derived from desorption *versus* that from active Hg methylation, however there is ample evidence that active methylation played an important role, particularly under the active heating treatment in 2019. Active warming significantly increased THg concentrations in porewaters in the moss-dominated site but not in the sedge-dominated site. An explanation is that active warming plots in the moss-dominated site had a larger increased soil temperature (+4.5°C) than that in the sedge-dominated site (+3.8°C), leading to an enhancement of SOM decomposition and more releases of THg. Additionally, the peat in the sedge-dominated fen will be inherently more decomposable than the more recalcitrant *Sphagnum*-dominated peat at the moss site.

Measured MeHg concentrations are controlled by both Hg methylation and demethylation (Ullrich et al., 2001), and the measurements made as part of this study cannot determine the relative importance of each of these in regulating net MeHg concentrations in porewaters. Although both may be considered a largely biologically-mediated process in the sub-surface environment, and as such are regulated by temperature as a first-order control, it has been shown that relatively higher temperatures tend to favor the Hg methylation reaction (Canario et al., 2007; St Pierre et al., 2014; Hudelson et al., 2020) while relatively lower temperatures tend to favor MeHg demethylation (Ramlal et al., 1993). Active warming in this study may have warmed soil temperatures into a more optimal range for Hg methylation than demethylation in both fens. The relative fraction of THg that is MeHg (%MeHg) is often used as an indication of net MeHg production in sediment when comparing among sites (Paranjape and Hall, 2017). The overall higher %MeHg in the moss-dominated peatland is consistent with relatively high %MeHg reported in these types of wetlands relative to other methylating environments (Yu et al., 2010). Indeed, % MeHg in the moss-dominated fen is 2–10 times higher than that in the sedge-dominated fen, and is almost certainly due to its high aromatic fraction of DOM and deeply reducing conditions. DOM especially with high aromaticity plays an important role in increasing the mobility and transport of Hg and the bioaccessibility of IHg (Ravichandran, 2004; Hall et al., 2008). Soil interactions with surface water and ground water in the sedge-dominated fen would maintain both the vascular plant community, and a relatively higher redox environment than in the moss-dominated system. The lower water table levels and the deeply reducing conditions in the moss-dominated site can apply more nutrients (such as $SO_4^{2-}$) by oxidation under hydrological fluctuation conditions, leading to a significant increase in MeHg production, given that the addition of the more limited $SO_4^{2-}$increases net Hg methylation (Branfireun et al., 1999;

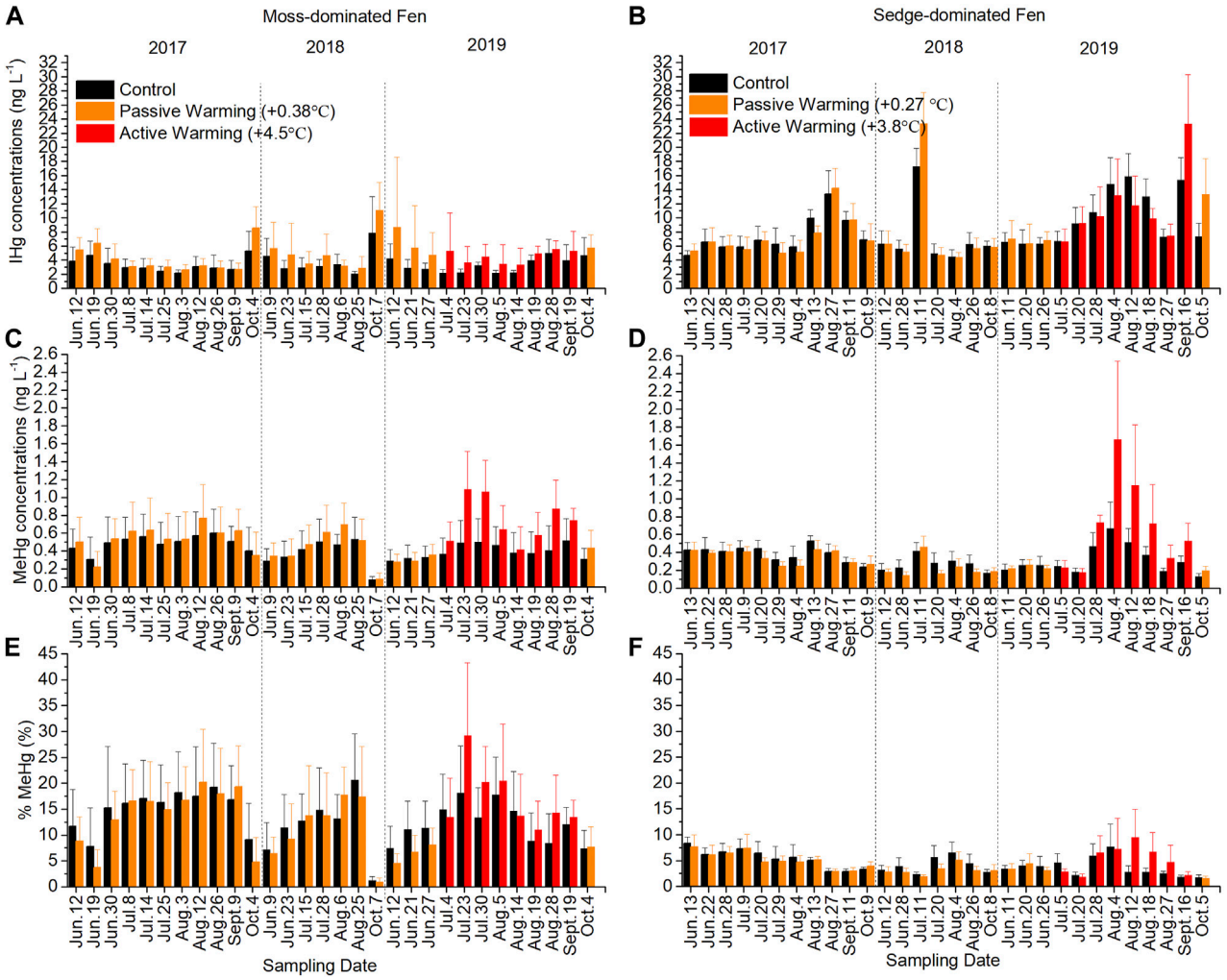


FIGURE 3
Concentrations of inorganic mercury (IHg) and methylmercury (MeHg) and the proportion of total Hg (THg) as MeHg (%MeHg) in pore waters in the control and warmed plots in the moss-dominated fen and the sedge-dominated fen over the experiment. Pore water IHg concentrations in **(A)** the moss-dominated fen and **(B)** the sedge-dominated fen; pore water MeHg concentrations in **(C)** the moss-dominated fen and **(D)** the sedge-dominated fen; % MeHg changes in pore waters in **(E)** the moss-dominated fen and **(F)** the sedge-dominated fen. Colors are different plot treatments: black for the control plots; orange for the passively warmed plots; red for the actively warmed plots. Bars are mean values and whiskers are ± one standard deviation.

Mitchell et al., 2008b). Despite active warming increasing both the THg and MeHg concentrations in porewater in the moss-dominated site, the relatively greater increase in MeHg concentrations resulted in a large increase in %MeHg, strongly suggesting active methylation of porewater IHg. Although the sedge-dominated site showed a stronger impact of active warming on absolute porewater MeHg concentrations, the % MeHg remained relatively low because that the relatively high absolute porewater IHg concentrations consistently measured at this site may offset the changes of increased MeHg concentrations. The substantial increase in MeHg concentrations and decreased IHg concentrations in warmed plots relative to controls in the sedge-dominated site could be a reflection of the net conversion of dissolved IHg to MeHg at this site.

Sulfate is an important but limiting nutrient for the dominant Hg methylator, the SRB, in boreal peatlands (Branfireun et al., 1999; Mitchell et al., 2008b). Rising temperature stimulates SRB metabolism with consumption of $SO_4^{2-}$ (Holmer and Storkholm, 2001), while drier conditions increase the oxidation of reduced sulfur compounds (Mandernack et al., 2000). Warming had no direct significant effects on $SO_4^{2-}$ concentrations in the moss-dominate site but did in the sedge-dominated site. The sedge-dominated site is relatively more $SO_4^{2-}$-rich due to groundwater and surface water connections with a generally higher water table, and this generally higher availability alone may have been responsible for an observable significant effect at this site. The more $SO_4^{2-}$ limited, and strongly reducing conditions in the moss-dominated fen indeed may have resulted in a much more rapid cycling of available $SO_4^{2-}$ such that any warming related increase in $SO_4^{2-}$ availability was not measurable. The significant time × warming treatment interaction in both sites suggested that $SO_4^{2-}$ concentrations were controlled by both seasonal changes in environmental conditions and warming treatments. The peak summer months generally bring about lower water table levels

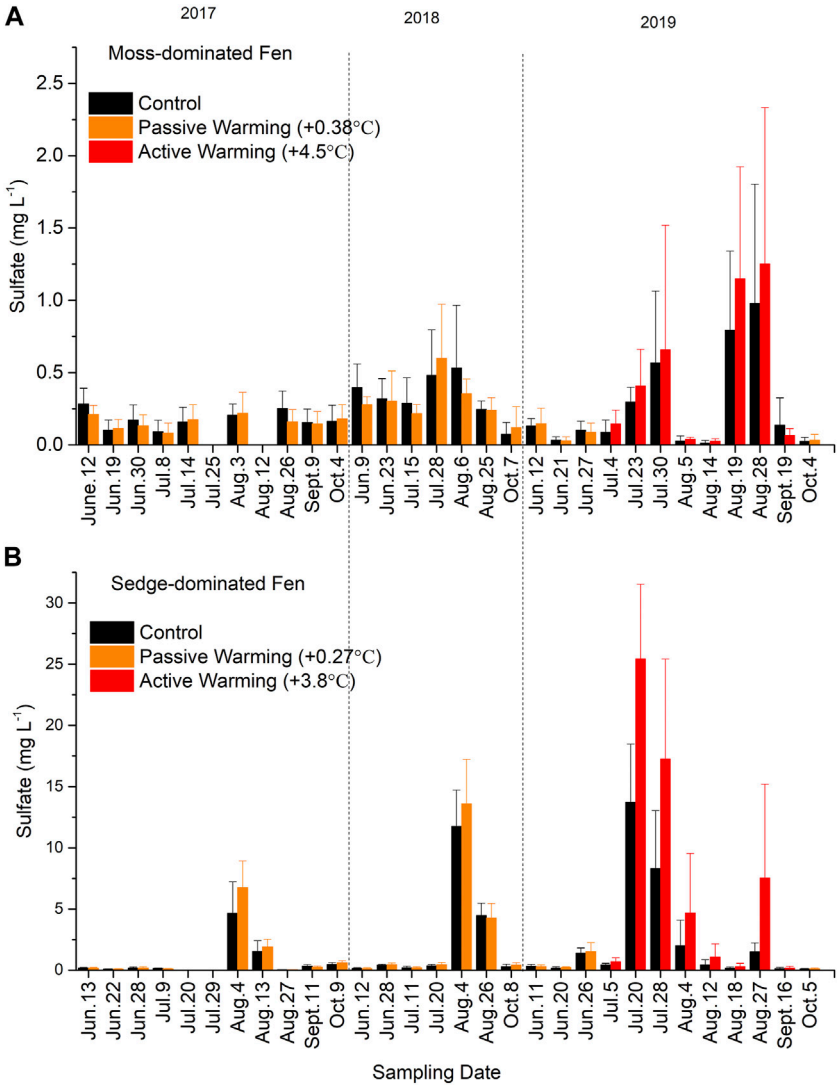


FIGURE 4
Sulfate ($SO_4^{2-}$) concentrations in **(A)** the moss-dominated fen and **(B)** the sedge-dominated fen. Colors are different plot treatments: black for the control plots; orange for the passively warmed plots; red for the actively warmed plots. Bars are mean values and whiskers are ± one standard deviation. Note differences in *y*-axis scales.

and lower surface soil moistures due to lower rainfall amounts and higher evapotranspiration rates. Thus, the higher $SO_4^{2-}$ concentrations in July and August across all years, especially in 2019, were partially attributed to the oxidative release of reduced sulfur compounds from peat soils (Rydin et al., 2013). Although higher $SO_4^{2-}$ concentrations and more oxic conditions may appear contradictory to the observed concomitant increases in MeHg concentrations, this was likely a function of the sampling approach in the experimental plots. A single fully integrating 50 cm well was used to sample porewater chemistry. During periods of the lower water table and oxidation of reduced sulphur compounds, $SO_4^{2-}$ becomes available in the upper peat profile and at the oxic-anoxic interface, stimulating Hg methylation in the deeper saturated zone, all of which is sampled together by the integrated closed Teflon well. Enhanced net MeHg production under warming conditions is not just a function of increased microbial metabolism but also increased $SO_4^{2-}$ availability due to the drying.

Overall microbial metabolism and Hg availability may be also increased by warming-induced changes to DOM quantity and quality. There is no doubt that warming increases microbial metabolism (Comeau, 2008), with a subsequent increase in decomposition. However, there was a non-significant increase in warming on DOC concentrations at both sites. A plausible explanation is that warmer conditions may enhance decomposition rates corresponding with increases in the emissions of $CO_2$ (Dorrepaal et al., 2009; Schuur et al., 2015). At the moss-dominated site, there were no significant differences in mean $SUVA_{254}$ values and other fluorescence indices between warming plots and control plots, possibly reflecting the contribution of both higher and lower molecular weight (more and less aromatic) compounds from SOM decomposition and microbial biomass or plant root exudates, respectively.

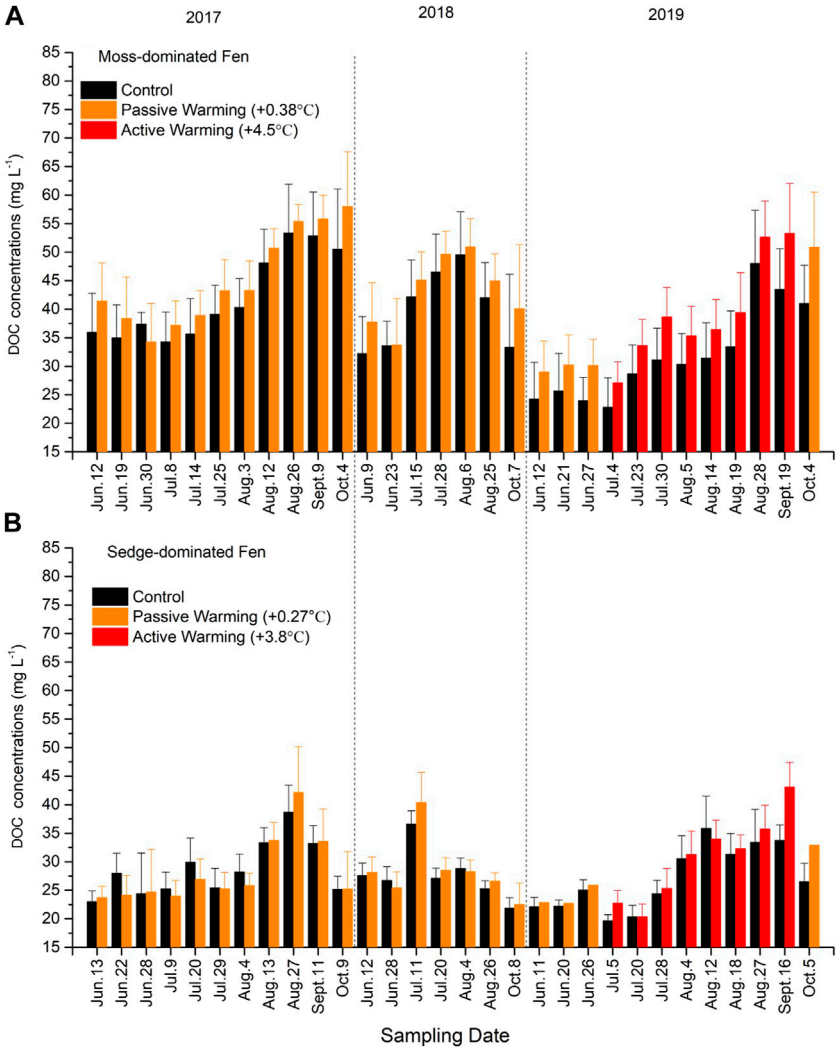


FIGURE 5
Dissolved organic carbon (DOC) concentrations in **(A)** the moss-dominated fen and **(B)** the sedge-dominated fen. Colors are different plot treatments: black for the control plots; orange for the passively warmed plots; red for the actively warmed plots. Bars are mean values and whiskers are ± one standard deviation.

At the sedge-dominated fen, warming significantly decreased $SUVA_{254}$ values over time and significantly increased BIX index. These trends indicate a larger input of plant-derived lower molecular weight DOM and bacterial biomass. This is entirely consistent with the fact that this fen vegetation community is overwhelmingly dominated by *Carex* spp. which has been shown to increase in biomass at this site in response to even passive warming in the plots (Lyons et al., 2020). Further, Lyons and Lindo (2020) used phospholipid fatty acid (PLFA) analysis to show that the sedge-dominated fen microbial community was bacterially-dominated, whereas the moss-dominated fen was fungal-dominated. The significant difference in bacterial abundance is a parsimonious explanation for the observed effects on DOM quality indices in the sedge-dominated fen and not the moss-dominated site; over the short duration of the experiment, the much higher "ecosystem metabolism" of the sedge-dominated site allowed for changes to manifest more quickly. The rapid response of the bacteria-dominated microbial community in the sedge-dominated fen coupled with the increased above and belowground biomass of the dominant *Carex* spp. and the increased delivery of root exudates and relatively labile litter inputs suggests that sedge-dominated systems could be more important sites of Hg methylation in a warmer world. The potential trajectory of moss-dominated fens toward sedge-dominated systems under climate change (Dieleman et al., 2015) raises concerns about northern peatlands more generally becoming more potent sites of Hg methylation because of shifts in plant community composition, in addition to weaker carbon sinks (Wu and Roulet, 2014).

Our results indicate that climate change-induced ground warming will increase MeHg concentrations in the porewaters of northern peatlands, and that the degree of this increase

**TABLE 2** Measures of specific ultraviolet absorbance at 254 nm ($SUVA_{254}$, L mg $C^{-1}$ $mL^{-1}$) and fluorescence indices (FI, $HIX_{EM}$, and BIX) in pore waters under the ground warming treatment at moss- and sedge-dominated sites. Passive warming was from June to October in 2017, 2018 and 2019; active warming was from July to September in 2019. Control and Experimental Plot data are paired by year. Values are presented as mean ± standard deviation.

| | Moss-dominated fen | | | Sedge-dominated fen | | |
|---|---|---|---|---|---|---|
| | Control plots | Passively warmed plots | Actively warmed plots | control plots | Passively warmed plots | Actively warmed plots |
| $SUVA_{254}$ | 4.40 ± 0.48 | 4.55 ± 0.61 | | 4.33 ± 0.53 | 4.29 ± 0.55 | |
| | 5.30 ± 0.47 | | 5.17 ± 0.46 | 5.55 ± 0.47 | | 5.31 ± 0.50 |
| FI | 1.32 ± 0.06 | 1.33 ± 0.07 | | 1.51 ± 0.09 | 1.51 ± 0.09 | |
| | 1.31 ± 0.04 | | 1.31 ± 0.05 | 1.50 ± 0.04 | | 1.53 ± 0.04 |
| $HIX_{EM}$ | 0.93 ± 0.04 | 0.93 ± 0.05 | | 0.93 ± 0.03 | 0.93 ± 0.03 | |
| | 0.92 ± 0.02 | | 0.93 ± 0.03 | 0.92 ± 0.01 | | 0.91 ± 0.01 |
| BIX | 0.41 ± 0.03 | 0.40 ± 0.03 | | 0.50 ± 0.04 | 0.51 ± 0.04 | |
| | 0.43 ± 0.02 | | 0.43 ± 0.01 | 0.53 ± 0.03 | | 0.56 ± 0.03 |

depends in part on peatland type. This increase is driven by not just the expected increase in microbial metabolism which will speed up other biogeochemical cycles in addition to Hg methylation, but also warming-induced increased availability of other reactants required for methylation, including $SO_4^{2-}$, labile DOM, and bioavailable IHg. This experiment may represent a transient response to pulse warming treatment, however the size of the pool of available sulfur, OM and IHg in peatlands along with the consistency of the findings here with other work related to warming induced peatland changes strongly suggest that the enhancement of MeHg production in these systems under future warming is both likely to occur, and is likely to be sustained. Ultimately the implications of this increased MeHg production on downstream aquatic systems is a function of MeHg export from these sites of methylation. summer streamflow from northern peatlands will likely decrease as a function of future warming and lower water tables, potentially offsetting the negative impacts of higher rates of MeHg production within the peatland itself.

## Data availability statement

The raw data supporting the conclusion of this article will be made available by the authors, without undue reservation.

## Author contributions

All authors contributed to the editing of the final manuscript; ZL and BB designed and initiated with BRACE experiment, TS collected and analysed samples, conducted data analysis and interpretation, and wrote the draft manuscript.

## Funding

The Funding was provided by the Natural Sciences and Engineering Research Council of Canada (NSERC) Discover Grants program (# 217046-2009 [BB], # 05901–2019 [ZL]), Research Tools and Infrastructure (# 458702-2014 [ZL and BB]), and Strategic Partnership Grants program (# 479026-2015 [BB and ZL]).

## Acknowledgments

We thank numerous field crews and technicians from the Ontario Ministry of Natural Resources and Forestry for their help in establishing the experimental system at these two remote peatland sites, including James McLaughlin who was instrumental in overseeing our continued site success. We would also like to thank several undergraduate and graduate students for field support (Bayley Germain, Jing Tian, Caitlyn Lyons, Madelaine Anderson, and Ericka James).

## Conflict of interest

The authors declare that the research was conducted in the absence of any commercial or financial relationships that could be construed as a potential conflict of interest.

## Publisher's note

# References


Bloom, N. (1989). Determination of picogram levels of methylmercury by aqueous phase ethylation, followed by cryogenic gas chromatography with cold vapour atomic fluorescence detection. *Can. J. Fish. Aquatic Sci.* 46, 1131–1140. doi:10.1139/f89-147

Branfireun, B. A., Roulet, N. T., Kelly, C. A., and Rudd, J. W. M. (1999). *In situ* sulphate stimulation of mercury methylation in a boreal peatland: Toward a link between acid rain and methylmercury contamination in remote environments. *Glob. Biogeochem. Cycles* 13, 743–750. doi:10.1029/1999gb900033

Brigham, M. E., Wentz, D. A., Aiken, G. R., and Krabbenhoft, D. P. (2009). Mercury cycling in stream ecosystems. 1. water column chemistry and transport. *Environ. Sci. Technol.* 43, 2720–2725. doi:10.1021/es802694n

Buttler, A., Robroek, B. J. M., Laggoun-Defarge, F., Jassey, V. E. J., Pochelon, C., Bernard, G., et al. (2015). Experimental warming interacts with soil moisture to discriminate plant responses in an ombrotrophic peatland. *J. Veg. Sci.* 26, 964–974. doi:10.1111/jvs.12296

Canario, J., Branco, V., and Vale, C. (2007). Seasonal variation of monomethylmercury concentrations in surface sediments of the Tagus Estuary (Portugal). *Environ. Pollut.* 148, 380–383. doi:10.1016/j.envpol.2006.11.023

Ci, Z. J., Peng, F., Xue, X., and Zhang, X. S. (2020). Permafrost thaw dominates mercury emission in Tibetan thermokarst ponds. *Environ. Sci. Technol.* 54, 5456–5466. doi:10.1021/acs.est.9b06712

Clarkson, T. W., and Magos, L. (2006). The toxicology of mercury and its chemical compounds. *Crit. Rev. Toxicol.* 36, 609–662. doi:10.1080/10408440600845619

Coleman-Wasik, J., Engstrom, D. R., Mitchell, C. P. J., Mitchell, E. B., Monson, B. A., Balogh, S. J., et al. (2015). The effects of hydrologic fluctuation and sulfate regeneration on mercury cycling in an experimental peatland. *J. Geophys. Research-Biogeosciences* 120, 1697–1715. doi:10.1002/2015jg002993

Comeau, Y. (2008). "Microbial metabolism," in *Biological wastewater treatment: principles, modelling and design* (London: IWA Publishing), 9–32.

Dieleman, C. M., Branfireun, B. A., McLaughlin, J. W., and Lindo, Z. (2015). Climate change drives a shift in peatland ecosystem plant community: Implications for ecosystem function and stability. *Glob. Change Biol.* 21, 388–395. doi:10.1111/gcb.12643

Dieleman, C. M., Lindo, Z., McLaughlin, J. W., Craig, A. E., and Branfireun, B. A. (2016). Climate change effects on peatland decomposition and porewater dissolved organic carbon biogeochemistry. *Biogeochemistry* 128, 385–396. doi:10.1007/s10533-016-0214-8

Dorrepaal, E., Toet, S., van Logtestijn, R. S. P., Swart, E., van de Weg, M. J., Callaghan, T. V., et al. (2009). Carbon respiration from subsurface peat accelerated by climate warming in the subarctic. *Nature* 460, 616–619. doi:10.1038/nature08216

Driscoll, C. T., Mason, R. P., Chan, H. M., Jacob, D. J., and Pirrone, N. (2013). Mercury as a global pollutant: Sources, pathways, and effects. *Environ. Sci. Technol.* 47, 4967–4983. doi:10.1021/es305071v

Fellman, J. B., Hood, E., and Spencer, R. G. M. (2010). Fluorescence spectroscopy opens new windows into dissolved organic matter dynamics in freshwater ecosystems: A review. *Limnol. Oceanogr.* 55, 2452–2462. doi:10.4319/lo.2010.55.6.2452

Fleming, E. J., Mack, E. E., Green, P. G., and Nelson, D. C. (2006). Mercury methylation from unexpected sources: Molybdate-inhibited freshwater sediments and an iron-reducing bacterium. *Appl. Environ.* 72, 457–464. doi:10.1128/AEM.72.1.457-464.2006

Gilmour, C. C., Henry, E. A., and Mitchell, R. (1992). Sulfate stimulation of mercury methylation in freshwater sediments. *Environ. Sci. Technol.* 26, 2281–2287. doi:10.1021/es00035a029

Gilmour, C. C., Podar, M., Bullock, A. L., Graham, A. M., Brown, S. D., Somenahally, A. C., et al. (2013). Mercury methylation by novel microorganisms from new environments. *Environ. Sci. Technol.* 47, 11810–11820. doi:10.1021/es403075t

Haitzer, M., Aiken, G. R., and Ryan, J. N. (2003). Binding of mercury (II) to aquatic humic substances: Influence of pH and source of humic substances. *Environ. Sci. Technol.* 37, 2436–2441. doi:10.1021/es026291o

Hall, B. D., Aiken, G. R., Krabbenhoft, D. P., Marvin-DiPasquale, M., and Swarzenski, C. M. (2008). Wetlands as principal zones of methylmercury production in southern Louisiana and the Gulf of Mexico region. *Environ. Pollut.* 154, 124–134. doi:10.1016/j.envpol.2007.12.017

Hamelin, S., Amyot, M., Barkay, T., Wang, Y. P., and Planas, D. (2011). Methanogens: Principal methylators of mercury in lake periphyton. *Environ. Sci. Technol.* 45, 7693–7700. doi:10.1021/es2010072

Helbig, M., Waddington, J. M., Alekseychik, P., Amiro, B. D., Aurela, M., Barr, A. G., et al. (2020). Increasing contribution of peatlands to boreal evapotranspiration in a warming climate. *Nat. Clim. Change* 10, 555–560. doi:10.1038/s41558-020-0763-7

Holmer, M., and Storkholm, P. (2001). Sulphate reduction and sulphur cycling in lake sediments: A review. *Freshw. Biol.* 46, 431–451. doi:10.1046/j.1365-2427.2001.00687.x–

Hudelson, K. E., Drevnick, P. E., Wang, F. Y., Armstrong, D., and Fisk, A. T. (2020). Mercury methylation and demethylation potentials in Arctic lake sediments. *Chemosphere* 248, 126001. doi:10.1016/j.chemosphere.2020.126001

Hurley, J. P., Krabbenhoft, D. P., Cleckner, L. B., Olson, M. L., Aiken, G. R., and Rawlik, P. S. (1998). System controls on the aqueous distribution of mercury in the northern Florida Everglades. *Biogeochemistry* 40, 293–311. doi:10.1023/a:1005928927272

IPCC (2018). "Summary for policymakers, in " *Global warming of 1.5°C. An IPCC special report on the impacts of global warming of 1.5°C above pre-industrial levels and related global greenhouse gas emission pathways, in the context of strengthening the global response to the threat of climate change, sustainable development, and efforts to eradicate poverty*. Editors V. P. Masson-Delmotte, H.-O. Zhai, D. Portner, J. Roberts, P. R. Skea, A. Shukla, et al. (Geneva, Switzerland: World Meteorological Organization), 32

Kerin, E. J., Gilmour, C. C., Roden, E., Suzuki, M. T., Coates, J. D., and Mason, R. P. (2006). Mercury methylation by dissimilatory iron-reducing bacteria. *Appl. Environ. Microbiol.* 72, 7919–7921. doi:10.1128/aem.01602-06

King, J. K., Saunders, F. M., Lee, R. F., and Jahnke, R. A. (1999). Coupling mercury methylation rates to sulfate reduction rates in marine sediments. *Environ. Toxicol. Chem.* 18, 1362–1369. doi:10.1002/etc.5620180704

Kolari, T. H. M., Sallinen, A., Wolff, F., Kumpula, T., Tolonen, K., and Tahvanainen, T. (2021). Ongoing fen-bog transition in a Boreal Aapa mire inferred from repeated field sampling, aerial images, and landsat data. *Ecosystems* 25, 1166–1188. doi:10.1007/s10021-021-00708-7

Krabbenhoft, D. P., and Sunderland, E. M. (2013). Global change and mercury. *Science* 341, 1457–1458. doi:10.1126/science.1242838

Liang, L., Horvat, M., and Bloom, N. S. (1994). An improved speciation method for mercury by GC/CVAFS after aqueous phase ethylation and room temperature precollection. *Talanta* 41, 371–379. doi:10.1016/0039-9140(94)80141-x

Liem-Nguyen, V., Skyllberg, U., and Bjorn, E. (2017). Thermodynamic modeling of the solubility and chemical speciation of mercury and methylmercury driven by organic thiols and micromolar sulfide concentrations in boreal wetland soils. *Environ. Sci. Technol.* 51, 3678–3686. doi:10.1021/acs.est.6b04622

Lyons, C. L., Branfireun, B. A., McLaughlin, J., and Lindo, Z. (2020). Simulated climate warming increases plant community heterogeneity in two types of boreal peatlands in north-central Canada. *J. Veg. Sci.* 31, 908–919. doi:10.1111/jvs.12912

Lyons, C. L., and Lindo, Z. (2020). Above- and belowground community linkages in boreal peatlands. *Plant Ecol.* 221, 615–632. doi:10.1007/s11258-020-01037-w

MacMillan, G. A., Girard, C., Chetelat, J., Laurion, I., and Amyot, M. (2015). High methylmercury in Arctic and Subarctic ponds is related to nutrient levels in the warming eastern Canadian Arctic. *Environ. Sci. Technol.* 49, 7743–7753. doi:10.1021/acs.est.5b00763

Mäkiranta, P., Laiho, R., Mehtätalo, L., Straková, P., Sormunen, J., Minkkinen, K., et al. 2018. Responses of phenology and biomass production of boreal fens to climate warming under different water-table level regimes. *Glob. Change Biol.*, 24: 944–956. doi:10.1111/gcb.13934

Mandernack, K. W., Lynch, L., Krouse, H. R., and Morgan, M. D., (2000). Sulfur cycling in wetland peat of the New Jersey Pinelands and its effect on stream water chemistry. *Geochimica Cosmochimica Acta*, 64, 3949–3964.

Mastný, J., Kastovska, E., Barta, J., Chronakova, A., Borovec, J., Santruckova, H., et al. (2018). Quality of DOC produced during litter decomposition of peatland plant dominants. *Soil Biol. Biochem.*, 121, 221–230. doi:10.1016/j.soilbio.2018.03.018

McPartland, M. Y., Montgomery, R. A., Hanson, P. J., Phillips, J. R., Kolka, R., and Palik, B. (2020). Vascular plant species response to warming and elevated carbon dioxide in a boreal peatland. *Environ. Res. Lett.* 15, 124066. doi:10.1088/1748-9326/abc4fb

Mergler, D., Anderson, H. A., Chan, L. H. M., Mahaffey, K. R., Murray, M., Sakamoto, M., et al. (2007). Methylmercury exposure and health effects in humans: A worldwide concern. *Ambio* 36, 3–11. doi:10.1579/0044-7447(2007)36[3:meahei]2.0.co;2

Mitchell, C. P. J., Branfireun, B. A., and Kolka, R. K. (2008b). Assessing sulfate and carbon controls on net methylmercury production in peatlands: An *in situ* mesocosm approach. *Appl. Geochem.* 23, 503–518. doi:10.1016/j.apgeochem.2007.12.020

Mitchell, C. P. J., Branfireun, B. A., and Kolka, R. K. (2008a). Total mercury and methylmercury dynamics in upland-peatland watersheds during snowmelt. *Biogeochemistry* 90, 225–241. doi:10.1007/s10533-008-9246-z

Mu, C. C., Schuster, P. F., Abbott, B. W., Kang, S. C., Guo, J. M., Sun, S. W., et al. (2020). Permafrost degradation enhances the risk of mercury release on Qinghai-Tibetan Plateau. *Sci. Total Environ.* 708. doi:10.1016/j.scitotenv.2019.135127

Paranjape, A. R., and Hall, B. D. (2017). Recent advances in the study of mercury methylation in aquatic systems. *Facets* 2, 85–119. doi:10.1139/facets-2016-0027

Ramlal, P. S., Kelly, C. A., Rudd, J. W. M., and Furutani, A. (1993). Sites of methyl mercury production in remote Canadian shield. *Can. J. Fish. Aquatic Sci.* 50, 972–979. doi:10.1139/f93-112

Ravichandran, M. (2004). Interactions between mercury and dissolved organic matter: A review. *Chemosphere* 55, 319–331. doi:10.1016/j.chemosphere.2003.11.011

Rydin, H., Jeglum, J. K., and Bennett, K. D. (2013). *The biology of peatlands*. Oxford, United Kingdom: Oxford University Press.

Schaefer, K., Elshorbany, Y., Jafarov, E., Schuster, P. F., Striegl, R. G., Wickland, K. P., et al. (2020). Potential impacts of mercury released from thawing permafrost. *Nat. Commun.* 11, 4650. doi:10.1038/s41467-020-18398-5

Schuur, E. A. G., McGuire, A. D., Schadel, C., Grosse, G., Harden, J. W., Hayes, D. J., et al. (2015). Climate change and the permafrost carbon feedback. *Nature* 520, 171–179. doi:10.1038/nature14338

Skyllberg, U., (2008). Competition among thiols and inorganic sulfides and polysulfides for Hg and MeHg in wetland soils and sediments under suboxic conditions: Illumination of controversies and implications for MeHg net production. *J. Geophys. Research:Biogeosciences*, 113, G00C03. doi:10.1029/2008JG000745

St Pierre, K. A., Chetelat, J., Yumvihoze, E., and Poulain, A. J. (2014). Temperature and the sulfur cycle control monomethylmercury cycling in high Arctic coastal marine sediments from Allen Bay, Nunavut, Canada. *Environ. Sci. Technol.* 48, 2680–2687. doi:10.1021/es405253g

Streets, D. G., Horowitz, H. M., Lu, Z. F., Levin, L., Thackray, C. P., and Sunderland, E. M. (2019). Global and regional trends in mercury emissions and concentrations. *Atmos. Environ.* 201, 417–427. doi:10.1016/j.atmosenv.2018.12.031

Tarnocai, C. (2009). The impact of climate change on Canadian peatlands. *Can. Water Resour. J.* 34, 453–466. doi:10.4296/cwrj3404453

Ullrich, S. M., Tanton, T. W., and Abdrashitova, S. A. (2001). Mercury in the aquatic environment: A review of factors affecting methylation. *Crit. Rev. Environ. Sci. Technol.* 31, 241–293. doi:10.1080/20016491089226

US EPA (1996). "Sampling ambient water for trace metals at EPA water quality criteria levels, " in *U.S. environmental protection agency office of water engineering and analysis division (4303)* (Washington, D. C.) 20460.

Weishaar, J. L., Aiken, G. R., Bergamaschi, B. A., Fram, M. S., Fujii, R., and Mopper, K. (2003). Evaluation of specific ultraviolet absorbance as an indicator of the chemical composition and reactivity of dissolved organic carbon. *Environ. Sci. Technol.* 37, 4702–4708. doi:10.1021/es030360x

Wu, J. H., and Roulet, N. T. (2014). Climate change reduces the capacity of northern peatlands to absorb the atmospheric carbon dioxide: The different responses of bogs and fens. *Glob. Biogeochem. Cycles* 28, 1005–1024. doi:10.1002/2014gb004845

Xia, K., Skyllberg, U. L., Bleam, W. F., Bloom, P. R., Nater, E. A., and Helmke, P. A. (1999). X-ray absorption spectroscopic evidence for the complexation of Hg (II) by reduced sulfur in soil humic substances. *Environ. Sci. Technol.* 33, 257–261. doi:10.1021/es980433q

Yang, Z. M., Fang, W., Lu, X., Sheng, G. P., Graham, D. E., Liang, L. Y., et al. (2016). Warming increases methylmercury production in an Arctic soil. *Environ. Pollut.* 214, 504–509. doi:10.1016/j.envpol.2016.04.069

Yu, R. Q., Adatto, I., Montesdeoca, M. R., Driscoll, C. T., Hines, M. E., and Barkay, T. (2010). Mercury methylation in Sphagnum moss mats and its association with sulfate-reducing bacteria in an acidic Adirondack forest lake wetland. *FEMS Microbiol. Ecol.* 74, 655–668. doi:10.1111/j.1574-6941.2010.00978.x

Zhang, H., Valiranta, M., Piilo, S., Amesbury, M. J., Aquino-Lopez, M. A., Roland, T. P., et al. (2020). Decreased carbon accumulation feedback driven by climate-induced drying of two southern boreal bogs over recent centuries. *Glob. Change Biol.* 26, 2435–2448. doi:10.1111/gcb.15005

frontiers | Frontiers in Environmental Science

TYPE Original Research
PUBLISHED 09 August 2023
DOI 10.3389/fenvs.2023.1191909



OPEN ACCESS

EDITED BY
Wei He,
China University of Geosciences, China

REVIEWED BY
M. Dolores Basallote,
University of Huelva, Spain
Željka Fiket,
Ruđer Bošković Institute, Croatia

*CORRESPONDENCE
Kaisa Forsyth,
kaisa.forsyth@gmail.com
Mathieu Pédrot,
mathieu.pedrot@univ-rennes.fr

RECEIVED 22 March 2023
ACCEPTED 25 July 2023
PUBLISHED 09 August 2023

CITATION
Forsyth K, Dia A, Marques R, Prudêncio MI, Diamantino C, Carvalho E, Russo D, Dionisio I, Davranche M, Bouhnik-Le-Coz M and Pédrot M (2023), Bioconcentration and translocation of rare earth elements in plants collected from three legacy mine sites in Portugal. *Front. Environ. Sci.* 11:1191909. doi: 10.3389/fenvs.2023.1191909



# Bioconcentration and translocation of rare earth elements in plants collected from three legacy mine sites in Portugal

Kaisa Forsyth[1]*, Aline Dia[1], Rosa Marques[2,3], Maria Isabel Prudêncio[2,3], Catarina Diamantino[4], Edgar Carvalho[4], Dulce Russo[2,3], Isabel Dionisio[2,3], Melanie Davranche[1], Martine Bouhnik-Le-Coz[1] and Mathieu Pédrot[1]*

[1]Univ. Rennes, CNRS, Géosciences Rennes, UMR 6118, Rennes, France, [2]Centro de Ciências e Tecnologias Nucleares (C[2]TN), Instituto Superior Técnico, Universidade de Lisboa, Bobadela, Portugal, [3]Departamento de Engenharia e Ciências Nucleares (DECN), Instituto Superior Técnico, Universidade de Lisboa, Bobadela, Portugal, [4]EDM—Empresa de Desenvolvimento Mineiro, S.A., Lisbon, Portugal

Rare earth elements (REE), a group of emerging contaminants with commercial and technological applications, share many physical and chemical characteristics and have thus been used as accurate tracers of various environmental samples. They have been shown to increase in receiving waters following the dissolution of host-rock material during mining activities. In this study, spontaneous vegetation and related media were collected from three Portuguese legacy mine sites in November 2020 to evaluate the phytoavailability and fate of REE. Water, soil and plant data were analyzed in the context of the 1) prevailing geochemical context, 2) the mining context, and 3) plant effects. This study presents the REE signatures for different plant species and links the signatures to a potential source of bioavailable REE. The REE accumulated in plant tissue seems to reflect the REE signature of surface waters in the mining areas, showing enrichment in middle REE. Although the soils, sediments, and waters in this study had similar features, certain plants seemed better adapted to translocating Light REE and Eu over others. Given that REE are readily available within the field conditions of a mining site, this study shows how plant physiology and biologic preference towards particular REE contribute to the fractionation of REE and create a unique signature dependent on plant type.

KEYWORDS

**rare earth elements, acid mine drainage, abandoned mines, plant, soil, water, bioaccumulation, transfer factor**

## 1 Introduction

The rare earth elements (REE) are comprised of 17 elements: the lanthanoid series (La, Ce, Pr, Nd, Pm, Sm, Eu, Gd, Tb, Dy, Ho, Er, Tm, Yb, and Lu), plus Y and Sc (Pan et al., 2020). They can be characterized by similar chemical properties and closely related geochemical behaviors, resulting in similar distributions within the Earth's crust (Taylor and McLennan, 1985). Though Y and Sc are officially defined as REE by the International Union of Pure and Applied Chemistry (IUPAC) (2005), the lanthanoid series (La to Lu) share electrical and thermodynamic properties (Joshi et al., 2018) and a unique electron configuration which

results in lanthanide contraction. Therefore, this paper will only consider La-Lu when referencing the REE series.

Since the initial discovery of REE in 1794, they have become a critical part of the world economy (U.S. Geological Survey, 2022). Their versatile applications in industry, medical services, agriculture, and many other domains (Bau and Dulski, 1996; Tyler, 2004; Binnemans et al., 2013; Migaszewski and Gałuszka, 2015; Van Gosen et al., 2017) have inevitably led to the elevated release of REE in the environment (Li et al., 2013; Merschel and Bau, 2015) and an increased risk of occupational exposures (Rim et al., 2013). Yet the environmental risks related to REE have so far received little attention, overshadowed as they are by economic and geopolitical considerations. Evidence suggesting their potential toxicity (Pagano et al., 2015; Wakabayashi et al., 2016; Gong et al., 2021) has consequently led to REE being categorized as "emerging contaminants," potentially making the anomalous supply of REE in the environment a major challenge for the years to come.

Historically the management of mining wastes has posed a risk to the environment, with many sites leaving a legacy of significant pollution to the surrounding environment (Perez-Lopez et al., 2010; Li et al., 2013; Soyol-Erdene et al., 2018). Economically valuable resources have often been mined, generating major anthropogenic waste streams and spurring geogenic pollution, exemplified by Acid Mine Drainage (AMD). AMD is characterized by the oxidation of iron-sulfide minerals leading to the perpetual formation of sulfuric acid, concomitant with an increase in soluble metal concentrations (Johnson and Hallberg, 2003; Herman and Maier, 2009). Several countries such as Australia, Bolivia, China, France, Germany, India, Portugal, Romania, Spain, Sweden, and the United States (Akcil and Koldas, 2006; Casiot et al., 2009; Grawunder et al., 2014; Strosnider et al., 2014; Marquez et al., 2018, and references therein) are impacted by AMD, making it a global concern. These mine waste sites, with large quantities of metals solubilized by AMD and mining practices, provide valuable insights into the behavior of REE in the environment. Because of their ubiquitous distribution in Earth's crust, the dissolution of host-rock material during local mining activities has been shown to increase REE in receiving waters (Ferreira da Silva et al., 2009; Perez-Lopez et al., 2010; Prudêncio et al., 2015; Soyol-Erdene et al., 2018), even when the resources being mined are not REE.

While there are 199 cataloged abandoned mines in Portugal, this study focuses on three sites: São Domingos, Lousal, and Quinta do Bispo. These sites have been chosen as subjects of study due to their long history of mining activity in a variety of geologic contexts with different stages of remediation efforts in place. Though the context for each of these mines is vastly different, they share previously observed high REE concentration levels. Each site demonstrates anthropogenically driven changes to geochemistry as São Domingos and Lousal are subject to AMD evolution from waste rock piles, while low-grade uranium ores from Quinta do Bispo have been processed using *in situ* leaching (ISL). The Lousal site boasts a passive treatment system in an effort to remediate tailing leachate and AMD. Though no such treatment systems were in place at the other two sites as of November 2020, all three were monitored regularly with future remediation projects planned by Empresa de Desenvolvimento Mineiro (EDM). Since the geochemistry and background of each mine are unique, we are afforded the opportunity to study various control parameters, making them ideal targets for this investigation of the uptake and fractionation of REE by spontaneous vegetation as well as the concentration in corresponding soils and waters.

Plants potentially play a vital role in the fate and transport of REE (Tyler, 2004). Although some studies have suggested phytoremediation strategies to stabilize and remove REE from contaminated soils (Lima and Ottosen, 2021), the topic has been the subject of limited study. To date two plant types, *Dichranopteris dichotoma* (Chour et al., 2018; Liu et al., 2018) and *Phytolacca Americana* (Liu et al., 2018), have been identified as candidates for REE recovery when combined with enhanced extraction using electrokinetic methods (Lima and Ottosen, 2021).

The origin of REE fractionation in plant tissue is still subject to many questions as well. Very few authors have published on the entire REE series and their impact on the planted environment, instead opting to study a selection of REE considered representative of the LREE (light rare earth elements), MREE (middle rare earth elements), and HREE (heavy rare earth elements). However, the stability constants formed between individual REE and compatible ions vary (Millero, 1992), potentially creating differences in the bioavailability of REE in the natural environment, thus demonstrating the importance of studying the entire REE series. Moreover, while some studies have concluded that the geologic context and soil weathering are critical factors influencing plant REE uptake (Laul and Weimer, 1982; Pisciotta et al., 2017), others have suggested that a combination of plant type and geologic context is important to note in determining the phyto-availability of REE (Gałuszka et al., 2020).

Through the analysis of water, soil, and plant samples, this study presents REE signatures. The implication of each signature is discussed in the context of the environmental compartment, the geochemical background, and the mining influences. Using the bioconcentration and translocation factors, this study presents data on REE phyto-availability and fractionation.

## 2 Materials and methods

Nine water samples, 13 soil/aquatic sediment samples and 12 plant samples were recovered in November 2020 from three different legacy mine sites (Table 1) located in Portugal. Samples were collected from both inside and outside of mining sites to assess the legacy of mining activity. Site management and remediation is currently supervised by EDM, a State-owned enterprise, under a concession contract concluded with the Portuguese State for the environmental recovery of degraded mining areas (approved in Decree-Law n° 198-A/2001, 6/7/2001).

### 2.1 Field site description and collected samples

The sample locations and types are reported in Table 1 and mapped in Figure 1. The geological characteristics of the sampling sites and the descriptions of the samples collected are detailed in the following section.

#### 2.1.1 São Domingos

São Domingos, located in Southern Portugal, has been an established mining area since Chalcolithic times. Copper and

**TABLE 1 Coordinates for all samples collected from mine areas in Portugal (São Domingos, Lousal and Quinta do Bispo).**

| Mine site | Sample type | Sample ID | Latitude | Longitude |
|---|---|---|---|---|
| São Domingos Mine | Water | Tapada Grande Reservoir, "uncontaminated" | N 37°40′10.2″ | W 7°30′25.2″ |
| | Water | Pt. 1: São Domingos, "contaminated" | N 37°39′34.0″ | W 7°30′19.9″ |
| | Water | Pt. 2: São Domingos, "contaminated" | N 37°39′11.3″ | W 7°30′34.5″ |
| | Plant/Soil | *Cistus ladanifer*[a] | N 37°40′10.2″ | W 7°30′25.2″ |
| | Plant/Soil | *Cistus ladanifer* | N 37°39′34.0″ | W 7°30′19.9″ |
| | Plant/Soil | *Cistus ladanifer* | N 37°39′37.4″ | W 7°30′19.1″ |
| | Plant/Soil | *Erica andevalensis* | N 37°39′11.3″ | W 7°30′34.5″ |
| Quinta do Bispo | Water | Pt. 1: flooded open pit mine, "contaminated" | N 40°34′42.7″ | W 7°46′22.0″ |
| | Plant/Soil | *Salix* sp. | N 40°34′37.5″ | W 7°46′24.1″ |
| | Soil | Unplanted | N 40°34′37.5″ | W 7°46′24.1″ |
| | Plant/Soil | *Pteridium aquilinum*[a] | N 40°34′39.1″ | W 7°46′38.0″ |
| | Soil | Unplanted | N 40°34′39.1″ | W 7°46′38.0″ |
| | Plant/Soil | *Pteridium aquilinum* | N 40°34′40.3″ | W 7°46′16.6″ |
| | Plant/Soil | *Retama sphaerocarpa* | N 40°34′40.3″ | W 7°46′16.6″ |
| | Soil | Unplanted | N 40°34′40.3″ | W 7°46′16.6″ |
| Lousal Mine | Water | Uncontaminated water from Albufeira da Barragem da Tapada supplemented to passive treatment | N 38°02′15.1″ | W 8°25′31.1″ |
| | Water | Pt. 1: Leachate containment for tailings, "contaminated" | N 38°02′17.2″ | W 8°25′25.8″ |
| | Water | Pt. 2: Mixing pond for leachate and diluting water | N 38°02′15.6″ | W 8°25′25.4″ |
| | Water | Pt. 3: First treatment pool lined with limestone | N 38°02′10.2″ | W 8°25′36.4″ |
| | Water | Pt. 4: 6th treatment pool with plants established | N 38°02′10.7″ | W 8°25′18.3″ |
| | Plant/Sediment | *Juncus acutus*[a] | N 38°02′15.1″ | W 8°25′31.1″ |
| | Plant/Sediment | *Typha Latifolia*[a] | N 38°02′15.1″ | W 8°25′31.1″ |
| | Plant/Sediment | *Typha Latifolia* | N 38°02′10.7″ | W 8°25′18.3″ |
| | Plant/Sediment | *Juncus acutus* | N 38°02′10.7″ | W 8°25′18.3″ |

[a]Samples collected from outside of the mining area.

sulfur ores were the dominant resources extracted from São Domingos mine till its closure in 1966 (Pérez-López et al., 2010). São Domingos covers 50 $km^2$ of land in the Iberian Pyrite Belt (IPB) (Quental et al., 2002), an area infamously impacted by mining and the resulting AMD. The volcanogenic massive sulfides (VMS) in the IPB are rich in pyrite ($FeS_2$) with inclusions of chalcopyrite ($CuFeS_2$), sphalerite ((Zn,Fe)S), galena (PbS) and other polymetallic sulfide minerals. As the VMS deposits are exposed to the atmosphere, Fe(II) is oxidized to Fe(III) and S is oxidized to $SO_4^{2-}$, forming $H_2SO_4$ in surface waters. The perpetual cycle of AMD has been a proven challenge for environmental recovery efforts. EDM's strategy for rehabilitation prioritizes 1) the diversion of clean waters, 2) sealing and confinement of the mine waste deposits to prevent further AMD generation, 3) passive treatment of AMD, and 4) decontamination of the downstream Mosteirão River Valley. In order to mitigate the volume of contaminated waters, diversion of uncontaminated surface waters, as part of the first intervention, has already been completed. Following remediation, EDM intends to preserve the heritage of São Domingos and promote tourism.

The climate of São Domingos can be described as a temperate Mediterranean Köppen climate type with dry and hot summers (*Csa*) with an average annual air temperature of 17.5°C (Estatal de Meteorología (España) and Instituto de Meteorologia (Portugal), 2011). On average 500 mm of precipitation accumulates over the course of a year (Estatal de Meteorología (España) and Instituto de Meteorologia (Portugal), 2011). Species collected from São Domingos include: *Cistus ladanifer* and *Erica andevalensis,* both were prevalent species growing in the sampling area. *Erica andevalensis* is a metallophyte species endemic to the IPB, typically found growing on tailing piles or close to AMD-impacted surface waters (Cabezudo and Rivera, 1980). Since *Erica andevalensis* is identified as a vulnerable species (Law 8/2003 on Andalusian Wild Fauna and Flora) in Junta de

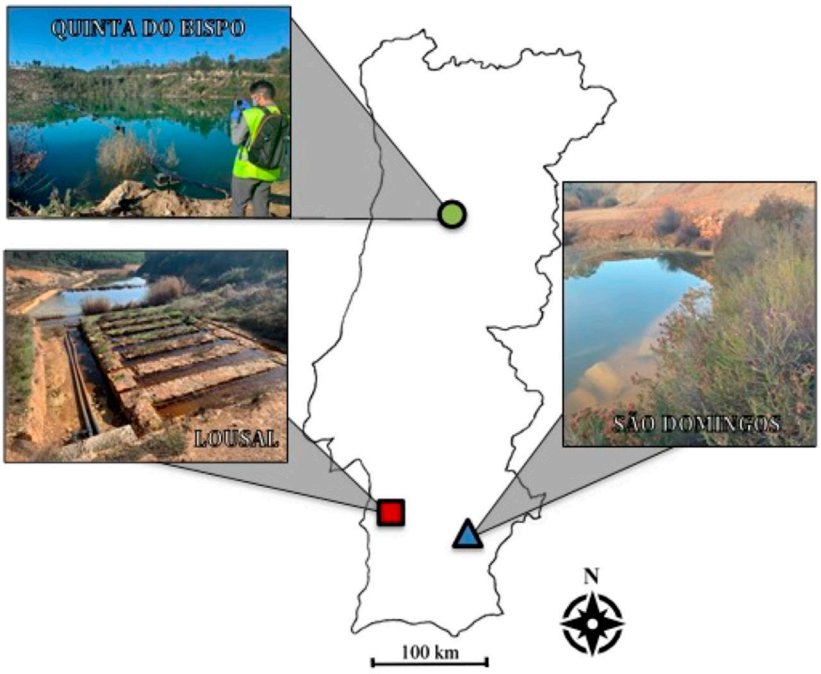


| Sample Type | Number of Observations (n) |
|---|---|
| Water | 9 |
| Soil | 13 |
| Above-ground Tissue | 11 |
| Below-ground Tissue | 11 |

FIGURE 1
Map of the sample sites with the number of observations for each sample type (n).

Andalucia: Consejeria de Medio Ambiente's list of threatened flora (Santa-Bárbara Carrascosa and Valdés, 2008/2008), this plant is subject to special protections.

### 2.1.2 Lousal

Lousal is an example of a legacy mine site under remediation and culturally revitalized as an educational center (Relvas, 2014). Located in the IPB of Southern Portugal, all mining activity ended at Lousal in 1988 (Relvas, 2014) when the extraction of S, Cu, and Zn from the polymetallic massive sulfide deposit became less profitable. Long established for the extraction of VMS ores, much like São Domingos, Lousal is impacted by AMD (Ferreira da Silva et al., 2009). In 2010, a passive treatment system consisting of 17 basins was built as part of EDM's first phase of treatment works. The treatment system collects leachate from a sealed tailing pile. The leachate is supplemented with water from Albufeira da Barragem da Tapada reservoir during dry seasons to maintain the wetland system. Basins are structured in a cascade with a limestone barrier between each basin constituting a permeable dike and HDPE geomembrane lining underneath to contain treatment effluent until discharge into Corona Creek, a tributary of Sado River. In the first treatment stage, five basins are devoted to the neutralization, precipitation, and sedimentation of the leachate mixture. The consecutive basins are planted with macrophytes, which remediate the metal loading (Al, As, Cu, Fe, and Zn) from the tailing pile (Empresa de Desenvolvimento Mineiro [EDM] and Direcção Geral de Energia e Geologia [DGEG], 2011). According to the measurements made during the sampling campaign, by the time the effluent reaches Corona Creek for discharge the pH is increased from 2.3 to 3.2.

The climate of Lousal is similar to that of São Domingos, however Lousal accumulates 600 mm of rainfall annually on average (Estatal de Meteorología (España) and Instituto de Meteorologia (Portugal), 2011). The treatment system is dominated by aquatic species such as: *Phragmites australis*, *Typha latifolia*, and *Juncus acutus*. Due to sampling constraints and the large rooting system associated with *Phragmites australis*, only *Typha latifolia* and *Juncus acutus* were collected for analysis.

### 2.1.3 Quinta do Bispo

Quinta do Bispo is a legacy uranium mine site hosted in Hercynian granite and meta-sedimentary deposits (Ramalho et al., 2009) in Northern Portugal. Unlike São Domingos and Lousal, Quinta do Bispo is not subject to the geogenic phenomenon of AMD. Quinta do Bispo was Portugal's largest open pit mine (European Commission Directorate-General for Energy, 2012). Between 1979 and 1987, 460,000 tons of ore were

excavated, resulting in a 75-m deep pit (Ramalho et al., 2009). Later, in 1992 the open pit was used to extract low-grade uranium ores (300–500 ppm) using ISL, which employs strong acids—such as sulfuric acid—to leach precious metals from ore. The exploitation of hydrothermally deposited uranium seams has left the nearby surface waters with contamination from extraction processes (Pereira, 2014). Environmental remediation of ISL practices is ongoing at Quinta do Bispo. This site was selected for study because the lanthanide series has similar physiochemical characteristics to the actinide series.

The climate of Quinta do Bispo can be described by a temperate Mediterranean Köppen climate type with a dry and temperate summer (*Csb*) characterized by an average air annual temperature of 15°C and 1,400 mm annual rainfall (Estatal de Meteorología España and Instituto de Meteorologia Portugal, 2011). Due to site conditions being conducive to sample access the Quinta do Bispo site is the focus of the comparison between planted and unplanted soil environments. Species collection was limited to plants with large biomass and high prevalence on-site. Species collected included: *Salix sp.*, *Pteridium aquilinum* and *Retama sphaerocarpa*.

## 2.2 Sample recovery and analyses

All materials used for the recovery of major cation and trace metal analysis were prepared in a clean room and decontaminated using a 24 h nitric acid (1.5 M $HNO_3$) wash at 45°C, followed by a 24 h wash with deionized ultrapure water (18 MΩ-cm) at 45°C.

### 2.2.1 Water samples

*In situ* physiochemical water quality parameters were measured during sample collection using a Aquaread AP-2000 multimeter with an AquaPlus 2000 dynamic luminescence quenching optical dissolved oxygen (DO) combination electrical conductivity (EC) and temperature electrode, and a 3MPK1 silver chloride combination pH and oxidizing-reducing potential (ORP) probe. The ORP was converted to Eh by interpolating the half-cell potential of the reference electrode using manufacture provided potentials at variable temperatures.

For laboratory analyses, approximately 60 mL of sample were filtered through 0.2 µm polyethersulfone (PES) filters capable of resisting deterioration when exposed to low pH solutions. Filtered samples were collected and separated into two Nalgene bottles, one for dissolved organic carbon (DOC) and anion analysis, and one for major cation and trace metal analysis. Bottles for major cation and trace metal analysis were preserved with 2% $HNO_3$ to maintain the integrity of the metals within the sample. The aliquots of sample reserved for dissolved organic carbon and anion analysis were kept refrigerated to preserve the integrity of analytes.

Major and trace cation concentrations were determined in water samples by ICP-MS (Agilent 7700x) using rhenium and rhodium as internal standards (Yéghicheyan et al., 2019). The international geostandard SLRS-6 was used to verify the validity and reproducibility of the results.

Dissolved Organic Carbon (DOC) and major anion concentrations of water samples were analyzed by Shimadzu TOC Analyzer, and by Dionex ICS-5000 ion chromatograph with an AS11 HC column (Dionex Method 123), respectively.

### 2.2.2 Plant samples

Plant samples were processed and analyzed in two mass fractions representative of the above-ground and below-ground tissues. Specimens from each species were collected within a 1-m radius and combined to represent one sample point. The above ground tissues were freeze dried and lyophilized, while below-ground tissue was washed with deionized water (18 MΩ-cm), and then dried in a 50°C oven for 4 days, and ground using a zircon ball-mill.

Above-ground plant samples were digested on a hot-plate using an adaption of the Krishnamurty (1976) method, whereas below-ground plant samples were digested more aggressively using a microwave (Anton Paar Multiwave 7000) with a modification of the preprogramed "organic" digestion method. Major and trace cation concentrations were determined using ICP-MS (Agilent 7700x) following an analogous protocol to the one performed on water samples, but with Tomato Leaves standard 1573a (NIST® SRM®) as a reference material for confirmation of the validity and reproducibility of results. Methodological error was determined using triplicate analysis of each sample.

### 2.2.3 Soil/aquatic sediment samples

Soils and aquatic sediments were collected from the same areas as the plant roots—representative of the rhizosphere - samples were dried at 40°C for 48 h and sieved to recover the <2 mm fraction. In addition to the rhizosphere soils collected for each plant, three bulk soils, identified by areas with no overlying vegetation, were collected from the Quinta do Bispo site.

Soil/aquatic sediment sample major and trace cation concentrations were analyzed by ICP-MS with alkaline fusion in the CNRS National SARM Analytical facility (https://sarm.cnrs.fr/index.html/) following the procedure described in Carignan et al. (2001), whereas soil/aquatic sediment texture, $pH_{water}$, $pH_{KCl}$, cationic exchange capacity ($CEC_{Metson}$), and organic matter (OM) content were determined by LABOCEA. LABOCEA employed standard methods to determine extractable cations by ammonium acetate agitation at pH 7 (NF X 31-108) (Metson, 1956) and OM content by dry combustion of sample carbon (NF ISO 10694).

## 2.3 Data handling

In order to compare the enrichment or depletion of REE as a whole series, they are generally normalized to a standard set of values. For this study we normalized REE concentrations in soil and water samples to Taylor and McLennan (1989)'s Upper Continental Crust (UCC) values. Elements were further classified into three groups, the light REE (LREE) which range from elements La to Nd, middle REE (MREE) Sm to Tb, and heavy REE (HREE) Dy to Lu. For soil, sediment, and aqueous samples the Ce anomaly (Ce*) and Eu anomaly (Eu*) were calculated using a linear extrapolation of UCC-normalized REE, Eqs. 1, 2 respectively:

$$Ce^{*} = \frac{2\left(Ce_{UCC}\right)}{La_{UCC} + Pr_{UCC}} \tag{1}$$

$$Eu^{*} = \frac{2\left(Eu_{UCC}\right)}{Sm_{UCC} + Gd_{UCC}} \tag{2}$$

For comparisons of plant samples, the bioconcentration factor (BCF) and translocation factor (TF) were calculated using Eqs. 3, 4, accordingly, where [$REE_{AG}$] is the concentration of REE in the above-ground tissue (mg $kg^{-1}$) [$REE_{BG}$] is the concentration of REE in the below-ground tissue (mg $kg^{-1}$), and [$REE_{soil}$] is the concentration of REE in the soil or aquatic sediment collected from the plant rhizosphere (mg $kg^{-1}$). The resulting BCF and TF values are dimensionless ratios. The BCF is reflective of the plant's ability to accumulate an element from the soil/aquatic sediment and TF is reflective of the ability for the plant to translocate elements from the rooting system to aerial tissue. The Ce* and Eu* for plant samples were determined using BCF values calculated from Eqs 1, 2, instead of UCC-normalized values:

$$BCF = \frac{[REE_{AG}]}{[REE_{Soil}]} \quad (3)$$

$$TF = \frac{[REE_{AG}]}{[REE_{BG}]} \quad (4)$$

For statistical treatment, standard diagnostic tests were performed to determine whether data needed transformation. If a transformation was required, the box-cox method for transformation was used to determine the best fit. Data passing diagnostic tests were then tested with an Analysis of Variance (ANOVA), for statistical significance the $p$-value was limited to $p < 0.05$. The number, n, of all datasets analyzed is reported in Figure 1. Missing data are handled as random, allowing the analysis of imbalanced datasets, particularly soils and aquatic sediments. Post-hoc testing was completed using Tukey Honestly Significantly Difference (Tukey HSD).

# 3 Results

In the following section the REE concentrations and associated chemistry are presented for samples representing the water, soil/aquatic sediment, and plant environmental compartments.

## 3.1 Water sample REE signature

*In situ* physicochemical water quality parameters are displayed in Supplementary Table S1. Waters collected from outside of São Domingos and Lousal were circumneutral, pH 7.1 and pH 6.7, accordingly. Similar Eh values were observed for water collected from outside of São Domingos and Lousal, +397 mV and +360 mV, respectively. Of the water samples collected from inside of the mining sites, the open pit at Quinta do Bispo had the highest pH, 5.1. The sample collected at Quinta do Bispo still had an oxidizing Eh of +524 mV. Samples collected from the São Domingos River Valley display a pH ranging from 2.4 to 2.9 and were strongly oxidizing with an Eh ranging from +691 mV to +723 mV. Similarly, samples collected from the Lousal treatment system had a pH ranging from 2.3 to 3.0 with an Eh ranging from +615 mV to +808 mV.

The EC for the samples collected from the mining areas tended to be higher than the EC observed outside of the mining areas. The range of DOC for the samples collected ranges from 0.45 mg·$L^{-1}$–9.71 mg·$L^{-1}$. Supplementary Table S1 presents the concentrations of anions, measured in aqueous samples. The dominant inorganic anion observed in the mining sites was sulfate, in contrast to the dominant anion outside of the mining area which was chloride. The presence of sulfate is anticipated as sulfuric acid is generated through AMD and used during ISL.

Upper Continental Crust (UCC) normalized aqueous REE patterns are displayed in Figure 2 while REE concentrations are tabulated in Table 2. The aqueous samples collected from outside of the mining area contained less REE than the samples collected from inside of the mining areas. The samples collected outside of the mining area exhibited depletion of LREE relative to both the MREE and HREE. The depletion of LREE was punctuated by a negative Ce anomaly (Ce*) for samples collected outside the mining area. Samples collected from the Lousal passive treatment system had the highest REE concentrations with 628.84 μg·$L^{-1}$ associated with the leachate treatment tank. The sample collected from the sixth treatment pool showed a marked decrease in dissolved REE with 238.68 μg·$L^{-1}$. Aqueous samples collected from the AMD areas also contained higher concentrations of REE than in the open pit at Quinta do Bispo, perhaps indicating that AMD is a more potent mobilizer of REE than ISL. There were some similarities between the aqueous REE patterns, all mines showed a MREE enrichment as compared to the LREE and HREE. In addition to the MREE concavity, samples collected from São Domingos and Quinta do Bispo had a skewed pattern, with MREE > HREE > LREE. The open pit sample from Quinta do Bispo also exhibited a strong positive Eu anomaly (Eu*), not shared by the other sites.

## 3.2 Soil/aquatic sediment REE signature

A summary of major cation concentrations for water and soils/aquatic sediments reported in Supplementary Tables S2, S3, respectively. Table 3 displays the REE concentration of each individual soil. When evaluating soil REE concentrations there were three effects considered: 1) Prevailing geochemical context, 2) the mining context, and 3) rhizosphere effects.

### 3.2.1 Geochemical context

All of the water and soil/aquatic sediment sample data across all of the sites were used to make a correlation matrix and determine if any particular chemical couplings controlled REE behavior. As evidenced from Pearson's correlations, HREE (Dy through Lu) in the soil have significant positive correlations ($p < 0.05$) with major cations such as Ca, Mg, and Mn. This correlation is also present in the water samples collected. Though no correlation between Fe concentration and REE was evident in soil samples, there was a correlation between Fe and REE in the water samples. These correlations are further contextualized in the results section which details how compatible cations may interact with REE.

Physiochemical characteristics of the soil/aquatic sediment were also taken into consideration for site geochemistry. Samples display contrasting pH, $pH_{KCl}$, $CEC_{Metson}$, and OM concentrations (Supplementary Table S4). All of these characteristics can vary widely based on biotic and abiotic factors. The soils collected from São Domingos had high $CEC_{Metson}$ and OM, while Lousal sediments had the lowest $CEC_{Metson}$ and OM content.

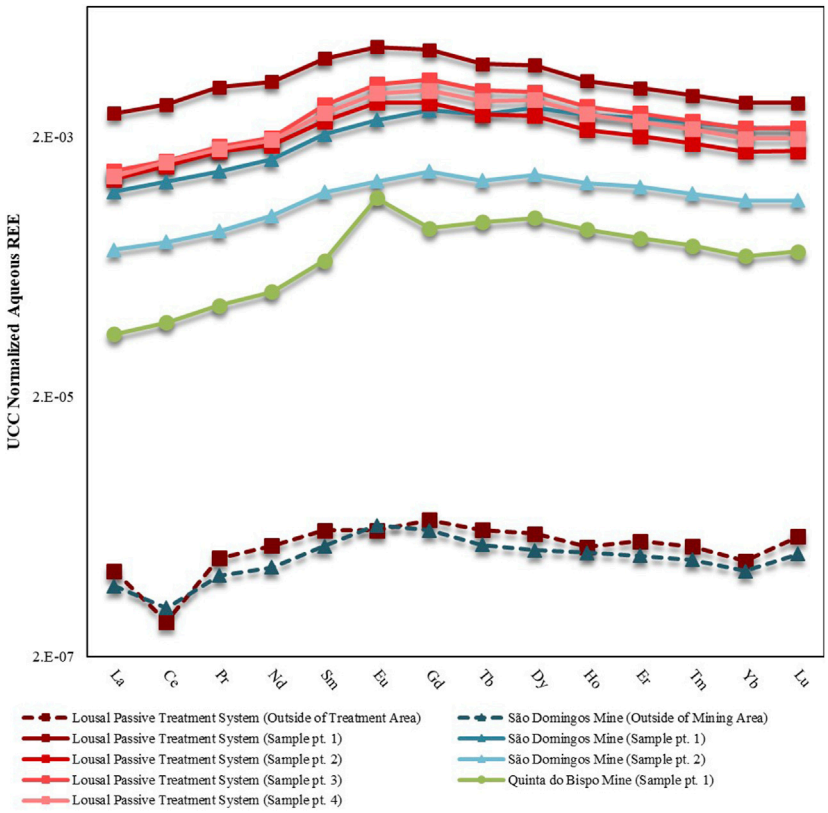


FIGURE 2
UCC-normalized REE patterns for aqueous samples collected from mine areas in Portugal (São Domingos, Lousal and Quinta do Bispo). Separate sampling points are distinguished using the abbreviation pt. Solid lines represent the samples collected inside of the mine, whereas dashed lines represent samples collected outside of the mining areas. Data for samples collected in São Domingos, Lousal and Quinta do Bispo are displayed by triangle, square and circle markers, respectively.

### 3.2.2 Mining context

Based on the mining site there are distinct differences in the levels of REE enrichment observed at each site (Figure 3). Soil samples collected from Quinta do Bispo had the highest concentrations of REE (161–231 mg·kg$^{-1}$), whereas aquatic sediment samples collected from Lousal exhibited the lowest concentrations (76–94 mg·kg$^{-1}$) (Table 3). Statistically there was no difference between REE concentrations observed at Quinta do Bispo and São Domingos ($p < 0.05$). Similarly, there was no statistically significant difference between soils collected from São Domingos and aquatic sediments collected from Lousal ($p < 0.05$) with regards to the total REE concentrations. Quinta do Bispo and São Domingos share similarities in their environmental remediation status, since these legacy mine sites were both mitigated and maintained by EDM with environmental remediation planned in the near future. São Domingos and Lousal also share similarities, as both sites are in the IPB and subject to AMD.

Both Quinta do Bispo and São Domingos had statistically significantly higher LREE and MREE concentrations than Lousal. There was no statistical difference between the HREE for each of the mining sites. This can be attributed to the large spread of HREE concentrations. For Quinta do Bispo, a majority of the REE signatures show an enrichment of LREE and MREE with lower values of HREE when normalized to the UCC. One of the samples collected from Quinta do Bispo also displayed a positive Eu*, as opposed to the other Quinta do Bispo soil samples which display a negative Eu*. The REE signature for soils collected from São Domingos shows that the LREE and MREE had lower values than the HREE, with two of the samples showing significant enrichment. All of the aquatic sediment samples collected from Lousal were depleted in LREE, MREE, and HREE with respect to the UCC. The REE signatures for samples collected from Lousal display lower LREE values and higher MREE and HREE values.

There was no statistically significant difference for the soil LREE, MREE, HREE, or total REE concentrations among samples collected from inside or outside of the mining areas. As per the heterogeneous nature of soil, perhaps the spread of data between samples collected from inside and outside of the mining area is too large to make a distinction between the influences of the mining area without also taking into consideration the geochemical context. This is further highlighted by the fact that the REE signature for the soil sample collected from outside of Sao Domingos does not match samples collected from inside of the same site. The sample collected from outside of the mining area features depletion of the LREE and enrichment of the MREE and HREE with respect to the UCC, along with a negative Ce*. Due to sampling constraints encountered in this study there was not enough sample replication to determine the combined effects of mining and the surrounding geochemistry.

**TABLE 2 Concentrations of REE in aqueous samples from mine areas in Portugal (São Domingos, Lousal and Quinta do Bispo). Separate sampling points are distinguished using the abbreviation pt. followed by a brief description of the sample location. Concentrations are reported in μg $L^{-1}$; Ce and Eu anomalies (Ce* and Eu*, respectively) are also reported as dimensionless values.**

| Mine site | Description | La | Ce | Pr | Nd | Sm | Eu | Gd | Tb | Dy | Ho | Er | Tm | Yb | Lu | ΣREE | LREE | MREE | HREE | Ce* | Eu* |
|---|---|---|---|---|---|---|---|---|---|---|---|---|---|---|---|---|---|---|---|---|---|
| São Domingos Mine | Tapada Grande Reservoir[a] | 0.021 | 0.030 | 0.006 | 0.025 | 0.006 | 0.002 | 0.007 | 0.001 | 0.005 | 0.001 | 0.003 | 0.000 | 0.002 | 0.000 | 0.110 | 0.083 | 0.021 | 0.007 | 0.61 | 1.24 |
| | Pt. 1: São Domingos River Valley | 22.7 | 58.2 | 7.71 | 35.1 | 9.46 | 2.39 | 12.2 | 1.93 | 11.8 | 2.35 | 6.46 | 0.855 | 5.18 | 0.748 | 177 | 124 | 37.8 | 15.6 | 0.99 | 1.02 |
| | Pt. 2: São Domingos River Valley | 8.13 | 19.9 | 2.67 | 12.9 | 3.40 | 0.801 | 4.13 | 0.593 | 3.59 | 0.710 | 1.91 | 0.241 | 1.43 | 0.208 | 60.6 | 43.57 | 12.50 | 4.50 | 0.96 | 0.99 |
| Quinta do Bispo Mine | Pt. 1: Flooded open pit | 1.83 | 4.78 | 0.718 | 3.36 | 1.01 | 0.598 | 1.51 | 0.283 | 1.67 | 0.311 | 0.763 | 0.096 | 0.535 | 0.084 | 17.5 | 10.7 | 5.07 | 1.79 | 0.92 | 2.19 |
| Lousal Mine | Uncontaminated water from Albufeira da Barragem da Tapada supplemented to passive treatment[a] | 0.027 | 0.024 | 0.008 | 0.037 | 0.008 | 0.002 | 0.009 | 0.001 | 0.006 | 0.001 | 0.004 | 0.000 | 0.002 | 0.001 | 0.130 | 0.096 | 0.026 | 0.008 | 0.36 | 0.91 |
| | Pt. 1: Tailing pile leachate containment | 91.7 | 227 | 34.5 | 139 | 36.1 | 8.71 | 35.7 | 4.69 | 25.1 | 4.34 | 11.0 | 1.38 | 8.12 | 1.18 | 629 | 493 | 110 | 26.0 | 0.90 | 1.14 |
| | Pt. 2: Mixing lagoon for leachate and supplemental water | 28.4 | 76.7 | 11.0 | 44.9 | 11.9 | 3.25 | 13.9 | 1.91 | 10.2 | 1.82 | 4.69 | 0.588 | 3.41 | 0.501 | 213 | 161 | 41.2 | 11.0 | 0.96 | 1.17 |
| | Pt. 3: First treatment basin | 32.9 | 83.7 | 12.0 | 51.5 | 15.9 | 4.49 | 21.0 | 2.94 | 15.6 | 2.75 | 7.02 | 0.878 | 5.16 | 0.756 | 257 | 180 | 59.9 | 16.6 | 0.94 | 1.13 |
| | Pt. 4: 6th treatment basin, beginning of planted basins | 30.0 | 82.7 | 11.5 | 49.4 | 13.8 | 3.81 | 17.4 | 2.44 | 13.5 | 2.41 | 6.07 | 0.762 | 4.28 | 0.622 | 239 | 174 | 51.0 | 14.1 | 0.99 | 1.13 |

[a]Samples collected from outside of the mining area.





10.3389/fenvs.2023.1191909

**TABLE 3 The REE concentrations for all rhizosphere soils from mine areas in Portugal (São Domingos, Lousal and Quinta do Bispo) given in mg kg$^{-1}$, as well as the Ce and Eu anomalies (Ce* and Eu*, respectively) given as dimensionless values.**

| Mine site | ID sample | La | Ce | Pr | Nd | Sm | Eu | Gd | Tb | Dy | Ho | Er | Tm | Yb | Lu | ΣREE | LREE | MREE | HREE | Ce* | Eu* |
|---|---|---|---|---|---|---|---|---|---|---|---|---|---|---|---|---|---|---|---|---|---|
| São Domingos Mine | *Cistus ladanifer*[a] | 16.0 | 26.6 | 4.76 | 20.8 | 5.71 | 1.22 | 6.35 | 1.05 | 6.40 | 1.34 | 3.50 | 0.493 | 3.07 | 0.470 | 97.7 | 68.1 | 14.3 | 15.3 | 0.69 | 0.95 |
| | *Cistus ladanifer* | 32.0 | 63.6 | 7.40 | 27.8 | 5.01 | 1.04 | 3.96 | 0.645 | 4.20 | 0.897 | 2.51 | 0.389 | 2.65 | 0.394 | 152 | 131 | 10.7 | 11.0 | 0.94 | 1.09 |
| | *Cistus ladanifer* | 34.0 | 71.1 | 8.11 | 30.3 | 5.99 | 1.21 | 5.21 | 0.860 | 5.40 | 1.13 | 3.08 | 0.470 | 3.02 | 0.457 | 170 | 144 | 13.3 | 13.6 | 0.98 | 1.02 |
| | *Erica andevalensis* | 31.3 | 60.9 | 7.19 | 26.6 | 4.91 | 0.976 | 3.65 | 0.581 | 3.66 | 0.771 | 2.16 | 0.342 | 2.37 | 0.372 | 146 | 126 | 10.1 | 9.67 | 0.93 | 1.08 |
| Quinta do Bispo | *Salix sp.* | 46.9 | 93.0 | 11.5 | 43.3 | 8.94 | 2.12 | 7.92 | 1.23 | 7.15 | 1.36 | 3.53 | 0.512 | 3.23 | 0.463 | 231 | 195 | 20.2 | 16.3 | 0.91 | 1.19 |
| | *Pteridium aquilinum*[a] | 33.9 | 69.3 | 8.16 | 29.7 | 5.63 | 0.695 | 4.26 | 0.641 | 3.65 | 0.739 | 2.02 | 0.302 | 2.06 | 0.308 | 161 | 141 | 11.2 | 9.08 | 0.95 | 0.67 |
| | *Pteridium aquilinum* | 38.8 | 76.3 | 9.14 | 33.0 | 6.60 | 0.826 | 5.12 | 0.764 | 4.36 | 0.853 | 2.27 | 0.336 | 2.16 | 0.296 | 181 | 157 | 13.3 | 10.3 | 0.92 | 0.67 |
| | *Retama sphaerocarpa* | 36.0 | 72.1 | 8.45 | 30.7 | 5.97 | 0.747 | 4.47 | 0.654 | 3.73 | 0.745 | 1.98 | 0.294 | 1.92 | 0.267 | 168 | 147 | 11.8 | 8.94 | 0.94 | 0.68 |
| Lousal Mine | *Juncus acutus*[a] | 20.9 | 38.3 | 4.53 | 16.7 | 3.27 | 0.679 | 2.68 | 0.432 | 2.68 | 0.555 | 1.52 | 0.230 | 1.52 | 0.227 | 94.2 | 80.4 | 7.07 | 6.73 | 0.90 | 1.08 |
| | *Juncus Acutus* | 14.6 | 30.3 | 3.64 | 14.1 | 2.89 | 0.619 | 2.55 | 0.418 | 2.73 | 0.581 | 1.63 | 0.256 | 1.69 | 0.255 | 76.3 | 62.7 | 6.48 | 7.14 | 0.95 | 1.07 |

[a]Samples collected from outside of the mining area.





10.3389/fenvs.2023.1191909

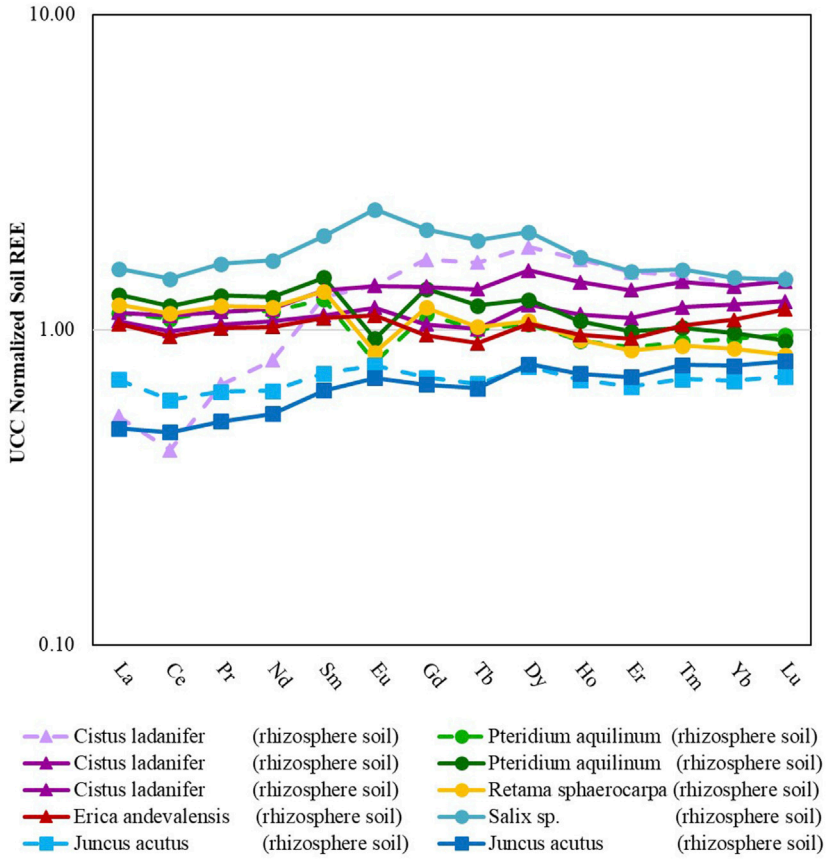


FIGURE 3
Rare earth element patterns for different rhizosphere soils from mine areas in Portugal (São Domingos, Lousal and Quinta do Bispo). Dashed lines represent soils collected outside of the mining areas. Data from soils collected in São Domingos, Lousal and Quinta do Bispo are displayed by triangle, square and circle markers, respectively.

### 3.2.3 Rhizosphere effects

A comparison of the rhizosphere versus bulk soils was possible at the Quinta do Bispo site (Supplementary Table S5) and shows that the rhizosphere and bulk soils display similar patterns. This comparison should also show whether plants selectively depleted or enriched REE from the soil. There was ultimately no statistical difference for the LREE, MREE, HREE, or Total REE in soils collected from the plant rhizosphere when compared with bulk soils. This would indicate that the plant does not influence the soil REE observed in the area.

## 3.3 Plant sample REE signature

When considering the responses of plant REE concentration, BCF, and TF there were three main effects investigated: 1) Prevailing geochemical context, 2) the mining context, and 3) the plant type.

### 3.3.1 Geochemical context

There was no statistical difference between the BCF (Figure 4) or the TF of the Total REE (Figure 5) observed in samples collected from Quinta do Bispo, São Domingos, or Lousal. This would indicate that the geological background did not influence the uptake of REE. However, this conclusion is difficult to support, since among the plants collected from each site there were no shared species for comparison. Therefore, a potential area for expansion of this study could be to research REE in the same plant species found at different mining sites. Such a task may prove difficult since the spontaneous vegetation is specific to the growth conditions of the individual site. In the discussion section comparisons from literature are presented in order to account for some of the differences seen across plant types collected in different geological conditions.

### 3.3.2 Mining context

While it is difficult to make conclusions about the effects of geochemistry on the bioaccumulation of REE in plants, there were some differences in plants collected from inside of the mining site when compared with plants collected from outside of the mining site (Figure 4).

In general, the BCF and REE concentrations (Table 4) were elevated for plants collected from inside of the mining areas, when compared with plants collected from outside of the mining areas (approximately 76% more REE in the plants recovered from inside of the mining areas), indicating an enhancement in the uptake and bioconcentration of REE from the soil into the above-ground tissue. Specifically, the MREE and HREE were taken up at a greater rate when the plant was collected from inside of the mining area (94% more MREE and 106% more HREE, as

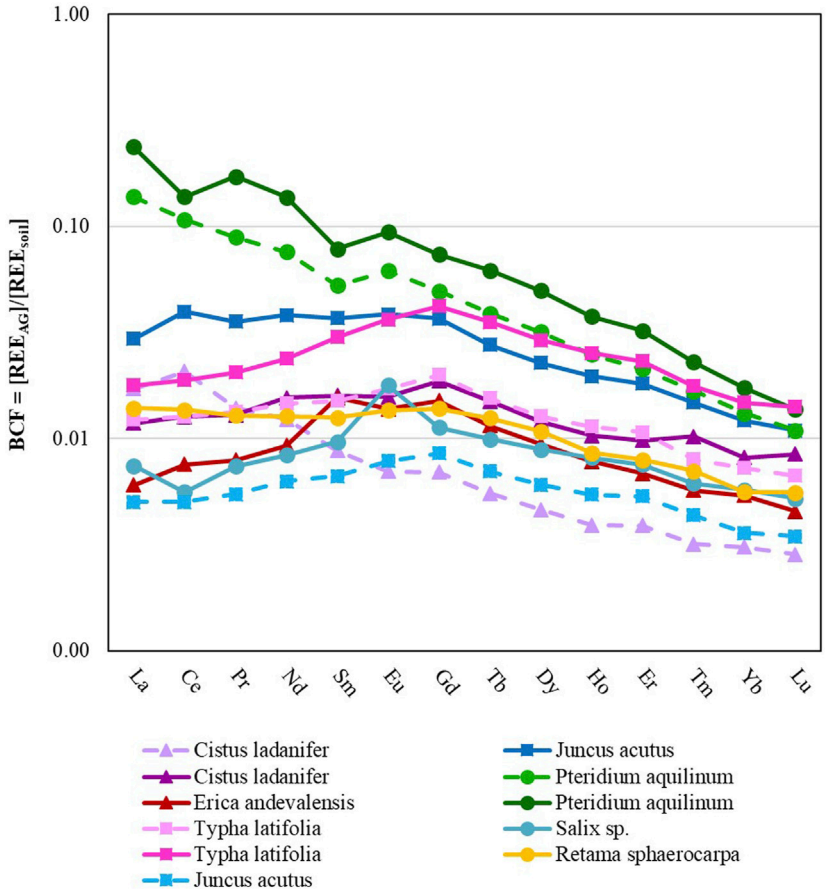


FIGURE 4
Plant BCF versus REE for above-ground tissue. Solid lines represent plant samples collected from inside of the mining sites while dashed lines represent samples collected from outside of the mining sites. Data from plants collected in São Domingos, Lousal and Quinta do Bispo (Portugal) are displayed by triangle, square and circle markers, respectively.

compared with the LREE which was elevated by 75%). More specifically, plants had an elevated BCF ($p < 0.05$) for Sm, Eu, Gd, Tb, Dy, Ho, Er, Yb, and Lu, when collected from inside of the mining area. However, there was also no significant difference between the TF of samples collected inside vs. outside of the mining area. In summary, mining increased the bioavailability of all REE, in particular elevating the BCF for MREE and HREE over LREE. This increased availability of REE did not translate to an increased TF.

### 3.3.3 Plant type

*Pteridium aquilinum* showed the greatest affinity for REE, accumulating 27.3 mg·kg$^{-1}$ of REE in the above-ground tissue. Similar to other studies, many of the plant types collected show higher concentrations of REE associated with the below ground-tissue as opposed to the above-ground tissue (Babula et al., 2009), with the exception of *P. aquilinum* which accumulated more La, Ce, and Pr in the above-ground plant tissue than in the below-ground plant tissue. Of the plants collected with replication (*P. aquilinum*, *Cistus ladanifer*, *Typha latifolia*, and *Juncus acutus*), plant type played a statistically significant role ($p < 0.05$) in the BCF of La, Ce, Nd, Sm, Eu, Gd, Tb, Dy, Ho, Er, Tm, and Yb. *P. aquilinum* had a significantly higher BCF for all of the aforementioned elements except for Ho. For Ho, *P. aquilinum* had similar rates of accumulation to *T. latifolia*, but had higher accumulation rates when compared to *J. acutus* and *C. ladanifer*. *T. latifolia* also had a higher BCF when compared to *C. ladanifer* for Dy and Ho, and a higher BCF when compared to *J. acutus* for Tm.

Of the REE accumulated in *P. aquilinum*, the LREE tended to concentrate at a higher rate than MREE, and both LREE and MREE tended to concentrate more than the HREE. Lanthanum was three orders of magnitude more concentrated than Lu. Similarly, the *C. ladanifer* sample collected from outside of the mine exhibited the same downward trend of LREE>MREE>HREE. This trend was not conserved across all plant types. *T. Latifolia* and *Erica andevalensis* demonstrated a MREE concave pattern instead, MREE>LREE = HREE. The BCF of *J. acutus* and *Retama sphaerocarpa* displayed a pattern where LREE = MREE>HREE.

Three plant samples had a positive Eu*: the *Salix sp.* sample and both of the *P. aquilinum* samples. All of these samples were collected from Quinta do Bispo. This anomaly accounts for the initial soil Eu* as the plant tissue is normalized to the native soil when evaluating the BCF. Additionally, there was a positive Eu* for the TF, so though modest amounts of Eu* were incorporated into the below-ground tissue from the soil, there was a preferential transport and accumulation of Eu into the aerial plant tissue.

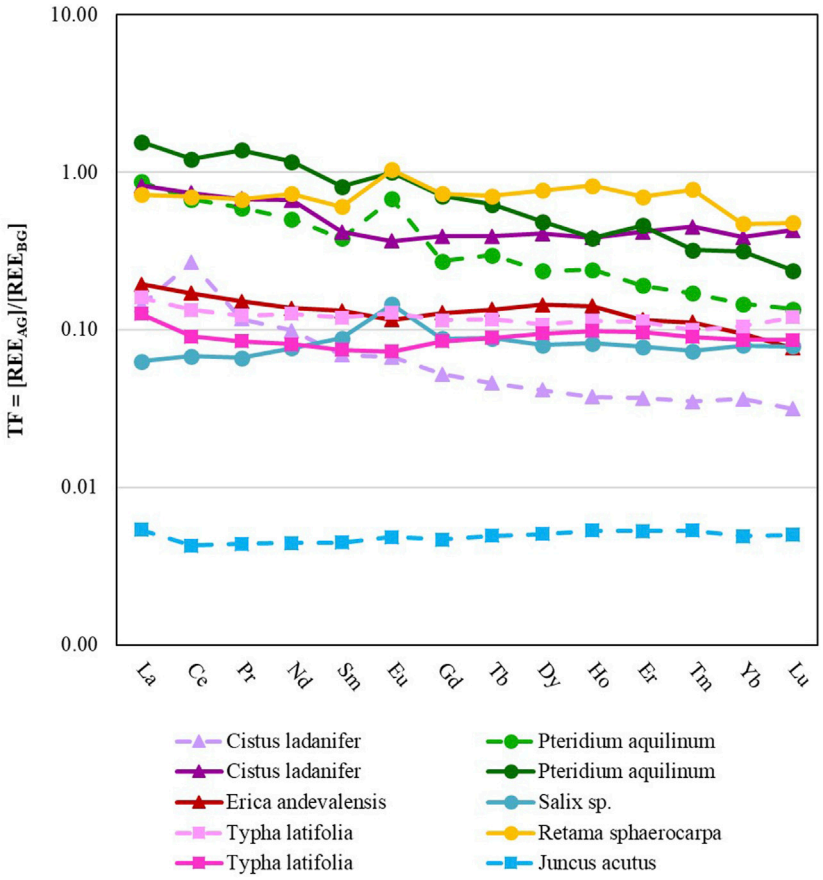


FIGURE 5
Plant TF versus REE. Solid lines represent plant samples collected from inside of the mining sites while dashed lines represent samples collected from outside of the mining sites. Data from plants collected in São Domingos, Lousal and Quinta do Bispo (Portugal) are displayed by triangle, square and circle markers, respectively.

Moreover, the *C. ladanifer* sample collected from outside of the São Domingos mining area had a positive Ce* in the above-ground tissue and negative Ce* in the below-ground plant tissue, which is matched with a high TF for Ce. The total concentration of Ce in the plant tissue was not in fact inordinately high and when normalized to UCC values shows no such anomaly. This observation is matched with soil and water samples collected from the same area showing Ce depletion as well. In this particular sample, Ce was accumulated in the above-ground tissue of the plant at a higher rate and the root anomaly is an artifact of less plant-available Ce in the rhizosphere.

There are three distinct groups of TF rates (Figure 5). The highest TF is seen for both of the *P. aquilinum* (collected from both inside and outside of the Quinta do Bispo mining area), *C. ladanifer* (collected from inside of the São Domingos mining area), and *R. sphaerocarpa* (collected from inside of the Quinta do Bispo mining area). The middle group consisted of the *C. ladanifer* collected from outside of the mining area, *T. latifolia*, *Salix sp*., and *E. andevalensis*. The TF of the middle group was 3 times lower than the highest TF group. The lowest TF was observed in *J. acutus*, which had large quantities of REE associated with the below-ground tissue. Low TF resulted in low accumulation of REE in the above-ground tissue. The TF for *J. acutus* was 177 times less than the TF recorded for plants in the highest TF group. This observation indicates that a majority of the REE remained stabilized within the below-ground tissue of *J. acutus*. Plant type had a significant effect on the TF of total REE and LREE, but had no effect on the MREE and HREE. REE was preferentially translocated in the following order: LREE>MREE>HREE for select plants, particularly *C. ladanifer* and *P. aquilinum* samples. Many of the other plant samples have no relative slope regarding the TF for LREE, MREE, and HREE.

# 4 Discussion

## 4.1 Geochemical and mining context

Though none of the studied mines targeted the extraction of REE ores, REE can be distributed throughout silicate, carbonate, oxide, phosphate, and oxyhydroxide (Migaszewski and Gałuszka, 2015) minerals, which are susceptible to dissolution under low pH conditions or changes in reduction/oxidation conditions (Cao et al., 2001; Mihajlovic et al., 2017). The MREE enrichment in aqueous samples is a typical signature of AMD (Perez-Lopez et al., 2010). The pH range and Eh observed for both São Domingos and Lousal are also consistent with the geochemical context of AMD (Dold, 2014). The pH observed in Quinta do Bispo was relatively high when

**TABLE 4 Concentration of REE in above-ground and below-ground plant tissues (μg kg$^{-1}$) collected on mine areas in Portugal (São Domingos, Lousal and Quinta do Bispo) as well as the Ce and Eu anomalies (Ce* and Eu*, respectively).**

| Above-ground tissue | | | | | | | | | | | | | | | | | | | | | |
|---|---|---|---|---|---|---|---|---|---|---|---|---|---|---|---|---|---|---|---|---|---|
| Mine site | ID sample | La | Ce | Pr | Nd | Sm | Eu | Gd | Tb | Dy | Ho | Er | Tm | Yb | Lu | ΣREE | LREE | MREE | HREE | Ce* | Eu* |
| São Domingos Mine | *Cistus ladanifer*[a] | 275 | 552 | 66.4 | 257 | 50.2 | 8.59 | 44.2 | 5.78 | 29.6 | 5.24 | 13.6 | 1.57 | 9.4 | 1.34 | 1320 | 1150 | 109 | 60.9 | 1.33 | 0.89 |
| | *Cistus ladanifer* | 379 | 809 | 96.0 | 433 | 80.1 | 16.3 | 74.3 | 9.70 | 50.7 | 9.26 | 24.6 | 3.99 | 21.6 | 3.33 | 2010 | 1720 | 180 | 113 | 1.03 | 0.91 |
| | *Erica andevalensis* | 189 | 460 | 56.9 | 247 | 76.7 | 13.5 | 55.1 | 6.70 | 34.5 | 6.03 | 14.8 | 1.96 | 12.8 | 1.69 | 1177 | 953 | 152 | 71.8 | 1.08 | 0.90 |
| Quinta do Bispo | *Salix sp.* | 349 | 521 | 85.4 | 363 | 86.7 | 38.0 | 89.5 | 12.2 | 63.7 | 11.1 | 26.7 | 3.16 | 18.5 | 2.42 | 1670 | 1320 | 226 | 126 | 0.75 | 1.70 |
| | *Pteridium aquilinum*[a] | 4700 | 7470 | 729 | 2260 | 298 | 43.0 | 212 | 24.9 | 116 | 18.5 | 43.2 | 5.07 | 27.1 | 3.38 | 16000 | 15200 | 578 | 214 | 0.95 | 1.21 |
| | *Pteridium aquilinum* | 9200 | 10500 | 1570 | 4550 | 518 | 77.7 | 379 | 47.4 | 218 | 32.2 | 73.7 | 7.72 | 37.5 | 4.07 | 27300 | 25900 | 1020 | 373 | 0.67 | 1.24 |
| | *Retama sphaerocarpa* | 503 | 989 | 109 | 393 | 75.2 | 10.2 | 62.2 | 8.19 | 40.5 | 6.40 | 15.8 | 2.07 | 10.8 | 1.49 | 2230 | 2000 | 156 | 77.0 | 1.02 | 1.03 |
| Lousal Mine | *Juncus acutus*[a] | 105 | 194 | 24.8 | 105 | 21.8 | 5.34 | 22.9 | 3.03 | 16.3 | 3.03 | 8.14 | 1.00 | 5.47 | 0.79 | 516 | 428 | 53.1 | 34.7 | 0.96 | 1.04 |
| | *Typha latifolia*[a] | 257 | 487 | 60.6 | 245 | 49.6 | 11.7 | 53.6 | 6.71 | 34.2 | 6.32 | 16.3 | 1.84 | 11.1 | 1.52 | 1240 | 1050 | 122 | 71.2 | 0.99 | 0.98 |
| | *Typha latifolia* | 262 | 574 | 75.0 | 336 | 87.2 | 22.6 | 108 | 14.9 | 79.6 | 14.8 | 37.9 | 4.52 | 25.1 | 3.61 | 1650 | 1250 | 232 | 165 | 0.98 | 1.01 |
| | *Juncus acutus* | 433 | 1202 | 130 | 539 | 107 | 23.9 | 94.2 | 11.6 | 62.1 | 11.4 | 29.7 | 3.78 | 20.6 | 2.79 | 2670 | 2300 | 237 | 130 | 1.22 | 1.05 |
| **Below-ground tissue** | | | | | | | | | | | | | | | | | | | | | |
| Mine Site | ID Sample | La | Ce | Pr | Nd | Sm | Eu | Gd | Tb | Dy | Ho | Er | Tm | Yb | Lu | ΣREE | LREE | MREE | HREE | Ce* | Eu* |
| São Domingos Mine | *Cistus ladanifer*[a] | 1920 | 2060 | 566 | 2600 | 726 | 128 | 849 | 126 | 714 | 140 | 370 | 45.1 | 259 | 42.5 | 10500 | 7140 | 1830 | 1570 | 0.65 | 0.80 |
| | *Cistus ladanifer* | 462 | 1090 | 142 | 653 | 192 | 44.4 | 190 | 24.8 | 125 | 24.0 | 59.0 | 8.8 | 55.7 | 7.77 | 3080 | 2350 | 451 | 280 | 1.02 | 0.99 |
| | *Cistus ladanifer* | 559 | 1120 | 136 | 526 | 117 | 20.3 | 95.0 | 16.8 | 89.5 | 14.1 | 42.9 | 3.6 | 32.8 | 4.01 | 2780 | 2340 | 249 | 187 | 0.95 | 0.89 |
| | *Erica ladanifer* | 975 | 2700 | 376 | 1790 | 580 | 116 | 431 | 49.8 | 240 | 42.7 | 128 | 17.5 | 135 | 22.0 | 7610 | 5850 | 1180 | 585 | 1.06 | 1.01 |
| Quinta do Bispo | *Salix sp.* | 5560 | 7640 | 1290 | 4730 | 983 | 263 | 1020 | 139 | 794 | 136 | 341 | 43.2 | 234 | 30.9 | 23200 | 19200 | 2400 | 1580 | 0.71 | 1.04 |
| | *Pteridium aquilinum*[a] | 5390 | 11100 | 1230 | 4500 | 784 | 63.5 | 779 | 83.5 | 491 | 76.8 | 226 | 29.7 | 185 | 25.0 | 25000 | 22200 | 1710 | 1030 | 1.04 | 0.57 |
| | *Pteridium aquilinum* | 5930 | 8670 | 1140 | 3900 | 638 | 77.7 | 535 | 76.1 | 449 | 84.1 | 160 | 24.1 | 119 | 17.1 | 21800 | 19600 | 1330 | 854 | 0.82 | 0.94 |
| | *Retama sphaerocarpa* | 700 | 1420 | 161 | 538 | 124 | 9.8 | 85.0 | 11.6 | 52.9 | 7.76 | 22.7 | 2.7 | 22.9 | 3.13 | 3160 | 2820 | 231 | 112 | 1.02 | 0.66 |
| Lousal Mine | *Juncus acutus*[a] | 19500 | 45400 | 5650 | 23600 | 4890 | 1110 | 4910 | 614 | 3230 | 569 | 1543 | 189 | 1115 | 157 | 112000 | 94100 | 11500 | 6800 | 1.09 | 0.98 |
| | *Typha latifolia*[a] | 1600 | 3640 | 491 | 1930 | 415 | 91.6 | 464 | 57.7 | 315 | 55.1 | 144 | 18.4 | 105 | 12.6 | 9340 | 7660 | 1030 | 651 | 1.03 | 0.90 |
| | *Typha latifolia* | 2080 | 6350 | 885 | 4150 | 1170 | 310 | 1270 | 167 | 842 | 150 | 394 | 50.3 | 291 | 41.7 | 18100 | 13500 | 2900 | 1770 | 1.09 | 1.11 |

[a] Samples collected from outside of the mining area.





10.3389/fenvs.2023.1191909

compared with the pH of São Domingos and Lousal. This is most likely due to the fact that sulfate mineral oxidation or AMD is negligible in the surrounding geology (Carvalho et al., 2005) and the ISL methods employed at Quinta do Bispo ended in 1999 (European Commission Directorate-General for Energy, 2012). The saturation of cations and anions in waste streams, represented by the EC measured in aqueous samples, favors the precipitation of metals (Nieto et al., 2007), and is therefore also a parameter used to evaluate the precipitation/dissolution dynamics at these sites. Low pH, high EC, and elevated sulfate concentrations were indicative of the geogenic and anthropogenic dissolution of primary minerals inside of the three legacy mine sites. These geochemical changes were induced by AMD processes or ISL practices.

In addition to dissolution, processed REE were susceptible to sorption and desorption processes, which were evaluated in this study based on the $CEC_{Metson}$ and OM content of soils and aquatic sediments. A soil with higher $CEC_{Metson}$ and OM content has a high metal loading capacity, whereas a soil with a low $CEC_{Metson}$ and OM content has less potential metal-sorbing surfaces, thus the metal holding capacity of soils collected from São Domingos is higher and the metal holding capacity of aquatic sediments collected from Lousal is lower. The sediments collected from Lousal had lower concentrations of REE indicative of the lower metal holding capacity of these sediments relative to the other sampled sites. As a result, Lousal also displayed the highest aqueous REE concentrations.

All of the samples collected from inside of the mining sites are considered impaired simply on the basis of having low pH (pH < 6.5) (Baker et al., 1990). As Baker et al. (1990) reported, biological diversity is lost starting at pH < 6.5, and an interruption of nutrient cycling at pH < 5.0. While pH directly impacts the ecology of a system, the increased metal solubility and bioavailability caused by acidification (Baker et al., 1990; Cao et al., 2001; Batista et al., 2013) can also induce toxicity (Baker et al., 1990; Plante, 2007; Batista et al., 2013).

Inorganic anions typically associated with REE complexation include: $SO_4^{2-}$, $PO_4^{3-}$, $Cl^-$, $CO_3^{2-}$, and $F^-$ (Millero, 1992; Vaziri Hassas et al., 2021). As stated in the results, the mining areas were dominated by sulfate. A study by Zhimang et al. (2000) implicates sulfates in the bioavailability of REE to plants, mainly showing that REE accumulation in below-ground tissue is limited by sulfate. Secondary sulfate salts such as jarosite and alunogen have been shown to be temporary stabilizers of polyvalent cations (including REE) in AMD (Ferreira et al., 2021). Subsequent solubilization of metals associated with jarosite, alunogen, and other secondary sulfate minerals has been implicated as a cause for delayed revegetation (Ferreira et al., 2021). This demonstrates that plants growth in mining environments is dependent on the prevailing geochemistry, as primary and secondary minerals constitute a source or sink for potentially toxic metals.

Aside from sulfates being a sink for REE, sulfates have also been implicated in the selective partitioning of REE in soils and waters (Ferreira da Silva et al., 2009; Welch et al., 2009; Grawunder et al., 2014; Soyol-Erdene et al., 2018). REE have even been suggested as tracers of mining pollution due to their unique MREE-enriched signature in mining wastes (Merten et al., 2005; Perez-Lopez et al., 2010). This signature is presumably due to sulfate and sulfate intermediates showing higher stability in complexation with MREE (Perez-Lopez et al., 2010) and precipitation/sorption processes occluding LREE (Liu et al., 2019) and HREE (Byrne and Li, 1995) from solution, paired with dissolution/desorption of MREE-enriched Fe and S minerals (Welch et al., 2009; Perez-Lopez et al., 2010; Grawunder et al., 2014). The occurrence of a correlation between REE and Fe, as seen in the water samples collected in this study, may indicate that Fe-mineral dissolution contributes to the soluble REE in these systems (Cao et al., 2001; Merten, 2005; Prudêncio et al., 2015; Prudêncio et al., 2017; Riley and Dutrizac, 2017; Liu et al., 2022). Many geochemical factors may contribute to the observed high REE concentrations and unique MREE enrichment in AMD surface waters, a detailed study on REE speciation is still needed.

The DOC concentrations anticipated in AMD waters should be low as acidic pH promotes an increase of organic aggregation, inducing a decrease of their colloidal stability (Johnson and Hallberg, 2003; Pédrot et al., 2009). Though limited amounts of DOC and OM are associated with AMD systems, no broad generalizations can be made about the fractionation of REE by organics, which is specific to the type of organic matter. Organic matter forms a significant sink for REE, both as a sorbing surface and as a bridging ligand (Byrne and Li, 1995; Pourret et al., 2007). Organic ligands make a more stable complex with HREE, causing HREE to deplete from solution into complexes with sediment surface ligands (Byrne and Li, 1995). More complex organics, such as humic substances, have been shown to produce a fractionation of MREE enrichment over both LREE and HREE, specifically in natural systems characterized by a high metal loading like the sites studied (Pourret et al., 2007; Pédrot et al., 2008).

The oxidation state of REE is generally trivalent, with the exception of $Eu^{2+}$ and $Ce^{4+}$. In this study, a negative Ce* was associated with samples collected from outside the mining areas. Geochemically, the waters collected from outside of the mining area are less oxidizing and have a higher pH. Therefore, the speciation of metals may vary between waters collected from inside of the mining area versus those collected from outside of the mining area. The negative Ce* observed in surface waters collected from outside of the mining areas is indicative of preferential $Ce^{4+}$ sorption to the solid phase, which is typical of circumneutral pH waters under oxidizing conditions (Bau, 1999).

The positive Eu* in liquors and ores associated with the open-pit can be attributed to the hydrothermal deposit where the $Eu^{2+}$ oxidations state is preferentially incorporated into high-temperature hydrothermal seams over the other REE, leading to enriched Eu concentrations (Sverjensky, 1984; Danielson et al., 1992). The proceeding ISL processes increased mobilization of all REE contained in the Eu-enriched ore, accordingly producing an enrichment of Eu in the remaining liquor and analogous waste rock. This mechanism explains the positive Eu* seen in the open-pit water sample and the *Salix sp.* rhizosphere soil, which was collected from the waste rock pile. All other soil samples collected from Quinta do Bispo had a negative Eu*. Consequently, the conclusion can be drawn that the soils collected from the surrounding material were depleted in Eu as it was partitioned into the hydrothermal seam. Thus, in the soil samples collected from the surrounding areas, there is a negative Eu* corresponding to this partition.

## 4.2 Plant influences

In order for a plant type to be considered a REE hyperaccumulator, the REE concentration in the above ground-tissue must exceed 1,000 $\mu g \cdot g^{-1}$ (Liu et al., 2018). None of the plants collected in this study met the hyperaccumulator definition. Liu et al. (2018) acknowledges the importance of plant biomass, as high

biomass can accrue significant amounts of REE. The concentrations of REE observed in the collected plants do not show any particular elevation or depletion when compared with other studies of plant REE (Wyttenbach et al., 1998; Liang et al., 2008; Migaszewski and Gałuszka, 2015). The *P. aquilinum* plant species did accumulate more REE than any other plant type: though this figure represents 6–53 times the amount accumulated by the other plant samples in the present study, the pteridophyte sample is not remarkably high. Pteridophytes are generally known to accumulate much higher concentrations of REE over other plant types (Tyler, 2004). *P. aquilinum* also tended to concentrate certain REE at a higher level in the above-ground tissue than in the below-ground tissue. Wang et al. (1997) made a similar observation in *Dicranopteris dichotoma*, another pteridophyte, which accumulated more REE in the above-ground tissue than in the below-ground tissue.

As mentioned in the materials and methods section, the BCF is reflective of biological occlusion or assimilation of particular REE from the surrounding media. The closer the BCF value is to 1, the closer the plant concentrations reflect the soil concentrations. In this study, any uptake of REE by the plant was insignificant in comparison with the soil pool. This was proven by a comparison of bulk and rhizosphere soils which showed no depletion or enrichment dependent on plant growth, and further supported by the BCF which for most plants was much less than 1.

The BCF can also be looked at in terms of slope and anomaly, indicating the effects of soil speciation and plant species selectivity towards the assimilation of particular REE into the above-ground tissue. Ultimately this study showed that for certain plant types (*P. aquilinum*), above-ground tissues were enriched in LREE relative to the surrounding soil. This finding is congruent with previous research, which demonstrated that LREE tend to be enriched in the above-ground tissue of plants compared to the MREE and HREE (Wang et al., 1997; Fu et al., 1998; Liang et al., 2008; Gonzalez et al., 2014). This may have to do with the plant's affinity to uptake LREE (Brioschi et al., 2012) and porewater chemistry restricting available HREE (Millero, 1992; Byrne and Li, 1995; Fu et al., 1998; Tyler, 2004; Brioschi et al., 2012). However, this pattern was not maintained across all plant types. In fact, *T. latifolia* and *Salix* sp. showed an MREE-enrichment compared with LREE and HREE, supported by Wyttenbach et al. (1998).

*Salix sp.* and *P. aquilinum* had positive Eu* in their BCF signatures. Positive Eu* in plant tissue has been observed in other studies (Durães et al., 2014; Krzcuik and Gałuszka, 2019; Krzciuk and Gałuszka, 2020). There are a couple of to-date unconfirmed hypotheses on why plants may have Eu*. Potentially $Eu^{3+}$ is transformed to $Eu^{2+}$ and is taken up by plants under the redox conditions of the rhizosphere. This may be a result of diurnal patterns, which dictate oxygen supply to the roots (Krzcuik and Gałuszka, 2020), or it may be related to the acquisition of other essential nutrients; such as Fe, which is reduced at the root dermis (Marschner and Rö;mheld, 1994; Wyttenbach et al., 1998). In both scenarios, the supply of Eu and the redox conditions are a vital control on the bioavailability of Eu. Many authors (Wang et al., 2012; Brioschi et al., 2013; Durães et al., 2014; Thomas et al., 2014) have suggested that the origin of positive Eu* in plants is the result of $Eu^{2+}$ substitution for an essential plant nutrient such as $Ca^{2+}$ due to the similarity in ionic radius (Shannon, 1976). All of the above-ground tissue REE concentrations positively correlate with above-ground tissue $Ca^{2+}$ concentrations for this study.

The investigation of the TF can be used to make conclusions about the transfer and relative accumulation of REE in and to different parts of the plant. In this study, the REE transfer from below-ground tissue to above-ground tissue did not relate to the geochemistry or mining context. It was only reflective of plant type differences. The subsequent enrichment in the LREE seen in the *C. ladanifer* and *P. aquilinum* plants is then an artifact of the preferential translocation of LREE into the above-ground tissue. Fu et al. (1998) posited that preferential uptake and translocation of REE in a pteridophyte was related to plant Si processes and that *in situ* recrystallization of Si would allow for substitution of MREE and HREE occluding the larger ionic radius of LREE, leaving the LREE more mobile and able to reach the distal and aerial tissues. Evidence supporting this may be seen in the strong positive correlation between all of the REE and Si (Supplementary Table S6) among all samples collected in this study.

Combining the information presented on the BCF enrichment of MREE with the lack of a TF MREE enrichment, it can be concluded that the MREE fractionation into the above-ground plant tissue, observed in *T. latifolia* and *Salix sp.*, originates from the preferential uptake of MREE in the below-ground tissue. While the total bioavailable pool of metals can include the soil (water-soluble, ligand-exchangeable, and organic or carbonate bound metals), the dissolved metals in water are typically thought of as readily bioavailable (Adriano, 2001; Di Bonito et al., 2008). These dissolved concentrations could explain the elevated MREE in plants, as the enrichment of the MREE in plant tissue mirrors the enrichment of MREE in surface waters impacted by mining.

The information presented may show that the MREE enrichment seen in the roots is an artifact of the soluble REE pool in these mine sites, whereas the LREE enrichment and Eu* in the above ground plant tissue demonstrates plant-specific fractionation. Thus, this study provides evidence that the REE pattern displayed by each plant may result from an interaction between the plant type and growth medium. This conclusion is contrary to one posited by Laul and Weimer (1982). Laul and Weimer (1982) studied a selection of biological samples and concluded that the REE patterns closely resembled their growth medium when normalized to chrondrites, however the REE patterns for plants were never normalized to the soil media to confirm enrichment or depletion, which would have obviated any preferential uptake of specific REE. Wang et al. (1997) similarly found that the concentration of REE in most plants collected from sites with REE-rich ores had similar patterns to the soils they were collected from, but also notes an accumulation of LREE over HREE. Pisciotta et al. (2017) made a similar conclusion that the plant tissue reflected the geochemistry of the collection site, however this conclusion was based on one plant type in one geochemical context. Another study by Krzcuik and Gałuszka (2020) showed that plants generally had a similar pattern for uptake regardless of the land usage, proving quite the opposite of earlier studies by Laul and Weimer (1982) and Pisciotta (2017), since this would mean that regardless of geochemical background, plants had a certain physiological signature for REE-uptake. In the context of Krzcuik and Gałuszka (2020) it should be noted that

researchers did find some differences based on collection of samples inside or outside of AMD areas. A study conducted by Barbera et al. (2021) actually showed that a planted system when spiked with REE did not necessarily lead to increased uptake of REE into the above-ground tissue. Barbera et al. (2021) instead shows increased REE concentration in the below ground tissue with limited transfer of REE into the above-ground tissue. Wyttenbach et al. (1998) similarly refuted the idea that the growth media was completely responsible for REE fractionation in above-ground tissues. Thus, there is evidence to support claims from each of these previous studies and create a more cohesive theory that both geochemical background and plant type contribute to REE patterns in plant tissues. The results from the present study seem to indicate that some plant types may be reflective of the area geochemistry, whereas others may show increased fractionation of soil REE, which demonstrates the importance of capturing many plant species in differing contexts.

## 5 Conclusion

Using samples from three Portuguese legacy mine sites, this study reaffirms previous findings that AMD waters tend to be enriched in MREE as compared with LREE and HREE. Through the coupled recovery of water, soil and plant samples, this research contributes to a growing body of work proving that 1) the substrate plays a role in the fractionation of REE into plant tissue and 2) the plant type can also contribute to REE fractionation.

Samples collected from inside of the mining sites had elevated dissolved REE concentrations in water samples, matched with a higher BCF in plant samples. This demonstrates the importance of the dissolved metal pool on the bioavailability of REE. Further sampling and identification of chemical speciation is recommended as the signatures for REE indicate some differences amongst soil types leading to differences in REE bioavailability. There were also no statistical differences in the BCF for plants based on the site in which they were collected from. This combined with the elevation of MREE in plant tissue may indicate that the dissolved REE pool plays a more significant role in plant REE uptake than the soil mineral REE. The concentration of REE in the soils collected from the rhizosphere and bulk soils were not statistically different, showing that the soil pool of REE in the plant rhizosphere was not significantly depleted when compared with unplanted soils.

Differences in uptake may be due to plant physiology as well. This hypothesis is supported by the fact that although the soils, aquatic sediments, and waters in this study had similar features, certain plants, such as *P. aquilinum*, seemed better adapted to extracting particular REE over others. Though it was anticipated that plant types commonly used in passive treatment systems, such as *J. acutus*, would perform best in extracting REE, very little REE was associated with the above-ground mass of these plants. Though the REE share physiochemical properties, there was observed preferential transfer of LREE and Eu into the aerial parts of certain plants. Thus, the unique geochemical context in which MREE is enriched in the dissolved phase, when combined with the preferential translocation of LREE and Eu based on plant type, creates each plant's REE signature.

## Data availability statement

The original contributions presented in the study are included in the article/Supplementary Material, further inquiries can be directed to the corresponding authors.

## Author contributions

AD and MD were responsible for funding acquisition. MP, RM, DR, CD, and KF organized sample retrieval. ID prepared plant samples for analysis. KF and ML performed laboratory analysis of the samples. KF compiled sample analysis and drafted the original manuscript. AD and MP significantly contributed to the revision of the manuscript. CD, EC, and RM read, edited, and approved the manuscript. All authors contributed to the article and approved the submitted version.

## Funding

This project has received funding from the European Union's Horizon 2020 research and innovation program under the Marie Sklodowska-Curie Grant Agreement No. 857989 (PANORAMA project). This publication is also supported by the European Union through the European Regional Development Fund (FEDER), the French ministry of Higher Education and Research, the French Region of Brittany and Rennes Métropole.

## Acknowledgments

The authors are grateful for the support of the GeOHeLiS analytical platform of Rennes University with technical support from Maxime Pattier and Patrice Petitjean.

## Conflict of interest

Access to legacy mine sites for sampling was provided by EDM, a State owned enterprise, under a legal regime of concession contract concluded with the Portuguese State for the environmental recovery of degraded mining areas (approved in Decree-Law no. 198-A/2001 and 6/7/2001).

## Publisher's note



## Supplementary material

The Supplementary Material for this article can be found online at: https://www.frontiersin.org/articles/10.3389/fenvs.2023.1191909/full#supplementary-material

# References


Adriano, D. C. (2001). "Bioavailablity of trace elements," in *Trace elements in terrestrial environments*. Editor D. C. Adriano (New York: Springer), 61–89.

Akcil, A., and Koldas, S. (2006). Acid mine drainage (AMD): Causes, treatment and case studies. *J. Clean. Prod.* 14 (12-13), 1139–1145. doi:10.1016/j.jclepro.2004.09.006

Babula, P., Adam, V., Opatrilova, R., Zehnalek, J., Havel, L., and Kizek, R. (2009). "Uncommon heavy metals, metalloids and their plant toxicity: A review," in *Organic farming, pest control and remediation of soil pollutants sustainable agriculture reviews*. Editor E. Lichtfouse (Dordrecht: Springer). doi:10.1007/978-1-4020-9654-9_14

Baker, J. P., Bernard, D. P., Christensen, S. W., Sale, M. J., Freda, J., Heltcher, K., et al. (1990). *Biological effects of changes in surface water acid-base chemistry*. Washington, D.C.: United States: Department of Energy. doi:10.2172/7255574

Barbera, M., Zuddas, P., Palazzolo, E., and Saiano, F. (2021). The distribution of rare earth elements discriminates the growth substrate of *Vitis vinifera L. Chemosphere* 266, 128993. doi:10.1016/j.chemosphere.2020.128993

Batista, M. J., de Oliveira, D. P. S., Abreu, M. M., Locutura, J., Shepherd, T., Matos, J., et al. (2013). Sources, background and enrichment of lead and other elements: Lower Guadiana River. *Geoderma* 193-194, 265–274. doi:10.1016/j.geoderma.2012.08.033

Bau, M., and Dulski, P. (1996). Anthropogenic origin of positive gadolinium anomalies in river waters. *Earth Planet. Sci. Lett.* 143, 245–255. doi:10.1016/0012-821x(96)00127-6

Bau, M. (1999). Scavenging of dissolved yttrium and rare earths by precipitating iron oxyhydroxide: Experimental evidence for Ce oxidation, Y-Ho fractionation, and lanthanide tetrad effect. *Geochim. Cosmochim. Acta.* 63, 67–77. doi:10.1016/s0016-7037(99)00014-9

Binnemans, K., Jones, P. T., Blanpain, B., Van Gerven, T., Yang, Y., Walton, A., et al. (2013). Recycling of rare earths: A critical review. *J. Clean. Prod.* 51, 1–22. doi:10.1016/j.jclepro.2012.12.037

Brioschi, L., Steinmann, M., Lucot, E., Pierret, M. C., Stille, P., Prunier, J., et al. (2013). Transfer of rare earth elements (REE) from natural soil to plant systems: Implications for the environmental availability of anthropogenic REE. *Plant Soil* 366, 143–163. doi:10.1007/s11104-012-1407-0

Byrne, R. H., and Li, B. (1995). Comparative complexation behavior of the rare earths. *Geochim. Cosmochim. Acta.* 59 (22), 4575–4589. doi:10.1016/0016-7037(95)00303-7

Cabezudo, B., and Rivera, J. (1980). Notas taxonómicas y corológicas sobre la Flora de Andalucía Occidental. *Lagascalia* 9 (2), 219–248.

Cao, X., Chen, Y., Wang, X., and Deng, X. (2001). Effects of redox potential and pH value on the release of rare earth elements from soil. *Chemosphere* 44, 655–661. doi:10.1016/s0045-6535(00)00492-6

Carignan, J., Hild, P., Mevelle, G., Morel, J., and Yeghicheyan, D. (2001). Routine analyses of trace elements in geological samples using flow injection and low pressure on-line liquid chromatography coupled to ICP-ms: A study of geochemical reference materials br, DR-N, UB-N, AN-G and gh. *Newsl* 25 (2-3), 187–198. doi:10.1111/j.1751-908x.2001.tb00595.x

Carvalho, F. P., Madruga, M. J., Reis, M. C., Alves, J. G., Oliveira, J. M., Gouveia, J., et al. (2005). "Radioactive survey in former uranium mining areas of Portugal," in *Environmental contamination from uranium production facilities and their remediation* (Vienna, Austria: International Atomic Energy Agency), 29–40.

Casiot, C., Egal, M., Elbaz-Poulichet, F., Bruneel, O., Bancon-Montigny, C., Cordier, M., et al. (2009). Hydrological and geochemical control of metals and arsenic in a Mediterranean river contaminated by acid mine drainage (the Amous River, France); preliminary assessment of impacts on fish (*Leuciscus cephalus*). *Appl. Geochem.* 24 (5), 787–799. doi:10.1016/j.apgeochem.2009.01.006

Chour, Z., Laubie, B., Morel, J. L., Tang, Y., Qiu, R., Simonnot, M. O., et al. (2018). Recovery of rare earth elements from Dicranopteris dichotoma by an enhanced ion exchange leaching process. *Chem. Eng. Process. – Process Intensif.* 130, 208–213. doi:10.1016/j.cep.2018.06.007

International Union of Pure and Applied Chemistry (2005). Editors N. G. Connelly, T. Damhus, R. M. Hartshorn, and A. T. Hutton (Cambridge, U.K.: IUPAC).*Nomenclature of inorganic chemistry*

Danielson, A., Möller, P., and Dulski, P. (1992). The europium anomalies in banded iron formations and the thermal history of the oceanic crust. *Geol* 97, 89–100. doi:10.1016/0009-2541(92)90137-t

Di Bonito, M., Breward, N., Crout, N., Smith, B., and Young, S. (2008) "Chapter ten – overview of selected soil pore water extraction methods for the determination of potentially toxic elements in contaminated soils: Operational and technical aspects," in *environmental geochemistry* , eds. B. de Vivo, H. E. Belkin, and A. Lima (Amsterdam, NL: Elsevier), 213–249.

Dold, B. (2014). Evolution of acid mine drainage formation in sulphidic mine tailings. *Minerals* 4, 621–641. doi:10.3390/min4030621

Durães, N., Ferreira da Silva, E., Bobos, I., and Ávila, P. (2014). Rare earth elements fractionation in native vegetation from the moncorvo iron mines, NE Portugal. *Procedia Earth Planet. Sci.* 10, 376–382. doi:10.1016/j.proeps.2014.08.064

Empresa de Desenvolvimento Mineiro and Direcção Geral de Energia e Geologia (2011). *The legacy of abandoned mines: The context and the action in Portugal*. Lisboa, Portugal: EDM.

Estatal de Meteorología (España) and Instituto de Meteorologia (Portugal) (2011). *Iberian climate atlas*. Madrid, Spain: Estatal de Meteorologia.

European Commission Directorate-General for Energy (2012). *Uranium sites environmental radioactivity and discharge monitoring and part of national monitoring system for environmental radioactivity: Portugal*. Article 35 Technical Report – PT-11/01 (Brussels, Belgium: European Commision).

Ferreira da Silva, E., Bobos, I., Xavier Matos, J., Patinha, C., Reis, A. P., and Cardoso Fonseca, E. (2009). Mineralogy and geochemistry of trace metals and REE in volcanic massive sulfide host rocks, stream sediments, stream waters and acid mine drainage from the Lousal mine area (Iberian Pyrite Belt, Portugal). *Appl. Geochem.* 24 (3), 383–401. doi:10.1016/j.apgeochem.2008.12.001

Ferreira, R. A., Pereira, M. F., Magalhães, J. P., Maurício, A. M., Caçador, I., and Martin-Dias, S. (2021). Assessing local acid mine drainage impacts on natural regeneration-revegetation of São Domingos mine (Portugal) using a mineralogical, biochemical, and textural approach. *Sci. Total Environ.* 755 (1), 142825–142916. doi:10.1016/j.scitotenv.2020.142825

Fu, F., Akagi, T., and Shinotsuka, K. (1998). Distribution pattern of rare earth elements in Fern. *Biol. Trace Elem. Res.* 64, 13–26. doi:10.1007/bf02783321

Gałuszka, A., Migaszewski, Z. M., Pelc, A., Trembaczowski, A., Dołęgowska, S., and Michalik, A. (2020). Trace elements and stable sulfur isotopes in plants of acid mine drainage area: Implications for revegetation of degraded land. *J. Environ. Sci.* 94, 128–136. doi:10.1016/j.jes.2020.03.041

Gong, B., He, E., Romero-Freire, A., Ruan, J., Yang, W., Zhang, P., et al. (2021). Do essential elements (Pa and Fe) have mitigation roles in the toxicity of individual and binary mixture of yttrium and cerium in *Triticum aestivum*? *J. Hazard. Mater.* 416, 125761. doi:10.1016/j.jhazmat.2021.125761

Gonzalez, V., Vignati, D. A. L., Leyval, C., and Giamberini, L. (2014). Environmental fate and ecotoxicity of lanthanides: Are they a uniform group beyond chemistry? *Environ. Int.* 7, 148–157. doi:10.1016/j.envint.2014.06.019

Grawunder, A., Merten, D., and Büchel, G. (2014). Origin of middle rare earth element enrichment in acid mine drainage-impacted areas. *Environ. Sci. Pollut. Res.* 21, 6812–6823. doi:10.1007/s11356-013-2107-x

Herman, D. C., and Maier, R. M. (2009). "Consequences of biogeochemical cycles gone wrong," in *Environmental microbiology*. Editors R. M. Maier, I. L. Pepper, and C. P. Gerba (Amsterdam, NL: Elsevier), 319–333.

Johnson, D. B., and Hallberg, K. B. (2003). The microbiology of acidic mine waters. *Res. Microbiol.* 154, 466–473. doi:10.1016/s0923-2508(03)00114-1

Joshi, M., Chandrasekar, A., and Ghanty, T. K. (2018). Theoretical investigation of M@Pb122-and M@Sn122- zintyl clusters (M=$Lr^{n+}$, $Lu^{n+}$, $La^{3+}$, $Ac^{3+}$ and n= 0, 1, 2, 3. *Phys. Chem. Chem. Phys.* 20, 15253–15272. doi:10.1039/c8cp01056k

Krishnamurty, K. V., Shpirt, E., and Reddy, M. M. (1976). Trace metal extraction of soils and sediments by nitric acid-hydrogen peroxide. *At. Absorpt. Newsl.* 15 (3), 68–70.

Krzciuk, K., and Gałuszka, A. (2020). Presence and possible origin of positive Eu anomaly in shoot samples of Juncus effusus L. *J. Trace Elem. Med. Biol.* 58, 126432. doi:10.1016/j.jtemb.2019.126432

Krzciuk, K., and Gałuszka, A. (2019). Seasonal changes in concentrations of trace elements and rare earth elements in shoot samples of Juncus effusus L. collected from natural habitats in the Holy Cross Mountains, south-central Poland. *Chemosphere* 219, 954–960. doi:10.1016/j.chemosphere.2018.12.062

Laul, J. C., and Weimer, W. C. (1982). "Behavior of REE in geological and biological systems," in *The rare earths in modern science and technology*. Editors G. J. McCarthy, J. J. Rhyne, and H. B. Silber (New York: Plenum Press), 531–535.

Li, X., Chen, Z., Chen, Z., and Zhang, Y. (2013). A human health risk assessment of rare earth elements in soil and vegetables from a mining area in Fujian Province, Southeast China. *Chemosphere* 93, 1240–1246. doi:10.1016/j.chemosphere.2013.06.085

Liang, T., Ding, S., Song, W., Chong, Z., Zhang, C., and Li, H. (2008). A review of fractionations of rare earth elements in plants. *J. Rare Earths.* 26, 7–15. doi:10.1016/s1002-0721(08)60027-7

Lima, A. T., and Ottosen, L. (2020). Recovering rare earth elements from contaminated soils: Critical overview of current remediation technologies. *Chemosphere* 265, 129163. doi:10.1016/j.chemosphere.2020.129163

Liu, C., Yuan, M., Liu, W. S., Guo, M. N., Huot, H., Tang, Y. T., et al. (2018). "Element case studies: Rare earth elements," in *Agromining: Farming for metals - extracting unconventional resources using plants*. Editors A. van der Ent, G. Echevarria, A. J. M. Baker, and J. L. Morel Cham, Switzerland.

Liu, H., Guo, H., Pourret, O., Wang, Z., Liu, M., Zhang, W., et al. (2022). Geochemical signatures of rare earth elements and yttrium exploited by acid solution mining around an ion-adsorption type deposit: Role of source control and potential for recovery. *Sci. Total Environ.* 804, 150241. doi:10.1016/j.scitotenv.2021.150241

Liu, W. S., Guo, M. N., Liu, C., Yuan, M., Chen, X. T., Huot, H., et al. (2019). Water, sediment and agricultural soil contamination from an ion-adsorption rare earth mining area. *Chemosphere* 216, 75–83. doi:10.1016/j.chemosphere.2018.10.109

Marquez, J., Pourret, O., Faucon, M. P., Weber, S., Hoàng, T., and Martinez, R. (2018). Effect of cadmium, copper and lead on the growth of rice in the coal mining region of Quang Ninh, cam-pha (Vietnam). *Sustainability* 10, 1758. doi:10.3390/su10061758

Marschner, H., and Römheld, V. (1994). Strategies of plants for acquisition of iron. *Plant Soil* 165 (2), 261–274. doi:10.1007/bf00008069

Merschel, G., and Bau, M. (1995). Rare earth elements in the aragonitic shell of freshwater mussel Corbicula fluminea and the bioavailability of anthropogenic lanthanum,samarium and gadolinium in river water. *Sci. Total Environ.* 533, 91–101. doi:10.1016/j.scitotenv.2015.06.042

Merten, D., Geletneky, J., Bergmann, H., Haferburg, G., Kothe, E., and Büchel, G. (2005). Rare earth element patterns: A tool for understanding processes in remediation of acid mine drainage. *Chem. Erde* 65 (S1), 97–114. doi:10.1016/j.chemer.2005.06.002

Metson, A. J. (1956). *Methods of chemical analysis for soil survey samples*. New Zealand: New Zealand Department of Scientific and Industrial Research.

Migaszewski, Z. H., and Gałuszka, A. (2015). The characteristics, occurrence, and geochemical behavior of rare earth elements in the environment: A review. *Environ. Sci. Technol.* 45, 429–471. doi:10.1080/10643389.2013.866622

Mihajlovic, J., Stärk, H., and Rinklebe, J. (2017). Rare earth elements and their release dynamics under pre-definite redox conditions in a floodplain soil. *Chemosphere* 181, 313–319. doi:10.1016/j.chemosphere.2017.04.036

Millero, F. J. (1992). Stability constants for the formation of rare earth inorganic complexes as a function of ionic strength. *Geochim. Cosmochim. Acta.* 56, 3123–3132. doi:10.1016/0016-7037(92)90293-r

Nieto, J. M., Sarmiento, A. M., Olías, M., Canovas, C. R., Riba, I., Kalman, J., et al. (2007). Acid mine drainage pollution in the tinto and odiel rivers (iberian pyrite Belt, SW Spain) and bioavailability of the transported metals to the Huelva estuary. *Int* 33 (4), 445–455. doi:10.1016/j.envint.2006.11.010

Pagano, G., Aliberti, F., Guida, M., Oral, R., Siciliano, A., Trifuoggi, M., et al. (2015). Rare earth elements in human and animal health: State of art and research priorities. *Environ. Res.* 142, 215–220. doi:10.1016/j.envres.2015.06.039

Pan, J., Nie, T., Vaziri Hassas, B., Rezaee, M., Wen, Z., and Zhou, C. (2020). Recovery of rare earth elements from coal fly ash by integrated physical separation and acid leaching. *Chemosphere* 248, 126112. doi:10.1016/j.chemosphere.2020.126112

Pédrot, M., Dia, A., Davranche, M., Bouhnik-Le Coz, M., Henin, O., and Gruau, G. (2008). Insights into colloid-mediated trace element release at the soil/water interface. *J. Colloid Interface Sci.* 325, 187–197. doi:10.1016/j.jcis.2008.05.019

Pédrot, M., Dia, A., and Davranche, M. (2009). Double pH control on humic substance-borne trace elements distribution in soil waters as inferred from ultrafiltration. *J. Colloid Interface Sci.* 339, 390–403. doi:10.1016/j.jcis.2009.07.046

Pereira, R., Barbosa, S., and Carvalho, F. P. (2014). Uranium mining in Portugal: A review of the environmental legacies of the largest mines and environmental and human health impacts. *Environ. Geochem. Health.* 36, 285–301. doi:10.1007/s10653-013-9563-6

Pérez-López, R., Delgado, J., Nieto, J. M., and Márquez-García, B. (2010). Rare earth element geochemistry of sulphide weathering in the São Domingos mine area (iberian pyrite Belt): A proxy for fluid–rock interaction and ancient mining pollution. *Chem. Geol.* 276 (1-2), 29–40. doi:10.1016/j.chemgeo.2010.05.018

Pisciotta, A., Tutone, L., and Saiano, F. (2017). Distribution of YLOID in soil-grapevine system (Vitis vinifera L) as tool for geographical characterization of agro-food products. A two years case study on different grafting combinations. *Food Chem.* 221, 1214–1220. doi:10.1016/j.foodchem.2016.11.037

Plante, A. F. (2007). "Soil biogeochemical cycling of inorganic nutrients and metals," in *Soil microbiology, ecology, and biochemistry*. Editor E. A. Paul (Amsterdam, NL: Elsevier), 389–432.

Pourret, O., Davranche, M., Gruau, G., and Dia, A. (2007). Rare earth elements complexation with humic acid. *Chem. Geol.* 243, 128–141. doi:10.1016/j.chemgeo.2007.05.018

Prudêncio, M. I., Valente, T., Marques, R., Braga, S. M. A., and Pamplona, J. (2015). Geochemistry of rare earth elements in a passive treatment system built for acid mine drainage remediation. *Chemosphere* 138, 691–700. doi:10.1016/j.chemosphere.2015.07.064

Prudêncio, M. I., Valente, T., Marques, R., Sequeira Braga, M. A., and Pamplona, J. (2017). Rare earth elements, iron and manganese in ochre-precipitates and wetland soils of a passive treatment system for acid mine drainage. *Sci* 17, 932–935. doi:10.1016/j.proeps.2017.01.024

Quental, L., Bourguignon, A., Sousa, A. J., Batista, M. J., Brito, M. G., Tavares, T., et al. (2002). *MINEO Southern Europe environment test site: Contamination impact mapping and modelling — final Report*. Report No. IST-1999-10337 (Alfragide, Portugal: Information Society Technologies). Available at: http://hdl.handle.net/10400.9/3268.

Ramalho, E., Carvalho, J., Barbosa, S., and Monteiro Santos, F. A. (2009). Using geophysical methods to characterize an abandoned uranium mining site, Portugal. *J. Appl. Geophys.* 67, 14–33. doi:10.1016/j.jappgeo.2008.08.010

Relvas, J. M. R. S., Pinto, A., Fernandes, C., Matos, J. X., Vieira, A., Mendonça, A., et al. (2014). Lousal: An old mine, a recent dream. A new reality. *Comun. Geol.* 101 (I), 1345–1347.

Riley, E., and Dutrizac, J. E. (2017). The behaviour of the rare earth elements during the precipitation of ferrihydrite from sulphate media. *Hydrometallurgy* 172, 69–78. doi:10.1016/j.hydromet.2017.05.004

Rim, K. T., Koo, K. H., and Park, J. S. (2013). Toxicological evaluations of rare earths and their health impacts to workers: A literature review. *Saf. Health A. T. Work* 4 (1), 12–26. doi:10.5491/shaw.2013.4.1.12

Santa-Bárbara Carrascosa, C., and Valdés, B. (2008). *Guía de la Flora y Vegetación del Andévalo: Faja Pirítica España-Portugal (P, Silva, Trans)*. Junta de Andalucia Consejería de Medio Ambiente y Ordenación del Territorio.

Shannon, R. D. (1976). Revised effective ionic radii and systematic studies of interatomic distances in halides and chalcogenides. *Acta Crystallogr. A* 32, 751–767. doi:10.1107/s0567739476001551

Soyol-Erdene, T. O., Valente, T., Grande, J. A., and de la Torre, M. L. (2018). Mineralogical controls on mobility of rare earth elements in acid mine drainage environments. *Chemosphere* 205, 317–327. doi:10.1016/j.chemosphere.2018.04.095

Strosnider, W. H. J., Llanos López, F. S., LaBar, J. A., Palmer, K. J., and Nairn, R. W. (2014). Unabated acid mine drainage from cerro rico de Potosí, Bolivia: Uncommon constituents of concern impact the rio pilcomayo headwaters. *Environ. Earth Sci.* 71, 3223–3234. doi:10.1007/s12665-013-2734-z

Sverjensky, D. A. (1984). Europium redox equilibria in aqueous solution. *Earth Planet. Sci. Lett.* 67, 70–78. doi:10.1016/0012-821x(84)90039-6

Taylor, S. R., and McLennan, S. M. (1985). *The continental crust: Its composition and evolution*. Oxford, U.K.: Blackwell.

Thomas, P. J., Carpenter, D., Boutin, C., and Allison, J. E. (2014). Rare earth elements (REEs) effects on germination and growth of selected crop and native plant species. *Chemosphere* 96, 57–66. doi:10.1016/j.chemosphere.2013.07.020

Tyler, C. (2004). Rare earth elements in soil and plant systems - a review. *Plant Soil* 267, 191–206. doi:10.1007/s11104-005-4888-2

U.S. Geological Survey (2022). "Rare earths," in *Mineral commodity summaries 2022: U.S. Geological Survey*. (Reston, VA: U.S. Geological Survey), 134–135. doi:10.3133/mcs2022

Van Gosen, B. S., Verplanck, P. L., Seal, R. R., Long, K. R., and Gambogi, J.II (2017). "Chapter O: Rare-earth elements," in *Critical mineral resources of the United States—economic and environmental geology and prospects for future supply*. Editors K. J. Schulz, J. H. DeYoung, R. R. Seal, and D. C. Bradley (Reston, VA: U.S. Geological Survey), 1–31. doi:10.3133/pp1802O

Vaziri Hassas, B., Rezaee, M., and Pisupati, S. V. (2021). Effect of various ligands on the selective precipitation of critical and rare earth elements from acid mine drainage. *Chemosphere* 280, 130684. doi:10.1016/j.chemosphere.2021.130684

Wakabayashi, T., Ymamoto, A., Kazaana, A., Nakano, Y., Nojiri, Y., and Kashiwazaki, M. (2016). Antibacterial, antifungal and nematicidal activities of rare earth ions. *Biol. Trace Elem. Res.* 174 (2), 464–470. doi:10.1007/s12011-016-0727-y

Wang, C., Zhang, K., He, M., Jiang, C., Tian, L., Tian, Y., et al. (2012). Mineral nutrient imbalance, DNA lesion and DNA-protein crosslink involved in growth retardation of Vicia faba L. seedlings exposed to lanthanum ions. *J. Environ. Sci.* 24, 214–220. doi:10.1016/s1001-0742(11)60760-2

Wang, Y. Q., Sun, J. X., Chen, H. M., and Guo, F. Q. (1997). Determination of the contents and distribution characteristics of REE in natural plants by NAA. *J. Radioanal. Nucl. Chem.* 219 (1), 99–103. doi:10.1007/bf02040273

Welch, S. A., Christy, A. G., Isaacson, L., and Kirste, D. (2009). Mineralogical control of rare earth elements in acid sulfate soils. *Geochim. Cosmochim. Acta.* 73, 44–64.

Wyttenbach, A., Furrer, V., Schelppi, P., and Tobler, L. (1998). Rare earth elements in soil and soil-grown plants. *Plant Soil* 199, 267–273. doi:10.1023/a:1004331826160

Yéghicheyan, D., Aubert, D., Bouhnik-Le Coz, M., Chmeleff, J., Delpoux, S., Djouraev, I., et al. (2019). A new interlaboratory characterisation of silicon, rare earth elements and twenty-two other trace element concentrations in the natural river water certified reference material SLRS-6 (NRC-CNRC). *Geostand. Geoanal. Res.* 43 (3), 475–496. doi:10.1111/ggr.12268

Zhimang, G., Xiaorong, W., Jing, C., Liansheng, W., and Lemei, D. (2000). Effects of sulfate on speciation and bioavailability of rare earth elements in nutrient solution. *Chem. Speciat. Bioavailab.* 12 (2), 53–58. doi:10.3184/095422900782775544

frontiers | Frontiers in Environmental Science

TYPE Review
PUBLISHED 28 August 2023
DOI 10.3389/fenvs.2023.1198856



OPEN ACCESS

EDITED BY
Marta Sebastian,
Institut de Ciències del Mar, Spain

REVIEWED BY
Peter Leslie Croot,
University of Galway, Ireland
Cristina Schultz,
Northeastern University, United States

*CORRESPONDENCE
Maryam R. Al-Shehhi,
maryamr.alshehhi@ku.ac.ae

RECEIVED 02 April 2023
ACCEPTED 11 August 2023
PUBLISHED 28 August 2023

CITATION
Ismail KA and Al-Shehhi MR (2023), Applications of biogeochemical models in different marine environments: a review.
*Front. Environ. Sci.* 11:1198856.
doi: 10.3389/fenvs.2023.1198856



# Applications of biogeochemical models in different marine environments: a review

Kaltham A. Ismail and Maryam R. Al-Shehhi*

Department of Civil, Infrastructure and Environmental Engineering, Khalifa University, Abu Dhabi, United Arab Emirates

Marine biogeochemical models are an effective tool for formulating hypothesis and gaining mechanistic understanding of how an ecosystem functions. This paper presents a comprehensive review of biogeochemical models and explores their applications in different marine ecosystems. It also assesses their performance in reproducing key biogeochemical components, such as chlorophyll-a, nutrients, carbon, and oxygen cycles. The study focuses on four distinct zones: tropical, temperate, polar/subpolar, and high nutrient low chlorophyll (HNLC). Each zone exhibits unique physical and biogeochemical characteristics, which are defined and used to evaluate the models' performance. While biogeochemical models have demonstrated the ability to simulate various ecosystem components, limitations and assumptions persist. Thus, this review addresses these limitations and discusses the challenges and future developments of biogeochemical models. Key areas for improvement involve incorporating missing components such as viruses, archaea, mixotrophs, refining parameterizations for nitrogen transformations, detritus representation, and considering the interactions of fish and zooplankton within the models.

KEYWORDS

**marine biogeochemistry, tropical, subtropical, polar, carbon cycle, biogeochemical models, chlorophyll-a**

## 1 Introduction

Marine biogeochemistry concerns the interactions between physical, geological, chemical, and biological processes that influence the cycling of key elements and organisms within the oceans, along the ocean floor and water column, and between the ocean and the atmosphere (Achterberg, 2014). Carbon (C) is one of the primary elements in marine biogeochemistry owing to its importance in both the Earth's climate and living organisms. The other important elements considered include nitrogen, oxygen, phosphorous, silicon, and iron. When these become limiting in the marine environment, they affect the growth of phytoplankton and consequently of zooplankton that graze them (Dutkiewicz et al., 2020). Phytoplankton play a critical role in the biogeochemical cycling through their carbon and nutrient fixation during the photosynthesis process (Munhoven, 2013),whereas, zooplankton consume phytoplankton as one of their primary sources of food and process a significant portion of carbon and nutrients (Ford et al., 2018). Thus, modelling the biogeochemistry of the ocean is an important step toward understanding its primary productivity and eutrophication, as well as the cycling and variability of nutrients (Malone and Newton, 2020). The availability of nutrients along with other physical factors such as light and temperature drives ocean's primary productivity (Ford et al., 2018). However, the

excessive/unbalanced enrichment of water with nutrients (eutrophication) can result in accelerating growth of phytoplankton yielding to unfavourable disturbance to the balance of organisms in the water as well as water quality (Malone and Newton, 2020). Therefore, over the last two decades, marine biogeochemical models have been developed and widely utilized to explore how primary production responds to physical environment disturbances (e.g., El Nino, surface light, temperature increase) at a variety of temporal and spatial scales. Many of these models have originated from the pioneering efforts carried out by Steele in 1958 (Steele, 1958). In his plankton-based model, the assumption was made that the mixed layer is biologically homogeneous, with physical mixing rates (due to factors like wind, tides, and currents) being faster than the growth rate of organisms. The assumption of a homogeneous mixed layer may not hold for deep mixed layers, like the northeast Atlantic Ocean, where increased depth leads to greater light limitation instead of nutrient limitation. Phytoplankton growth occurs near the surface, where light is abundant despite the deep mixed layer. Thus, physical mixing alone cannot overcome the density differences between nutrient-rich deep water and the surface layer. As a result, nutrient depletion may occur in the surface layer, which can restrict organism growth and decrease primary production rates. Hence, Riley revised Steele's model by assuming that the depth of the euphotic zone fluctuates with chlorophyll-a (Chl-*a*) content (Chl-*a* influences depth of PAR through shading) rather than being fixed arbitrarily (Riley, 1965). It is important to note that light attenuation is also influenced by other particles and water properties within the water column, which can contribute to the overall light availability for photosynthetic activity. Riley's model also assumes an increase in the carbon: Chl-*a* ratio with the decrease in nutrient availability. More recently, most of the new models have used nitrogen as fundamental currency and accounted for a simplified food web that distinguishes phytoplankton and zooplankton, along with a regeneration network that incorporates detritus, dissolved organic nitrogen, and several nutrients. The classical NPZD (Nutrients, Phytoplankton, Zooplankton, and Detritus) approach, developed by Fasham et al. (1990)., is one of the earliest and most widely cited biogeochemical models. These main four compartments include biotic (e.g., phytoplankton, zooplankton) and abiotic (e.g., ammonium, nitrate, dissolved organic/inorganic carbon (DOC/DIC), particulate organic carbon (POC)) elements) (Sarmiento et al., 1993).The simplest form of NPZD is presented in Equations 1–4.

$$\frac{dDIN}{dt} = -Uptake + Remineralisation \quad (1)$$

$$\frac{dP}{dt} = (I - m - g)P \quad (2)$$

$$\frac{dZ}{dt} = (gZ - hZ)P \quad (3)$$

$$\frac{dD}{dt} = \mathrm{mP} + \mathrm{hZP} - \mathrm{rD} \quad (4)$$

Where dDIN/dt, dP/dt, dZ/dt, and dD/dt are rate of change of nutrient, phytoplankton, zooplankton, and detritus respectively. DIN is the dissolved inorganic nutrient. Uptake is the rate at which phytoplankton consumes nutrients. Remineralisation is the rate at which organic matter is breaking down into nutrients. I is growth rate of phytoplankton due to light and nutrient availability. m is phytoplankton mortality rate. g is zooplankton grazing rate on phytoplankton. h is zooplankton mortality rate. mP and hZP are the rate of detritus generation due to phytoplankton and zooplankton mortality respectively. r is the rate at which detritus (D) is remineralized into nutrients.

The most applied form of nutrient uptake by phytoplankton is the Michaelis-Menten/Monod saturation function, which relates phytoplankton's growth rates to the concentration of a limiting nutrient (Monod, 1949). However, Droop approach (Droop, 1973; Droop, 1983) suggested that the growth rate is more likely dependent on cells' internal rather than the external concentration of nutrients, and cells could absorb more nutrients than are required for growth (luxury uptake of nutrients) (John and Flynn, 2000; Cherif and Loreau, 2010). Hence, the growth of phytoplankton can be described by a function of internal concentration (quota model-(Droop, 1973; Droop, 1983)). In addition, it is argued that the growth rate is determined by the most limiting process, either light limitation or nutrient uptake, permitting for switching between the two (Franks, 2002).

Recently developed ocean biogeochemical models with increased complexity can accommodate more than 70 state variables (Follows et al., 2007) (Figure 1). In addition to these models, several other biogeochemical models have focused on the inorganic carbon cycle. For instance, the Hamburg model of the oceanic carbon cycle (HAMOCC) was initially a pure inorganic carbon cycle model and was utilized to evaluate both the inorganic carbon cycle and the ocean model residence time properties (Maier-Reimer and Hasselmann, 1987). The Hadley Centre Ocean Carbon Cycle (HadOCC) model which was primarily developed for global climate studies is another example of a carbon cycle model which incorporates the full suite of biogeochemical processes (Cox et al., 2000).

Despite the importance of phytoplankton in carbon fixation in the surface ocean, direct measurements of their carbon biomass are rare, and that multiple factors, including physical processes and microbial activity, contribute to carbon export and remineralization in the oceanic carbon cycle (Hood et al., 2006). Chlorophyll (Chl-*a*) which is a pigment present in phytoplankton to photosynthesize is commonly used to estimate phytoplankton biomass. Chlorophyll has distinctive optical properties (Macintyre et al., 2000) and is controlled by a complex interplay of physiologic, oceanographic, and ecological ocean factors (Sverdrup, 1953; Wroblewski et al., 1988). Furthermore, the relationship between chlorophyll concentration and phytoplankton biomass is nonlinear and the ratio of chlorophyll to biomass varies by an order of magnitude under photoacclimation (Fennel, 2003; Cullen, 2015). Several biogeochemical models (Moore et al., 2002; Aumont and Bopp, 2006; Follows et al., 2007; Vichi et al., 2007), although not all of them, use a parameterization of photoacclimation to take into account changes in the phytoplankton biomass to chlorophyll ratio (Geider et al., 1997).

Along with Chl-*a* as being an important state variable in the biogeochemical models, macronutrients such as nitrogen, phosphorous, silica (necessary for diatom phytoplankton), and micronutrient iron play a significant role in phytoplankton growth and Chl-*a* production. These nutrients exist in the oceans with varying concentrations due to a variety of factors including

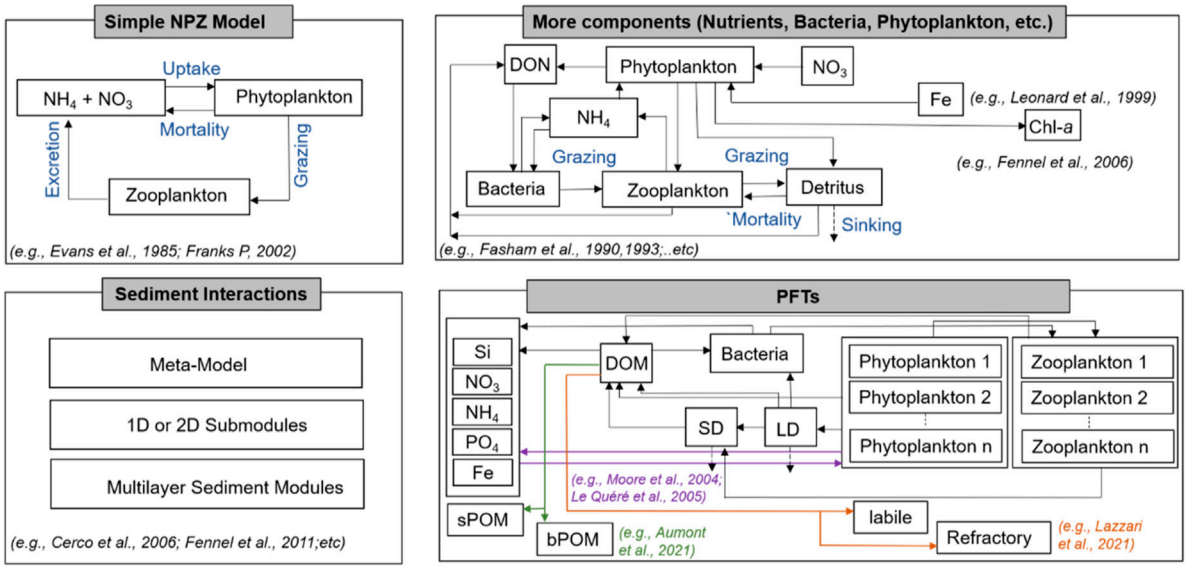


FIGURE 1
Schematic representation of the ocean biogeochemical models varying in complexity from the most basic NPZ form to those with more state variables and processes (high complexity). The labelled rectangular boxes are model variables, and processes are represented by arrows. Sediment interactions are represented which is comprised of different approaches.

regional variations in nutrient sources, physical processes like ocean currents and mixing, biological uptake and recycling, the impact of atmospheric deposition, and terrestrial runoff. In addition, seasonal fluctuations, upwelling events, and nutrient limitation regimes (Anderson et al., 2002; Smith, 2006; Davis et al., 2015; Yang et al., 2017) can have an impact on nutrient availability, which increases the geographical and temporal variability in nutrient concentrations across oceanic regions. Due to the increase of anthropogenic activities, coastal ecosystems receive high levels of nitrogen and phosphorous leading to eutrophication. Excessive nutrient enrichment can result in algal blooms (Chl-*a* concentrations above 40 g $L^{-1}$) (Clarke et al., 2009). Ecosystems in various regions, such as the Baltic Sea (Vahtera et al., 2007; Rönnberg and Bonsdorff, 2016), Chesapeake Bay (Murphy et al., 2022), and the Gulf of Mexico (Rabalais et al., 2002), have experienced imbalances due to eutrophication, including oxygen depletion, loss of biodiversity, and negative effects on fish and shellfish populations.

Eutrophication can cause frequent hypoxia or anoxia (Officer et al., 1984; Naqvi et al., 2000; Soetaert and Middelburg, 2009) emphasizing the need for biogeochemical models in monitoring water quality and alerting ecosystem managers of pollution incidents (Fennel et al., 2019). These models simulate and predict fluctuations in water quality indicators, considering primary production, oxygen levels, and nutrient dynamics. By utilizing field observations and real-time monitoring data, these models can provide valuable insights to mitigate ecological imbalances promptly (Piehl et al., 2022).

In addition to macronutrients, iron is a major limiting nutrient in high latitudes seas, such as the subarctic Pacific Ocean, Southern Ocean, and southern Indian Ocean (Miller et al., 1991; Moore et al., 2004; Hamilton et al., 2020). In many regions, the atmosphere serves as the primary source of iron, which is transported as aerosols and often associated with soil dust (Fung et al., 2000; Sarthou et al., 2003). However, Iron sources can vary in different regions, including coastal Antarctica. It is essential to note that dust is not the predominant source of iron in all regions. In coastal areas, such as coastal Antarctica, diverse sources, including glacial melt and diagenesis, are considered to understand the origins of iron (Gerringa et al., 2012; Sherrell et al., 2018; Dinniman et al., 2020). Dissolved oxygen is another crucial state variable in ocean biogeochemical models, impacting the ecological and biogeochemical structure of marine ecosystems (Wilson et al., 2019). Oxygen depletion and hypoxia can occur due to factors like nutrient loading and insufficient oxygen replenishment. In regions where oxygen levels decrease significantly, known as hypoxic regions, the intensification of hypoxia leads to denitrification and the formation of oxygen minimum zones (OMZs) (Stramma et al., 2010; Stramma et al., 2009; Stramma et al., 2008; Karstensen et al., 2008; Levin and Breitburg, 2015; Lachkar et al., 2016; Lachkar et al., 2019; Lachkar et al., 2020; Levin, 2018; Grégoire et al., 2021). Coastal zones or upwelling regions are typical locations for these hypoxic regions in the ocean (Gobler and Baumann, 2016).

Biogeochemical models have been used in various ecosystems of the world ocean, and for the purpose of our study, we have classified the regions into four distinct zones: tropical, temperate, polar/subpolar, and HNLC. The tropical zone spans approximately 40% of the Earth's surface, stretching from the Tropics of Cancer (latitude 23.5°N) to the Tropic of Capricorn (latitude 23.5°S) (Val et al., 2023). The zone is primarily defined by consistently high temperatures with a sea surface temperature above 20°C and an abundance of sunlight, which leads to high primary production and nutrient cycling. However, there may be some variation in precipitation patterns, humidity levels, and cloud cover across different regions within the tropical zone, which can influence

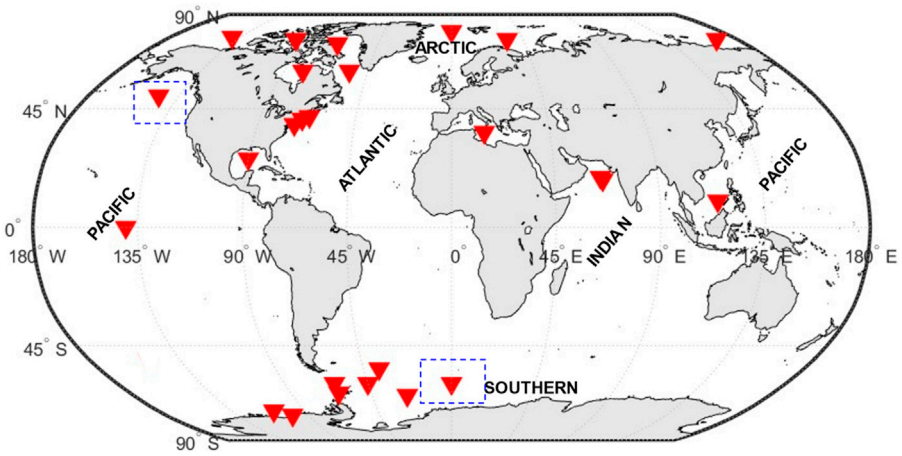


FIGURE 2
World ocean map with the indicated climatic zones presented in this study. The symbols on the map indicate regions where biogeochemical modeling studies, discussed in the review, have been conducted. Boxes with dashed outline are regions where HNLC zone mentioned in the text.

local climate conditions (Lønborg et al., 2021). However, temperate regions are those with latitudes from 35° to 50° North and South and is marked by moderate sea surface temperatures and seasonal variations in nutrient availability and primary production (Lønborg et al., 2021). In tropical coastal waters, sea surface temperatures typically range between 20°C and 32°C. Temperate coastal waters, on the other hand, have a wider temperature range, ranging from 0°C to 25°C, with greater seasonal variation than tropical locations. Although seasonal variations are still noticeable in tropical coastal waters, they are not primarily driven by temperature (Eyre and Balls, 1999). The polar/subpolar zone is covering the Arctic and Antarctic regions (the areas between 60 degrees and the poles) and is defined by low sea surface temperatures usually range from −1°C and 14.7°, sea ice cover, and limited sunlight, leading to low primary production and nutrient cycling (Schultz, 1995). Finally, the HNLC (High Nutrient Low Chlorophyll) zones are regions where the abundance of phytoplankton biomass (or Chl-*a*) is low and almost constant, and macronutrients, in particular nitrates, are never considerably depleted (Edwards et al., 2004). These regions constitute more than 20% of the global ocean (Martin et al., 1994) and is found in areas where iron availability is low and limits the growth of phytoplankton, which are the base of the marine food web. The HNLC zones are found in areas of the Southern Ocean, the equatorial Pacific, and parts of the North Pacific and North Atlantic, Figure 2.

Herein, we describe existing biogeochemical models used to study various ecosystems for the present state in the global oceans at the regional and global scale, and assess their performance, strengths, uncertainties and limitations in estimating several biochemical components, including Chl-*a*, macronutrients (e.g., nitrate, phosphate, silicate), micronutrients (iron), carbon and oxygen cycles. This paper begins with a section that describes different modelling approaches, components, assumptions and structure. Then, the assessment of applications of these models in different ecosystems of the global oceans are discussed.

## 2 Biogeochemical modelling approaches

The existing biogeochemical models are categorized herein by their different level of complexity in terms of the number of phytoplankton functional types (PFTs), different forms of inorganic and organic matter, physics, and deep sediments incorporation.

### 2.1 Classical NPZD approach

The classical NPZD approach is an improvement of the NPZ (Evans et al., 1985; Franks, 2002) which considers a single variable for each compartment (nutrients - phytoplankton - zooplankton - detritus, sometimes including a different compartment for bacteria) neglecting the differences between the different biological types (Fasham et al., 1990; Fasham, 1993; McGillicuddy et al., 1995b). In this approach, nitrogen is typically considered a limiting nutrient because it is a necessary component of chlorophyll, nucleic acids, and proteins, all of which are important for the growth of phytoplankton and photosynthesis (Liefer et al., 2019). Also, compared to other nutrients, nitrogen availability is frequently limited, which can have an adverse effect on the entire food web by limiting phytoplankton development (Bristow et al., 2017). The detritus component accounts for the organic matter pool, which is derived from faecal materials, the fraction non-assimilated by grazing zooplankton and phytoplankton decay. The detritus is recycled by bacteria and degraded to dissolved organic nitrogen, or digested by zooplankton (Leles et al., 2016). The process through which autotrophic organisms, including phytoplankton, produce organic matter by converting sunlight and nutrients into biomass referred as primary production. Contrarily, in secondary production, organic matter is consumed by heterotrophic creatures like zooplankton, which graze on primary producers or consume other organisms.

## 2.2 Improving nitrogen and carbon flux and adding other elements

Modifications have been made in the classical NPZD approaches to improve the estimation of nitrogen and carbon flux (Fennel et al., 2006), with the addition of variable Chl-*a* and introducing a nitrogen-based nutrient-phytoplankton-heterotroph model which is of intermediate complexity with respect to Fasham's and McGillicuddy's models (Fasham et al., 1990; McGillicuddy et al., 1995a). Although nitrate is considered one of the most important limiting nutrients for the growth of phytoplankton biomass and primary production in open ecosystems; in some locations, such as the equatorial Pacific, North Pacific, and the Southern Ocean, nitrate ($NO_3$) levels may exceed 4 μM (central Pacific) and phytoplankton biomass is low (Chai et al., 1996). The high nitrate and low Chl-*a* (HNLC) conditions observed in these regions are commonly associated with limited iron availability (Leonard et al., 1999; Pitchford and Brindley, 1999; Venables and Moore, 2010).

Nevertheless, in high-latitude areas, other factors besides the iron deficiency may also inhibit phytoplankton growth. Low temperatures (Rhee and Gotham, 1981), imbalanced nutritional stoichiometry (Gerhard et al., 2022), short days and prolonged cloud cover (ChrEilertsen and Degerlund, 2010), and grazing pressure (Dale et al., 1999) from higher trophic levels are some examples of these constraints. Leonard et al., 1999 accounted for iron limitation (nutrient compartment) in his extended NPZD model with the employment of nine compartments. The model incorporated iron partitioning into new iron and regenerated iron, as well as dissolved iron bioavailability in the marine environment. Following these developments, Galbraith developed the Biogeochemistry with Light Iron Nutrients and Gases (BLING) model, also based on NPZD (Galbraith et al., 2009). This model employs a specific approach to isolate the global impact of iron on two major features of photosynthesis: maximum light-saturated photosynthesis rates and photosynthetic efficiency. The model uses sophisticated parameterizations or algorithms to separate and quantify the impact of iron on these distinct components. These sophisticated formulations take into account various factors and processes, such as iron uptake mechanisms, iron limitation effects, and biochemical reactions, to provide a detailed understanding of how iron affects photosynthetic process. The model also considers an implicit representation (without explicitly modeling it as a separate parameter or variable) of the growth rate of phytoplankton.

The proportion of the main elements in most biogeochemical models is commonly described with a constant elemental ratio (stoichiometry): 106 C (carbon):16 N (nitrogen):1 P (phosphorous) (Redfield, 1933). This ratio is the most widely used stoichiometric reference for planktonic nutrient limitation (Ptacnik et al., 2010). Hence, biogeochemical models may consider simple growth formulations with constant C: Nutrients stoichiometry or neglect photo-acclimation by considering a constant Chl:C ratio. The classical Michaelis Menten equations are the simplest representation of phytoplankton growth (Monod, 1949) assuming a constant stoichiometric ratio between nitrogen, phosphorous, and carbon (Redfield, 1933; Ho et al., 2003; Quigg et al., 2003; Quigg et al., 2011; Finkel et al., 2006; Finkel et al., 2006). The Redfield ratio has been modified to take into account observed differences from the conventional ratio. As study by (Anderson and Sarmiento, 1994) have been conducted to analyse nutrient data and evaluate the variability of nutrient ratios under different conditions in several regions. Their research emphasizes the significance of taking into account context-specific elements that can affect nutrient stoichiometry, such as nutrient availability, microbial community composition, and ecological interactions Biogeochemical models that incorporate these modified formulations of the Redfield ratio use specific units (nitrogen, phosphorus, or carbon currency) to represent phytoplankton biomass and these models can generally be utilized for global scale studies (Aumont and Bopp, 2006; Follows et al., 2007a; Dutkiewicz et al., 2009). On the other hand (Droop, 1983), has more advanced and complex growth formulations which account for the dynamics of phytoplankton cell internal quota (Klausmeier et al., 2004; Bougaran et al., 2010; Bernard, 2011; Mairet et al., 2011; Wang et al., 2022). Thus, phytoplankton biomass in Droop's model (Droop, 1983) is represented by at least two state variables, typically carbon and nitrogen currency. Different versions of Droop's model have been embedded and utilized in 1D (Lancelot et al., 2000; Allen et al., 2002; Lefe et al., 2003; Mongin et al., 2003; Blackford et al., 2004; Salihoglu et al., 2008) and 3D (Tagliabue and Arrigo, 2005; Vichi et al., 2007; Vichi and Masina, 2009; Vogt et al., 2010) marine biogeochemical models. In these models, Chl-*a* dynamics can be also defined with various levels of complexity. The ratio of Chl: C can be constant (non-photo-acclimation), or prognostic with a dynamic behaviour (Flynn and Flynn, 1998; Geider et al., 1998; Ross and Geider, 2009) or diagnostic with an empirical (Bernard, 2011) and mechanistic relationships (Geider and Platt, 1986; Doney et al., 1996; Bissett et al., 1999). These approaches vary in terms of their level of complexity, assumptions, and underlying mechanisms employed. The constant Chl:C ratio method is the simplest, assuming no acclimation or variation in Chl-*a* concentration. Prognostic techniques enable dynamic modifications of the Chl-*a*:C ratio, capturing phytoplankton's adaptation to changing environmental conditions. Both empirical and mechanistic diagnostic techniques estimate Chl-*a* content based on observational or mechanistic correlations, respectively, without explicitly modelling the physiological processes. Each method provides information about the regulation of Chl-*a* dynamics and their ecological implications in marine ecosystems.

Other complexities have been added to the simple NPZD model, including 1) dissolved organic nitrogen in order to allow for a comprehensive representation of a significant nitrogen pool, particularly in regions where high primary productivity is observed (Hood et al., 2001; Druon et al., 2010), 2) oxygen cycle which is known to be an essential component to represent the oxygen minimum zone caused by excessive denitrification (Naqvi et al., 2000; Codispoti et al., 2001).

## 2.3 Increasing the biological complexity

Unlike the simple NPZD, more complex models include different phytoplankton functional types (PFTs) and at least 15 state variables (e.g., Gregg, 2000; Gregg et al., 2003; Moore et al., 2004; Le Quéré et al., 2005; Dutkiewicz et al., 2009; Stock et al., 2014b; Wright et al., 2021; Luo et al., 2022). Considering a range of plankton groups and increasing the number of variables

allows for a more thorough assessment of ecological interactions. Table 2 provides a summary of the models presented in this section, emphasizing their key characteristics and improvements. Here, we expand on the interpretation of each model improvement and discuss the relevance of increasing the number of variables.

The incorporation of Plankton Functional Types (PFTs) in biogeochemical models has been pursued to improve the accuracy of marine ecosystem representations (Anderson, 2005). Notably, the integration of additional complexity beyond NPZD models presents challenges, including limited understanding of ecology, data constraints, and the need to consolidate diversity within functional groups (Anderson, 2005). This approach is exemplified in biogeochemical models such as ERSEM (European Regional Seas Ecosystem Model) versions 1 and 2 (Baretta et al., 1995; Baretta-Bekker et al., 1997; Blackford et al., 2004). ERSEM adopts a functional role-based classification of biotic groups, categorizing phytoplankton as producers, bacteria as decomposers, and zooplankton as consumers, employing a general lower trophic approach. This approach is similar to the functional roles in an NPZD model, where each component has specific functions within the nutrient dynamics and planktonic community interactions. However, what distinguishes ERSEM from other NPZD models is its comprehensive integration of ecosystem-specific processes and interactions, allowing for a more tailored representation of biotic groups and their functions. The division of the food web into three functional categories is based on traits, including silica uptake, maximum growth rate, and nutrient affinity. The ERSEM model was initially applied to the North Sea to study the seasonal cycling of nutrients (i.e., nitrogen, phosphorous, silica, carbon). ERSEM was later modified to produce the Biogeochemical Flux Model (BFM), which accounts for the Chemical Functional Families (CFFs) in the state variables. The CFFs is split into living, non-living, and inorganic states (Vichi et al., 2007).

The Pelagic Interactions Scheme for Carbon and Ecosystem Studies (PISCES) is another example of a simple PFT model adapted from HAMOCC (Aumont et al., 2003) and extensively and widely applied in more than a hundred studies directly or indirectly (Aumont et al., 2015) The NASA Ocean Biogeochemical Model (NOBM) is a PFT model coupled with the Ocean-Atmosphere Spectral Irradiance Model (OASIM) (Gregg, 2001; Gregg et al., 2009) and is capable of simulating global-scale biogeochemical cycles. Additionally, the PlankTOM model describes the lower trophic level of marine ecosystems and has various extensions with different numbers of PFTs (Le Quéré et al., 2005; Kwiatkowski et al., 2014).

The Model of Ecosystem Dynamics, nutrient Utilization, Sequestration and Acidification (MEDUSA) includes the biogeochemical cycles of iron, silicon, and nitrogen as well as small and large plankton size classes (Yool et al., 2011; 2013). MEDUSA focuses on the biological sequestration of carbon in the deep ocean. Similarly, the Tracers of Phytoplankton with Allometric Zooplankton (TOPAZ), developed by Dunne et al., 2010, focuses on simulating the interactions among phytoplankton and allometric zooplankton, emphasizing their roles within the ecosystem dynamics.This model has been implemented in several studies (Jung, et al., 2019a; Bronselaer et al., 2020; Sharada et al., 2020) and extended in the Carbon, Ocean Biogeochemistry and Lower Trophics (COBALT) model, which improves the planktonic food web dynamics resolution to examine the influence of climate on the flow of energy from phytoplankton to fish (Stock et al., 2014a). Since the planktonic food web representation in TOPAZ is highly idealized due to an implicit representation of zooplankton and bacteria, COBALT addressed these limitations by including three explicit zooplankton groups and bacteria with a mechanistic parametrization of the impacts of these groups on the biogeochemistry (Stock et al., 2014b).

The DARWIN biogeochemical model is a more complex PFT model allowing for several different configurations and number of PFTs. It is initially developed to study *Prochlorococcus* species (Follows et al., 2007b) and later applied to global distributions of phytoplankton (Dutkiewicz et al., 2015; Lo et al., 2019). Nevertheless, the Regulated Ecosystem Model (REcoM) is based on a functional group approach (Schourup-Kristensen et al., 2014) and has also been commonly used in the Southern Ocean studies (Taylor et al., 2013; Losch et al., 2014; Hauck and Völker, 2015).

The complexity of the aforementioned PFT models depends on the number of the independent elements, processes parameterization (e.g., shape of functional responses, number of parameters, linear vs. nonlinear) along with the number of PFTs considered (Ford et al., 2018). As the number of PFTs increases, the complexity of the model increases as well. Generally, adding complexity to the model does not necessarily improve the model's performance as the addition of complexity will require validation of each component of the ecosystem. Even under ideal circumstances, biogeochemical observations are lacking for full spatiotemporal coverage. As a result, the validity of additional processes is sometimes simply determined by how much they contribute to certain quantities like the total chlorophyll content (Ford et al., 2018). These studies comparing models of varying complexity have typically concluded that increasing model complexity does not always result in an increase in model skill (Friedrichs et al., 2007; Kriest et al., 2010; Ward et al., 2013; Kwiatkowski et al., 2014; Xiao and Friedrichs, 2014).

## 2.4 The addition of several classes of organic matter and bacteria

Bacteria play a key role in their contribution in the microbial loop, particularly in the recycling of dissolved organic matter (DOM) and provide a linkage between the higher trophic level and the dynamics of DOM (Pauer et al., 2014). In biogeochemical models studying dissolved organic matter (DOM) dynamics, various classes of organic matter, along with chemical elements and Plankton Functional Types (PFTs), have been incorporated. DOM is divided into three distinct pools based on its lability: labile DOM, semi-labile DOM, and refractory DOM. Labile DOM consists of organic molecules with a lifespan ranging from minutes to days. Semi-labile DOM undergoes decomposition over a period of 1–20 years and typically accumulates above a seasonal or permanent pycnocline. Refractory DOM, the most abundant component, exhibits the longest residence time in the water column, persisting for tens of thousands of years (Carlson and Hansell, 2015; Osterholz et al., 2015).

The ratios of DOC:DON vary among different DOM pools. The refractory DOM pool has a ratio of 3511:202, whereas the labile DOM pool has a ratio of 199:20 (Hopkinson and Vallino, 2005). These ratios indicate the relative amounts of dissolved organic carbon to dissolved organic nitrogen within each pool. It is essential to consider these ratios when incorporating DOM dynamics into biogeochemical models.

DOM in the oceans is an important input to the biogeochemical cycle, with the ocean's DOC pool serving as the biosphere's largest storage facility for reduced organic carbon (Hansell et al., 2009). Labile and, to a lesser extent, semi-refractory pools are driven by microbial reactions. In the microbial loop, the DOC-bacteria pathway constitutes a primary mechanism through which primary production is eitherrespired to $CO_2$, directed to higher trophic levels, or transformed into refractory compounds. However, the refractory DOC is transported deep into the ocean (Anderson, 1999; Kahler and Koeve, 2001).

The aforementioned different forms of organic matter have been incorporated into some biogeochemical models. For instance, the semi-labile DOC and semi-labile dissolved organic nitrogen (DON) have been included in biogeochemical models that focus on regions known of their high primary productivity, particularly coastal and continental shelves regions (Druon et al., 2010; Fennel, 2010; Xue et al., 2013). These areas are potential sites for sediment denitrification and organic carbon transport to the open ocean (Devol and Christensen, 1993; Rao et al., 2007; Fennel et al., 2008; Druon et al., 2010). Another study by Schartau et al. (2007) considered the labile DOM exudation and extracellular POC formation. This process occurs during the growth of phytoplankton in which the assimilation of dissolved inorganic carbon (DIC) by phytoplankton is exuded as DOC, which is simultaneously converted into extracellular POC. A significant proportion of extracellular POC is available as transparent exopolymer particles (TEP), which consist mainly of dissolved polysaccharides (PCHO). PCHO exudation is associated with high consumption of DIC that is not directly measurable from the use of dissolved inorganic nitrogen (DIN), a phenomenon known as carbon overconsumption (Toggweiler, 1993).

## 2.5 Benthic-pelagic coupling

Sediment processes have been also integrated into the pelagic biogeochemical models to investigate the impact of atmospheric conditions on the ecosystem dynamics, the distribution of sediments processes in the water column, and the nitrogen budget derivation (Soetaert et al., 2001; 2000; Arthur et al., 2016; Ehrnsten et al., 2019; Kearney et al., 2020). The lack of sediment regeneration of nutrients in the biogeochemical model may lead to underestimating primary productivity (Liu et al., 2007). Adding a representation of marine sediment in biogeochemical models is important, particularly in shallow water regions like shelves, where strong vertical mixing occurs. This inclusion helps to accurately account for nutrient recycling from sediments to surface waters, preventing the underestimation of productivity (Yool et al., 2013). However, it is crucial to emphasize that in many models, sediment is represented as a boundary condition with simplistic representation, and even global models that address diagenesis frequently lack a thorough representation of the benthic ecosystem.

While incorporating sediment interactions in biogeochemical models is important to understand the linkages between sediment diagenetic processes and the global carbon cycle (Middelburg, 2018; Snelgrove et al., 2018), many models use an oversimplified representation of sediment. Several regional models have been developed to examine specific areas of the ocean at different timescales, yielding important insights into biogeochemical processes. These models such as (Soetaert et al., 2000) and the Ecological ReGional Ocean Model with vertically resolved sediments (ERGOM SED 1.0) (Radtke et al., 2019) also add to the discussion of sediment representation and its effects on oceanic and coastal ecosystems. For example, in a coastal environment (Reed et al., 2011), investigated the dynamics of sedimentary phosphorus and the development of bottom-water hypoxia. Furthermore, the relationship between sediment dynamics and biogeochemical cycling was examined by (Radtke et al., 2019).

Marine sediments representation in the biogeochemical model can be parametrized using a meta-model that is based on the downward fluxes of organic matter (Middelburg et al., 1996), a sediment box module which uses simple 1D or 2D submodules in the pelagic model to represent a simple interaction of the water column with the sedimentary pools (Yool et al., 2013), or multilayer sediment modules with chemically active sediment layers (Heinze and Maier-Reimer, 1999). Most of the biogeochemical models utilize sediment box modules or meta-models to examine eutrophication (Cerco et al., 2006; Soetaert and Middelburg, 2009; Fennel et al., 2011) or hypoxia in several regions, such as Tokyo Bay (Sohma et al., 2008), the Baltic Sea (Reed et al., 2011) and the North Sea (Lancelot et al., 2005; Meire et al., 2013).

# 3 Applications of biogeochemical models

The aforementioned models have been applied to resolve biochemical components including Chl-*a*, macronutrients (nitrogen, phosphorous, silica), micronutrients (iron), carbon and oxygen in different regions of the world's ocean. Here, we will focus on the application of these biogeochemical models in four zones as described in the introduction section. Detailed assessments of the capabilities of these models along with their complexity through the addition of more components are provided here and summarized in Table 1. Further, the common statistical metrics for model assessment used in the analysed studies are illustrated in Table 2. To provide a comprehensive analysis of the model performance, Taylor diagrams (Taylor, 2001) are employed in various biogeochemical modelling studies. Taylor Diagrams are graphical tools that show several model performance metrics at the same time, providing an illustration of the model's ability to capture observed data patterns. They can assist in comparing and ranking various models based on correlation, root mean square error, and standard deviation (Jolliff et al., 2009). We have added also a graphical illustration of the model's performance separated for each zone along with their temporal scale and type of observational data used to validate the model variables, see Figures 3–7.

**TABLE 1 Overview of the biogeochemical models reviewed in this work showing their model approach, physical model, resolution, Nutrient/element cycling, the number of the living/non-living components and sediments formulation.**

| Ocean | Zone | Model approach | Physical model | Resolution* | | Nutrient/element cycling* | | | | | | Living/non-living components | | | | | | Sediments |
|---|---|---|---|---|---|---|---|---|---|---|---|---|---|---|---|---|---|---|
| | | | | Vertical layers | Horizontal | Fe | N | P | Si | $O_2$ | C | # of phytoplankton | # of zooplankton | # of detritus | # of bacteria | DOM | POM | |
| Global | | NOBM[1] | GCM | | | + | + | | + | | | 4 | 1 | 2 | | | | No |
| Global | | HAMOCC5[2] | LSG | | | + | | + | + | | + | 2 | 2 | 1 | | + | | Balance |
| Global | | ERSEM[3] | GOTM | | | + | + | + | + | + | + | 4 | 3 | 1 | 1 | + | + | Meta-mod |
| Global | | Moore[4] | CCSM | | | + | + | + | + | + | + | 4 | 1 | 1 | | + | | Meta-mod |
| Global | | Moore[5] | CCSM | | | + | + | + | + | + | + | 4 | 1 | 2 | | | | No |
| Global | | PlankTOM[6] | NEMO | | | + | + | | + | + | + | 3 | 2 | 7 | | | | No |
| Global | | PISCES[7] | NEMO | | | + | + | + | + | + | + | 2 | 2 | 3 | | + | + | Meta-mod |
| Global | | DARWIN[8] | MITgcm | | | + | + | + | + | + | + | 8 | 2 | 2 | | + | + | Meta-mod |
| Global | | PlankTOM[9] | NEMO | | | + | + | + | + | + | + | 6 | 3 | 3 | 1 | | | No |
| Global | | PISCES[10] | NEMO | | | + | + | + | + | | + | 2 | 2 | 2 | | + | + | Meta-mod |
| Global | | Moore[11] | NCAR-CSM1 | | | + | + | + | + | + | + | 4 | 1 | 2 | | | | No |
| Global | | TOPAZ/ PISCES[12] | NEMO | | | + | + | + | + | + | + | TOPAZ:3 PISCES: 2 | PISCES:2 | | | | | Meta-Mod |
| Atlantic | Tropical | Fasham[13] | MOM | | | | + | | | | | 1 | 1 | 1 | | | | No |
| Atlantic | Subtropical | Fasham[14] | ROMS | | | | + | | | | + | 1 | 1 | 1 | | | | Meta-Mod |
| Atlantic | Subtropical | Fasham[15] | ROMS | | | | + | | | | + | 1 | 1 | 4 | | + | | Meta-Mod |
| Atlantic | Subtropical | Fasham[16] | ROMS | | | | + | | | | | 1 | 1 | 2 | | + | | Meta-Mod |
| Atlantic | Subtropical | BFM[17] | OGCM-MED16 | | | | + | + | + | + | | 4 | 4 | 1 | 1 | | | No |
| Atlantic | Subtropical | ERSEM[18] | POM | | | | + | + | + | + | + | 4 | 3 | | 1 | + | + | Meta-Mod |
| Atlantic | Subtropical | ERSEM[19] | POM | | | | + | + | + | + | + | 4 | 3 | | 1 | + | + | Meta-Mod |
| Indian | Tropical | Fasham[20] | OGCM | | | | + | | | | | 1 | 1 | 1 | 1 | + | | No |
| Indian | Tropical | ERSEM[21] | Princeton/ Mellor–Yamada | | | | + | + | + | | + | 4 | 3 | 2 | 1 | + | + | Meta-Mod |
| Indian | Tropical | McCreary[22] | Four-layer model | | | | + | | | | | 1 | 1 | 1 | | | | No |

(Continued on following page)





10.3389/fenvs.2023.1198856

**TABLE 1 (*Continued*) Overview of the biogeochemical models reviewed in this work showing their model approach, physical model, resolution, Nutrient/element cycling, the number of the living/non-living components and sediments formulation.**

| Ocean | Zone | Model approach | Physical model | Resolution* | | Nutrient/element cycling* | | | | | | Living/non-living components | | | | | | Sediments |
|---|---|---|---|---|---|---|---|---|---|---|---|---|---|---|---|---|---|---|
| | | | | Vertical layers | Horizontal | Fe | N | P | Si | $O_2$ | C | # of phytoplankton | # of zooplankton | # of detritus | # of bacteria | DOM | POM | |
| Indian | Tropical | Fasham[23] | MOM | | | | + | | | | | 1 | 1 | 1 | | | | No |
| Indian | Tropical | PISCES[24] | NEMO | | | + | + | + | + | | | 2 | 2 | 3 | | | | Meta-Mod |
| Indian | Tropical | PISCES[25] | NEMO | | | | + | | + | | | 2 | 2 | 3 | | | | No |
| Indian | Tropical | McCreary[26] | Six-layer model | | | | + | | | + | | 1 | 1 | 2 | | | | No |
| Indian | Tropical | Fasham[27] | ROMS | | | | + | | | + | | 1 | 1 | 1 | | | | Meta-Mod |
| Indian | Tropical | ERSEM[28] | GOTM | | | + | + | + | + | + | + | 4 | 3 | 1 | 1 | + | + | Meta-Mod |
| Indian | Tropical | Fasham[29] | ROMS | | | | + | | | + | | 1 | 1 | 1 | 1 | | | Meta-Mod |
| Indian | Tropical | PISCES[30] | ROMS | | | + | + | + | + | | | 2 | 2 | 3 | | | | Meta-Mod |
| Indian | Tropical | NOBM[31] | OGCM | | | | + | | | | | 4 | 1 | 3 | | | | No |
| Indian | Tropical | TOPAZ[32] | MOM | | | + | + | + | + | | + | 3 | | 1 | + | + | | Sed-Box |
| Indian | Tropical | Fasham[33] | ROMS | | | | + | | | + | | 1 | 1 | 1 | | | | Meta-Mod |
| Southern | HNLC | PlankTOM[34] | NEMO | | | | + | + | + | + | + | 6 | 3 | 3 | 1 | | | Meta-Mod |
| Southern | HNLC | NOBM[35] | OGCM | | | | + | | + | | + | 4 | 1 | 3 | | | | No |
| Southern | HNLC | DARWIN[36] | MITgcm | | | + | | | | | | 2 | 2 | | | | | No |
| Southern | HNLC | PISCES[37] | NEMO | | | + | + | + | + | | | 2 | 2 | 2 | | + | | Meta-Mod |
| Southern | Polar | DARWIN[38] | MITgcm | | | | + | + | + | | + | 6 | 2 | | | + | | Meta-Mod |
| Southern | Polar | Chai[39] | ROMS | | | + | + | | + | | | 2 | 2 | 2 | 1 | | | Meta-Mod |
| Southern | HNLC | TOPAZ[40] | ESM2M | | | | + | | | | + | 3 | | 2 | | | | Sed-Box |
| Arctic | Polar | PISCES[41] | MITgcm | | | | | | | | + | 2 | 2 | 2 | | + | | No |
| Arctic | Polar | 21 biogeochemical models[42] c) | - | | | | | | | | | | | | | | | |
| Arctic | Polar | REcoM2[43] | FESOM | | | + | + | | + | | + | 2 | 1 | 1 | | | | Meta-Mod |
| Arctic | Polar | BLING[44] | NEMO | | | + | | + | | + | | | | | | + | | No |
| Arctic | Polar | DARWIN[45] | MITgcm | | | + | + | + | + | | + | 5 | 2 | | | | | No |

(Continued on following page)





10.3389/fenvs.2023.1198856

**TABLE 1 (*Continued*) Overview of the biogeochemical models reviewed in this work showing their model approach, physical model, resolution, Nutrient/element cycling, the number of the living/non-living components and sediments formulation.**

| Ocean | Zone | Model approach | Physical model | Resolution* | | Nutrient/element cycling* | | | | | | Living/non-living components | | | | | | Sediments |
|---|---|---|---|---|---|---|---|---|---|---|---|---|---|---|---|---|---|---|
| | | | | Vertical layers | Horizontal | Fe | N | P | Si | $O_2$ | C | # of phytoplankton | # of zooplankton | # of detritus | # of bacteria | DOM | POM | |
| Pacific | Tropical | Leonard[46] | OGCM | | | + | + | | | | | 1 | 1 | 1 | | | | Model-layer |
| Pacific | Tropical | Chai[47] | ROMS | | | | + | | + | | | 2 | 2 | 2 | | | | Balance |
| Pacific | Subtropical | Fasham[48] | ROMS | | | | + | + | | | | 1 | 1 | 2 | | | | No |
| Pacific | Tropical | Fasham[49] | ROMS | | | | + | | | + | + | 1 | 1 | 4 | | | | No |
| Pacific | Tropical | PISCES[50] | ROMS | | | + | + | + | + | | | 2 | 2 | 3 | | | | Meta-Mod |
| Pacific | Tropical | TOPAZ[51] | GOTM | | | | + | + | + | + | + | 3 | | 1 | | | | Sed-Box |
| Pacific | Tropical | Chai[52] | ROMS | | | | + | + | + | + | + | 2 | 2 | 3 | | | + | Meta-Mod |
| Pacific | Tropical | Fasham[53] | ROMS | | | | + | + | | | | 1 | 1 | 2 | | | | No |
| Pacific | Tropical | Kearney[54] | Bering 10K ROMS | | | + | + | | | | | 2 | 5 | 2 | | | | Model-layer |
| Pacific | HNLC | Chai[55] | ROMS | | | + | + | + | + | + | | 2 | 2 | 4 | | | | No |

[1] (Gregg et al., 2003), [2] (Aumont et al., 2003), [3] (Blackford et al., 2004), [4] (Moore et al., 2004), [5] (Moore et al., 2004), [6] (Buitenhuis et al., 2013), [7] (Aumont et al., 2015), [8] (Dutkiewicz et al., 2015), [9] (Andrews et al., 2017), [10] (Aumont et al., 2015), [11] (Pant et al., 2018), [12] (Jung et al., 2019a). [13] (Oschlies and Garçon, 1999), [14] (Fennel et al., 2008), [15] (Druon et al., 2010), [16] (Xue et al., 2013). [17] (Lazzari et al., 2016). [18] (Kalaroni et al., 2019). [19] (Kalaroni et al., 2020). [20] (Ryabchenko et al., 1998). [21] (Blackford and Burkill, 2002). [22] (Hood et al., 2006), [23] (Kawamiya and Oschlies, 2003). [24] (Koné et al., 2009). [25] (Resplandy et al., 2011). [26] (McCreary et al., 2013). [27] (Lachkar et al., 2017). [28] (Sankar et al., 2018). [29] (Lachkar et al., 2019). [30] (Guieu et al., 2019). [31] (Das et al., 2019). [32] (Sharada et al., 2020). [33] (Lachkar et al., 2020). [34] (Le Quéré et al., 2016). [35] (Trull et al., 2018). [36] (Uchida et al., 2019). [37] (Person et al., 2019). [38] (Lo et al., 2019). [39] (Jiang et al., 2019). [40] (Bronselaer et al., 2020). [41] (Manizza et al., 2011). [42] (Babin et al., 2016). [43] (Schourup-Kristensen et al., 2018). [44] (Castro de la Guardia et al., 2019). [45] (Manizza et al., 2012). [46] (Christian et al., 2001). [47] (Xiu and Chai, 2011). [48] (Gan et al., 2014). [49] (Ji et al., 2017). [50] (Vergara et al., 2017). [51] (Jung et al., 2019b). [52] (Ma et al., 2019). [53] (Lu et al., 2020). [54] (Kearney et al., 2020), [55] (Zhang et al., 2021). *For the surface nutrients: dark orange: 0.8≤r < 1; Bias: < 0.5; RMSD <0.2, Medium orange: 0.5 ≤r < 0.8; 0.5≤Bias< 1; 0.5< RMSD <0.2 and Light orange: r < 0.5; Bias ≥ 1; RMSD ≥0.5. *For the vertical resolution: dark blue: > 50 layers, medium blue: 20<layers< 50, light blue: < 20 layers. *For the horizontal resolution: dark blue: < 0.1degrees, medium blue: 0.1<degrees<0.5 and light blue: >0.5 degrees. For the chlorophyll (Chl): dark green. DOM, dissolved organic matter. POM, particulate organic matter.





10.3389/fenvs.2023.1198856

**TABLE 2 The common statistical metrics for model assessment used in the analysed studies.**

| Method | Description | Equation |
|---|---|---|
| RMSE | Calculate the model's error between the predicted data ($y_i$) and the observational data ($x_i$). | $\sqrt{\sum_{i=1}^{n}\frac{(x_i-y_i)^2}{n}}$ |
| R | Correlation coefficient which determines how linearly connected the observations are to their model equivalents. r = 1 means a perfect correlation or relationship. r = 0 means there is no relationship, and r < 0 indicates that the two data are negatively correlated. | $\frac{\sum_{i=1}^{n}(x_i-\overline{x_i})(y_i-\overline{y_i})}{\sqrt{\sum(x_i-\overline{x_i})^2\sum(y_i-\overline{y_i})^2}}$ |
| $R^2$ | Coefficient of determination (between 0 and 1) which measures how well the model predicts the observed data. As it is closer to 1 means strong correlation while closer to 0 means weak correlation between the predicted and observed data. It is defined | $\frac{n(\sum_{i=1}^{n}x_iy_i)-(\sum_{i}^{n}x_i)(\sum_{i}^{n}y)}{\sqrt{[n\sum_{i=1}^{n}x_i^2-(\sum_{i=1}^{n}x_i)^2]n\sum_{i=1}^{n}y_i^2-(\sum_{i=1}^{n}y_i)^2]}}$ |
| Bias | Bias is to what degree the model overestimates (bias>0) or underestimates (bias<0) the observed data. | $\frac{1}{n}\sum_{i=1}^{n}(x_i-y_i)$ |

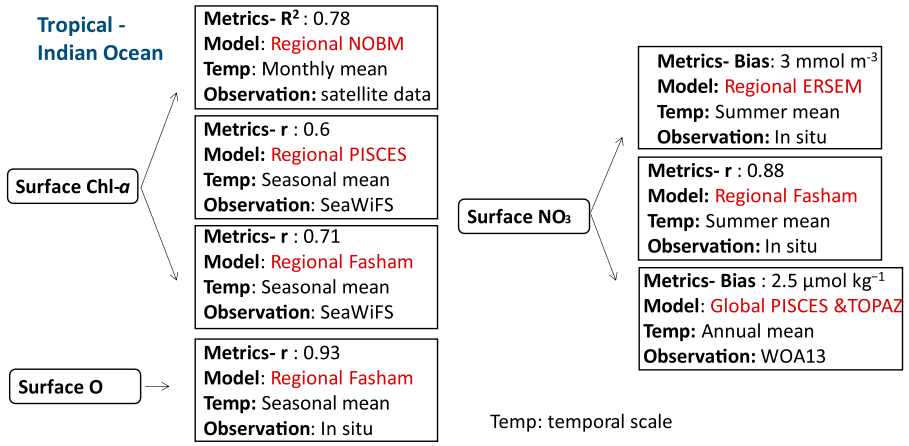


FIGURE 3
Biogeochemical variables performance for some of the models applied in the tropical ecosystems along with their temporal scale and type of observational data used to validate the model components.

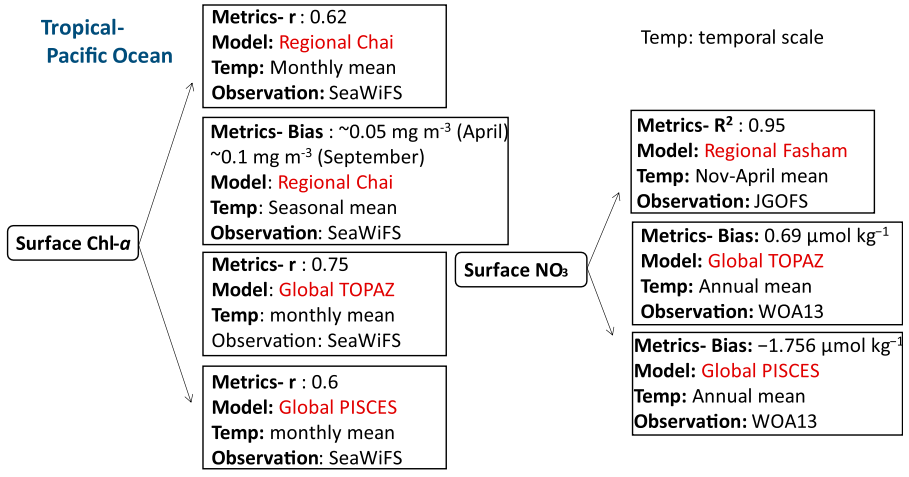


FIGURE 4
Biogeochemical variables performance for some of the models applied in the tropical Pacific ecosystems along with their temporal scale and type of observational data used to validate the model components.

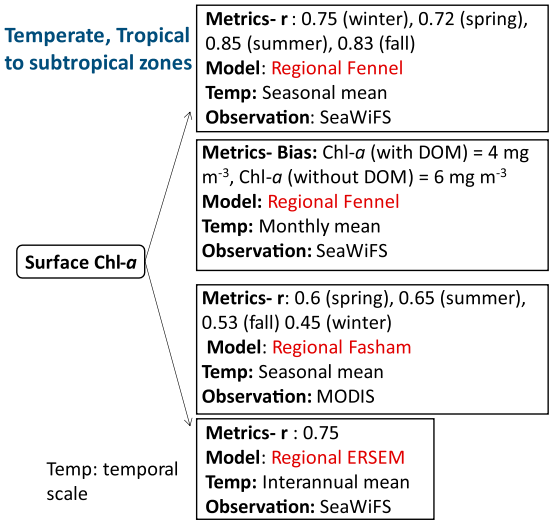


FIGURE 5
Biogeochemical variables performance for some of the models applied in the temperate, and tropical to subtropical ecosystems along with their temporal scale and type of observational data used to validate the model components.

## 3.1 Tropical zones

The aforementioned biogeochemical models have been applied in various tropical seas due to their high dynamism and significant biogeochemical activity, making them among the most active zones in the ocean (Lønborg et al., 2021). This section encompasses multiple regions, including the tropical Indian Ocean (specifically the Arabian Sea), the South China Sea, the tropical Pacific Ocean, and the oxygen minimum zone in the Arabian Sea. One prime example of a tropical ecosystem is the Indian Ocean, which experiences the world's most significant monsoon system caused by the seasonal warming and cooling of massive air masses (Wiggert et al., 2005). In winter and summer, the wind patterns near the ocean change, with the southwest monsoon (SWM) providing half of the year's wind and the northeast monsoon (NEM) providing the other half (Wiggert et al., 2005). The dynamics of the Arabian Sea's (the most extensively studied ecosystem in the Indian Ocean) phytoplankton bloom clearly show a temporal alignment with the southwest monsoon and northeast monsoon (Madhupratap et al., 1996; Wiggert et al., 2005). Strong south-westerly winds during the summer propel coastal upwelling and offshore movement of entrained nutrients, which promote the Arabian Sea's observed phytoplankton blooms (Brock and Mcclain, 1992; Hitchcock et al., 2000; Lierheimer and Banse, 2002). Modest north-easterly winds during the winter carry cool, dry air from the Tibetan Plateau over the northern Arabian Sea (Huang, 2010). Additionally, convective mixing during NEM entrains nutrients and promotes biological activity north of 15°N (Madhupratap et al., 1996). Thus, primary productivity and nutrients budgets in the Arabian Sea, spanning a temporal scale of seasonal variations and a spatial scale ranging from 5°S to 27°N are highly impacted by the seasonal cycle and mesoscale impacts (Resplandy et al., 2011). The primary production in terms of surface Chl-*a* production in the Arabian Sea is widely studied using several types of ocean biogeochemical models. For example, the estimated surface Chl-*a* by PISCES coupled to the Nucleus for European Modelling of the Ocean (NEMO) is compared with the weekly climatology of SeaWiFS (Sea-viewingWide Field-of-view Sensor Data). The PISCES-NEMO reproduced surface Chl-*a* levels of more than 0.2 mg $m^{-3}$ during the NEM. It also predicted the maximum intensity of surface Chl-*a*, which exceeds 0.5 mg $m^{-3}$, but underpredicted surface Chl-*a* by 30%–50% north of 20°N. This bias was found in other studies and may be attributed to the lack of diurnal layer mixing (Kawamiya and Oschlies, 2003; Wiggert et al., 2006; Koné et al., 2009). The bias in the bloom dynamics is explained by the lack of deepening of the mixed layer and nutrient feed (Wiggert et al., 2006), and light limitation (Koné et al., 2009). Another cause of inconsistencies in the PISCES model (Resplandy et al., 2011) is partially linked to the underprediction of silicate input from the Sea of Oman. PISCES

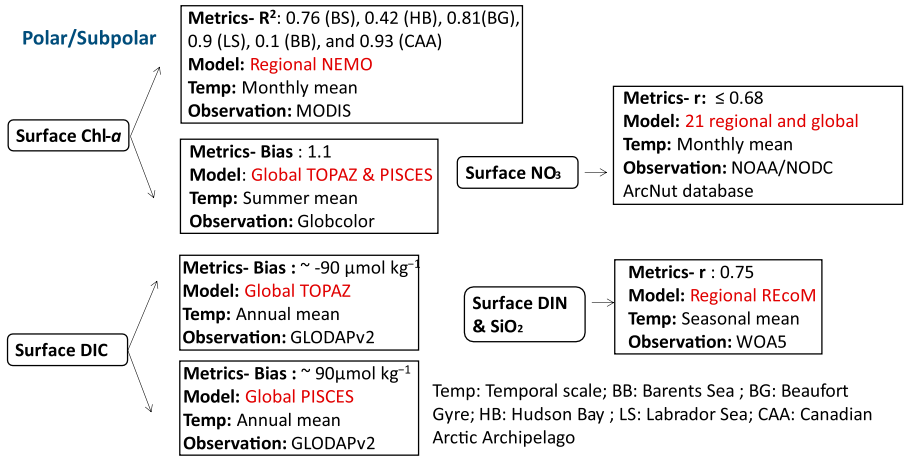


FIGURE 6
Biogeochemical variables performance for some of the models applied in the polar/subpolar ecosystems along with their temporal scale and type of observational data used to validate the model components.

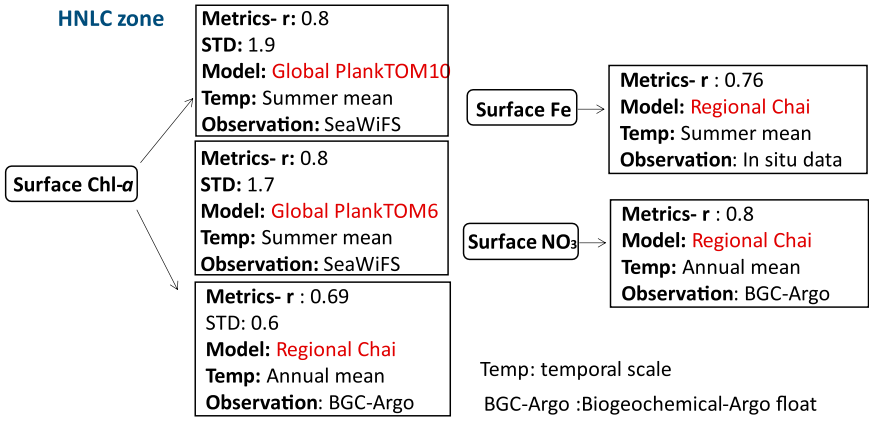


FIGURE 7
Biogeochemical variables performance for some of the models applied in the HNLC zone along with their temporal scale and type of observational data used to validate the model components.

captured the observed high surface Chl-*a* along the coasts of Somalia and southwestern India, reaching values higher than 0.4 mg $m^{-3}$ during the SWM. On the other hand, it underestimated Chl-*a* in Oman. These inconsistencies can be attributed to the overprediction of the offshore advection by the Great Whirl and the Socotra Passage, resulting in an excessive outflow of warmer and oligotrophic waters from the Aden Gulf. Therefore, PISCES-NEMO showed better agreement with observations (seasonal SeaWiFS data) for the surface Chl-*a* distribution than in (Koné et al., 2009) with a correlation coefficient (r) around 0.6. These comparisons encompass a spatial scale ranging from 30°S to 30°N and from 30°E to 120°E, with a focus on seasonal variations. In addition to PISCES, the PFT model NOBM coupled with the oceanic general circulation and radiative forcing model was able to capture the intra-seasonal variability of the Indian summer monsoon, specifically focusing on the spatial scale of the Bay of Bengal (BOB) (6°–22° N; 80°–100° E) and Arabian Sea (AS) (3°–17° N; 55°–73.5° E) in the North Indian Ocean. The study showed important differences between the two regions indicating that the Arabian Sea is richer in nutrients than the Bay of Bengal with a coefficient of determination ($R^2$) around 0.78 for the monthly mean surface Chl-*a* (Das et al., 2019). Furthermore, surface Chl-*a* is reproduced by Fasham-ROMS (Regional Ocean Modeling System), in the study region, which extends in latitude from 5°S to 30°N and in longitude from 34°E to 78°E. The performance of the model is evaluated by comparing its outputs with seasonal SeaWiFs observations, resulting in correlation coefficient ranging from 0.69 in summer to 0.74 in winter (Lachkar et al., 2017).

In addition to surface Chl-*a* estimation, surface nitrogen content in the Arabian Sea is estimated by the European Regional Seas Ecosystem Model (ERSEM) coupled with a 1D Princeton/ Mellor–Yamada (Blackford and Burkill (2002). The model performance was assessed at three stations located at 19°N 59°E, 16°N 62°E, and 8°N 67°E, covering a seasonal timescale. The coupled model has a bias for surface nitrate concentration (3 mmol $m^{-3}$) and lacks horizontal advective processes, which might be enhanced by including diurnal physical processes (horizontal advection, vertical mixing, or tidal currents). Another study by using Fasham-ROMS indicated a correlation coefficient (r) of 0.88 with observation for surface nitrate in summer. Nitrogen is not the only limiting nutrient affecting phytoplankton growth in the Arabian Sea and the ignorance of other components such as iron may underestimate nitrogen budget in the region. Iron, as an important limiting nutrient in the Arabian Sea, plays a significant role in facilitating nitrogen fixation, which is a crucial process driving biological productivity. However, nitrogen fixation is not taken into account in the NPZD, which may amplify the impact of denitrification on the nitrogen budgets in the Arabian Sea (Lachkar et al., 2017). A few studies have been conducted to examine the effect of iron limitation on global biogeochemical processes, including those in the Indian Ocean. For instance, studies using PFT approach, such as PISCES-ROMS and TOPAZ-MOM (Jung et al., 2019b) have explored the implications of iron limitation on various aspects, including macronutrient availability and ecosystem dynamics. Unlike the previous version of PISCES in (Aumont and Bopp, 2006), this version incorporated new parametrizations for iron chemistry and nitrogen fixation. PISCES exhibited a better iron estimate than TOPAZ, whereas TOPAZ showed larger bias with observation (SeaWiFS) (1.5 nMol $m^{-3}$) (Jung et al., 2019b).

Another prominent feature of the Arabian Sea is its oxygen minimum zone which is noted for its low oxygen concentrations (<4 mmol/$m^{-3}$) at depths of 150–1,250 m in the central part of the Arabian Sea. Thus, the dynamics of the oxygen minimum zone (OMZ) at spatial coordinates (65°E, 13°N) is studied by applying ERSEM coupled with General Ocean Turbulence Model (GOTM). The model incorporates most of the biogeochemical processes driving the dynamics of OMZ with the inclusion of denitrification process which was not considered in Butenschön et al. (2016). ERSEM-GOTM ignores the episodic intrusion of oxygen within the OMZ which may play a role in maintaining aerobic microorganisms. Therefore, the aerobic biomass within the OMZ is maintained by the residual initial conditions (Sankar et al., 2018). In addition, the model is unable to reproduce meso-zooplankton at depth, and the discrepancy between the estimates and the climatological seasonal cycles of nutrients and oxygen at

depth might be due to the absence of lateral circulation in the model. Further studies on the OMZs in the Arabian Sea were investigated by Lachkar using a simple NPZD approach with the addition of the oxygen cycle (Fasham- ROMS) (Lachkar et al., 2017; Lachkar et al., 2019; Lachkar et al., 2020). Fasham-ROMS indicated that the primary productivity and OMZ are highly impacted by monsoon wind intensification, with an overall high correlation coefficient (r) 0.93 for oxygen (both seasons) in the upper layer. While the model's horizontal grid resolution of 1/12° and vertical grid consisting of 32 sigma layers allow for some representation of eddy dynamics, the resolution may still be too coarse to fully capture all eddy processes.The OMZ intensity (oxygen concentration) has also been overestimated because of the underestimation of the northern Arabian Sea ventilation. Studies on OMZ in the Arabian Gulf are still limited.

In addition to the Indian Ocean, some parts of the Pacific Ocean are also located in the tropical zone, and south China Sea, which is the largest marginal seas of the West Pacific Ocean (Qi-zhou et al., 1994), is an example of an ecosystem that belongs to this region. Similar to the Arabian Sea, this region is largely controlled by seasonal monsoon circulation. Strong northeast (NE) winter monsoon and weaker southeast (SE) summer monsoon predominate at the sea surface of the South China Sea (SCS) (Qi-zhou et al., 1994; Li et al., 2021). Studies have shown a clear response of Chl-*a* and temperature of the upper oceanic conditions to atmospheric forcing in the SCS (Sun et al., 2009; Sun et al., 2010; Yang et al., 2010; Zhao et al., 2014). Estimates of the mean surface Chl-*a* has been reported with varying performances. A correlation coefficient (r) of 0.85 for the annual mean surface Chl-*a* is obtained by (Jung et al., 2019b) using both global PISCES and TOPAZ coupled to NEMO representing surface Chl-*a* concentration conditions (i.e., phytoplankton blooms) in the tropical Pacific. Furthermore, the monthly mean surface Chl-*a* was determined by PISCES-NEMO and TOPAZ-NEMO (Jung et al., 2019b) with r equal to 0.6 and 0.75, respectively. However, both models overpredicted the zonal averaged Chl-*a* in the Pacific Ocean east of Japan by 67%, primarily because of errors in the Kuroshio current path, as seen in low-resolution models (Gnanadesikan et al., 2002; Dutkiewicz et al., 2005; Aumont and Bopp, 2006). Nevertheless, the regional Chai's NPZD model (Chai et al., 1996) configured for the central South China Sea was modified by adding phosphate, silicate, dissolved oxygen, DIC, two phytoplankton groups (diatoms, small phytoplankton) and their chlorophyll components (Chl1 and Chl2) has shown a correlation coefficient of approximately 0.62 for the monthly mean surface Chl-*a* in the SCS compared to SeaWiFS data (Ma et al., 2019). Other NPZD models were also applied in the tropical Pacific seas (SCS) to study the physical processes of mesoscale eddies' impacts on biology such as in (Xiu and Chai, 2011). The study covered the entire Pacific Ocean, spanning from 45°S to 65°N and from 99°E to 70°W. The model exhibited a bias of approximately 0.05 mg $m^{-3}$ (April) and ~0.1 mg $m^{-3}$ (September) for mean surface Chl-*a* concentrations when compared to SeaWiFS data for the respective months.

Other biogeochemical components such as nutrients including nitrate, phosphate, silicate, and iron have been estimated using global ocean biogeochemical models in the Pacific region. Higher positive bias for nutrients is obtained using the global TOPAZ-NEMO model compared to PISCES-NEMO in the Southern Pacific Ocean using the same physical model setup. With bias of 4.5 μmol $kg^{-1}$,0.32 μmol $kg^{-1}$, and 16 μmol $kg^{-1}$ for nitrate, phosphate, and silicate respectively, with a higher positive bias in the central and southern Pacific for silicate (8 μmol $kg^{-1}$). With regards to a NPZD based approach, Fasham-ROMS exhibited the impact of physical processes, such as lateral and vertical fluxes, as well as vertical diffusion in the shelf water, on nutrient distribution in the SCS (Ji et al., 2017; Lu et al., 2020) showing a reasonable linearity between the model estimates and field observations (JGOFS: a global, multidisciplinary program with participants from over 20 countries) for surface nitrate with $R^2$: 0.95 (Ji et al., 2017). In (Ji et al., 2017), the model domain focused on the northwestern Pacific (NWP) region (3°–52°N, 98°–158°E), while in (Lu et al., 2020), the model domain extended from approximately 0.95°N, 99°E in the southwest corner to around 50°N, 147°E in the northeast corner.

With regards to iron, low surface concentrations of iron were predicted in the North and North Central Pacific, while high concentrations were predicted in the North and Equatorial Indian Ocean using global NOBM (Gregg et al., 2003). The model domain considered spans from approximately −84°S to 72°N latitude in increments of 1.25° longitude by 2/3° latitude. The overall correlation coefficient for the annual mean iron with *in situ* data is 0.86 and the reason for the iron overprediction is attributed to the lack of scavenging, excessive remineralization, and slow detritus sinking rate.

## 3.2 Temperate, and tropical to subtropical zones

Compared to the tropical zones, the temperate zone is characterized by moderate climate with mean annual temperatures. Average monthly air temperatures in the temperate zone typically exceed 10°C during the warmest months while water temperatures generally remain above −3°C, with a minimum around ~-2°C. (Trewartha and Horn, 1980). In contrast, the subtropical zones, located between the tropical and temperate zones, are characterized by hot summers and moderate winters. Some parts of the North Atlantic Ocean comprises both temperate and varying tropical to subtropical zones. Biogeochemical studies in this region have focused on understanding primary productivity in continental shelves and coastal areas, which are highly productive ecosystems and are significantly influenced by human activities (Economidou, 1982; Fennel, 2010). Additionally, air-sea $CO_2$ fluxes in coastal waters exhibit greater variability and larger amplitudes compared to fluxes in the open ocean (Tsunogai et al., 1999; Cai et al., 2003; Thomas et al., 2004). For instance, in the Mid Atlantic Bight, located in the central region of the eastern U.S. continental shelf, high primary productivity rates, sediment denitrification, and strong residual circulation contribute to the region's significance as a potential source of organic carbon export to the open ocean (Druon et al., 2010). In the Northwest North Atlantic and other ecosystems within the region, many studies have utilized simple NPZD models to investigate the influence of physical processes on biological dynamics, rather than aiming to capture the full complexity of ecological interactions. Therefore, this section covers both coastal areas and open sea regions of the Mid

Atlantic Bight, northeastern US continental shelves, Georges Bank, Gulf of Mexico, and Mediterranean waters. An example of such modeling approach is demonstrated in (Fennel et al., 2008), where the distribution of Chl-*a*, an indicator of productivity in the Atlantic regions, is predicted using a NPZD model. The model is coupled with a high-resolution physical model ROMS, which incorporates accurate descriptions of physical processes and an explicit representation of inorganic carbon chemistry and air-sea gas exchange of $CO_2$ (Fennel et al., 2008). The model's inclusion of tides in ROMS improves the seasonal mean surface Chl-*a* representations, showing good agreement with SeaWiFS climatology in Georges Bank (correlation coefficients: 0.75 in winter, 0.72 in spring, 0.85 in summer, and 0.83 in fall) (Fennel et al., 2008). In another study by Druon et al., 2010, Fennel's model (Fennel et al., 2008) was further enhanced by incorporating a dissolved organic matter (DOM) module to investigate organic carbon dynamics in the North-eastern U.S. continental shelves. The model demonstrated good agreement with monthly satellite data, particularly in the inner shelf and on Georges Bank, attributing this agreement to tidal mixing and continuous nutrient suppl (Bias: Chl-*a* (with DOM) = 4 mg $m^{-3}$, Chl-*a* (without DOM) = 6 mg $m^{-3}$). The inclusion of the DOM module improved the model by capturing the role of dissolved organic matter in nutrient cycling and its influence on primary production in the North-eastern U.S. continental shelf. In a separate study by (Xue et al., 2013), phosphate cycling was omitted from Fennel's model (Fennel et al., 2011) because previous studies (Rabalais et al., 2002) showed that the primary production is generally nitrogen limited in the Louisiana-Texas shelf in the Gulf of Mexico. Therefore, the correlation coefficient of the seasonal mean of simulated and observed (MODIS: Moderate Resolution Imaging Spectroradiometer) surface Chl-*a* for the spring, summer, fall and winter were 0.6, 0.65, 0.53, 0.45 respectively. The simulated data successfully captured the high concentration of surface Chl-*a* in coastal areas close to main rivers, such as the Bay of Campeche, Campeche Bank, and the Louisiana-Texas shelf, whereas Chl-*a* concentrations were very low in the deep ocean. It is important to note that while Louisiana/Texas shelf in the Gulf of Mexico, as discussed in Xue et al. (2013), falls outside the tropics, the Gulf of Mexico circulation does include tropical latitudes. This reference to the Gulf of Mexico was mentioned to highlight the omission of phosphate cycling in Fennel's model due to nitrogen limitation in the primary production observed in the Louisiana-Texas shelf (Rabalais et al., 2002). In contrast to continental shelves and coastal areas of the Mid Atlantic Bight, some areas of the Atlantic Ocean and the Mediterranean Sea shows limitation of phosphate rather than nitrogen. The Mediterranean Sea encompasses the most oligotrophic ecosystems in the global ocean, with low nutrient and low chlorophyll content (Krom et al., 1991; Durrieu et al., 2011; Thingstad et al., 2014), being characterised by strong seasonality as well as highly dynamic system in terms of physics and biology (Ortenzio et al., 2009; Christaki et al., 2011). This limitation of phosphate was modelled using ERSEM which accounts for variable stoichiometric formulation in phytoplankton cells allowing the adaptation of internal N:P quota to different limiting environments (Lazzari et al., 2016). ERSEM reproduced the seasonal cycle and the observed patterns of surface Chl-*a* and inorganic nutrients in the Mediterranean Sea (MS). The interannual variability of Chl-*a* showed an agreement of r: 0.75 with SeaWiFS observation for the MS. However, the model underestimates phytoplankton blooms in the western basin of the MS while overestimates the blooms in the eastern basin during spring chlorophyll peaks. This discrepancy is attributed to the overestimation/underestimation of the winter mixing intensity by the physical model (Kalaroni et al., 2019). The spatial variability of the simulated surface Chl-*a* was assessed by calculating the correlation coefficient (r) between the model outputs and SeaWiFS observations. The correlation coefficient (r) was found to be 0.64, indicating a moderate positive linear association between the two datasets. The standard deviation of the spatial model variability was computed to be lower than 1 (normalised), suggesting relatively low dispersion of Chl-*a* values across the Mediterranean Sea. The temporal variability, on the other hand, was evaluated using unbiased root mean square differences (RMSDs) for the annual mean surface spatial and temporal variability. The RMSD value for the annual mean surface spatial variability was 0.78, indicating the average magnitude of differences between the model simulations and the observed data. Likewise, the RMSD value for the annual mean surface temporal variability was 0.68, suggesting the average magnitude of differences between the model simulations and the observed data over time. Lower RMSD values indicate better agreement in terms of both spatial and temporal variations.

## 3.3 Polar/subpolar and seasonally stratified zones

The effects of climate change, such as a considerable decrease in ice extent and rising sea levels, can exacerbate stratification in polar and subpolar regions (Farmer et al., 2021). In addition, changes to the global climate system are anticipated to have a significant impact on polar and subpolar marine ecosystems through their effects on water temperature and sea ice cover hence affecting marine production and carbon cycle (Gibson et al., 2020). This section covers the Arctic Ocean, Antarctic Peninsula, Drake Passage, Scotia Sea, northern Weddell Sea, South Georgia, Barents Sea, Hudson Bay, Beaufort Gyre, Labrador Sea, Baffin Bay, Canadian Arctic Archipelago, Russian shelves (East Siberian Sea), and the Dotson Ice Shelf in West Antarctica, along with the adjacent Amundsen Sea Polynya. Several ocean biogeochemical studies in the polar region focused on the effect of climate change on the carbon cycle (MCGUIRE et al., 2009; Terhaar et al., 2021; 2019; 2020; Negrete-garcía et al., 2019; Bruhwiler et al., 2021) and nutrients dynamics (Hátún et al., 2017; Randelhoff et al., 2018; 2019; Tuerena et al., 2021). Therefore, carbon is estimated using biogeochemical models with the inclusion of an explicit representation of the DIC component, such as PISCES-MIT general circulation model (MITgcm), which have been used to qualitatively examine the carbon cycle in the Arctic Ocean and have demonstrated their capacity to capture observed seasonal and regional changes in dissolved $pCO_2$ (Manizza et al., 2011). PISCES-MITgcm represented summer levels of surface $pCO_2$ in the Canadian Archipelago (200–250 µatm) correctly, but underestimated $pCO_2$ spring values (~300 µatm) relative to observations (Carbon Dioxide in the Atlantic (CARINA) data set (Jutterstrom et al., 2010))

(400–450 µatm). The lack of riverine POC and the impact of terrestrial carbon resulting from coastal erosion in the model resulted in the underprediction of the observed carbon levels. Additionally, sedimentation and resuspension processes, which may be important to enrich the water column with carbon hence impacting air-sea gas exchange, were neglected in the model. When comparing PISCES-NEMO and TOPAZ-NEMO (Jung et al., 2019b) for annual mean (averaged over all depths) DIC, TOPAZ-NEMO's results agreed with observation ($r > 0.95$), and the zonally averaged surface content was better represented by TOPAZ-NEMO in the Northern Hemisphere (bias $< 10\ \mu mol\ kg^{-1}$). However, surface mean DIC reproduced by TOPAZ and PISCES showed a bias of −90 and 90 respectively with GLobal Ocean Data Analysis Project version 2 (GLODAPv2 (Lauvset et al., 2016)).

In addition, a modified version of Chai's model (Chai et al., 1996) coupled to ROMS is applied over a model domain that spans the Antarctic Peninsula, Drake Passage, Scotia Sea, northern Weddell Sea, and South Georgia, indicating that dominant iron sources in the Scotia Sea are derived from sediments in the Antarctic Peninsula shelf along with the South Orkney Plateau (Jiang et al., 2019). In addition to these sources, the Antarctic Circumpolar Current, the northern side of the Weddell Gyre, upwelling, atmospheric dust deposition, and icebergs are the common sources of iron in the Southern Ocean (Jiang et al., 2019). However, the monthly means of iron levels estimated by the modified Chai's model have shown an average overestimation by 0.26 nM, deviating from the observed average value of 0.35 nM, resulting in r: 0.76.

On the other hand, the representation of the monthly observed nitrate, mixed layer depth, as well as euphotic layer depth is reproduced in the Arctic region using a skill assessment of 21 regional and global coupled biogeochemical models based on a phytoplankton functional types, including PISCES, PlankTOM, COBALT, TOPAZ, HAMOCC, BIOMASS, MEDUSA, ERSEM, PELAGOS, PISCES and NOBM (Babin et al., 2016). Most of these models have shown a positive bias for depth-averaged nitrates, explaining the overestimation of nitrates in the upper layer ($r \leq 0.68$), and none of these models were able to represent accurately the variability in field measurements (NOAA/NODC ArcNut database (Codispoti et al., 2013)). However, REcoM with its variable stoichiometry for phytoplankton's growth and nutrient cycling (Geider et al., 1998), coupled with a high-resolution physical model: Finite Element Sea Ice-Ocean Model (FESOM), exhibited a correlation coefficient of ($r = 0.75$) for spatial seasonal surface values of both dissolved inorganic nitrogen (DIN) and silicate (Schourup-Kristensen et al., 2018). The simulated DIN concentration indicated low levels in the Russian shelves (East Siberian Sea) with the exception of the Lena Delta in which the nutrients are added to the water by the riverine supply.

As for the representation of Chl-*a* in polar ecosystems, the original version of BLING coupled with NEMO was used to study monthly high surface Chl-*a* levels (i.e., blooms) in the high-latitude eastern North Atlantic and the central Arctic (Castro de la Guardia et al., 2019). This model is compared with MODIS observations and showed $R^2$: 0.76, 0.42, 0.81, 0.9, 0.1, and 0.93 in the Barents Sea (BB), Hudson Bay (HB), Beaufort Gyre (BG), Labrador Sea (LS), Baffin Bay (BB), and Canadian Arctic Archipelago (CAA) respectively. However, it underestimated the spring bloom by 1.7 mg $m^{-3}$ and the fall bloom by 0.7 mg $m^{-3}$ in the BB, likely because it did not take into account nutrients from riverine input. Furthermore, the model exhibited a tendency to overpredict the spring blooms in Hudson Bay (HB) and Baffin Bay (BB) by approximately 0.5 mg $m^{-3}$ and 0.3 mg $m^{-3}$ respectively, occurring about a month earlier than expected (March instead of April). This discrepancy might be attributed to the underprediction of sea ice concentration. Additionally, the REcoM model exhibited a bias of 1.1 mg $m^{-3}$ in predicting widespread subsurface chlorophyll maxima in the central Arctic Ocean, as compared to the mean summer surface Chl-*a* data obtained from Globcolor observations (Schourup-Kristensen et al., 2018).

Moreover, the MITgcm-REcoM model is used to investigate the impact of sea ice on phytoplankton blooms and surface dissolved inorganic carbon (DIC) in the ocean coastal-shelf-slope ecosystem west of the Antarctic Peninsula (Schultz et al., 2019). The study area encompasses a vast region ranging from 74.7°S, 95°W in the southwest to 55°S, 55.6°W in the northeast. Simulation results were compared with ocean color observations, and research ship surveys from the Palmer Long-Term Ecological Research (LTER) program. The Palmer LTER data and MODIS/SeaWifs data showed significant discrepancies in the study of the interannual variability of the phytoplankton bloom, with correlations for surface Chl-*a* in different sub-regions ranging from 0.52 to 0.73. While late summer retreat years displayed positive or low negative anomalies, early sea-ice retreat years primarily displayed negative or neutral anomalies in Chl-*a*. The model demonstrated the influence of sea-ice dynamics on phytoplankton dynamics by indicating an earlier bloom and lower Chl-*a* concentrations (relative to climatology) in years with early retreat of sea ice, resulting in lower chlorophyll concentrations at the end of the summer. Conversely, in years with late retreat of sea ice, the model showed greater Chl-*a* concentrations later in the season. Despite discrepancies between the model and observations, the model captured the temporal shifts in bloom timing during years characterized by high or low ice extent. Additionally, the model reproduced overall seasonal anomalies in dissolved inorganic carbon (DIC), which are related to seasonal net community production (NCP).

DARWIN is another model that has been used to study regional phytoplankton distribution in the Southern Ocean (Lo et al., 2019). The model was customized to improve its accuracy by increasing the affinity of phytoplankton for nutrients, adding two distinct size classes of diatoms, and considering two different life stages for Phaeocystis (single-cell vs. colonial). These improvements increased the agreement between the simulated coccolithophore and diatom levels with the *in-situ* observations. However, the model inaccurately simulated monthly diatoms and haptophytes, including small non-silicified phytoplankton, in the Ross Sea. Additionally, the model overestimated small non-silicified phytoplankton in this region, resulting in a general mean absolute error for diatoms and haptophytes of 0.74 mg $m^{-3}$ and 0.22 mg $m^{-3}$, respectively. This inconsistency can be partially attributed to inaccuracies in representing PFT phenology and distribution, and the potential impact of iron limitation should also be considered. The representation of co-existing coccolithophores and Phaeocystis remains a challenge, and any small changes in DARWIN physiological parameters can lead to either Phaeocystis or coccolithophores loss. Furthermore, the explicit representation of

sea-ice algae, which is important for accurately modeling ice-covered regions, has not been adequately incorporated.

In addition to studying Arctic and Antarctic phytoplankton dynamics, researchers have also been investigating the role of polynyas in polar ecosystems. Polynyas, which refer to expansive openings in the sea ice cover, play a crucial role in facilitating the exchange of heat, moisture, and gases between the atmosphere and the ocean (Maqueda et al., 2004; Dieckmann and Hellmer, 2009). Moreover, they drive patterns of ocean circulation, contribute to nutrient cycling, and influence ecosystem dynamics in polar regions (Maqueda et al., 2004). The rapid melting beneath the Dotson Ice Shelf (DIS) in West Antarctica, caused by warm, saline Circumpolar Deep Water (CDW) intrusions, has a significant impact on the adjacent Amundsen Sea Polynya (ASP) and its biology. Further, studies focusing on polynyas has garnered significant attention due to their substantial impact (Fichefet and Goosse, 1999; Hunke and Ackley, 2001; Wu et al., 2003). A recent study by (Twelves et al., 2020) using a coupled MITgcm-BLING model examined the effect of ice shelf melting on net primary production (NPP). The results show that melting ice shelves enhances upper ocean iron concentrations, which increases NPP. The study highlights how phytoplankton self-shading delays the bloom and reduces peak NPP while simultaneously emphasizing that changes in CDW intrusion regulate the horizontal dispersion of iron-rich meltwater, thereby impacting NPP levels.

## 3.4 High nutrient low chlorophyll (HNLC) zones

Biogeochemical models applied in this zone are mostly based on PFT approach which account for at least two plankton species. The section covers the Subarctic northeast Pacific at Ocean Station Papa (OSP), HNLC areas of the Southern Ocean, and the Southern Ocean (Antarctic Circumpolar Current region). Surface Chl-*a* concentrations are low in this region caused by iron limitation (Edwards et al., 2004). More recently (Zhang et al., 2021), used an extended version of the Chai's model (CoSiNE-Fe) that incorporated iron cycling to investigate phytoplankton dynamics at the Ocean Station Papa (OSP) in the subarctic northeast Pacific (50°N, 145°W). The model was able to demonstrate a strong correlation between nitrate and the averaged depth-integrated Chl-*a* in the upper 200 m of the water column, with correlation coefficients of 0.8 and 0.69, respectively, compared to observations from a Biogeochemical-Argo float (BGC-Argo). The model's performance was also evaluated using root-mean-square differences (RMSDs), which were 0.65 and 0.98 for nitrate and averaged depth-integrated Chl-*a* (in the upper 200 m), respectively.

However, the global PFT-based model PlankTOM10 coupled to NEMO was used to evaluate the role of grazing versus iron limitation in HNLC areas of the Southern Ocean (Le Quéré et al., 2016). PlankTOM10 was able to reproduce annual mean surface Chl-*a* estimates with a correlation coefficient (r) around 0.8 in the summer season when macro-zooplankton grazing is more intense. While this suggests that microzooplankton grazing may be a significant factor contributing to the low Chl-*a* concentrations observed in HNLC areas, it is important to note that high growth of phytoplankton can coexist with grazing (Lu¨rling, 2021). While both PlankTOM10 and PlankTOM6 share similar formulations, the former encompasses a greater number of plankton groups. These models yielded comparable outcomes for the annual mean surface Chl-*a* concentrations, demonstrating a correlation coefficient (r) of approximately 0.8 when compared with SeaWiFS satellite data. PlankTOM10, in particular, displayed slightly better performance to PlankTOM6 in terms of seasonal surface Chl-*a* distribution, with a bias of only 1.2%.

In contrast, DARWIN-MITgcm (Dutkiewicz et al., 2015) captured significant spatial variability in the annual mean surface Chl-a across the global oceans. Despite this, the model exhibited a relatively lower correlation coefficient of around 0.55 and tended to overestimate surface Chl-a concentration, particularly in the Southern Ocean.

Surface nitrate concentration, on the other hand, is high relative to surface Chl-*a* production in the HNLC zone (Edwards et al., 2004) and the global PlankTOM10 model predicted slightly lower (by 5%) of annual mean surface nitrate concentrations than observations World Ocean Atlas 2009 (Garcia et al., 2006; Le Quéré et al., 2016). Biases in the PlankTOM10 model can indeed be attributed to various limitations, including simplified overwintering strategies for zooplankton, coarse representation of iron (Fe) dynamics, the absence of certain organic matter types such as semi-refractory organic matter, and the exclusion of ecosystem pathways like viral lysis. Additionally, the model's omission of specific zooplankton groups like salps, pteropods, and auto- and mixotrophic dinoflagellates can also contribute to biases in its predictions.

Although iron is required at low concentrations for phytoplankton growth, the lack of its sources in the HNLC zone particularly the Southern Ocean highly impact the primary productivity and phytoplankton composition. For example, in the simplified version of DARWIN biogeochemical model (Dutkiewicz et al., 2009), which consists of two species (diatoms and small phytoplankton), coupled with MITgcm model, suggested that iron supply to the surface layer of the open Southern Ocean (Antarctic Circumpolar Current region) is highly driven by eddies (Uchida et al., 2019). Eddies can improve vertical mixing, influencing the upwelling of iron from deeper waters. This transport of iron from subsurface reservoirs to the sunlit layer where phytoplankton thrive can stimulate their growth and productivity. Therefore, to improve the accuracy of iron fluxes in the Southern Ocean, it is important to consider the role of eddies in addition to the atmospheric source. In particular, the inverse energy cascade caused by meso- and sub-mesoscale baroclinic instabilities plays a crucial role in determining iron distributions (Person et al., 2019).

Additionally, a recent study by Fu (2022) which used an inverse biogeochemical model with phosphorus, carbon, and oxygen Modules (Wang et al., 2019) to investigate the effects of ocean iron fertilization (OIF) in high nutrient low chlorophyll (HNLC) regions, specifically the Southern Ocean, North Pacific, and eastern equatorial Pacific. The findings revealed that OIF led to increased productivity, causing a downward transfer of nutrients and carbon to deeper waters. This process was accompanied by improved efficiency of the soft tissue pump and an increased in the $CO_2$ uptake. However, these positive effects were counterbalanced by a decrease in global mean oxygen levels and an expansion of oxygen minimum zones, suggesting potential consequences for ocean

oxygenation and the development of hypoxic conditions. Notably, the study used (Wang et al., 2019) biogeochemical model and exhibited strong agreement with observations (GLODAPv2), showing correlation coefficients of 0.92 for dissolved inorganic phosphorus (DIP), 0.93 for dissolved inorganic carbon (DIC), and 0.85 for oxygen ($O_2$). Interestingly, a comprehensive investigation conducted by (Bianchi et al., 2022) revealed the specific role of nitrogen cycling within the oxygen minimum zone (OMZ) of the HNLC Pacific Ocean, highlighting its implications for ecosystem dynamics. A new nitrogen cycling model was developed and specifically designed for integration into an ocean biogeochemical model, aiming to explore the impact of different nitrogen transformation processes on the biogeochemistry of the Eastern Tropical South Pacific OMZ. The model successfully captured typical OMZ conditions, providing valuable insights into the sensitivity of nitrogen transformations to environmental factors. However, it should be noted that while the model explicitly resolved N chemical tracers and their transformations, it did not directly incorporate the microbial communities responsible for these reactions, potentially limiting the understanding of the crucial role of microbes. Additionally, the model did not explicitly account for the conversion of dissolved $CO_2$ to organic matter through chemolithotrophy due to the relatively small rates compared to organic matter remineralization in the upper ocean, posing challenges in achieving a more comprehensive integration between chemolithotrophy and the carbon cycle.

## 4 Limitations and future developments

Although the aforementioned biogeochemical models performed well in several ecosystems, they have been modified and improved over the years by incorporating more components and processes to improve their reliability and predictability. Even in the most recent and advanced biogeochemical research, however, some limits remain. This section discusses the limitations of the existing biogeochemical models applied in several oceans, as well as recommendations for future modeling studies.

The absence of viruses in current biogeochemical models is a noteworthy drawback that demands more attention. Viruses play an important role in marine ecosystems by controlling microbial population numbers and altering the dynamics of nutrient and carbon cycling (Weitz and Wilhelm, 2012; Mateus, 2017). Their ability to infect and lyse bacteria and other microbes leads to the release of intracellular organic materials, which other species can then uptake (Zhao et al., 2019). Incorporating viruses into biogeochemical models may help us gaining a deeper understanding of how ecosystems work and the complex connections that exist between the different components of the microbial community (Weitz et al., 2015). These models may more accurately represent the intricate feedback systems that control nutrient availability, primary productivity, and carbon sequestration in the oceans by taking the viral impact into account. Furthermore, viruses can alter the variety and dominance of species by profoundly altering the structure and makeup of microbial communities (Tran and Anantharaman, 2021). Their impact on community dynamics and adaptability to environmental changes emphasizes how crucial they are in determining the stability and resiliency of the ecosystem.

In addition to not properly representing viruses, biogeochemical models often neglect the inclusion of archaea, despite their important role in ammonia oxidation processes. Archaea are important in ammonia oxidation and have the ability to affect nitrogen cycling, according to studies by (Urakawa et al., 2010; Yakimov et al., 2011). Similarly, mixotrophs, organisms capable of both photosynthetic and heterotrophic feeding, are often overlooked in biogeochemical models. Studies by (Stoecker et al., 2017; Edwards, 2019; Faure et al., 2019; Wilken et al., 2019) have revealed mixotrophs' ecological importance and possible impact on nutrient dynamics and ecosystem functioning. Unfortunately, most models do not treat mixotrophs as distinct Plankton Functional Types (PFTs), limiting our understanding of their contributions.

Furthermore, autotrophic bacteria such as nitrifying bacteria which carry out two-step nitrification processes are oversimplified in many biogeochemical models. These types of bacteria compete with the photosynthesizers for inorganic carbon and their current representation may underestimate or overestimate the primary productivity in the ocean. In addition, the detritus component is not well classified in many marine biogeochemical models and the representation of organic matter is not fully considered, leading to a possible under/overestimation of organic matter. Although the most intricate models include more components, they omit some important processes, including day-night cycles, zooplankton's diurnal migration (Ford et al., 2018). The omission of fish from biogeochemical models represent another significant area that needs exploration. Fish play an important part in the recycling and regeneration of nutrients within marine environments (Mcintyre et al., 2007). Thus, incorporating their interactions with other ecosystem components, such as feeding patterns and nutrient excretion, would provide valuable insights into nutrient dynamics and enhance our understanding of ecosystem functioning. Furthermore, the omission or simplification of benthic (e.g., Lazzari et al., 2016; Kalaroni et al., 2020) and sea ice components in biogeochemical models can hinder accurate predictions of ecosystem responses to environmental changes, thereby affecting the carbon and nutrient cycling assessment.

Biogeochemical models commonly simplify the representation of nitrogen (N) transformations, failing to capture the complexity of the underlying network of N reactions and their controlling factors. In the case of $N_2O$ cycling, many models rely on oversimplified parameterizations that consider $N_2O$ production solely from nitrification or aerobic respiration, while neglecting the important $N_2O$ sources and sinks associated with denitrification (Suntharalingam and Sarmiento, 2000; Jin and Gruber, 2003; Nevison et al., 2003; Manizza et al., 2012). The comprehensive consideration of nitrite cycling in the presence of low oxygen conditions, encompassing the concurrent processes of nitrite production from nitrate dissimilatory reactions, reduction to $N_2O$ and $N_2$ via denitrification and anammox, and subsequent reoxidation to nitrate, is insufficiently addressed (Lam and Kuypers, 2011; Kalvelage et al., 2013; Babbin et al., 2014; Babbin et al., 2015; Buchwald et al., 2015; Babbin et al., 2017).

In summary, although many biogeochemical models are able to simulate certain phenomenon/conditions, in certain regions of the global oceans they may underpredict/overpredict concentrations of some

components that can be largely dependent on other missing elements mentioned above. Therefore, biogeochemical models could be improved through the inclusion of dissolved organic carbon (labile, semi-labile, refractory), mixotrophic functional groups, viruses which in turn improve the representation of plankton functional groups, heterotrophic and microbial food web. While assessing biogeochemical models for current conditions reveals model biases, it does not always explain how they behave outside of the observed conditions (Fennel et al., 2022). Nevertheless, adding complexity does not always guarantee improved model performance or changes in rates. For example, Luo et al. (2022) found that while the drivers of export rate can change with the addition of an extra zooplankton component like tunicates, the total export amount may not vary significantly.

Obtaining comprehensive and high-quality data for model initialization and parameterization continues to be a challenge, with limited accessible sources available. Moreover, the challenges associated with data acquisition in polar regions make it difficult to effectively compare models with the available data. These challenges are primarily related to factors such as sea ice and cloud cover, which often result in substantial gaps in the coverage of remote sensing data.

Improvement in the zooplankton component may help further in constraining processes that regulate Chl-*a* distribution in the models (Clerc et al., 2021; Ratnarajah et al., 2023). Moreover, re-considering simulations of under-ice and near-ice phytoplankton blooms in the cold ecosystems by defining the photosynthesis irradiance curve for each phytoplankton group and allowing seasonal plasticity in the model parameters may increase the reliability of models applied in Arctic regions (Kearney et al., 2020). Most of the current models use a simplified, single-size detritus component, but in fact, detritus consists of different sizes and sinking rates, which may result in significant limitations in some regions (Ford et al., 2018). Considering different types of detrital matter with various timescales in the remineralization process would produce a more realistic model output for the organic matter.

## 5 Conclusion

This review presents different biogeochemical models applied to various ecosystems of the world's ocean. Most of these widely used ocean biogeochemical models are an extension of NPZD models and have undergone several modifications and developments which increased their complexity in terms of number of PFTs, organic matter, physics, and sediments interactions. We divided the oceans into four zones, tropical, temperate and varying from tropical to subtropical, polar/subpolar, and HNLC zones to review the biogeochemical modelling studies been done on the biogeochemical components in these regions separately. Estimation of biogeochemical model variables, such as Chl-*a*, nutrients, carbon and oxygen in various ecosystems have shown varying performances. The varying performances for these biogeochemical model variables are dependent on the features of the ecosystems and the resolution of the physical environment. In the tropical and subtropical ecosystems, seasonal variations are highly strong and have a great impact on the biogeochemical cycles in these regions. These regions are known to be the most productive ecosystems in the ocean and nutrients can be supplied to the open ocean from the coastal enriched nutrients. Due to considerable decrease in ice extent and rising sea levels caused by climate change, the Arctic/Antarctic region experiences rapid changes in the physical and biological ecosystems. This is observed in the changes of the Arctic carbon and nutrients cycles. Ocean biogeochemical models play a critical role in climate studies, particularly in regions that are prone to experiencing high variations in extreme climates. The increase in carbon and nitrogen concentrations in the biosphere, resulting from anthropogenic activities, has the potential to disrupt biogeochemical cycles. This alteration of biogeochemical cycles can have wide-ranging impacts, making biodiversity, food security, and water quality more susceptible to the impacts of climate change.

## Author contributions

KI and MA-S defined the content of the manuscript. KI prepared the manuscript and MA-S contributed in conceptualization, revisions and improvements. All authors contributed to the article and approved the submitted version.

## Acknowledgments

The authors would like to thank Khalifa University for the financial support. This paper is under the project of modelling the biogeochemistry of the Arabian Gulf waters.

## Conflict of interest

The authors declare that the research was conducted in the absence of any commercial or financial relationships that could be construed as a potential conflict of interest.

## Publisher's note



## References

Achterberg, E. P. (2014). Grand challenges in marine biogeochemistry. *Front. Mar. Sci.* 1, 1–5. doi:10.3389/fmars.2014.00007

Allen, J. I., Somerfield, P. J., and Siddorn, J. (2002). Primary and bacterial production in the Mediterranean Sea: a modelling study. *J. Mar. Syst.* 34, 473–495. doi:10.1016/s0924-7963(02)00072-6

Anderson, L. A., and Sarmiento, J. L. (1994). Redfield ratios of remineralization determined by nutrient data analysis. *Glob. Biogeochem. Cycles* 8, 65–80. doi:10.1029/93gb03318

Anderson, R., and Williams, P. J. l. B. (1999). A one-dimensional model of dissolved organic carbon cycling in the water column incorporating combined biological-

photochemical decomposition. *Refract. Mater. Amador* 13, 337–349. doi:10.1029/1999gb900013

Anderson, T. R. (2005). Plankton functional type modelling: running before we can walk. *J. Plankton Res.* 27, 1073–1081. doi:10.1093/plankt/fbi076

Andrews, O., Buitenhuis, E., Le Quéré, C., and Suntharalingam, P. (2017). Biogeochemical modelling of dissolved oxygen in a changing ocean. *Phil. Trans. R. Soc. A* 375, 20160328. doi:10.1098/rsta.2016.0328

Anderson, D. M., Patricia, G., and Burkholder, J. M. (2002). Harmful algal blooms and eutrophication: nutrient sources, composition, and consequences. *Estuaries* 25, 704–726. doi:10.1007/BF02804901

Arthur, C., Ioanna, A., Karline, S., Ioanna, A., and Karline, S. (2016). Integrating sediment biogeochemistry into 3D oceanic models: a study of benthic-pelagic coupling in the black sea. *Ocean. Model* 101, 83–100. doi:10.1016/j.ocemod.2016.03.006

Aumont, O., and Bopp, L. (2006). Globalizing results from ocean *in situ* iron fertilization studies. *Glob. Biogeochem. Cycles* 20, 1–15. doi:10.1029/2005GB002591

Aumont, O., Ethé, C., Tagliabue, A., Bopp, L., and Gehlen, M. (2015). PISCES-v2: an ocean biogeochemical model for carbon and ecosystem studies. *Geosci. Model Dev. Discuss.* 8, 1375–1509. doi:10.5194/gmdd-8-1375-2015

Aumont, O., Maier-Reimer, E., Blain, S., and Monfray, P. (2003). An ecosystem model of the global ocean including Fe, Si, P colimitations. *Glob. Biogeochem. Cycles* 17, 1745. doi:10.1029/2001gb001745

Babbin, A. R., Bianchi, D., Jayakumar, A., and Ward, B. B. (2015). Rapid nitrous oxide cycling in the suboxic ocean. *Sci. (80-. )* 348, 1127–1129. doi:10.1126/science.aaa8380

Babbin, A. R., Keil, R. G., Devol, A. H., and Ward, B. B. (2014). Organic matter stoichiometry, flux, and oxygen control nitrogen loss in the Ocean. *Sci. (80-. )* 344, 406–408. doi:10.1126/science.1248364

Babbin, A. R., Peters, B. D., Casciotti, K. L., Ward, B. B., and Widner, B. (2017). Multiple metabolisms constrain the anaerobic nitrite budget in the Eastern Tropical South Pacific. *Glob. Biogeochem. Cycles* 31, 258–271. doi:10.1002/2016GB005407

Babin, M., Buitenhuis, E. T., Chevallier, M., Mora, L. D., and Dessert, M. (2016). Net primary productivity estimates and environmental variables in the Arctic Ocean. *Assess. coupled physical-biogeochemical models* 2016, 1–35. doi:10.1002/2016JC011993

Baretta, J. W., Ebenhöh, W., and Ruardij, P. (1995). The European regional seas ecosystem model, a complex marine ecosystem model. *Neth. J. Sea Res.* 33, 233–246. doi:10.1016/0077-7579(95)90047-0

Baretta-Bekker, J. G., Baretta, J. W., and Ebenhöh, W. (1997). Microbial dynamics in the marine ecosystem model ERSEM II with decoupled carbon assimilation and nutrient uptake. *J. Sea Res.* 38, 195–211. doi:10.1016/S1385-1101(97)00052-X

Bernard, O. (2011). Hurdles and challenges for modelling and control of microalgae for CO 2 mitigation and biofuel production. *IFAC* 43, 667–678. doi:10.3182/20100705-3-BE-2011.00111

Bianchi, D., Mccoy, D., and Yang, S. (2022). Formulation, optimization and sensitivity of NitrOMZv1. 0, a biogeochemical model of the nitrogen cycle in oceanic oxygen minimum zones. *Geosci. Model Dev.* 16 (12), 3581–3609. doi:10.5194/gmd-16-3581-2023

Bissett, W. P., Walsh, J. J., Dieterle, D. A., and Carder, K. L. (1999). Carbon cycling in the upper waters of the sargasso sea: i. numerical simulation of differential carbon and nitrogen fluxes. *Deep. Res. Part I Oceanogr. Res. Pap.* 46, 205–269. doi:10.1016/S0967-0637(98)00062-4

Blackford, J. C., Allen, J. I., and Gilbert, F. J. (2004). Ecosystem dynamics at six contrasting sites: a generic modelling study. *J. Mar. Syst.* 52, 191–215. doi:10.1016/j.jmarsys.2004.02.004

Blackford, J. C., and Burkill, P. H. (2002). Planktonic community structure and carbon cycling in the Arabian Sea as a result of monsoonal forcing: the application of a generic model. *J. Mar. Syst.* 36, 239–267. doi:10.1016/S0924-7963(02)00182-3

Bougaran, G., Bernard, O., and Sciandra, A. (2010). Modeling continuous cultures of microalgae colimited by nitrogen and phosphorus. *J. Theor. Biol.* 265, 443–454. doi:10.1016/j.jtbi.2010.04.018

Bristow, L. A., Mohr, W., Ahmerkamp, S., and Kuypers, M. M. M. (2017). Nutrients that limit growth in the ocean. *Curr. Biol.* 27, R474–R478. doi:10.1016/j.cub.2017.03.030

Brock, J. C., and Mcclain, C. R. (1992). Interannual variability in phytoplankton blooms observed in the northwestern Arabian Sea during the southwest monsoon. *J. Geophys. Res. Oceans* 97, 733–750. doi:10.1029/91JC02225

Bronselaer, B., Russell, J. L., Winton, M., Williams, N. L., Key, R. M., Dunne, J. P., et al. (2020). Importance of wind and meltwater for observed chemical and physical changes in the Southern Ocean. *Nat. Geosci.* 13, 35–42. doi:10.1038/s41561-019-0502-8

Bruhwiler, L., Parmentier, F.-J. W., Crill, P., Leonard1, M., and Palmer, P. I. (2021). The arctic carbon cycle and its response to changing climate. *Curr. Clim. Chang. Rep.* 7, 14–34. doi:10.1007/s40641-020-00169-5

Buchwald, C., Santoro, A. E., Stanley, R. H. R., and Casciotti, K. L. (2015). Global biogeochemical cycles of the eastern tropical north paci fi c off Costa Rica. *Glob. Biogeochem. Cycles* 2015, 2061–2081. doi:10.1002/2015GB005187

Butenschön, M., Clark, J., Aldridge, J. N., Icarus Allen, J., Artioli, Y., Blackford, J., et al. (2016). ERSEM 15.06: a generic model for marine biogeochemistry and the ecosystem dynamics of the lower trophic levels. *Model Dev.* 9, 1293–1339. doi:10.5194/gmd-9-1293-2016

Buitenhuis, E. T., Hashioka, T., and Quéré, C. Le. (2013). Combined constraints on global ocean primary production using observations and models. *Glob. Biogeochem. Cycles* 27 (3), 847–858. doi:10.1002/gbc.20074

Cai, W., Wang, Z. A., and Wang, Y. (2003). The role of marsh-dominated heterotrophic continental margins in transport of $CO_2$between the atmosphere, the land-sea interface and the ocean: the role of marsh-dominated heterotrophic continental margins. *Geophys. Res. Lett.* 30 (16), 1849. doi:10.1029/2003GL017633

Carlson, C. A., and Hansell, D. A. (2015). DOM sources, sinks, reactivity, and budgets. *Biogeochem. Mar. Dissolved Org. Matter* 2015, 65–126. doi:10.1016/B978-0-12-405940-5.00003-0

Castro de la Guardia, L., Garcia-Quintana, Y., Claret, M., Hu, X., Galbraith, E. D., and Myers, P. G. (2019). Assessing the role of high-frequency winds and Sea Ice loss on arctic phytoplankton blooms in an Ice-Ocean-biogeochemical model. *J. Geophys. Res. Biogeosciences* 124, 2728–2750. doi:10.1029/2018JG004869

Cerco, C. F., Noel, M. R., and Kim, S. C. (2006). Three-dimensional management model for lake Washington, Part II: eutrophication modeling and skill assessment. *Lake Reserv. Manag.* 22, 115–131. doi:10.1080/07438140609353889

Chai, F., Lindley, S. T., and Barber, R. T. (1996). Origin and maintenance of a high nitrate condition in the equatorial Pacific. *Deep. Res. Part II Top. Stud. Oceanogr.* 43, 1031–1064. doi:10.1016/0967-0645(96)00029-X

Cherif, M., and Loreau, M. (2010). Towards a more biologically realistic use of Droop ' s equations to model growth under multiple nutrient limitation. *Oikos* 119 (6), 897–907. doi:10.1111/j.1600-0706.2010.18397.x

Christian, J. R., Verschell, M. A., Murtugudde, R., Busalacchi, A. J., and McClain, C. R. (2001). Biogeochemical modelling of the tropical Pacific Ocean. I: Seasonal and interannual variability. *Deep-Sea Res. Part I Top. Stud. Oceanogr.* 49 (1–3), 509–543. doi:10.1016/S0967-0645(01)00110-2

ChrEilertsen, H., and Degerlund, M. (2010). Phytoplankton and light during the northern high-latitude winter. *J. Plankton Res.* 32 (6), 899–912. doi:10.1093/plankt/fbq017

Christaki, U., Wambeke, F., Lagaria, A., Prieur, L., Grattepanche, J., Pujo-Pay, M., et al. (2011). Microbial food webs and metabolic state across oligotrophic waters of the Mediterranean Sea during summer. *Biogeosciences* 8, 1839–1852. doi:10.5194/bg-8-1839-2011

Clarke, R. A., Stanley, C. D., Macleod, B. W., and Mcneal, B. L. (2009). Relationship of seasonal water quality to chlorophyll a concentration in lake manatee, Florida. *Lake Reserv. Manag.* 13, 253–258. doi:10.1080/07438149709354316

Clerc, C., Aumont, O., and Bopp, L. (2021). Should we account for mesozooplankton reproduction and ontogenetic growth in biogeochemical modeling. *Theor. Ecol.* 14, 589–609. doi:10.1007/s12080-021-00519-5

Codispoti, L. A., Brandes, J. A., Christensen, J. P., Devol, A. H., Naqvi, S. W. A., Paerl, H. W., et al. (2001). The oceanic fixed nitrogen and nitrous oxide budgets: moving targets as we enter the anthropocene? *Sci. Mar.* 65, 85–105. doi:10.3989/scimar.2001.65s285

Codispoti, L. A., Kelly, V., Thessen, A., Matrai, P., Suttles, S., Hill, V., et al. (2013). Synthesis of primary production in the Arctic Ocean: 3 Nitrate and phosphate based estimates of net community production. *Prog. Oceanogr.* 110, 126–150. doi:10.1016/j.pocean.2012.11.006

Cox, P. M., Betts, R. A., Jones, C. D., Spall, S. A., and Tollerdell, I. J. (2000). Erratum: acceleration of global warming due to carbon-cycle feedbacks in a coupled climate model. *Nature* 408, 750. doi:10.1038/35047138

Cullen, J. J. (2015). Subsurface chlorophyll maximum layers: enduring enigma or mystery solved. *Ann. Rev. Mar. Sci.* 7, 207–239. doi:10.1146/annurev-marine-010213-135111

Dale, T., Rey, F., and Heimdal, B. R. (1999). Seasonal development of phytoplankton at a high latitude oceanic site. *Sarsia* 84, 419–435. doi:10.1080/00364827.1999.10807347

Das, D., Chakrabarty, M., Goswami, S., Basu, D., and Chaudhuri, S. (2019). Impact of intra-seasonal oscillations of Indian summer monsoon on biogeochemical constituents of North Indian Ocean. *Theor. Appl. Climatol.* 136, 839–848. doi:10.1007/s00704-018-2518-1

Davis, T. W., Bullerjahn, G. S., Tuttle, T., Mckay, R. M., and Watson, S. B. (2015). Effects of increasing nitrogen and phosphorus concentrations on phytoplankton community growth and toxicity during *planktothrix* blooms in sandusky Bay, lake erie. *Lake Erie 4840 South State Road.* 49, 7197–7207. doi:10.1021/acs.est.5b00799

Devol, A. H., and Christensen, J. P. (1993). Benthic fluxes and nitrogen cycling in sediments of the continental margin of the eastern North Pacific. *J. Mar. Res.* 51, 345–372. doi:10.1357/0022240933223765

Dieckmann, G. A., and Hellmer, H. (2009). "The importance of sea ice: an overview," in *Sea ice*. Editors D. N Thomas and G. S Dieckmann. second ed (Oxford: Wiley-Blackwell, Wiley-Blackwell), 1–22.

Dinniman, M. S., St-laurent, P., Arrigo, K. R., Hofmann, E. E., and Dijken, G. L. V. (2020). Analysis of iron sources in antarctic continental shelf waters. *Analysis Iron Sources Antarct. Cont. Shelf Waters* 125, 2019jc015736. doi:10.1029/2019jc015736

Doney, S. C., Glover, D. M., and Najjar, R. G. (1996). A new coupled, one-dimensional biological-physical model for the upper ocean: applications to the JGOFS Bermuda Atlantic Time-series study (BATS) site. *Deep. Res. Part II Top. Stud. Oceanogr.* 43, 591–624. doi:10.1016/0967-0645(95)00104-2

Droop, M. R. (1983). 25 Years of algal growth kinetics A personal view. *Bot. Mar. XXVI* 26, 99–112. doi:10.1515/botm.1983.26.3.99

Droop, M. R. (1973). Some thoughts on nutrient limitation in algae. *J. Phycol.* 9, 264–272. doi:10.1111/j.1529-8817.1973.tb04092.x

Druon, J. N., Mannino, A., Signorini, S., McClain, C., Friedrichs, M., Wilkin, J., et al. (2010). Modeling the dynamics and export of dissolved organic matter in the Northeastern U.S. continental shelf. *Estuar. Coast. Shelf Sci.* 88, 488–507. doi:10.1016/j.ecss.2010.05.010

Dunne, J., Gnanadesikan, A., Sarmiento, J. L., Slater, R. D., and Hiscock, M. R. (2010). Efficiency of small scale carbon mitigation by patch iron fertilization. *Biogeosciences Suppl.* 7, 3593–3624. doi:10.5194/bg-7-3593-2010

Durrieu, G. X., Madron, D., Guieu, C., Sempéré, R., Conan, P., Cossa, D., et al. (2011). Marine ecosystems' responses to climatic and anthropogenic forcings in the Mediterranean. *Prog. Oceanogr.* 91, 97–166. doi:10.1016/j.pocean.2011.02.003

Dutkiewicz, S., Baird, M., and Chai, F. (2020). *Synergy between ocean colour and biogeochemical/ecosystem models*.

Dutkiewicz, S., Follows, M. J., and Bragg, J. G. (2009). Modeling the coupling of ocean ecology and biogeochemistry. *Glob. Biogeochem. Cycles* 23, 1–15. doi:10.1029/2008GB003405

Dutkiewicz, S., Follows, M. J., and Parekh, P. (2005). Interactions of the iron and phosphorus cycles: a three-dimensional model study. *Glob. Biogeochem. Cycles* 19, 1–22. doi:10.1029/2004GB002342

Dutkiewicz, S., Hickman, A. E., Jahn, O., Gregg, W. W., Mouw, C. B., and Follows, M. J. (2015). Capturing optically important constituents and properties in a marine biogeochemical and ecosystem model. *Biogeosciences* 12, 4447–4481. doi:10.5194/bg-12-4447-2015

Economidou, E. (1982). The ecological value of coastal ecosystems coastal ecosystems. *Ekistics* 49, 98–101.

Edwards, A. M., Platt, T., and Sathyendranath, S. (2004). The high-nutrient, low-chlorophyll regime of the ocean: limits on biomass and nitrate before and after iron enrichment. *Ecol. Model.* 71, 103–125. doi:10.1016/j.ecolmodel.2003.06.001

Edwards, K. F. (2019). Mixotrophy in nanoflagellates across environmental gradients in the ocean. *Mix. nanoflagellates across Environ. gradients ocean* 116, 6211–6220. doi:10.1073/pnas.1814860116

Ehrnsten, E., Norkko, A., Timmermann, K., and Gustafsson, B. G. (2019). Benthic-pelagic coupling in coastal seas – modelling macrofaunal biomass and carbon processing in response to organic matter supply. *J. Mar. Syst.* 196, 36–47. doi:10.1016/j.jmarsys.2019.04.003

Evans, G. T., Parslow, J. S., Evans, G. T., and Parslow, J. S. (1985). A model of annual plankton cycles. Deep Sea Research Part B. *Oceanogr. Lit. Rev.* 32 (9), 759. doi:10.1016/0198-0254(85)92902-4

Eyre, B., and Balls, P. (1999). A Comparative Study of Nutrient Behavior along the Salinity Gradient of Tropical and Temperate Estuaries REFERENCES Linked references are available on JSTOR for this article: you may need to log in to JSTOR to access the linked references. *A Comp.* 22, 313–326. doi:10.2307/1352987

Farmer, J. R., Sigman, D. M., Granger, J., Underwood, O. M., Fripiat, F., Cronin, T. M., et al. (2021). Arctic Ocean stratification set by sea level and freshwater inputs since the last ice age. *Nat. Geosci.* 14, 684–689. doi:10.1038/s41561-021-00789-y

Fasham, M. J. R., Ducklow, H. W., and McKelvie, S. M. (1990). A nitrogen-based model of plankton dynamics in the oceanic mixed layer. *J. Mar. Res.* 48, 591–639. doi:10.1357/002224090784984678

Fasham, M. J. R. (1993). Modelling the marine biota. *Glob. Carbon Cycle, I* 1993, 457–504. doi:10.1007/978-3-642-84608-3_19

Faure, E., Not, F., Benoiston, A.-S., Labadie, K., Bittner, L., and Ayata, S.-D. (2019). Mixotrophic protists display contrasted biogeographies in the global ocean. *ISME J.* 13, 1072–1083. doi:10.1038/s41396-018-0340-5

Fennel, K., and Boss, E. (2003). Subsurface maxima of phytoplankton and chlorophyll: steady-state solutions from a simple model. *Limnol. Oceanogr.* 48, 1521–1534. doi:10.4319/lo.2003.48.4.1521

Fennel, K., Gehlen, M., Brasseur, P., Brown, C. W., Ciavatta, S., Cossarini, G., et al. (2019). Advancing marine biogeochemical and ecosystem reanalyses and forecasts as tools for monitoring and managing ecosystem health. *Front. Mar. Sci.* 6, 1–9. doi:10.3389/fmars.2019.00089

Fennel, K., Hetland, R., Feng, Y., and DiMarco, S. (2011). A coupled physical-biological model of the northern Gulf of Mexico shelf: model description, validation and analysis of phytoplankton variability. *Biogeosciences Discuss.* 8, 121–156. doi:10.5194/bgd-8-121-2011

Fennel, K., Mattern, J. P., Doney, S. C., Bopp, L., Moore, A. M., Wang, B., et al. (2022). Ocean biogeochemical modelling. *Nat. Rev.* 2, 76. doi:10.1038/s43586-022-00154-2

Fennel, K. (2010). The role of continental shelves in nitrogen and carbon cycling: northwestern North Atlantic case study. *Ocean. Sci.* 6, 539–548. doi:10.5194/os-6-539-2010

Fennel, K., Wilkin, J., Levin, J., Moisan, J., O'Reilly, J., and Haidvogel, D. (2006). Nitrogen cycling in the middle atlantic Bight: results from a three-dimensional model and implications for the North Atlantic nitrogen budget. *Glob. Biogeochem. Cycles* 20, 20. doi:10.1029/2005GB002456

Fennel, K., Wilkin, J., Previdi, M., and Najjar, R. (2008). Denitrification effects on air-sea CO2 flux in the coastal ocean: simulations for the northwest North Atlantic. *Geophys. Res. Lett.* 35, L24608. doi:10.1029/2008GL036147

Fichefet, T., and Goosse, H. (1999). A numerical investigation of the spring Ross Sea polynya. *A Numer. investigation spring Ross Sea polynya* 26, 1015–1018. doi:10.1029/1999gl900159

Finkel, Z. V., Quigg, A., Raven, J. A., Schofield, O. E., and Falkowski, P. G. (2006). Irradiance and the elemental stoichiometry of marine phytoplankton. *Irradiance Elem. Stoichiom. Mar. Phytoplankt.* 51, 2690–2701. doi:10.4319/lo.2006.51.6.2690

Flynn, K. J., and Flynn, K. (1998). Release of nitrite by marine dinoflagellates: development of a mathematical simulation. *Mar. Biol.* 130, 455–470. doi:10.1007/s002270050266

Follows, M. J., Dutkiewicz, S., Grant, S., and Chisholm, S. W. (2007a). Emergent biogeography of microbial communities in a model ocean. *Science* 80, 1843–1846. doi:10.1126/science.1138544

Follows, M. J., Dutkiewicz, S., Grant, S., and Chisholm, S. W. (2007b). Emergent biogeography of microbial communities in a model ocean. *Sci. (80-. )* 315, 1843–1846. doi:10.1126/science.1138544

Ford, D., Kay, S., McEwan, R., Totterdell, I., and Gehlen, M. (2018). Marine biogeochemical modelling and data assimilation for operational forecasting, reanalysis, and climate research. *New Front. Oper. Oceanogr.* 2018, 625–652. doi:10.17125/gov2018.ch22

Franks, P. (2002). *NPZ Models of Plankton Dynamics: Their construction,coupling with physics, and application*.

Friedrichs, M. A. M., Dusenberry, J. A., Anderson, L. A., Armstrong, R. A., Chai, F., Christian, J. R., et al. (2007). Assessment of skill and portability in regional marine biogeochemical models: role of multiple planktonic groups. *J. Geophys. Res. Ocean.* 112, C08001. doi:10.1029/2006JC003852

Fung, I. Y., Meyn, S. K., Tegen, I., Doney, S. C., John, J. G., and Bishop, J. K. B. (2000). Iron supply and demand in the upper ocean. *Glob. Biogeochem. Cycles* 14, 281–295. doi:10.1029/1999gb900059

Fu, W., and Wang, W.-L. (2022). Biogeochemical equilibrium responses to maximal productivity in high nutrient low chlorophyll regions. *J. Geophys. Res. Biogeosciences* 127, e2021JG006636. doi:10.1029/2021JG006636

Galbraith, E. D., Gnanadesikan, A., Dunne, J. P., and Hiscock, M. R. (2009). Regional impacts of iron-light colimitation in a global biogeochemical model. *Biogeosciences Discuss.* 6, 7517–7564. doi:10.5194/bgd-6-7517-2009

Gan, J., Lu, Z., Cheung, A., Dai, M., Liang, L., Harrison, P. J., et al. (2014). Assessing ecosystem response to phosphorus and nitrogen limitation in the Pearl River plume using the Regional Ocean Modeling System (ROMS). *J. Geophys. Res. Oceans* 119, 8858–8877. doi:10.1002/2014JC009951

Garcia, H. E., Locarnini, R. A., Boyer, T. P., and Antonov, J. I. (2006). NOAA Atlas NESDIS 63 WORLD OCEAN ATLAS 2005 volume 3: dissolved oxygen. *Apparent Oxyg. Util. Oxyg. Satur.* 3.

Geider, R. J., MacIntyre, H. L., and Kana, T. M. (1998). A dynamic regulatory model of phytoplanktonic acclimation to light, nutrients, and temperature. *Limnol. Oceanogr.* 43, 679–694. doi:10.4319/lo.1998.43.4.0679

Geider, R. J., MacIntyre, H. L., and Kana, T. M. (1997). Dynamic model of phytoplankton growth and acclimation: responses of the balanced growth rate and the chlorophyll a:carbon ratio to light, nutrient-limitation and temperature. *Mar. Ecol. Prog. Ser.* 148, 187–200. doi:10.3354/meps148187

Geider, R. J., and Platt, T. (1986). A mechanistic model of photoadaptation in microalgae. *Mar. Ecol. Prog. Ser.* 30, 85–92. doi:10.3354/meps030085

Gerhard, M., Striebel, M., Schlenker, A., and Hillebrand, H. (2022). Environmental stoichiometry mediates phytoplankton diversity effects on communities' resource use efficiency and biomass. *J. Ecol.* 110, 430–442. doi:10.1111/1365-2745.13811

Gerringa, L. J. A., Alderkamp, A.-C., Laan, P., Thuro´czy, C.-E., Baar, H. J. W., Mills, M. M., et al. (2012). Iron from melting glaciers fuels the phytoplankton blooms in Amundsen Sea (Southern Ocean): iron biogeochemistry. *Deep. Res. II J.* 76, 16–31. doi:10.1016/j.dsr2.2012.03.007

Gibson, G., Weijer, W., Jeffery, N., and Wang, S. (2020). Relative impact of Sea Ice and temperature changes on arctic marine production. *JGR Biogeosciences* 125. doi:10.1029/2019JG005343

Gnanadesikan, A., Slater, R. D., Gruber, N., and Sarmiento, J. L. (2002). Oceanic vertical exchange and new production: a comparison between models and observations. *Deep Sea Res. Part II Top. Stud. Oceanogr.* 49, 363–401. doi:10.1016/s0967-0645(01)00107-2

Gobler, C. J., and Baumann, H. (2016). Hypoxia and acidification in ocean ecosystems: coupled dynamics and effects on marine life. *Biol. Lett.* 1, 20150976. doi:10.1098/rsbl.2015.0976

Gregg, W. W. (2000). *A coupled ocean general circulation, biogeochemical, and radiative model of the global oceans. Seasonal distributions of ocean chlorophyll and nutrients*.

Gregg, W. W., Casey, N. W., O'Reilly, J. E., and Esaias, and W. E. (2009). An empirical approach to ocean color data: reducing bias and the need for post-launch radiometric re-calibration. *Remote Sens. Environ*. 113, 1598–1612. doi:10.1016/j.rse.2009.03.005

Gregg, W. W., Ginoux, P., Schopf, P. S., and Casey, N. W. (2003). Phytoplankton and iron: validation of a global three-dimensional ocean biogeochemical model. *Deep. Res. Part II Top. Stud. Oceanogr.* 50, 3143–3169. doi:10.1016/j.dsr2.2003.07.013

Gregg, W. W. (2001). Tracking the SeaWiFS record with a coupled physical/biogeochemical/radiative model of the global oceans. *Deep. Res. Part II Top. Stud. Oceanogr.* 49, 81–105. doi:10.1016/S0967-0645(01)00095-9

Grégoire, M., Garçon, V., Garcia, H., Breitburg, D., Isensee, K., Oschlies, A., et al. (2021). A Global Ocean oxygen database and Atlas for assessing and predicting deoxygenation and ocean health in the open and coastal ocean. *Ocean* 8, 1–29. doi:10.3389/fmars.2021.724913

Guieu, C., Al Azhar, M., Aumont, O., Mahowald, N., Levy, M., Ethé, C., et al. (2019). Major impact of dust deposition on the productivity of the arabian sea. *Geophys. Res. Lett.* 46 (12), 6736–6744. doi:10.1029/2019GL082770

Hamilton, D. S., Moore, J. K., Arneth, A., Bond, T. C., Carslaw, K. S., Hantson, S., et al. (2020). Impact of changes to the atmospheric soluble iron deposition flux on Ocean Biogeochemical cycles in the anthropocene. *Glob. Biogeochem. Cycles* 34, 1–22. doi:10.1029/2019GB006448

Hansell, D. A., Carlson, C. A., Repeta, D. J., and Schlitzer, R. (2009). Dissolved organic matter in the ocean a controversy stim ulates new insights. *Oceanogr. Wash. D. C).* 22, 202–211. doi:10.5670/oceanog.2009.109

Hátún, H., Somavilla, R., Rey, F., Johnson, C., Mathis, M., Mikolajewicz, U., et al. (2017). The subpolar gyre regulates silicate concentrations in the North Atlantic. *Sci. Rep.* 7, 1–9. doi:10.1038/s41598-017-14837-4

Hauck, J., and Völker, C. (2015). Rising atmospheric CO 2 leads to large impact of biology on Southern Ocean CO 2 uptake via changes of the Revelle factor. *Geophys. Res. Lett.* 42, 1459–1464. doi:10.1002/2015GL063070

Heinze, C., Maier-Reimer, E., Winguth, A. M. E., and Archer, D. (1999). A global oceanic sediment model for long-term climate studies. *Glob. Biogeochem. Cycles* 13, 221–250. doi:10.1029/98gb02812

Hitchcock, G. L., Key, E. L., and Masters, J. (2000). The fate of upwelled waters in the Great Whirl, August 1995. *Whirl* 47, 1605–1621. doi:10.1016/s0967-0645(99)00156-3

Ho, T., Quigg, A., Zoe, V., Milligan, A. J., Falkowski, P. G., Morel, M. M., et al. (2003). The elemental composition of some marine phytoplankton. *J. Phycol.* 1159, 1145–1159. doi:10.1111/j.0022-3646.2003.03-090.x

Hood, R. R., Bates, N. R., Capone, D. G., and Olson, D. B. (2001). Modeling the effect of nitrogen fixation on carbon and nitrogen fluxes at BATS. *Deep Sea Res. Part II Top. Stud. Oceanogr.* 48, 1609–1648. doi:10.1016/S0967-0645(00)00160-0

Hood, R. R., Laws, E. A., Armstrong, R. A., Bates, N. R., Brown, C. W., Carlson, C. A., et al. (2006). Pelagic functional group modeling: progress, challenges and prospects. *Deep. Res. II* 53, 459–512. doi:10.1016/j.dsr2.2006.01.025

Hopkinson, C. S., and Vallino, J. J. (2005). Efficient export of carbon to the deep ocean through dissolved organic matter. *Lett. Nat.* 433, 142–145. doi:10.1038/nature03191

Huang, K. (2010). Indian Ocean Biogeochemical processes and ecological variability. *General & Introd. Earth Sci.* 91, 2–3.

Hunke, C., and Ackley, S. F. (2001). A numerical investigation of the 1997-1998. *Ronne Polynya* 106, 22,373–22,382. doi:10.1002/9781119828242.ch13

Jiang, M., Measures, C. I., Barbeau, K. A., Charette, M. A., Gille, S. T., Hatta, M., et al. (2019). Fe sources and transport from the Antarctic Peninsula shelf to the southern Scotia Sea. *Deep-Sea Res. Part I, Oceanogr. Res. Pap.* 150, 103060. doi:10.1016/J.DSR.2019.06.006

Ji, X., Liu, G., Gao, S., Wang, H., and Zhang, M. (2017). Temporal and spatial variability of the carbon cycle in the east of China's seas: a three-dimensional physical-biogeochemical modeling study. *Acta Oceanol. Sin.* 36, 60–71. doi:10.1007/s13131-017-0977-3

Jin, X., and Gruber, N. (2003). Offsetting the radiative benefit of ocean iron fertilization by enhancing N2O emissions. *Geophys. Res. Lett.* 30, 1–4. doi:10.1029/2003GL018458

John, E. H., and Flynn, K. J. (2000). Modelling phosphate transport and assimilation in microalgae. *how much Complex. is warranted ?* 125, 145–157. doi:10.1016/s0304-3800(99)00178-7

Jolliff, J. K., Kindle, J. C., Shulman, I., Penta, B., Friedrichs, M. A. M., Helber, R., et al. (2009). Summary diagrams for coupled hydrodynamic-ecosystem model skill assessment. *J. Mar. Syst.* 76, 64–82. doi:10.1016/j.jmarsys.2008.05.014

Jung, H. C., Moon, B. K., Lee, H., Choi, J. H., Kim, H. K., Park, J. Y., et al. (2019b). Development and assessment of NEMO(v3.6)-TOPAZ(v2), a coupled Global Ocean biogeochemistry model. *J. Atmos. Sci.* 56, 411–428. doi:10.1007/s13143-019-00147-4

Jung, H. C., Moon, B. K., Wie, J., Park, H. S., Lee, J., and Byun, Y. H. (2019a). A single-column ocean biogeochemistry model (GOTM–TOPAZ) version 1.0. *Model Dev* 12, 699–722. doi:10.5194/gmd-12-699-2019

Jutterstrom, S., Anderson, L. G., Bates, N. R., Bellerby, R., Johannessen, T., Jones, E. P., et al. (2010). Arctic Ocean data in CARINA. *Earth Syst. Sci. Data* 2, 71–78. doi:10.5194/essd-2-71-2010

Kahler, P., and Koeve, W. (2001). Marine dissolved organic matter: can its C: n ratio explain carbon overconsumption. *Deep Sea Research Part I Oceanographic Research Papers* 48, 49–62. doi:10.1016/s0967-0637(00)00034-0

Kalaroni, S., Tsiaras, K., Petihakis, G., Economou-Amilli, A., and Triantafyllou, G. (2019). Modelling the Mediterranean pelagic ecosystem using the POSEIDON ecological model. Part I: nutrients and chlorophyll-a dynamics. *Deep. Res. Part II Top. Stud. Oceanogr.* 171, 104647. doi:10.1016/j.dsr2.2019.104647

Kalaroni, S., Tsiaras, K., Petihakis, G., Economou-Amilli, A., and Triantafyllou, G. (2020). Modelling the mediterranean pelagic ecosystem using the POSEIDON ecological model. Part II: biological dynamics. *Deep. Res. Part II Top. Stud. Oceanogr.* 171, 104711. doi:10.1016/j.dsr2.2019.104711

Kalvelage, T., Lavik, G., Lam, P., Contreras, S., Arteaga, L., Löscher, C. R., et al. (2013). Nitrogen cycling driven by organic matter export in the South Pacific oxygen minimum zone. *Nat. Geosci.* 6, 228–234. doi:10.1038/ngeo1739

Karstensen, J., Stramma, L., and Visbeck, M. (2008). Oxygen minimum zones in the eastern tropical Atlantic and Pacific oceans. *Prog. Oceanogr.* 77, 331–350. doi:10.1016/j.pocean.2007.05.009

Kawamiya, M., and Oschlies, A. (2003). An eddy-permitting, coupled ecosystem-circulation model of the Arabian Sea: comparison with observations. *J. Mar. Syst.* 38, 221–257. doi:10.1016/S0924-7963(02)00241-5

Kearney, K., Hermann, A., Cheng, W., Ortiz, I., and Aydin, K. (2020). A coupled pelagic-benthic-sympagic biogeochemical model for the bering sea: documentation and validation of the BESTNPZ model (v2019.08.23) within a high-resolution regional ocean model. *Geosci. Model Dev.* 13, 597–650. doi:10.5194/gmd-13-597-2020

Klausmeier, C. A., Litchman, E., Drive, F., and Levin, S. A. (2004). Phytoplankton growth and stoichiometry under multiple nutrient limitation. *Limnol. Oceanogr.* 49, 1463–1470. doi:10.4319/lo.2004.49.4_part_2.1463

Koné, V., Aumont, O., Lévy, M., and Resplandy, L. (2009). Physical and biogeochemical controls of the phytoplankton seasonal cycle in the Indian ocean: a modeling study. *Geophys. Monogr. Ser.* 185, 147–166. doi:10.1029/2008GM000700

Kriest, I., Khatiwala, S., and Oschlies, A. (2010). Towards an assessment of simple global marine biogeochemical models of different complexity. *Prog. Oceanogr.* 86, 337–360. doi:10.1016/j.pocean.2010.05.002

Krom, M. D., Kress, N., Brenner, S., and Gordon, L. I. (1991). Phosphorus limitation of primary productivity in the eastern Mediterranean Sea. *Limnology and Oceanography* 36, 424–432. doi:10.4319/lo.1991.36.3.0424

Kwiatkowski, L., Yool, A., Allen, J. I., Anderson, T. R., Barciela, R., Buitenhuis, E. T., et al. (2014). IMarNet: an ocean biogeochemistry model intercomparison project within a common physical ocean modelling framework. *Biogeosciences* 11, 7291–7304. doi:10.5194/bg-11-7291-2014

Lachkar, Z., Lévy, M., and Smith, K. S. (2019). Strong intensification of the Arabian Sea oxygen minimum zone in response to arabian Gulf warming. *Geophys. Res. Lett.* 46, 5420–5429. doi:10.1029/2018GL081631

Lachkar, Z., Lévy, M., and Smith, S. (2017). Intensification and deepening of the Arabian Sea Oxygen Minimum Zone in response to increase in Indian monsoon wind intensity. *Biogeosciences Discuss* 2017, 1–34. doi:10.5194/bg-2017-146

Lachkar, Z., Mehari, M., Azhar, M. A., Lévy, M., and Smith, S. (2020). Fast local warming is the main driver of recent deoxygenation in the northern Arabian Sea. *Biogeosciences* 18, 5831–5849. doi:10.5194/bg-18-5831-2021

Lachkar, Z., Smith, S., Lévy, M., and Pauluis, O. (2016). Eddies reduce denitrification and compress habitats in the Arabian Sea. *Geophys. Res. Lett.* 43, 9148–9156. doi:10.1002/2016GL069876

Lam, P., and Kuypers, M. M. M. (2011). Microbial nitrogen cycling processes in oxygen minimum zones. *Ann. Rev. Mar. Sci.* 3, 317–345. doi:10.1146/annurev-marine-120709-142814

Lancelot, C., Hannon, E., Becquevort, S., Veth, C., and De Baar, H. J. W. (2000). Modeling phytoplankton blooms and carbon export production in the Southern Ocean: dominant controls by light and iron in the Atlantic sector in Austral spring 1992. *Deep. Res. Part I Oceanogr. Res. Pap.* 47, 1621–1662. doi:10.1016/S0967-0637(00)00005-4

Lancelot, C., Spitz, Y., Gypens, N., Ruddick, K., Becquevort, S., Rousseau, V., et al. (2005). Modelling diatom and Phaeocystis blooms and nutrient cycles in the southern Bight of the North Sea: the MIRO model. *Mar. Ecol. Prog. Ser.* 289, 63–78. doi:10.3354/meps289063

Lauvset, S. K., Key, R. M., Olsen, A., Heuven, S., Lin, X., Schirnick, C., et al. (2016). A new global interior ocean mapped climatology: the 1 ∘ × 1 ∘ GLODAP version 2. *Earth Syst. Sci. Data* 8, 325–340. doi:10.5194/essd-8-325-2016

Lazzari, P., Solidoro, C., Salon, S., and Bolzon, G. (2016). Spatial variability of phosphate and nitrate in the Mediterranean Sea: a modeling approach. *Deep. Res. Part I Oceanogr. Res. Pap.* 108, 39–52. doi:10.1016/j.dsr.2015.12.006

Le Quéré, C., Buitenhuis, E. T., Moriarty, R., Alvain, S., Aumont, O., Bopp, L., et al. (2016). Role of zooplankton dynamics for Southern Ocean phytoplankton biomass andglobal biogeochemical cycles. *Ocean phytoplankton biomass and global biogeochemical cycles* 13, 4111–4133. doi:10.5194/bg-13-4111-2016

Le Quéré, C., Sciences, G., Sciences, E., Vi, P., Jussieu, P., Villefranche, O., et al. (2005). Ecosystem dynamics based on plankton functional types for global ocean biogeochemistry models. *Glob. Chang. Biol.* 2005, 2016–2040. doi:10.1111/j.1365-2486.2005.1004.x

Lefe, N., Taylor, A. H., Gilbert, F. J., and Geider, R. J. (2003). Modeling carbon to nitrogen and carbon to chlorophyll a ratios in the ocean at low latitudes: evaluation of the role of physiological plasticity. *Limnol. Oceanogr.* 48, 1796–1807. doi:10.4319/lo.2003.48.5.1796

Leles, S. G., Valentin, J. L., and Figueiredo, G. M. (2016). Evaluation of the complexity and performance of marine planktonic trophic models. *An. Acad. Bras. Cienc.* 88, 1971–1991. doi:10.1590/0001-3765201620150588

Leonard, C. L., McClain, C. R., Murtugudde, R., Hofmann, E. E., and Harding, L. W. (1999). An iron-based ecosystem model of the central equatorial Pacific. *J. Geophys. Res. Ocean.* 104, 1325–1341. doi:10.1029/1998jc900049

Levin, L. A., and Breitburg, D. L. (2015). Linking coasts and seas to address ocean deoxygenation. *Nat. Publ. Gr.* 5, 401–403. doi:10.1038/nclimate2595

Levin, L. A. (2018). *Emergence of open ocean deoxygenation*.

Li, X., Wang, C., and Lan, J. (2021). Role of the South China sea in southern China rainfall: meridional moisture flux transport. *Clim. Dyn.* 56, 2551–2568. doi:10.1007/s00382-020-05603-w

Liefer, J. D., Garg, A., Fyfe, M. H., Irwin, A. J., Benner, I., Brown, C. M., et al. (2019). The macromolecular basis of phytoplankton C: n: p under nitrogen starvation. *Front. Microbiol.* 10, 763–816. doi:10.3389/fmicb.2019.00763

Lierheimer, L. J., and Banse, K. (2002). Seasonal and interannual variability of phytoplankton pigment in the laccadive (lakshadweep) sea as observed by the coastal zone color scanner. *Proc. Indian Acad. Sci. (Earth Planet Sci.)* 111, 163–185. doi:10.1007/BF02981144

Liu, K. K., Chen, Y. J., Tseng, C. M., Lin, I. I., Liu, H. B., and Snidvongs, A. (2007). The significance of phytoplankton photo-adaptation and benthic-pelagic coupling to primary production in the South China Sea: observations and numerical investigations. *Deep. Res. Part II Top. Stud. Oceanogr.* 54, 1546–1574. doi:10.1016/j.dsr2.2007.05.009

Lo, S., Dutkiewicz, S., Losch, M., Oelker, J., Soppa, M., Trimborn, S., et al. (2019). On modeling the Southern Ocean phytoplankton functional types. *Biogeosciences Discuss* 2019, 1–37. doi:10.5194/bg-2019-289

Lønborg, C., Müller, M., Butler, E. C. V., Jiang, S., Ooi, S. K., Trinh, D. H., et al. (2021). Nutrient cycling in tropical and temperate coastal waters: is latitude making a difference? *Estuar. Coast. Shelf Sci.* 262, 107571. doi:10.1016/j.ecss.2021.107571

Losch, M., Strass, V., Cisewski, B., Klaas, C., and Bellerby, R. G. J. (2014). Ocean state estimation from hydrography and velocity observations during EIFEX with a regional biogeochemical ocean circulation model. *J. Mar. Syst.* 129, 437–451. doi:10.1016/j.jmarsys.2013.09.003

Lu, Z., Gan, J., Dai, M., Zhao, X., and Hui, C. R. (2020). Nutrient transport and dynamics in the South China sea: a modeling study. *Prog. Oceanogr.* 183, 102308. doi:10.1016/j.pocean.2020.102308

Luo, J. Y., Stock, C. A., Henschke, N., Dunne, J. P., and Brien, T. D. O. (2022). Global ecological and biogeochemical impacts of pelagic tunicates. *Prog. Oceanogr.* 205, 102822. doi:10.1016/j.pocean.2022.102822

Lurling, M. (2021). Grazing resistance in phytoplankton. *REYNOLDS' Leg. Grazing* 3, 237–249. doi:10.1007/s10750-020-04370-3

Ma, W., Xiu, P., Chai, F., and Li, H. (2019). Seasonal variability of the carbon export in the central South China Sea. *Ocean Dyn* 69, 955–966. doi:10.1007/s10236-019-01286-y

Macintyre, H. L., Kana, T. M., and Geider, R. J. (2000). The effect of water motion on short-term rates of photosynthesis by marine phytoplankton. *Trends Plant Sci* 5, 12–17. doi:10.1016/S1360-1385(99)01504-6

Madhupratap, M., Kumar, S. P., Bhattathiri, P. M. A., Kumar, M. D., Raghukumar, S., Nair, K. K. C., et al. (1996). Mechanism of the biological response to winter cooling in the northeastern Arabian Sea. *Arabian Sea* 384, 549–552. doi:10.1038/384549a0

Maier-Reimer, E., and Hasselmann, K. (1987). Transport and storage of CO2 in the ocean ——An inorganic ocean-circulation carbon cycle model. *Clim. Dyn.* 2, 63–90. doi:10.1007/BF01054491

Mairet, F., Bernard, O., Masci, P., Lacour, T., and Sciandra, A. (2011). Modelling neutral lipid production by the microalga Isochrysis aff. galbana under nitrogen limitation. *Bioresour. Technol.* 102, 142–149. doi:10.1016/j.biortech.2010.06.138

Malone, T. C., and Newton, A. (2020). The globalization of cultural eutrophication in the coastal ocean: causes and consequences. *Front. Mar. Sci.* 7, 1–30. doi:10.3389/fmars.2020.00670

Manizza, M., Follows, M. J., Dutkiewicz, S., Menemenlis, D., Mcclelland, J. W., Hill, C. N., et al. (2011). A model of the Arctic Ocean carbon cycle. *A Model of the Arctic Ocean carbon cycle* 116, 120200–C12119. doi:10.1029/2011JC006998

Manizza, M., Keeling, R. F., and Nevison, C. D. (2012). On the processes controlling the seasonal cycles of the air–sea fluxes of O<sub>2</sub> and N<sub>2</sub>O: a modelling study. *Tellus B Chem. Phys. Meteorol.* 64, 18429. doi:10.3402/tellusb.v64i0.18429

Maqueda, M. A. M., Willmott, A. J., and Biggs, N. R. T. (2004). Polynya dynamics: a review of observations and modeling. *Journal of Geophysical Research Oceans* 42, 116. doi:10.1029/2002RG000116

Martin, J. H., Coale, K. H., Johnson, K. S., Fitzwater, S. E., Gordon, R. M., Tanner, S. J., et al. (1994). Testing the iron hypothesis in ecosystems of the equatorial Pacific Ocean. *Nature* 371, 123–129. doi:10.1038/371123a0

Mateus, M. D. (2017). Bridging the gap between knowing and modeling viruses in marine systems-An upcoming frontier. *Front. Mar. Sci.* 3, 1–16. doi:10.3389/FMARS.2016.00284

McCreary, J. P., Yu, Z., Hood, R. R., Vinaychandran, P. N., Furue, R., Ishida, A., et al. (2013). Dynamics of the Indian-Ocean oxygen minimum zones. *Prog. Oceanogr.* 112–113, 15–37. doi:10.1016/j.pocean.2013.03.002

McGillicuddy, D. J., McCarthy, J. J., and Robinson, A. R. (1995a). Coupled physical and biological modeling of the spring bloom in the North Atlantic (I): model formulation and one dimensional bloom processes. *Deep. Res. Part I* 42, 1313–1357. doi:10.1016/0967-0637(95)00034-4

McGillicuddy, D. J., Robinson, A. R., and McCarthy, J. J. (1995b). Coupled physical and biological modelling of the spring bloom in the North Atlantic (II): three dimensional bloom and post-bloom processes. *Deep. Res. Part I* 42, 1359–1398. doi:10.1016/0967-0637(95)00035-5

Mcguire, A. D., Leifanderson, G., Guo, T. R. C. S. D. L., Hayes, D. J., Heimann, M., Lorenson, T. D., et al. (2009). Sensitivity of the carbon cycle in the Arctic to climate change. *Ecol. Monogr.* 79, 523–555. doi:10.1890/08-2025.1

Mcintyre, P. B., Jones, L. E., Flecker, A. S., and Vanni, M. J. (2007). Fish extinctions alter nutrient recycling in tropical freshwaters. *Proc. Natl. Acad. Sci. U. S. A.* 104, 4461–4466. doi:10.1073/pnas.0608148104

Meire, L., Soetaert, K. E. R., and Meysman, F. J. R. (2013). Impact of global change on coastal oxygen dynamics and risk of hypoxia. *Biogeosciences* 10, 2633–2653. doi:10.5194/bg-10-2633-2013

Middelburg, J. J. (2018). Reviews and syntheses: to the bottom of carbon processing at the seafloor. *Reviews and syntheses the bottom of carbon processing A. T. the seafloor* 15, 413–427. doi:10.5194/bg-15-413-2018

Middelburg, J. J., Soetaert, K., Herman, P. M. J., and Heip, C. H. R. (1996). Denitrification in marine sediments: a model study. *Global Biogeochem. Cycles* 10, 661–673. doi:10.1029/96GB02562

Miller, C. B., Frost, B. W., Wheeler, P. A., Land-y, , M. R., Welschmeyer, N., and Powell, T. M. (1991). Ecological dynamics in the subarctic Pacific, a possibly iron-limited ecosystem. *Grazing control* 36, 1600–1615. doi:10.4319/lo.1991.36.8.1600

Mongin, M., Nelson, D. M., Pondaven, P., Brzezinski, M. A., and Tréguer, P. (2003). Simulation of upper-Ocean Biogeochemistry with a flexible-composition phytoplankton model: c, N and Si cycling in the western sargasso sea. *Deep Sea Research Part I Oceanographic Research Papers* 50, 1445–1480. doi:10.1016/j.dsr.2003.08.003

Monod, J. (1949). The growth of bacterial cultures. *Annu. Rev. M* 3, 371–394. doi:10.1146/annurev.mi.03.100149.002103

Moore, J. K., Doney, S. C., Kleypas, J. A., Glover, D. M., and Fung, I. Y. (2002). An intermediate complexity marine ecosystem model for the global domain. *Deep. Res. Part II Top. Stud. Oceanogr.* 49, 403–462. doi:10.1016/S0967-0645(01)00108-4

Moore, J. K., Doney, S. C., and Lindsay, K. (2004). Upper ocean ecosystem dynamics and iron cycling in a global three-dimensional model. *Global Biogeochem. Cycles* 18, 1–21. doi:10.1029/2004GB002220

Munhoven, G. (2013). Mathematics of the total alkalinity–pH equation – pathway to robust and universal solution algorithms: the SolveSAPHE package v1.0.1. *Model Dev* 6, 1367–1388. doi:10.5194/gmd-6-1367-2013

Murphy, R. R., Keisman, J., Harcum, J., Karrh, R. R., Lane, M., Perry, E. S., et al. (2022). Nutrient improvements in Chesapeake Bay: direct E ff ect of load reductions and implications for coastal management. *Environ Sci Technol* 56 (1), 260–270. doi:10.1021/acs.est.1c05388

Naqvi, S. W. A., Jayakumar, D. A., Narvekar, P. V., Naik, H., Sarma, V. V. S. S., D'Souza, W., et al. (2000). Increased marine production of N2O due to intensifying anoxia on the Indian continental shelf. *Nature* 408, 346–349. doi:10.1038/35042551

Negrete-garcía, G., Lovenduski, N. S., Hauri, C., Krumhardt, K. M., and Lauvset, S. K. (2019). Sudden emergence of a shallow aragonite saturation horizon in the Southern Ocean. *Nat. Clim. Chang.* 9, 313–317. doi:10.1038/s41558-019-0418-8

Nevison, C., Butler, J. H., and Elkins, J. W. (2003). Global distribution of $N_2O$ and the $\Delta N_2O$-AOU yield in the subsurface ocean. *Global Biogeochem. Cycles* 17, 1–18. doi:10.1029/2003GB002068

Oschlies, A., and Garçon, V. (1999). An eddy-permitting coupled physical-biological model of the North Atlantic. 1. Sensitivity to advection numerics and mixed layer physics. *Glob. Biogeochem. Cycles* 13 (1), 135–160. doi:10.1029/98GB02811

Officer, C. B., Biggs, R. B., Taft, J. L., Cronin, L. E., Tyler, M. A., and Boynton, W. R. (1984). Chesapeake Bay anoxia: origin, development, and significance. *Science (80)* 223, 22–27. doi:10.1126/science.223.4631.22

Ortenzio, F. D., Alcal, M. R., Biologica, O., Dohrn, S. Z. A., and Comunale, V. (2009). On the trophic regimes of the Mediterranean Sea: a satellite analysis. *Biogeosciences* 6, 139–148. doi:10.5194/bg-6-139-2009

Osterholz, H., Niggemann, J., Giebel, H. A., Simon, M., and Dittmar, T. (2015). Inefficient microbial production of refractory dissolved organic matter in the ocean. *Nat. Commun.* 6, 7422. doi:10.1038/ncomms8422

Pant, V., Moher, J., and Seelanki, V. (2018). Multi-decadal variations in the oceanic CO2 uptake and biogeochemical parameters over the northern and southern high latitudes. *Polar Sci.* 18, 102–112. doi:10.1016/j.polar.2018.05.008

Pauer, J. J., DePetro, P. A., Anstead, A. M., and Lehrter, J. C. (2014). Application of a one-dimensional model to explore the drivers and lability of carbon in the northern Gulf of Mexico. *Ecol. Modell.* 294, 59–70. doi:10.1016/j.ecolmodel.2014.09.007

Person, R., Aumont, O., Madec, G., Vancoppenolle, M., Bopp, L., and Merino, N. (2019). Sensitivity of ocean biogeochemistry to the iron supply from the Antarctic Ice Sheet explored with a biogeochemical model. *Biogeosciences* 16, 3583–3603. doi:10.5194/bg-16-3583-2019

Piehl, S., Friedland, R., Heyden, B., Leujak, W., Neumann, T., and Schernewski, G. (2022). Modeling of water quality indicators in the western Baltic SeaSea: seasonal oxygen deficiency. *Environ. Model. Assess.* 28, 429–446. doi:10.1007/s10666-022-09866-x

Pitchford, J. W., and Brindley, J. (1999). Iron limitation, grazing pressure and oceanic high nutrient-low chlorophyll (HNLC) regions. *J. Plankton Res.* 21, 525–547. doi:10.1093/plankt/21.3.525

Ptacnik, R., Andersen, T., and Tamminen, T. (2010). Performance of the Redfield ratio and a family of nutrient limitation indicators as thresholds for phytoplankton N vs. P limitation. *P Limitation* 13, 1201–1214. doi:10.1007/s10021-010-9380-z

Qi-zhou, H., Wen-zhi, W., Li, y. S., and Li, C. W. (1994). Current characteristics of the south china sea. *Oceanology of China Seas* 1, 39–47. doi:10.1007/978-94-011-0862-1_5

Quigg, A., Finkel, Z. V., Irwin, A. J., Rosenthal, Y., Ho, T., Reinfelder, J. R., et al. (2003). The evolutionary inheritance of elemental stoichiometry in marine phytoplankton. *Nature* 291, 291–294. doi:10.1038/nature01953

Quigg, A., Irwin, A. J., and Finkel, Z. V. (2011). Evolutionary inheritance of elemental stoichiometry in phytoplankton. *Proc Biol Sci* 278 (1705), 526–534. doi:10.1098/rspb.2010.1356

Rabalais, N. N., Turner, R. E., and Wiseman, W. J. (2002). Gulf of Mexico hypoxia, a.k.a, The dead zone. *Annu. Rev. Ecol. Syst.* 33, 235–263. doi:10.1146/annurev.ecolsys.33.010802.150513

Radtke, H., Lipka, M., Bunke, D., Morys, C., Woelfel, J., Cahill, B., et al. (2019). Ecological ReGional Ocean Model with vertically resolved sediments (ERGOM SED 1. 0): coupling benthic and pelagic biogeochemistry of the south-western Baltic Sea. *Geoscientific Model Development* 12, 275–320. doi:10.5194/gmd-12-275-2019

Randelhoff, A., Oziel, L., Massicotte, P., Bécu, G., Lacour, L., Dumont, D., et al. (2019). The evolution of light and vertical mixing across a phytoplankton ice-edge bloom. *Elementa Science of the Anthropocene* 7, 20. doi:10.1525/elementa.357

Randelhoff, A., Reigstad, M., Chierici, M., Sundfjord, A., Ivanov, V., Cape, M., et al. (2018). Seasonality of the physical and biogeochemical hydrography in the inflow to the Arctic Ocean through fram strait. *Front. Mar. Sci.* 5, 1–16. doi:10.3389/fmars.2018.00224

Rao, A. M. F., McCarthy, M. J., Gardner, W. S., and Jahnke, R. A. (2007). Respiration and denitrification in permeable continental shelf deposits on the South Atlantic Bight: rates of carbon and nitrogen cycling from sediment column experiments. *Cont. Shelf Res.* 27, 1801–1819. doi:10.1016/j.csr.2007.03.001

Ratnarajah, L., Abu-alhaija, R., Atkinson, A., Batten, S., Bax, N. J., Bernard, K. S., et al. (2023). Monitoring and modelling marine zooplankton in a changing climate. *Nat Commun* 14 (1), 564. doi:10.1038/s41467-023-36241-5

Redfield, A. C. (1933). On the proportions of organic derivatives in sea water and their relation to the composition of plankton. *James Johnstone Meml* 1933, 176–192.

Reed, D. C., Slomp, C. P., and Gustafsson, B. G. (2011). Sedimentary phosphorus dynamics and the evolution of bottom-water hypoxia: a coupled benthic-pelagic model of a coastal system. *Limnol. Oceanogr.* 56, 1075–1092. doi:10.4319/lo.2011.56.3.1075

Resplandy, L., Lévy, M., Madec, G., Pous, S., Aumont, O., and Kumar, D. (2011). Contribution of mesoscale processes to nutrient budgets in the Arabian Sea. *J. Geophys. Res. Ocean.* 116, 2011JC007006. doi:10.1029/2011JC007006

Rhee, G.-Y., and Gotham, I. (1981). The effect of environmental factors on phytoplankton growth: temperature and the interactions of temperature with nutrient limitation1: temperature-nutrient interactions. *Limnol. Oceanogr.* 26, 635–648. doi:10.4319/lo.1981.26.4.0635

Riley, G. A. (1965). A mathematical model of regional variations in plankton. *Limnol. Oceanogr.* 10, R202–R215. doi:10.4319/lo.1965.10.suppl2.r202

Rönnberg, C., and Bonsdorff, E. (2016). Baltic Sea eutrophication: area-specific ecological consequences Baltic Sea eutrophication: area-specific ecological consequences. *Developments in Hydrobiology* 2016, 0920. doi:10.1007/978-94-017-0920-0

Ross, O. N., and Geider, R. J. (2009). New cell-based model of photosynthesis and photo-acclimation: accumulation and mobilisation of energy reserves in phytoplankton. *Mar. Ecol. Prog. Ser.* 383, 53–71. doi:10.3354/meps07961

Ryabchenko, V. A., Gorchakov, A., and Fasham, M. J. R. (1998). Seasonal dynamics and biological productivity in the Arabian Sea Euphotic Zone as simulated by a three-dimensional ecosystem model. *Glob. Biogeochem. Cycles* 12 (3), 501–530. doi:10.1029/98GB01183

Salihoglu, B., Garc, V., Oschlies, A., and Lomas, M. W. (2008). Influence of nutrient utilization and remineralization stoichiometry on phytoplankton species and carbon export: a modeling study at bats. *A modeling study A. T. BATS* 55, 73–107. doi:10.1016/j.dsr.2007.09.010

Sankar, S., Polimene, L., Marin, L., Menon, N. N., Samuelsen, A., Pastres, R., et al. (2018). Sensitivity of the simulated oxygen minimum zone to biogeochemical processes at an oligotrophic site in the Arabian Sea. *Ecol. Modell.* 372, 12–23. doi:10.1016/j.ecolmodel.2018.01.016

Sarmiento, J. L., Fasham, M. J. R., Slater, R. D., Ducklow, H. W., and Williams, R. (1993). Ecosystem behavior at Bermuda station "S" and ocean weather station "India": a general circulation model and observational analysis. *Global Biogeochem. Cycles* 7, 379–415. doi:10.1029/92gb02784

Sarthou, G., Baker, A. R., Blain, S., Achterberg, E. P., Boye, M., Bowie, A. R., et al. (2003). Atmospheric iron deposition and sea-surface dissolved iron concentrations in the eastern Atlantic Ocean. *Ocean* 50, 1339–1352. doi:10.1016/S0967-0637(03)00126-2

Schartau, M., Engel, A., Schröter, J., Thoms, S., Völker, C., and Wolf-Gladrow, D. (2007). Modelling carbon overconsumption and the formation of extracellular particulate organic carbon. *Biogeosciences Discuss* 4, 13–67. doi:10.5194/bgd-4-13-2007

Schourup-Kristensen, V., Sidorenko, D., Wolf-Gladrow, D. A., and Völker, C. (2014). A skill assessment of the biogeochemical model REcoM2 coupled to the finite element sea-ice ocean model (FESOM 1.3), Geosci. *Model Dev. Discuss.* 7, 4153–4249. doi:10.5194/gmdd-7-4153-2014

Schourup-Kristensen, V., Wekerle, C., Wolf-Gladrow, D. A., and Völker, C. (2018). Arctic Ocean biogeochemistry in the high resolution FESOM 1.4-REcoM2 model. *Prog. Oceanogr.* 168, 65–81. doi:10.1016/j.pocean.2018.09.006

Schultz, C., Doney, S. C., Kavanaugh, M. T., and Schofield, O. (2019). Modeling phytoplankton blooms and inorganic carbon responses to sea-ice variability in the West antarctic Peninsula. *Journal of Geophysical Research Biogeosciences* 2019, 1–21. doi:10.1029/2020JG006227

Schultz, J. (1995). *The ecozones of theWorld: The ecological divisions of the geosphere.*

Sharada, M. K., Kalyani Devasena, C., and Swathi, P. S. (2020). Iron limitation study in the North Indian Ocean using model simulations. *J. Earth Syst. Sci.* 129, 93. doi:10.1007/s12040-020-1361-9

Sherrell, R. M., Sherrell, R. M., Annett, A. L., Fitzsimmons, J. N., Roccanova, V. J., and Meredith, M. P. (2018). Subject areas: author for correspondence: a ' shallow bathtub ring ' of local sedimentary iron input maintains the palmer deep biological hotspot on the West antarctic Peninsula shelf. *PHILOSOPHICAL TRANSACTIONS A* 376, 20170171. doi:10.1098/rsta.2017.0171

Smith, V. H. (2006). Responses of estuarine and coastal marine phytoplankton to nitrogen and phosphorus enrichment. *Limnol. Oceanogr.* 51, 377–384. doi:10.4319/lo.2006.51.1_part_2.0377

Snelgrove, P. V. R., Soetaert, K., Solan, M., Thrush, S., Wei, C. L., Danovaro, R., et al. (2018). Global carbon cycling on a heterogeneous seafloor. *Trends Ecol. Evol.* 33, 96–105. doi:10.1016/j.tree.2017.11.004

Soetaert, K., Herman, P. M. J., Middelburg, J. J., Heip, C., Smith, C. L., Tett, P., et al. (2001). Numerical modelling of the shelf break ecosystem: reproducing benthic and pelagic measurements. *Deep. Res. Part II Top. Stud. Oceanogr.* 48, 3141–3177. doi:10.1016/S0967-0645(01)00035-2

Soetaert, K., and Middelburg, J. J. (2009). *Eutrophication in coastal ecosystems*. doi:10.1007/978-90-481-3385-7

Soetaert, K., Middelburg, J. J., Herman, P. M. J., and Buis, K. (2000). On the coupling of benthic and pelagic biogeochemical models. *Earth Sci. Rev.* 51, 173–201. doi:10.1016/S0012-8252(00)00004-0

Sohma, A., Sekiguchi, Y., Kuwae, T., and Nakamura, Y. (2008). A benthic-pelagic coupled ecosystem model to estimate the hypoxic estuary including tidal flat-Model description and validation of seasonal/daily dynamics. *Ecol. Modell.* 215, 10–39. doi:10.1016/j.ecolmodel.2008.02.027

Steele, J. H. (1958). the quantitative ecology of marine phytoplankton. *Biol. Rev.* 34, 129–158. doi:10.1111/j.1469-185X.1959.tb01287.x

Stock, C. A., Dunne, J. P., and John, J. G. (2014a). Drivers of trophic amplification of ocean productivity trends in a changing climate. *Biogeosciences Discussions* 11 (7), 11331–11359. doi:10.5194/bgd-11-11331-2014

Stock, C. A., Dunne, J. P., and John, J. G. (2014b). Global-scale carbon and energy flows through the marine planktonic food web: an analysis with a coupled physical-biological model. *Prog. Oceanogr.* 120, 1–28. doi:10.1016/j.pocean.2013.07.001

Stoecker, D. K., Hansen, P. J., Caron, D. A., and Mitra, A. (2017). Mixotrophy in the marine plankton. *Mixotrophy in the Marine Plankton* 9, 311–335. doi:10.1146/annurev-marine-010816-060617

Stramma, L., Johnson, G. C., Sprintall, J., and Mohrholz, V. (2008). Expanding oxygen-minimum zones in the tropical oceans. *Science* 80, 655–658. doi:10.1126/science.1153847

Stramma, L., Schmidtko, S., Levin, L. A., and Johnson, G. C. (2010). Ocean oxygen minima expansions and their biological impacts. *Deep. Res. Part I* 57, 587–595. doi:10.1016/j.dsr.2010.01.005

Stramma, L., Visbeck, M., Brandt, P., Tanhua, T., and Wallace, D. (2009). Deoxygenation in the oxygen minimum zone of the eastern tropical North Atlantic. *Geophys. Res. Lett.* 36, 206077–206115. doi:10.1029/2009GL039593

Sun, D., Li, Y., and Wang, Q. (2009). A unified model for remotely estimating chlorophyll a in Lake Taihu, China, based on SVM and *in situ* hyperspectral data. *IEEE Trans. Geosci. Remote Sens.* 47, 2957–2965. doi:10.1109/TGRS.2009.2014688

Sun, L., Yang, Y., Xian, T., Lu, Z., and Fu, Y. (2010). Strong enhancement of chlorophyll a concentration by a weak typhoon. *Marine Ecology Progress Series* 404, 39–50. doi:10.3354/meps08477

Suntharalingam, P., and Sarmiento, J. L. (2000). Factors governing the oceanic nitrous oxide distribution' Simulations with an ocean general circulation model. *Global Biogeochem. Cycles* 14, 429–454. doi:10.1029/1999gb900032

Sverdrup, H. U. (1953). On conditions for the vernal blooming of phytoplankton. *ICES J. Mar. Sci.* 18, 287–295. doi:10.1093/icesjms/18.3.287

Tagliabue, A., and Arrigo, K. R. (2005). Iron in the Ross Sea: 1. Impact on CO 2 fluxes via variation in phytoplankton functional group and non-redfield stoichiometry. *J. Geophys. Res.* 110, 1–15. doi:10.1029/2004JC002531

Taylor, K. E. (2001). Summarizing multiple aspects of model performance in a single diagram. *J. Geophys. Res.* 106, 7183–7192. doi:10.1029/2000jd900719

Taylor, M. H., Losch, M., and Bracher, A. (2013). On the drivers of phytoplankton blooms in the antarctic marginal ice zone: a modeling approach: marginal ice zone phytoplankton blooms. *A modeling approach* 118, 63–75. doi:10.1029/2012JC008418

Terhaar, J., Kwiatkowski, L., and Bopp, L. (2020). Emergent constraint on Arctic Ocean acidification in the twenty-first century. *Nature* 582, 379–383. doi:10.1038/s41586-020-2360-3

Terhaar, J., Orr, J. C., Ethé, C., Regnier, P., and Bopp, L. (2019). Simulated Arctic Ocean response to doubling of riverine carbon and nutrient delivery. *Global Biogeochemical Cycles* 33, 1048–1070. doi:10.1029/2019GB006200

Terhaar, J., Torres, O., Bourgeois, T., and Kwiatkowski, L. (2021). Arctic Ocean acidification over the 21st century co-driven by anthropogenic carbon increases and freshening in the CMIP6 model ensemble. *Biogeosciences* 18, 2221–2240. doi:10.5194/bg-18-2221-2021

Thingstad, T. F., Thingstad, T. F., Krom, M. D., Mantoura, R. F. C., Groom, S., Herut, B., et al. (2014). Nature of phosphorus limitation in the ultraoligotrophic eastern mediterranean. *Nature of Phosphorus Limitation in the Ultraoligotrophic Eastern Mediterranean* 309, 1068–1071. doi:10.1126/science.1112632

Thomas, H., Bozec, Y., Elkalay, K., and Baar, H. J. W. (2004). Enhanced open ocean storage of CO2 from shelf sea pumping. *Science* 304 (5673), 1005–1008. doi:10.1126/science.1095491

Toggweiler, J. (1993). Carbon overconsumption. *Nature* 363, 210–211. doi:10.1038/363210a0

Tran, P. Q., and Anantharaman, K. (2021). Biogeochemistry goes viral: towards a multifaceted approach to study viruses and biogeochemical cycling. *mSystems* 6, e0113821–e0113825. doi:10.1128/msystems.01138-21

Trewartha, G. T., and Horn, L. H. (1980). *An introduction to climate*. New York: McGraw-Hill.

Trull, T. W., Passmore, A., Davies, D. M., Smit, T., Berry, K., and Tilbrook, B. (2018). Distribution of planktonic biogenic carbonate organisms in the southern ocean south of Australia: A baseline for ocean acidification impact assessment. *Biogeosciences* 15 (1), 31–49. doi:10.5194/bg-15-31-2018

Tsunogai, S., Watanabe, S., and Sato, T. (1999). Tellus B: chemical and Physical Meteorology Is there a " continental shelf pump " for the absorption of atmospheric CO 2? *Tellus B Chemical and Physical Meteorology* 51, 701–712. doi:10.3402/tellusb.v51i3.16468

Tuerena, R. E., Hopkins, J., Buchanan, P. J., Ganeshram, R. S., Norman, L., Von, A. W.-J., et al. (2021). An arctic strait of two halves: the changing dynamics of nutrient uptake and limitation across the fram strait. *Global Biogeochem. Cycles* 35, 1–20. doi:10.1029/2021GB006961

Twelves, A. G., Goldberg, D. N., Henley, S. F., Mazloff, M. R., and Jones, D. C. (2020). Self-shading and meltwater spreading control the transition from light to iron limitation in an antarctic coastal polynya. *J. Geophys. Res. Ocean.* 126, 1–28. doi:10.1029/2020JC016636

Uchida, T., Balwada, D., Abernathey, R., McKinley, G., Smith, S., and Lévy, M. (2019). The contribution of submesoscale over mesoscale eddy iron transport in the open Southern Ocean. *J. Adv. Model. Earth Syst.* 11, 3934–3958. doi:10.1029/2019MS001805

Urakawa, H., Martens-habbena, W., David, A., Urakawa, H., Martens-habbena, W., and Stahl, D. A. (2010). High abundance of ammonia-oxidizing *archaea* in coastal waters, determined using a modified DNA extraction method. *Appl Environ Microbiol* 76 (7), 2129–2135. doi:10.1128/AEM.02692-09

Vahtera, E., Conley, D. J., Gustafsson, B. G., Kuosa, H., Pitkänen, H., Savchuk, O. P., et al. (2007). Internal ecosystem feedbacks enhance nitrogen-fixing cyanobacteria internal ecosystem feedbacks enhance nitrogen-fixing cyanobacteria blooms and complicate. *Management in the Baltic Sea* 2007, 7447. doi:10.1579/0044-7447

Val, A. L., Almeida-val, V., and Randall, D. J. (2023). Tropical environment. *Tropical environment* 21, 21001–21045. doi:10.1016/S1546-5098(05)21001-4

Venables, H., and Moore, C. M. (2010). Phytoplankton and light limitation in the Southern Ocean: learning from high-nutrient, high-chlorophyll areas. *J. Geophys. Res.* 115, C02015. doi:10.1029/2009jc005361

Vergara, O. A., Echevin, V., Sepúlveda, H. H., and Quinones, R. A. (2017). Controlling factors of the seasonal variability of productivity in the southern humboldt current system (30–40°S): A biophysical modeling approach. *Cont. Shelf Res.* 148, 89–103. doi:10.1016/j.csr.2017.08.013

Vichi, M., and Masina, S. (2009). Biogeosciences Skill assessment of the PELAGOS global ocean biogeochemistry model over the period. *Biogeosciences* 2009, 1980–2000. doi:10.5194/bgd-6-3511-2009

Vichi, M., Pinardi, N., and Masina, S. (2007). A generalized model of pelagic biogeochemistry for the global ocean ecosystem. Part I: theory. *J. Mar. Syst.* 64, 89–109. doi:10.1016/j.jmarsys.2006.03.006

Vogt, M., Vallina, S. M., Buitenhuis, E. T., Bopp, L., and Quéré, C. L. (2010). Simulating dimethylsulphide seasonality with the dynamic green Ocean Model PlankTOM5. *Ocean Model PlankTOM5* 115, C06021–21. doi:10.1029/2009JC005529

Wang, H., Garcia, P. V., Ahmed, S., and Heggerud, C. M. (2022). Mathematical comparison and empirical review of the Monod and Droop forms for resource-based population dynamics. *Ecol. Modell.* 466, 109887. doi:10.1016/j.ecolmodel.2022.109887

Wang, W., Moore, J. K., Martiny, A. C., and François, W. (2019). Convergent estimates of marine nitrogen fixation. *Nature* 566, 205–211. doi:10.1038/s41586-019-0911-2

Ward, B. A., Schartau, M., Oschlies, A., Martin, A. P., Follows, M. J., and Anderson, T. R. (2013). When is a biogeochemical model too complex? Objective model reduction and selection for North Atlantic time-series sites. *Prog. Oceanogr.* 116, 49–65. doi:10.1016/j.pocean.2013.06.002

Weitz, J. S., Stock, C. A., Wilhelm, S. W., Bourouiba, L., Coleman, M. L., Buchan, A., et al. (2015). A multitrophic model to quantify the effects of marine viruses on microbial food webs and ecosystem processes. *ISME J* 9, 1352–1364. doi:10.1038/ismej.2014.220

Weitz, J. S., and Wilhelm, S. W. (2012). Ocean viruses and their effects on microbial communities and biogeochemical cycles. *Biol. Rep.* 4, 17–19. doi:10.3410/B4-17

Wiggert, J. D., Hood, R. R., Banse, K., and Kindle, J. C. (2005). Monsoon-driven biogeochemical processes in the Arabian Sea. *Prog. Oceanogr.* 65, 176–213. doi:10.1016/j.pocean.2005.03.008

Wiggert, J. D., Murtugudde, R. G., and Christian, J. R. (2006). Annual ecosystem variability in the tropical Indian Ocean: results of a coupled bio-physical ocean general circulation model. *Deep. Res. Part II Top. Stud. Oceanogr.* 53, 644–676. doi:10.1016/j.dsr2.2006.01.027

Wilken, S., Yung, C. C. M., Hamilton, M., Hoadley, K., Nzongo, J., Eckmann, C., et al. (2019). The need to account for cell biology in characterizing predatory mixotrophs in aquatic environments. *Philos Trans R Soc Lond B Biol Sci* 374 (1786), 20190090. doi:10.1098/rstb.2019.0090

Wilson, J., Ucharm, G., and Beman, J. M. (2019). Climatic, physical, and biogeochemical changes drive rapid oxygen loss and recovery in a marine ecosystem. *Sci Rep* 9 (1), 16114–16212. doi:10.1038/s41598-019-52430-z

Wright, R. M., Quéré, C. L., Buitenhuis, E., Pitois, S., and Gibbons, M. J. (2021). Role of jellyfish in the plankton ecosystem revealed using a global ocean biogeochemical model. *Biogeosciences* 18, 1291–1320. doi:10.5194/bg-18-1291-2021

Wroblewski, J. S., Sarmiento, J. L., and Flierl, G. R. (1988). An Ocean basin scale model of plankton dynamics in the North Atlantic: 1. Solutions for the climatological oceanographic conditions in may. *Global Biogeochem. Cycles* 2, 199–218. doi:10.1029/GB002i003p00199

Wu, X., Budd, W. F., and Allison, I. (2003). Modelling the impacts of persistent Antarctic polynyas with an atmosphere – sea-ice general circulation model. *Deep Sea Research Part II Topical Studies in Oceanography* 50, 1357–1372. doi:10.1016/S0967-0645(03)00072-9

Xiao, Y., and Friedrichs, M. A. M. (2014). Using biogeochemical data assimilation to assess the relative skill of multiple ecosystem models in the mid-atlantic Bight: effects of increasing the complexity of the planktonic food web. *Biogeosciences* 11, 3015–3030. doi:10.5194/bg-11-3015-2014

Xiu, P., and Chai, F. (2011). Modeled biogeochemical responses to mesoscale eddies in the South China Sea. *J. Geophys. Res. Ocean.* 116, C10006. doi:10.1029/2010JC006800

Xue, Z., He, R., Fennel, K., Cai, W. J., Lohrenz, S., and Hopkinson, C. (2013). Modeling ocean circulation and biogeochemical variability in the Gulf of Mexico. *Modeling ocean circulation and biogeochemical variability in the Gulf of Mexico* 10, 7219–7234. doi:10.5194/bg-10-7219-2013

Yakimov, M. M., Cono, V. L., Smedile, F., Deluca, T. H., Ciordia, S., Ferna, M., et al. (2011). Contribution of crenarchaeal autotrophic ammonia oxidizers to the dark

primary production in Tyrrhenian deep waters (Central Mediterranean Sea). *Central Mediterranean Sea* 5, 945–961. doi:10.1038/ismej.2010.197

Yang, J. R., Lv, H., Isabwe, A., Liu, L., Yu, X., Chen, H., et al. (2017). Disturbance-induced phytoplankton regime shifts and recovery of cyanobacteria dominance in two subtropical reservoirs. *Water Res* 120, 52–63. doi:10.1016/j.watres.2017.04.062

Yang, Y., Sun, L., Liu, Q., Tao, X., and Fu, Y. F. (2010). The biophysical responses of the upper ocean to the typhoons Namtheun and Malou in 2004. *Res . Letts . Corresponding author address* 31, 4559–4568. doi:10.1080/01431161.2010.485140

Yool, A., Popova, E. E., and Anderson, T. R. (2011). MEDUSA-1.0: a new intermediate complexity plankton ecosystem model for the global domain. *Geosci. Model Dev.* 4, 381–417. doi:10.5194/gmd-4-381-2011

Yool, A., Popova, E. E., and Anderson, T. R. (2013). MEDUSA-2.0: an intermediate complexity biogeochemical model of the marine carbon cycle for climate change and ocean acidification studies. *Geosci. Model Dev. Discuss.* 6, 1259–1365. doi:10.5194/gmdd-6-1259-2013

Zhang, H. R., Wang, Y., Xiu, P., Qi, Y., Chai, F., and Hu, Y. C. (2021). Spherical center axial hinge knee prosthesis causes lower contact stress on tibial insert and bushing compared with biaxial hinge knee prosthesis. *Front. Mar. Sci.* 8, 1–8. doi:10.1016/j.knee.2021.01.005

Zhao, J., Temimi, M., Ghedira, H., and Hu, C. (2014). Exploring the potential of optical remote sensing for oil spill detection in shallow coastal waters-a case study in the Arabian Gulf. *Opt. Express* 22, 13755. doi:10.1364/oe.22.013755

Zhao, Z., Schmitt-kopplin, M. G. P., Zhan, Y., Zhang, R., Chen, F., Jiao, N., et al. (2019). Microbial transformation of virus-induced dissolved organic matter from picocyanobacteria: coupling of bacterial diversity and DOM chemodiversity. *ISME J* 13, 2551–2565. doi:10.1038/s41396-019-0449-1

Zoefinkel, V., Beardall, J., Flynn, K. J., Quigg, A., Rees, T. A. V., and Raven, A. J. A. (2010). Phytoplankton in a changing world: cell size and elemental stoichiometry. *J. Plankton Res.* 32, 119–137. doi:10.1093/plankt/fbp098

frontiers | Frontiers in Environmental Science

TYPE Review
PUBLISHED 15 February 2024
DOI 10.3389/fenvs.2024.1326158



OPEN ACCESS

EDITED BY
Marta Sebastian,
Institut de Ciències del Mar, CSIC, Spain

REVIEWED BY
Antti Juhani Rissanen,
Tampere University, Finland
Yi Zhai,
Berkeley Lab (DOE), United States

*CORRESPONDENCE
Claudia Rojas,
claudia.rojas@uoh.cl

RECEIVED 22 October 2023
ACCEPTED 29 January 2024
PUBLISHED 15 February 2024

CITATION
Lavergne C, Cabrol L, Cuadros-Orellana S, Quinteros-Urquieta C, Stoll A, Yáñez C, Tapia J, Orlando J and Rojas C (2024), Rising awareness to improve conservation of microorganisms in terrestrial ecosystems: advances and future directions in soil microbial diversity from Chile and the Antarctic Peninsula.
*Front. Environ. Sci.* 12:1326158.
doi: 10.3389/fenvs.2024.1326158



# Rising awareness to improve conservation of microorganisms in terrestrial ecosystems: advances and future directions in soil microbial diversity from Chile and the Antarctic Peninsula

Céline Lavergne[1,2], Léa Cabrol[3,4], Sara Cuadros-Orellana[5], Carolina Quinteros-Urquieta[1,6], Alexandra Stoll[7,8], Carolina Yáñez[9], Joseline Tapia[10], Julieta Orlando[4,11] and Claudia Rojas[12,13]*

[1]HUB Ambiental UPLA, Laboratorio Observatorio de Ecología Microbiana, Laboratory of Aquatic Environmental Research, Laboratorio de Geografía Ambiental & Palinología, Universidad de Playa Ancha, Valparaíso, Chile, [2]Departamento de Ciencias y Geografía, Facultad de Ciencias Naturales y Exactas, Universidad de Playa Ancha, Valparaíso, Chile, [3]Aix-Marseille University, University Toulon, CNRS, IRD, M.I.O. UM 110, Mediterranean Institute of Oceanography, Marseille, France, [4]Millennium Institute Biodiversity of Antarctic and Subantarctic Ecosystems (BASE), Santiago, Chile, [5]Centro de Biotecnología de los Recursos Naturales, Facultad de Ciencias Agrarias y Forestales, Universidad Católica del Maule, Talca, Chile, [6]Doctorado Interdisciplinario en Ciencias Ambientales, Facultad de Ciencias Naturales y Exactas, Universidad de Playa Ancha, Valparaíso, Chile, [7]Laboratorio de Microbiología Aplicada, Centro de Estudios Avanzados en Zonas Áridas, La Serena, Chile, [8]Instituto de Investigación Multidisciplinario en Ciencia y Tecnología, Universidad de La Serena, La Serena, Chile, [9]Grupo Ecología Microbiana de la Rizósfera (EMRi), Laboratorio de Microbiología, Instituto de Biología, Facultad de Ciencias, Pontificia Universidad Católica de Valparaíso, Valparaíso, Chile, [10]Departamento de Ciencias Geológicas, Facultad de Ingeniería y Ciencias Geológicas, Universidad Católica del Norte, Antofagasta, Chile, [11]Laboratory of Microbial Ecology, Department of Ecological Sciences, Faculty of Sciences, Universidad de Chile, Santiago, Chile, [12]Laboratory of Soil Microbial Ecology and Biogeochemistry (LEMiBiS), Institute of Agri-Food, Animal and Environmental Sciences (ICA3), Universidad de O'Higgins, San Fernando, Chile, [13]Center of Applied Ecology and Sustainability (CAPES), Santiago, Chile

Soil ecosystems are important reservoirs of biodiversity, as they are the most diverse habitat on Earth. Microbial biodiversity plays key roles in many ecosystem services, including the support to biogeochemical cycles. However, despite great advances in the understanding of the role of soil microbiota in providing benefits to nature and humankind, there is still much knowledge to be gained from understudied areas across the globe. Indeed, underrepresentation of the Global South in ecological studies has been suggested as an important gap that could compromise global solutions to conservation and the current biodiversity and climate crisis. In the Southern hemisphere, the southwest of South America, which includes Chile, runs behind the rest of the continent on studies related to soil microbial diversity and ecosystem functions. Therefore, to gain a better understanding of the global biodiversity and environment crisis, essential perspectives and knowledge from underrepresented regions need to be acknowledged to avoid biases in the scientific community. The main objective of this work is to understand how soil microbial diversity has been studied in Chile and the Antarctic Peninsula since 1975 to identify main knowledge gaps and funding opportunities for future research. Our survey consists of 343 articles representing 1,335 sampling points from Continental Chile to the Antarctic

Peninsula. It revealed a better representation of articles studying bacterial and fungal diversity in the extreme regions of Chile funded by both international funds and the National Agency for Research and Development (ANID). To study microbial diversity, cultivation-based methods are still the most commonly used, whereas molecular studies are increasing but insufficiently applied. We have identified and argued the need to enhance collaborative multi- and interdisciplinary efforts, fundings for sequencing effort, and long-term studies to provide robust and informative knowledge about soil microbial communities.

KEYWORDS

**global south, biogeography, microbial ecology, biodiversity, soil diversity, Chile, bibliometrics**

## 1 Introduction

Soil ecosystems are important reservoirs of biodiversity, as they are the most diverse habitat on Earth (Anthony et al., 2023). This biodiversity varies from microscopic constituents such as bacteria, archaea, fungi, and viruses, up to macroscopic life, all of which can spend their entire or part of their life cycle within the soil environment (FAO, 2020). Recently, it has been estimated that up to 50% and 90% of all bacteria and fungi identified on Earth are present in soil ecosystems, respectively (Anthony et al., 2023). It is indeed the soil spatial and temporal heterogeneity, along with characteristics missing in other microbial habitats (e.g., rhizosphere environments or spatial isolation within soil aggregate microhabitats), which contributes to this considerable variety of life (Jansson and Hofmockel, 2018). At a local scale, this diversity is mainly driven by soil physicochemical properties (e.g., pH and soil organic carbon) (Fierer, 2017), while spatial patterns at a global scale have been attributed to variations in plant composition and climate conditions, in addition to soil properties (Bardgett and van der Putten, 2014). It has also been pointed out that species richness belowground does not follow the same trend as aboveground biodiversity (Bardgett and van der Putten, 2014).

Microbial biodiversity plays key roles in many soil functions, which in turn results in important soil ecosystem services (Wall et al., 2012). In addition to the contribution to biogeochemical cycles, among others (Bardgett and van der Putten, 2014), soil microorganisms have been recognized as important drivers of ecosystem multifunctionality (i.e., ecosystem functions and services) in terrestrial environments at a global scale (Delgado-Baquerizo et al., 2016). Due to their wide range of functional capacities and their adaptation to diverse (including extreme) conditions, soil microorganisms offer potential biotechnological applications for food or pharmaceutical production. Despite great advances in the understanding of the role of soil microbiota in providing benefits to nature and humankind, much knowledge is needed to better comprehend its specific role in particular soil processes (Jansson and Hofmockel, 2018). Nowadays, global awareness of the soil biodiversity transcendence in ecosystem functioning not only encourages the scientific community to further decipher soil microbial roles in the environment (i.e., from a genetic to a functional diversity level) (Bardgett and van der Putten, 2014; Jansson and Hofmockel, 2018), but also to contribute from academia with appropriate knowledge and technological solutions beyond academia. This is particularly important to support policymakers and stakeholders in their attributions to encourage sustainable soil management practices to preserve such biodiversity, functioning and associated ecosystem services (Cavicchioli et al., 2019).

In a global context, many of the studies conducted on soil biodiversity have taken place either in temperate ecosystems of the northern hemisphere (Guerra et al., 2020) or mainly in agroecosystems (Hartmann and Six, 2022). In ecology, this underrepresentation of the Global South has been suggested as an important gap that could compromise global solutions to conservation and the current biodiversity and climate crisis (Maas et al., 2021). In the Southern hemisphere, the southwest of South America, which includes Chile, particularly lacks studies on soil microbial diversity and ecosystem functions, as opposed to those conducted in the northern part of the continent (Guerra et al., 2020). The ecological significance of this region is beyond local, as Chile has been considered as a "biogeographic island" (Scherson et al., 2017), because it is surrounded by natural barriers (Altiplano, Atacama Desert, Los Andes Mountains, Pacific Ocean, Patagonian ice fields, Southern Ocean and Antarctica) that result in the evolution of a unique biota (Villagrán and Hinojosa, 1997; Villagrán and Armesto, 2005). The large latitudinal gradient characteristic of the Chilean territory, results in biogeographical and climatic conditions favoring the development of a rich and varied biodiversity, with 31,000 native species reported (Ministerio del Medio Ambiente–Chile, 2018) and around 25% of them endemic (up to >50% for fishes, amphibians, reptiles, and plants) (Ministerio del Medio Ambiente–Chile, 2018). Moreover, Chile host one of the five Mediterranean biomes on Earth, which is considered one of the 36 worldwide global hotspots of conservation priority due to its endemism and a high degree of habitat loss, mainly due to the conversion and replacement of the native vegetation (Fuentes et al., 2019). Therefore, to gain a better understanding of the global biodiversity and environment crisis, as it has been previously reinforced (Nielsen et al., 2017; Nuñez et al., 2019), essential perspectives and knowledge from underrepresented regions need to be acknowledged to avoid biases in the scientific community (Maas et al., 2021). This is particularly critical in zone of the globe such as Chile, where unprecedented climatic anomalies such as incomparable droughts are expected to occur sooner than anticipated and increase in frequency in the next 30 years regardless of emission scenarios (Satoh et al., 2022).

In Chile recent efforts documenting the state of knowledge of soil biodiversity have pointed out disparities on soil taxa and

ecosystem functions studied (Marín et al., 2022). Other national surveys have reported the distribution of soil organic carbon (Pfeiffer et al., 2020), and provided a gridded database on soil physical and hydraulic properties (Dinamarca et al., 2023), contributing to a better understanding of the environmental variables that could affect microbial diversity. Here, we complement these efforts by presenting a compilation and an in-depth analysis of additional aspects of soil microbial biodiversity studies conducted in Chile and the Antarctic Peninsula. In this systematic review, we have included the Antarctic Peninsula due to the scientific significance for Chile, reflected in specific financing programs developed to support research at this place. Moreover, we considered that it was important to incorporate this area because of administrative, geological, and biological connections with the continental territory. Thus, the area to cover includes diverse biomes, from the Atacama Desert to Antarctica, which adds complexity to the literature search and data analysis. Moreover, we add data generated in the past 50 years, which is challenging due to considerable changes in methodology registered overtime. The present review is the collective effort of a multidisciplinary group of researchers (microbiologists, ecologists, geneticists, soil scientists, and geologists), and the data we present herein may serve as a guide to decision-makers regarding environmental conservation efforts, agroecosystems development, research funding, among others. The main objective of this work is to understand how soil microbial diversity has been studied in Chile and the Antarctic Peninsula since 1975 to identify main knowledge gaps and funding opportunities for future research.

## 2 Historical context of research and funding development contributing to the study of (soil) microbial diversity in Chile

The formal study of microorganisms in Chile began in the 1880s, with the foundation of the Histology and Pathological Anatomy Laboratories, in the Faculty of Medicine of the University of Chile (Rodríguez, 1992; Osorio, 2010). Microbiology was, at that moment, limited to bacteriological studies focusing on infectious pathologies (Seeger and Espinoza, 2008). In 1927, the Agronomic Institute was transferred to the University of Chile as the Faculty of Agronomy and Veterinary Medicine (Agronomia, 2023) and in 1953, microbiologists from the Bacteriological Institute of Chile created the first Chilean Association of Microbiology (ACHM) now named Chilean Society of Microbiology (SOMICH) (Osorio, 2015). Along with SOMICH, the Society of Ecology of Chile (SOCECOL) and the Chilean Society of Soil Science (SCHCS) founded in the 70's have greatly contributed to the study of soil biodiversity in the Chilean territory. In terms of documentation of soil studies in Chile, in 1968, a soil map was published as one of the first efforts to show a classification of soils with taxonomic and cartographic units, with the aim to contribute to an adequate agricultural soil management (Alcayaga, 1968). Later, in 1992, the Map of Associations of Large Soil Groups in Chile gathered information from numerous soil studies carried out in Chile since the 1960s (Luzio and Alcayaga, 1992). Related to soils and biodiversity, the work on Mediterranean-type ecosystems (di Castri and Mooney, 1973) and microbial activity in this type of climate (Schaefer, 1973) are among the earliest documented works paving the way to the study of soil microbial diversity in Chile.

Funding formalization to support research, scientific and technological development in Chile is reflected by the creation of several institutions and instruments. The Chilean Economic Development Agency (*Corporación de Fomento de la Producción*—CORFO) was created in 1939 to link research and productive development (Nazer Ahumada, 2016). Based on the Antarctic Treaty (signed on 1 December 1959, in Washington), the Chilean Antarctic Institute (*Instituto Antártico Chileno*—INACH) was established in 1963 to promote advances in Antarctic science (Ministerio de Relaciones Exteriores - Chile, 1966). The following year, the Institute of Agricultural Research (*Instituto de Investigaciones Agropecuarias*—INIA) (Quesada, 2016) was created. In 1953, the United Nations Economic Commission for Latin America and the Caribbean (ECLA, *Comisión Económica para América Latina y el Caribe*—CEPAL recommended the creation of a coordinating institution for technological research, with fiscal funds available (CEPAL—Comisión Económica para América Latina, 1953). From this, the National Commission of Scientific and Technological Research (*Comisión Nacional de Investigación Científica y Tecnológica*—CONICYT), currently the National Research and Development Agency (*Agencia Nacional de Investigación y Desarrollo*—ANID) was founded in 1966 (Ministerio de Educación - Chile, 2018). The latter agency was created in 2018 with the objective of becoming a coordinating and funding hub for the advancement of science and technology in the national context, with a new institutional framework that created the Ministry of Science, Technology, Knowledge and Innovation (MinCTC&I) (Ministerio de Educación - Chile, 2018).

The first CONICYT (currently ANID) program was created in 1971 (Zárate et al., 2022); later, in 1981 the *Fondo Nacional de Desarrollo Científico y Tecnológico (FONDECYT)* was launched, hence funding research projects since 1982 (Figure 1). This funding was developed as a competitive grant to support fundamental and applied science (Zárate et al., 2022), with the objective to maintain and strengthen national capacity for high quality research (Benavente et al., 2012). The National Fund for Scientific and Technological Development (*Fondo de Fomento al Desarrollo Científico y Tecnológico*—FONDEF) was created in 1991 to promote collaboration between academia and private sector by financing research in applied sciences (Benavente et al., 2012). Other relevant sources of research funding in Chile include the Millennium Science Initiative Program (Programa Iniciativa Científica Milenio) created in 1999 to finance research in the areas of Social and Natural Sciences. Since 2011, the Millennium Initiative is part of the MinCTC&I, and until 2013 it has supported 13 Millennium Institutes in the Natural and Exact Sciences and 15 Millennium Nucleus in the same areas (Ministerio de Ciencia Tecnología Conocimiento e Innovación, 2023). It is worth noticing that only two Institutes (Millennium Institute—BASE, Millennium Institute—SECOS) and three Nucleus (Millennium Nucleus—UPWELL, Millennium Nucleus—NUTME, and Millennium Nucleus—LiLi) specially focus on biodiversity, ecology and/or conservation mainly on aquatic related

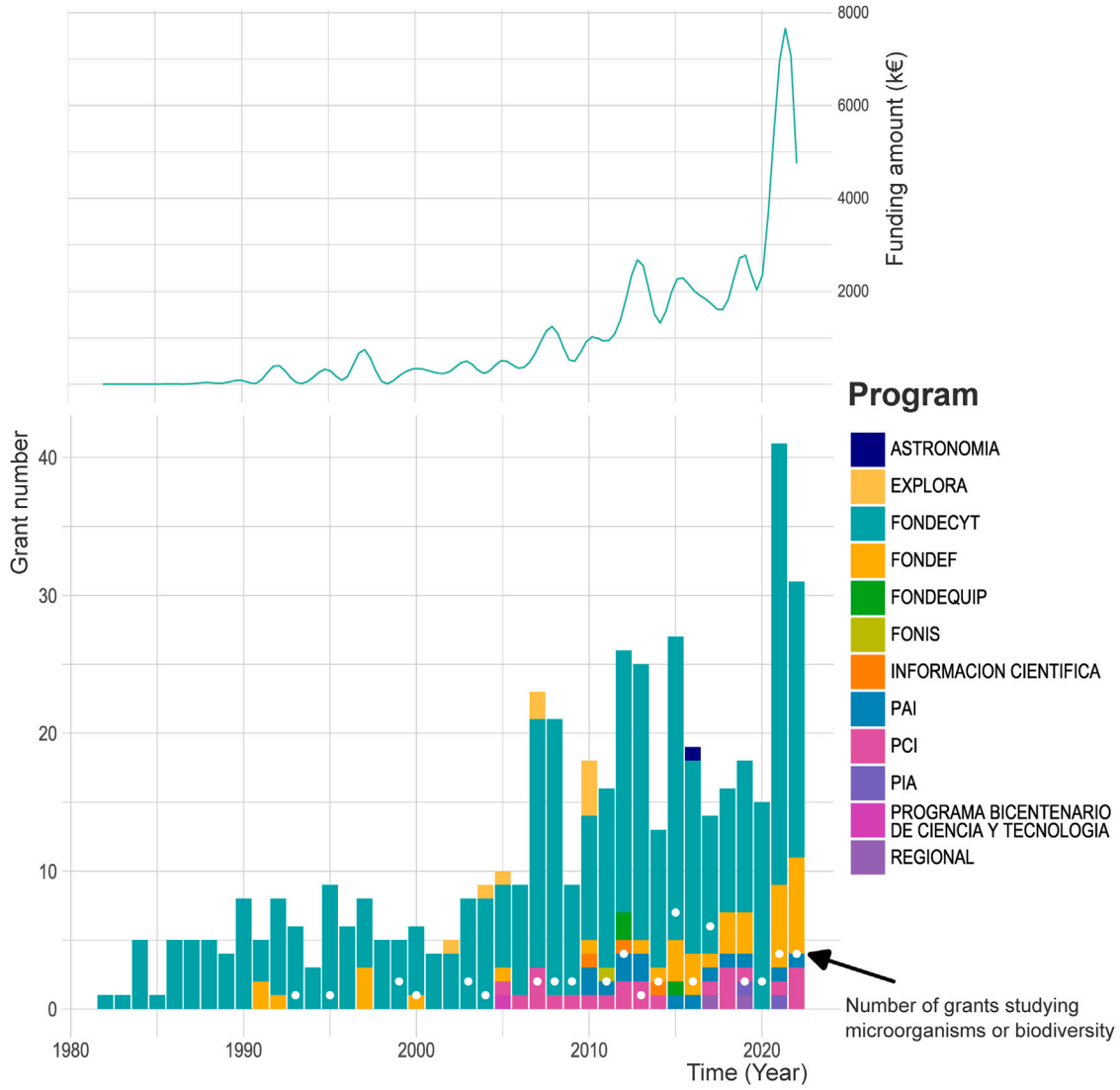


FIGURE 1
Number of soil-related research grants funded by Chilean National Agency for Research and Development (ANID). White points represented the number of grants corresponding to projects focusing on soil microorganisms or biodiversity. Dataset extracted and filtered from https://github.com/ANID-GITHUB/Historico-de-Proyectos-Adjudicados. ASTRONOMIA:Grant for scientific projects in Astronomy; EXPLORA: *Programa Nacional de Divulgación y Valoración de la Ciencia y la Tecnología*/National program for science and technology outreach; FONDECYT: *Fondo Nacional de Desarrollo Científico y Tecnológico;* FONDEF: *Fondo de Fomento al Desarrollo Científico y Tecnológico*/National fund for scientific and technological development; FONDEQUIP: *Programa de Equipamiento Científico y Tecnológico*/National fund for scientific and technological equipment; FONIS: *Fondo Nacional de Investigación y Desarrollo en Salud*/National Fund for Research and Development in Health sciences; INFORMACION CIENTIFICA: Fund for strengthening the national scientific journals; PAI: *Programa de Atracción e Inserción de Capital Humano Avanzado*/Advanced human capital attraction and insertion program; PCI: *Programa de cooperación internacional*/International cooperation program; PIA: Programa de investigación asociativa/Associative research program; PROGRAMA BICENTENARIO DE CIENCIA Y TECNOLOGIA: Bicentennial program for sciences and technology; REGIONAL = National fund for the implementation of regional science and technology research centers.

ecosystems (except LiLi) (Ministerio de Ciencia Tecnología Conocimiento e Innovación, 2023). In addition, another instrument created under ANID is the *Centros Basales* with the aim to strengthen Chile's scientific capabilities towards greater social and economic development (ANID—Agencia Nacional de Investigación y Desarrollo, 2023). By 2024, out of the 19 *Centros Basales,* two (CAPES and IEB) concentrate their research on ecology, biodiversity, and sustainability.

Even with all this battery of programs and institutions, FONDECYT has remained the most important horizontal mechanism for funding scientific research in Chile (Benavente et al., 2012) (Figure 1). Despite the undoubted contribution to the national scientific development, it has also been recognized that up to 60% of funding from this program has been granted to only two, out of the 30 Universities belonging to the *Consejo de Rectores de las Universidades Chilenas* (*CRUCH*), both in the capital of Chile (Parada, 1999). Since 1981, ANID has funded 473 projects related to soil science (including "terrestrial" or "soil" terms in the title of the project), of which 50 have focused on soil biodiversity and/or microorganism studies (Figure 1, white dots). Of such

studies, 46% have been led by the sole University of La Frontera, in the Araucanía administrative region, representing a total of 2,171 k€ accumulated since 1981.

# 3 Methodology

## 3.1 Literature search

We created a dataset following the method described by Guerra et al. (2020) adapted to our topic of interest. Briefly, we collected published literature on studies of soil microbial biodiversity. For this literature search, we conducted independent searches in the Web of Knowledge (WOS), the SCOPUS and the PUBMED databases on 23 June 2023, within papers published between 1975 and 2023. For the first search, we used the keywords (soil OR sand) AND ("Antarctic Peninsula" OR Chile*) AND (*bacteria* OR fung* OR *archaea* OR vir* OR microbi* OR metagen* OR metatranscript* OR metataxon* OR genom*) using the "Topic" search option, which includes title, abstract, author keywords, and Keywords Plus. Chile has strong commitments for the conservation and study of the Antarctic Peninsula. In this context, this territory was included in our study because of administrative, geological, and biological connections as well as scientific relevance for the country.

## 3.2 Rationale of data selection

The initial search returned 1,424 publications, which were further manually selected based on the following inclusion criteria: 1) soil samples excluding biocrusts, marine and lacustrine sediments (the "sand*" keyword being not selective enough to exclude sediments); 2) *in situ* soil samples were not modified by researchers before analysis (e.g., excluding microcosm or mesocosm incubation); 3) in the case of study after atypical events that may have caused a major change on natural microbial communities (e.g., following a wildfire), the study was only considered if they also provided a control point; 4) study was conducted in the Chilean claimed territory (including Antarctic Peninsula) (the "Chile*" keyword being not selective enough to exclude studies outside Chile); 5) only original studies (i.e., reviews were excluded); 6) only studies with diversity data (i.e., studies with only microbial activity measurements were excluded). The list of selected publications based on the criteria previously described is available in Mendeley data repository at: 10.17632/vxpjcjfvth.1.

## 3.3 Data handling

Among the 1,424 studies returned by the performed search, a total of 343 articles fitted the scope according to the criteria described in the methodological section. These 343 articles represented 1,335 sampling points where microbial biodiversity was studied in soils from Chile and the Antarctic Peninsula.

All the statistical analysis and figures were performed with the R software version 4.3.1 (R Core Team, 2021) using the R studio version 2023.09.0. The main packages used for the analysis of the dataset related to data frame manipulation, generation of the figures and visual purposes are listed with the corresponding references as supplementary information (see details in the Supplementary Table S1).

The sampling sites were classified into seven macrozones, grouping the administrative regions of Chile, to provide a spatial interpretation of the results (Figure 2): North (17°S–29°S: Arica y Parinacota, Tarapacá, Antofagasta, and Atacama), Central (29°S–34°S: Coquimbo, Valparaíso, and Metropolitana), Central-South (34°S–38°S: O'Higgins, Maule, Ñuble, and Biobío), South (38°S–44°S: Araucanía, Los Ríos, and Los Lagos including Chiloe island), Austral (44°S–56°S: Aysén and Magallanes y la Antártica Chilena including Tierra del Fuego and Cape Horn), Insular (i.e., Chilean islands not considered in other regions including Easter Island, Juan Fernandez Archipelago), and the Antarctic Peninsula; two studies did not exhibit the information and hence were classified as "Non provided".

The methodology used in every selected article was clustered into 23 groups (Table 1).

The main objective of every article was reported and clustered into eight categories, named application potential, climate change, extreme environments, new species, effect of disturbance, functionality insights, biogeography, and others (which included descriptive surveys, biotic interactions, bioprospective studies, and paleomicrobiology surveys) (Supplementary Figure S1). A maximum of three categories was attributed to every single study; thus, a single article can contribute to more than one category.

# 4 Towards a better understanding of soil microbial communities in Chile and the Antarctic Peninsula

## 4.1 Historical and geographical trends

From a historical point of view, the first study reporting microbial diversity in soils from Chile (and the Antarctic Peninsula), within the time frame of this study (1975–2023), was documented in 1977 (Figure 2). It described two new fungal species from subantarctic Magallanes ecoregion and Antarctic Peninsula (Caretta and Piontelli, 1977). Later, from 1977 to 2005, we found few publications related to the scope of our study, with zero to two reports per year matching our research criteria. The exception to this was observed in 2002 when five studies were conducted in the South of Chile, in the South-Central area ($n$ = 2), Easter Island, and Antarctic Peninsula. Four out of these five studies focused on fungal biodiversity, while the Antarctic study described microalgal communities. From 2005 onwards, the number increased exponentially to reach 11 studies per year between 2010–2015 and 25 per year between 2015–2023. Noticeably, the South and Austral territories were the most studied areas in 1985, 1992, 2011, 2013, 2014, and 2016, accumulating 43 surveys until 2016. This tendency changed between 2017 and 2021, when the focus shifted to the Northern zone of Chile, particularly to the Atacama Desert, recognized as an analog of the soils on Mars since 2003 approximately; thus, as a relevant extreme ecosystem for the discovery of life (Azua-Bustos et al., 2012; Azua-Bustos et al., 2022).

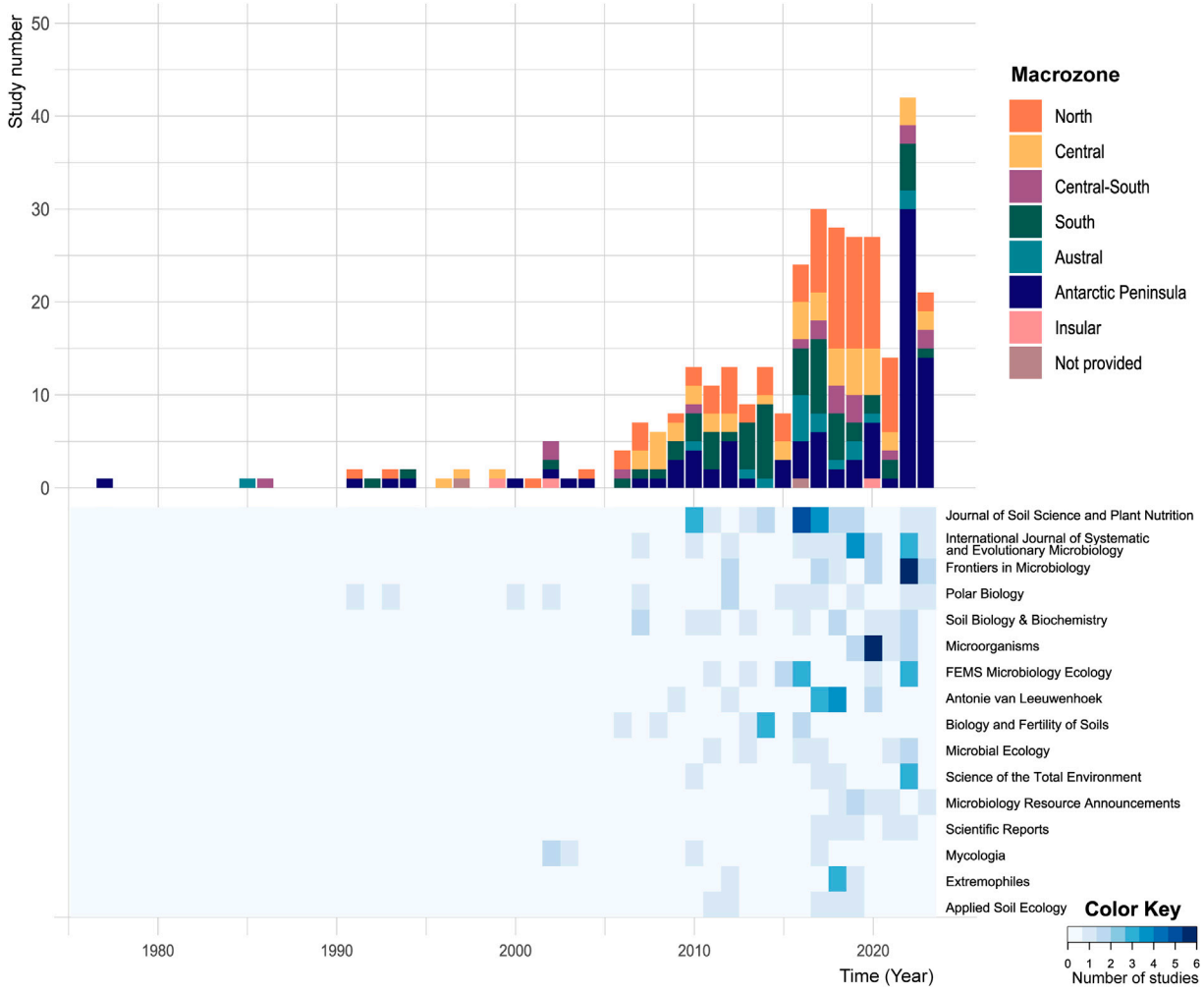


FIGURE 2
Number of studies focusing on soil microbiome diversity in Chile and Antarctic Peninsula. Top panel: number of soil microbial diversity studies per year and per Chilean macrozone. Bottom panel: number of soil microbial diversity studies published per year in the 16 most frequent scientific journals (only showing journals with more than five publications in total).

Lately, since 2022, studies from the Antarctic Peninsula have increased, both in proportions (60.6% of the studies per year) and absolute number of studies (i.e., $n$ = 30 in 2022 and $n$ = 14 in 2023).

The unique and extreme conditions of the Atacama Desert have been recognized globally due to its ecological niches, resulting in microbial life of scientific, technological, and conservation relevance (Bull et al., 2016; Contador et al., 2020). Our findings add to previous reports at the national scale, highlighting this site as one of the most studied places in Chile in terms of soil microbial diversity (Marín et al., 2022). The Atacama Desert, located within the dry subtropical climate belt, has been recognized as the driest and oldest desert on our planet, where no altitudinal movement has been detected since the end of the Jurassic (150 million years ago) (Hartley et al., 2022) and a cold marine upwelling current since at least the early Cenozoic is present (Azua-Bustos et al., 2012). Descriptions of the Atacama Desert soil microbiota date back to 1966 when NASA sought basic information on desert environments to develop and test instruments for the Viking Mission in 1976 (Cameron et al., 1966). Since this NASA mission provided inconclusive results about the existence of life on Mars, no sites were described during the 1980s (Azua-Bustos et al., 2012). Later, from the early 1990s, we identified two studies reporting the diversity of halophilic bacteria in this extreme environment (Prado et al., 1991; Prado et al., 1993). Then, in 2000, the extreme conditions of the Atacama Desert for the development of life were reported using light and solar UV-B radiation experiments (Dose et al., 2001). A milestone in the investigation of microorganisms from the Atacama Desert was published in 2003 by the group led by Chris McKay, who obtained comparable results as the experiments performed in the Viking Landers missions on Mars, this time with samples taken in the Yungay area (80 km from Antofagasta). They found active decomposition of organic species in these soils and extremely low, but still level of, culturable bacteria in the samples, which validated the Atacama Desert as a Mars analog. (McKay et al., 2003; Navarro-González et al., 2003).

TABLE 1 Categories and details of the techniques reported in the current survey.

| Categories | Techniques |
|---|---|
| CLONES | Includes the whole cloning-sequencing approach |
| CULTURE | Enrichment and isolation |
| DETERMINATION-HYPHAE | - |
| DETERMINATION-SPORES | - |
| DGGE | Denaturing gradient gel electrophoresis |
| FLOW CYTOMETRY | Cell detection and counting by flow cytometry |
| GENOMICS | Whole genome sequencing of a single taxa |
| INCUBATIONS | Included only if a non-disturbed initial sampling was provided in studies including inoculation of soil pots, greenhouse assay, microcosms, mesocosms, incubation vials, bioreactors, *in situ* soil inoculation, *in situ* soil chambers |
| METABARCODING | Amplicon sequencing of 16S rRNA, 18S rRNA gene ITS gene or other functional genes at the whole community level, through 454 pyrosequencing or Illumina MiSeq |
| METAGENOMICS | Shotgun metagenomic sequencing |
| MICROARRAY | Life Detector Chip containing 300 antibodies, oligonucleotide probes GeoChip for functional genes, PhyloChip for strain taxonomic identification |
| MICROSCOPY | - |
| OTHER FINGERPRINTS | Nucleic acid-based fingerprints, including Temperature gradient gel electrophoresis—TGGE, Amplified ribosomal DNA restriction analysis—ARDRA, Single-strand conformation polymorphism—SSCP, BOX-PCR, Most probable number PCR—MPN-PCR, Southern blot |
| PCR | - |
| PHYSIOLOGY | Individual enzymatic activity or microbial metabolic activities of a global pathway; Biolog ecoplates--bacteria, archaea and micro-eukaryotes; community-level physiological profiling—CLPP; biodegradation assays; substrate utilization; antimicrobial activities; production of biochemical components; Plant growth-promoting capabilities—PGP |
| PIGMENTS | - |
| PLFA | Fatty acid-based profiles |
| qPCR | Gene abundance or expression of targeted genes by quantitative PCR |
| RESPIRATION | It is one class of "PHYSIOLOGY" |
| SEQUENCING | Gene or gene fragment sequencing on individual populations obtained after culture or fingerprint such as DGGE band |
| SIDEROPHORES | - |
| T-RFLP | Terminal restriction fragment-length polymorphism |
| TOXICITY ASSAYS | Exposition to UV-C, heavy metal |

## 4.2 Main taxa and ecosystems studied

According to our search, out of the targeted microorganisms (i.e., bacteria, archaea, fungi, other microorganisms) studied in Chile and the Antarctic Peninsula, bacteria represent 73% of the studies, followed by fungi with 38% of the studies (Figure 3). Studies focusing on bacteria were common in the North macrozone, representing 30.2% of the study, while articles reporting fungi biodiversity made up 63.6% of the sampling sites at Antarctic and South macrozone. Interestingly, archaeal communities were the main objective of only one study where two archaeal metagenome-assembled genomes (MAGs) were reconstructed (Santos et al., 2021), while two studies focused on the ammonia-oxidizing bacteria and archaea in Central Chile (Bustamante et al., 2012) and the Antarctic Peninsula (Han et al., 2013).

The surveyed ecosystems in the selected publications were representative of the main biomes and/or land use of the region across macrozones (Figure 4). Desert and salt flat reports represented up to 87.8% of the studies conducted in the North of Chile (corresponding to Arica y Parinacota, Tarapacá, Antofagasta, and Atacama administrative regions), which represents the driest territory in the country, with desertic arid to semi-arid climates. The central zone (corresponding to the Coquimbo and Valparaíso regions, and the Metropolitan region, where Santiago, the capital of the country is located), with the highest population density in Chile, encompassed the greatest diversity of ecosystems studied, including scrublands and human-impacted ecosystems (e.g., urban and industrial). In the South-Central area (O'Higgins, Maule, Ñuble and Biobío regions) and Southern territory (La Araucanía, Los Lagos, Los Ríos regions), 86.8% of the selected studies focused on agricultural, forest, and grassland ecosystems, which is consistent with the main land uses at these places. Indeed, the Maule, Ñuble, Biobío, and Araucanía regions have the highest annual and permanent crop area (around 350,000 Ha

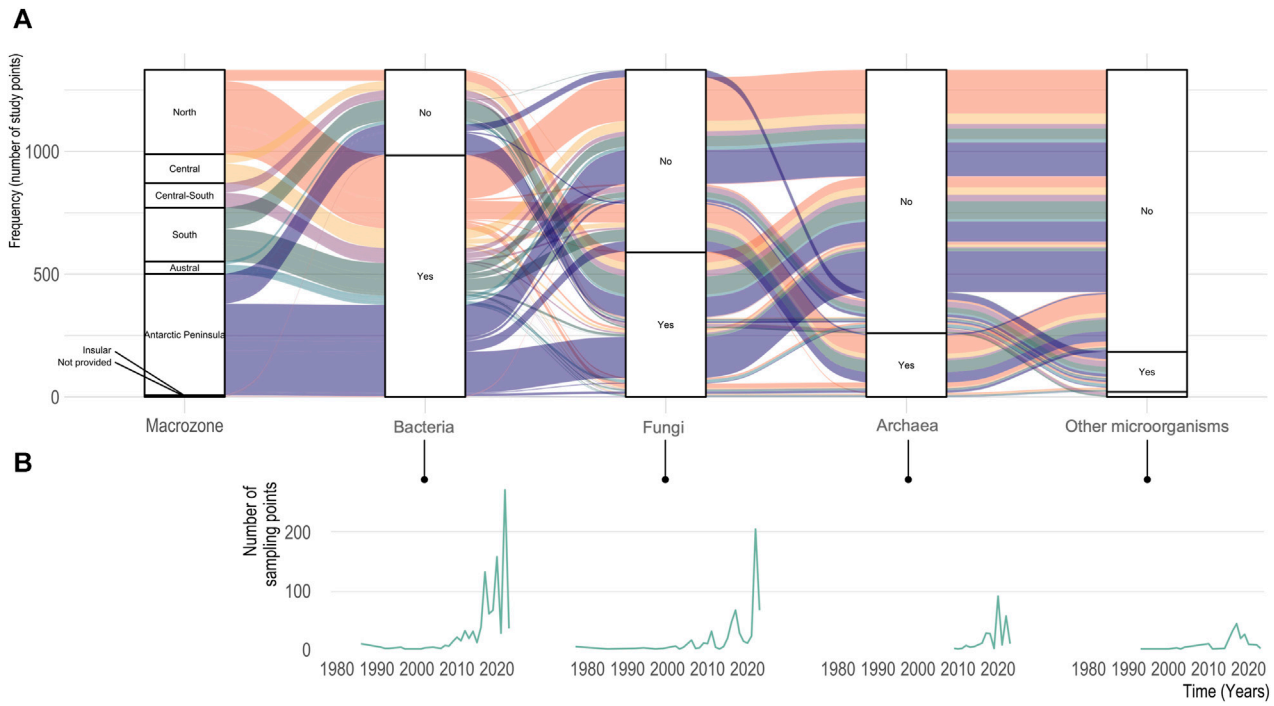


FIGURE 3
Type of microorganisms studied from soils in Chile and the Antarctic Peninsula. **(A)**. Frequency based on the number of sampling points (n = 1,335 sampling points from 343 studies) is given for Bacteria, Archaea, Fungi and Other microorganisms by Chilean Macrozone (first clustering and color). Color for macrozone is similar to Figure 2 and Figure 3. **(B)**. Evolution of the number of sampling points studied per year for every microorganism group considered in this study.

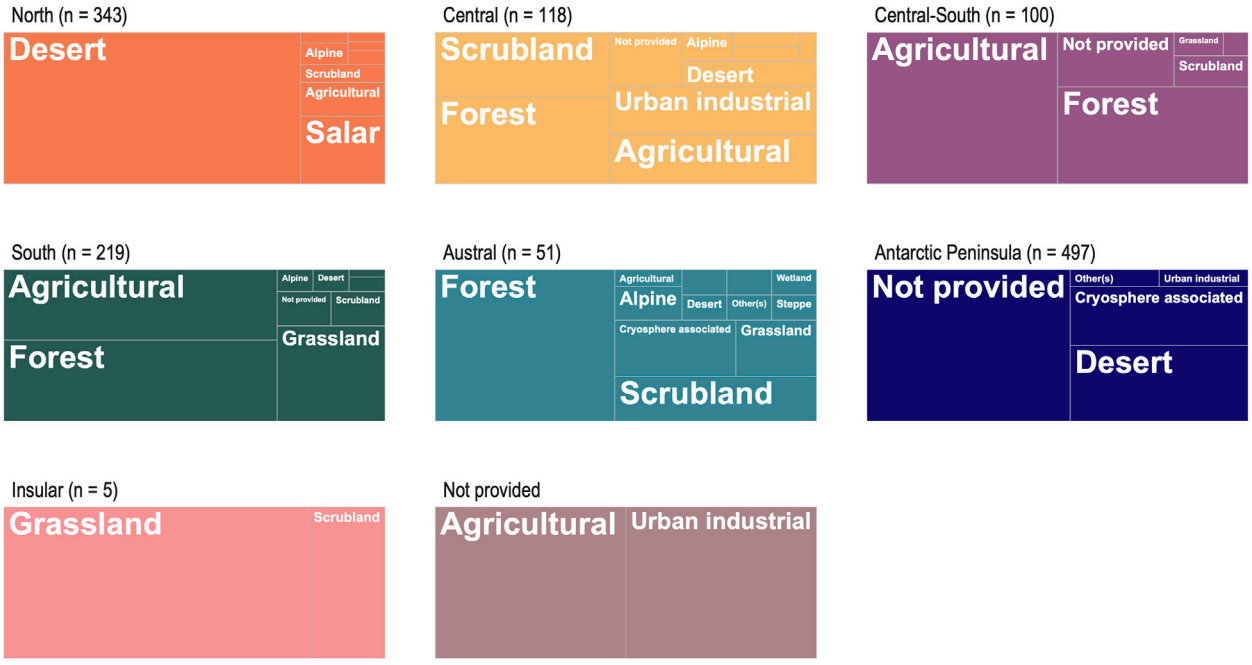


FIGURE 4
Main soil use categories for each macrozone. The number of sampling points per macrozone is indicated between brackets.

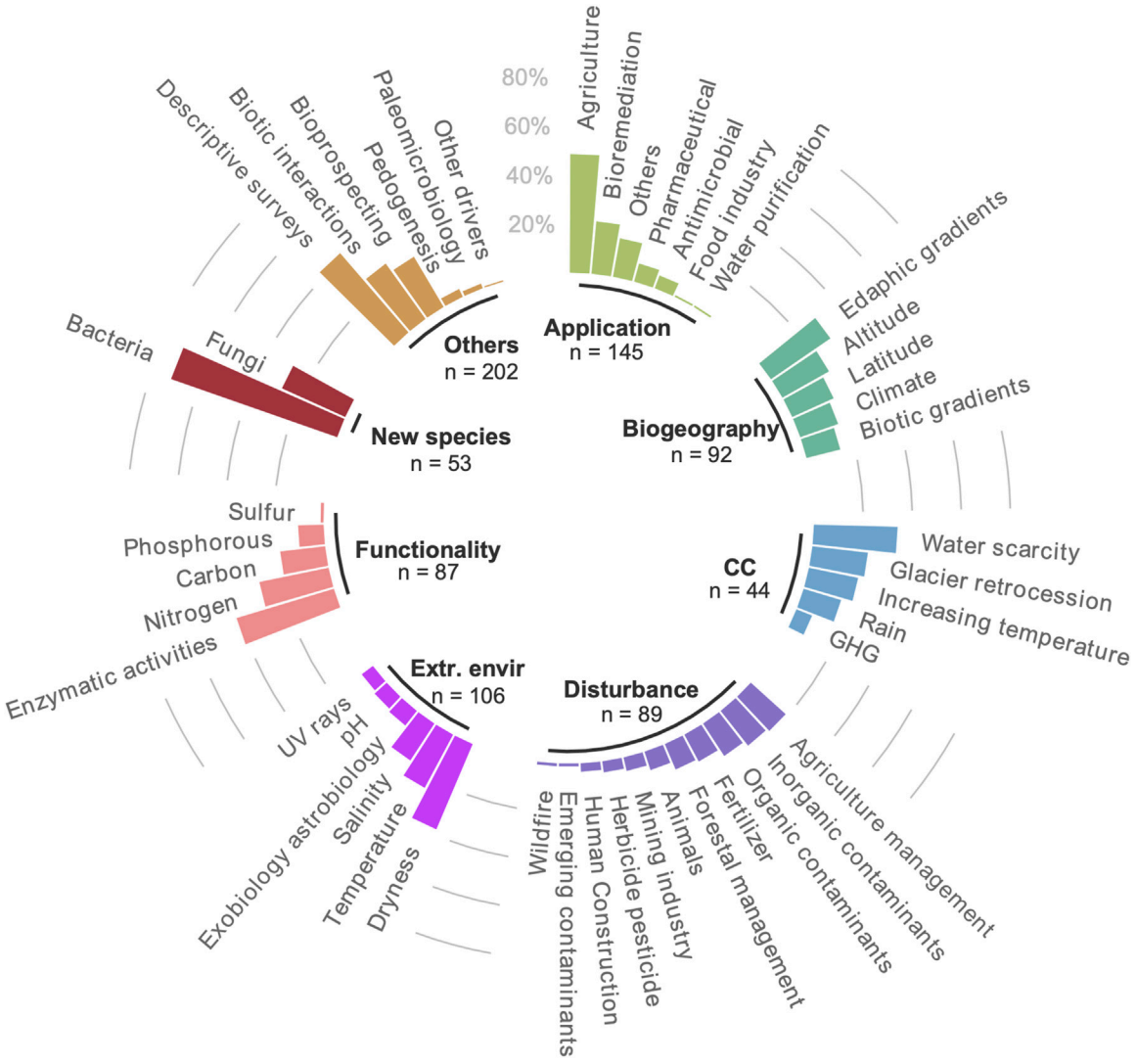


FIGURE 5
Proportion of studies addressing one of the main research scopes identified in this dataset. A single study can match several (sub) categories. CC: climate change; GHG: greenhouse gas; Extr. Env.: extreme environments.

each) and forest plantation area [500,000–980,000 Ha each; ODEPA—Oficina de Estudios y Políticas Agrarias (2019)] in the country. Finally, forest and scrubland studies dominated in the Austral macrozone (Aysén and Magallanes regions) which is in line with the highest area of native forest reported in the Los Lagos, Aysén, and Magallanes y la Antártica Chilena regions [2,400,000–4,400,000 Ha each; ODEPA—Oficina de Estudios y Políticas Agrarias (2019)].

# 5 Main research scope and funding for the study of soil microbial diversity in Chile and the Antarctic Peninsula

## 5.1 Main scopes of the soil microbial diversity studies

Out of the eight research scopes categories used in this survey (Figure 5), 202 articles focused on studies including descriptive, biotic interactions, bioprospecting studies, and paleomicrobiology surveys (shown as Others in Figure 5). Descriptive studies, focusing mainly on the identification of novel species of bacteria and fungi, represented about 40% of these surveys. The second most abundant category corresponded to biotechnological applications (shown as Application in Figure 4), with 145 out of 343 of the articles identified in our study. Half of the biotechnological applications relate to the agricultural sector, with an important focus on plant growth-promoting rhizobacteria (PGPR), which can enhance plant growth by a wide variety of mechanisms like phosphate solubilization, siderophore production, biological nitrogen fixation, phytohormone production, antifungal activity, induction of resistance to pathogen toxins, promotion of beneficial symbioses, etc. (Bhattacharyya and Jha, 2012). PGPRs offer an attractive way to replace the use of chemical fertilizers or pesticides for the development of sustainable agriculture. In our survey, agricultural application studies focus on crops of interest for Chile or on the adaptation to harsh climatic conditions (e.g., Fuentes et al., 2020;

Meza et al., 2022). Another important sector of application is the use of soil microorganisms for bioremediation of contaminated sites, especially by oil (e.g., Serrano and Leiva, 2017; Vázquez et al., 2017), as well as the use of microbial consortia naturally adapted to specific conditions (e.g., low temperature) for bioenergy (methane) production (Aguilar Muñoz et al., 2022). Several extremophilic strains have also been isolated, especially from Antarctic ecosystems, and evaluated for their capacity to produce enzymes of commercial interest, acting as biocatalysts able to carry out reactions at nonstandard conditions (Cabrera and Blamey, 2018; Espina et al., 2022).

Another important focus of the articles selected was the adaptation to extreme environments with 106 studies. This included conditions including dryness, temperature, and salinity, all of which are typical extreme conditions found in the desert and salt flats of Northern Chile (e.g., Paulino-Lima et al., 2013; Pulschen et al., 2015). These studies are of particular interest for astrobiology and take place in the Atacama Desert, reflecting the relevance of extreme environments at a global scale in the search for life. Indeed, in 2003, the European Science Foundation (ESF) launched support for the Investigating Life in Extreme Environments (ILEE) initiative, highlighting the need for a coordinated, interdisciplinary approach to future "Life in extreme environments" (LEXEN) research. The Coordinating Action for Research on the Study of Life in Extreme Environments (CAREX) was developed between 2008 and 2011 and had four priority areas: 1) contributions of life in extreme environments to biogeochemical cycles and responses to environmental change, 2) stressful environments—responses, adaptation, and evolution, 3) biodiversity, bioenergetics and interactions in extreme environments, and 4) life and habitability (Martins et al., 2017).

The biogeographic distribution of soil microorganisms and how it is related to latitudinal, altitudinal, edaphic, climatic, or biotic (e.g., vegetation cover) gradients also took an important proportion of the studies, with 92 of them focusing on this topic. The peculiar geographic and geomorphological context of Chile, with considerable latitudinal and altitudinal gradients, reflected over more than 4,000 km of expansion from North to South, and few hundred kilometers starting from the Pacific Ocean up to >6,000 m a.s.l in the Andes Cordillera, resulting in more than 20 climatic regimes in the country (ODEPA—Oficina de Estudios y Políticas Agrarias, 2019). These unique natural gradients represent a remarkable diversity of ecosystems to explore soil microbial diversity patterns. In our survey, 20 studies focused on altitudinal gradients (e.g., Renny et al., 2017; Rodríguez-Echeverría et al., 2021) and 17 on the influence of latitudinal variation (e.g., Marín et al., 2017; Knief et al., 2020).

Lastly, studies on disturbance, functionality, and climate change were represented by 89, 87, and 44 studies, respectively. Not surprisingly, within the effect of climate change, in Chile, the main research scope was the effect of water scarcity (linked to increased aridity), on soil microbiomes (Neilson et al., 2017) followed by glacial retreat effects on soil microbial communities (Fernández-Martínez et al., 2017). Within the environmental and anthropogenic disturbances identified in our survey, the majority were related to agriculture management, bringing new insights about how to prevent soil degradation (Ramírez et al., 2020) or leaching (Cardenas et al., 2013). The high proportion of studies assessing the impact of inorganic contaminants (mainly metals) can be related to the importance of the mining activity in Chile (e.g., Altimira et al., 2012; Carvajal et al., 2023).

## 5.2 Sources of fundings

Out of the reported sources financing research on soil microbial diversity in Chile (23 studies did not provide such information), international funding supported 53% of the studies (Figure 6), of which 59% was dedicated to studies in continental Chile. FONDECYT was the main national financial support, funding 28.7% of the studies (i.e., $n$ = 141). This Chilean research grant represents the earliest national funding instrument supporting soil microbial diversity studies, with publications acknowledging this from 1992 until the present. The second most important pecuniary source with 8.9% of the studies funded is the so-called "Others" category that includes funding from universities or regional government, bilateral cooperation projects between CONICYT and equivalent foreign research agencies (e.g., Argentina, United Kingdom, Spain), programs funded by ANID that favor the insertion into the academia, Education Quality, and Equity Improvement Program (MECESUP Program) and private companies (e.g., Agroenergía Ingeniería Genética S.A, Anglo American Sur Ltda.). Overall, 25.5% of the Antarctic studies involving Chilean institutions were financed or co-financed by the Chilean Antarctic Institute (INACH). Interestingly, although INACH was founded in 1964 and started to finance research in 1995, only in 2016 did the first study on soil microbial diversity in Antarctica receive financial support from this institution (Figure 6).

# 6 From cultivation to omics techniques

Culture was the most employed methodology (46.4% of the studies; Figure 7), followed by sequencing (27.7% of the studies) and physiological-based approaches (23.3% of the studies). Since 1975, cultivation-based methods have allowed the detection and description of soil microorganisms in Chile. This technique remained the unique approach for microorganism exploration until 1997 and nowadays it is still used, often in combination with other methods (Figure 7). In our survey, 15.5% of the studies ($n$ = 53) allowed the isolation/culture of 61 new microbial taxa (40 bacteria and 21 fungi). This input represents a great contribution to scientific knowledge on soil biodiversity, as these contributed to better comprehend the diversity of Actinobacteria (Idris et al., 2017), Micromonospora (Carro et al., 2018) and Actinomycetes (Okoro et al., 2009). Additionally, they revealed functions still not described in various genus such as biodegradation of chlorinated aromatic compounds (Fulthorpe et al., 1996), metal-chelating compound production (Machuca et al., 2007), tolerance to UV-C (Paulino-Lima et al., 2013), biomineralization of Li-containing nanomaterials by Li-resistant bacteria (Bruna et al., 2022), degradation of PAH (Gran-Scheuch et al., 2020) and antiproliferative activity against a colon cancer cell line (Pavón et al., 2023). The new strains were mainly isolated from the North macrozone (50.9% of the studies, $n$ = 30) and the

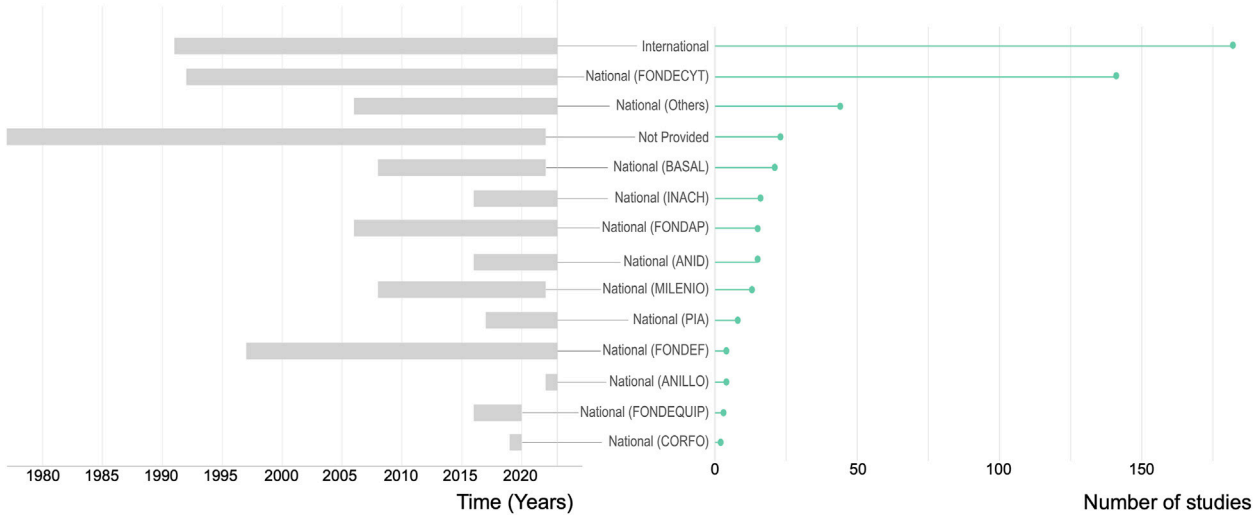


FIGURE 6
Timeline and importance of funding sources. Left panel: timeline of funding sources considering that one single study can be supported by one or more funding sources. Right panel: quantitative importance of funding sources expressed as the number of studies funded.

Antarctic Peninsula (23.7% of the studies, $n$ = 14). In the other macrozones, the remaining 9 studies described mainly new fungal species or genus ($n$ = 10) such as the new genus *Nothophytophthora gen. nov.* (Jung et al., 2017). or *Podospora selenospora* sp. *nov.* discovered from the Ao horizon of a Chilean xerophilic forest soil of the Central-South region (Stchigel et al., 2002).

In 1997, we began to observe the first culture-independent studies using DNA sequencing, cloning, and amino-acid-based fingerprint techniques (Figure 7). The evolution and change of methods allowed to study new aspects of microbial communities. The metabarcoding of a target gene used as a proxy of diversity (mainly 16S rRNA gene for prokaryotes, ITS gene for fungi, and 18S rRNA gene for eukaryotes) began to appear in 2012 in our dataset. Despite the recent incorporation of metabarcoding at the national context, this is the third most used technique with a total of 79 (23%) studies, revealing a very fast spreading of this low-cost high-throughput technique providing access to the whole diversity of a community, overpassing the culture biases and limitations. Indeed, most of the data reported for archaea came from studies using metabarcoding approaches based on sequencing of the 16S rRNA genes. The improvement on sequencing technologies and the decrease of cost resulted in an increase of the use of metagenomic techniques since 2017 (both Illumina MiSeq and Oxford Minion). Metabarcoding, metagenomic or metranscriptomic data were available from the Central, Central-South and Austral regions in a total of no more than 81 sampling points. Continental Chile only accounted for 52.2% of all the sampling points (i.e., 291 sampling points) where high throughput sequencing techniques are applied (Supplementary Figure S4). In our survey, we detected 10 studies using shot-gun sequencing since 2017, with four of them published in 2022 (Figure 7). This technique provides access to the full genomic content of a community, which is useful for functional insights and reveals the metabolic potential of a community, by overpassing the PCR-based biases of metabarcoding. Hence, genomes of uncultured microorganisms can be reconstructed through the generation of MAGs) to explore new putative functions or genes (Hernández et al., 2020). Also, complete genomes of previously isolated strain can be provided (Valenzuela-Heredia et al., 2020; Núñez-Montero et al., 2023). Yet, this approach is based on community DNA, and does not specifically target active microorganisms through their RNA. Based on the publication revised in this survey, no metatranscriptomic study has been reported for the study of microbial diversity in soils from Chile. The difference in soil microbial community representation by culture-dependent and culture-independent approaches has been extensively reported (e.g., Stefani et al., 2015; Hinsu et al., 2021), even in the Chilean Andean highlands (Maza et al., 2019) resulting in the identification of some taxa overrepresented by culture-dependent techniques compared to high throughput sequencing. Also, through cultivation, Hinsu et al. (2021) showed the detection of a large proportion of amplicon sequence variants (ASVs) not retrieved by 16S rRNA gene metabarcoding, suggesting the need to associate different approaches and methodologies. Importantly, 62.7% of the studies combined two or more methodological approaches to provide a more complete picture of microbial diversity. It is interesting to note the efforts to go beyond a sole description, by coupling diversity surveys based on molecular data with functional approaches such as the measurement of diverse enzymatic activities make up 23.3% of the studies (Figure 7).

## 7 Future directions and opportunities to study soil microorganisms in Chile

There is a widely recognized interest for microorganisms from extreme environments due to their potential biotechnological applications such as enzyme production under extreme conditions, biomass conversion, biobased products, sustainable industrial processes, or prospection of life on extraterrestrial

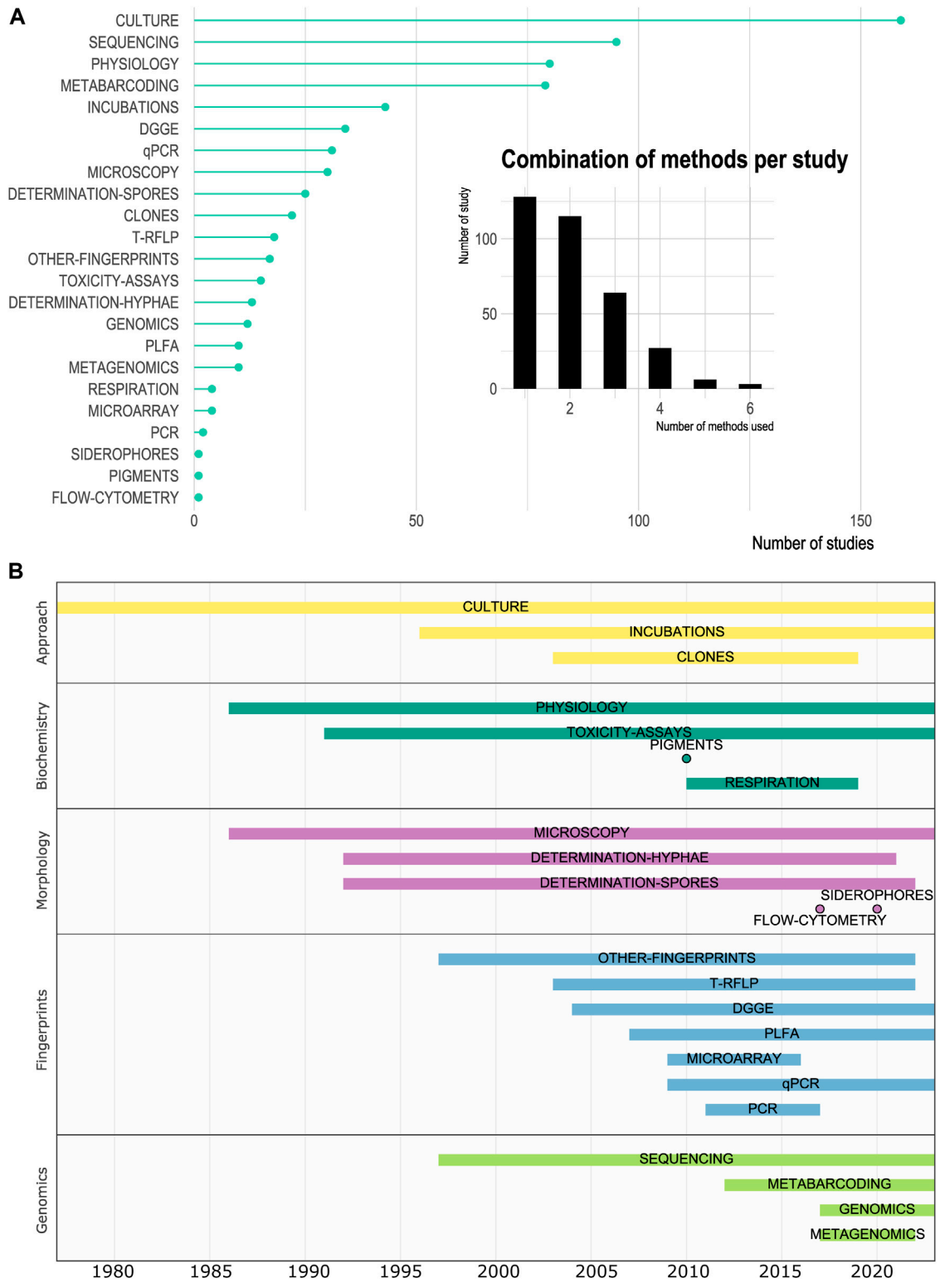


FIGURE 7
Chronological and quantitative analysis of the methods used to study microbial diversity in soils. **(A)**. Identification and frequency of methodologies used in soil microbial diversity studies. Number of studies using at least one of the listed techniques. The inserted barplot presented the number of different methods used per study. **(B)**. Timeline of the methodologies clustered in categories partly defined according to Hatzenpichler et al. (2020).

habitats, as reviewed in different parts of the world (e.g., Krüger et al., 2018; Kochhar et al., 2022; Schultz et al., 2023). In Chile, extremophilic microorganisms inhabiting unique environmental conditions in Chilean ecosystems have been studied, together with their potential for biotechnological applications (Azua-Bustos and González-Silva, 2014; Anguita et al., 2018; Orellana et al., 2018; Leiva-Aravena et al., 2019). Indeed, Chile offers a particularly attractive natural laboratory in this perspective due to its multiple extreme ecosystems. The great range of edaphic conditions characterized by alkaline or acidic pH, high salt and metal concentrations, wide temperature gradients, water stress, and strong UV radiation of the high-altitude deserts, salt flats, and geysers in the north of Chile (Altiplano and Atacama Desert) represent a unique microbial reservoir of life of international interest. Soils influenced by high altitude glaciers, geothermal springs, and volcanic activity in the Andes mountains in Central Chile, are subjected to a wide temperature gradient and high metal concentrations. In the southern extreme of Chile microbial life thrives in extremely low temperatures associated with ice fields, cold lakes, and fjords in Patagonia and Antarctica. Therefore, beyond the clear and urgent need to increase the number of studies focusing on soil microbial diversity in the southern hemisphere and extreme ecosystems, through our survey, we identified three main directions for future research: 1) enhance multi- and interdisciplinary collaborations, 2) increase funding support for high-throughput sequencing approaches to study soil microbial diversity in Chile, and, 3) perform long-term studies.

## 7.1 Collaborative multi- and interdisciplinary studies

Soil ecosystem functioning is complex and depends on the interaction of biological processes, soil physical structure, chemical reactions, and geological context, among others. Therefore, soil microbial diversity can only be fully understood through the integration with these connected disciplines. Despite some efforts to combine soil microbial diversity and geochemical data (e.g., Mandakovic et al., 2018; Aponte et al., 2022; Barret et al., 2022; Aguado-Norese et al., 2023), integrated studies are scarce. As an example, in our survey the type of soil was rarely explicitly indicated, despite the great diversity of soil orders identified in Chile (Casanova et al., 2013). In 73.8% of cases, the type of soil was not described or not identified, which hampers the possibilities of comparisons and raises the need for greater interdisciplinary collaboration among ecologists, microbiologists, and soil scientists to deeper characterize soil ecosystems as living bodies.

Even within biological sciences, interactions are rare, as shown by the low proportion of studies (16.3%) addressing biotic interactions with other components of biodiversity, despite the importance of microorganisms in soil food web both above- and below-ground feedback. Finally, social sciences and humanities are absent from our survey. As a result, the multidisciplinary wide scope journals such as Science of the Total Environment and Scientific Reports only accounted for 6 and 5 studies, respectively (Figure 2). This reinforced a lack of interdisciplinarity as the main journals chosen for publication are highly specialized. Yet, they need to be included in biodiversity studies to provide historical, sociological, or economical perspectives of soil use, as well as to integrate traditional knowledge. Future directions in soil microbial diversity studies should involve tight collaboration with different disciplines to provide a more global picture of ecosystem functioning from different perspectives. Therefore, it seems to us to integrate not only knowledge from natural science related fields but also social science in particular within the new generation of scientists and stakeholders is critical. We hence fully agree with what Timmis et al. (2020) called "the need for microbial literacy" and consider that multidisciplinary teams of microbiologists, microbial ecologists and social scientist should promote, through the collaboration, the access of this knowledge to the society (Bradshaw, 2021). This is critical if complex multi-component concerns such as climate change impact are to be addressed. A possible orientation towards this direction can be encouraged by funding criteria, with the development of interdisciplinary research calls, such as the new "Exploration Call" from Chilean ANID, aiming at contributing to the development and consolidation of disruptive, novel, high-uncertainty scientific-technological research. Finally, as revealed by our survey, the use of soil as a reservoir of microbial resources for potential biotechnological applications is of strong interest in continental Chile, especially in extreme remote regions. However, these prospective studies barely involve traditional knowledge and local communities who live in these places and benefit from ecosystem services provided by uniquely adapted microbial communities. Hence, as a perspective, we consider that a compromise between resource use and conservation should be accounted for in future research, relying on more dialogue and inclusion of local communities.

## 7.2 Increase and decentralize funding for high-throughput sequencing

As shown in our survey, soil microbial diversity is spatially heterogeneous across Chile, with some highly represented regions (namely, the most extreme ones) and others under-represented, such as the insular and the Austral regions. Funding should promote the development of studies in under-represented ecosystems.

On one hand, at a global scale, south-north collaborations are a way to improve funding availability and stimulate global-impact research (Baker, 2023). However, we observed in our survey that more than 30% of the soil microbial diversity studies conducted in the northern regions of Chile did not involve any Chilean institution (Supplementary Figures S2, S3), highlighting a very strong international interest in the Atacama Desert as an analog for the search for life on Mars and a lack of local collaborations. To improve our knowledge using cutting-edge techniques and propose suitable protection measures/solutions, it is necessary to maintain and strengthen south-north collaborations even between high-income countries in science. Moreover, Chile, as most Latin American countries, is considered a high-income country by the World

Bank (World Bank Group, 2020) and the Organization for Economic Co-operation and Development (OECD, 2022). However, in 2020, only 0.33% of the gross domestic product (GDP) of the country was dedicated to research and development, while in Europe, on average 2.23% of the GDP support scientific research (Eurostat, 2023), ranging from 0.46% to 3.44% depending on the country.

On the other hand, at a national scale, we consider that incrementation and decentralization of funding for sequencing is urgently needed to continue supplying the universal microbial genetic archives from Chilean terrestrial ecosystems. In Chile, the FONDEQUIP (Fund for Scientific and Technological Equipment) program alone has allowed for the acquisition and implementation of 10 DNA sequencing platforms, six of which are in Santiago. At a global scale, omic observatories are flourishing, but the global south is generally less covered, and our survey demonstrates that local efforts may be integrated into global networks. For example, shotgun environmental DNA sequencing would provide valuable data combined with culture and functional inputs. Amplicon thoughput sequencing methods are now common in soil microbial studies in Chile, but our review shows that they appeared relatively late in the national context compared to worldwide studies. The same happens with metagenomics reported for the first time in 2017 in our survey, while metatranscriptomics studies are absent despite their rapid development in other parts of the world. This delay could be due to the prohibitively high costs of these techniques, resulting in the need to wait until they become more affordable as occurred previously with amplicon sequencing. This limitation could be overpassed with enhanced specific funding encouraging the use of state-of-the-art techniques.

### 7.3 Long term studies

Another gap that has been identified during our survey is the lack of long-term studies. As pointed out by Cavicchioli et al. (2019) long-term monitoring is needed as they allow to identify patterns between biological parameters and climatic variables or gradual changes that cannot be detected with single sampling events. As an example, Hartmann et al. (2015) demonstrated the effect of conventional *versus* organic agriculture on soil microbial diversity (bacteria and fungi) over 20 years of monitoring in Switzerland. Also, along a 7-year survey, Wu et al. (2022) evaluated the effect of warming temperatures on bacterial, fungal and protistan diversity and interactions in an old-field tall-grass prairie in Oklahoma (United States). In our survey, we retrieved only one long-term study, reported by Aguilera et al. (2016). It conducted a 25-year study bringing new insights about the effect of precipitation regime changes and presence of small mammals on bacterial and fungal communities in a semi-arid shrubland of the Bosque Fray (Jorge National Park). One factor that limits the realization of long-term studies is the scarcity of mid- to long-term fundings almost nonexistent in Chile. The ANID BASAL and FONDAP are the two funding tools available for research centers in Chile for 5 years projects (renewable for 5 more years). Two centers with BASAL fundings (CAPES and IEB) focus on biodiversity and ecology at the time of writing and may have the capacity to produce long-term dataset, hence filling the important gap for terrestrial microbial ecology in Chile.

## 8 Conclusion

Through a comprehensive review of 343 articles studying soil microbial diversity from Chile and the Antarctic Peninsula, we revealed a strong interest in applied microbiology to improve agriculture practices and the study of extreme environments. The deep analysis of the main fundings and the evolution of methodologies used to study microbial community diversity in this territory, provided recommendations for future research in this field. We emphasized the need for multi- and interdisciplinary efforts to increase knowledge on soil microbial diversity not only for academia but also to bring this to local communities and stakeholders. We suggested some future funding directions adapted to the use of cutting-edge techniques. Finally, we argue the urgent need to begin long-term studies, crucial in a global change context. Our work contributes both to global and local awareness on the importance of soil microbial biodiversity in Chile and the Antarctic Peninsula. Indeed, the geographic region we cover here, with its unique biodiversity and variety of biomes, might serve as a natural laboratory where, for example, the effect of climate anomalies on soil microbial diversity can be evaluated sooner than elsewhere.

## Author contributions

CL: Conceptualization, Data curation, Writing–original draft, Formal Analysis, Funding acquisition, Investigation, Visualization. LC: Conceptualization, Data curation, Investigation, Writing–original draft, Writing–review and editing. SC-O: Conceptualization, Data curation, Investigation, Writing–original draft, Writing–review and editing, Visualization. CQ-U: Conceptualization, Data curation, Investigation, Writing–original draft. AS: Conceptualization, Data curation, Writing–review and editing. CY: Conceptualization, Data curation, Investigation, Writing–review and editing. JO: Conceptualization, Data curation, Writing–review and editing. JT: Conceptualization, Data curation, Writing–review and editing. CR: Conceptualization, Data curation, Writing–original draft, Writing–review and editing, Funding acquisition.

## Funding

The author(s) declare financial support was received for the research, authorship, and/or publication of this article. CL has been supported by ANID FONDECYT 11201072 and ANID InES I + D 2021 (INID210013). S. Cuadros-Orellana acknowledges ANID FONDECYT 1201692, ANID FONDEQUIP EQM210185 and ANID FONDEF ID23I10049 support. CQ-U has been funded by ANID BECA DOCTORADO NACIONAL 21221130, FONDECYT 11170566, FONDECYT 1211977, NODO 220002 and Fondo UPLA: CNE 23-20. CR acknowledges ANID FONDECYT 11180869 and ANID PIA/BASAL FB0002. LC acknowledges support from ANID FONDECYT 1211672 and INACH RT09-12. JO and LC acknowledged support from ANID–Millennium Science Initiative Program–ICN 2021_002.

## Acknowledgments

Authors particularly acknowledge the preliminary discussions with the founding members of the first Chilean Microbial Ecology Network (Red Chilena de Ecología Microbiana, RECHEM). We are also grateful to Constanza Soto for her help in the dataset generation. CL and CR also acknowledge the support frame under the project URO RED 21992 [Plan de Fortalecimiento de Universidades del Estado (CUECH)].

## Conflict of interest

The authors declare that the research was conducted in the absence of any commercial or financial relationships that could be construed as a potential conflict of interest.

## Publisher's note

All claims expressed in this article are solely those of the authors and do not necessarily represent those of their affiliated organizations, or those of the publisher, the editors and the reviewers. Any product that may be evaluated in this article, or claim that may be made by its manufacturer, is not guaranteed or endorsed by the publisher.

## Supplementary material

The Supplementary Material for this article can be found online at: https://www.frontiersin.org/articles/10.3389/fenvs.2024.1326158/full#supplementary-material

## References

Agronomia (2023). Facultad de Ciencias Agronómicas Universidad de Chile. Historia. Available: https://agronomia.uchile.cl/facultad/la-facultad/historia (Accessed October 14, 2023).

Aguado-Norese, C., Cárdenas, V., Gaete, A., Mandakovic, D., Vasquez-Dean, J., Hodar, C., et al. (2023). Topsoil and subsoil bacterial community assemblies across different drainage conditions in a mountain environment. *Biol. Res.* 56 (1), 35–15. doi:10.1186/s40659-023-00445-2

Aguilar-Muñoz, P., Lavergne, C., Chamy, R., and Cabrol, L. (2022). The biotechnological potential of microbial communities from Antarctic soils and sediments: application to low temperature biogenic methane production. *J. Biotechnol.* 351, 38–49. doi:10.1016/j.jbiotec.2022.04.014

Aguilera, L. E., Armas, C., Cea, A. P., Gutiérrez, J. R., Meserve, P. L., and Kelt, D. A. (2016). Rainfall, microhabitat, and small mammals influence the abundance and distribution of soil microorganisms in a Chilean semi-arid shrubland. *J. Arid. Environ.* 126, 37–46. doi:10.1016/j.jaridenv.2015.11.013

Alcayaga, S. (1968). "Los mapas de suelos," in *Publicación técnica N°1. Series 1968* (Santiago de Chile: CORFO).

Altimira, F., Yáñez, C., Bravo, G., González, M., Rojas, L. A., and Seeger, M. (2012). Characterization of copper-resistant bacteria and bacterial communities from copper-polluted agricultural soils of central Chile. *BMC Microbiol.* 12, 193. doi:10.1186/1471-2180-12-193

Anguita, J. M., Rojas, C., Pastén, P. A., and Vargas, I. T. (2018). A new aerobic chemolithoautotrophic arsenic oxidizing microorganism isolated from a high Andean watershed. *Biodegradation* 29, 59–69. doi:10.1007/s10532-017-9813-x

ANID—Agencia Nacional de Investigación y Desarrollo (2023). Centros Basales. Available: https://anid.cl/centros-e-investigacion-asociativa/centros-basales/ (Accessed October 14, 2023).

Anthony, M. A., Bender, S. F., and van der Heijden, M. G. A. (2023). Enumerating soil biodiversity. *Proc. Natl. Acad. Sci. U.S.A.* 120 (33), e2304663120. doi:10.1073/pnas.2304663120

Aponte, H., Galindo-Castañeda, T., Yáñez, C., Hartmann, M., and Rojas, C. (2022). Microbial community-level physiological profiles and genetic prokaryotic structure of burned soils under Mediterranean sclerophyll forests in central Chile. *Front. Microbiol.* 13, 824813. doi:10.3389/fmicb.2022.824813

Averill, C., Anthony, M. A., Baldrian, P., Finkbeiner, F., van den Hoogen, J., Kiers, T., et al. (2022). Defending earth's terrestrial microbiome. *Nat. Microbiol.* 7 (11), 1717–1725. doi:10.1038/s41564-022-01228-3

Azua-Bustos, A., and González-Silva, C. (2014). Biotechnological applications derived from microorganisms of the Atacama Desert. *BioMed Res. Int.* 2014, 1–7. doi:10.1155/2014/909312

Azua-Bustos, A., González-Silva, C., and Fairén, A. G. (2022). The Atacama Desert in northern Chile as an analog model of Mars. *Front. Astron. Space Sci.* 8. doi:10.3389/fspas.2021.810426

Azua-Bustos, A., Urrejola, C., and Vicuña, R. (2012). Life at the dry edge: microorganisms of the Atacama Desert. *FEBS Lett.* 586 (18), 2939–2945. doi:10.1016/j.febslet.2012.07.025

Baker, S. (2023). North-south publishing data show Stark inequities in global research. *Nature* 624 (7991), S1. doi:10.1038/d41586-023-03901-x

Bardgett, R. D., and van der Putten, W. H. (2014). Belowground biodiversity and ecosystem functioning. *Nature* 515 (7528), 505–511. doi:10.1038/nature13855

Barret, M., Gandois, L., Thalasso, F., Martinez Cruz, K., Sepulveda Jauregui, A., Lavergne, C., et al. (2022). A combined microbial and biogeochemical dataset from high-latitude ecosystems with respect to methane cycle. *Sci. Data* 9 (1), 674. doi:10.1038/s41597-022-01759-8

Benavente, J. M., Crespi, G., Figal Garone, L., and Maffioli, A. (2012). The impact of national research funds: a regression discontinuity approach to the Chilean FONDECYT. *Res. Policy* 41 (8), 1461–1475. doi:10.1016/j.respol.2012.04.007

Bhattacharyya, P. N., and Jha, D. K. (2012). Plant growth-promoting rhizobacteria (PGPR): emergence in agriculture. *World J. Microbiol. Biotechnol.* 28 (4), 1327–1350. doi:10.1007/s11274-011-0979-9

Bradshaw, A. (2021). Microbiological literacy and the role of social science: a response to Timmis et al. *Environ. Microbiol.* 23 (11), 6350–6354. doi:10.1111/1462-2920.15808

Bruna, N., Galliani, E., Oyarzún, P., Bravo, D., Fuentes, F., and Pérez-Donoso, J. M. (2022). Biomineralization of lithium nanoparticles by Li-resistant Pseudomonas rodhesiae isolated from the Atacama salt flat. *Biol. Res.* 55 (1), 12. doi:10.1186/s40659-022-00382-6

Bull, A. T., Asenjo, J. A., Goodfellow, M., and Gómez-Silva, B. (2016). The Atacama Desert: technical resources and the growing importance of novel microbial diversity. *Annu. Rev. Microbiol.* 70, 215–234. doi:10.1146/annurev-micro-102215-095236

Bustamante, M., Verdejo, V., Zúñiga, C., Espinosa, F., Orlando, J., and Carú, M. (2012). Comparison of water availability effect on ammonia-oxidizing bacteria and archaea in microcosms of a Chilean semiarid soil. *Front. Microbiol.* 3, 282. doi:10.3389/fmicb.2012.00282

Cabrera, M. Á., and Blamey, J. M. (2018). Biotechnological applications of archaeal enzymes from extreme environments. *Biol. Res.* 51, 37. doi:10.1186/s40659-018-0186-3

Cameron, R. E., Gensel, D. R., and Blank, C. B. (1966). "Soil studies—desert microflora. Xii. Abundance of microflora in soil samples from the Chile Atacama Desert," in *Supporting research and advanced developments, space programs summary no. 37–38* (Pasadena, CA: Jet Propulsion Lab, NASA), 140–147.

Cardenas, L. M., Hatch, D. J., Scholefield, D., Jhurreea, D., Clark, I. M., Hirsch, P. R., et al. (2013). Potential mineralization and nitrification in volcanic grassland soils in Chile. *Soil Sci. Plant Nutr.* 59 (3), 380–391. doi:10.1080/00380768.2013.789395

Caretta, G., and Piontelli, E. (1977). Microsporum magellanicum and Cunninghamella Antarctica, new species isolated from Australia and Antarctic soil of Chile. *Sabouraudia* 15 (1), 1–10. doi:10.1080/00362177785190021

Carro, L., Razmilic, V., Nouioui, I., Richardson, L., Pan, C., Golinska, P., et al. (2018). Hunting for cultivable Micromonospora strains in soils of the Atacama Desert. *Antonie Leeuwenhoek* 111 (8), 1375–1387. doi:10.1007/s10482-018-1049-1

Carvajal, M., Jeldres, P., Vergara, A., Lobaina, E., Olivares, M., Meza, D., et al. (2023). Bioremoval of copper by filamentous fungi isolated from contaminated soils of Puchuncaví-Ventanas Central Chile. *Environ. Geochem. Health* 45 (7), 4275–4293. doi:10.1007/s10653-023-01493-z

Casanova, M., Salazar, O., Seguel, O., and Luzio, W. (2013). *The soils of Chile*. Dordrecht, Netherlands: Springer.

Cavicchioli, R., Ripple, W. J., Timmis, K. N., Azam, F., Bakken, L. R., Baylis, M., et al. (2019). Scientists' warning to humanity: microorganisms and climate change. *Nat. Rev. Microbiol.* 17 (9), 569–586. doi:10.1038/s41579-019-0222-5

CEPAL—Comisión Económica para América Latina (1953). *Investigación tecnológica y formación de técnicos en América Latina. Estudio preliminar de prueba referente a*

*Chile preparado por la Secretaría Ejecutiva con la cooperación de un grupo de expertos*. Rio de Janeiro: Naciones Unidas.

Contador, C. A., Veas-Castillo, L., Tapia, E., Antipan, M., Miranda, N., Ruiz-Tagle, B., et al. (2020). Atacama database: a platform of the microbiome of the Atacama Desert. *Antonie Leeuwenhoek* 113 (2), 185–195. doi:10.1007/s10482-019-01328-x

Delgado-Baquerizo, M., Maestre, F. T., Reich, P. B., Jeffries, T. C., Gaitan, J. J., Encinar, D., et al. (2016). Microbial diversity drives multifunctionality in terrestrial ecosystems. *Nat. Commun.* 7, 10541. doi:10.1038/ncomms10541

di Castri, F., and Mooney, H. (1973). *Mediterranean type ecosystems, ecological studies 7*. Berlin, Germany: Springer-Verlag.

Dinamarca, D. I., Galleguillos, M., Seguel, O., and Faúndez Urbina, C. (2023). CLSoilMaps: a national soil gridded database of physical and hydraulic soil properties for Chile. *Sci. Data* 10 (1), 630. doi:10.1038/s41597-023-02536-x

Dose, K., Bieger-Dose, A., Ernst, B., Feister, U., Gómez-Silva, B., Klein, A., et al. (2001). Survival of microorganisms under the extreme conditions of the Atacama Desert. *Orig. Life Evol. Biosph.* 31 (3), 287–303. doi:10.1023/a:1010788829265

Espina, G., Muñoz-Ibacache, S. A., Cáceres-Moreno, P., Amenabar, M. J., and Blamey, J. M. (2022). From the discovery of Extremozymes to an enzymatic product: roadmap based on their applications. *Front. Bioeng. Biotechnol.* 9, 752281. doi:10.3389/fbioe.2021.752281

Eurostat (2023). Gross domestic expenditure on research and development 2022. Statistic Explained. Available: https://ec.europa.eu/eurostat/statistics-explained/index.php?title=R%26D_expenditure&oldid=551418#Gross_domestic_expenditure_on_R.26D (Accessed December 21, 2023).

FAO (2020). *State of knowledge of soil biodiversity – status, challenges and potentialities, summary for policymakers*. Rome: FAO.

Fernández-Martínez, M. A., Pérez-Ortega, S., Pointing, S. B., Allan Green, T. G., Pintado, A., Rozzi, R., et al. (2017). Microbial succession dynamics along glacier forefield chronosequences in Tierra del Fuego (Chile). *Polar Biol.* 40 (10), 1939–1957. doi:10.1007/s00300-017-2110-7

Fierer, N. (2017). Embracing the unknown: disentangling the complexities of the soil microbiome. *Nat. Rev. Microbiol.* 15 (10), 579–590. doi:10.1038/nrmicro.2017.87

Fuentes, A., Herrera, H., Charles, T. C., and Arriagada, C. (2020). Fungal and bacterial microbiome associated with the rhizosphere of native plants from the Atacama Desert. *Microorganisms* 8 (2), 209. doi:10.3390/microorganisms8020209

Fulthorpe, R. R., Rhodes, A. N., and Tiedje, J. M. (1996). Pristine soils mineralize 3-chlorobenzoate and 2,4-dichlorophenoxyacetate via different microbial populations. *Appl. Environ. Microbiol.* 62 (4), 1159–1166. doi:10.1128/aem.62.4.1159-1166.1996

Gran-Scheuch, A., Ramos-Zúñiga, J., Fuentes, E., Bravo, D., and Pérez-Donoso, J. M. (2020). Effect of co-contamination by PAHs and heavy metals on bacterial communities of diesel contaminated soils of South Shetland Islands, Antarctica. *Microorganisms* 8 (11), 1749. doi:10.3390/microorganisms8111749

Guerra, C. A., Heintz-Buschart, A., Sikorski, J., Chatzinotas, A., Guerrero-Ramírez, N., Cesarz, S., et al. (2020). Blind spots in global soil biodiversity and ecosystem function research. *Nat. Commun.* 11 (1), 3870. doi:10.1038/s41467-020-17688-2

Han, J., Jung, J., Park, M., Hyun, S., and Park, W. (2013). Short-term effect of elevated temperature on the abundance and diversity of bacterial and archaeal amoA genes in Antarctic soils. *J. Microbiol. Biotechnol.* 23 (9), 1187–1196. doi:10.4014/jmb.1305.05017

Hartley, A. J., Chong, G., Houston, J., and Mather, A. E. (2022). 150 million years of climatic stability: evidence from the Atacama Desert, northern Chile. *J. Geol. Soc.* 162 (3), 421–424. doi:10.1144/0016-764904-071

Hartmann, M., Frey, B., Mayer, J., Mader, P., and Widmer, F. (2015). Distinct soil microbial diversity under long-term organic and conventional farming. *ISME J.* 9 (5), 1177–1194. doi:10.1038/ismej.2014.210

Hartmann, M., and Six, J. (2022). Soil structure and microbiome functions in agroecosystems. *Nat. Rev. Earth Environ.* 4 (1), 4–18. doi:10.1038/s43017-022-00366-w

Hatzenpichler, R., Krukenberg, V., Spietz, R. L., and Jay, Z. J. (2020). Next-generation physiology approaches to study microbiome function at single cell level. *Nat. Rev. Microbiol.* 18 (4), 241–256. doi:10.1038/s41579-020-0323-1

Hernández, M., Vera-Gargallo, B., Calabi-Floody, M., King, G. M., Conrad, R., and Tebbe, C. C. (2020). Reconstructing genomes of carbon monoxide oxidisers in volcanic deposits including members of the class Ktedonobacteria. *Microorganisms* 8 (12), 1880. doi:10.3390/microorganisms8121880

Hinsu, A., Dumadiya, A., Joshi, A., Kotadiya, R., Andharia, K., Koringa, P., et al. (2021). To culture or not to culture: a snapshot of culture-dependent and culture-independent bacterial diversity from peanut rhizosphere. *PeerJ* 9, e12035. doi:10.7717/peerj.12035

Idris, H., Goodfellow, M., Sanderson, R., Asenjo, J. A., and Bull, A. T. (2017). Actinobacterial rare biospheres and dark matter revealed in habitats of the Chilean Atacama Desert. *Sci. Rep.* 7 (1), 8373. doi:10.1038/s41598-017-08937-4

Jansson, J. K., and Hofmockel, K. S. (2018). The soil microbiome-from metagenomics to metaphenomics. *Curr. Opin. Microbiol.* 43, 162–168. doi:10.1016/j.mib.2018.01.013

Jorquera, M. A., Inostroza, N. G., Lagos, L. M., Barra, P. J., Marileo, L. G., Rilling, J. I., et al. (2014). Bacterial community structure and detection of putative plant growth-promoting rhizobacteria associated with plants grown in Chilean agro-ecosystems and undisturbed ecosystems. *Biol. Fertil. Soils* 50 (7), 1141–1153. doi:10.1007/s00374-014-0935-6

Jung, T., Scanu, B., Bakonyi, J., Seress, D., Kovacs, G. M., Duran, A., et al. (2017). Nothophytophthora gen. nov., a new sister genus of Phytophthora from natural and semi-natural ecosystems. *Persoonia* 39, 143–174. doi:10.3767/persoonia.2017.39.07

Knief, C., Bol, R., Amelung, W., Kusch, S., Frindte, K., Eckmeier, E., et al. (2020). Tracing elevational changes in microbial life and organic carbon sources in soils of the Atacama Desert. *Glob. Planet. Change* 184, 103078. doi:10.1016/j.gloplacha.2019.103078

Kochhar, N., Shrivastava, S., Ghosh, A., Rawat, V. S., Sodhi, K. K., Kumar, M., et al. (2022). Perspectives on the microorganism of extreme environments and their applications. *Curr. Res. Microb. Sci.* 3, 100134. doi:10.1016/j.crmicr.2022.100134

Krüger, A., Schäfers, C., Schröder, C., and Antranikian, G. (2018). Towards a sustainable biobased industry–highlighting the impact of extremophiles. *New Biotechnol.* 40, 144–153. doi:10.1016/j.nbt.2017.05.002

Leiva-Aravena, E., Leiva, E., Zamorano, V., Rojas, C., Regan, J. M., and Vargas, I. T. (2019). Organotrophic acid-tolerant microorganisms enriched from an acid mine drainage affected environment as inoculum for microbial fuel cells. *Sci. Total Environ.* 678, 639–646. doi:10.1016/j.scitotenv.2019.05.003

Luzio, W., and Alcayaga, S. (1992). Mapa de asociaciones de grandes grupos de suelos de Chile. *Agric. Téc.* 52 (4), 347–353.

Maas, B., Pakeman, R. J., Godet, L., Smith, L., Devictor, V., and Primack, R. (2021). Women and global south strikingly underrepresented among top-publishing ecologists. *Conserv. Lett.* 14 (4). doi:10.1111/conl.12797

Machuca, A., Pereira, G., Aguiar, A., and Milagres, A. M. (2007). Metal-chelating compounds produced by ectomycorrhizal fungi collected from pine plantations. *Lett. Appl. Microbiol.* 44 (1), 7–12. doi:10.1111/j.1472-765X.2006.02046.x

Mandakovic, D., Rojas, C., Maldonado, J., Latorre, M., Travisany, D., Delage, E., et al. (2018). Structure and co-occurrence patterns in microbial communities under acute environmental stress reveal ecological factors fostering resilience. *Sci. Rep.* 8 (1), 5875. doi:10.1038/s41598-018-23931-0

Marín, C., Aguilera, P., Oehl, F., and Godoy, R. (2017). Factors affecting arbuscular mycorrhizal fungi of Chilean temperate rainforests. *J. Soil Sci. Plant Nutr.* 17 (4), 966–984. doi:10.4067/s0718-95162017000400010

Marín, C., Rubio, J., and Godoy, R. (2022). Chilean blind spots in soil biodiversity and ecosystem function research. *Austral Ecol.* 47 (7), 1372–1381. doi:10.1111/aec.13232

Martins, Z., Cottin, H., Kotler, J. M., Carrasco, N., Cockell, C. S., de la Torre Noetzel, R., et al. (2017). Earth as a tool for astrobiology—a European perspective. *Space Sci. Rev.* 209 (1-4), 43–81. doi:10.1007/s11214-017-0369-1

Maza, F., Maldonado, J., Vásquez-Dean, J., Mandakovic, D., Gaete, A., Cambiazo, V., et al. (2019). Soil bacterial communities from the Chilean Andean highlands: taxonomic composition and culturability. *Front. Bioeng. Biotechnol.* 7, 10. doi:10.3389/fbioe.2019.00010

McKay, C. P., Friedmann, E. I., Gómez-Silva, B., Cáceres-Villanueva, L., Andersen, D. T., and Landheim, R. (2003). Temperature and moisture conditions for life in the extreme arid region of the Atacama desert: four years of observations including the el niño of 1997-1998. *Astrobiology* 3 (2), 393–406. doi:10.1089/153110703769016460

Meza, C., Valenzuela, F., Echeverría-Vega, A., Gomez, A., Sarkar, S., Cabeza, R. A., et al. (2022). Plant-growth-promoting bacteria from rhizosphere of Chilean common bean ecotype (Phaseolus vulgaris L.) supporting seed germination and growth against salinity stress. *Front. Plant. Sci.* 13, 1052263. doi:10.3389/fpls.2022.1052263

Ministerio de Ciencia Tecnología Conocimiento e Innovación (2023). Iniciativa científica Milenio. Available: https://www.iniciativamilenio.cl/institutos-y-nucleos-milenio [Accessed 14 October 2023].

Ministerio de Educación - Chile (2018). Ley 21105, de 13 de agosto de 2018. Crea el Ministerio de Ciencia, Tecnología, Conocimiento e Innovación. Available: https://www.bcn.cl/leychile/navegar?idNorma=1121682 [Accessed 5 September 2023].

Ministerio del Medio Ambiente - Chile (2018). "Biodiversidad de Chile," in *Patrimonio y desafíos* (Santiago de Chile: Ministerio del Medio Ambiente - Chile), 430.

Ministerio de Relaciones Exteriores - Chile (1966). Ley 16592, de 21 de diciembre de 1966. Crea Dirección de Fronteras y Límites del Estado. Available: https://www.bcn.cl/leychile/navegar?idNorma=28558 (Accessed October 18, 2023).

Navarro-González, R., Rainey, F. A., Molina, P., Bagaley, D. R., Hollen, B. J., de la Rosa, J., et al. (2003). Mars-like soils in the Atacama Desert, Chile, and the dry limit of microbial life. *Science* 302 (5647), 1018–1021. doi:10.1126/science.1089143

Nazer Ahumada, R. (2016). La Corporación de Fomento a la Producción y la modernización económica de Chile. 1939-1970. *Rev. Gest. Pública* 5 (2), 283–316. doi:10.22370/rgp.2016.5.2.2223

Neilson, J. W., Califf, K., Cardona, C., Copeland, A., van Treuren, W., Josephson, K. L., et al. (2017). Significant impacts of increasing aridity on the arid soil microbiome. *mSystems* 2 (3), e00195-16. doi:10.1128/mSystems.00195-16

Nielsen, M. W., Alegria, S., Börjeson, L., Etzkowitz, H., Falk-Krzesinski, H. J., Joshi, A., et al. (2017). Opinion: gender diversity leads to better science. *Proc. Natl. Acad. Sci. U.S.A.* 114 (8), 1740–1742. doi:10.1073/pnas.1700616114

Nuñez, M. A., Barlow, J., Cadotte, M., Lucas, K., Newton, E., Pettorelli, N., et al. (2019). Assessing the uneven global distribution of readership, submissions and publications in applied ecology: obvious problems without obvious solutions. *J. Appl. Ecol.* 56 (1), 4–9. doi:10.1111/1365-2664.13319

Núñez-Montero, K., Rojas-Villalta, D., Hernández-Moncada, R., Esquivel, A., and Barrientos, L. (2023). Genome sequence of Pseudomonas sp. strain So3.2b, isolated from a soil sample from robert island (antarctic specially protected area 112), antarctic. *Antarct. Microbiol. Resour. Announce.* 12 (3), e0116722. doi:10.1128/mra.01167-22

ODEPA—Oficina de Estudios y Políticas Agrarias (2019). *Panorama de la agricultura chilena*. Santiago, Chile: Ministerio de Agricultura. ODEPA.

OECD (2022). OECD economic surveys: Chile. https://www.oecd-ilibrary.org/economics/oecd-economic-surveys-chile_19990847.

Okoro, C. K., Brown, R., Jones, A. L., Andrews, B. A., Asenjo, J. A., Goodfellow, M., et al. (2009). Diversity of culturable actinomycetes in hyper-arid soils of the Atacama Desert, Chile. *Antonie Leeuwenhoek* 95 (2), 121–133. doi:10.1007/s10482-008-9295-2

Orellana, R., Macaya, C., Bravo, G., Dorochesi, F., Cumsille, A., Valencia, R., et al. (2018). Living at the frontiers of life: extremophiles in Chile and their potential for bioremediation. *Front. Microbiol.* 9, 2309. doi:10.3389/fmicb.2018.02309

Osorio, C. (2015). Historia de la ensenanza de la microbiologia en Chile: Centros formadores. *Rev. Chil. Infectol.* 32 (4), 447–452. doi:10.4067/S0716-10182015000500012

Osorio, C. G. (2010). The history of microbiology in Chile: about the origin of experimental bacteriology. *Rev. Med. Chile* 138 (7), 913–919. doi:10.4067/s0034-98872010000700019

Parada, R. J. (1999). Variables discriminantes en fondecyt. *Estud. Soc. (Santiago)* 100, 163–173.

Paulino-Lima, I. G., Azua-Bustos, A., Vicuña, R., González-Silva, C., Salas, L., Teixeira, L., et al. (2013). Isolation of UVC-tolerant bacteria from the hyperarid Atacama Desert, Chile. *Microb. Ecol.* 65 (2), 325–335. doi:10.1007/s00248-012-0121-z

Pavón, A., Corsini, G., Orellana, P., Calisto, N., Navarro, L., Wiese, G., et al. (2023). Identification of Antarctic soil bacteria exhibiting antiproliferative activity against a colon cancer cell line. *Int. J. Morphol.* 41 (1), 286–296. doi:10.4067/s0717-95022023000100286

Pfeiffer, M., Padarian, J., Osorio, R., Bustamante, N., Olmedo, G. F., Guevara, M., et al. (2020). CHLSOC: the Chilean soil organic carbon database, a multi-institutional collaborative effort. *Earth Syst. Sci. Data* 12 (1), 457–468. doi:10.5194/essd-12-457-2020

Prado, B., del Moral, A., and Campos, V. (1993). Distribution and types of heterotrophyc halophilic flora from Salar de Atacama, Chile. *Toxicol. Environ. Chem.* 38 (3-4), 163–166. doi:10.1080/02772249309357887

Prado, B., Del Moral, A., Quesada, E., Ríos, R., Monteoliva-Sanchez, M., Campos, V., et al. (1991). Numerical taxonomy of moderately halophilic Gram-negative rods isolated from the Salar de Atacama, Chile. *Syst. Appl. Microbiol.* 14 (3), 275–281. doi:10.1016/s0723-2020(11)80381-4

Pulschen, A. A., Rodrigues, F., Duarte, R. T., Araujo, G. G., Santiago, I. F., Paulino-Lima, I. G., et al. (2015). UV-resistant yeasts isolated from a high-altitude volcanic area on the Atacama Desert as eukaryotic models for astrobiology. *MicrobiologyOpen* 4 (4), 574–588. doi:10.1002/mbo3.262

Quesada, C. F. (2016). Institucionalización científica y financiamiento filantrópico. El Convenio Universidad de Chile-Universidad de California y la Fundación Ford (1965-1975). *Fronteras* 3 (1), 125–148.

Ramírez, P. B., Fuentes-Alburquenque, S., Díez, B., Vargas, I., and Bonilla, C. A. (2020). Soil microbial community responses to labile organic carbon fractions in relation to soil type and land use along a climate gradient. *Soil Biol. biochem.* 141, 107692. doi:10.1016/j.soilbio.2019.107692

R Core Team (2021). *R: a language and environment for statistical computing*. Vienna, Austria: R Foundation for Statistical Computing.

Renny, M., Acosta, M. C., Cofré, N., Domínguez, L. S., Bidartondo, M. I., and Sersic, A. N. (2017). Genetic diversity patterns of arbuscular mycorrhizal fungi associated with the mycoheterotroph Arachnitis uniflora Phil. (Corsiaceae). *Phil. (Corsiaceae). Ann. Bot.* 119 (8), 1279–1294. doi:10.1093/aob/mcx023

Rodríguez, M. (1992). La microbiología en Chile: su desarrollo a la luz de un siglo de existencia. *Rev. Med. Chile* 120, 463–470.

Rodríguez-Echeverría, S., Delgado-Baquerizo, M., Morillo, J. A., Gaxiola, A., Manzano, M., Marquet, P. A., et al. (2021). Azorella cushion plants and aridity are important drivers of soil microbial communities in Andean ecosystems. *Ecosystems* 24 (7), 1576–1590. doi:10.1007/s10021-021-00603-1

Santos, A., Bruna, P., Martinez-Urtaza, J., Solís, F., Valenzuela, B., Zamorano, P., et al. (2021). Two archaeal metagenome-assembled genomes from El Tatio provide new insights into the Crenarchaeota phylum. *Genes* 12 (3), 391. doi:10.3390/genes12030391

Satoh, Y., Yoshimura, K., Pokhrel, Y., Kim, H., Shiogama, H., Yokohata, T., et al. (2022). The timing of unprecedented hydrological drought under climate change. *Nat. Commun.* 13 (1), 3287. doi:10.1038/s41467-022-30729-2

Schaefer, P. (1973). "Microbial activity under seasonal conditions of drought in Mediterranean climates," in *Mediterranean type ecosystems, ecological studies 7*. Editors F. Di Castri and H. Mooney (Berlin, Germany: Springer-Verlag), 191–198.

Scherson, R. A., Thornhill, A. H., Urbina-Casanova, R., Freyman, W. A., Pliscoff, P. A., and Mishler, B. D. (2017). Spatial phylogenetics of the vascular flora of Chile. *Mol. Phylogenet. Evol.* 112, 88–95. doi:10.1016/j.ympev.2017.04.021

Schultz, J., dos Santos, A., Patel, N., and Rosado, A. S. (2023). Life on the edge: bioprospecting extremophiles for astrobiology. *J. Indian Inst. Sci.* 103, 721–737. doi:10.1007/s41745-023-00382-9

Seeger, M., and Espinoza, F. (2008). Highlights of Latin American microbiology: the 19th ALAM congress. *Int. Microbiol.* 11, 289–292. doi:10.2436/20.1501.01.74

Serrano, J., and Leiva, E. (2017). Removal of arsenic using acid/metal-tolerant sulfate reducing bacteria: a new approach for bioremediation of high-arsenic acid mine waters. *Water* 9 (12), 994. doi:10.3390/w9120994

Stchigel, A. M., Calduch, M., Guarro, J., and Zaror, L. (2002). A new species of Podospora from soil in Chile. *Mycologia* 94 (3), 554–558. doi:10.1080/15572536.2003.11833221

Stefani, F. O., Bell, T. H., Marchand, C., De La Providencia, I. E., El Yassimi, A., St-Arnaud, M., et al. (2015). Culture-dependent and-independent methods capture different microbial community fractions in hydrocarbon-contaminated soils. *PloS one* 10 (6), e0128272. doi:10.1371/journal.pone.0128272

Timmis, K., Timmis, J., and Jebok, F. (2020). The urgent need for microbiology literacy in society: children as educators. *Microb. Biotechnol.* 13 (5), 1300–1303. doi:10.1111/1751-7915.13619

Valenzuela-Heredia, D., Henríquez-Castillo, C., Donoso, R., Lavín, P., Pavlov, M. S., Franchi, O., et al. (2020). Complete genome sequence of Pseudomonas chilensis strain ABC1, isolated from soil. *Microbiol. Resour. Announce.* 9 (39), e00775-20. doi:10.1128/MRA.00775-20

Vázquez, S., Monien, P., Pepino Minetti, R., Jürgens, J., Curtosi, A., Villalba Primitz, J., et al. (2017). Bacterial communities and chemical parameters in soils and coastal sediments in response to diesel spills at Carlini Station, Antarctica. *Sci. Total Environ.* 605-606, 26–37. doi:10.1016/j.scitotenv.2017.06.129

Villagrán, C., and Armesto, J. J. (2005). "Fitogeografía histórica de la cordilera de la costa de Chile," in *Historia, biogeografía y ecología de los bosques costeros de Chile*. Editors C. Smith-Ramírez, J. J. Armesto, and C. Valdovinos (Santiago: Editorial Universitaria), 99–115.

Villagrán, C., and Hinojosa, F. (1997). Historia de los bosques del sur de Sudamérica, II: análisis fitogeográfico. *Rev. Chil. Hist. Nat.* 70, 241–267.

D. H. Wall, R. D. Bardgett, V. Behan-Pelletier, J. E. Herrick, T. H. Jones, K. Ritz, et al. (2012). *Soil ecology and ecosystem services* (New York, United States of America: Oxford University Press).

World Bank Group (2020). Economy profile of Chile. Available: https://Archive.Doingbusiness.Org/En/Data/Exploreeconomies/Chile (Accessed December 21, 2023).

Wu, L., Zhang, Y., Guo, X., Ning, D., Zhou, X., Feng, J., et al. (2022). Reduction of microbial diversity in grassland soil is driven by long-term climate warming. *Nat. Microbiol.* 7 (7), 1054–1062. doi:10.1038/s41564-022-01147-3

Zárate, M. S., Sierra, D., and Goldflam, M. (2022). Orígenes y desarrollo de una política científica nacional en Chile: conicyt, 1967-1981. *Hist. Cienc. Saude-Manguinhos* 29 (4), 953–972. doi:10.1590/S0104-59702022000400005

# Frontiers in Environmental Science

**Explores the anthropogenic impact on our natural world**

An innovative journal that advances knowledge of the natural world and its intersections with human society. It supports the formulation of policies that lead to a more inhabitable and sustainable world.

---

## Discover the latest Research Topics

See more →

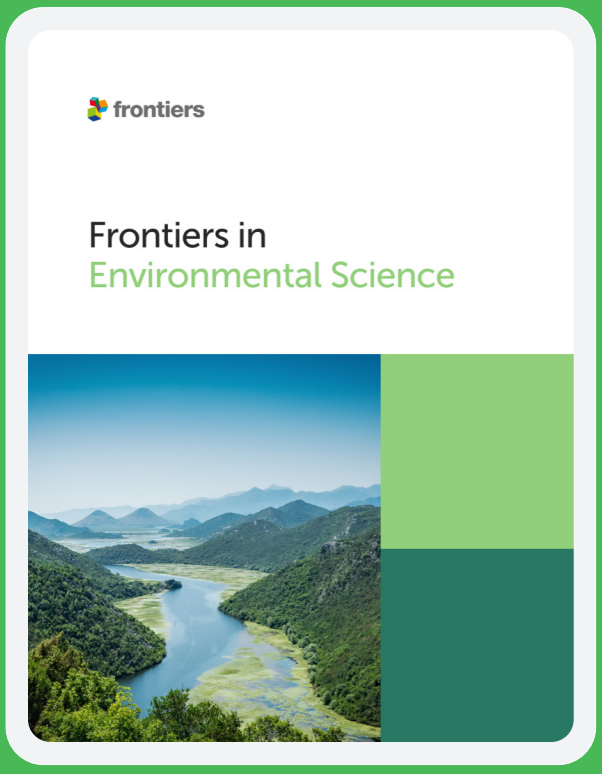


**Frontiers**

Avenue du Tribunal-Fédéral 34
1005 Lausanne, Switzerland
frontiersin.org

**Contact us**

+41 (0)21 510 17 00
frontiersin.org/about/contact